

UC Irvine

UC Irvine Electronic Theses and Dissertations

Title

Cobalt-Catalyzed Hydrogen Atom Transfer-Initiated Radical-Polar Crossover Alkene Hydrofunctionalizations

Permalink

<https://escholarship.org/uc/item/8t12x3nq>

Author

Touney, Eric

Publication Date

2021

Peer reviewed|Thesis/dissertation

UNIVERSITY OF CALIFORNIA,
IRVINE

Cobalt-Catalyzed Hydrogen Atom Transfer-Initiated Radical–Polar Crossover Alkene
Hydrofunctionalizations

DISSERTATION

submitted in partial satisfaction of the requirements
for the degree of

DOCTOR OF PHILOSOPHY

in Chemistry

by

Eric Edward Touney

Dissertation Committee:
Professor Sergey V. Pronin, Chair
Professor Vy M. Dong
Professor Christopher D. Vanderwal

2021

Portions of Chapter 2 were reprinted with permission from:
Touney, E. E.; Foy, N. J.; Pronin, S. V. *J. Am. Chem. Soc.* **2018**, *140*, 16982.
© 2018 American Chemical Society

Portions of Chapter 3 were reprinted with permission from:
Discolo, C. A.; Touney, E. E.; Pronin, S. V. *J. Am. Chem. Soc.* **2019**, *141*, 17527.
© 2019 American Chemical Society

© 2021 Eric Edward Touney

DEDICATION

To Grandma Touney,
the best Scrabble player I know.

TABLE OF CONTENTS

	Page
List of Figures	viii
List of Schemes	ix
List of Tables	xiv
Acknowledgments	xvi
Vita	xix
Abstract of the Dissertation	xx
Chapter 1: A Review of Cobalt-Catalyzed Hydrogen Atom Transfer-Initiated Alkene Hydrofunctionalizations	1
1.1 An Introduction to Metal-Hydride-Mediated Hydrogen Atom Transfer Reactions	1
1.1.1 Brønsted Acid-Catalyzed Alkene Hydrofunctionalizations	
1.1.2 Metal-Hydride-Mediated Hydrogen Atom Transfer Alkene Hydrofunctionalizations	2
1.2 A Brief History of Cobalt Hydride-Mediated HAT Alkene Hydrofunctionalizations	3
1.2.1 Origins of MHAT Alkene Hydrofunctionalizations	3
1.2.2 Mukaiyama's Cobalt-Catalyzed HAT Hydration of Unactivated Alkenes	5
1.2.3 Carreira's Cobalt-Catalyzed HAT Hydrohydrazination of Unactivated Alkenes	9
1.2.4 Carreira's Cobalt-Catalyzed HAT Hydroazidation of Unactivated Alkenes	11
1.2.5 Carreira's Cobalt-Catalyzed HAT Hydrocyanation of Unactivated Alkenes	13
1.2.6 Carreira's Cobalt-Catalyzed HAT Hydrochlorination of Unactivated Alkenes	14
1.2.7 Shenvi's Cobalt-Catalyzed HAT Hydrogenation of Unactivated Alkenes	17
1.2.8 Herzon's Cobalt-Catalyzed HAT Hydrogenation of Unactivated Alkenes	19
1.2.9 Shenvi's Cobalt-Catalyzed HAT Alkene Isomerization	21

1.2.10 Herzon's Cobalt-Mediated HAT Hydropyridylation of Unactivated Alkenes	24
1.2.11 Shenvi's Dual-Catalytic HAT Hydroarylation of Unactivated Alkenes	26
1.3 Cobalt-Catalyzed HAT Radical–Polar Crossover Alkene Hydrofunctionalizations	28
1.3.1 An Introduction to MHAT Radical–Polar Crossover Hydrofunctionalizations	28
1.3.2 Conspectus	30
1.3.3 Shigehisa's Intermolecular HAT Radical–Polar Crossover Hydroalkoxylation	30
1.3.4 Shigehisa's Intramolecular HAT Radical–Polar Crossover Hydroamination	33
1.3.5 Shigehisa's Synthesis of Oxygen Heterocycles via HAT Radical–Polar Crossover	34
1.3.6 Shigehisa's Intramolecular HAT Radical–Polar Crossover Hydroarylation	37
1.3.7 Shigehisa's Intramolecular HAT Radical–Polar Crossover Hydrothiolation	39
1.3.8 Shigehisa's Synthesis of Cyclic Carbamates and Ureas via HAT Radical–Polar Crossover	41
1.3.9 Shigehisa's Asymmetric HAT Radical–Polar Crossover Hydroalkoxylation	43
1.3.10 Shigehisa's Synthesis of Cyclic Guanidines via HAT Radical–Polar Crossover	47
1.3.11 Zhu's Intermolecular HAT Radical–Polar Crossover Hydroacyloxylation	48
1.3.12 Zhu's Photoredox-Enabled Radical–Polar Crossover Hydrofunctionalizations	51
1.3.13 Akai's Intermolecular HAT Radical–Polar Crossover Hydroamination	53
1.3.14 Vanderwals's HAT Radical–Polar Crossover Bicyclizations	55
1.3.15 Vanderwals's Stereocontrolled Synthesis of Abietane Diterpenoids via HAT Radical–Polar Crossover Polyene Cyclization	57
1.4 References and Notes	60

Chapter 2: Catalytic Radical–Polar Crossover Reactions of Allylic Alcohols	65
2.1 Introduction	65
2.2 Strategy for Catalytic Radical–Polar Crossover Reactions of Allylic Alcohols	66
2.3 Reaction Optimization	69
2.3.1 Substrate Selection	69
2.3.2 Optimization of Reaction Conditions for Radical–Polar Crossover Hydrofunctionalization	70
2.3.3 Optimization of Catalysts for Radical–Polar Crossover Hydrofunctionalization	72
2.4 Substrate Scope	73
2.5 Mechanistic Studies	77
2.5.1 Catalyst Control Suggests Participation of Electrophilic Alkylcobalt Intermediates	77
2.5.2 Diastereoselectivity of Ring Expansion is Catalyst Dependent	77
2.5.3 Diastereoselectivity of Ag(I) Promoted Ring Expansions of Bromohydrins	79
2.6 Solvent Dependent HAT Radical–Polar Crossover Hydrofunctionalizations of 1,1-Disubstituted Alkenes	81
2.7 Conclusions and Outlook	83
2.8 Experimental Section	
2.8.1 Materials and Methods	84
2.3.2 Experimental Procedures	55
2.9 References and Notes	119

Chapter 3: Catalytic Asymmetric Radical–Polar Crossover Hydroalkoxylation	122
3.1 Introduction	122
3.2 Strategy for Catalytic Asymmetric Radical–Polar Crossover Hydroalkoxylation	123
3.3 Key Precedents for Method Development	125
3.3.1 Jackman’s Stereoselective Deuterocobaltation	125
3.3.2 Gridnev’s Stereoselective Hydrocobaltation	126
3.3.3 Halpern’s Stereospecific Displacement of Alkylcobalt(IV) Complexes	127
3.3.4 Shigehisa’s Intramolecular HAT Radical–Polar Crossover Hydroalkoxylation	128
3.4 Strategy Design	130
3.5 Catalyst Optimization	133
3.6 Substrate Scope	136
3.7 Mechanistic Studies	137
3.7.1 Eyring Analysis	137
3.7.2 Arene Property Correlations	141
3.7.3 Rationalizing the Influence of Substrate Structure on Enantioselectivity	142
3.7.4 Proposed Mechanism for Catalytic Asymmetric Radical–Polar Crossover Hydroalkoxylation	145
3.8 Derivatization of Epoxide 3.61	147
3.9 Conclusions and Outlook	147
3.10 Experimental Section	148
3.10.1 Materials and Methods	148
3.10.2 Experimental Procedures	150
3.5 References and Notes	190

Chapter 4: Catalytic Radical–Polar Crossover Ritter Reactions of Trisubstituted and Tetrasubstituted Alkenes	194
4.1 Introduction	194
4.2 Strategy for a Catalytic Radical–Polar Crossover Ritter Reactions	198
4.3 Catalyst Optimization	200
4.3.1 Catalyst Optimization for Hydroamidation of Tetrasubstituted Alkene 4.41	200
4.3.2 Catalyst Optimization for Hydroamidation of Trisubstituted Alkene 4.51	202
4.4 Substrate Scope	204
4.5 Mechanistic Studies	207
4.5.1 Elucidating the Origin of Hydration Products	207
4.5.2 Hydrogen Evolution Studies	208
4.6 Conclusions and Outlook	212
4.7 Experimental Section	212
4.7.1 Materials and Methods	212
4.7.2 Experimental Procedures	214
4.8 References and Notes	299
Appendix A: NMR Spectra for Chapter 2	303
Appendix B: NMR Spectra for Chapter 3	363
Appendix C: NMR Spectra for Chapter 4	426
Appendix D: Chiral GC-FID Data	544
Appendix E: Chiral SFC Data	563

LIST OF FIGURES

	Page
Figure 1.1 Cobalamine and its Artificial Mimics	4
Figure 3.1 Retrosynthetic Strategy for Exploring Co(II) Salen Ligand Chemical Space	132
Figure 3.2 Eyring Analysis Supports Pi-Stacking Interactions in Enantiodetermining Step	138
Figure 3.3 Representation of Putative Alkylcobalt(IV) Intermediate Derived From Catalyst 3.59 and Substrate 3.51	141
Figure 3.4 Linear Correlation of Arene Properties with Enantioselectivity	142
Figure 3.5 Proposed Influence of Substrate Structural Features on Stereochemical Outcomes	144
Figure 4.1 Retrosynthetic Strategy for Exploring Co(II) Salen Ligand Chemical Space	199

LIST OF SCHEMES

	Page
Scheme 1.1 Brønsted Acid-Catalyzed Hydrofunctionalization	1
Scheme 1.2 Metal-Hydride-Mediated Hydrogen Atom Transfer Hydrofunctionalizations	2
Scheme 1.3 Okamoto and Oka's Catalytic Styrene Hydrations	5
Scheme 1.4 Mukaiyama's 1 st Generation Cobalt-Catalyzed Hydration of Unactivated Alkenes	6
Scheme 1.5 Mukaiyama's Optimized Cobalt-Catalyzed Aerobic Hydration of Unactivated Alkenes	7
Scheme 1.6 General Catalytic Cycles for a Cobalt-Catalyzed Mukaiyama-Type Alkene Hydrofunctionalization	8
Scheme 1.7 Carreira's Cobalt-Catalyzed HAT Hydrohydrazination of Unactivated Alkenes	9
Scheme 1.8 Substrate Scope and Proposed Catalytic Cycle of Carreira's Cobalt-Catalyzed HAT Hydrohydrazination	10
Scheme 1.9 Carreira's Cobalt-Catalyzed HAT Hydroazidation	12
Scheme 1.10 Carreira's Cobalt-Catalyzed HAT Hydrocyanation	13
Scheme 1.11 Carreira's Cobalt-Catalyzed HAT Hydrochlorination	15
Scheme 1.12 Proposed Mechanism of Carreira's Cobalt-Catalyzed HAT Hydrochlorination and Deuterium Labeling Studies	16
Scheme 1.13 Shenvi's HAT-Mediated Alkene Hydrogenation	18
Scheme 1.14 Herzon's Cobalt-Catalyzed HAT Hydrogenation	20
Scheme 1.15 Shenvi's Cobalt-Catalyzed HAT Alkene Isomerization	22
Scheme 1.16 Catalyst Effects and Proposed Mechanism for Shenvi's Cobalt-Catalyzed HAT Alkene Isomerization	23

Scheme 1.17 Herzon's Cobalt-Mediated HAT Hydropyridylation	24
Scheme 1.18 Herzon's Scope of Competent Pyridinium Coupling Partners	25
Scheme 1.19 Proposed Mechanism of Shenvi's Dual-Catalytic HAT Hydroarylation	26
Scheme 1.20 Representative Substrate Scope of Shenvi's Dual-Catalytic HAT Hydroarylation	27
Scheme 1.21 A General Mechanism for MHAT-Mediated Radical–Polar Crossover Alkene Hydrofunctionalization	29
Scheme 1.22 Proposed Mechanism of Shigehisa's HAT Radical–Polar Crossover Hydroalkoxylation	31
Scheme 1.23 Representative Scope of Shigehisa's HAT Radical–Polar Crossover Hydroalkoxylation	32
Scheme 1.24 Shigehisa's Intramolecular HAT Radical–Polar Crossover Hydroamination	33
Scheme 1.25 Protecting Group Identity Influences Reaction Outcomes	34
Scheme 1.26 Shigehisa's HAT Radical–Polar Crossover Synthesis of Oxygen Heterocycles	35
Scheme 1.27 Mechanistic Studies of HAT Radical–Polar Crossover Synthesis of Oxygen Heterocycles	36
Scheme 1.28 Shigehisa's Intramolecular HAT Radical–Polar Crossover Hydroarylation	38
Scheme 1.29 Shigehisa's HAT Radical–Polar Crossover Hydrothiolation	39
Scheme 1.30 Representative Scope of Shigehisa's HAT Radical–Polar Crossover Hydrothiolation	40
Scheme 1.31 Shigehisa's Synthesis of Cyclic Carbamates and Ureas via Radical–Polar Crossover	42
Scheme 1.32 Shigehisa's Asymmetric HAT Radical–Polar Crossover Hydroalkoxylation	43

Scheme 1.33 Representative Substrate Scope for Shigehisa's Asymmetric HAT Radical–Polar Crossover Hydroalkoxylation	44
Scheme 1.34 Proposed Mechanism for Shigehisa's Asymmetric HAT Radical–Polar Crossover Hydroalkoxylation	46
Scheme 1.35 Shigehisa's Synthesis of Cyclic Guanidines via Radical–Polar Crossover	47
Scheme 1.36 Proposed Mechanism of Zhu's Radical–Polar Crossover Hydroacyloxylation	49
Scheme 1.37 Representative Substrate Scope for Zhu's HAT Radical–Polar Crossover Hydroacyloxylation	50
Scheme 1.38 Zhu's Proposed Mechanism for Photoredox-Coupled HAT Radical–Polar Crossover	52
Scheme 1.39 Akai's Intermolecular HAT Radical–Polar Crossover Hydroamination	54
Scheme 1.40 Vanderwal's HAT Radical–Polar Crossover Bicyclizations	55
Scheme 1.41 Mechanistic Investigations of Vanderwal's HAT Radical–Polar Crossover Bicyclizations	56
Scheme 1.42 Vanderwal's Stereocontrolled HAT Radical–Polar Crossover Bicyclizations	58
Scheme 1.43 Vanderwal's Synthesis of Abietane Diterpenoids	59
Scheme 2.1 Strategy for Catalyst-Controlled HAT Radical–Polar Crossover Alkene Hydrofunctionalization	66
Scheme 2.2 Halpern's Stereoinvertive Displacement of Alkylcobalt(IV) Complexes	67
Scheme 2.3 Reaction Pathways Available to Tertiary Allylic Alcohols	68
Scheme 2.4 Proposed Ring Expansion of Vinylcyclohexanols to Cycloheptanones	69
Scheme 2.5 Takemoto's Iodine(III)-Promoted Ring Expansions of Bromohydrins	78
Scheme 2.6 Proposed Hydrofunctionalization Mechanism for Catalyst 2.27	79

Scheme 2.7 Silver(I)-Promoted Ring Expansion of Bromohydrins 2.69 and 2.70	80
Scheme 2.8 Proposed Hydrofunctionalization Mechanism for Catalysts 2.32 and 2.33	80
Scheme 2.9 Proposed Mechanism for Hydrofunctionalization of 1,1-Disubstituted Alkenes	81
Scheme 3.1 Yamada's Stereoselective HAT Hydrofunctionalization of α,β -Unsaturated Carboxamides	122
Scheme 3.2 Strategy for Asymmetric HAT Radical–Polar Crossover Alkene Hydrofunctionalization	124
Scheme 3.3 Jackman's Stereoselective Deuterocobaltation	126
Scheme 3.4 Gridnev's Stereoselective Hydrocobaltation	127
Scheme 3.5 Halpern's Stereospecific Nucleophilic Displacement of Alkylcobalt(IV) Complexes	128
Scheme 3.6 Shigehisa's Intramolecular HAT Radical–Polar Crossover Hydroalkoxylation	129
Scheme 3.7 Strategy for Asymmetric HAT Radical–Polar Crossover Hydroalkoxylation	130
Scheme 3.8 Synthetic Strategy for Preparing Enantioenriched Co(II) Salen Catalysts	133
Scheme 3.9 Proposed Mechanism for the Catalytic Asymmetric Radical–Polar Crossover Hydroalkoxylation	145
Scheme 3.10 Derivatization of Epoxide 3.61	147
Scheme 4.1 The Ritter Reaction and a General Mechanism	194
Scheme 4.2 Select Examples from Carreira's Cobalt-Catalyzed Hydrohydrazination and Hydroazidation	195
Scheme 4.3 Initial Studies of the Catalytic Radical–Polar Crossover Ritter Reaction	196
Scheme 4.4 Select Examples from Relevant Radical–Polar Crossover Hydrofunctionalizations	197

Scheme 4.5 Strategy for a HAT Radical–Polar Crossover Ritter Reaction	200
Scheme 4.6 Isotope Labeling Experiments Using H ₂ ¹⁸ O	207
Scheme 4.7 Deuterium Labeling Experiments Using D ₂ O	208
Scheme 4.8 Proposed Mechanism for Background Consumption of Silane and Oxidant Without Formation of Hydrogen Gas	211

LIST OF TABLES

	Page
Table 2.1 Effect of Reaction Conditions on the Radical–Polar Crossover Hydrofunctionalization of Alcohol 2.25	71
Table 2.2 Effect of Catalyst Structure on the Radical–Polar Crossover Hydrofunctionalization of Alcohol 2.25	72
Table 2.3 Effect of Temperature on the Radical–Polar Crossover Hydrofunctionalization of Alcohol 2.36	73
Table 2.4 Substrate Scope of the Cobalt-Catalyzed Epoxidation and Semipinacol Rearrangement	75
Table 2.5 Effect of Catalyst Structure on the Radical–Polar Crossover Semipinacol Rearrangement of Alcohol 2.65	78
Table 2.6 Effect of Reaction Conditions on the Radical–Polar Crossover Hydrofunctionalization of Alcohol 2.79	82
Table 3.1 Catalyst Structure-Activity Relationships for Asymmetric HAT Radical–Polar Crossover Hydroalkoxylation	135
Table 3.2 Substrate Scope for the Catalytic Asymmetric HAT Radical–Polar Crossover Hydroalkoxylation	137
Table 4.1 Effect of Catalyst Structure on the HAT Radical–Polar Crossover Ritter Reaction of Tetrasubstituted Alkene 4.41	201
Table 4.2 Effect of Catalyst Structure on the HAT Radical–Polar Crossover Ritter Reaction of Trisubstituted Alkene 4.51	203
Table 4.3 Preliminary Substrate Scope of the HAT Radical–Polar Crossover Ritter Reaction	206

Table 4.4 Excess Water Experiments	208
Table 4.5 Hydrogen Evolution Studies	210

ACKNOWLEDGMENTS

First, I would like to extend my sincere gratitude and appreciation to my supervisor, Professor Sergey V. Pronin. I joined your lab in hopes of performing challenging research, and after five years I have to say my expectations were certainly exceeded. I am extremely proud of what the cobalt program has blossomed into, and I have to thank you for providing me with such a fantastic opportunity early into my graduate career. Research was often frustrating, clear trends often failed to materialize, and enantioselectivities were often low, but your contagious enthusiasm for chemistry has always kept me motivated to run the next reaction or try the next idea. Congratulations on achieving tenure, and I very much look forward to seeing what exciting new projects the future holds.

I would like to thank my committee members, Professor Christopher D. Vanderwal and Professor Vy M. Dong for taking the time to review my dissertation and for providing me the privilege of not only serving on my defense committee, but my candidacy exam committee as well. My conversations with you both have only ever been insightful and positive experiences, and I'm honored to have had you both monitoring my progress. Moreover, you've both fostered intellectually stimulating research environments in your own labs that has always made interacting with your graduate students a rewarding experience in and of itself.

To my current and former colleagues in the Pronin lab, I admire each and every one of you and I look forward to keeping up with your careers in the future. You are all some of the most insightful, industrious, and talented individuals I have ever met and I have only improved as a scientist as a result of working with you all. I would like to extend a special thanks to Dr. David T. George for helping me develop good research habits and acting as a mentor early on in my graduate career. I would also like to thank Nicholas J. Foy, Dr. Christopher A. Discolo, Riley E.

Cooper, and Sarah E. Bredenkamp for their incredibly hard work and contributions to the projects we have worked on together.

I would like to acknowledge my undergraduate research advisor at the University of Wisconsin-Madison, Professor Jennifer M. Schomaker, for giving me the opportunity to join her lab and offering me an incredible amount of independence. Your support while applying to internships, graduate school, and the NSF has been very much appreciated. To Dr. Ryan Van Hoveln, thank you for taking me under your wing and teaching me the fundamentals of research. I cannot express how much of an impact your mentorship has had on my development as a scientist and I am truly grateful for all of the guidance you have offered to me over the past seven years. Your students at Indiana State University should consider themselves very lucky. Additionally, you were the impetus for my now sizable collection of rubber ducks, so thank you for inspiring that entertaining hobby as well. I would also like to thank fellow Schomaker graduate students Dr. Steve C. Schmid and Dr. Joshua R. Corbin for their guidance and friendship as well as Professor Tehshik P. Yoon and Dr. Brian J. Esselman for sparking my love of organic chemistry through their lectures.

To my friends in the Pronin group, Dr. Stephen D. Holmbo, Dr. Christopher A. Discolo, Will Thomas, Nick Foy, and Sarah Bredenkamp, thank you for providing me with a support system and a necessary outlet to distract myself from lab. Without your company, both inside lab and out, I would have almost certainly not completed graduate school. Whether it be watching Nicolas Cage movies until 3 am, crying from laughing so hard at the absolute absurdity of topics we would discuss, or simply venting about research, your friendship has been invaluable. I would also like to acknowledge my friends outside of the Pronin lab, including Ryan Kozlowski, Anna Love, Alexander Valdes, Alexander Lu, and Brenna Norton-Baker. The group chats, late night Rock

Band jam sessions, and board game hangouts have been some of my fondest memories from graduate school and I am not sure completing classes and oral exams without losing my sanity would have been possible without your friendship.

To Leah, thank you for being a truly incredible partner. Graduate school has been one of the most difficult things I have ever done, but I'm so glad that it brought me to you. No matter how busy things get you always find time to grab coffee with me. Even when all of my reactions failed for a week in a row, I can rely on you to make me laugh every day when we get home. When I need to stay in lab late to run last minute reactions or write, you are always understanding. You have been my greatest source of joy over the past three years, and I am so thankful for all of the unconditional support you have given me. I love you and I'm so proud of you and everything you've accomplished.

Finally, to my parents and brother, thank you for the continual love and support you have given me throughout graduate school. I don't get to see you all nearly enough, and the last year and half has been especially difficult due to travel restrictions, but I'm looking forward to seeing you all in a few weeks. Thank you for the phone calls, the spontaneous gifts, and granting me the leeway to occasionally rant about politics uninterrupted.

VITA

ERIC TOUNEY

EDUCATION

University of California-Irvine Irvine, CA
Ph.D., Organic Chemistry 2016–2021
GPA: 3.83

University of Wisconsin-Madison Madison, WI
B.Sc. Chemistry (Honors) 2011–2016
B.Sc. Biochemistry
GPA: 3.57

RESEARCH EXPERIENCE

Pronin Lab Irvine, CA
• Graduate Student, Organic Chemistry, University of California-Irvine Dec 2016–Present
Supervised by Professor Sergey V. Pronin

Schomaker Lab Madison, WI
• Undergraduate Researcher, Organic Chemistry, University of Wisconsin-Madison 2014–2016
Supervised by Professor Jennifer M. Schomaker

Merck Research Laboratories Kenilworth, NJ
• Summer Intern, Drug Discovery and Medicinal Chemistry, Merck & Co. Summer 2015
Supervised by Dr. Dmitri Pissarnitski

PUBLICATIONS

- Discolo, C. A.*; **Touney, E. E.***; Pronin, S. V. Catalytic Asymmetric Radical-Polar Crossover Hydroalkoxylation. *J. Am. Chem. Soc.* **2019**, *141*, 17527–17532. (*equally contributing authors)
- **Touney, E. E.**; Foy, N. J.; Pronin, S. V. Catalytic Radical-Polar Crossover Reactions of Allylic Alcohols. *J. Am. Chem. Soc.* **2018**, *140*, 16982–16987.
- **Touney, E. E.**; Van Hoveln, R.; Buttke, C. T.; Freidberg, M. D.; Guzei, I. A.; Schomaker, J. M. Heteroleptic Nickel Complexes for the Markovnikov-Selective Hydroboration of Styrenes. *Organometallics* **2016**, *35*, 3436–3439.

PRESENTATIONS

- **Touney, E. E.**; Discolo, C. A.; Pronin, S. V. Development of Asymmetric Radical-Polar Crossover Hydrofunctionalizations. 2020 ACS DOC Graduate Research Symposium (Presentation). (Cancelled due to COVID-19)
- **Touney, E. E.**; Van Hoveln, R.; Schomaker, J. M. Nickel-Catalyzed Hydroboration of Styrenes. Presented at the 18th University of Wisconsin-Madison Undergraduate Symposium, April 2016 (Poster).

AWARDS

- 2020 Allergan Graduate Fellowship
- NSF GRFP Honorable Mention (2018)

ABSTRACT OF THE DISSERTATION

Cobalt-Catalyzed Hydrogen Atom Transfer-Initiated Radical–Polar Crossover Alkene Hydrofunctionalizations

by

Eric Edward Touney

Doctor of Philosophy in Chemistry

University of California, Irvine, 2021

Professor Sergey V. Pronin

Chapter 1 contains a thorough overview of cobalt-catalyzed hydrogen atom transfer (HAT)-initiated alkene hydrofunctionalizations with special attention given to radical–polar crossover reactions. The chapter begins with a general mechanistic discussion of metal-hydride-initiated HAT radical reactions. A historical perspective on the origins of the field is then provided, including work by bioinorganic chemists, inorganic chemists, and seminal work by Mukaiyama. Key contributions from the Carreira, Shenvi, and Herzon labs are highlighted. The second half of Chapter 1 contains an exhaustive review of all published cobalt-catalyzed HAT-initiated radical–polar crossover alkene hydrofunctionalizations to date.

Chapter 2 describes our lab’s strategy for developing a catalytic radical–polar crossover reaction under strong catalyst control. Direct conversion of tertiary allylic alcohols to epoxides or semipinacol rearrangement products could be achieved with judicious choice of cobalt(II) salen catalyst. Bifurcation of reaction pathways suggests the participation of electrophilic alkylcobalt(IV) intermediates. Evaluating the stereochemical outcomes of analogous bromohydrin expansions provided insight into which complexes promote the formation of alkylcobalt(IV) intermediates. Preliminary studies into solvent dependent radical–polar crossover

hydrofunctionalizations of tertiary allylic alcohols bearing 1,1-disubstituted alkenes are described as well.

In Chapter 3, efforts that led to the development of a catalytic asymmetric HAT radical–polar crossover hydroalkoxylation are summarized. Catalyst structure-activity relationships were revealed that lead to the synthesis of a series of novel scalemic cobalt(II) salen complexes containing extended aromatic systems. Our protocol proved successful for converting a variety of cyclic tertiary allylic alcohols to the corresponding epoxides with high levels of enantioselectivity. Analysis of thermodynamic parameters and arene properties suggest that stabilizing noncovalent cation– π interactions within the cobalt(II) salen catalyst are essential to asymmetric induction.

Chapter 4 describes recent efforts by our lab to develop a catalytic radical–polar crossover variant of the Ritter reaction. Long-standing limitations to substrate scope within the field of cobalt-catalyzed HAT radical–polar crossover hydrofunctionalizations are discussed. Strategic ligand design facilitated the development of cobalt(II) salen complexes capable of efficiently engaging trisubstituted and tetrasubstituted alkenes to afford *tert*-alkyl acetamide products. Isotope labeling and excess water experiments identified that nucleophilic capture of electrophilic intermediates by water was competitive with the desired hydroamidation. Hydrogen evolution studies confirmed that formation of hydrogen gas is a competitive pathway that contributes to background consumption of oxidant and silane.

Chapter 1: A Review of Cobalt-Catalyzed Hydrogen Atom Transfer-Initiated Alkene Hydrofunctionalizations

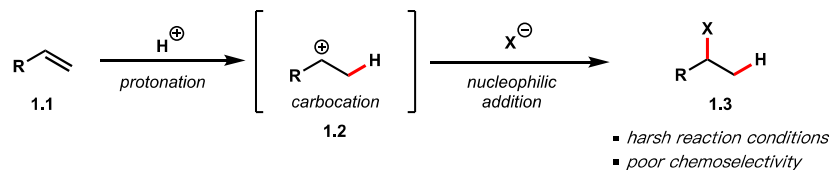
1.1 An Introduction to Metal-Hydride-Mediated Hydrogen Atom Transfer Reactions

1.1.1 Brønsted Acid-Catalyzed Alkene Hydrofunctionalizations

Markovnikov-selective hydrofunctionalizations of simple, unactivated alkenes are an invaluable tool to construct carbon-heteroatom bonds. Traditionally, these transformations have been performed by treating alkenes with Brønsted acids in the presence of polar nucleophiles (Scheme 1.1).¹ Initial protonation of the alkene **1.1** by a Brønsted acid catalyst occurs on the least substituted terminus of the carbon-carbon double bond, resulting in Markovnikov-selective formation of the more substituted, thermodynamically stable carbocation **1.2**. Nucleophilic addition into the carbocation by a polar nucleophile produces the final hydrofunctionalized product **1.3**.

1.3.

Scheme 1.1 Brønsted-acid catalyzed hydrofunctionalization



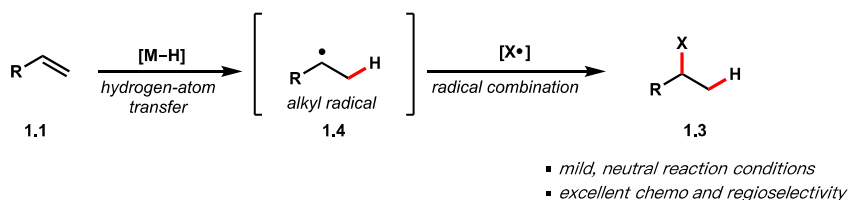
While Brønsted acid catalysis is arguably the most straightforward way to perform Markovnikov-selective hydrofunctionalizations of alkenes, the approach has significant disadvantages. Given the low basicity of alkenes, decidedly harsh strong Brønsted acids are required to access the requisite carbocation intermediates. Furthermore, unstabilized carbocations are exceedingly reactive, high energy species. Not only are their lifetimes estimated to be around a single bond vibration², they also contain superacidic C–H bonds (pK_a ≈ -17).³ As one could imagine, favorably protonating an alkene to a carbocation while keeping other, more basic functional groups intact has proven to be a persistent limitation to the broader application of

Markovnikov-selective acid-catalyzed alkene hydrofunctionalizations. Additionally, deleterious side reactions such as alkyl shifts, hydride shifts, competing nucleophilic additions, alkene isomerization, or back reaction to the starting alkene further complicates reaction planning.⁴

1.1.2 Metal-Hydride-Mediated Hydrogen Atom Transfer Alkene Hydrofunctionalizations

Metal-hydride-mediated hydrogen atom transfer (MHAT) reactions have garnered significant attention in recent decades as a highly chemoselective means for hydrofunctionalization of alkenes with Markovnikov regioselectivity.^{5,6} Typical metal-hydride HAT reactions are characterized by initial delivery of a hydrogen atom from a metal-hydride to the least substituted terminus of an alkene **1.1** resulting in the formation of a substituted alkyl radical **1.4** (Scheme 1.2).⁷ The alkyl radical intermediate can then be engaged with a radical acceptor to afford Markovnikov hydrofunctionalization products **1.3** mirroring those produced by Brønsted acid catalysis.

Scheme 1.2 Metal-hydride-mediated hydrogen-atom transfer (HAT) hydrofunctionalizations



However, when contrasted with traditional Brønsted acid-catalysis, the advantages of MHAT alkene hydrofunctionalizations are immediately apparent. Primarily, MHAT reactions have broad functional group tolerance, as metal-hydrides are exceptionally chemoselective towards reacting with alkenes via HAT versus any other functional group capable of accepting a hydrogen atom.⁸ This selectivity can be attributed to the rapid kinetics of HAT from metal-hydrides onto alkenes.⁹ Another origin of chemoselectivity is the thermodynamic favorability of

HAT by metal-hydride species containing weak M–H bonds (< 50 kcal/mol BDFE).^{7,8,10} Examples of such metal-hydrides are those derived from complexes of cobalt, iron, and manganese bearing acetylacetonate (acac), dipivaloylmethanato (dpm), dimethylglyoxime (dmg), porphyrin, or salen ligands.¹¹

Another distinct benefit of MHAT hydrofunctionalizations is that they proceed with near exclusive Markovnikov regioselectivity. The high degree of regioselectivity can be attributed to the sensitivity of metal-hydrides to steric encumbrance as well as the stability of the resulting alkyl radical that reflect the relative energies of the associated transition states. MHAT hydrofunctionalizations also benefit from the intermediacy of alkyl radicals, which are both lower in energy and have longer lifetimes than their respective carbocationic counterparts.¹² Alkyl radicals can also be tuned electronically to react faster or slower with electron-rich or electron-deficient radical acceptors, giving them a more robust reaction profile than solely electrophilic carbocations.¹³ Other general advantages of MHAT hydrofunctionalizations include neutral reaction conditions that are compatible with functional groups sensitive to acid, base, reductants and oxidants, standard pressures, and operative temperatures rarely falling outside the range between 0 °C and room temperature.

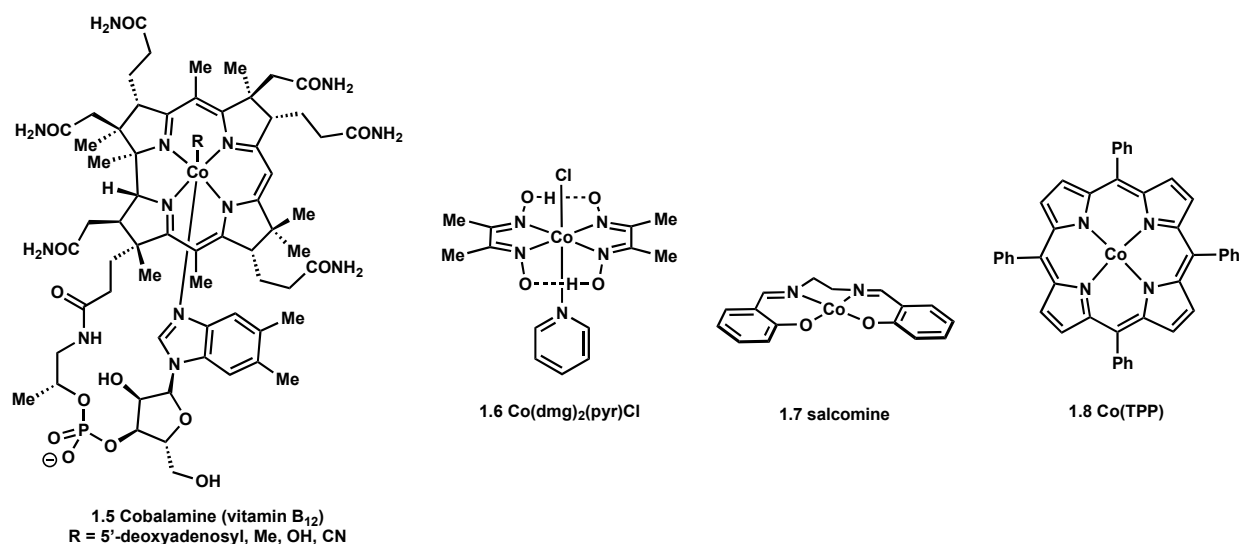
1.2 A Brief History of Cobalt Hydride-Mediated HAT Alkene Hydrofunctionalizations

1.2.1 Origins of MHAT Alkene Hydrofunctionalizations

The field of metal-hydride-mediated HAT chemistry derives its origin from contributions by bioinorganic chemists studying the cofactor ligands of metalloenzymes beginning in the 1960's. Biomolecules such as heme protein oxygenases have long been the focus of study by bioinorganic chemists for their ability to perform oxidations of organic substrates by incorporation of molecular

O₂ with exquisite control.¹⁴ Following the structural elucidation of heme protein cytochrome P-450¹⁵, organic chemists developed structural mimics of the central Fe(II/III) porphyrin reaction center in the hopes of performing similarly controlled hydrations of alkenes.¹⁶ To this day, complexes derived from these ligands are pervasive throughout MHAT literature. Likewise, early studies by bioinorganic chemists found that the necessary reaction components for metalloenzyme oxidations are a first row transition metal, organic ligands, an oxidant such as O₂, a reductant such as NADH, and an organic substrate.¹⁷ This general reagent list has guided MHAT reaction design for decades.

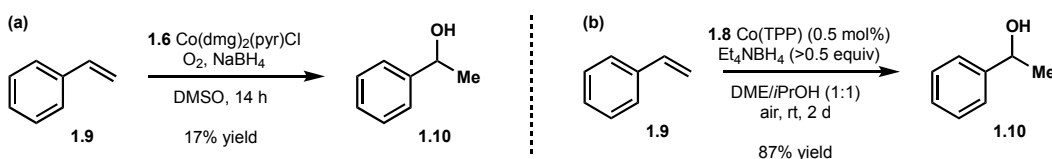
Figure 1.1. Cobalamine and its artificial structural mimics



A biomolecule of particular relevance to the history of cobalt-hydride HAT reaction development is coenzyme B₁₂ **1.5**. Since its structural elucidation in 1965, coenzyme B₁₂ has inspired chemists to develop structural mimics of the embedded corrin ring cofactor (**Figure 1.1**).¹⁸ Investigations by Schrauzer focused on probing the reactivity of the coenzyme B₁₂ alkylcobalt bond and developing cofactor models that could facilitate similar alkyl–metal bond formation such as Co(dmgl)₂(pyr)Cl **1.6** among other glyoxime complexes.¹⁹ Cobalt glyoxime complexes found

their first synthetic application as catalysts in a 1981 report by Okamoto and Ota detailing a catalytic Markovnikov hydration of styrenes **1.9** to benzylic alcohols **1.10** (**Scheme 1.3a**).²⁰ Yields of hydration were improved by using a cobalt tetraphenylporphyrin (TPP) catalyst **1.8** in a second generation method disclosed a few years later (**Scheme 1.3b**).²¹ Although not suggested as a possible mechanism at the time of publication, Okamoto's aerobic styrene hydrations are among the first cobalt-catalyzed MHAT alkene hydrofunctionalizations published. The lack of metal-hydride HAT invocation will be a common theme throughout this brief historical overview of cobalt-catalyzed HAT hydrofunctionalizations. Despite a sizable collection of published work by inorganic chemists studying the hydrogenation²² and hydroformylation²³ of alkenes by metal-hydrides using $\text{Co}_2(\text{CO})_x$ complexes and high pressures of hydrogen gas, as well as Jack Halpern first postulating MHAT as an operative mechanism in his studies of anthracene hydrogenation using syngas and $\text{Co}_2(\text{CO})_8$ in 1975, it was not until recently that hydrogen atom transfer by metal-hydrides to alkenes was invoked explicitly as an operative mechanism by organic chemists.²⁴

Scheme 1.3 Okamoto and Oka's catalytic styrene hydrations

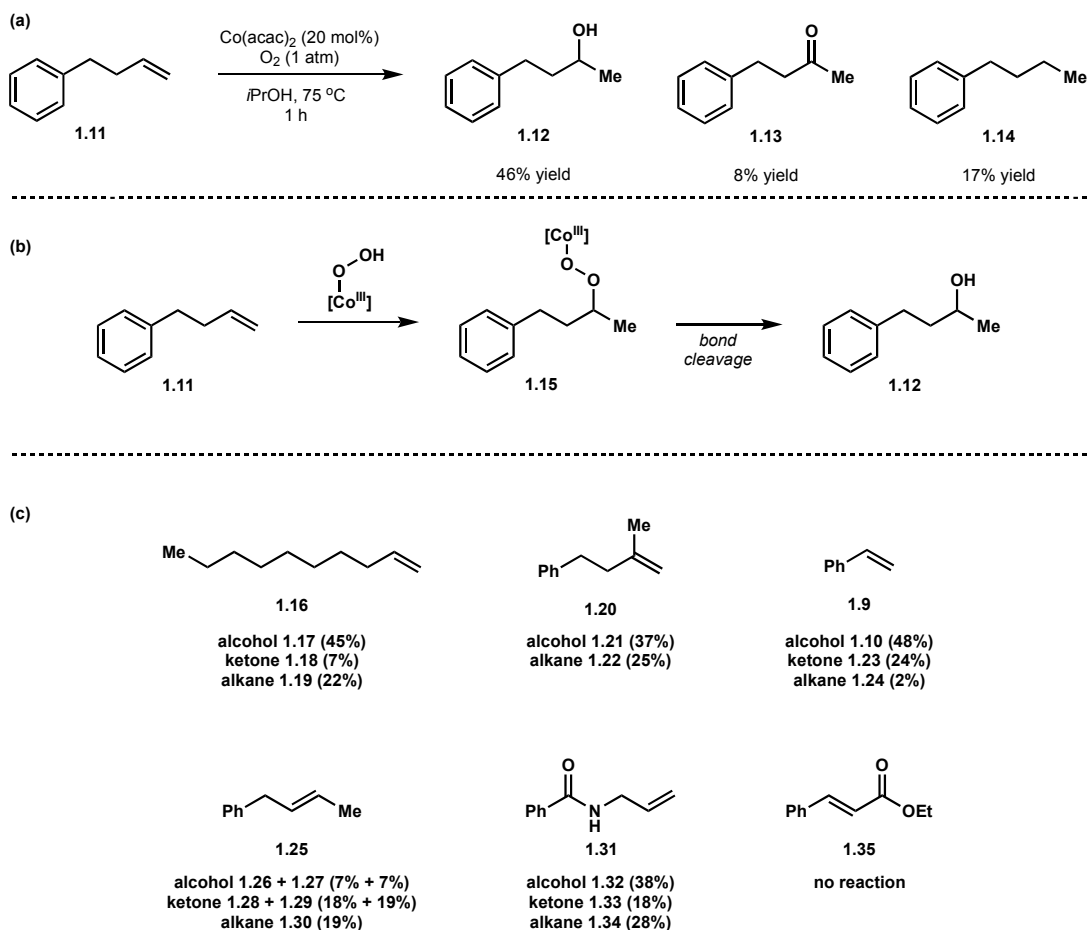


1.2.2 Mukaiyama's Cobalt-Catalyzed HAT Hydration of Unactivated Alkenes

Building upon the large body of work investigating aerobic transition metal-catalyzed alkene hydrations^{20,21,25–27}, Mukaiyama published the first general and highly regioselective cobalt-catalyzed HAT hydration of unactivated olefins in 1989 (**Scheme 1.4a**).²⁸ The authors found that treating 4-phenylbutene **1.11** with catalytic $\text{Co}(\text{acac})_2$ in *i*PrOH, that acts as both solvent and reductant, under an atmosphere of O_2 afforded the corresponding alcohol **1.12** and ketone **1.13**

products in good yields with exclusive Markovnikov regioselectivity. The authors propose *i*-PrOH as the hydride source and cleavage of cobalt-peroxide **1.5** as the source of the newly formed C–O bond (**Scheme 1.4b**).

Scheme 1.4 Mukaiyama's 1st generation cobalt-catalyzed hydration of unactivated alkenes

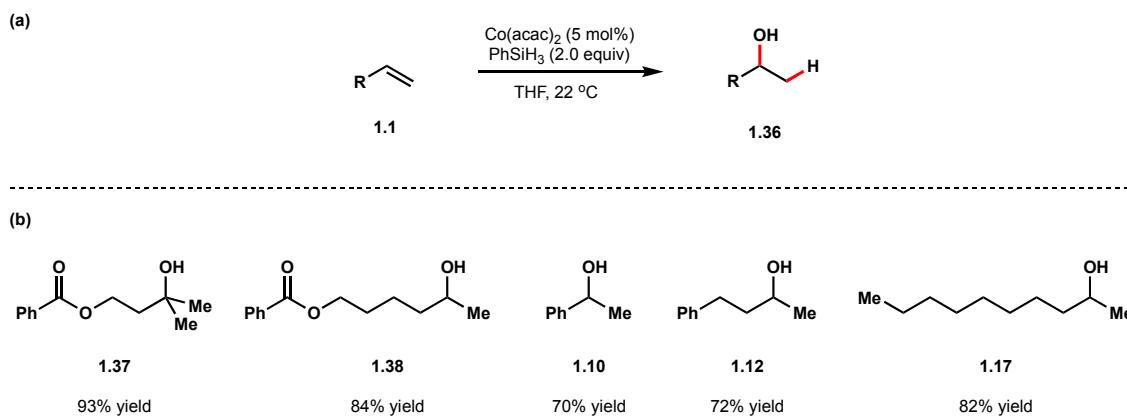


While previous transition metal-catalyzed aerobic hydrations were largely limited to styrenyl substrates, this was the first related method that could reliably hydrofunctionalize unactivated alkenes. A brief substrate scope revealed that the method was applicable to several electronically neutral alkenes (**Scheme 1.4c**). In all cases oxidation products were afforded with exclusive Markovnikov regioselectivity with the exception of 1,2-disubstituted alkene **1.25** which produced an equimolar mixture of regioisomeric alcohols and ketones. Interestingly, α,β -

unsaturated ester **1.35** was not engaged. Some drawbacks of this initial report are significant amounts of hydrogenation **1.14**, high temperatures, and high catalyst loadings.

Subsequent investigations of catalyst electronics, solvent effects, and reductants led Mukaiyama and Isayama to publish optimized conditions for what many now recognize as the quintessential Mukaiyama hydration.²⁹ The authors disclosed that treating unactivated alkenes with Co(acac)₂ and phenylsilane in a solvent of THF under an atmosphere of O₂ at ambient temperature furnished high yields of alcohols with exclusive Markovnikov regioselectivity (**Scheme 1.5a**) Use of phenylsilane as the hydride source was a significant departure from Mukaiyama's first generation method, and allowed for much higher yields of the desired alcohols while lowering catalyst loading and reaction temperature. Notably, if diphenylsilane was used instead of phenylsilane, the proposed O–O bond cleavage could be interrupted and peroxysilane products isolated directly. A brief survey of unactivated alkenes highlighted the regioselectivity and chemoselectivity of these mild conditions (**Scheme 1.5b**).

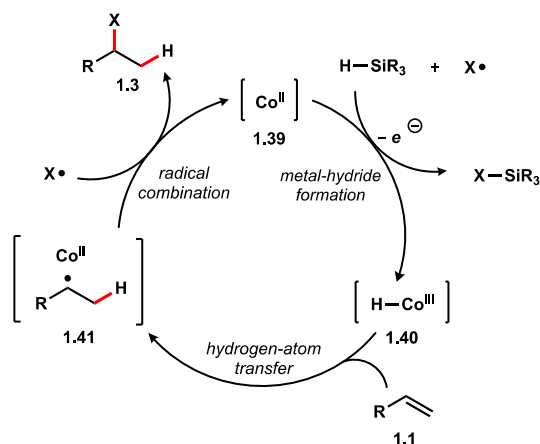
Scheme 1.5 Mukaiyama's optimized cobalt-catalyzed aerobic hydration of unactivated alkenes



The Mukaiyama hydration has seen wide synthetic application in complex molecule synthesis due to its mild conditions, broad functional group tolerance, and generally high efficiency. Unfortunately, an equally rigorous investigation into elucidating the mechanism of

Mukaiyama-type reactions has not been undertaken, likely due to the fleeting nature of the metal-hydride, alkylradical, alkylmetal, and metalloradical intermediates. However, mechanistic studies by Nojima³⁰ focusing on cobalt-catalyzed hydroperoxidations of alkenes in addition to recent efforts by the Shenvi lab³¹ have laid the foundation for a general cobalt-hydride HAT alkene hydrofunctionalization mechanism (**Scheme 1.6**). The general catalytic cycle for a Mukaiyama-type alkene hydrofunctionalization is as follows: 1) Initial formation of a Co(III)–H species **1.40** by single-electron oxidation of Co(II) **1.39** followed by transmetalation with a hydride source. 2) HAT from Co(III)–H **1.40** to the least substituted terminus of the alkene **1.1** resulting in the formation of a solvent-caged alkylradical-metalloradical pair **1.41**. 3) Dissociation of the alkylradical-metalloradical pair, which allows for capture of the alkyl radical by a radical acceptor to afford the desired Markovnikov hydrofunctionalization product **1.3** in addition to turning over the Co(II) catalyst **1.39**. It is presumed all reactions discussed in Chapter 1.2 up to this point and going forward follow a general mechanism resembling **Scheme 1.6**.

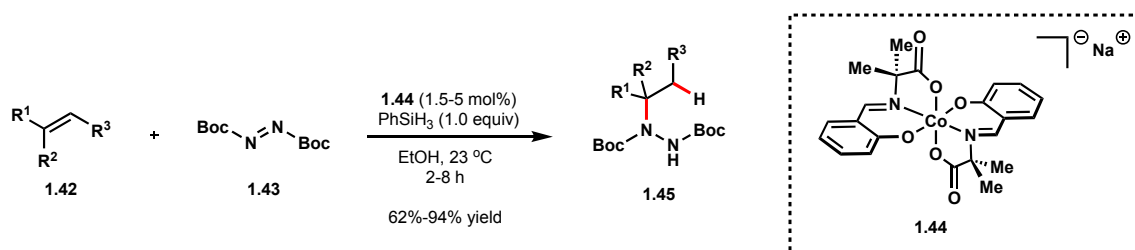
Scheme 1.6 General catalytic cycle for a cobalt-catalyzed Mukaiyama-type alkene hydrofunctionalization



1.2.3 Carreira's Cobalt-Catalyzed HAT Hydrohydrazination of Unactivated Alkenes

Taking direct inspiration from Mukaiyama, the Carreira lab published a series of cobalt-catalyzed HAT hydrofunctionalizations throughout the 2000's detailing the construction of C–N^{32,33}, C–C^{34,35}, and C–X³⁶ bonds. The first installment of this series was a mild hydrohydrazination of unactivated alkenes (**Scheme 1.7**).³² Realizing that Mukaiyama's hydration products likely arose from capture of O₂, Carreira proposed addition into a N₂ equivalent would furnish C–N bonds. Preliminary catalyst screening with cobalt complexes previously shown to promote Mukaiyama hydration such as Co(acac)₂ and Co(dpm)₂ in the presence of silane and diethyl azodicarboxylate (DEAD) failed to afford any desired product. However, Co(III) precatalyst **1.44** bearing unique Schiff base ligands managed to afford 35% yield of the hydrohydrazination product **1.46** with exclusive Markovnikov regioselectivity. Further optimization using **1.44** in the presence of PhSiH₃ and bulkier di-*tert*-butyl azodicarboxylate **1.43** in EtOH produced hydrohydrazination in 85% yield as a single regioisomer. It is worth noting that producing high yields of Boc-protected amines is a testament to the mild nature of cobalt HAT hydrofunctionalizations and a similar transformation would likely not be possible under Brønsted acid-catalysis.

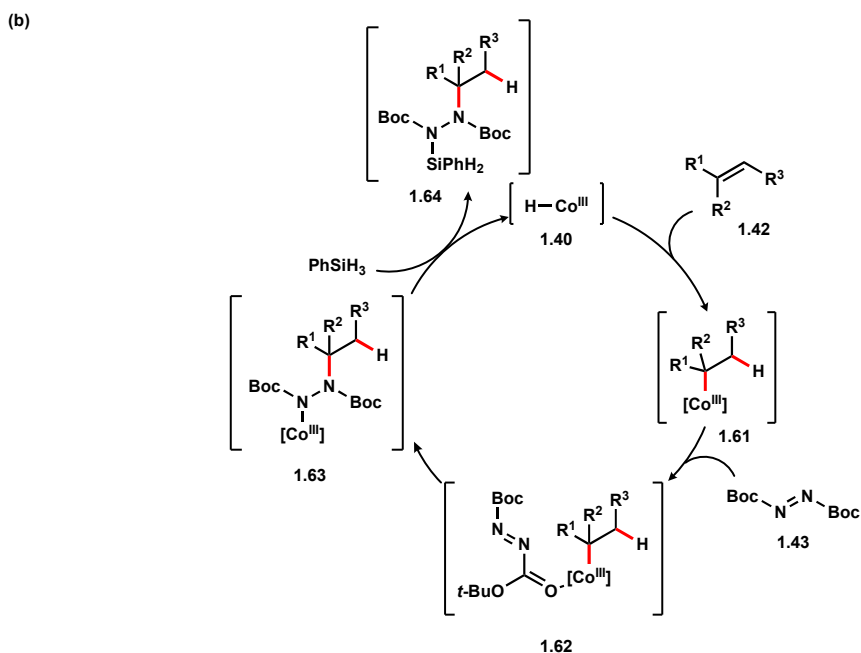
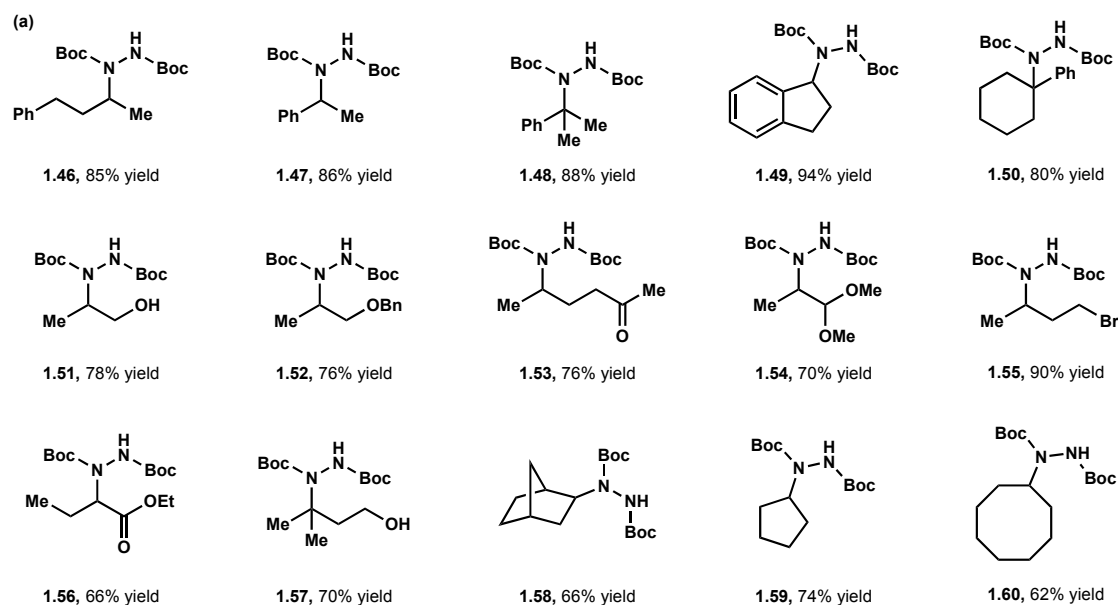
Scheme 1.7 Carreira's cobalt-catalyzed HAT hydrohydrazination



The reaction was applied to a wide variety of alkenes with diversity in both substitution and functional handles (**Scheme 1.8a**). Acyclic and cyclic styrenyl alkenes were competent

substrates (**1.46–1.50**). Monosubstituted alkenes bearing functionality such as alcohols, benzyl ethers, ketones, acyclic acetals, and halides were tolerated (**1.51–1.55**). Unlike Mukaiyama's seminal publication, Carreira was able to engage α,β -unsaturated esters (**1.56**). Prenyl groups were engaged successively (**1.57**) as well as medium sized rings (**1.58–1.60**). In all cases, products were formed as a single regioisomer at the position that most stabilizes the intermediate alkyl radical.

Scheme 1.8 Substrate scope and proposed catalytic cycle of Carreira's cobalt-catalyzed HAT hydrohydrazination



Carreira proposed the mechanism commences with initial hydrometallation to produce a tertiary alkyl cobalt species **1.61** (**Scheme 1.8b**). Coordination to **1.43** then furnishes cobalt hydrazide **1.62**. Subsequent σ bond metathesis regenerates cobalt hydride and affords a *N*-silylated hydrofunctionalization intermediate that hydrolyzes to the desired product upon workup.

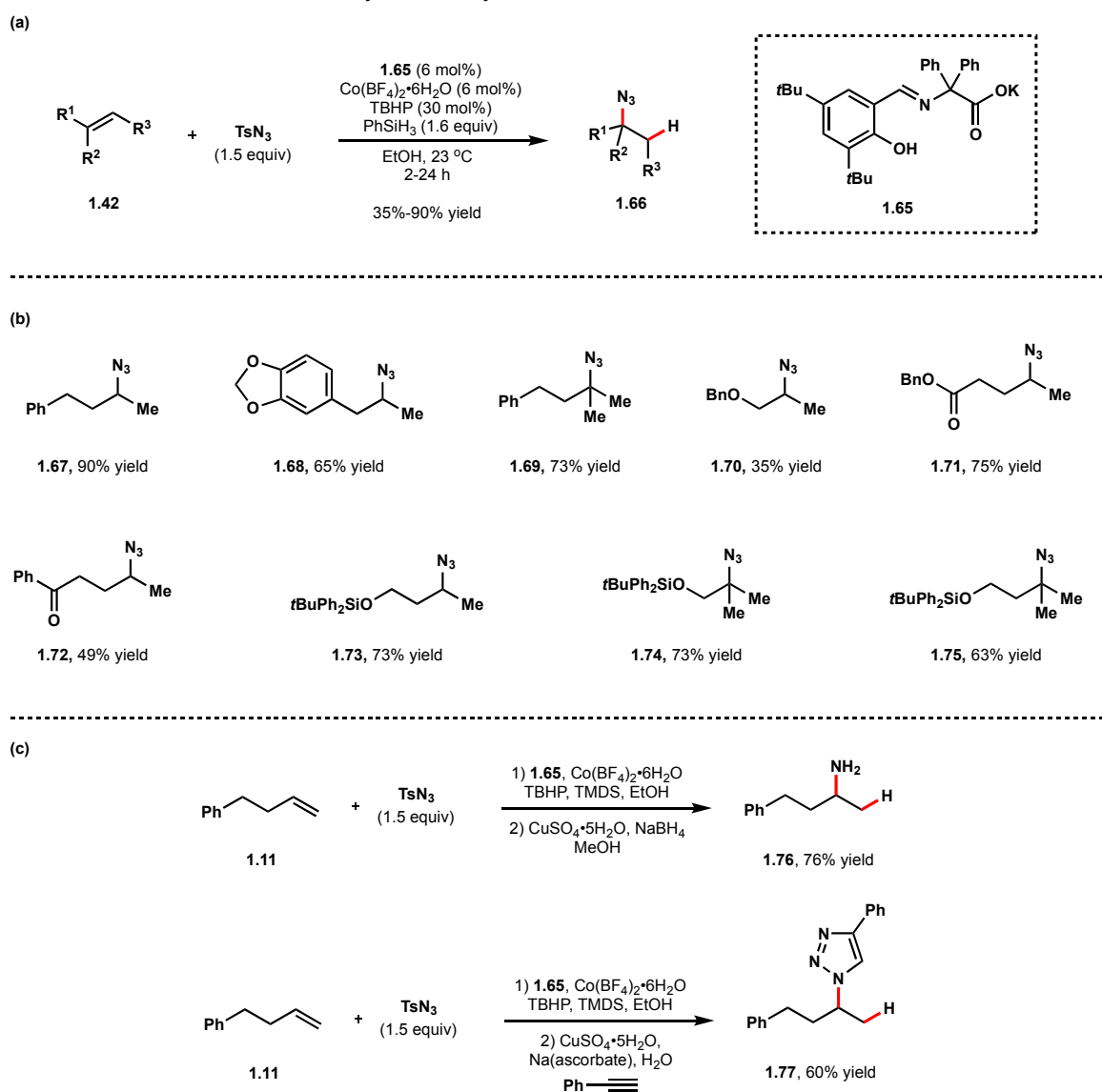
1.2.4 Carreira's Cobalt-Catalyzed HAT Hydroazidation of Unactivated Alkenes

Carreira's second cobalt-catalyzed HAT reaction detailed conditions for a mild hydroazidation of unactivated alkenes (**Scheme 1.9a**).³³ Tosyl azide was chosen as the nitrogen source due to its commercial availability and ease of handling. During the course of screening catalysts, the authors remarked on difficulty reproducing yields due to inconsistent batch quality while preparing catalysts. To bypass this problem, the active catalyst was generated *in situ* by addition of a Co(II) salt and Schiff base ligand to the reaction mixture as separate components. Optimization efforts found that Co(BF₄)₂·6H₂O and ligand **1.65** provided the best yields. Tert-butyl hydroperoxide (TBHP) additive was needed to prevent the occurrence of induction periods and excessively long reaction times. TBHP has been well precedented to accelerate MHAT reactions, likely by acting as a co-oxidant to convert Co(II) to Co(III) and break up redox inactive Co(II) dimers.³⁷ PhSiH₃ generally afforded the highest yields, but produced significant hydrogenation byproducts. Tetramethyldisiloxane (TMDS) attenuated hydrogenation, but often at the cost of overall yield.

Optimized procedure in hand, the authors explored a brief substrate scope (**Scheme 1.9b**). Arenes bearing mono and geminal disubstituted alkenes were compatible (**1.67–1.69**). In contrast to their previous report, benzylic ethers performed poorly (**1.70**). Benzyl esters and ketones delivered good and moderate yields of azide, respectively (**1.71–1.72**). Allylic and homoallylic

silyl ethers bearing monosubstituted, 1,1-disubstituted, and trisubstituted alkenes were all compatible substrates (**1.73-1.75**). A significant drawback of the hydroazidation is the intolerance of unprotected alcohols despite the reaction being ran in ethanol. To showcase the utility of their method, the authors converted azide **1.67** to primary amine **1.76** by reduction with $\text{CuSO}_4 \cdot 5\text{H}_2\text{O}$ and NaBH_4 as well as triazole **1.77** with a Cu(I) azide-alkyne cycloaddition (**Scheme 1.9c**).^{38,39} A second generation hydroazidation and mechanistic investigation were the subject of later publications.^{40,41}

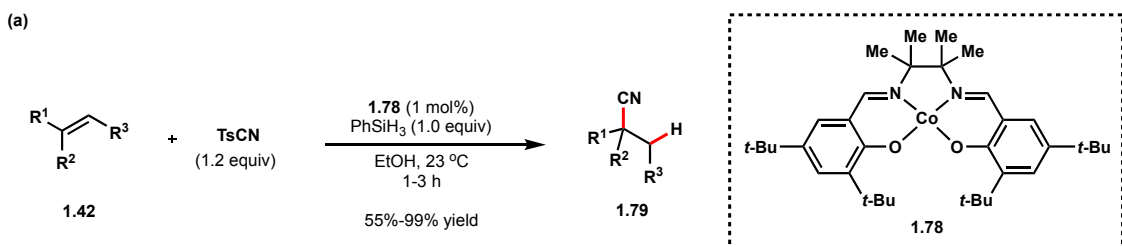
Scheme 1.9 Carreira's cobalt-catalyzed HAT hydroazidation



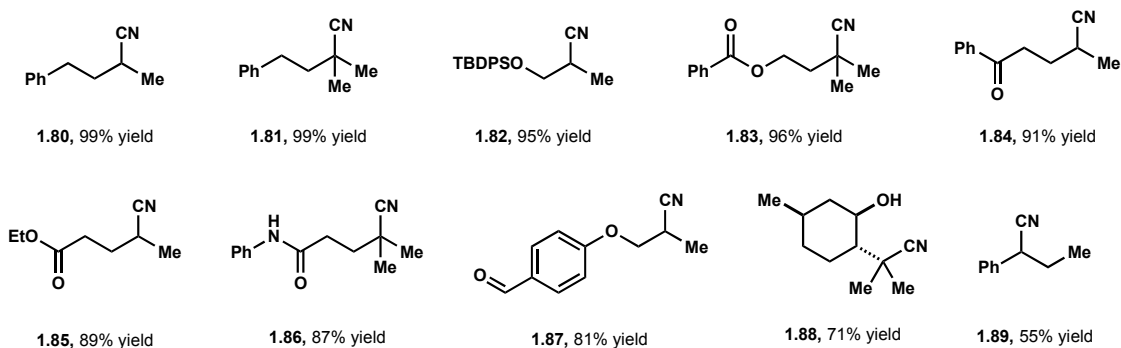
1.2.5 Carreira's Cobalt-Catalyzed HAT Hydrocyanation of Unactivated Alkenes

In 2007 the Carreira lab shifted their focus away from C–N bond formation and published a Markovnikov selective construction of C–C bonds via mild hydrocyanation of unactivated alkenes with *p*-toluenesulfonyl cyanide (**Scheme 1.10a**).³⁴ Mild and regioselective generation of new C–C bonds bearing versatile functional handles from common alkenes is a powerful retrosynthetic transform. Hydrocyanation is particularly desirable as nitriles can be further elaborated by hydrolysis, reduction, and alkylation. Previous alkene hydrocyanation methods were largely limited to activated alkenes, required elevated temperatures, and relied on strong Lewis acids such as AlCl₃.⁴² In contrast, the mild nature of cobalt-catalyzed alkene hydrocyanation makes it a more robust method in terms of both functional group tolerance and retrosynthetic utility.

Scheme 1.10 Carreira's cobalt-catalyzed HAT hydrocyanation



(b)



Reaction optimization commenced by screening previously used cobalt catalysts **1.44** and Co(BF₄)₂•6H₂O/ligand **1.65** mixture which afforded low yields of hydrocyanation in 29% and 19%, respectively. Application of Co(salen) catalysts improved yields significantly and eliminated

the need for TBHP additives. Catalyst **1.78** bearing a tetramethyl ethylenediamine backbone provided near quantitative yields of hydrocyanation. PhSiH₃ was determined to be the superior hydride source, as more heavily substituted and less reactive silanes resulted in lower yields and longer reaction times. The hydrocyanation protocol was compatible with a variety of alkene substitution and functional groups (**Scheme 1.10b**). Electronically neutral alkenes (**1.80–1.81**), silyl ethers (**1.82**), acyl groups (**1.83**), ketones (**1.84**), esters (**1.85**), amides (**1.86**), aldehydes (**1.87**), and alcohols (**1.88**) were all well tolerated and delivered high yields of hydrocyanation as a single regioisomer. The authors report that substrates containing endocyclic double bonds were not engaged.

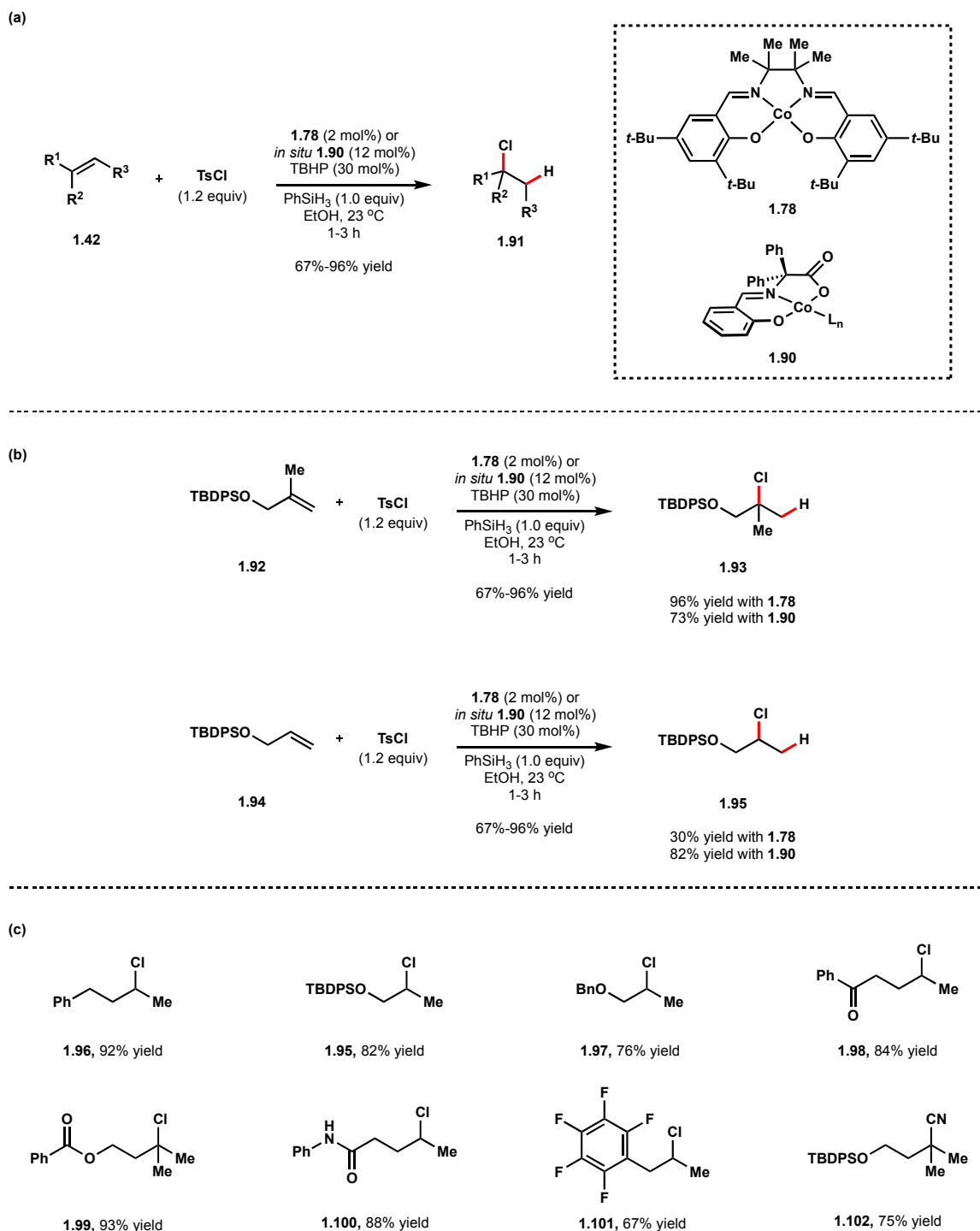
1.2.6 Carreira's Cobalt-Catalyzed HAT Hydrochlorination of Unactivated Alkenes

In 2008 the Carreira group expanded their cobalt-catalyzed hydrofunctionalization manifold to the direct Markovnikov hydrochlorination of alkenes (**Scheme 1.11a**).³⁶ Cobalt-catalyzed hydrochlorination is a particularly compelling example of the utility of MHAT alkene hydrofunctionalizations because it stands in direct contrast to the forcing conditions of alkene hydrochlorination catalyzed by HCl.⁴³ Methods to regioselectively prepare diverse arrays of alkyl chlorides in a straightforward fashion have great value, as alkyl chlorides are useful intermediates for further elaboration by nucleophilic substitution or metalation.

Similar to their previous reports, the Carreira lab used *p*-toluenesulfonyl chloride as their radical acceptor and Cl atom source, PhSiH₃ as a reductant, and a solvent of EtOH. The authors note that catalyst efficiency exhibited significant dependence on alkene substitution, as salen catalyst **1.78** delivered near quantitative yields of 3° alkyl chloride **1.93** but only afforded 30% yield of 2° alkyl chloride **1.95** (**Scheme 1.11b**). In stark contrast, *in situ* catalyst **1.90** showed little

discrimination, producing **1.93** and **1.95** in 73% and 82% yield, respectively. With this knowledge, a series of secondary alkyl chlorides (**1.95-1.98**) were prepared using **1.90** while tertiary alkyl chlorides (**1.99-1.102**) were produced using **1.78** (Scheme 1.11c).

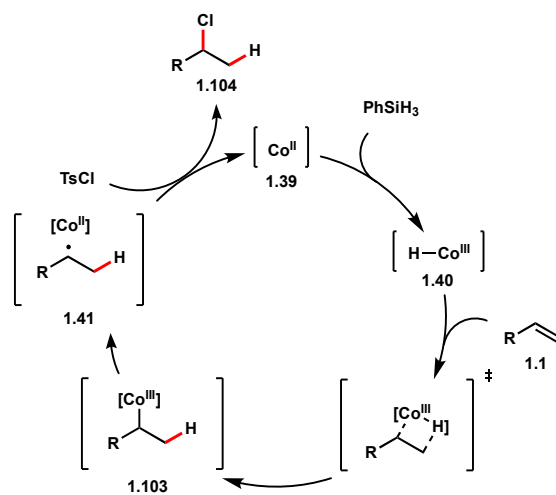
Scheme 1.11 Carreira's cobalt-catalyzed HAT hydrochlorination



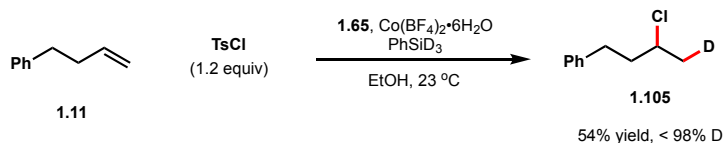
A full mechanism is proposed for the cobalt-catalyzed hydrochlorination (**Scheme 1.12a**). The mechanism commences with formation of Co(III)–H **1.40** by reaction of Co(II) with PhSiH₃, no commentary on the oxidant is made. Concerted Markovnikov hydrometallation of the alkene with Co(III)–H to form secondary alkylcobalt species **1.103** is then suggested. Homolysis of the C–Co(III) bond releases an alkyl radical that then engages TsCl to produce the hydrochlorination product **1.104** and turn over Co(II). Deuterium labeling studies using PhSiD₃ confirmed that the newly incorporated H/D atom originates exclusively from silane, although HAT is not suggested (**Scheme 1.12b**). Whereas Mukaiyama demonstrated the regioselectivity and generality of MHAT hydrofunctionalizations, Carreira’s contributions to the field highlight the wide range of bond connections and retrosynthetic possibilities offered through cobalt-hydride-mediated HAT alkene hydrofunctionalizations. Additionally, invaluable insights were gleaned into the nuances of catalyst selection, substrate limitations, and broader reaction design.

Scheme 1.12 Proposed mechanism of Carreira’s cobalt-catalyzed HAT hydrochlorination and deuterium labeling studies

(a)



(b)



1.2.7 Shenvi's Cobalt-Catalyzed HAT Hydrogenation of Unactivated Alkenes

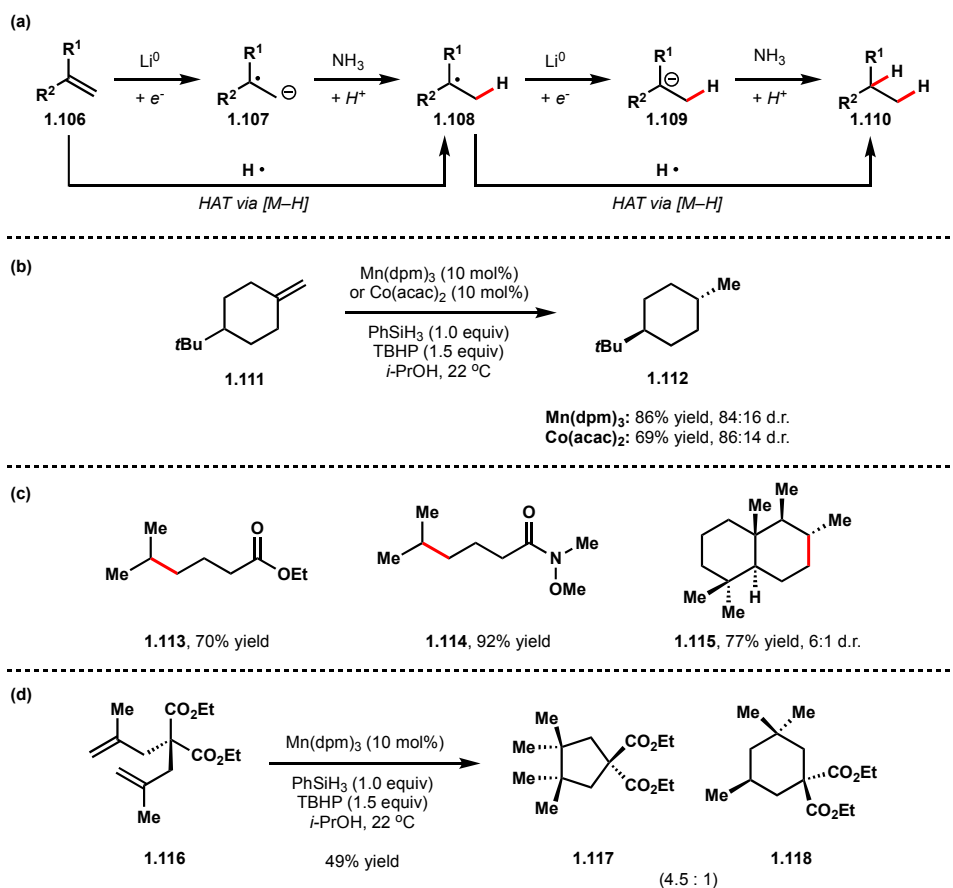
In 2014 the Shenvi lab developed a method for MHAT hydrogenation structured around the propensity of metal-hydrides to perform HAT.⁴⁴ The group identified a scarcity of alkene hydrogenation methods that are reliably diastereoselective for the thermodynamically favored product. Dissolving metal reduction has traditionally filled the niche for thermodynamic controlled alkene reduction (**Scheme 1.13a**).⁴⁵ However, the functional group tolerance of dissolving metal reductions is restricted, as the harsh conditions needed to access the requisite high energy intermediates, such as radical anions, reduce most other functional handles preferentially to alkenes. The Shenvi group identified that first-row transition metal-hydrides can mildly access carbon-centered radicals via low energy HAT to alkenes. They proposed the alkyl radical could then abstract a hydrogen atom from a second equivalent of metal-hydride to afford the desired thermodynamic hydrogenation product.

Guided by this mechanistic framework, the authors successively developed a thermodynamically controlled MHAT-mediated alkene hydrogenation catalyzed by Mn or Co (**Scheme 1.13b**). Conditions are similar to those in previously discussed literature, using catalytic $\text{Mn}(\text{dpm})_3$ or $\text{Co}(\text{acac})_2$, PhSiH_3 as the hydride source, TBHP as an oxidant, and *i*-PrOH as the solvent. Although both $\text{Mn}(\text{dpm})_3$ or $\text{Co}(\text{acac})_2$ reduced model substrate **1.111** to product **1.112** in comparable yields and diastereoselectivity, the substrate scope was conducted using $\text{Mn}(\text{dpm})_3$ primarily. Because this dissertation focuses on Co-catalyzed MHAT reactions, I will only address the entries ran using $\text{Co}(\text{acac})_2$ (**Scheme 1.13c**). The reduced bond is highlighted in red. Saturated ester **1.113** and Weinreb amide **1.114** were produced in good yield and high yield, respectively. Notably, the N–O bond of the Weinreb amide did not undergo bond homolysis. Traditional

platinum hydrogenation⁴⁸ failed to access terpene **1.115**, but the hydrogenation protocol using $\text{Co}(\text{acac})_2$ delivered **1.115** in 66% yield favoring the desired diastereomer in a 6:1 ratio.

Interrogation of the mechanism led Shenvi to explicitly propose HAT from a metal-hydride to an alkene as an operative elementary step in their hydrogenation. The authors noted that alkene substitution and electronics did not influence rates of starting material consumption, suggesting that alkylradical formation is occurring directly from the alkene rather than concerted hydrometallation followed by alkylmetal bond homolysis. Further evidence for participation of carbon-centered radicals is the facile 5-*exo*-trig cyclization of diene **1.116** to sterically encumbered **1.117** (Scheme 1.13d). Following this report and the suggestion by Boger that his iron-hydride alkene hydrofunctionalizations operate via HAT⁴⁹, contemporary MHAT hydrofunctionalization commonly invoke HAT as an operative elementary step.

Scheme 1.13 Shenvi's HAT-mediated hydrogenation



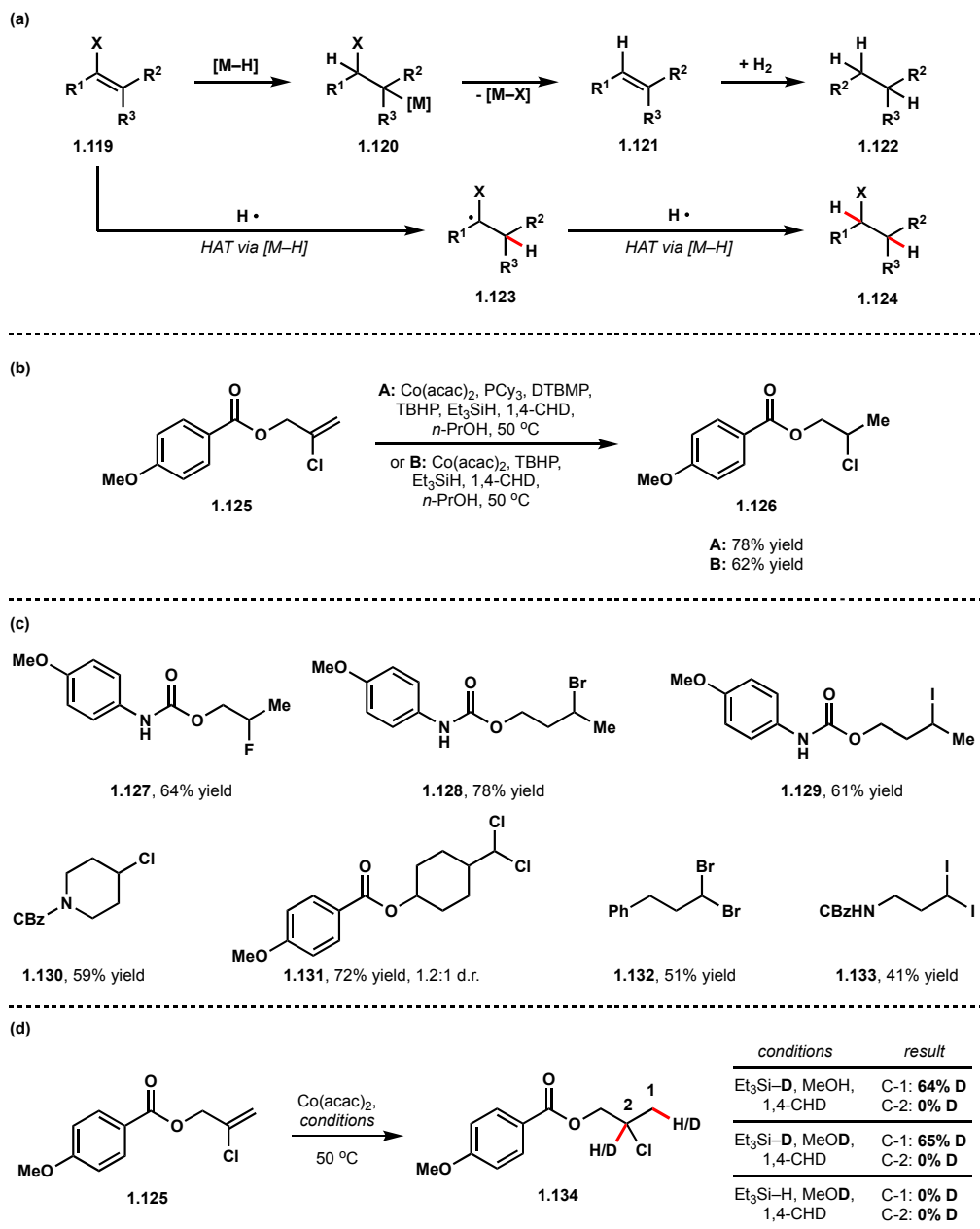
1.2.8 Herzon's Cobalt-Catalyzed HAT Hydrogenation of Unactivated Alkenes

Shortly after the publication of Shenvi's hydrogenation protocol, the Herzon laboratory disclosed their own Co-catalyzed HAT method to hydrogenate alkenyl halides to alkyl halides.⁵⁰ During their synthesis of (-)-acutimine⁵¹, the Herzon group noticed a lack of general methods to directly hydrogenate alkenyl halides to alkyl halides. A major roadblock preventing a general hydrogenation method is parasitic dehydrohalogenation that arises from β -elimination following hydrometallation of the alkenyl halide (**Scheme 1.14a**).⁵² Herzon speculated that dehydrohalogenation could be overcome by employing MHAT catalysis. Because HAT directly generates alkylradical intermediates from alkenes, deleterious elimination pathways that follow hydrometallation could be avoided. Similar to Shenvi's proposed hydrogenation mechanism, Herzon proposes initial HAT would directly access an α -haloradical that then abstracts a hydrogen atom from a second equivalent of metal-hydride to afford the desired alkyl halide.

Guided by an extensive body of metal-hydride hydrogenation literature, two optimized protocols for hydrogenation of alkenyl halides catalyzed by Co(acac)₂ were developed (**Scheme 1.14b**).⁵³ The first protocol is only effective for engaging 1,1-disubstituted alkenes and relies on activating agents tricyclohexylphosphine and 2,6-di-*tert*-butyl-4-methylpyridine (DTBMP). The second set of conditions is identical to the first, but forgoes tricyclohexylphosphine and DTBMP. Trisubstituted alkenes and geminal dihaloalkenes were reduced using the second protocol. Radical oxidation to ketones and dimerization were the observed major byproducts. Chloro, fluoro, bromo, and iodoalkenes were all cleanly reduced to the corresponding alkanes (**1.126-1.129**) (**Scheme 1.14c**). Endocyclic trisubstituted alkenes, typically a challenge to engage in HAT, were reduced in modest yield (**1.130**). Geminal dihaloalkenes were also competent, delivering dichloride **1.131**, dibromide **1.132**, and diiodide **1.133**.

Deuterium labeling studies confirmed that, consistent with past literature, the hydrogen atom incorporated at the least substituted terminus of the alkene originates from triethylsilane (Scheme 1.14d). No deuterium incorporation was observed at the most substituted terminus of the alkene, suggesting that the second hydrogen atom originates from 1,4-cyclohexadiene rather than a transient cobalt-hydride.

Scheme 1.14 Herzon's Co-catalyzed HAT hydrogenation



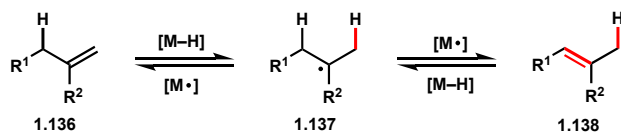
1.2.9 Shenvi's Cobalt-Catalyzed HAT Alkene Isomerization

In 2014 the Shenvi lab reported a series of MHAT-mediated alkene isomerizations catalyzed by Co(salen)Cl complexes and phenylsilane.³¹ They propose that following MHAT to a terminal alkene, the resulting metalloradical could abstract a hydrogen atom from the intermediate alkylradical to regenerate metal-hydride and furnish a more thermodynamically stable substituted internal alkene (**Scheme 1.15a**). The reaction is conditional upon the exclusion of external radical traps and reversible HAT.⁵⁴

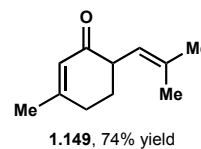
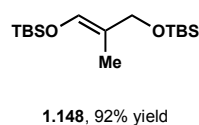
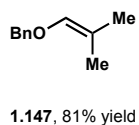
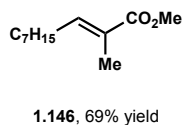
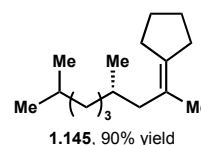
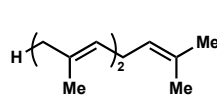
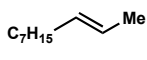
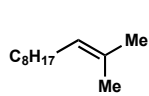
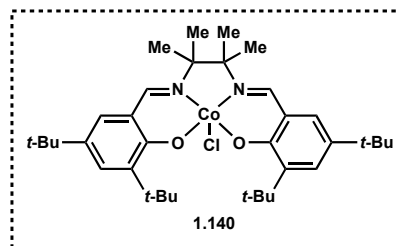
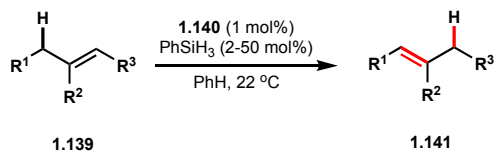
Optimized conditions delivered a series of thermodynamically stable alkenes from unactivated alkenes with broad functional group tolerance (**Scheme 1.15b**). 1,1-disubstituted alkenes were isomerized to trisubstituted alkenes (**1.142**). Monosubstituted alkenes were cleanly converted to 1,2-disubstituted alkenes favoring the *E* isomer (**1.143**). Preinstalled trisubstituted alkenes were not touched (**1.144**). Tetrasubstituted alkenes could be accessed (**1.145**). In a testament to the utility and chemoselectivity of Shenvi's isomerization, α,β -unsaturated esters (**1.146**), vinyl ethers (**1.147**), and silylenol ethers (**1.148**) could be prepared. The method was expanded to cycloisomerizations (**Scheme 1.15c**) Highly substituted cyclic systems, including heterocycles, bicycles, and tricycles, in high diastereoselectivity were accessed (**1.142–1.145**). MHAT to alkene **1.146** bearing a pendant cyclopropane initiated facile radical ring opening-radical annulation cascade to afford tricycle **1.147** (**Scheme 1.15d**). Analogous cycloisomerizations would be challenging using conventional transition metal catalysis due to the absence of strongly coordinating alkenes such as allenes and alkynes in addition to the presence of nitrogenous Lewis basic functionality such as imidazole **1.145**.^{55–57} Retrocycloisomerization of caryophyllene oxide **1.148** was also possible to enact in high yield (**Scheme 1.15e**).

Scheme 1.15 Shenvi's Co-catalyzed HAT alkene isomerization

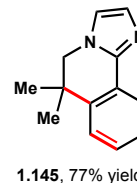
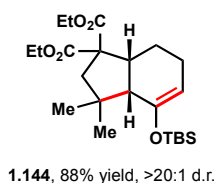
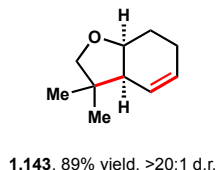
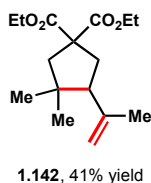
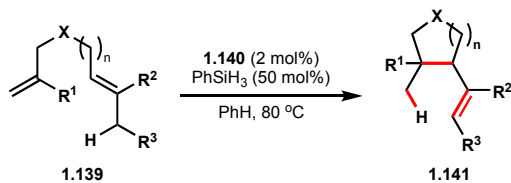
(a)



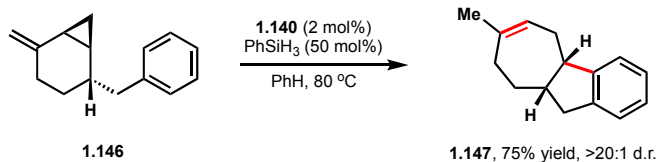
(b)



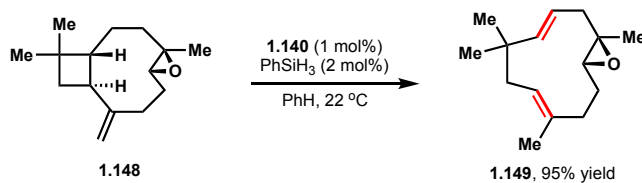
(c)



(d)

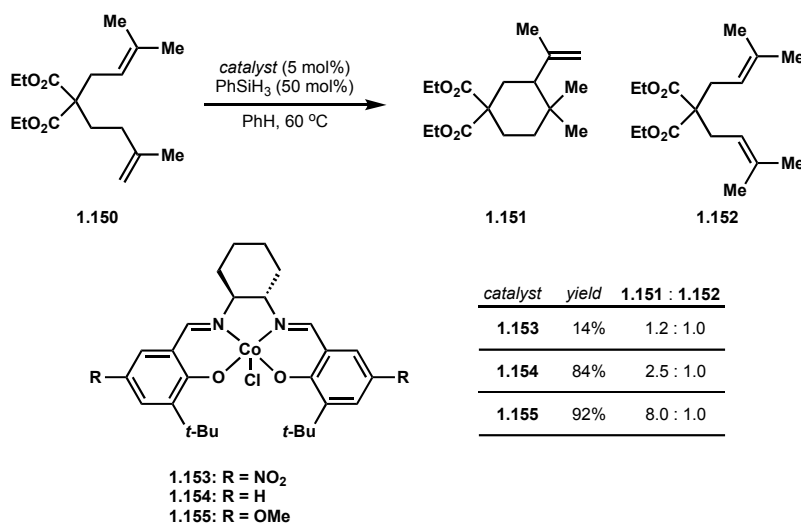


(e)

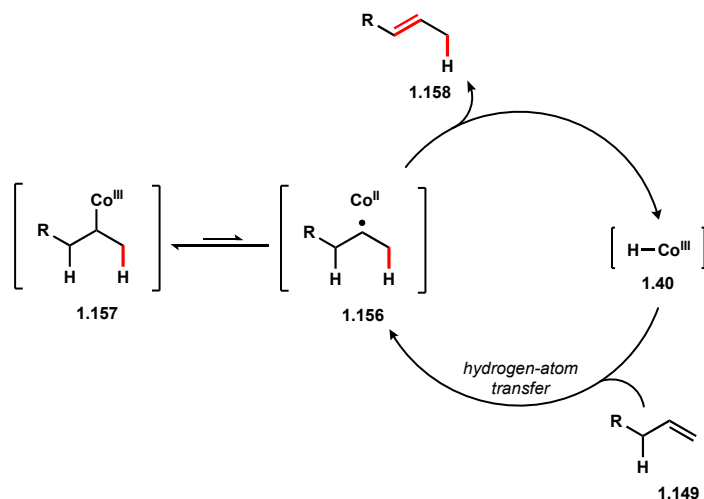


Scheme 1.16 Catalyst effects and proposed mechanism for Shenvi's Co-catalyzed HAT alkene isomerization

(a)



(b)



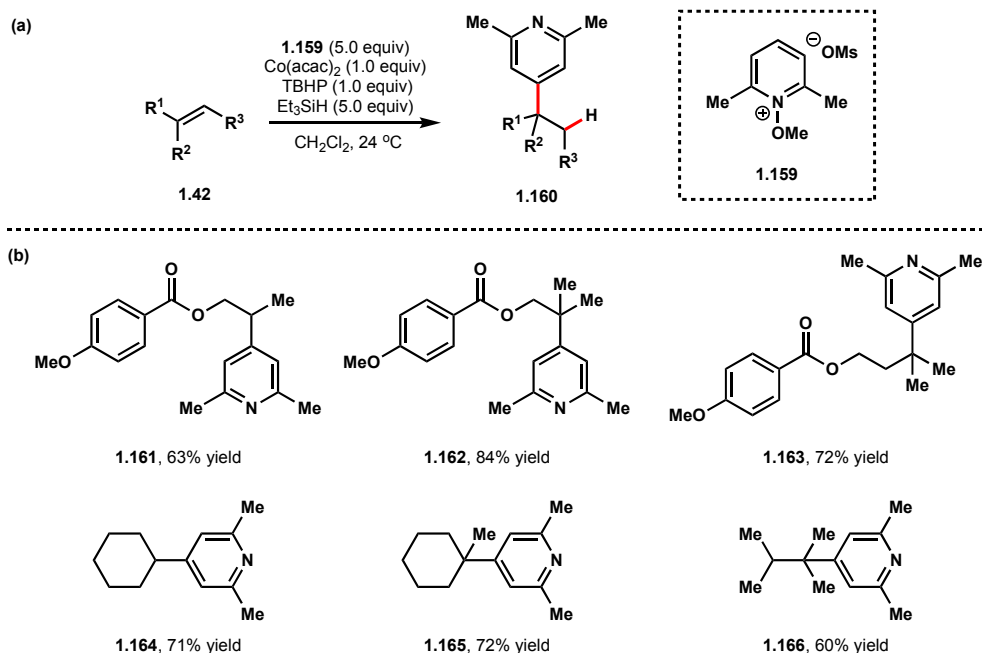
Reaction efficiency was highly dependent on the persistence of the nascent carbon-centered radical. Catalyst ligand electronics influenced the ratio of intramolecular radical cyclization versus alkene isomerization, with electron-poor catalysts suppressing radical cyclization as a function of highly reversible HAT, and electron-rich catalysts accelerating radical cyclization as a function of less reversible HAT (**Scheme 1.16a**).⁵⁸ Isomerization of terminal alkenes at room temperature with electron-rich catalysts proceeded in poor yield. However, efficiency was restored at elevated temperatures, suggesting that radical pair collapse to a

nonreactive alkylcobalt is behaving as a parasitic pathway at ambient temperature but is made reversible at higher temperatures (**Scheme 1.16b**).⁵⁹ This report details construction of some of the most complicated molecules prepared to date by HAT-mediated cobalt catalysis and represents the broad range of chemical space and strategic retrosynthetic disconnections that can be accessed by MHAT reactions. Additionally, Shenvi explicitly marries the mechanistic insights into MHAT gleaned by polymer and inorganic chemists with the Mukaiyama-type alkene hydrofunctionalizations developed by Mukaiyama and Carreira.

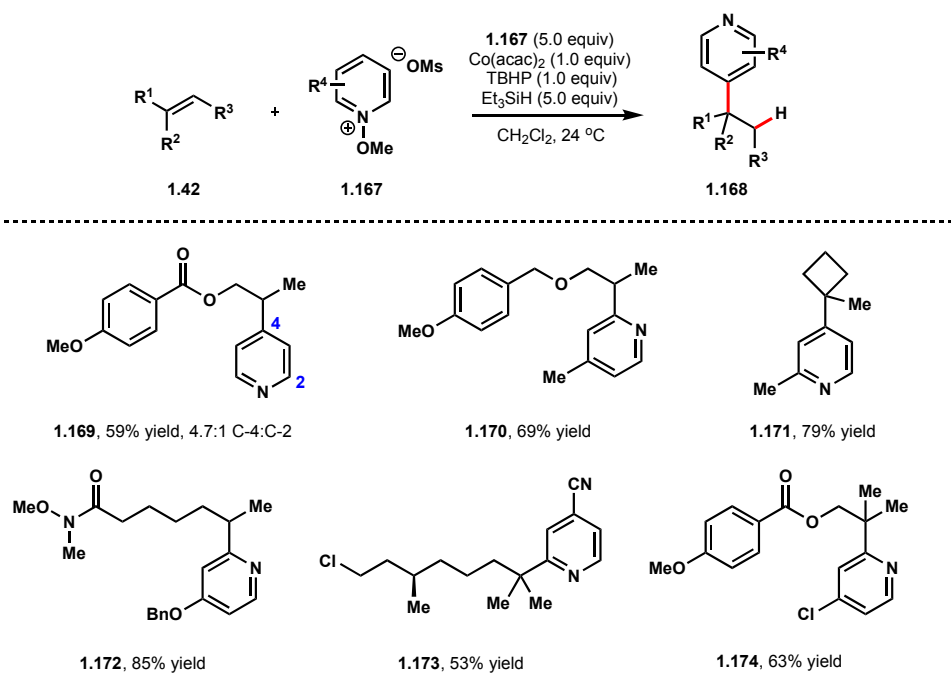
1.2.10 Herzon's Cobalt-Mediated HAT Hydroarylation of Unactivated Alkenes

In 2016 the Herzon lab published the first known intermolecular HAT-mediated hydroarylation of alkenes (**Scheme 1.17a**).⁶⁰ Previously reported transition metal-catalyzed alkene hydroarylations are prone to producing mixtures of isomers and limited by alkene substitution.⁶¹ However, the Markovnikov selective and chemoselective nature of MHAT lends itself to both reducing the complexity of isomeric mixtures as well as broadening alkene scope.

Scheme 1.17 Herzon's Co-mediated HAT hydroarylation



Scheme 1.18 Herzon's scope of competent pyridinium coupling partners



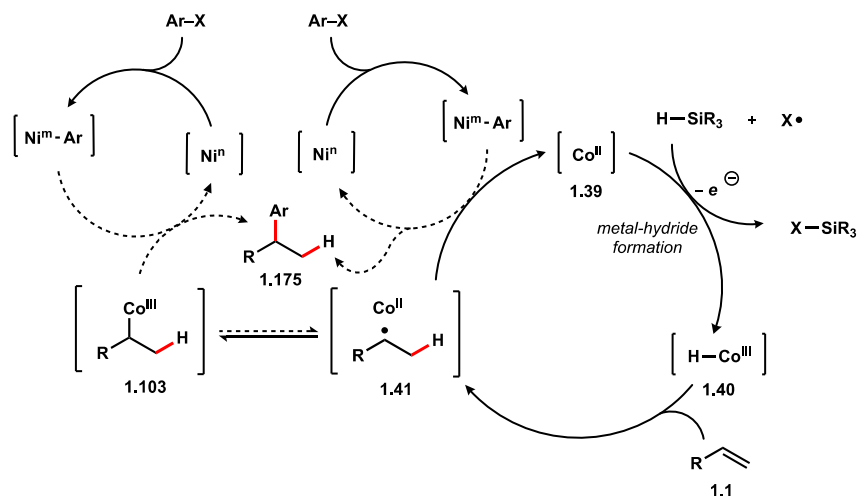
Modeling the Minisci reaction, activated 2,6-dimethyl pyridinium salts were chosen as radical acceptors.⁶² Optimized hydropyridylation conditions consisted of standard MHAT reagents, although stoichiometric amounts of Co(acac)₂ were required. Alkene scope was first surveyed (**Scheme 1.17b**). Acyclic monosubstituted (**1.161**), 1,1-disubstituted (**1.162**), and trisubstituted alkenes (**1.163**) were successfully converted to hydropyridylation products as single regioisomers in moderate to good yield. Cyclic 1,2-disubstituted (**1.164**) and trisubstituted (**1.165**) alkenes were likewise competent. Impressively, tetrasubstituted alkenes (**1.166**) underwent formal cross-coupling as well. Pyridinium scope was then interrogated to assess the regioselectivity of radical addition as well as functional group tolerance (**Scheme 1.18**). Radical addition into electronically neutral pyridinium salts favored C-4 addition (**1.169**). Regioselectivity of the radical addition into 4-methyl pyridinium salts was dependent upon radical substitution, as secondary radicals preferred C-2 addition (**1.170**) while tertiary radicals favored C-4 addition (**1.171**). 4-substituted pyridinium salts bearing electron-donating (**1.172**) and electron-withdrawing (**1.173**)

groups were selective for C-2 addition exclusively. Halogen substitution on the pyridinium salts was also tolerated (**1.174**), although yields dropped precipitously in the presence of bromide substitution both on the pyridinium and substrate. Consistent with other MHAT methods, functional groups such as esters, amides, and alkyl chlorides were left untouched.

1.2.11 Shenvi's Dual-Catalytic HAT Hydroarylation of Unactivated Alkenes

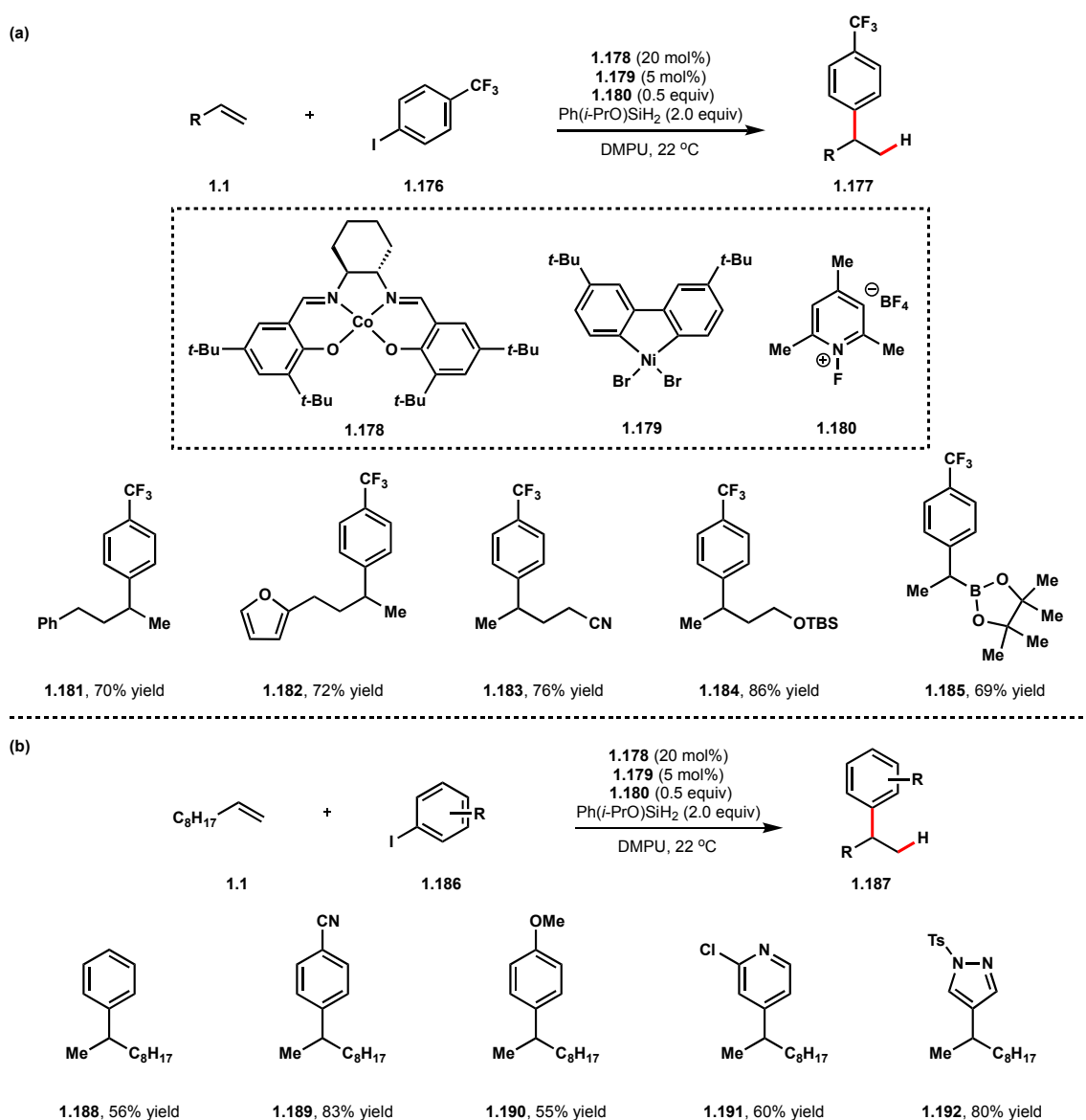
Transition metal catalyzed-cross coupling reactions are pervasive throughout organic chemistry for their robust functional group tolerance and ability to quickly build complexity.⁶³ Although there are a seemingly infinite amount of coupling partners available for cross coupling reactions, unactivated alkenes have largely remained unwilling participants.⁶⁴ It is known that nickel can intercept alkyl radicals and build new sp^3 - sp^2 C-C bonds by subsequent reductive elimination.⁶⁵ Shenvi proposed that intercepting the alkyl radicals generated by cobalt-catalyzed HAT to unactivated alkenes with nickel could provide a robust method to build branched hydroarylation products (**Scheme 1.19**). Transmetalation between nickel and an alkylcobalt species is also a viable proposed pathway. The lab reported their dual Co/Ni catalyzed hydroarylation between unactivated alkenes and iodoarenes in 2016.⁶⁶

Scheme 1.19 Proposed mechanism of Shenvi's dual-catalytic HAT hydroarylation



The optimized reaction conditions delivered a diverse range of branched arenes (**Scheme 1.20a**). Monosubstituted alkenes containing aryl substitution (**1.181**), furans (**1.182**), nitriles (**1.183**), and silyl ethers (**1.184**) were converted in good yields. The iodoarene fragment could also be decorated with electron-withdrawing and electron-donating groups (**1.188–1.190**) (**Scheme 1.20b**). Iodopyridines (**1.191**) and iodopyrazoles (**1.192**) were also competent coupling partners. The authors conclude the study with radical-clock experiments that implicate the participation of alkyl radical intermediates.

Scheme 1.20 Representative substrate scope of Shenvi's dual-catalytic HAT hydroarylation



Thanks to the work of Carreira, Shenvi, and Herzon, MHAT alkene hydrofunctionalizations have seen a renaissance in recent years. Metal-hydride-mediated HAT, once a reaction mode almost exclusively recognized by inorganic and polymer chemists for decades, is now readily accepted amongst organic chemists. The introduction of MHAT into the modern organic chemist's vernacular has enabled a new paradigm where alkenes can be treated as alkyl radical synthons.

1.3 Cobalt-Catalyzed HAT Radical–Polar Crossover Alkene Hydrofunctionalizations

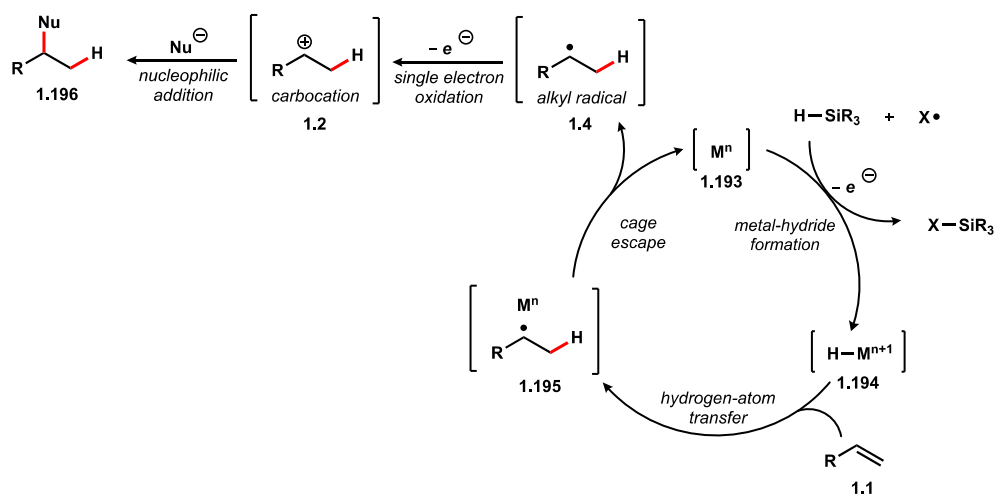
1.3.1 An Introduction to MHAT Radical–Polar Crossover Alkene Hydrofunctionalizations

Metal-hydride-mediated HAT radical reactions provide a highly chemoselective means for hydrofunctionalization of alkenes with Markovnikov selectivity. Previous research has focused primarily on directly engaging the alkyl radicals generated from initial HAT with atom and group-transfer reagents as well as trapping with metals for downstream cross-couplings. Recent efforts have focused on uniting MHAT with subsequent redox manipulations of the alkyl radical to afford corresponding anionic⁶⁷ or carbocationic⁶⁸ intermediates. Thus, radical–polar crossover.

As previously discussed, direct protonation of alkenes by Brønsted acid-catalysis has been the traditional method to access high energy carbocations from alkenes. Conditions requiring the use of acids strong enough to protonate alkenes are not amenable to use with a broad range of functional groups. However, combining the mild nature of MHAT with a similarly mild single-electron oxidation of alkyl radicals offers a way to chemoselectively and regioselectively access carbocations. Given the relatively low oxidation potentials of secondary and tertiary alkyl radicals⁶⁹ and propensity for electron transfer to proceed faster than nuclear vibrations⁷⁰, single-electron oxidation of alkyl radicals is a thermodynamically and kinetically favorable approach to access carbocationic intermediates. Because transition metal salts⁷¹ and complexes⁷² are capable

single-electron oxidants toward carbon-centered radicals, uniting MHAT with a similarly mild single-electron oxidation to chemoselectively and regioselectively access carbocations should prove robust. The profound implication of this new reaction manifold is that it should be possible to develop a mild radical–polar crossover alternative to any Brønsted acid-catalyzed alkene hydrofunctionalization.

Scheme 1.21 A general mechanism for MHAT-mediated radical–polar crossover alkene hydrofunctionalization



While many of the finer mechanistic details of metal-hydride-mediated HAT radical–polar crossover alkene hydrofunctionalizations are still currently unknown, under investigation, or highly context dependent, a general mechanism is outlined in **Scheme 1.21**: 1) Initial formation of $[M^{n+1}-H]$ **1.194** by single-electron oxidation of $[M^n]$ **1.193** followed by transmetalation with a hydride source.⁷³ 2) Regioselective HAT from $[M^{n+1}-H]$ **1.194** to the least substituted terminus of the alkene **1.1** results in formation of a solvent-caged alkyl radical-metalloradical pair **1.195**. 3) Dissociation of the carbon-centered radical from the solvent cage regenerates free $[M^n]$. 4) Single-electron oxidation of alkyl radical **1.4** generates a high energy carbocation **1.2**. 5) The reaction is terminated by capture of the carbocation with a polar nucleophile to form hydrofunctionalized product **1.196**. More complex factors that dictate reaction outcomes such as solvent cage effects,

radical pair collapse to alkylmetal intermediates, and participation of alkylmetal intermediates will be discussed at length in upcoming chapters.

1.3.2 Conspectus

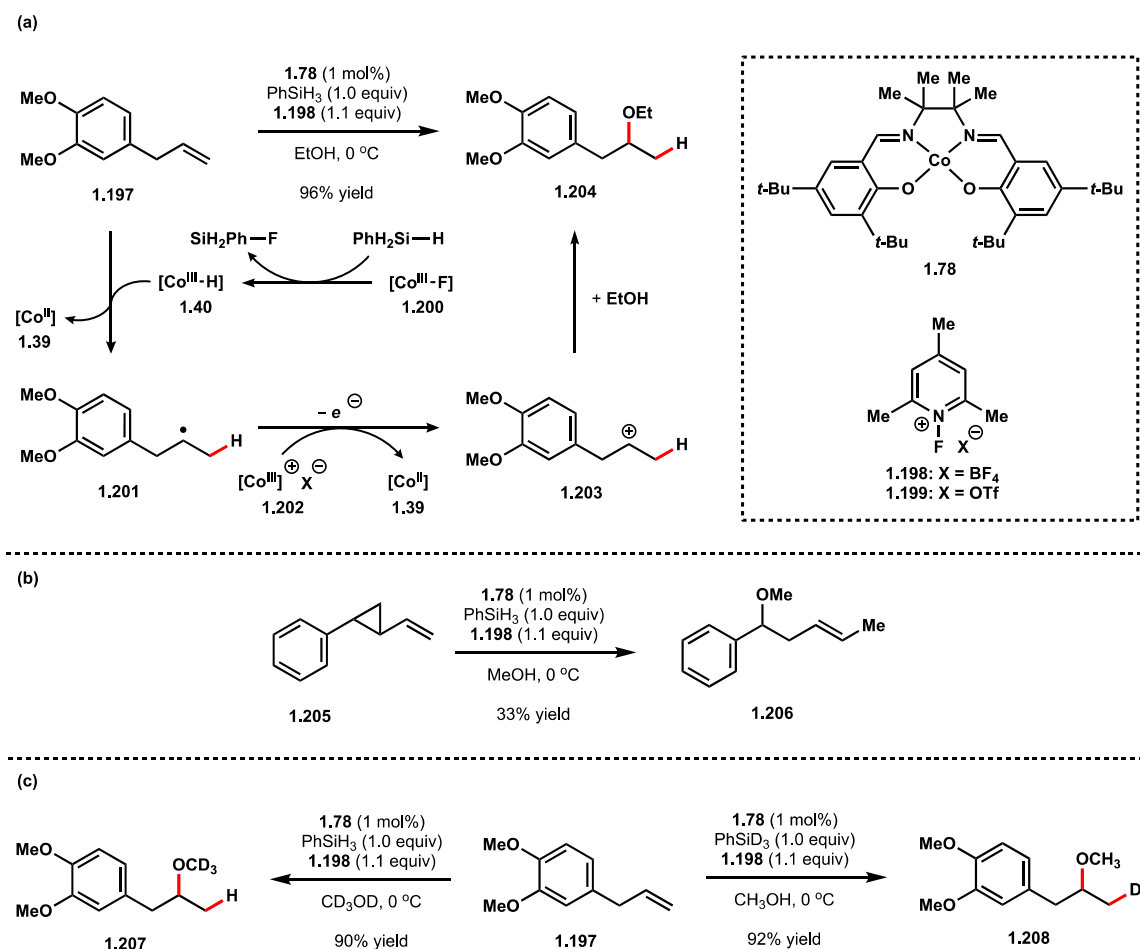
This section of Chapter 1 will serve as a review of all currently published cobalt-catalyzed HAT radical–polar crossover alkene hydrofunctionalizations to date. The work presented is organized by principal investigator, which coincidentally follows a loosely chronological structure. Beginning with Hiroki Shigehisa’s seminal intermolecular alkene hydroalkoxylation, the remainder of his numerous contributions to the field of MHAT radical–polar crossover will be summarized. Rong Zhu’s hydroacyloxylation methodology and his subsequent marrying of MHAT with photoredox catalysis will be detailed followed by brief summary of a report by Shuji Akai detailing intermolecular hydroamination of unactivated alkenes with benzotriazole. The review will conclude with a discussion of Christopher Vanderwal’s HAT radical–polar crossover polyene cyclizations and their applications towards natural product synthesis.

1.3.3 Shigehisa’s Intermolecular HAT Radical–Polar Crossover Hydroalkoxylation

The seminal report of cobalt-catalyzed HAT radical–polar crossover hydrofunctionalization was published by Shigehisa and co-workers in 2013.⁶⁸ Their manuscript describes a protocol for Markovnikov selective alkene hydroalkoxylation in alcoholic solvents (**Scheme 1.22a**). Optimized reaction conditions converted monosubstituted alkene **1.197** to the Markovnikov ethyl ester **1.203** in excellent yield. The authors invoke a radical–polar crossover mechanism that commenced with oxidation of two equivalents of Co(salen) catalyst **1.78** by *N*-fluorocollidinium salt **1.198** to provide cobalt(III) fluoride **1.200** and cationic cobalt(III) salt **1.202**.

Formation of a strong Si–F bond drives transmetalation of phenylsilane with **1.200** to generate the requisite cobalt(III) hydride **1.40** and fluorophenylsilane. They proposed cobalt(III) hydride **1.40** then engages alkene **1.1** via regioselective concerted hydrometallation followed by homolytic alkylcobalt bond scission to furnish secondary alkyl radical **1.201**. Shigehisa then suggested single-electron oxidation of radical **1.201** by cationic cobalt(III) salt **1.202** to afford carbocation **1.203** and regenerate cobalt(II). Nucleophilic addition into **1.203** by solvent produced ethyl ether **1.204**.

Scheme 1.22 Proposed mechanism of Shigehisa's HAT radical–polar crossover hydroalkoxylation

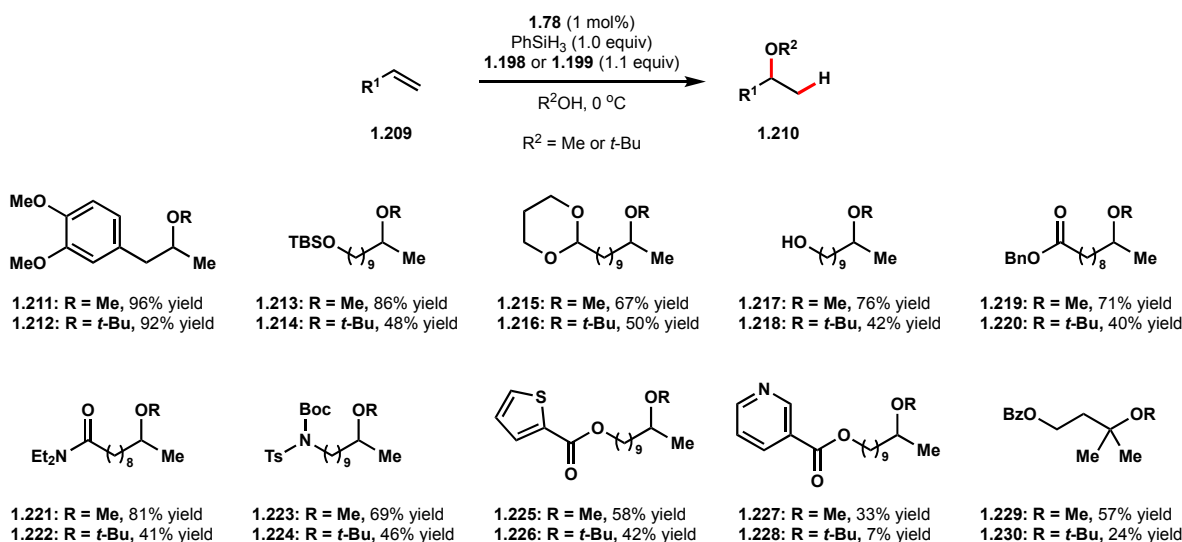


The authors provided support for their proposed mechanism with kinetic radical clock experiments and deuterium labeling studies. When subjected to the reaction conditions in a solvent of methanol, vinylcyclopropane **1.205** underwent ring opening and subsequent alkoxylation to

benzylic methyl ether **1.206**, suggesting the participation of radical intermediates although no mention of HAT was made (**Scheme 1.22a**). Deuterium labeling studies with deuterated phenylsilane and deuterated methanol confirmed the newly installed hydrogen atom originated from phenylsilane and the ether functionality was incorporated from solvent (**Scheme 1.22b**).

The hydroalkoxylation was applied to a broad range of monosubstituted alkenes to yield methyl and *tert*-butyl ethers. (**Scheme 1.23**). Model substrate **1.197** was converted to methyl and *tert*-butyl ethers in high yield (**1.211–1.212**). Acid sensitive functional groups like TBS ethers and acetals were converted in good to modest yield (**1.213–1.216**). Free alcohols, esters, and amides were likewise tolerated (**1.217–1.222**). Boc protected amines and thiophenes were preserved under the reaction conditions (**1.223–1.226**). Pyridine substitution was not well tolerated, which may not be surprising given the collidinium oxidants used (**1.227–1.228**). A trisubstituted alkene was converted to the tertiary ether albeit in moderate to poor yields (**1.229–1.230**). A subsequent report expanded the hydroalkoxylation of unactivated alkenes to use fluorinated alcohols as nucleophiles.⁷⁴ Although HAT was never explicitly invoked by the authors, hindsight marks this publication as the first cobalt-catalyzed radical–polar crossover alkene hydrofunctionalization.

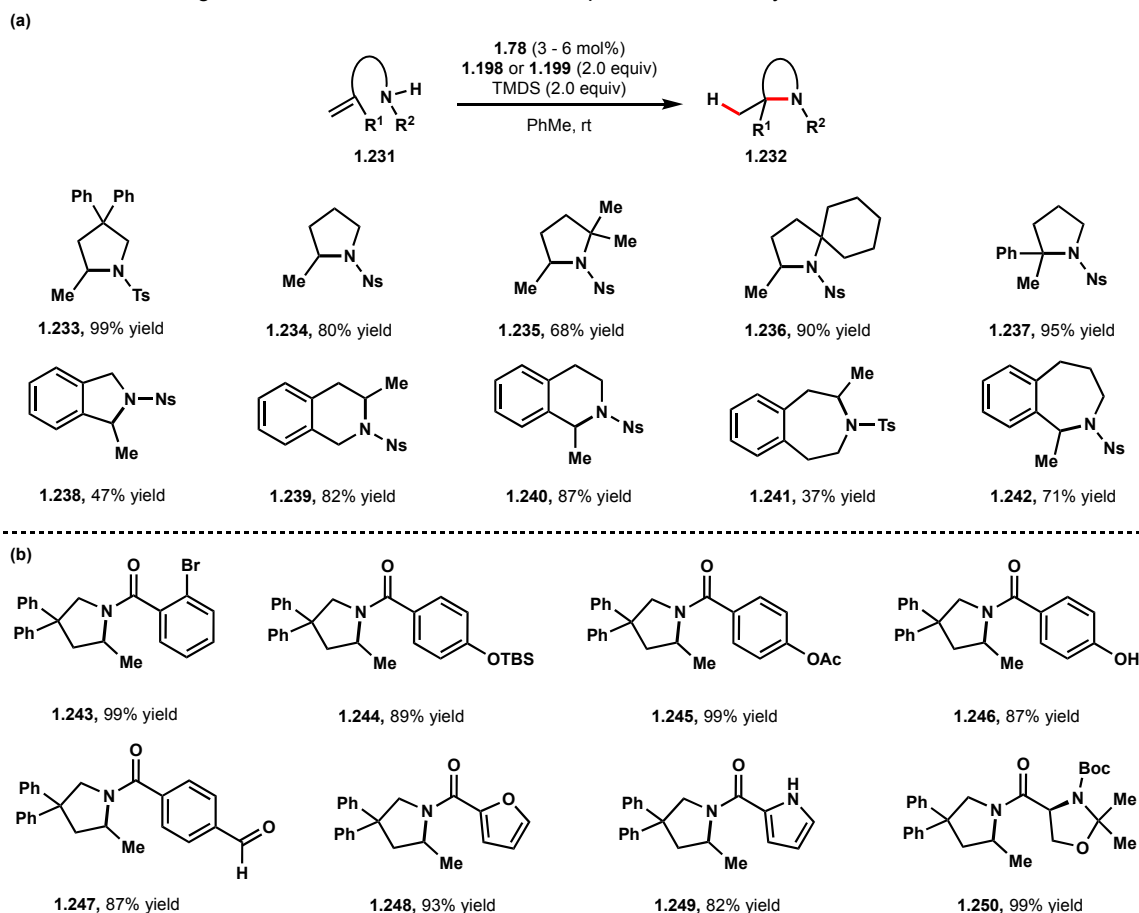
Scheme 1.23 Representative scope of Shigehisa's HAT radical–polar crossover hydroalkoxylation



1.3.4 Shigehisa's Intramolecular HAT Radical–Polar Crossover Hydroamination

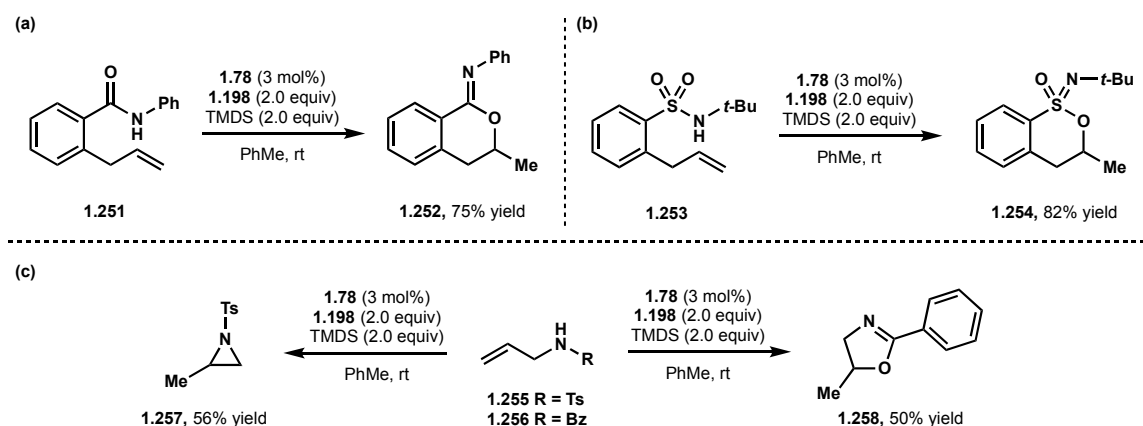
In 2014 the Shigehisa lab applied their HAT radical–polar crossover manifold towards the intramolecular hydroamination of unactivated alkenes (**Scheme 1.24**).⁷⁵ The authors proposed a mechanism analogous to that described in their hydroalkoxylation report, again invoking concerted hydrometallation and bond homolysis rather than HAT. Optimized reaction conditions were similar to those for hydroalkoxylation with the notable exception of toluene as solvent and the use of less reactive TMDS as the reductant. The substrate scope was largely limited to the formation of pyrrolidines and tetrahydroisoquinolines (**Scheme 1.24a**). Many of the ring closures were accelerated by the Thorpe-Ingold effect.⁷⁶ Protection of the nitrogen as an amide or carbamate was critical, although a broad range of functional groups could be embedded within the protecting group (**Scheme 1.24b**).

Scheme 1.24 Shigehisa's Intramolecular HAT radical–polar crossover hydroamination



Interestingly, reaction outcomes were highly dependent on protecting group identity. When protected with a phenyl group, *N*-phenylbenzamide **1.251** favored ring closure on the oxygen atom to furnish cyclic imine **1.252** (Scheme 1.25a). Likewise, *tert*-butyl sulfonamide **1.253** preferred closure on the oxygen atom (Scheme 1.25b). Tosyl protected allylamine **1.255** gave rise to aziridines while benzoyl protected allylamine **1.256** favored closure on oxygen to provide oxazolines (Scheme 1.25c).

Scheme 1.25 Protecting group identity influences reaction outcomes

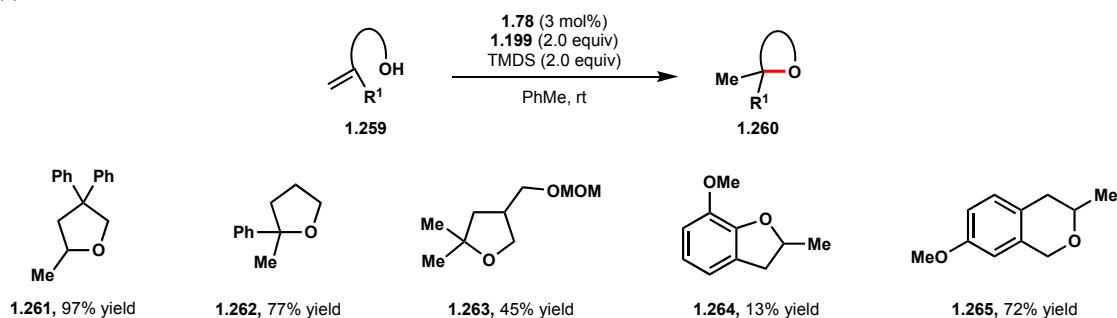


1.3.5 Shigehisa's Synthesis of Oxygen Heterocycles via HAT Radical–Polar Crossover

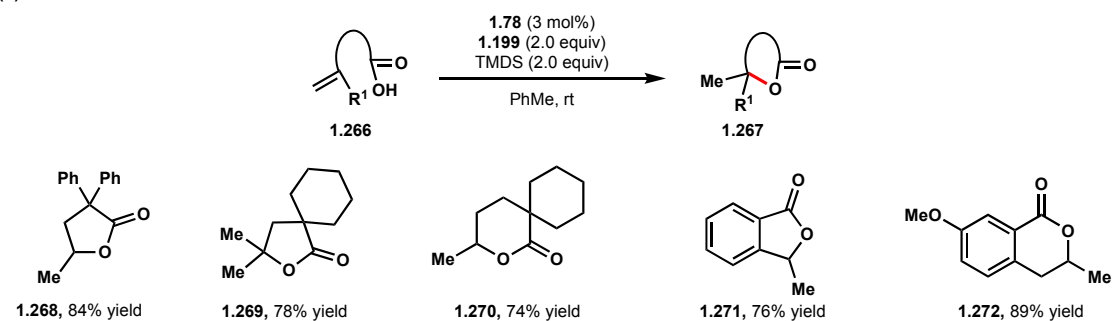
In 2016, the Shigehisa lab published an extensive report on cobalt-catalyzed HAT radical–polar crossover intramolecular closure of alcohols, carboxylic acids, and esters onto unactivated alkenes to synthesize a wide variety of saturated oxygen heterocycles (Scheme 1.26).⁷⁷ Notably, this is the first report by Shigehisa that explicitly invokes HAT as the operative elementary step to generate alkyl radical intermediates that are then oxidized to carbocations. Conditions are identical to previous reports from the Shigehisa lab, using *N*-fluorocollidinium triflate **1.199** as the oxidant and tetramethylethylenediamine substituted Co(II) salen catalyst **1.78**.

Scheme 1.26 Shigehisa's HAT radical–polar crossover synthesis of oxygen heterocycles

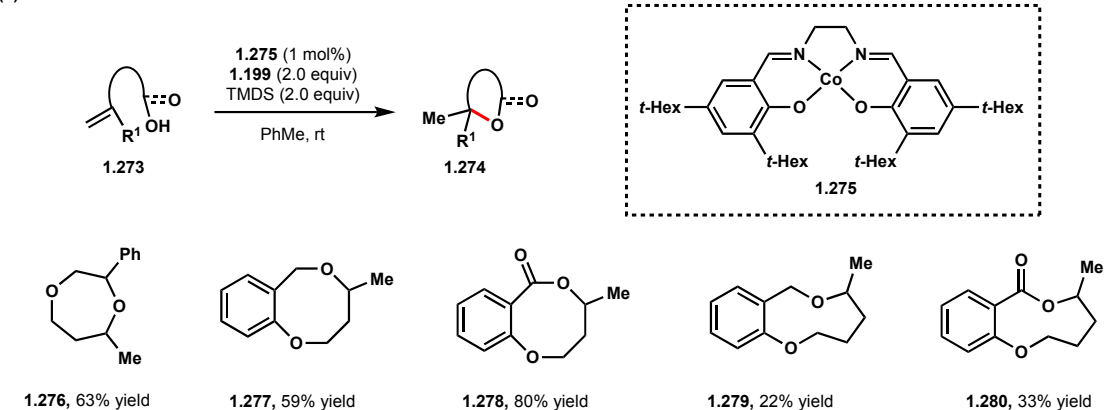
(a)



(b)



(c)

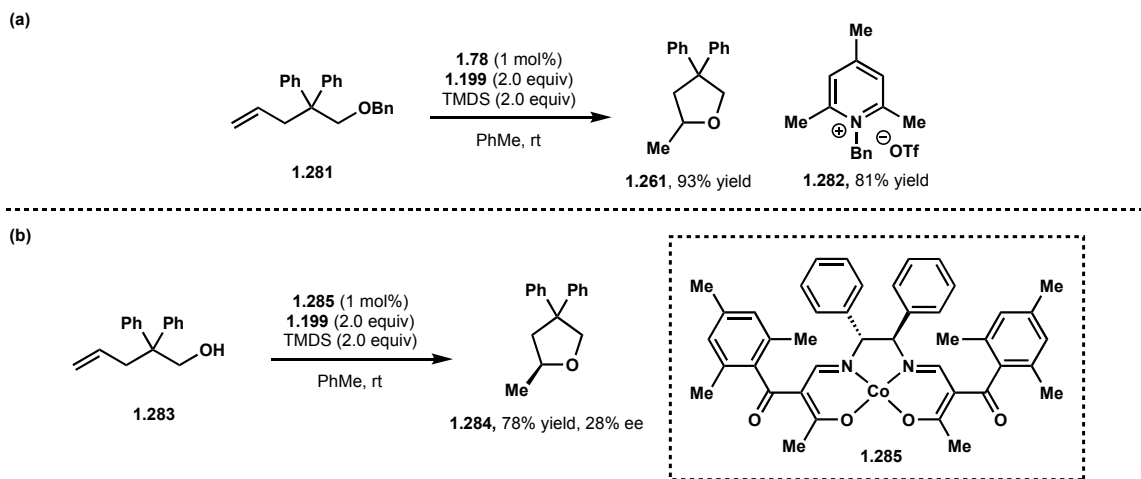


Primary alcohols with pendant terminal alkenes were readily cyclized to substituted tetrahydropyrans (**Scheme 1.26a**). Acyclic alcohols were reliant on geminal diphenyl and dimethyl substitution to drive ring closure. Phenols performed poorly, yielding dihydrobenzofurans in low yield. However, silyl and benzyl protection of the phenol boosted yields of benzofuran significantly. Benzylic alcohols closed readily to isochromanes. Carboxylic acids with pendant alkenes likewise underwent Thorpe-Ingold promoted ring closure to furnish lactones and

isochromanones (**Scheme 1.26b**). Catalyst optimization was required to construct oxygen containing macrocycles (**Scheme 1.26c**). The authors found that ethylenediamine based Co(II) salen catalyst **1.275** bearing *tert*-hexyl substitution on the salicylaldehyde motif effected macroetherification and macrolactonization to seven-membered rings in high yields. Ring closures to larger eight- and nine-membered rings proved inefficient.

The authors noted that when protected alcohols or esters were employed, collidinium salts bearing the corresponding protecting group were isolated as side products, suggesting that nucleophilic displacement or deprotonation of the intermediate oxonium by collidine is operative (**Scheme 1.27a**). Interestingly, when scalemic Co(II) β -ketoiminate catalyst **1.285** was applied to intramolecular hydroalkoxylation, mildly enantioenriched tetrahydropyran was isolated. (**Scheme 1.27b**) This is the first example of a MHAT radical reaction demonstrating any enantioselectivity. Strangely, Shigehisa did not propose alkylcobalt intermediates to explain the observed enantioselectivity, instead invoking achiral radical and carbocationic intermediates.

Scheme 1.27 Mechanistic studies of HAT radical–polar crossover synthesis of oxygen heterocycles



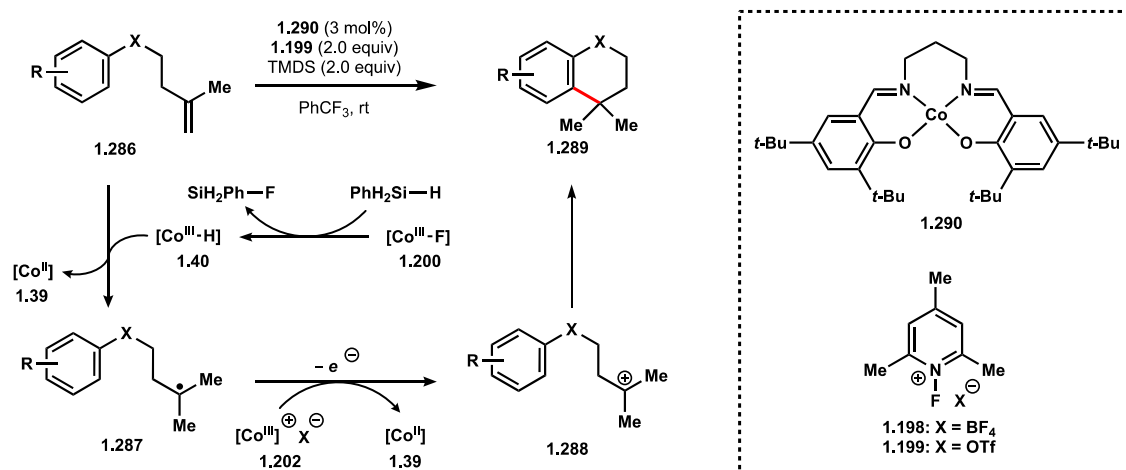
1.3.6 Shigehisa's Intramolecular HAT Radical–Polar Crossover Hydroarylation

In 2016, Shigehisa published an intramolecular cobalt-catalyzed HAT radical–polar crossover hydroarylation to rapidly construct α,α -dimethylbenzocycles.⁷⁸ The authors proposed a mechanism that begins with HAT from cobalt(III) hydride **1.40** to 1,1-disubstituted alkene **1.286** tethered to an arene (**Scheme 1.28a**). Oxidation of the resulting tertiary alkyl radical to a carbocation initiates cyclization by electrophilic aromatic substitution and forges a new carbon-carbon bond. Rearomatization produces the desired benzocycle **1.289**. Co(II) salen complex **1.290** bearing a propanediamine backbone was found to be the ideal hydroarylation catalyst. Isomerization to the trisubstituted was identified as the major side product.

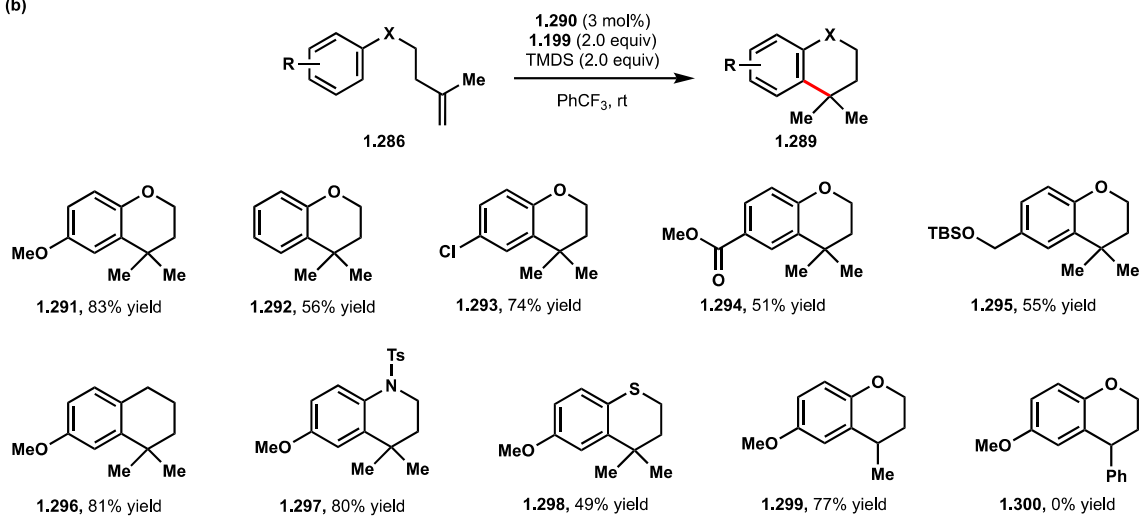
Optimized reaction conditions delivered a series of α,α -dimethylbenzocycles (**Scheme 1.28b**). Alkene scope was mostly limited to 1,1-disubstituted alkenes and entirely constrained to the formation of six-membered rings. Consistent with the participation of carbocationic intermediates, electron-donating group substitution on the arene was crucial for high yields of ring closure, while electron-withdrawing substituents depressed efficiency. Similarly, chromanes and tetrahydroquinolines were prepared in higher yields than corresponding tetrahydronaphthalene and thiochromane derivatives. Terminal alkenes that proceeded through unstabilized carbocations were appropriately engaged. Notably, the efficiency of ring closure for substrates that proceed through stabilized secondary carbocations was catalyst dependent. Optimized catalyst **1.290** failed to deliver **1.300** while tetramethyl catalyst **1.78** promoted the same hydroarylation in 88% yield. The authors do not elaborate further on the observed catalyst effects. To assess performance in the context of complex natural products, the hydroarylation protocol was applied to estrone derivative **1.301** to afford a 1.5:1 mixture of cyclization regioisomers (**Scheme 1.28c**). This method serves as a mild alternative to traditional acid-catalyzed Friedel-Crafts aromatic functionalization.

Scheme 1.28 Shigehisa's intramolecular HAT radical–polar crossover hydroarylation

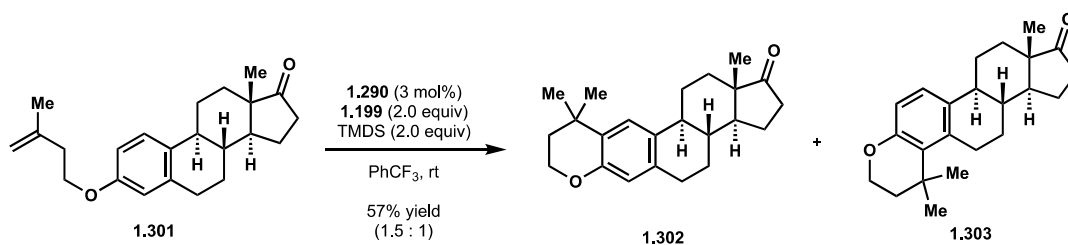
(a)



(b)



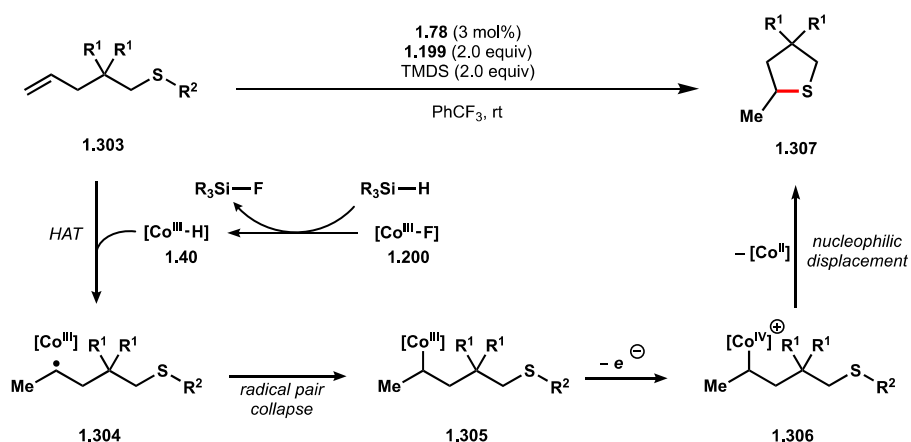
(c)



1.3.7 Shigehisa's Intramolecular HAT Radical–Polar Crossover Hydrothiolation

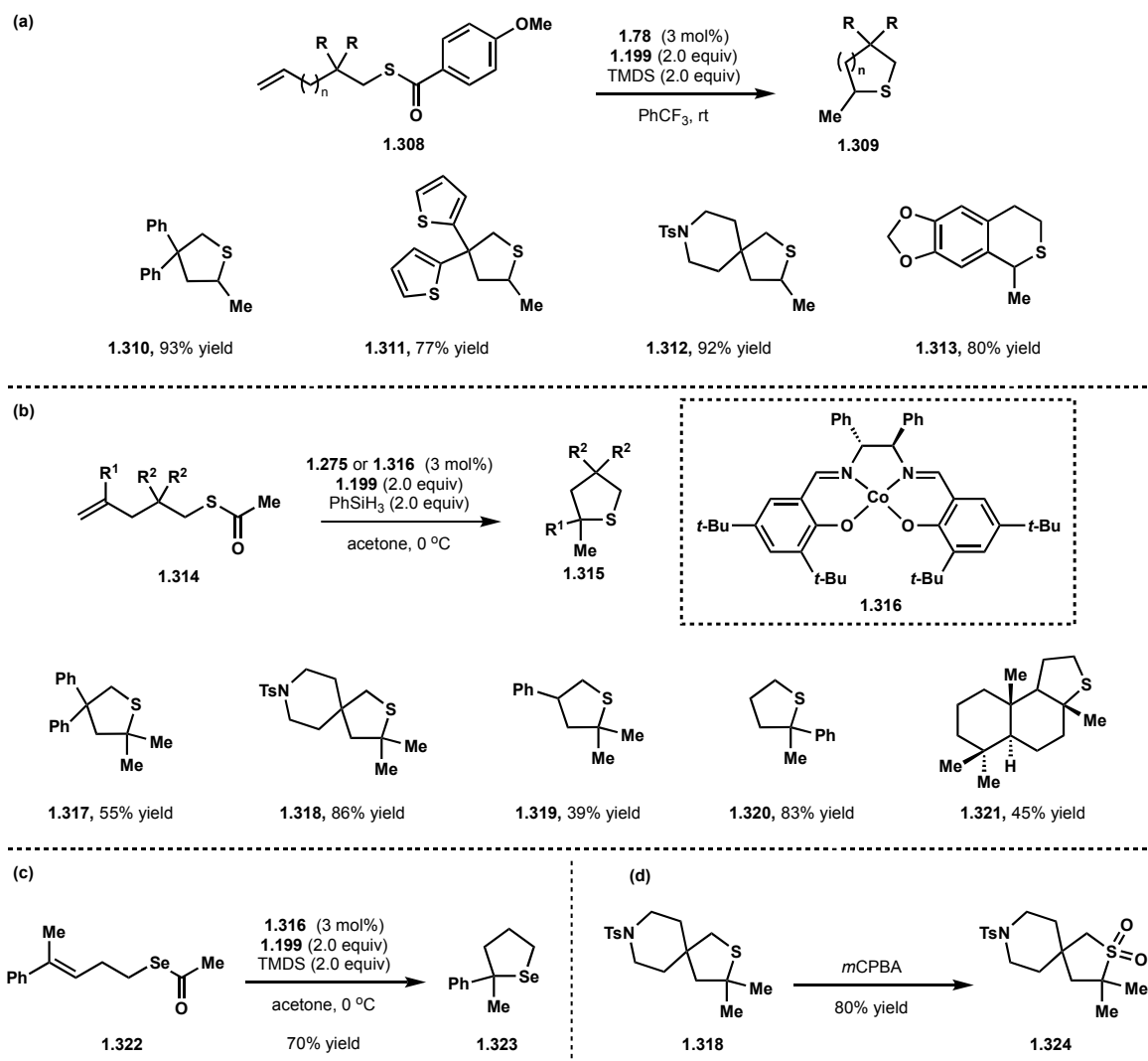
Intramolecular hydrothiolation of alkenyl thiols remains a challenging transformation with limited methods for synthetic chemists to utilize. Thiol-ene reactions have traditionally been employed to convert alkenyl thiols to saturated sulfur heterocycles with predominantly anti-Markovnikov regioselectivity.⁷⁹ Recently, Shigehisa disclosed a mild cobalt-catalyzed HAT radical–polar crossover hydrothiolation of alkenyl thiols that proceeds with exclusive Markovnikov selectivity.⁸⁰

Scheme 1.29 Shigehisa's radical–polar crossover hydrothiolation



In a departure from his previous mechanistic proposals, Shigehisa suggested that following HAT, the resulting solvent caged alkylradical–metalloradical pair **1.304** undergoes radical pair collapse to alkylcobalt(III) intermediate **1.305** (**Scheme 1.29**). Likely influenced by recent work from our lab^{81–82} and Shenvi⁸³ that suggest the participation of cationic alkylcobalt(IV) intermediates, Shigehisa proposed that single-electron oxidation of alkylcobalt(III) **1.305** gives rise to electrophilic alkylcobalt(IV) **1.306**. Nucleophilic displacement of Co(IV) delivers the desired heterocycle **1.307** and turns over Co(II).

Scheme 1.30 Representative scope of Shigehisa's radical-polar crossover hydrothiolation



The optimized conditions were first applied to the synthesis of 1-methyltetrahydrothiophenes from monosubstituted alkenes tethered to *para*-methoxybenzoyl protected thiols (**Scheme 1.30a**). Similar to prior methods, ring closures were reliant on Thorpe-Ingold effects and largely limited to five-membered rings (**1.310–1.312**). A succinct collection of isothiochromanes were synthesized in high yields (**1.313**). Broadening the alkene scope to 1,1-disubstituted alkenes required further reaction optimization. The solvent was switched to acetone and phenylsilane was applied as the reductant. Further investigation into catalysts found that 1,2-diphenylethylenediamine Co(II) salen catalyst **1.316** and *t*-hexyl substituted catalyst **1.275**

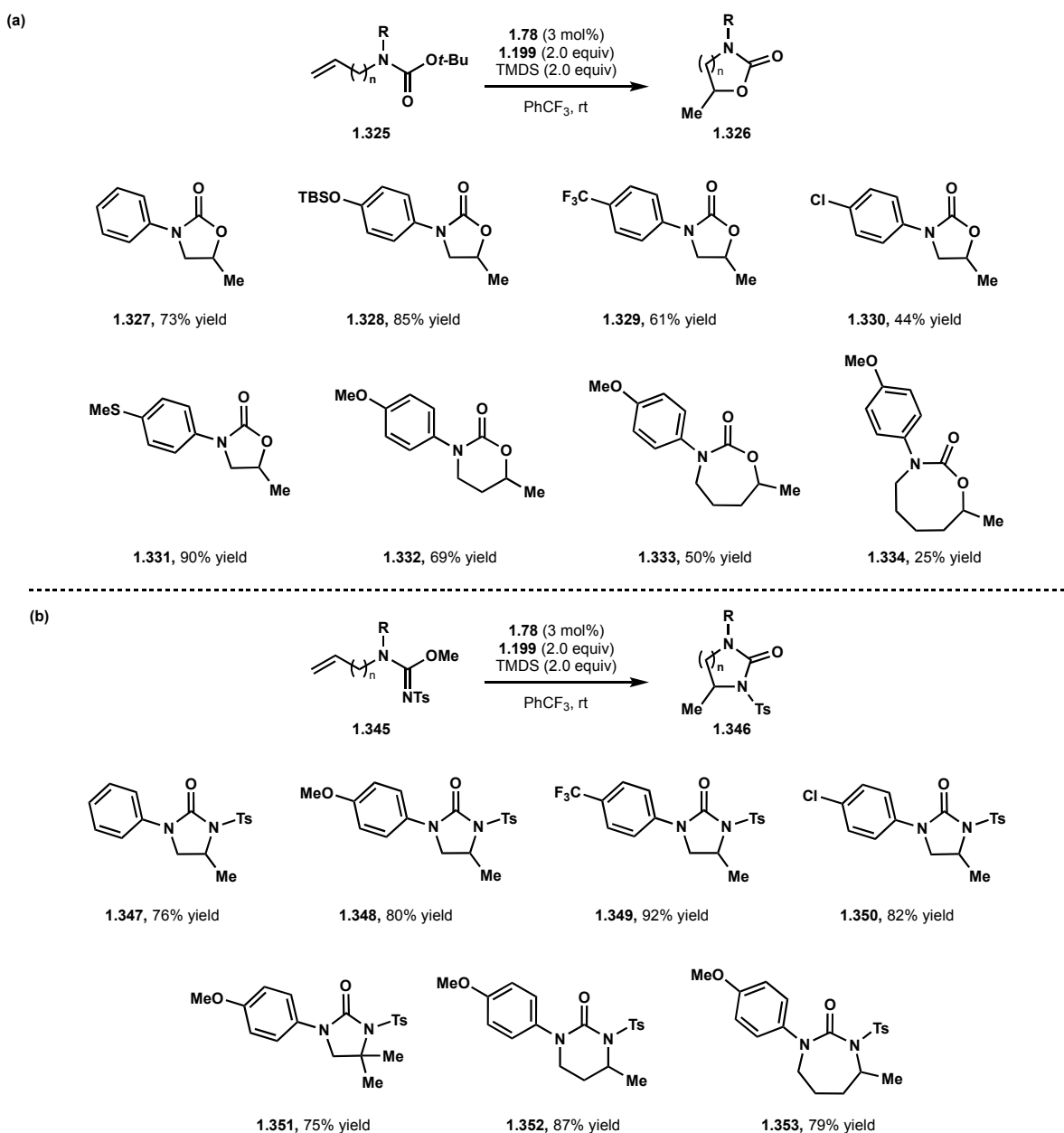
afforded the highest yields of ring closure (**Scheme 1.30b**). 2,2-Dimethyltetrahydrothiophenes were prepared with good efficiency (**1.317–1.319**). Geminal disubstitution was not required in cases where the alkene was styrenyl derived (**1.320**). Sesquiterpene thioambroxide **1.321** was synthesized in modest yield. The hydrothiolation protocol was adapted towards hydroselenolation of selenylester **1.322** to afford selenophane **1.323** in good yield. Sulfides and selenides are sensitive to oxidation, so their synthesis in the presence of *N*-fluorocollidinium oxidants is a testament to the mild nature and favorable kinetics of cobalt-catalyzed HAT hydrofunctionalizations. To emphasize this point, thiophane **1.318** was readily oxidized to sulfone **1.324** with *m*-chloroperoxybenzoic acid.

1.3.8 Shigehisa's Synthesis of Cyclic Carbamates and Ureas via Radical–Polar Crossover

Continuing their series of intramolecular HAT radical–polar crossover cyclizations, Shigehisa disclosed a method for the synthesis of cyclic carbamates and ureas from unactivated alkenes in 2020 (**Scheme 1.31**).⁸⁴ Optimized conditions were identical to those reported in Shigehisa's intramolecular hydroamination.⁷⁵ A series of *N*-phenyl Boc protected amines were converted efficiently to oxazolidinones (**Scheme 1.31a**). Electron-rich and electron-poor arenes were well tolerated (**1.327–1.329**), however arylhalide substitution depressed yields (**1.330**). Oxidation sensitive aryl sulfide motifs were left untouched during the course of cyclization (**1.331**). The hydrofunctionalization protocol was amenable towards the formation of six, seven, and eight-membered rings (**1.332–1.334**). Unsurprisingly, yields steadily fell as ring size increased. Alkene scope was limited to terminal alkenes. The authors next applied their protocol towards the synthesis of imidazolidinones from *N*-phenyl carbamimidates (**Scheme 1.31b**). Arene substitution on the nitrogen was assessed via installation of electron-donating and electron-

withdrawing groups, all of which were well tolerated (**1.347–1.349**). Interestingly, yields of substrates containing halogen substitution were significantly improved in the context of urea synthesis (**1.350**). 1,1-Disubstituted alkenes were competent substrates (**1.351**). Six and seven-membered imidazolidinones were accessed with high efficiency (**1.352–1.353**). The authors proposed a mechanism that proceeds through the intermediacy of electrophilic alkylcobalt(IV) species.

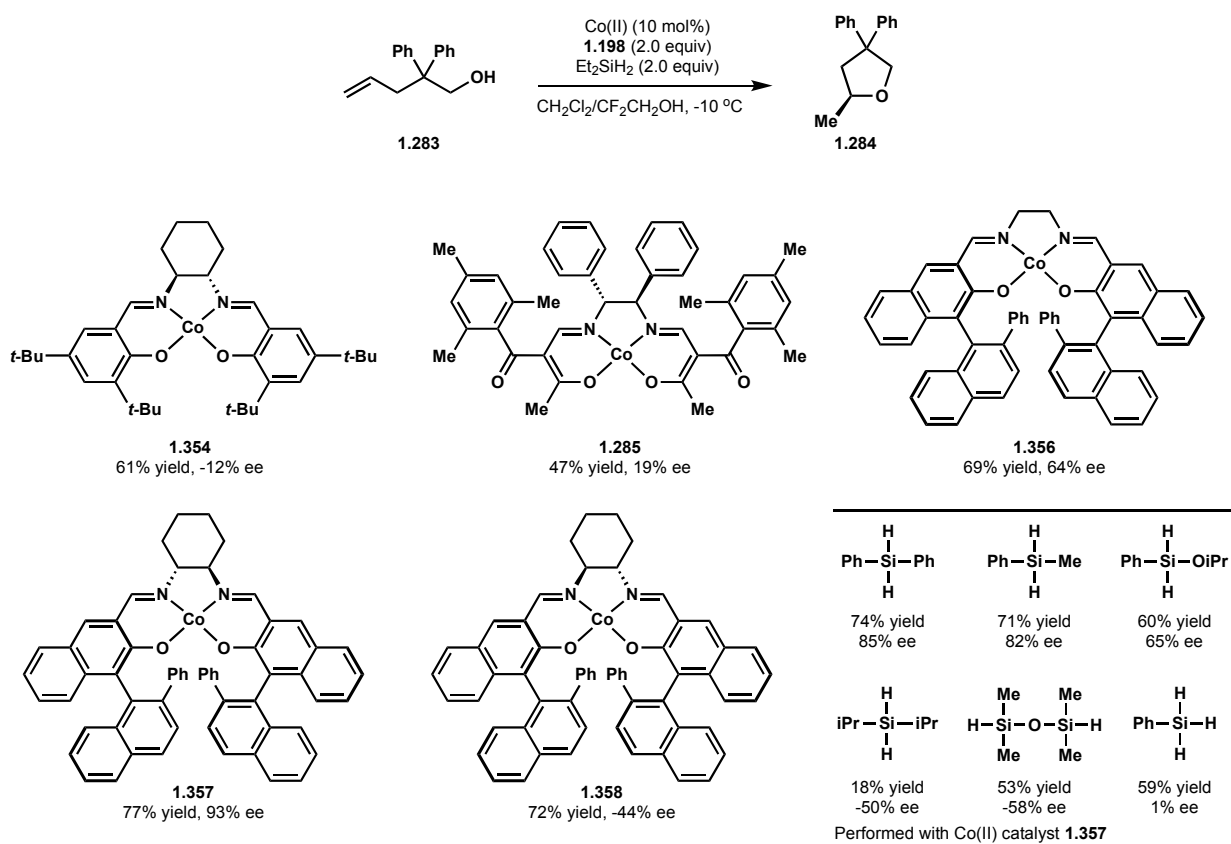
Scheme 1.31 Shigehisa's synthesis of cyclic carbamates and ureas via radical–polar crossover



1.3.9 Shigehisa's Asymmetric HAT Radical–Polar Crossover Hydroalkoxylation

Developing highly enantioselective variants of MHAT radical reactions is a multi-decade long challenge that has only been recently accomplished.^{82,85} Building upon the observation of mild enantioinduction during their 2016 study on the synthesis of saturated oxygen heterocycles, the Shigehisa lab recently published a full paper describing conditions for an asymmetric MHAT radical–polar crossover hydroalkoxylation.⁸⁶ An interesting feature of this reaction is that enantioselectivity was dependent on both catalyst structure and silane, typically considered an innocent bystander during the reaction other than acting as a hydride source.

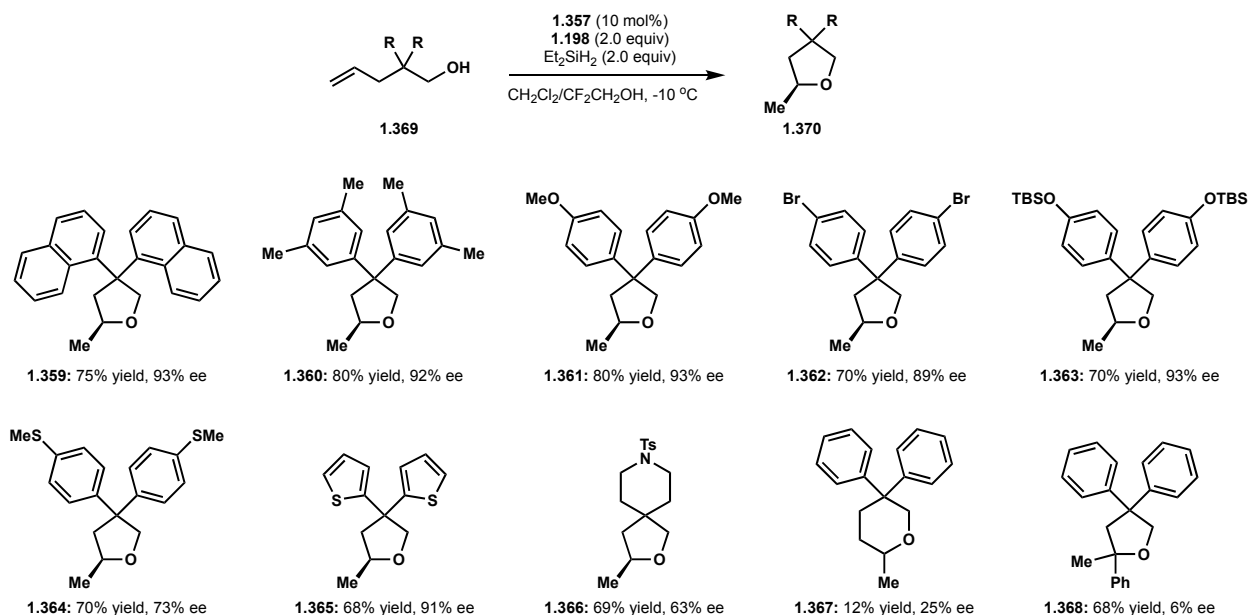
Scheme 1.32 Shigehisa's asymmetric HAT radical–polar crossover hydroalkoxylation



During optimization efforts, catalyst structure and silane led to interesting observations and trends (**Scheme 1.32**). Despite prior applications of Co(II) salen⁸⁷ and Co(II) β -ketoiminate⁸⁸ derived complexes towards enantioselective catalysis, modified binaphthyl Co(II) Katsuki⁸⁹

complexes afforded tetrahydrofuran **1.284** with the best enantioselectivities. Katsuki catalyst **1.357** bearing a cyclohexyl ethylenediamine backbone produced **1.284** with the highest asymmetric induction. Employing the opposite diastereomer of **1.357** by changing the stereochemical configuration of the cyclohexyl ethylenediamine backbone (**1.358**) produced the opposite enantiomer with eroded enantioselectivity. Enantioinduction and absolute configuration were both dependent on silane structure when used in conjunction with catalyst **1.357**. Secondary silanes bearing arene substitution such as diphenylsilane and methylphenylsilane afforded the *S* enantiomer of **1.284** in both good yield and enantioselectivity while alkylsilanes like diisopropylsilane and TMDS produced **1.284** in poor to modest yields but were moderately enantioselective for the *R* enantiomer. Phenylsilane produced a racemic mixture. Ultimately, diethylsilane was determined to be the best hydride source, providing **1.284** in 77% yield and 93% ee when paired with complex **1.357**.

Scheme 1.33 Representative substrate scope for Shigehisa's asymmetric HAT radical-polar crossover hydroalkoxylation



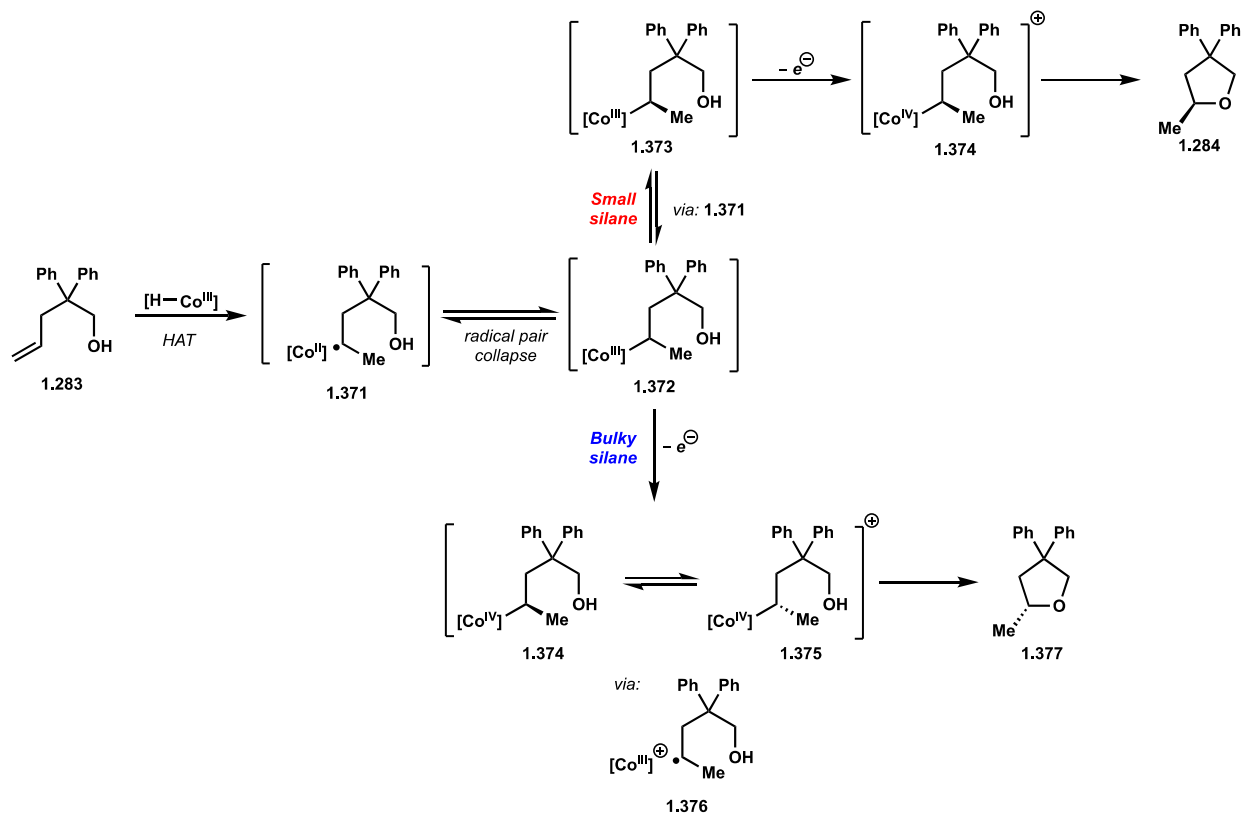
The substrate scope was limited to the formation of 2-methyl-4,4-diaryltetrahydrofurans (**Scheme 1.33**). Extended aromatic systems such as dinaphthyl **1.359** were prepared with high

yields and ee. Asymmetric induction was preserved with alkyl substituted (**1.360**), electron-rich (**1.361**), and electron-poor aromatics (**1.362**). Acid sensitive silyl ethers were likewise prepared with good yield and high enantioselectivity (**1.363**). Sulfides eroded enantioselectivity (**1.364**), perhaps due to oxidative degradation pathways. Heterocyclic substitution delivered high enantioselectivity (**1.365**), but yields were reduced. Diaryl substitution was essential for elevated levels of enantioinduction, as N-tosyl piperidine substitution delivered **1.366** in a modest 63% ee. Expanding ring size to tetrahydropyran products resulting in both severely depressed enantioinduction and yields (**1.367**). 1,1-disubstituted alkenes resulted in near racemic mixtures (**1.368**).

Shigehisa invokes a handful of potential mechanisms based on experiments with slow addition of silane. The authors noted that slowing addition of silane from 20 minutes to 4 hours reduced enantioselectivity. Extending silane addition over 80 hours inverted which enantiomer was favored, from 78% ee *S* to -14% ee *R*. These observations led Shigehisa to propose that at least two enantiodetermining steps are possible between at least two competing mechanistic pathways that are dependent upon silane concentration. Eyring analysis of the reaction using diethylsilane revealed a nonlinear plot, suggesting more than one operative enantiodetermining step weighted by temperature dependence. Taken together, Shigehisa proposed the following mechanism for asymmetric induction (**Scheme 1.34**): (1) Initial HAT by Co(III)–H to the alkene generates a solvent-caged alkylradical Co(II) metalloradical pair **1.371**. (2) Unselective radical pair collapse forms a racemic mixture of alkylcobalt(III) **1.372** as a resting state. (3a) When using a small silane, reversible radical chain disproportionation between alkylcobalt(III) **1.372** and diffusing carbon-centered radicals results in enantioenriched alkylcobalt(III) intermediate **1.373**. (4a) Subsequent oxidation to scalemic alkylcobalt(IV) **1.374** followed by stereospecific

intramolecular nucleophilic displacement results in enantioenriched (*S*) **1.284**. (3b) When using bulkier silane, radical chain disproportionation is suppressed, resulting in kinetic resolution of the racemic alkylcobalt(IV) species following single-electron oxidation. (4b) Nucleophilic displacement of the more reactive alkylcobalt(IV) diastereomer **1.375** leads to moderately enantioenriched (*R*) **1.377**.

Scheme 1.34 Proposed mechanism for Shigehisa's asymmetric HAT radical–polar crossover hydroalkoxylation

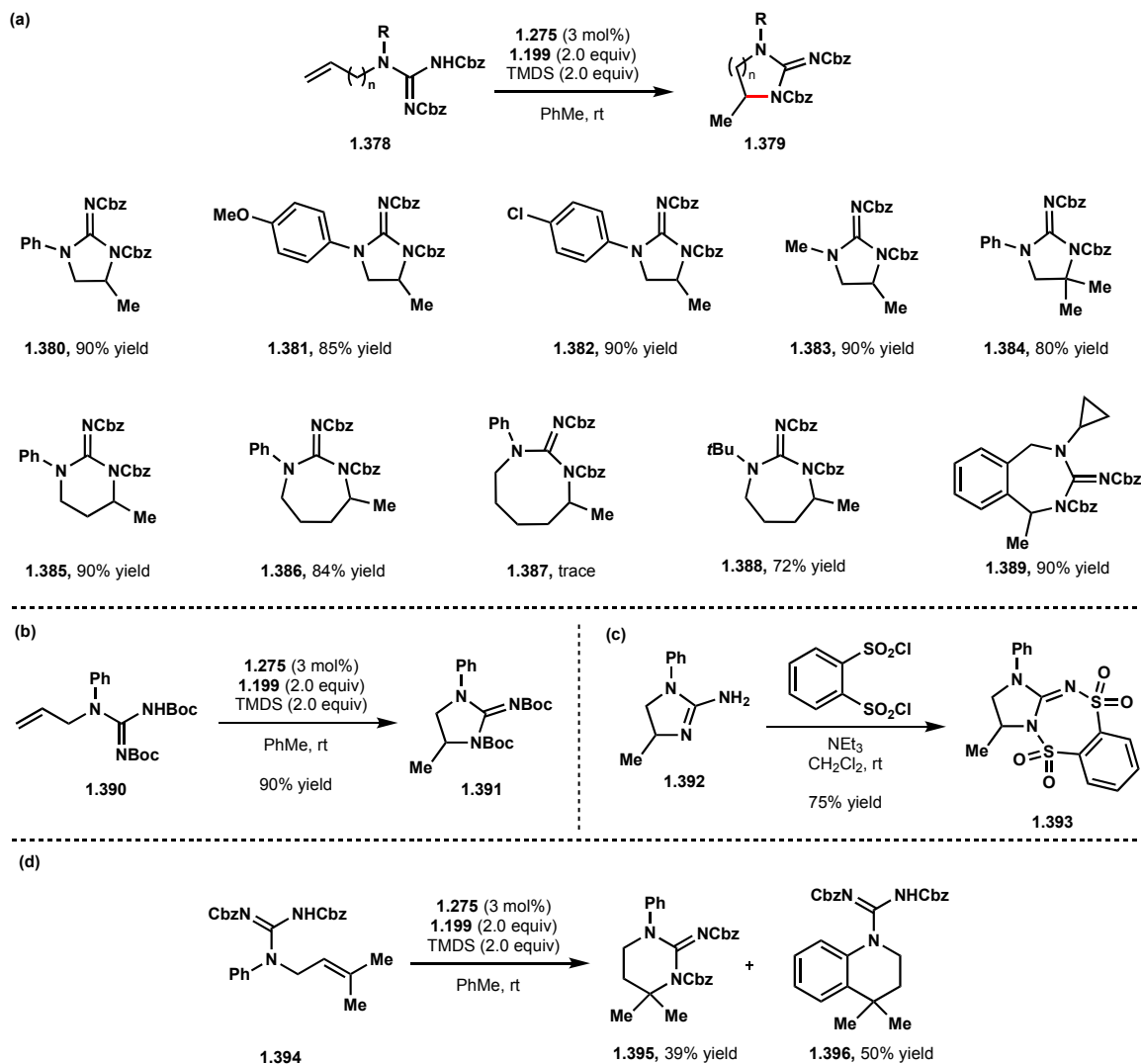


Shigehisa's asymmetric hydroalkoxylation is only the third reported asymmetric MHAT hydrofunctionalization. As one of the earliest reports of an enantioselective MHAT process, it is difficult to understate the significance this report contributes to the field of MHAT alkene hydrofunctionalizations.

1.3.10 Shigehisa's Synthesis of Cyclic Guanidines via HAT Radical–Polar Crossover

Shigehisa's most recent contribution to the field of HAT radical–polar crossover hydrofunctionalizations is a method for the synthesis of cyclic guanidines from alkenyl guanidines.⁹⁰ The synthesis of cyclic guanidines is well preceded, with a litany of preparative methods including intramolecular displacement⁹¹ and halocyclization⁹² as well as transition metal-catalysis using Ag,⁹³ Pd,⁹⁴ and Rh.⁹⁵ However, the synthesis of seven-membered guanidine rings remains underexplored.

Scheme 1.35 Shigehisa's synthesis of cyclic guanidines via radical–polar crossover

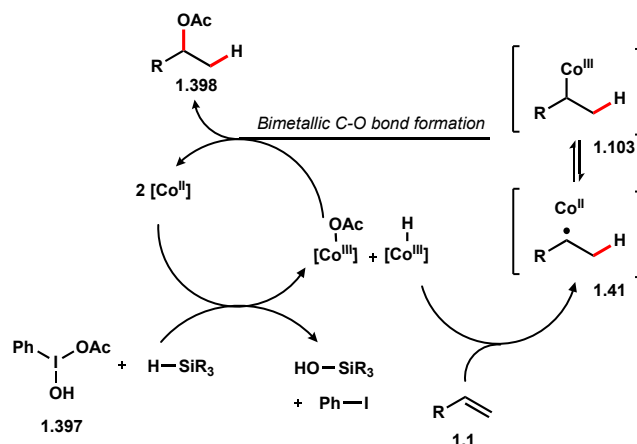


Optimized conditions delivered a variety of Cbz protected cyclic guanidines (**Scheme 1.35a**). Five-membered rings were formed in excellent yields and were tolerant of *N*-phenyl groups (**1.380**) bearing electron-rich functionality (**1.381**) and chloride substitution (**1.382**). Alkylated amines were compatible substrates (**1.383**). 1,1-Disubstituted alkenes were likewise efficient reaction partners (**1.384**). Ring closure to prepare six-membered (**1.385**) and seven-membered (**1.386**) cyclic guanidines was efficient while eight-membered rings (**1.387**) were formed in only trace amounts. *N*-alkylated guanidines were closed to seven-membered rings in good to excellent yields (**1.388–1.389**). To demonstrate broader functional group tolerance of the guanidine motif, Boc protected alkenyl guanidines were efficiently cyclized (**Scheme 1.35b**). Deprotected hydrofunctionalization product **1.392** was further derivatized with 1,2-benzenedisulfonyl dichloride to make dithiadiazepine **1.393** (**Scheme 1.35c**). Trisubstituted alkenes with *N*-phenyl substitution gave rise to mixtures of the desired ring closure onto nitrogen (**1.395**) as well as intramolecular Friedel-Crafts type hydroarylation (**1.396**) (**Scheme 1.35d**).

1.3.11 Zhu's Intermolecular HAT Radical–Polar Crossover Hydroacyloxylation

Rong Zhu's first contribution to the field of cobalt-catalyzed HAT radical–polar crossover hydrofunctionalization was a method for intermolecular hydroacyloxylation of unactivated alkenes published in 2019.⁹⁶ An advantage of this method is the use of accessible and easily diversifiable hypervalent iodine(III) reagents as oxidant, providing an alternative to the expensive and limited selection of *N*-fluorocollidinium salts utilized by Shigehisa.⁹⁷ Additionally, kinetic studies shed light on a more complex mechanistic picture suggested by Shigehisa and led Zhu to propose a novel bimetallic coupling pathway.

Scheme 1.36 Proposed mechanism for Zhu's radical-polar crossover hydroacyloxylation

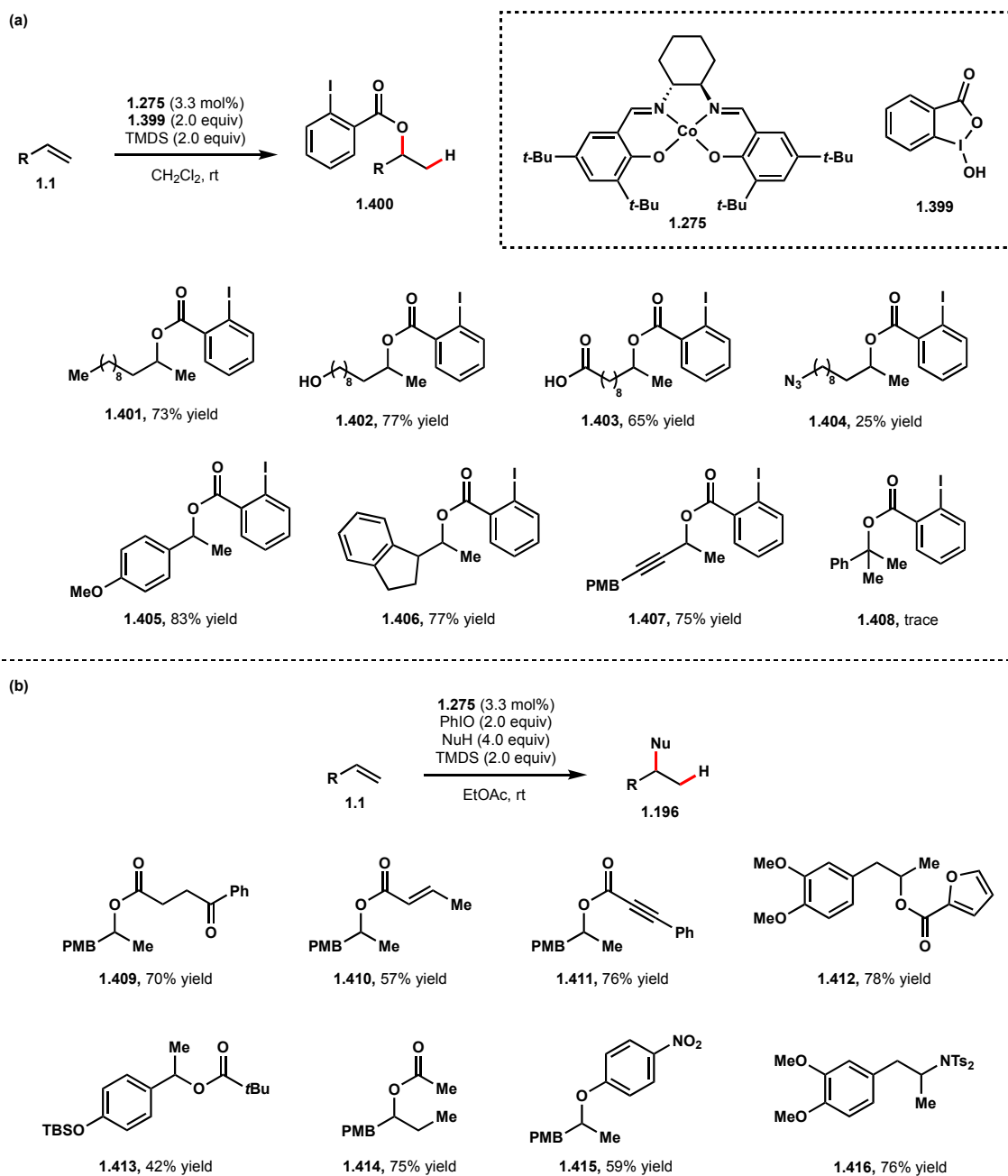


Zhu's mechanistic proposal commences with oxidation of two equivalents of cobalt(II) salen with silane and iodine(III) reagent **1.397** to an equivalent of cobalt(III) hydride and cobalt(III) acetate. The cobalt(III) hydride performs HAT onto an alkene and subsequently undergoes radical pair collapse to alkylcobalt(III) intermediate **1.103**. Bimetallic C–O bond formation between the alkylcobalt(III) and the cobalt(III) acetate species furnishes the hydroacyloxylation product **1.398** and returns the two equivalents of cobalt(II) salen. This proposal was supported by kinetic studies that demonstrated a second-order rate dependence on cobalt. Further details about how exactly the bimetallic coupling occurs were not provided, although Zhu speculated that a cooperative process similar to Jacobsens cobalt-catalyzed kinetic resolution of epoxides⁹⁸ or a transmetallation event similar to Shenvi's hydroarylation⁹⁹ may be occurring.

Optimized conditions using 1-hydroxy-1,2-benziodoxol-3(*H*)-one **1.399** as oxidant were used to screen compatible alkenes (**Scheme 1.37a**). Long-chained monosubstituted alkenes bearing alkyl (**1.401**), alcohol (**1.402**), and carboxylic acid (**1.403**) substitution were hydroacyloxylation in good yield. However, azides were poorly compatible with the reaction conditions (**1.404**). Styrenyl (**1.405**) and indenyl (**1.406**) alkenes were efficiently converted to the requisite hydrofunctionalization products. Interestingly, 1,3-enynes also proved to be viable

substrates for hydrofunctionalization (**1.407**). However, 1,1-disubstituted alkenes did not react productively, supporting Zhu's proposal that alkylcobalt(III) intermediates are participating, as tertiary alkylcobalts are disfavored intermediates compared to corresponding secondary alkylcobalt species.¹⁰⁰

Scheme 1.37 Representative substrate scope for Zhu's HAT radical-polar crossover hydroacyloxylation



The scope of nucleophile partners was then screened using paramethoxybenzene (PMB) derived alkenes (**Scheme 1.37b**). Addition of nucleophile and iodosobenzene produced the essential hypervalent iodine(III) oxidant transiently. Ketoacids (**1.409**), Michael acceptors (**1.410-1.411**), and carboxyfurans (**1.412**) were successively installed in good yield. Yields were depressed when bulky carboxylic acids were used (**1.413**). Simple acetate groups were installed onto 1,2-disubstituted alkenes (**1.414**). Expanding the reaction scope beyond acyloxy motifs, phenols (**1.415**) and secondary tosyl amines (**1.416**) were found to be compatible reaction partners and were installed in moderate to good yield. Like previous HAT mediated hydrofunctionalizations, all products were formed with excellent Markovnikov regioselectivity and functional group tolerance greatly exceeded that of a Brønsted acid-catalyzed process.

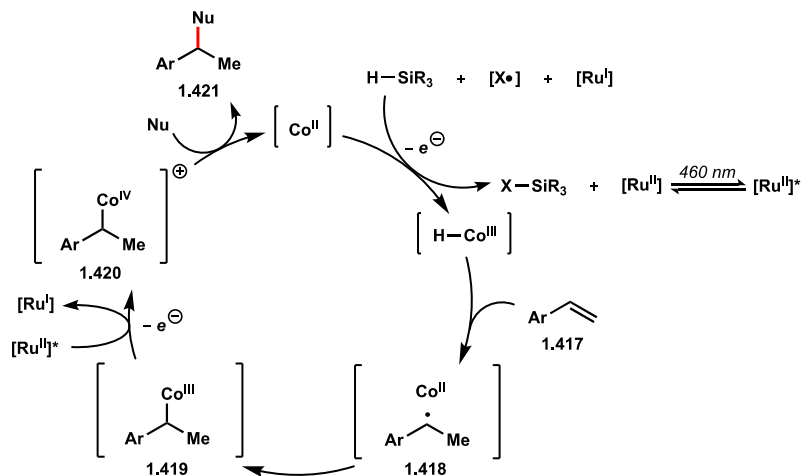
1.3.12 Zhu's Photoredox-Enabled HAT Radical–Polar Crossover Hydrofunctionalizations

Further investigations into alternative oxidation manifolds prompted the Zhu lab to develop a general platform for photoredox enabled HAT radical–polar crossover hydrofunctionalizations of styrenes.¹⁰¹ The authors proposed that chemical oxidants could be partly circumvented by using an excited state photocatalyst to oxidize alkylcobalt(III) intermediates to electrophilic alkylcobalt(IV) intermediates that could then engage in S_N2-type displacement by nucleophiles to afford Markovnikov hydrofunctionalization products (**Scheme 1.38a**). Brief screening of common photocatalysts and irradiation wavelengths identified Ru(bpy)₃²⁺ as the ideal photocatalyst. Stern–Volmer experiments conducted by exposure of an isolated alkylcobalt(III) salen complex derived from **1.275** to Ru(bpy)₃²⁺ and irradiation at 460 nm confirmed that excited state Ru(bpy)₃^{2+*} was readily quenched by alkylcobalt(III) salens. Tetramethylethylenediamine cobalt(II) salen **1.78** was found to be the best performing catalyst despite evidence that suggests alkylcobalt(III)

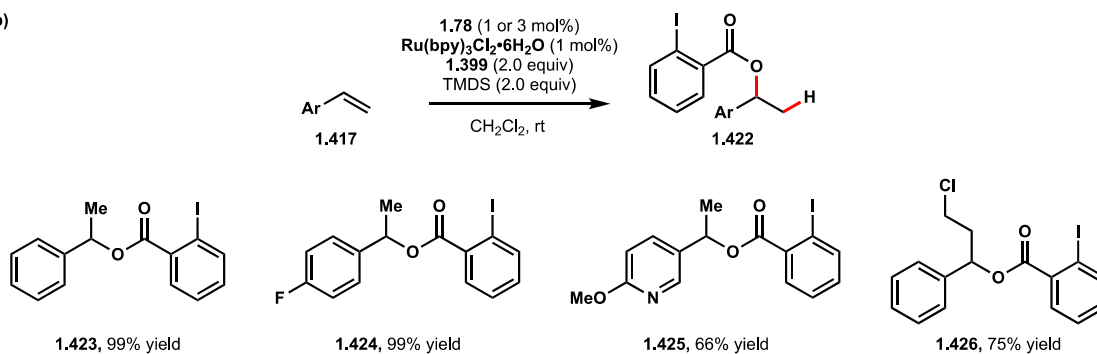
intermediates derived from **1.78** favor cobalt–carbon bond homolysis and subsequent cage escape.⁸¹

Scheme 1.38 Zhu's proposed mechanism for photoredox coupled HAT radical–polar crossover

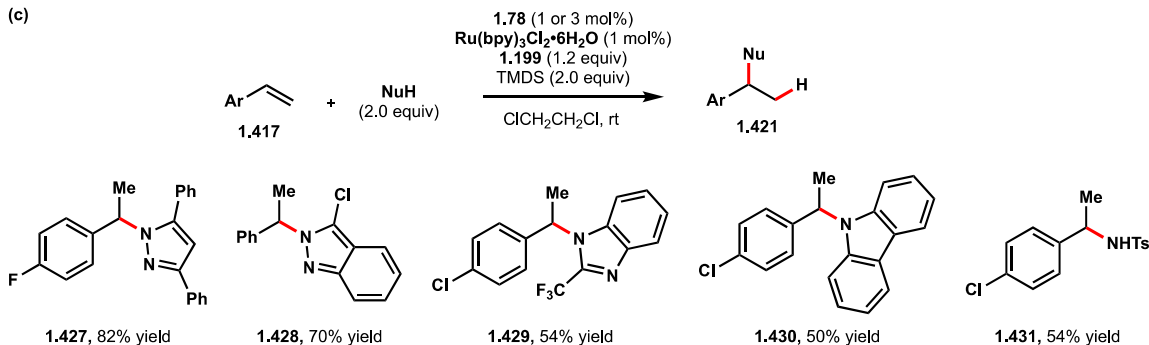
(a)



(b)



(c)



With optimized conditions in hand, a brief survey of vinyl arenes were hydroacyloxyated in the presence of hypervalent iodine(III) **1.399** (**Scheme 1.38b**). Products were prepared from styrene (**1.423**) and vinyl arylhalides (**1.424**) in near quantitative yield. Vinyl pyridines underwent

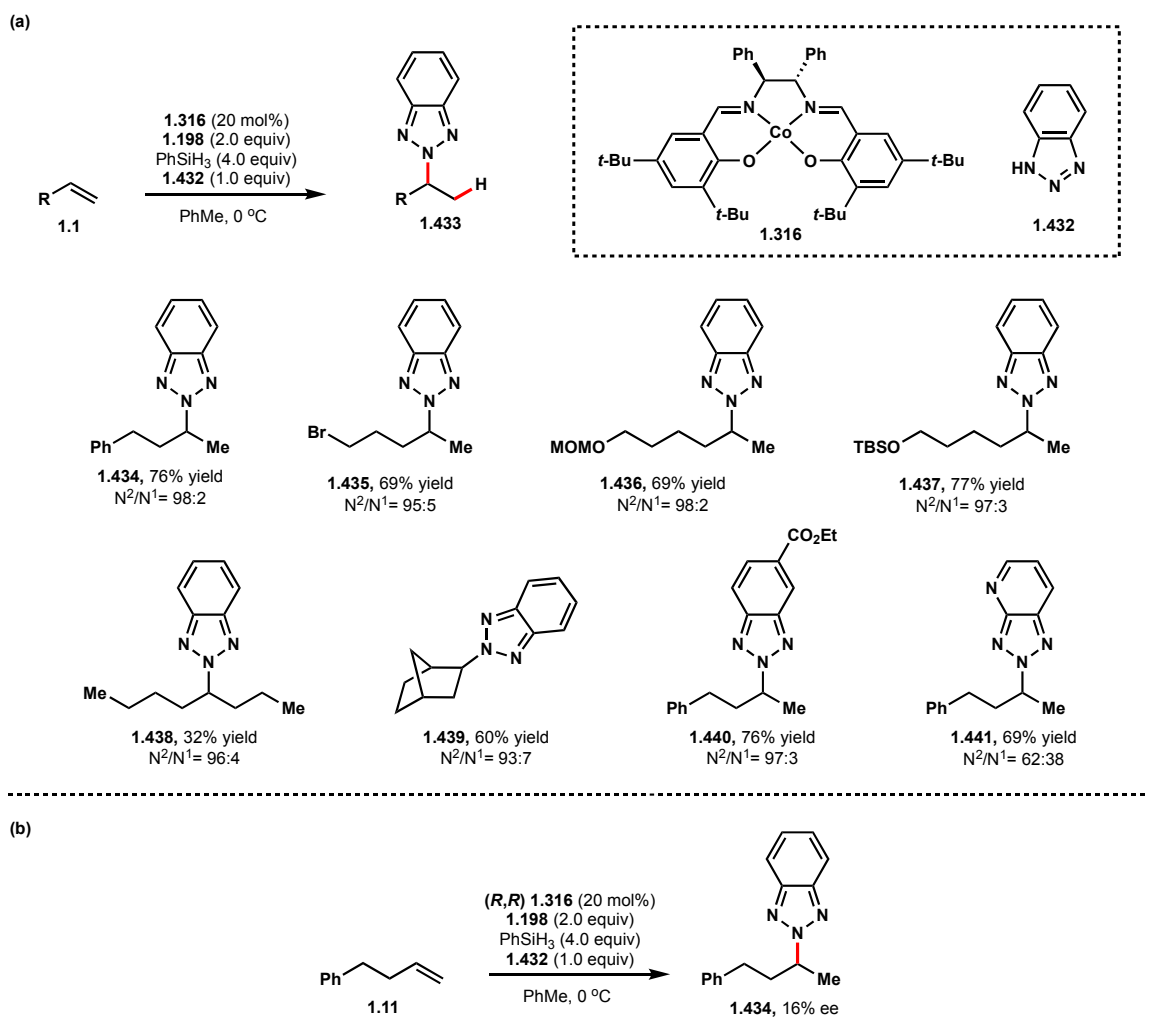
hydrofunctionalization in moderate yield (**1.425**) and 1,2-disubstituted alkenes were engaged efficiently (**1.426**). Exogenous nitrogen nucleophiles were then applied in combination with *N*-fluorocollidinium co-oxidant to afford hydroamination products (**Scheme 1.38c**). Pyrazoles (**1.427**) and indazoles (**1.428**) were installed in high yields while imidazoles (**1.429**), carbazoles (**1.430**), and sulfonamides (**1.431**) were only modestly incorporated. The marrying of photoredox and HAT hydrofunctionalization is an interesting new mode of reactivity, and although Zhu does not manage to get away completely from using hypervalent iodine(III) and *N*-fluorocollidinium co-oxidants, the reaction manifold clearly has potential for powerful new methods and mechanistic insight.

1.3.13 Akai's Intermolecular HAT Radical–Polar Crossover Hydroamination

Despite nearly a decade of HAT radical–polar crossover chemistry, methods to perform intermolecular Markovnikov hydroamination via cobalt catalysis remains limited to a few examples.^{96,101} Furthermore, selective *N*² alkylation of isobenzotriazoles remains a challenge. In an attempt to address both these limitations, Akai recently reported a HAT radical–polar crossover intermolecular hydroamination of unactivated alkenes using benzotriazoles as nucleophiles (**Scheme 1.39a**).¹⁰² In most cases, hydroamination products were formed with greater than 95:5 selectivity for alkylation on *N*². Linear monosubstituted alkenes bearing phenyl (**1.434**), bromine (**1.435**), and acid-sensitive functional handles (**1.436–1.437**) were delivered in good to moderate yields and *N*² selectivity was excellent in all cases. Acyclic 1,2-disubstituted alkenes were poorly engaged (**1.438**) but efficiency was improved when endocyclic 1,2-disubstituted alkenes were used (**1.439**). Electron-withdrawing substitution on the benzotriazole did not negatively influence reactivity (**1.440**). However, benzotriazoles derived from pyridine (**1.441**) reduced regioselectivity

significantly to a nearly 2:1 ratio of alkylation onto N^2 versus N^1 . Notably, when scalemic 1,2-diphenyl ethylenediamine cobalt(II) salen complex was used, some asymmetric induction was observed (**Scheme 1.39b**). This is the first example of catalytic asymmetric intermolecular HAT radical–polar crossover and will be sure to inspire efforts towards a highly enantioselective variant.

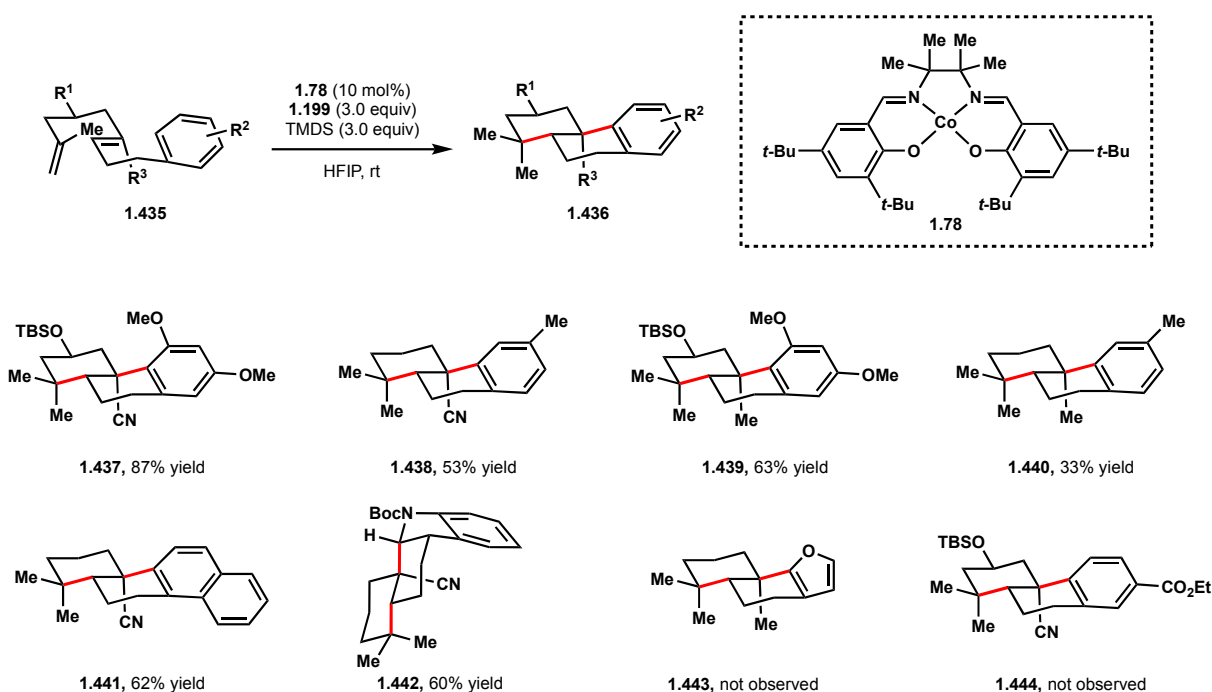
Scheme 1.39 Akai's intermolecular HAT radical–polar crossover hydroamination



1.3.14 Vanderwal's HAT Radical–Polar Crossover Bicyclization

Polyene cyclizations have been used for decades by chemists to rapidly construct structural complexity.¹⁰³ While the stereochemical outcomes of polycyclizations and broader reactivity patterns of substrates derived from geraniol are well established, predicting the behavior of polycyclization precursors containing electronically diverse alkene substitution is still not general. Realizing that metal-hydride HAT processes are known to reliably engage a broad range of alkenes, in 2020 the Vanderwal lab disclosed a cobalt-catalyzed HAT initiated radical–polar crossover polyene cyclization using electronically diverse alkenes.¹⁰⁴

Scheme 1.40 Vanderwal's HAT radical–polar crossover bicyclizations

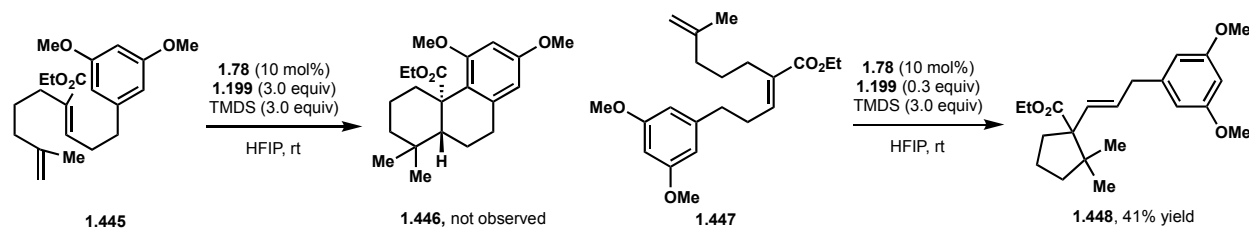


Optimized conditions delivered a series of electronically varied tricycles (**Scheme 1.40**). In all cases where cyclization was successful, products were formed as a single diastereomer and with trans stereochemistry about the ring junction of the decalin system. Precursors bearing electron-withdrawing nitrile groups and electron-rich arenes underwent cyclization in high yield (**1.437**). Removing electron density from the terminating arene reduced cyclization efficiency

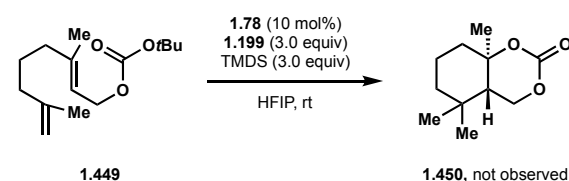
(**1.438**). Yields using precursors with the nitrile substituted for an electron-donating methyl group were further depressed (**1.439–1.440**). Naphthalene and indole groups were competent terminators (**1.441–1.442**) while furans (**1.443**) failed to deliver any detectable cyclization products. Installing electron-withdrawing functionality on the pendant arene shut down cyclization entirely (**1.444**).

Scheme 1.41 Mechanistic investigations on Vanderwal's HAT radical–polar crossover bicyclizations

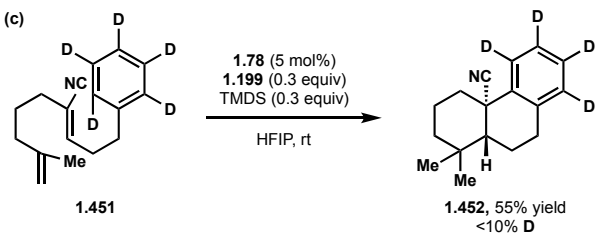
(a)



(b)



(c)



In an attempt to expand the scope of electron-withdrawing groups, acrylate ester **1.445** was subjected to the optimized reaction conditions (**Scheme 1.41a**). However, only a complex mixture of products was observed. The *E* isomer **1.447** likewise failed to deliver the desired tricycle, but rather primarily underwent 5-*exo*-trig radical cyclization to furnish cyclopentane **1.448**. Notably, substoichiometric amounts of oxidant were required to cyclize **1.447**, suggesting that back HAT is operating to regenerate cobalt hydride. A series of mechanistic studies were then conducted to probe when oxidation of the intermediate alkylradical occurs during cyclization. Attempts to cyclize carbonate **1.449** only produced hydrofluorination and isomerization products instead of the desired bicycle, suggesting that carbocationic intermediates are not involved (**Scheme 1.41b**).

Cyclization of pentadeuterated precursor **1.451** resulted in less than 10% deuterium incorporation at the geminal dimethyl groups on the decalin system of **1.452** (**Scheme 1.41c**). This

result implies that final single-electron oxidation of the conjugated cyclohexadienyl radical is followed by deprotonation to terminate the cyclization cascade. If the cyclization was purely radical, one might expect deuterium abstraction by cobalt(II) to generate a cobalt(III) deuteride that would then engage in deuterium atom transfer onto a second equivalent of substrate, resulting in appreciable deuterium incorporation at the terminal 1,1-disubstituted alkene. This report provides valuable mechanistic insights into MHAT-initiated polyene cyclization cascades and legitimizes the potential for broader application of MHAT radical–polar crossover hydrofunctionalization to natural product synthesis.

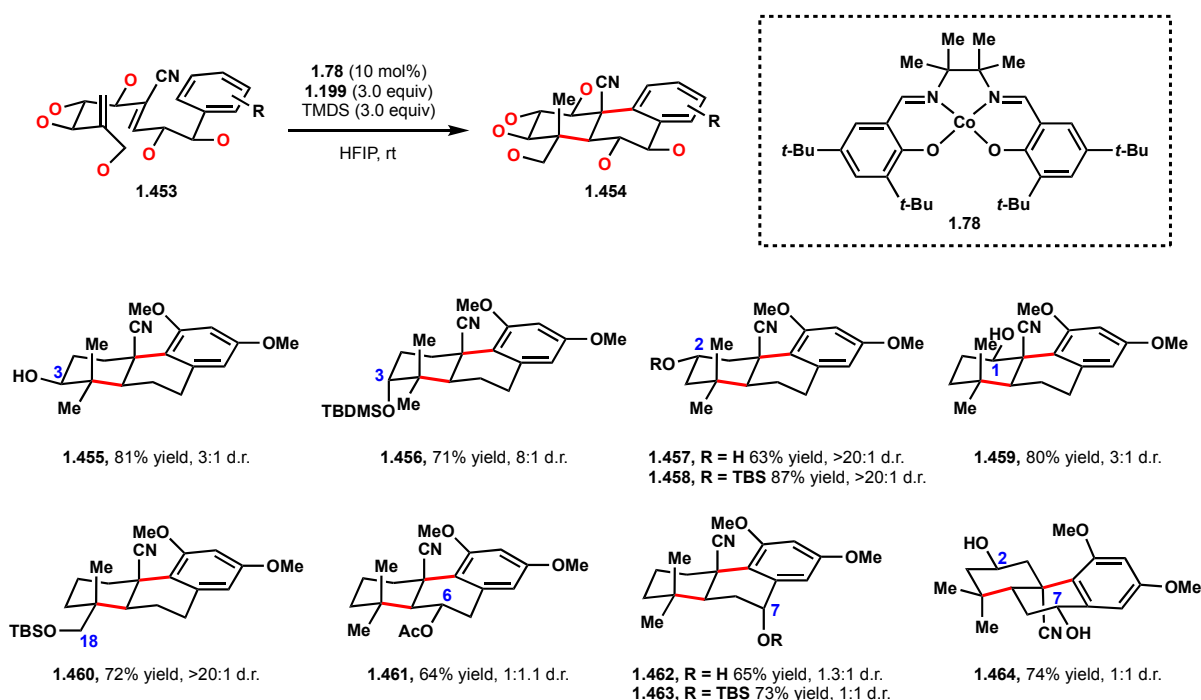
1.3.15 Vanderwal’s Stereocontrolled Synthesis of Abietane Diterpenoids via HAT Radical–Polar Crossover Polyene Cyclization

In 2021 the Vanderwal lab published an article detailing a systematic overview of the influence of oxidation pattern on the stereochemical outcomes of HAT-initiated radical–polar crossover bicyclization (**Scheme 1.42**).¹⁰⁵ The report concludes with a synthesis of abietane diterpenoids (+)-2-O-deacetyl plebedipene A, (+)-2-O-deacetyl plebedipene C, and (±)-plebedipene B.

Analysis commenced with investigating the stereochemical outcomes of HAT-initiated radical polar crossover cyclization of acrylonitrile influence of oxidation at C3. Free alcohols at C3 resulted in efficient cyclization favoring the equatorial diastereomer in a 3:1 ratio (**1.455**). However, protection of the C3 alcohol with a bulky *tert*-butyldimethylsilyl (TBS) group completely reversed selectivity to predominantly form the axial diastereomer in a 8:1 ratio (**1.456**). Oxidation at C2 resulted in cyclization to generate a single diastereomer in the case of both free alcohols (**1.457**) and TBS ethers (**1.458**). Diastereoselectivity was significantly eroded to 3:1

favoring the equatorial configuration at C1 when cyclization with free alcohols installed at C1 was attempted (**1.459**). Conversely, allylic oxidation at C18 produced **1.460** as a single diastereomer. Oxidation at C6 or C7 resulted in near equimolar mixtures of diastereomers regardless of substitution on the alcohol (**1.461–1.463**). Likewise, doubly oxygenated precursors delivered cyclization products as equimolar or near equimolar mixtures of diastereomers (**1.464**).

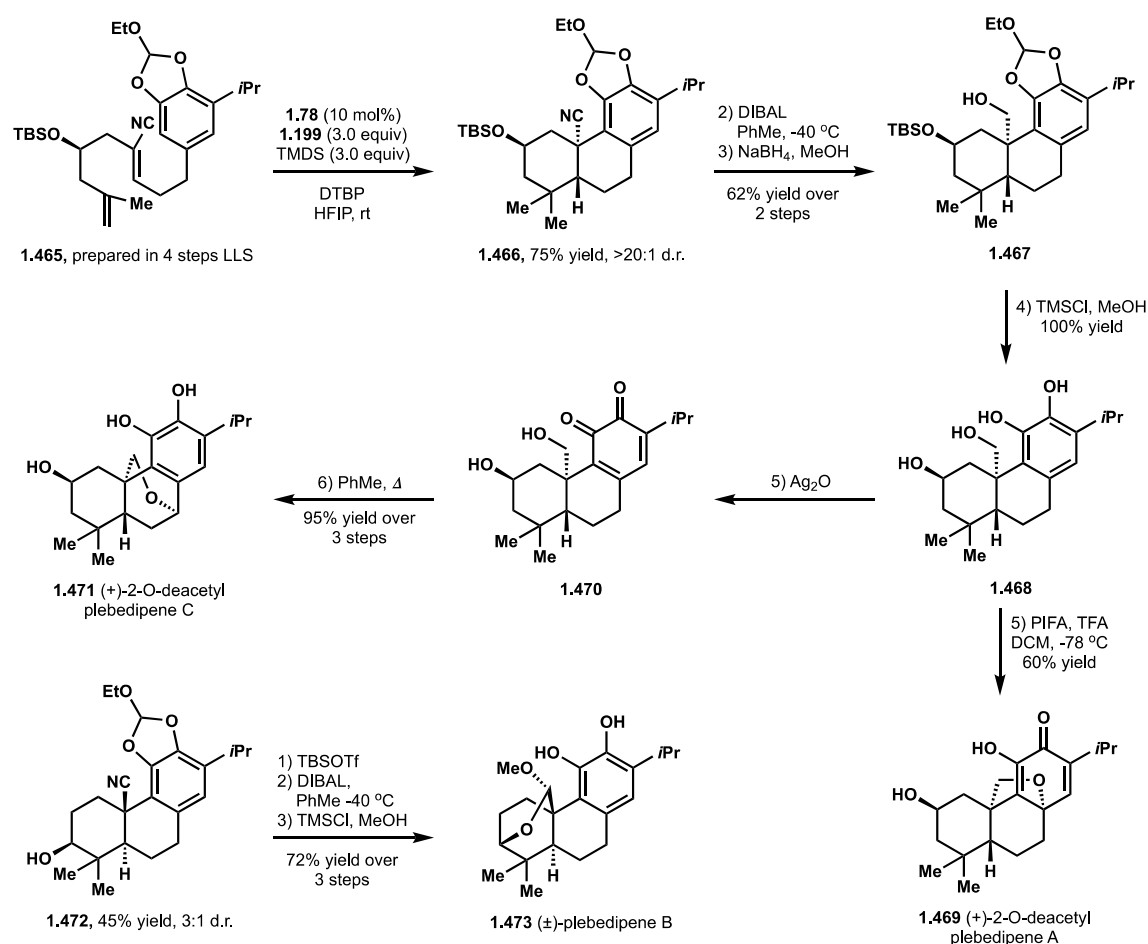
Scheme 1.42 Vanderwal's stereocontrolled HAT radical–polar crossover bicyclizations



The paper concludes with a concise and divergent synthesis of three highly oxygenated abietane diterpenoids (**Scheme 1.43**). Cyclization precursor **1.465** was first prepared in 4 steps longest linear sequence. Subjecting **1.465** to the HAT radical–polar crossover bicyclization furnished bicycle **1.466** as a single diastereomer in 75% yield. DIBAL reduction of the nitrile followed by a second reduction with sodium borohydride delivered alcohol **1.467** in 62% yield over 2 steps. Quantitative one pot deprotection of the TBS ether and orthoformate groups with trimethylsilyl chloride in methanol revealed tetraol **1.468** as a common intermediate for

diversification. Oxidative cyclization using hypervalent iodine converted **1.468** to (+)-2-O-deacetyl plebedipene A in a single step in 60% yield. Conversely, treatment of **1.468** with silver oxide delivered crude o-quinone **1.470** which was subsequently heated in toluene to cleanly afford (+)-2-O-deacetyl plebedipene C in 95% yield over 3 steps. (±)-plebedipene B was prepared in 72% yield over 3 steps from bicycle **1.472** through a sequence of TBS protection, DIBAL reduction, and concomitant orthoformate deprotection/acetal cyclization.

Scheme 1.43 Vanderwal's synthesis of abietane diterpenoids



1.4 References and Notes

1. Hennell, H. *Philos. Trans. R. Soc.* **1828**, *118*, 365.
2. Toteva, M. M.; Richard, J. P. *J. Am. Chem. Soc.* **1996**, *118*, 11434.
3. Reed, C. A. *Chem. Commun.* **2005**, 1669.
4. For a review of contemporary carbocation chemistry with an excellent summary of historical context see: Reddy, R. R.; Klumpp, D. A. *Chem. Rev.* **2013**, *113*, 6905 and references therein.
5. Hoffmann, R. W. *Chem. Soc. Rev.* **2016**, *45*, 577.
6. Crossley, S. W. M.; Obradors, C.; Martinez, R. M.; Shenvi, R. A. *Chem. Rev.* **2016**, *116*, 8912.
7. Shevick, S. L.; Wilson, C. V.; Kotesova, S.; Kim, D.; Holland, P.; Shenvi, R. A. *Chem. Sci.* **2020**, *11*, 12401.
8. Green, S. A.; Crossley, S. W. M.; Matos, J. L. M.; Vásquez-Céspedes, S.; Shevick, S. L.; Shenvi, R. A. *Acc. Chem. Res.* **2018**, *51*, 2628.
9. (a) Kim, D.; Rahaman, S. M. W.; Mercado, B. Q.; Poli, R.; Holland, P. L. *J. Am. Chem. Soc.* **2019**, *141*, 7473–7485. (b) Matos, J. L. M.; Green, S. A.; Chun, Y.; Dang, V. Q.; Dushin, R.; Richardson, P.; Chen, J.; Piotrowski, D.; Paegel, B.; Shenvi, R. A. *Angew. Chem., Int. Ed.* **2020**, *59*, 2. (c) Gonzalez, A. A.; Hoff, C. D. *J. Am. Chem. Soc.* **2008**, *130*, 4250.
10. For BDFE values of relevant M–H, C–H, and C–C bonds see: (a) Uddin, J.; Morales, C. M.; Maynard, J. H.; Landis, C. R. *Organometallics*, **2006**, *25*, 5566. (b) Luo, Y. R. *Comprehensive Handbook of Chemical Bond Energies*, CRC Press, Boca Raton, 1st edn, 2007. (c) Choi, J.; Pulling, M. E.; Smith, D. M.; Norton, J. R. *J. Am. Chem. Soc.* **2008**, *130*, 4250. (d) Blanksby, S. J.; Ellison, G. B. *Acc. Chem. Res.* **2003**, *36*, 255.
11. The M–H BDFE of the described metal-hydride species has not been measured directly due to their instability. Reference 9a describes computational BDFE estimations of relevant metal-hydrides. The weakest characterized metal-hydride has a M–H BDFE of 50.3 kcal/mol.^{9c}
12. Fleming, I. *Molecular Orbitals and Organic Chemical Reactions: Student Edition*, John Wiley & Sons Ltd, United Kingdom, 2009.
13. (a) Giese, B. *Angew. Chem., Int. Ed. Engl.* **1983**, *22*, 753. (b) Lewis, F. M.; Mayo, F. R.; Hulse, W. F. *J. Am. Chem. Soc.* **1945**, *67*, 1701. (c) Curran, D. P.; Eichenberger, E.; Collis, M.; Roepel, M. G.; Thoma, G. *J. Am. Chem. Soc.* **1994**, *116*, 4279. (d) Munger, K.; Fischer, H. *Int. J. Chem. Kinet.* **1985**, *17*, 809.
14. (a) Walsh, C. *Enzymatic Reaction Mechanisms*; W. H. Freeman and Co., 1979; Chapters 12–15. (b) Karlin, K. D.; Cruse, R. W.; Gultneh, Y.; Farooq, A.; Hayes, J. C.; Zubieta, J. *J. Am. Chem. Soc.* **1987**, *109*, 2668. (c) Kitajima, N.; Koda, T.; Hashimoto, S.; Kitagawa, T.; Morooka, Y. *J. Chem. Soc., Chem. Commun.* **1988**, 151.
15. (a) Klingenberg, M. *Arch. Biochem. Biophys.* **1958**, *75*, 376. (b) Omura, T.; Sato, R. *J. Biol. Chem.* **1964**, *239*, 2379.
16. (a) Tabushi, I.; Koga, N. *J. Am. Chem. Soc.* **1979**, *101*, 6456. (b) Punniyamurthy, T.; Velusamy, S.; Iqbal, J. *Chem. Rev.* **2005**, *105*, 2329. (c) Mansuy, D. *Pure Appl. Chem.* **1987**, *59*, 759.
17. Ullrich, V. *Angew. Chem., Int. Ed. Engl.* **1972**, *11*, 701.
18. (a) Hodgkin, D. C. *Proc. R. Soc. Lond.* **1945**, *A184*, 64. (b) Howard, J. A. K. *Nat. Rev. Mol. Cell Biol.* **2003**, *4*, 891.
19. (a) Schrauzer, G. N.; Kohnle, J. *Chem. Ber.* **1964**, *97*, 3056. (b) Schrauzer, G. N.; Windgassen, R. J. *Chem. Ber.* **1966**, *99*, 602. (c) Schrauzer, G. N.; Windgassen, R. J. *J. Am. Chem. Soc.* **1966**, *88*, 3738. (d) Schrauzer, G. N.; Windgassen, R. J. *J. Am. Chem. Soc.* **1967**, *89*, 1999.
20. Okamoto, T.; Oka, S. *Tetrahedron Lett.* **1981**, *22*, 2191.

21. Okamoto, T.; Oka, S. *J. Org. Chem.* **1984**, *49*, 1589.
22. (a) Wender, I.; Levine, R.; Orchin, M. *J. Am. Chem. Soc.* **1950**, *72*, 4375. (b) Wender, I.; Greenfield, H.; Orchin, M. *J. Am. Chem. Soc.* **1951**, *73*, 2656. (c) Friedman, S.; Metlin, S.; Svedi, A.; Wender, I. *J. Org. Chem.* **1959**, *24*, 1287.
23. (a) Adkins, H.; Krsek, G. *J. Am. Chem. Soc.* **1949**, *71*, 3051. (b) Bohnen, H.-W.; Cornils, B. *Adv. Catal.* **2002**, *47*, 1.
24. Feder, H. M.; Halpern, J. *J. Am. Chem. Soc.* **1975**, *97*, 7186.
25. Tabushi, I.; Koga, N. *J. Am. Chem. Soc.* **1979**, *101*, 6456.
26. Ohkatsu, Y.; Ohno, M.; Ooi, T.; Inoue, S. *Nippon Kagaku Kaishi* **1985**, 387.
27. (a) Zombeck, A.; Hamilton, D. E.; Drago, R. S. *J. Am. Chem. Soc.* **1982**, *104*, 6782. (b) Corden, B. B.; Drago, R. S.; Perito, R. P. *J. Am. Chem. Soc.* **1985**, *107*, 2903. (c) Hamilton, D. E.; Drago, R. S.; Zombeck, A. *J. Am. Chem. Soc.* **1987**, *109*, 374.
28. Mukaiyama, T.; Isayama, S.; Inoki, S.; Kato, K.; Yamada, T.; Takai, T. *Chem. Lett.* **1989**, *18*, 449.
29. Isayama, S.; Mukaiyama, T. *Chem. Lett.* **1989**, *18*, 1071.
30. (a) Tokuyasu, T.; Kunikawa, S.; Masuyama, A.; Nojima, M. *Org. Lett.* **2002**, *4*, 3595. (b) Tokuyasu, T.; Kunikawa, S.; McCullough, K. J.; Masuyama, A.; Nojima, M. *J. Org. Chem.* **2005**, *70*, 251.
31. Crossley, S. W. M.; Barabé, F.; Shenvi, R. A. *J. Am. Chem. Soc.* **2014**, *136*, 16788.
32. Waser, J.; Carreira, E. M. *J. Am. Chem. Soc.* **2004**, *126*, 5676.
33. Waser, J.; Nambu, H.; Carreira, E. M. *J. Am. Chem. Soc.* **2005**, *127*, 8294.
34. Gaspar, B.; Carreira, E. M. *Angew. Chem. Int. Ed.* **2007**, *46*, 4519.
35. Gaspar, B.; Carreira, E. M. *J. Am. Chem. Soc.* **2009**, *131*, 13214.
36. Gaspar, B.; Carreira, E. M. *Angew. Chem. Int. Ed.* **2008**, *47*, 5758.
37. Isayama, S. *Bull. Chem. Soc. Jpn.* **1990**, *63*, 1305.
38. Rao, H. S. P.; Siva, P. *Synth. Commun.* **1994**, *24*, 549.
39. Rostovtsev, V. V.; Green, L. G.; Fokin, V. V.; Sharpless, K. B. *Angew. Chem. Int. Ed.* **2002**, *41*, 2596.
40. Gaspar, B.; Waser, J.; Carreira, E. M. *Synthesis*, **2007**, *2007*, 3839.
41. Waser, J.; Gaspar, B.; Nambu, H.; Carreira, E. M. *J. Am. Chem. Soc.* **2006**, *128*, 11693.
42. (a) Nugent, W. A.; McKinney, R. J. *J. Org. Chem.* **1985**, *50*, 5370. (b) Casalnuovo, A. L.; RajanBabu, T. V.; Ayers, T. A.; Warren, T. H. *J. Am. Chem. Soc.* **1994**, *116*, 9869. (c) Keim, W.; Behr, A.; Lühr, H.-O.; Weisser, J. *J. Catal.* **1982**, *78*, 209. (d) Goertz, W.; Kamer, P. C. J.; van Leeuwen, P. V. N. M.; Vogt, D. *Chem. Commun.* **1997**, 1521.
43. Whitmore, F. C.; Johnston, F. *J. Am. Chem. Soc.* **1933**, *55*, 5020.
44. Iwasaki, K.; Wan, K. K.; Oppedisano, A.; Crossley, S. W. M.; Shenvi, R. A. *J. Am. Chem. Soc.* **2014**, *136*, 1300.
45. Johnson, W. S.; Bannister, B.; Bloom, B. M.; Kemp, A. D.; Pappo, R.; Rogier, E. R.; Szmuszkovicz, J. *J. Am. Chem. Soc.* **1953**, *75*, 2275.
46. Stork, G.; Darling, S. D. *J. Am. Chem. Soc.* **1960**, *82*, 1512.
47. Whitesides, G. M.; Ehmann, W. J. *J. Org. Chem.* **1970**, *35*, 3565.
48. Voorhees, V.; Adams, R. *J. Am. Chem. Soc.* **1922**, *44*, 1397.
49. (a) Ishikawa, H.; Colby, D. A.; Seto, S.; Va, P.; Tam, A.; Kakei, H.; Rayl, T. J.; Hwang, I.; Boger, D. L. *J. Am. Chem. Soc.* **2009**, *131*, 4904. (b) Barker, T. J.; Boger, D. L. *J. Am. Chem. Soc.* **2012**, *134*, 13588.
50. King, S. M.; Ma, X.; Herzon, S. B. *J. Am. Chem. Soc.* **2014**, *136*, 6884.

51. (a) King, S. M.; Calandra, N. A.; Herzon, S. B. *Angew. Chem. Int. Ed.* **2013**, *52*, 3642. (b) Calandra, N. A.; King, S. M.; Herzon, S. B. *J. Org. Chem.* **2013**, *78*, 10031.
52. Peterson, A. A.; Thoreson, K. A.; McNeill, K. *Organometallics* **2009**, *28*, 5982.
53. (a) Chung, S.-K.; *J. Org. Chem.* **1979**, *44*, 1014. (b) Sweany, R. L.; Halpern, J. *J. Am. Chem. Soc.* **1977**, *99*, 8335. (c) Roth, J. A.; Orchin, M. *J. Organomet. Chem.* **1979**, *182*, 299. (d) Sweany, R. L.; Comberrel, D. S.; Dombourian, M. F.; Peters, N. A. *J. Organomet. Chem.* **1981**, *216*, 37. (e) Nalesnik, T. E.; Freudenberg, J. H.; Orchin, M. *J. Mol. Catal.* **1982**, *16*, 43. (f) Roth, J. A.; Wiseman, P.; Ruzsala, L. *J. Organomet. Chem.* **1982**, *240*, 271. (g) Ungvary, F.; Marko, L. *Organometallics* **1982**, *1*, 1120. (h) Connolly, J. W. *Organometallics* **1984**, *3*, 1333. (i) Garst, J. F.; Bockman, T. M.; Batlaw, R. *J. Am. Chem. Soc.* **1986**, *108*, 1689. (j) Thomas, M. J.; Shackleton, T. A.; Wright, S. C.; Gillis, D. J.; Colpa, J. P.; Baird, M. C. *J. Chem. Soc., Chem. Commun.* **1986**, 312. (k) Wassink, B.; Thomas, M. J.; Wright, S. C.; Gillis, D. J.; Baird, M. C. *J. Am. Chem. Soc.* **1987**, *109*, 1995. (l) Choi, J.; Pulling, M. E.; Smith, D. M.; Norton, J. R. *J. Am. Chem. Soc.* **2008**, *130*, 4250.
54. Tang, L.; Papish, E. T.; Abramo, G. P.; Norton, J. R.; Baik, M.-H.; Friesner, R. A.; Rappé, A. *J. Am. Chem. Soc.* **2003**, *125*, 10093.
55. (a) Trost, B. M. *Angew. Chem., Int. Ed. Engl.* **1995**, *34*, 259. (b) Trost, B. M. *Acc. Chem. Res.* **2002**, *35*, 695. (c) Michelet, V.; Toullec, P. Y.; Genêt, J.-P. *Angew. Chem., Int. Ed.* **2008**, *47*, 4268.
56. Ojima, I.; Donovan, R. J.; Shay, W. R. *J. Am. Chem. Soc.* **1992**, *114*, 6580.
57. Okamoto, S.; Livinghouse, T. *J. Am. Chem. Soc.* **2000**, *122*, 1223.
58. Chiang, L.; Allen, L. E. N.; Alcantara, J.; Wang, M. C. P.; Storr, T.; Shaver, M. P. *Dalton Trans.* **2014**, *43*, 4295.
59. Morrison, D. A.; Davis, T. P.; Heuts, J. P.; Messerle, B.; Gridnev, A. A. *J. Polym. Sci. A: Polym. Chem.* **2006**, 6171.
60. Ma, X.; Herzon, S. B. *J. Am. Chem. Soc.* **2016**, *136*, 8718.
61. (a) Foley, N. A.; Lee, J. P.; Ke, Z.; Gunnoe, T. B.; Cundari, T. R. *Acc. Chem. Res.* **2009**, *42*, 585. (b) Andreatta, J. R.; McKeown, B. A.; Gunnoe, T. B. *J. Organomet. Chem.* **2011**, *696*, 305.
62. (a) Minisci, F.; Bernardi, R.; Bertini, F.; Galli, R.; Perchinummo, M. *Tetrahedron* **1971**, *27*, 3575. (b) Minisci, F. *Synthesis* **1973**, 1973.
63. Biffis, A.; Centomo, P.; Del Zotto, A.; Zecca, M. *Chem. Rev.* **2018**, *118*, 2249.
64. (a) Crisenza, G. E. M.; McCreanor, N. G.; Bower, J. F. *J. Am. Chem. Soc.* **2014**, *136*, 10258. (b) Crisenza, G. E. M.; Sokolova, O. O.; Bower, J. F. *Angew. Chem., Int. Ed.* **2015**, *54*, 14866. (c) Pan, S.; Ryu, N.; Shibata, T. *J. Am. Chem. Soc.* **2012**, *134*, 17474.
65. Tasker, S. Z.; Standley, E. A.; Jamison, T. F. *Nature*, **2014**, *509*, 299.
66. Green, S. A.; Matos, J. L. M.; Yagi, A.; Shenvi, R. A. *J. Am. Chem. Soc.* **2016**, *138*, 12779.
67. (a) Magnus, P.; Waring, M. J.; Scott, D. A. *Tetrahedron Lett.* **2000**, *41*, 9731. (b) Lo, J. C.; Yabe, Y.; Baran, P. S. *J. Am. Chem. Soc.* **2014**, *136*, 1304. (c) George, D. T.; Kuenstner, E. J.; Pronin, S. V. *J. Am. Chem. Soc.* **2015**, *137*, 15410. (d) Godfrey, N. A.; Schatz, D. J.; Pronin, S. V. *J. Am. Chem. Soc.* **2018**, *140*, 12770. (e) Thomas, W. P.; Schatz, D. J.; George, D. T.; Pronin, S. V. *J. Am. Chem. Soc.* **2019**, *141*, 12246.
68. Shigehisa, H.; Aoki, T.; Yamaguchi, S.; Shimizu, N.; Hiroya, K. *J. Am. Chem. Soc.* **2013**, *135*, 10306.
69. Fu, Y.; Liu, L.; Yu, H.-Z.; Wang, Y.-M.; Guo, Q.-X. *J. Am. Chem. Soc.* **2005**, *127*, 7227.

70. Anslyn, E. V.; Dougherty, D. A. *In Modern Physical Organic Chemistry*; University Science Books: United States of America, 2006, pp. 403–406.
71. Lande, S. S.; Kochi, J. K. *J. Am. Chem. Soc.* **1968**, *90*, 5196.
72. Kapturkiewicz, A.; Behr, B. *Inorg. Chim. Acta* **1983**, *69*, 247.
73. Ding, K.; Dugan, T. R.; Brennessel, W. W.; Bill, E.; Holland, P. L. *Organometallics* **2009**, *28*, 6650.
74. Shigehisa, H.; Kikuchi, H.; Hiroya, K. *Chem. Pharm. Bull.* **2016**, *64*, 371.
75. Shigehisa, H.; Koseki, N.; Shimizu, N.; Fujisawa, M.; Niitsu, M.; Hiroya, K. *J. Am. Chem. Soc.* **2014**, *136*, 13534.
76. Beesly, R. M.; Ingold, C. K.; Thorpe, J. F. *J. Chem. Soc., Trans.* **1915**, *107*, 1080.
77. Shigehisa, H.; Hayashi, M.; Ohkawa, H.; Suzuki, T.; Okayasu, H.; Mukai, M.; Yamazaki, A.; Kawai, R.; Kikuchi, H.; Satoh, Y.; Akane, F.; Hiroya, K. *J. Am. Chem. Soc.* **2016**, *138*, 10597.
78. Shigehisa, H.; Ano, T.; Honma, H.; Ebisawa, K.; Hiroya, K. *Org. Lett.* **2016**, *18*, 3622.
79. Scanlan, E. M.; Corcé, V.; Malone, A. *Molecules* **2014**, *19*, 19137.
80. Date, S.; Hamasaki, K.; Sunagawa, K.; Koyama, H.; Sebe, C.; Hiroya, K.; Shigehisa, H. *ACS Catal.* **2020**, *10*, 2039.
81. Touney, E. E.; Foy, N. J.; Pronin, S. V. *J. Am. Chem. Soc.* **2018**, *140*, 16982.
82. Discolo, C. A.; Touney, E. E.; Pronin, S. V. *J. Am. Chem. Soc.* **2019**, *141*, 17527.
83. Shevick, S. L.; Obradors, C.; Shenvi, R. A. *J. Am. Chem. Soc.* **2018**, *140*, 12056.
84. Nagai, T.; Mimata, N.; Terada, Y.; Sebe, C.; Shigehisa, H. *Org. Lett.* **2020**, *22*, 5522.
85. Shen, X.; Chen, X.; Chen, J.; Sun, Y.; Cheng, Z.; Lu, Z. *Nat. Comm.* **2020**, *11*, 783.
86. Ebisawa, K.; Izumi, K.; Ooka, Y.; Kato, H.; Kanazawa, S.; Komatsu, S.; Nishi, E.; Shigehisa, H. *J. Am. Chem. Soc.* **2020**, *142*, 13481.
87. Schaus, S. E.; Brandes, B. D.; Larrow, J. F.; Tokunga, M.; Hansen, K. B.; Gould, A. E.; Furrow, M. E.; Jacobsen, E. N. *J. Am. Chem. Soc.* **2002**, *124*, 1307.
88. Nagata, T.; Yoruzu, K.; Yamada, T.; Mukaiyama, T. *Angew. Chem., Int. Ed. Engl.* **1995**, *34*, 2145.
89. Niimi, T.; Uchida, T.; Irie, R.; Katsuki, T. *Adv. Synth. Catal.* **2001**, *343*, 79.
90. Ohuchi, S.; Koyama, H.; Shigehisa, H. *ACS Catal.* **2021**, *11*, 900.
91. Kim, H.-O.; Matthew, F.; Ogbu, C. *Synlett* **1999**, *1999*, 193.
92. Watanabe, M.; Okada, H.; Teshima, T.; Noguchi, M.; Kakehi, A. A. *Tetrahedron* **1996**, *52*, 2827.
93. Garlets, Z. J.; Silvi, M.; Wolfe, J. P. *Org. Lett.* **2016**, *18*, 2331.
94. Zavesky, B. P.; Babij, N. R.; Fritz, J. A.; Wolfe, J. P. *Org. Lett.* **2013**, *15*, 5423.
95. Gainer, M. J.; Bennett, N. R.; Takahashi, Y.; Looper, R. E. *Angew. Chem., Int. Ed.* **2011**, *50*, 684.
96. Zhou, X.-L.; Yang, F.; Sun, H.-L.; Yin, Y.-N.; Ye, W.-T.; Zhu, R. *J. Am. Chem. Soc.* **2019**, *141*, 7250.
97. Yoshimura, A.; Zhdankin, V. V. *Chem. Rev.* **2016**, *116*, 3328.
98. Ford, D. D.; Nielson, L. P. C.; Zuend, S. J.; Musgrave, C. B.; Jacobsen, E. N. *J. Am. Chem. Soc.* **2013**, *135*, 15595.
99. Shevick, S. L.; Obradors, C.; Shenvi, R. A. *J. Am. Chem. Soc.* **2018**, *140*, 12056.
100. Schrauzer, G. N.; Windgassen, R. J. *J. Am. Chem. Soc.* **1966**, *88*, 3738.
101. Sun, H.-L.; Yang, F.; Ye, W.-T.; Wang, J.-J.; Zhu, R. *ACS Catal.* **2020**, *10*, 4983.
102. Yahata, K.; Kaneko, Y.; Akai, S. *Org. Lett.* **2020**, *22*, 598.
103. Yoder, R. A.; Johnston, J. N. *Chem. Rev.* **2005**, *105*, 4730.

104. Vrubliauskas, D.; Vanderwal, C. D. *Angew. Chem. Int. Ed.* **2020**, *59*, 6115.
105. Vrubliauskas, D.; Gross, B. M.; Vanderwal, C. D. *J. Am. Chem. Soc.* **2021**, *143*, 2944.

Chapter 2: Catalytic Radical–Polar Crossover Reactions of Allylic Alcohols

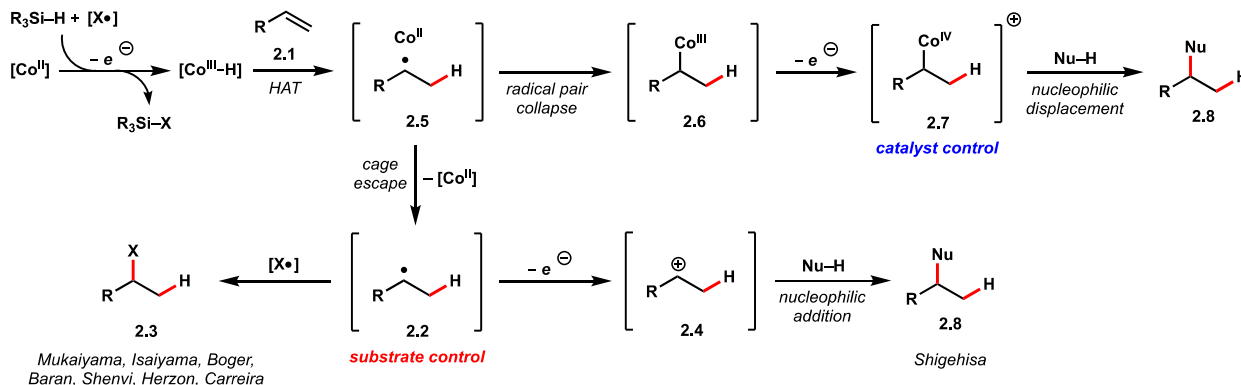
2.1 Introduction

Metal hydride-mediated radical reactions provide a highly chemoselective means for hydrofunctionalization of alkenes with Markovnikov selectivity.^{1–3} Previous research has focused primarily on directly engaging the alkyl radicals generated from initial hydrogen-atom transfer (HAT) with atom or group transfer reagents,⁴ trapping via addition into multiple bonds,⁵ as well as capture with metals to initiate cross couplings.⁶ Recently, the Shigehisa group has shown radical formation can be combined with single-electron oxidation to generate carbocationic intermediates that are competent at capturing heteroatom nucleophiles.⁷ This radical–polar crossover reactivity is an attractive alternative to the corresponding acid-catalyzed functionalization of alkenes due to enhanced chemoselectivity and functional group tolerance. However, catalyst control in the bond forming steps of HAT-initiated hydrofunctionalizations has been largely absent in the reported literature, a limitation that could potentially slow the pace and scope of future methods development.⁸ Establishing general and predictable relationships between catalyst structure and reactivity is sure to glean mechanistic insights that could accelerate the development of radical–polar crossover methods guided by strategic catalyst design.⁹ In this chapter, I describe our investigations that led to the development of the first example of a HAT-mediated radical–polar crossover alkene hydrofunctionalization under strong catalyst control.¹⁰

2.2 Strategy for Catalytic Radical–Polar Crossover Reactions of Allylic Alcohols

We sought to address the lack of catalyst-controlled radical–polar crossover reactions by developing a reaction manifold that proceeds through electrophilic alkyl metal intermediates (**Scheme 2.1**). Accomplishing this would require thorough understanding of the intermediates and elementary steps that occur following initial HAT to the alkene. Typical cobalt-catalyzed HAT hydrofunctionalizations commence by generation of cobalt(III) hydride by treatment of a cobalt(II) complex with a single-electron oxidant and silane as hydride source. Cobalt(III) hydride then engages an alkene **2.1** via hydrogen atom transfer to form a solvent caged alkyl radical–metalloradical pair **2.5**.^{11–12} Cage escape of cobalt(II) catalyst can then occur to release free alkyl radical **2.2**. Mukaiyama-type trapping of alkyl radical **2.2** with a radicalophile affords hydrofunctionalization product **2.3**. Conversely, a radical–polar crossover pathway involving single-electron oxidation of **2.2** to generate carbocationic intermediate **2.4** followed by capture with a polar nucleophile follows the mechanism for cobalt-catalyzed radical–polar crossover hydrofunctionalization proposed by Shigehisa.¹³ Both Mukaiyama-type radical and Shigehisa-type radical–polar crossover hydrofunctionalizations lack catalyst control because the cobalt catalyst is not directly involved in the bond forming step.

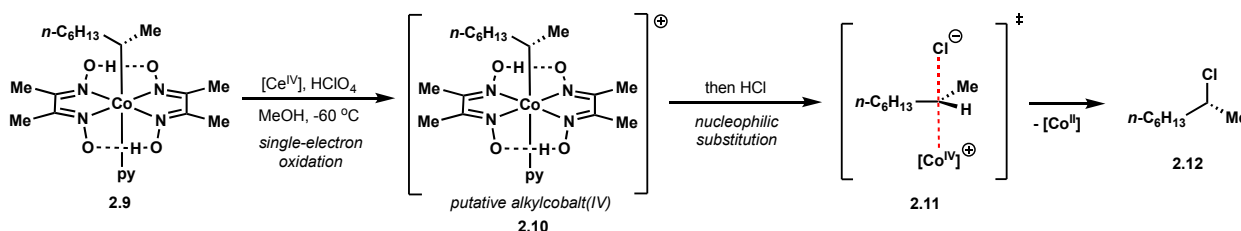
Scheme 2.1 Strategy for catalyst controlled HAT radical–polar crossover alkene hydrofunctionalization



Alternatively, instead of cage escape, radical pair collapse can occur within the solvent caged alkyl radical-metalloradical pair to deliver alkylcobalt(III) intermediate **2.6** containing a defined alkyl–metal bond. Alkylcobalt(III) species derived from radical pair collapse following HAT have been implicated in hydroformylations¹⁴ and more recently in reports of cobalt-catalyzed alkene isomerizations^{5f} and hydroarylations^{6c} published by the Shenvi lab. Single-electron oxidation of alkylcobalt(III) **2.6** is then expected to furnish electrophilic alkylcobalt(IV) **2.7**. Subsequent nucleophilic displacement of cobalt(IV) forms hydrofunctionalization product **2.8**. Direct involvement of alkylcobalt intermediates in the bond forming step renders this proposed reaction catalyst controlled.

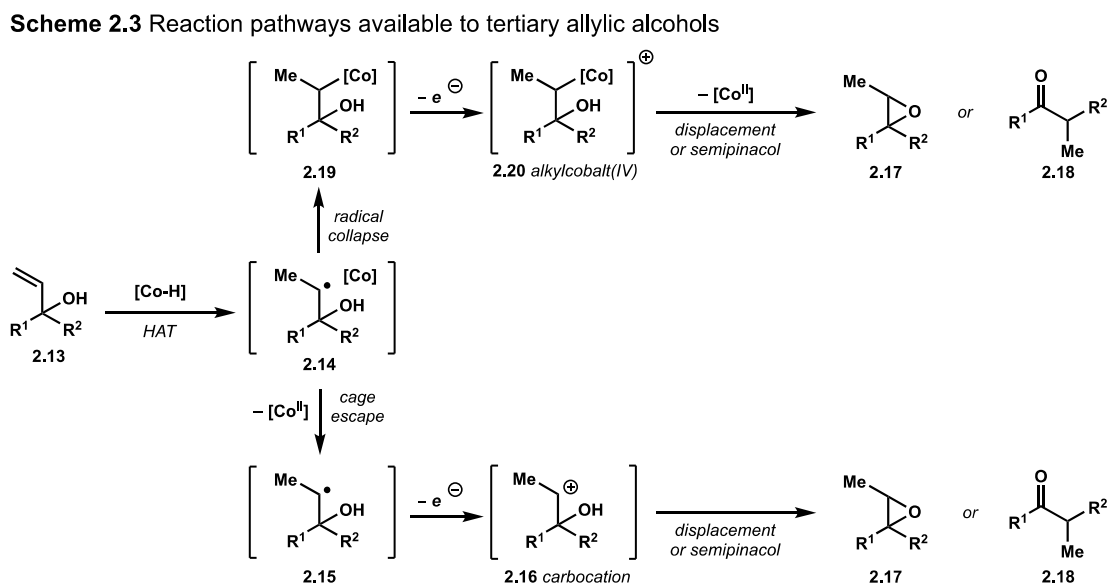
Halpern and coworkers have previously established that alkylcobalt(III) dimethylglyoxime complexes undergo single-electron oxidation to the corresponding cationic species aptly referred to as an alkylcobalt(IV).^{15,16} Kochi proposed similar intermediates arise as a function of capturing alkyl radicals with cationic alkylcobalt(III).¹⁷ Further investigations demonstrated that the putative alkylcobalt(IV) species undergoes facile stereospecific displacement by polar nucleophiles (**Scheme 2.2**).^{18–20} We hypothesized we could leverage similar electrophilic alkylcobalt(IV) intermediates as a functional handle for catalyst controlled radical–polar crossover alkene hydrofunctionalization.

Scheme 2.2 Halpern's stereoinvertive displacement of alkylcobalt(IV) complexes



One factor complicating our reaction development is that the expected products of catalyst-controlled nucleophilic displacement of alkylcobalt(IV) intermediates and Shigehisa-type

nucleophilic capture of carbocationic intermediates are indistinguishable from one another (**Scheme 2.1**). Thus, we required a scaffold where discriminatory bifurcation of reaction outcomes is possible between carbocationic and alkylcobalt(IV) pathways. Tertiary allylic alcohols are ideally positioned to address this problem as one could imagine multiple reaction pathways where formal protonation of the alkene leads to either epoxide formation **2.17** or semipinacol rearrangement **2.18** (**Scheme 2.3**). It was our hope that the carbocationic pathway would predominantly favor formation of either epoxides or semipinacol products while product distribution from the catalyst-controlled pathway could be tuned to favor the opposite outcome. Furthermore, HAT radical–polar crossover offers a unique opportunity to evaluate the reactivity of tertiary allylic alcohols. Direct access to the β -carbocationic framework **2.16** is incompatible with catalysis by Brønsted acid, as ionization of the alcohol outcompetes alkene protonation. However, the mild and chemoselective nature of HAT radical–polar crossover should bypass this complication.

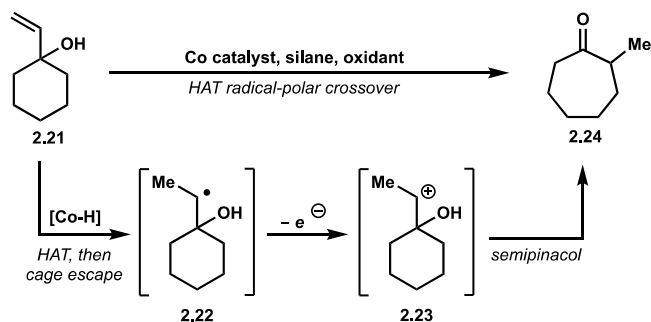


2.3 Reaction Optimization

2.3.1 Substrate Selection

Before optimization efforts could begin we had to first choose an appropriate tertiary allylic alcohol to use as a model substrate. 1-vinylcyclohexan-1-ols were an obvious choice due to the unique architecture of the 2-methylcycloheptanones we anticipated to arise from proposed semipinacol rearrangement (**Scheme 2.4**). Direct ring expansion of cyclic tertiary allylic alcohols is limited to cyclopropanols²¹ and cyclobutanols²² where expansion is driven primarily by release of ring strain.²³ Larger ring sizes have been accessed but prefunctionalization of the alkene is required.²⁴ More practically, 1-vinylcyclohexan-1-ols are simple to prepare by 1,2-addition of vinylmagnesium bromide to a parent cyclohexanone, a broad variety of which are commercially available. Monosubstituted alkenes would be most appropriate for catalyst control as they are well precedented to produce secondary alkyl radicals and secondary alkylcobalt intermediates following delivery of a hydrogen atom. Alkene substitution that gives rise to tertiary alkyl radicals following HAT is likely incompatible with catalyst control as tertiary alkylcobalt(III) complexes have yet to be characterized or fleetingly observed and are thus typically not invoked as reactive intermediates.²⁵ Ultimately, *cis*-4-phenyl-1-vinylcyclohexan-1-ol **2.25** was chosen as the model substrate.

Scheme 2.4 Proposed ring expansion of vinylcyclohexanols to cycloheptanones



2.3.2 Optimization of Reaction Conditions for Radical–Polar Hydrofunctionalization

Our investigations began by subjecting alcohol **2.25** to conditions similar to those developed by the Shigehisa lab (**Table 2.1**).⁷ Phenylsilane and tetramethyl ethylenediamine cobalt(II) salen catalyst **2.27** were logical starting points for hydride source and catalyst, respectively, as both have seen extensive use in MHAT hydrofunctionalizations.^{1,2} *N*-fluorocollidinium tetrafluoroborate salt **2.28** had been used successfully as a two-electron oxidant for HAT radical–polar crossover hydroalkoxylation, hydroaminations, and hydroacyloxylation.^{7,26,27} Concerned about competing intermolecular nucleophilic substitution, we opted to use dichloromethane as a decidedly non-nucleophilic solvent. To our great delight, the first set of conditions attempted delivered ring expansion product **2.26** in 25% yield as a 11:1 mixture of diastereomers favoring the *cis* arrangement **2.26a** (entry 1).

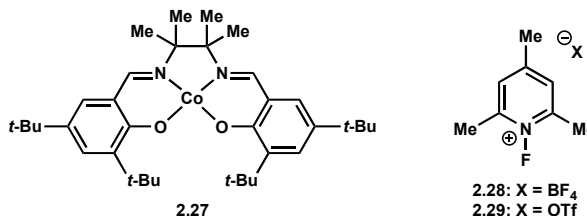
Encouraged by this early success, we next screened silane and oxidant. Switching to less reactive methylphenylsilane gave a mild improvement in yield, possibly due to improved oxidant solubility (entry 2). *N*-fluorocollidinium triflate **2.29** boosted efficiency to a modest 49% yield of semipinacol rearrangement (entry 3). In most cases, the remaining mass balance was composed of starting material, alkene hydrogenation, and oxidative cleavage of the vinyl group. Incomplete conversion was observed when less than 3 equivalents of oxidant and silane were applied. Silanes other than methylphenylsilane or TMDS also led to incomplete conversion. Other *N*-fluorinated oxidants such as *N*-fluoropyridinium triflate, *N*-fluoropyridinium tetrafluoroborate, Selectfluor, and *N*-fluorobenzenesulfonamide (NFSI) led to either low conversion or decomposition.

Realizing that solvent cage effects are likely influencing the reactivity of proposed carbocationic intermediates via solvation as well as manipulating the kinetics of radical pair collapse, we sought to assess the impact of solvent on reaction efficiency. In methanol yield fell

to 41% but diastereoselectivity curiously improved to 17:1 (entry 4). Isopropanol unexpectedly and dramatically increased yield of cycloheptanone **2.26** to 70% (entry 5). A 60% v/v mixture of *tert*-butanol in dichloromethane as solvent further improved performance and resulted in the highest diastereoselectivity observed, affording **2.26** as a single diastereomer (entry 6). Ultimately, acetone provided superior mass balance, generating **2.26** in 78% yield as a 16:1 mixture of diastereomers as well as epoxide product **2.30** in 12% yield (entry 7). Until this point epoxide products had never been formed in more than 5% yield, usually in amounts below the detection limit of ¹H NMR. However, 12% yield of epoxide gave us hope that the reaction could be selectively bifurcated. 1,1,3,3-Tetramethyldisloxane (TMDS) could be used interchangeably with methylphenylsilane but required increased reaction times (entry 8).

Table 2.1 Effect of reaction conditions on the radical–polar crossover hydrofunctionalization of alcohol **2.25**

entry	silane	oxidant	conditions	2.26 (%) ^a	d.r. (2.26a : 2.26b) ^a
1	PhSiH ₃	2.28	CH ₂ Cl ₂ , 0 °C	25	11:1
2	PhSiH ₂ Me	2.28	CH ₂ Cl ₂ , 0 °C	31	8:1
3	PhSiH ₂ Me	2.29	CH ₂ Cl ₂ , 0 °C	49	11:1
4	PhSiH ₂ Me	2.29	MeOH, 0 °C	41	17:1
5	PhSiH ₂ Me	2.29	<i>i</i> -PrOH, 0 °C	70	12:1
6	PhSiH ₂ Me	2.29	CH ₂ Cl ₂ : <i>t</i> BuOH (2:3), 0 °C	78	>20:1
7 ^c	PhSiH ₂ Me	2.29	(CH ₃) ₂ CO, 0 °C	78	16:1
8 ^c	TMDS	2.29	(CH ₃) ₂ CO, 0 °C	75	11:1

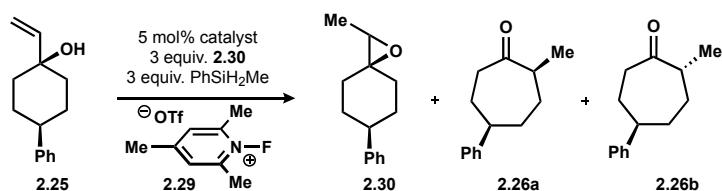


^aBased on an internal standard of mesitylene and determined by ¹H NMR. ^bUnless otherwise noted epoxide products were formed in <5% yield. ^cThe reaction also yielded 12% of epoxide product determined by ¹H NMR.

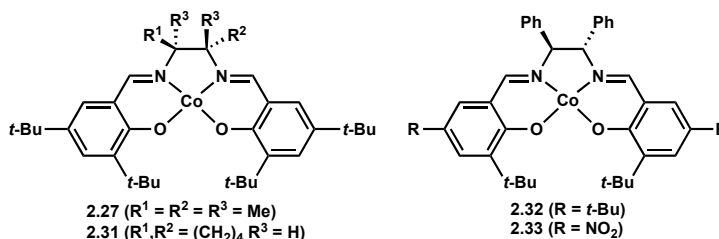
2.3.3 Optimization of Catalysts for Radical–Polar Crossover Hydrofunctionalization

Having validated the HAT radical–polar crossover semipinacol rearrangement of tertiary allylic alcohols (Table 2.2, entry 1), we next turned our attention towards optimizing the epoxidation pathway via catalyst control. Changing the structure of the salen ligand provided instructive trends. Catalyst 2.31 bearing a 1,2-cyclohexanediamine

Table 2.2 Effect of catalyst structure on the radical–polar crossover hydrofunctionalization of alcohol 2.25



entry	catalyst	conditions	2.30 (%) ^a	2.26 (%) ^a	d.r. (2.26a:2.26b) ^a
1	2.27	(CH ₃) ₂ CO, 0 °C	12	78	16:1
2	2.31	(CH ₃) ₂ CO, 0 °C	31	11	2.4:1
3	2.32	(CH ₃) ₂ CO, 0 °C	66	23	3.2:1
4	2.33	(CH ₃) ₂ CO, 0 °C	<1	63	1.5:1
5	2.32	(CH ₃) ₂ CO, -40 °C	65	15	3.2:1

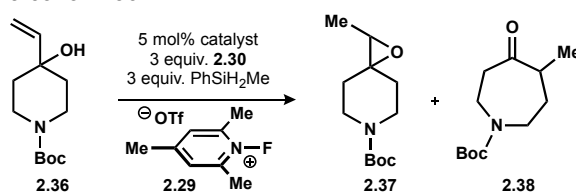


^aBased on internal standard of mesitylene and determined by ¹H NMR.

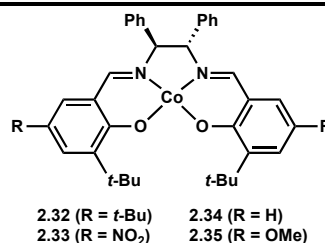
backbone formed epoxide 2.30 as the major product in 31% yield, but this improvement came at the cost of efficiency and selectivity, as the other major side products observed were starting material and hydrogenation (entry 2). Application of diphenyl ethylenediamine catalyst 2.32 more than doubled yield of epoxide to a respectable 66% (entry 3). Strikingly, performing the reaction in the presence of nitro-substituted catalyst 2.33 under otherwise identical conditions led to a complete reversal of selectivity to form semipinacol adduct 2.26 exclusively and with unusually poor diastereoselectivity (entry 4). Conducting the reaction at a lower temperature with catalyst 2.32 increased selectivity towards epoxide formation versus semipinacol from 2.9:1 to 4.3:1 (entry 5). The effect of temperature on product ratio is especially pronounced on the hydrofunctionalization of *N*-Boc protected 4-vinylpiperidin-4-ol 2.36 (Table 2.3, entries 1–2), the data for which was collected by my colleague Nicholas Foy. Astoundingly, upon lowering the

temperature from 0 °C to -40 °C, selectivity of epoxide **2.37** versus ketone **2.38** formation nearly tripled from 3.2:1 to 9.3:1. Nicholas validated that trends in product distribution for catalysts screened with alcohol **2.36** mirrored trends observed for alcohol **2.25**. He also investigated additional electronic and steric effects of salen structure on efficiency and product distribution. Content with the degree of catalyst control achieved, we turned our attention towards evaluating the generality of the catalyst controlled hydrofunctionalization.

Table 2.3 Effect of temperature and catalyst on the radical–polar crossover hydrofunctionalization of alcohol **2.36**^a



entry	catalyst	conditions	2.35 (%) ^b	2.36 (%) ^b
1	2.32	(CH ₃) ₂ CO, -40 °C	84	9
2	2.32	(CH ₃) ₂ CO, 0 °C	70	22
3	2.33	(CH ₃) ₂ CO, 0 °C	10	52
4	2.34	(CH ₃) ₂ CO, 0 °C	42	16
5	2.35	(CH ₃) ₂ CO, 0 °C	58	33
6	2.31	(CH ₃) ₂ CO, 0 °C	54	10
7	2.27	(CH ₃) ₂ CO, 0 °C	14	63



^aWork performed by NJF. ^bBased on internal standard of mesitylene and determined by ¹HNMR.

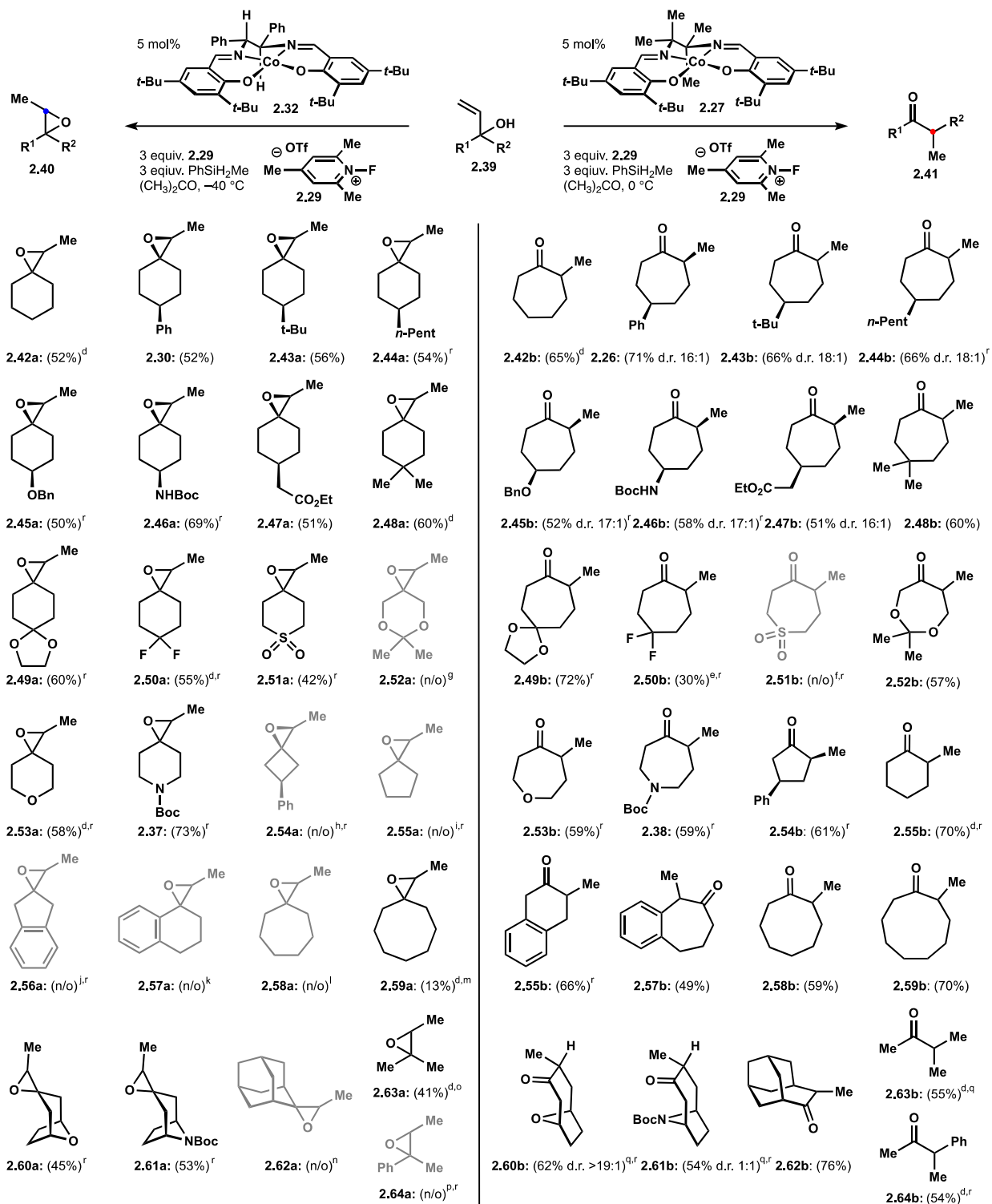
2.4 Substrate Scope

Bifurcation of the radical–polar crossover pathway allowed for selective transformation of various (dialkyl)vinylcarbinols to the corresponding epoxides and ketones (**Table 2.4**). It should be clarified that this collection of substrates was a function of work performed by myself and Nicholas Foy, and his contributions to **Table 2.4** are denoted within. 1-Vinylcyclohexan-1-ol and a series of 4-substituted aliphatic vinylcyclohexanols were readily converted to epoxides **2.42a–2.44a** in synthetically useful yields using catalyst **2.32**. Corresponding cycloheptanones **2.42b–2.44b** were efficiently produced in the presence of catalyst **2.27**. Substrates bearing a more diverse set of functional groups installed at the 4-position including benzyl ethers, Boc protected primary

amines, and esters were cleanly converted to epoxide (**2.45a–2.47a**) and ketone (**2.45b–2.47b**) products. Consistent with the results observed during optimization of **2.26**, ketones **2.43b–2.47b** were formed in a highly diastereoselective manner, unanimously favoring the *cis* arrangement.

4,4-Disubstituted cyclohexanol derivatives also participate in the radical–polar crossover hydrofunctionalization to produce the requisite epoxides (**2.48a–2.50a**) and ketones (**2.48b–2.50b**). Interestingly, we observed that electron-withdrawing substituents hinder alkyl migration. For example, regardless of catalyst used 4,4-difluoro epoxide **2.50a** was formed as the major product. This effect was especially pronounced for sulfonylpyranone derivative **2.51a**, where the corresponding ketone **2.51b** was never observed irrespective of catalyst identity. We attribute the bias toward epoxide formation as a function of inductive effects, where removal of electron density from the carbon-carbon σ bond framework via electron-withdrawing groups precludes the carbon-carbon bond migration necessary to afford ring expanded products. The opposite situation arose in the case of dioxepanone **2.52b**, which was the only product observed while the corresponding epoxide **2.52a** was not detected. This phenomenon is not as readily explainable, although we can offer conjecture. Perhaps the shorter C–O bonds embedded with the dioxane skeleton bring the 4,4-dimethyl substituents close enough to disrupt transient alkylcobalt intermediates, which are highly sensitive to sterics.²⁸ Alternatively, the oxygen atoms of the dioxane are polarity matched with the electrophilic carbon atom generated following HAT and single-electron oxidation. Donation of electron density through the oxygen lone pairs into the migrating C–C σ bond could accelerate 1,2-migration resulting in the observed selectivity for ring expansion. Heterocyclic vinyl carbinols derived from tetrahydropyranone and *N*-Boc piperidone behaved similarly to cyclohexanol analogues, delivering epoxides (**2.53a–2.37**) and ketones (**2.53b–2.38**) readily.

Table 2.4 Substrate scope of the cobalt-catalyzed epoxidation^{a,b} and semipinacol rearrangement^{a,c}



^aUnless otherwise noted, yields correspond to isolated, analytically pure material. ^bUnless otherwise noted, ratio of epoxide to ketone is $\geq 3:1$ (See experimental data for details). ^cUnless otherwise noted, ratio of ketone to epoxide is $\geq 4:1$ (See experimental data for details). ^dBased on internal standard of mesitylene and determined by ¹H NMR. ^eEpoxide **2.50a** is the major product (48% by ¹H NMR analysis). ^fEpoxide **2.51a** is the major product (32% by ¹H NMR analysis). ^gKetone **2.52b** is the major product (48% by ¹H NMR analysis). ^hKetone **2.54b** is the major product (97% by ¹H NMR analysis). ⁱKetone **2.55b** is the major product (90% by ¹H NMR analysis). ^jKetone **2.56b** is the major product (70% by ¹H NMR analysis). ^kKetone **2.57b** is the major product (74% by ¹H NMR analysis). ^lKetone **2.58b** is the major product (71% by ¹H NMR analysis). ^mKetone **2.59b** is the major product (41% by ¹H NMR analysis). ⁿKetone **2.62b** is the major product (80% by ¹H NMR analysis). ^oWith catalyst **2.35**. ^pKetone **2.64b** is the major product (73% by ¹H NMR). ^qWith catalyst **2.33**. ^rWork performed by NJF. n/o: not observed.

Cyclobutanols and cyclopentanols did not produce epoxide products (**2.54a–2.56a**) and both catalysts **2.27** and **2.32** afford good yields of cyclopentanone **2.54b** and cyclohexanones (**2.55b–2.56b**), respectively. The absence of epoxidation was unsurprising, as favorable strain release and near barrierless Wagner-Meerwein shift is kinetically facile compared to generating a strained spirocyclic epoxide adjoined to an already strained ring system. Similarly, benzofused allylic alcohols provide only semipinacol rearrangement (**2.57b**) likely due to the greater migratory aptitude of arenes as well as steric congestion hindering radical-pair collapse to form alkylcobalt intermediates. Cycloheptanols failed to deliver epoxide products as well, and only cyclooctanone **2.58b** was isolated. Morbid curiosity prompted us to subject cyclooctanols to the hydrofunctionalization conditions, resulting in predominant formation of cyclononanone **2.59b** regardless of catalyst, although a minor amount of epoxide **2.59a** was observed in the case of catalyst **2.32**.

Bicyclic epoxides **2.60a** and **2.61a** were readily prepared using the radical–polar crossover protocol in the presence of catalyst **2.32** while nitro catalyst **2.33** proved superior to catalyst **2.27** for ring expansion to ketones **2.60b** and **2.61b**. Strangely, catalyst **2.33** afforded **2.60b** as a single diastereomer while formation of **2.61b** lacked any diastereoselectivity. Adamantyl vinyl carbinols were efficiently converted to tricyclic ketone **2.62b** exclusively, producing no detectable amounts of epoxide **2.62a**. Acyclic allylic alcohols also acquiesced to the established bifurcation. Epoxide **2.63a** and isopropyl methyl ketone **2.63b** were obtained from 2-methyl-3-buten-2-ol, although electronics of the salen ligand were especially pronounced in this case, as the best performance for epoxidation and semipinacol rearrangement was achieved in the presence of catalysts **2.35** and **2.33**, respectively. Only semipinacol rearrangement product **2.64b** was obtained in the case of 2-phenylbut-3-en-2-ol, which is consistent with the high migratory aptitude of the phenyl substituent.

2.5 Mechanistic Studies

2.5.1 Catalyst Control Suggests Participation of Electrophilic Alkylcobalt Intermediates

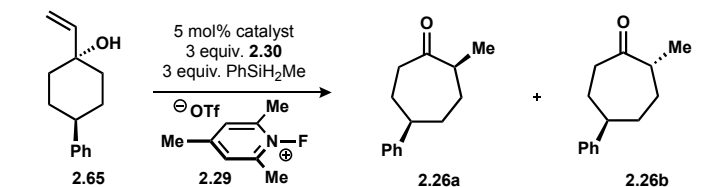
Catalyst control over the bifurcation of the radical–polar crossover hydrofunctionalization pathways implicates the participation of alkylcobalt complexes as electrophilic intermediates. If carbocations were the only electrophilic intermediates generated over the course of the reaction, as initially suggested by Shigehisa, one would anticipate product distribution to remain consistent independent of catalyst used. However, by keeping all other variables constant and only changing the structure of the salen ligand, product distribution can be controlled. These catalyst dependent outcomes demand that cobalt complexes are directly involved in the bond forming steps for at least one of the reaction pathways. We believe our observations are consistent with the participation of electrophilic alkylcobalt(IV) complexes as previously discussed in section 2.2.

2.5.2 Diastereoselectivity of Ring Expansion is Catalyst Dependent

In addition to catalyst control over reaction outcomes, we observed that the diastereoselectivity of ring expansion of alcohol **2.25** is dependent on catalyst structure. Catalyst **2.27** predominantly formed ketone **2.26** from alcohol **2.25** as a 16:1 mixture of diastereomers (Table 2.2, entry 1). Although diphenyl catalyst **2.32** favored epoxide formation, analysis of the minor product **2.26** produced showed that what little was made was generated with poor diastereoselectivity (Table 2.2, entry 3). Application of nitro substituted catalyst **2.33** converted alcohol **2.25** exclusively to ketone **2.26** albeit as a nearly equimolar mixture of diastereomers (Table 2.2, entry 4), a stark contrast to the high diastereoselectivity provided by catalyst **2.27** despite similar product distributions. Interestingly, application of epimeric 4-phenyl-1-

vinylcyclohexan-1-ol **2.65** resulted in exclusive and highly diastereoselective formation of *trans*-cycloheptanone **2.26b** irrespective of catalyst structure. (**Table 2.5**)

Table 2.5 Effect of catalyst structure on the radical–polar crossover semipinacol rearrangement of alcohol **2.65**

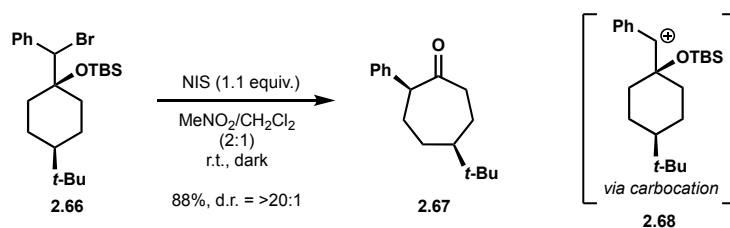


entry	catalyst	conditions	2.26 (%) ^a	d.r. (2.26a:2.26b) ^a
1	2.27	(CH ₃) ₂ CO, 0 °C	62	≤1:20
2	2.32	(CH ₃) ₂ CO, 0 °C	93	≤1:20
3	2.33	(CH ₃) ₂ CO, 0 °C	68	1:18

^aBased on internal standard of mesitylene and determined by ¹H NMR.

Catalyst control over semipinacol diastereoselectivity implicates the participation of alkylcobalt intermediates. If ring expansions proceeded solely through carbocationic intermediates diastereoselectivity should remain consistent independent of catalyst used. However, catalyst structure has dramatic influence over stereochemical outcomes, strongly suggesting that cobalt complexes are directly involved in the bond forming steps for at least some of the semipinacol rearrangements.

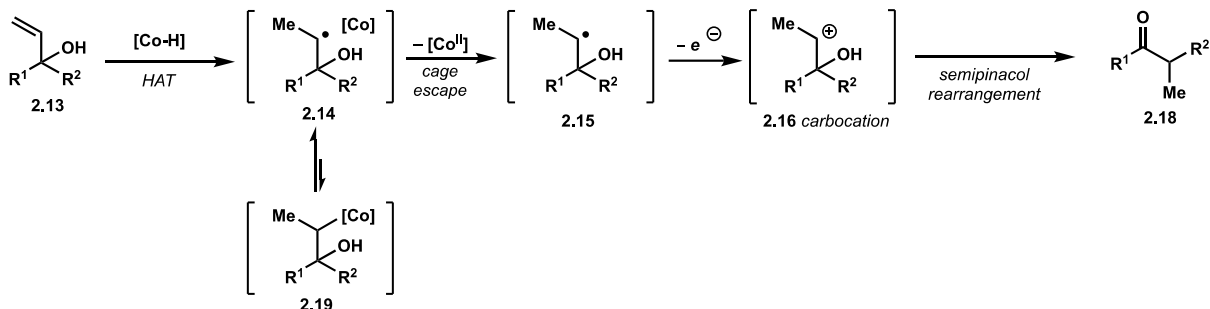
Scheme 2.5 Takemoto's iodine(I) promoted ring expansions of bromohydrins



To deconvolute what processes are under catalyst control we searched for relevant precedent in the literature. In 2014 the Takemoto lab reported a method for iodine(I) promoted ring expansions of *tert*-butyldimethylsilyl (TBS) protected bromohydrins to cycloheptanones

(Scheme 2.5).²⁹ They propose that their reactions proceed via the intermediacy of carbocation **2.68**. Notably, cycloheptanone products are generated with excellent diastereoselectivity. These results are reminiscent of the stereochemical outcomes observed with catalyst **2.27**. Acknowledging that elevated diastereoselectivity via carbocationic intermediates led to high diastereoselectivity, we propose by analogy that catalyst **2.27** is promoting semipinacol rearrangement of alcohol **2.25** through a predominantly carbocationic pathway as a result of direct oxidation of corresponding free alkyl radical intermediates (Scheme 2.6). Perhaps the steric bulk of the tetramethyl ethylenediamine backbone of catalyst **2.27** deters competing radical-pair collapse as well as destabilize alkylcobalt intermediates toward homolysis of the carbon-cobalt bond.³⁰

Scheme 2.6 Proposed hydrofunctionalization mechanism for catalyst **2.27**

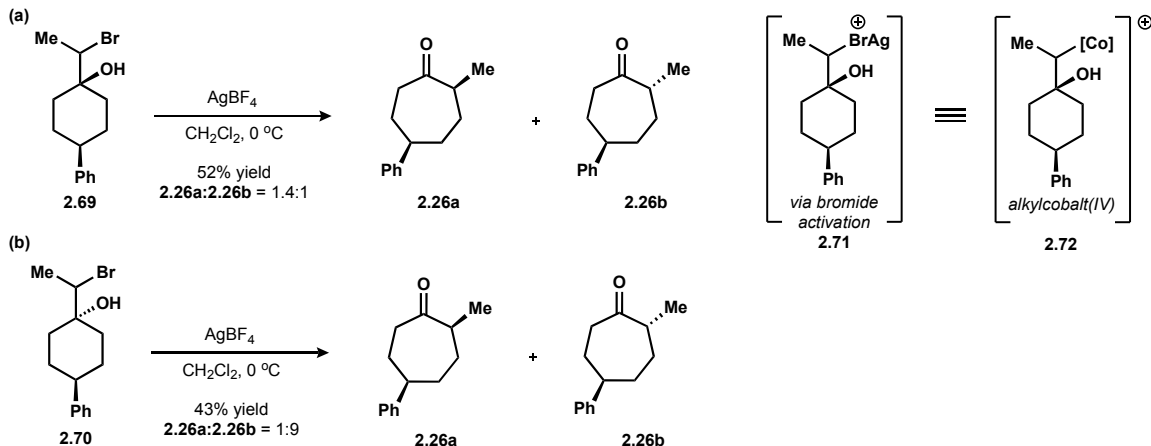


2.5.3 Diastereoselectivity of Ag(I) Promoted Ring Expansions of Bromohydrins

To approximate the diastereoselectivity of ring expansions that proceed through alkylcobalt(IV) intermediates, we evaluated the reactivity of bromohydrins. Silver(I) promoted semipinacol rearrangement of bromohydrins are not thought to proceed via carbocationic intermediates. Rather, formation of a silver bromide adduct weakens the carbon-bromine bond, activating it towards displacement. We posited that the weakened carbon-bromine bond of an activated bromohydrin may be analogous to the weak carbon-cobalt bond of an alkylcobalt(IV)

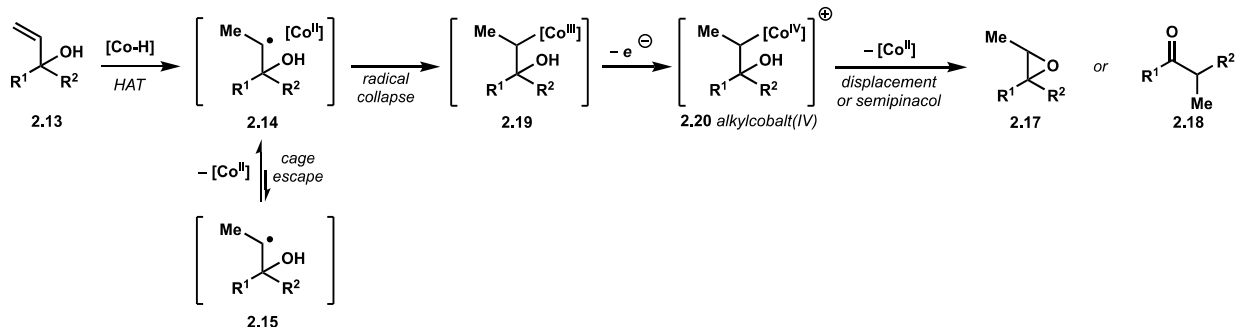
complex. Thus, bromohydrins derived from alcohols **2.25** and **2.65** were prepared and subjected to skeletal rearrangement by treatment with silver(I) tetrafluoroborate (**Scheme 2.7**).

Scheme 2.7 Silver(I) promoted ring expansion of bromohydrins **2.69** and **2.70**



Expansion of bromohydrin **2.69** delivered a 1.4:1 diastereomeric mixture of **2.26** favoring the *cis* arrangement. These results closely mirror the diastereoselectivity observed in ring expansions of alcohol **2.25** using catalyst **2.32** and **2.33**. Thus, we propose that both **2.32** and **2.33** promote radical–polar crossover mechanisms that proceed primarily through intermediates with alkylobalt character (**Scheme 2.8**). We attribute the disparity between selectivity for producing epoxides with **2.32** versus ketones with **2.33** to differing leaving group abilities associated with the nature of the arene fragments in the corresponding between alkylobalt(IV) intermediates. The electron-deficient nitro-substituted **2.33** should serve as a superior nucleofuge upon oxidation

Scheme 2.8 Proposed hydrofunctionalization mechanism for catalysts **2.32** and **2.33**



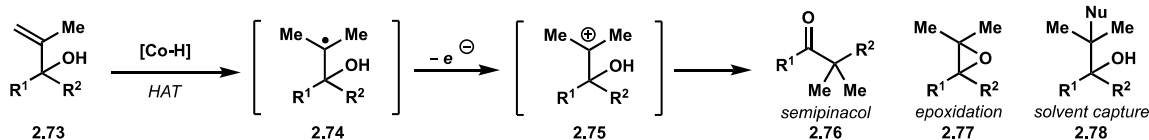
compared to the more stabilized alkylcobalt(IV) intermediate prepared from the relatively electron-rich ligand scaffold of **2.32**.³¹ Similar trends were previously observed in relevant Lewis acid-catalyzed reactions of unsaturated 1,2-diols.³²

Silver(I) promoted expansion of bromohydrin **2.68** delivered a 9:1 diastereomeric mixture of cycloheptanone **2.26** favoring the *trans* arrangement (**Scheme 2.7b**). Skeletal rearrangement of bromohydrin **2.68** is notably less diastereoselective than the corresponding cobalt-catalyzed expansions of alcohol **2.65**, suggesting that the radical–polar crossover ring expansion of **2.65** progresses through free radical oxidation to carbocations rather than alkylcobalt(IV) complexes. Consistently high diastereoselectivity for ring expansion of **2.65** irrespective of catalyst structure also implicates the participation of carbocations, but alkylcobalt(IV) pathways cannot be definitively ruled out.

2.6 Solvent Dependent HAT Radical–Polar Hydrofunctionalization of 1,1-Disubstituted Alkenes

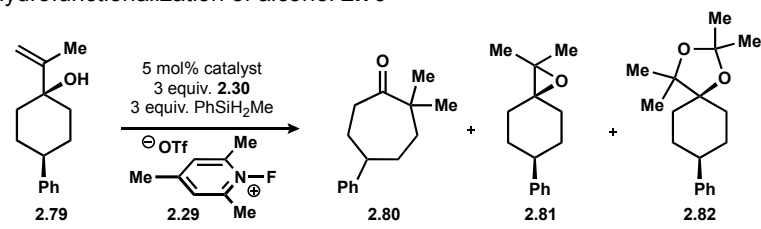
Parallel to our investigations of catalyst controlled hydrofunctionalization of (dialkyl)vinylcarbinols, we also probed the reactivity of tertiary allylic alcohols bearing 1,1-disubstituted alkenes. Realizing that we would likely not accomplish catalyst control over these substrates due to the proposed intermediacy of tertiary radicals, we were nevertheless interested in the potential scaffolds we could access including 2,2-dimethylcycloheptanones and tetrasubstituted epoxides (**Scheme 2.9**).

Scheme 2.9 Proposed mechanism for hydrofunctionalization of 1,1-disubstituted alkenes

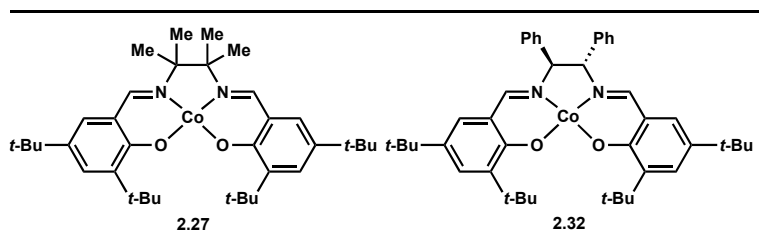


Intuitively, we first subjected allylic alcohol **2.79** to conditions optimized for the catalyst controlled radical–polar crossover hydrofunctionalization using catalyst **2.27** (Table 2.6, entry 1). To our surprise, the expected semipinacol rearrangement product was not observed. Instead, acetone **2.82** derived from intermolecular capture of acetone and subsequent cyclization onto the transient oxocarbenium was formed with great efficiency. Switching to a solvent of dichloromethane again left us surprised, as the major product identified was tetrasubstituted epoxide **2.81** while ketone **2.80** was only prepared nominally (entry 2). Application of catalyst **2.32** likewise produced epoxide **2.81** as the major product (entry 3), consistent with our speculation that the reaction would lack catalyst control. Admittedly, catalyst **2.32** greatly improved yield of ketone **2.80**, so catalyst control cannot be definitively excluded. 60% v/v *tert*-butanol in dichloromethane improved the ratio of epoxide **2.81** to ketone **2.80** (entry 4). In an attempt to

Table 2.6 Effect of reaction conditions on the radical–polar crossover hydrofunctionalization of alcohol **2.79**



entry	catalyst	conditions	2.80 (%) ^a	2.81 (%) ^a	2.82 (%) ^a
1	2.27	(CH ₃) ₂ CO, 0 °C	6	-	84
2	2.27	CH ₂ Cl ₂ , 0 °C	6	62	-
3	2.32	CH ₂ Cl ₂ , 0 °C	31	53	-
4	2.27	CH ₂ Cl ₂ : <i>t</i> BuOH (2:3), 0 °C	36	45	-
5	2.27	PhMe, 0 °C	-	56	-
6	2.27	C ₆ H ₁₂ , 0 °C	-	31	-
7	2.27	HFIP, 0 °C	59	2	-
8	2.32	HFIP, 0 °C	44	10	-



^aBased on internal standard of mesitylene and determined by ¹H NMR.

destabilize the intermediate carbocation towards 1,2-migration, toluene and cyclohexane were screened as solvents however both afforded epoxide **2.81** exclusively (entries 5–6). Ultimately, hexafluoroisopropanol (HFIP) was the only solvent identified that delivered ketone **2.80** as the major product (entry 7). The reaction demonstrated minimal catalyst dependence and **2.32** likewise formed ketone **2.80** predominantly (entry 8). These results are preliminary but offer a promising method for modular diversification of 1,1-disubstituted alkenes by careful choice of solvent.

2.7 Conclusions and Outlook

In summary, we have developed the first cobalt-catalyzed HAT-initiated radical–polar crossover alkene hydrofunctionalization under strong catalyst control. Tertiary allylic alcohols provide a unique scaffold to differentiate between alkylcobalt and carbocationic pathways. The reaction was general, and a broad range of (dialkyl)vinylcarbinols were selectively converted to epoxides or semipinacol rearrangement products with judicious choice of catalyst. This method facilitates the direct conversion of tertiary allylic alcohols to the corresponding epoxides, which is without precedent in the existing literature. Similarly, direct ring expansion of cyclic vinyl carbinols was previously limited to strained ring systems. Evaluation of the stereochemical outcomes of bromohydrin expansions led us to propose that reactions with catalysts bearing diphenyl ethylenediamine backbones proceed through electrophilic alkylcobalt(IV) intermediates. Preliminary results allow for solvent dependent hydrofunctionalizations of tertiary allylic alcohols bearing 1,1-disubstituted alkenes. Having established the participation of alkylcobalt intermediates, these findings provide a strong starting point for harnessing the stereoinvertive displacement of alkylcobalt(IV) complexes towards development of enantioselective radical–polar crossover reactions, which are described in Chapter 3.

2.8 Experimental Section

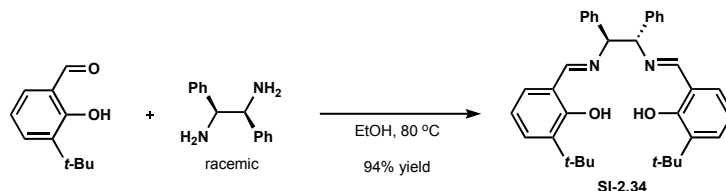
2.8.1 Materials and Methods

All reactions were carried out in flame-dried glassware under positive pressure of dry nitrogen unless otherwise noted. Reaction solvents including tetrahydrofuran (THF, Fisher, HPLC Grade), dichloromethane (DCM, Fisher, HPLC Grade), and toluene (Fisher, HPLC Grade) were dried by percolation through a column packed with neutral alumina and a column packed with a supported copper catalyst for scavenging oxygen (Q5) under positive pressure of argon. Acetone was dried over anhydrous powdered CaSO_4 overnight, distilled into a two-neck round bottom, and then transferred by cannula into a storage Schlenk. Solvents for extraction, thin layer chromatography (TLC), and flash column chromatography were purchased from Fischer (ACS Grade) and VWR (ACS Grade) and used without further purification. Chloroform- d and benzene- d_6 for ^1H and ^{13}C NMR analysis were purchased from Cambridge Isotope Laboratories and used without further purification. Commercially available reagents were used without further purification unless otherwise noted. Reactions were monitored by thin layer chromatography (TLC) using precoated silica gel plates (EMD Chemicals, Silica gel 60 F₂₅₄). Flash column chromatography was performed over silica gel (Acros Organics, 60 Å, particle size 0.04-0.063 mm). ^1H NMR and ^{13}C NMR spectra were recorded on Bruker DRX-500 (BBO probe), Bruker DRX-500 (TCI cryoprobe), Bruker AVANCE600 (TBI probe), and Bruker AVANCE600 (BBFO cryoprobe) spectrometers using residual solvent peaks as internal standards (CHCl_3 @ 7.26 ppm ^1H NMR, 77.00 ppm ^{13}C NMR; C_6H_6 @ 7.16 ppm ^1H NMR, 128.00 ppm ^{13}C NMR; $(\text{CD}_3)_2\text{CO}$ @ 2.05 ppm ^1H NMR, 29.84 ppm ^{13}C NMR; $(\text{CD}_3)_2\text{SO}$ @ 2.50 ppm ^1H NMR, 39.52 ppm ^{13}C NMR). High-resolution mass spectra (HRMS) were recorded on Waters LCT Premier TOF spectrometer with ESI and CI sources.

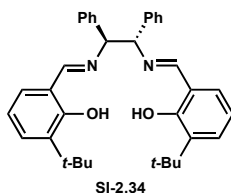
2.8.2 Experimental Procedures

Preparation of Co(II) salen complexes

Co(II) salen complexes **2.32**³³, **2.27**⁷, and **2.31**³⁴ are known. Ligands and Co(II) salen complexes were prepared according to the procedures of the Jacobsen group.³⁵



Ligand SI-2.34. 3-*tert*-butyl-3-hydroxybenzaldehyde (0.17 mL, 1.0 mmol) was added to a stirred solution of racemic 1,2-diphenylethylenediamine (106.2 mg, 0.5 mmol) in EtOH (5.0 mL, 0.2 M) at room temperature. The flask was equipped with a reflux condenser and the reaction was heated at 80 °C. After 2 h the reaction was removed from heat and concentrated in vacuo. The crude yellow oil was purified by flash chromatography using 2% v/v EtOAc/hexanes to afford 251.6 mg (94%) of **SI-2.34** as a pale yellow solid.



Ligand **SI-2.34**

¹H NMR (500 MHz, CDCl₃, 25 °C):

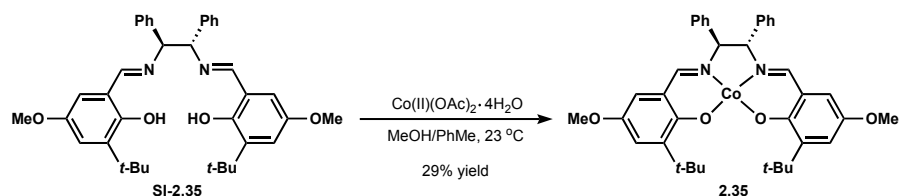
δ 13.77 (s, 2H)	6.72 (t, <i>J</i> = 7.6 Hz, 2H)
8.36 (s, 2H)	4.74 (s, 2H)
7.28-7.17 (m, 12H)	1.44 (s, 18H)
7.00 (dd, <i>J</i> = 7.6, 1.5 Hz, 2H)	

¹³C NMR (126 MHz, CDCl₃, 25 °C):

δ 166.9	130.1	127.6	34.8
160.3	129.7	118.6	29.4
139.6	128.4	117.9	
137.2	128.1	80.2	

HRMS (ESI) calculated for $C_{36}H_{40}N_2O_2$ $[M+Na]^+$: 555.2988, found: 555.3013

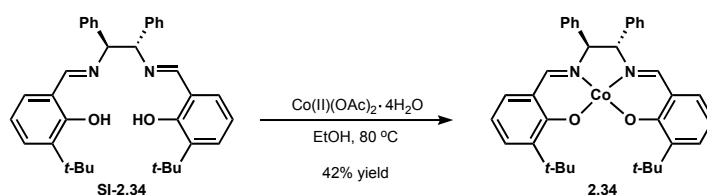
TLC: $R_f = 0.27$ (5% EtOAc/Hex)



Co(II) salen complex 2.35. A solution of $Co(II)(OAc)_2 \cdot 4H_2O$ (18.9 mg, 0.076 mmol) in degassed MeOH (2.3 mL, 0.033 M w.r.t. $Co(II)(OAc)_2 \cdot 4H_2O$) was added by cannula to a stirred solution of ligand **SI-2.35**³⁶ (44.9 mg, 0.32 mmol) in degassed dry toluene (0.76 mL, 0.1 M w.r.t. ligand) at room temperature. Dark coloration and precipitation observed immediately. The reaction was stirred for 2 h at room temperature, cooled to 0 °C, stirred for 20 min, and the dark brown Co(II) salen complex **2.35** was isolated (14.5 mg, 29% yield) by vacuum filtration and washing with cold MeOH (3 mL). Complex **2.35** was dried under vacuum overnight prior to use.

IR: 2953.54, 2360.97, 1617.30, 1593.98, 1532.60, 1493.66, 1452.71, 1419.40, 1403.87, 1383.47, 1355.10, 1324.96, 1147.94, 1111.48, 1162.97, 934.11, 812.84, 659.89 cm^{-1}

HRMS (ES) calculated for $C_{38}H_{42}CoN_2O_4$ $[M]^+$: 649.2477, found: 649.2471

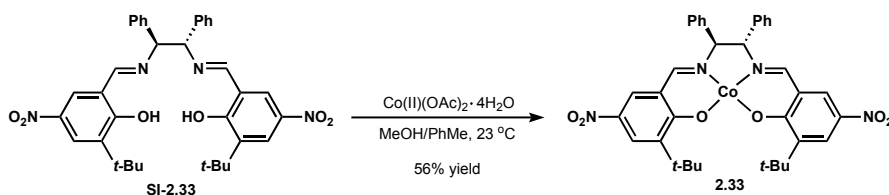


Co(II) salen complex 2.34. A solution of $Co(II)(OAc)_2 \cdot 4H_2O$ (124.5 mg, 0.5 mmol) in degassed EtOH (3.0 mL, 0.17 M w.r.t. $Co(II)(OAc)_2 \cdot 4H_2O$) was added by syringe to a stirred solution of ligand **SI-2.34** (266.4 mg, 0.5 mmol) in degassed EtOH (8.0 mL, 0.06 M w.r.t. ligand, 0.045 M total) at room temperature. Dark red coloration and precipitation observed upon addition of

Co(II)(OAc)₂·4H₂O. The flask was equipped with a reflux condenser and heated to 80 °C for 2 h. The reaction was removed from heat, cooled to 0 °C, stirred for 20 min, and the bright red Co(II) salen complex **2.34** was isolated (122.7 mg, 42% yield) by vacuum filtration and washing with cold EtOH (5 mL). Complex **2.34** was dried under vacuum overnight prior to use.

IR: 2950.08, 2908.88, 1588.76, 1529.67, 1492.72, 1453.07, 1385.58, 1314.02, 1198.51, 1146.60, 868.45, 751.62, 698.22 cm⁻¹

HRMS (ESI) calculated for C₃₈H₃₈CoN₂O₂ [M+Na]⁺: 612.2163, found: 612.2186

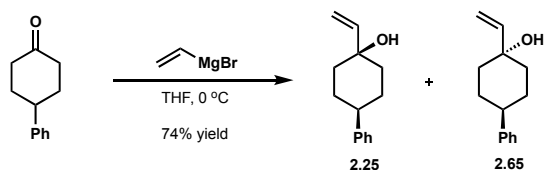


Co(II) salen complex 2.33. A solution of Co(II)(OAc)₂·4H₂O (79.7 mg, 0.32 mmol) in degassed MeOH (9.7 mL, 0.033 M w.r.t. Co(II)(OAc)₂·4H₂O) was added by cannula to a stirred solution of ligand **SI-2.33**³⁷ (200 mg, 0.32 mmol) in degassed dry toluene (3.2 mL, 0.1 M w.r.t. ligand) at room temperature. Red coloration and precipitation observed immediately. The reaction was stirred for 2 h at room temperature, cooled to 0 °C, stirred for 20 min, and the dark red-brown Co(II) salen complex **2.33** was isolated (121.1 mg, 56% yield) by vacuum filtration and washing with cold MeOH (5 mL). Complex **2.33** was dried under vacuum overnight prior to use.

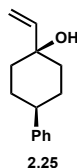
IR: 3543.88, 2955.53, 2359.14, 1626.35, 1588.27, 1558.45, 1297.26, 1278.80, 1260.28, 1228.82, 1200.73, 1182.11, 1102.47, 1027.36, 904.8, 857.3, 793.65, 696.61 cm⁻¹

HRMS (ESI) calculated for C₃₆H₃₆CoN₄O₆ [M]⁺: 679.1967, found: 679.1967

Preparation of starting materials



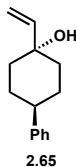
Allylic alcohols 2.25 and 2.65. A solution of vinylmagnesium bromide (20 mL of a 1.0 M solution in THF, 2.5 equiv) in THF (20 mL, 0.6 M w.r.t. Grignard reagent) was cooled to $0\text{ }^\circ\text{C}$. A solution of 4-phenylcyclohexanone (1.394 g, 8.0 mmol, 1.0 equiv.) in THF (20 mL, 0.6 M w.r.t. ketone, final reaction concentration 0.2 M) was added slowly. After 1 h, the reaction was quenched by the addition of saturated aqueous NH_4Cl (20 mL). The resulting mixture was extracted with Et_2O 3x 50 mL. The organics were washed with brine and dried over MgSO_4 . The crude material was purified by flash silica chromatography (gradient elution: 100% hexanes to 35% v/v Et_2O /hexanes) to yield 496.5 mg (31%) of **2.25** as glassy oil that solidified upon storage in the freezer, and 697.4 mg (43%) of **2.65** as a white solid. The spectral data of both diastereomers matched those reported in the literature.³⁸



Allylic alcohol **2.25**

^1H NMR (500 MHz, CDCl_3 , $25\text{ }^\circ\text{C}$):

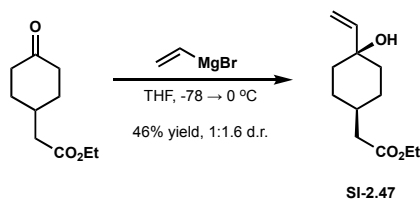
δ 7.32-7.29 (m, 2H)	2.51 (tt, $J = 12.3, 3.3$ Hz, 1H)
7.27-7.26 (m, 2H)	1.93 (qd, $J = 12.9, 3.6$ Hz, 2H)
7.22-7.18 (m, 1H)	1.76 (ddt, $J = 12.5, 5.5, 3.0$ Hz, 4H)
6.01 (dd, $J = 17.3, 10.7$ Hz, 1H)	1.66 (td, $J = 13.6, 4.1$ Hz, 2H)
5.29 (dd, $J = 17.4, 1.0$ Hz, 1H)	1.28 (s, 1H)
5.06 (dd, $J = 10.8, 0.9$ Hz, 1H)	



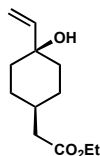
Allylic alcohol **2.65**

^1H NMR (500 MHz, CDCl_3 , 25 °C):

δ 7.30 (t, $J = 7.6$ Hz, 2H)	2.60 (tt, $J = 11.8, 3.7$ Hz, 1H)	1.58 (s, 1H)
7.20 (dd, $J = 15.4, 7.4$ Hz, 3H)	1.98 (d, $J = 11.9$ Hz, 2H)	
6.18 (dd, $J = 17.5, 10.8$ Hz, 1H)	1.91-1.87 (m, 2H)	
5.40 (d, $J = 17.5$ Hz, 1H)	1.74 (td, $J = 12.9, 3.5$ Hz, 2H)	
5.25 (d, $J = 10.9$ Hz, 1H)	1.68-1.62 (m, 2H)	1.58 (s, 1H)



Allylic alcohol SI-2.47. A solution of ethyl 2-(4-oxocyclohexyl)acetate (2.5 mmol, 0.44 mL) in THF (17 mL, 0.15M) was cooled to -78 °C in a dry ice/acetone bath. Vinylmagnesium bromide (2.75 mL of 1.0 M in THF, 2.75 mmol) was added to the flask slowly dropwise, stirred at -78 °C for 20 min, and then warmed to 0 °C. After 1 h, the reaction was quenched by the addition of sat. aq. NH_4Cl (30 mL) and the resulting mixture extracted with Et_2O 3x 30 mL. The organics were washed with brine and dried over MgSO_4 . Purification of the 1:1.6 mixture of diastereomers by flash column chromatography (gradient elution: 100% hexanes to 30% v/v EtOAc in hexanes) afforded **SI-2.47** in 22% yield (0.115 g, 0.54 mmol) as a clear colorless oil. The other diastereomer was isolated in 24% yield (0.127 g, 0.60 mmol).



SI-2.47

Allylic alcohol **SI-2.47**

^1H NMR (500 MHz; CDCl_3 , 25 °C):

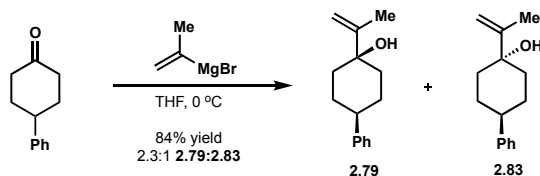
δ 5.93 (dd, $J = 17.4, 10.8$ Hz, 1H)	1.81-1.73 (m, 1H)	1.18 (s, 1H).
5.25-5.21 (m, 1H)	1.61 (d, $J = 11.0$ Hz, 3H)	
5.01 (d, $J = 10.8$ Hz, 1H)	1.55-1.49 (m, 2H)	
4.13 (d, $J = 7.1$ Hz, 2H)	1.47-1.39 (m, 2H)	
2.23 (d, $J = 7.1$ Hz, 2H)	1.25 (t, $J = 7.1$ Hz, 4H)	

^{13}C NMR (126 MHz; CDCl_3 , 25 °C):

δ 173.0	71.1	36.7	14.3
146.5	60.2	34.0	
111.2	41.7	27.7	

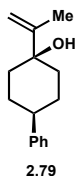
HRMS (ESI) calculated for $\text{C}_{12}\text{H}_{20}\text{O}_3$ $[\text{M}+\text{Na}]^+$: 235.1310, found: 235.1313

TLC: $R_f = 0.35$ (30% EtOAc/Hex)



Isopropenyl allylic alcohols 17. Isopropenylmagnesium bromide (4.53 mL of a 0.50 M solution in THF, 1.72 mmol) was added to 2.0 mL of cooled THF and left to stir for 20 min in an ice bath at 0 °C. A solution of 4-phenylcyclohexanone (0.100 g, 0.574 mmol) in THF (0.90 mL) was added slowly dropwise to the reaction and left to stir for 15 h. The reaction was quenched with 3.0 mL of saturated aqueous ammonium chloride and left to stir 10 minutes. The mixture was extracted three times with ether (45 mL combined), washed with brine (25 mL), dried over anhydrous

sodium sulfate, and concentrated under reduced pressure. The resulting diastereomers were separated by flash chromatography (gradient elution: 100% hexanes to 10% v/v diethyl ether in hexanes) in a 2.3:1 ratio of **2.79** to **2.83** in 84% total yield (0.104 g, 0.482 mmol).



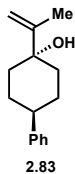
Allylic alcohol **2.79**

^1H NMR (500 MHz; CDCl_3):

δ 7.31-7.23 (m, 4H)	4.83 (t, $J = 1.3$ Hz, 1H)	1.85 (s, 3H)
7.20-7.17 (m, 1H)	2.49 (tt, $J = 12.3, 3.2$ Hz, 1H)	1.81-1.72 (m, 6H)
5.07 (s, 1H)	1.99-1.90 (m, 2H)	1.32 (s, 1H)

^{13}C NMR (126 MHz; CDCl_3):

δ 152.4	126.0	36.1
147.3	109.1	29.4
128.4	73.0	19.1
126.9	43.9	



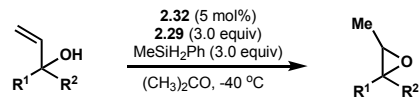
^1H NMR (500 MHz; CDCl_3):

δ 7.36-7.32 (m, 2H)	2.70 (tt, $J = 11.2, 3.8$ Hz, 1H)	1.74-1.68 (m, 2H)
7.27-7.23 (m, 3H)	2.33-2.29 (m, 2H)	1.67-1.59 (m, 2H)
5.19 (s, 1H)	1.96-1.93 (m, 2H)	1.52 (s, 1H)
5.14 (t, $J = 1.3$ Hz, 1H)	1.91 (d, $J = 0.6$ Hz, 3H)	

^{13}C NMR (126 MHz; CDCl_3):

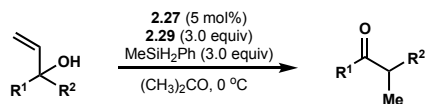
δ 147.1	126.1	36.5
146.6	113.4	31.3
128.4	73.7	18.9
127.0	43.6	

General procedure for the catalytic radical-polar crossover of allylic alcohols.



To a flame dried roundbottom flask charged with magnetic stir bar was added Co-salen catalyst **2.32** (0.05 equiv.) and oxidant **2.29** (3.0 equiv.). The roundbottom was placed under an atmosphere of argon. The allylic alcohol (1.0 equiv.) was added as a solution in dry acetone (0.1 M) and stirred until homogeneous. The resulting solution was sparged with argon and simultaneously subjected to sonication for 15 min. After cooling to -40 °C, MePhSiH₂ (3.0 equiv.) was added at a rate of 1 drop/10 s. The reaction quickly developed a bright orange color. After 1 h, the reaction was quenched by the addition of saturated aqueous NH₄Cl (2x reaction volume) and diluted with DCM (3 mL) and H₂O until homogeneous. The aqueous phase was extracted with DCM 3x 5 mL. The combined organics were washed with brine and dried over Na₂SO₄. The products were isolated using flash column chromatography.

Protocol 1: For epoxides that are co-polar on silica with their corresponding semi-pinacol side products. The crude reaction mixture was dissolved in MeOH (0.1 M) and cooled to 0 °C before treatment with NaBH₄ (10 equiv.). After warming to 20 °C for 30 min the mixture was diluted with H₂O (10 mL) and extracted with DCM 3x 5 mL. The organics were washed with brine and dried over Na₂SO₄.



To a flame dried roundbottom flask charged with magnetic stir bar was added Co-salen catalyst **2.33** or **2.27** (0.05 equiv.) and oxidant **2.29** (3.0 equiv.). The roundbottom was placed under an atmosphere of argon. The allylic alcohol (1.0 equiv.) was added as a solution in dry acetone (0.1 M) and stirred until homogeneous. The resulting solution was sparged with argon and simultaneously subjected to sonication for 15 min. After cooling to 0 °C, MePhSiH₂ (3.0 equiv.) was added at a rate of 1 drop/10 s. The reaction quickly developed a bright orange color. After 1 h, the reaction was quenched by the addition of saturated aqueous NH₄Cl (2x reaction volume) and diluted with DCM (3 mL) and H₂O until homogeneous. The aqueous phase was extracted with DCM 3x 5 mL. The combined organics were washed with brine and dried over Na₂SO₄. The products were isolated using flash column chromatography.

Protocol 2: For semi-pinacol products that are co-polar on silica with their corresponding epoxide side products. The crude reaction mixture was flushed through a plug of silica using 50% v/v CH₂Cl₂/hexanes and concentrated in vacuo. The material was dissolved in THF (0.2 M) and LiBr was added (10 equiv w.r.t epoxide component). The mixture was cooled to 0 °C and glacial acetic acid (12 equiv w.r.t epoxide component) was added. The reaction was left to warm to room temperature overnight then quenched with aqueous saturated NaHCO₃ and extracted with Et₂O 3x (10 mL portions). The organics were washed with brine, dried over Na₂SO₄, and concentrated in vacuo.

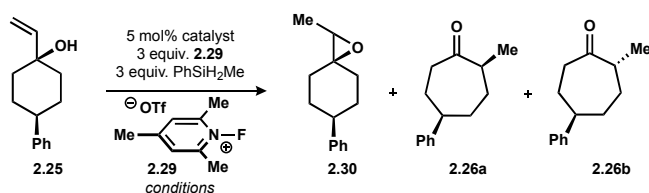
Note 1: In many cases, separation of the desired products from the silane byproducts was facilitated by including *ca.* 3 cm neutral alumina on top of the silica during chromatography. For some semi-pinacol adducts this protocol was found to epimerize the α -keto stereocenter.

Note 2: Variation of solvent mixtures from Hex/EtOAc to DCM/EtOAc or DCM/Et₂O often improved separation on silica of the epoxide and semi-pinacol products.

Note 3: When silane byproducts are inseparable from the desired products on silica: purified material was dissolved in MeCN (10 mL) and extracted with pentane (10 mL). The pentane layer was back-extracted 3x with MeCN. The recovery of material from this procedure was found to be variable depending on the compound.

Note 4: All product ratios are determined by integration of the crude ¹H NMR spectrum.

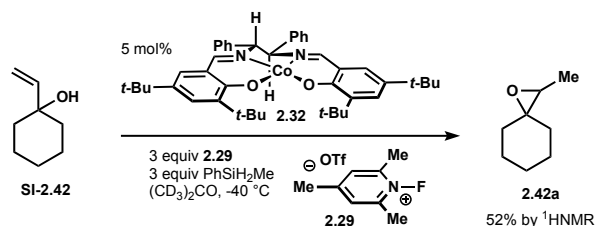
General procedure for optimization studies (Table 2.1 and Table 2.2)



Experimental Procedure: To a flame dried RBF charged with magnetic stir bar was added Co-salen catalyst (2.5 μ mol) and oxidant **2.29** (43.4 mg, 0.15 mmol). The RBF was placed under an atmosphere of argon. Allylic alcohol **2.25** (10.1 mg, 0.05 mmol) was added as a solution in dry solvent (0.5 mL, 0.1 M) and stirred until homogeneous. The resulting solution was sparged with argon and simultaneously subjected to sonication for 5 min. After cooling to the desired temperature, silane was added at a rate of 1 drop/10 s. The reaction quickly developed a bright orange color in most cases. After 2 h, the reaction was quenched by the addition of saturated aqueous NH₄Cl (2 mL) and diluted with DCM (3 mL) and H₂O until homogeneous. The aqueous phase was extracted with DCM 3x 5 mL. The combined organics were washed with brine, dried over Na₂SO₄ and concentrated. To the resulting dark-brown residue was added mesitylene (0.05 mmol, 7.0 μ L) and 0.7 mL CDCl₃.

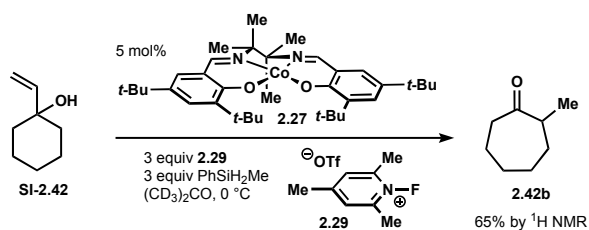
Determination of conversion & product ratios by 1H NMR analysis: The entirety of the sample was transferred to an NMR tube and a spectrum collected. The mesitylene singlet was set to 6.80 ppm and was integrated to 3.0. Quantification of the remaining starting vinylcyclohexanol **2.25** was accomplished by integration of the doublet of doublets at 6.18 ppm (dd, $J = 17.5, 10.8$ Hz, 1H). Quantification of the epoxide **2.30** produced was accomplished by integration of the quartet at 2.94 (q, $J = 5.6$ Hz, 1H). Quantification of semipinacol adduct **2.26a** produced was accomplished by integration of the doublet at 1.17 ppm ($J = 7.0$ Hz, 3H) and division of the integration by 3. Quantification of semipinacol adduct **2.26b** produced was accomplished by integration of the doublet at 1.12 ppm ($J = 7.0$ Hz, 3H) and division of the integration by 3.

Experimental Data

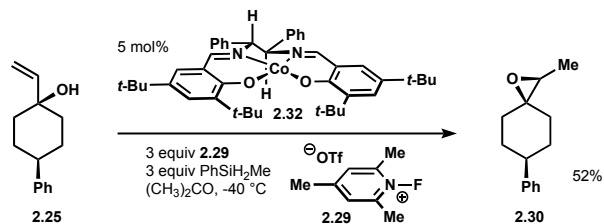


Epoxide 2.42a. Prepared according to “**General procedure for the catalytic radical-polar crossover of allylic alcohols.**” The reaction was performed with 0.3 mmol (86.8 mg) of **2.29**, 5 μmol (3.5 mg) of **2.32**, 0.3 mmol (41 μL) of MePhSiH₂, 0.1 mmol (13.4 μL) vinylcyclohexanol **SI-2.42** in a solvent of acetone-d₆ (0.1 M, 1.0 mL) producing a 3.1:1.0 ratio of **2.42a** to **2.42b**. After the reaction was determined complete by TLC, an internal standard of mesitylene (0.1 mmol, 13.9 μL) was added to the reaction flask. All contents of the flask were then removed and transferred to an NMR tube. Yield of **2.42a** (52%) was determined by ¹H NMR analysis, integrating against an internal standard. Contents in the NMR tube were then filtered through a plug of alumina using

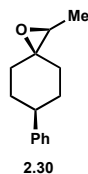
3 mL of CDCl₃ and a second spectra taken. Observed ¹H NMR peaks match those reported in the literature.³⁹



Cycloheptanone 2.42b. Prepared according to “**General procedure for the catalytic radical-polar crossover of allylic alcohols**”. The reaction was performed with 0.3 mmol (86.8 mg) of **2.29**, 5 μmol (3.0 mg) of **2.27**, 0.3 mmol (41 μL) of MePhSiH₂, 0.1 mmol (13.4 μL) vinylcyclohexanol **SI-2.42** in a solvent of acetone-d₆ (0.1 M, 1.0 mL) producing a 7.2:1.0 ratio of **2.42b** to **2.42a**. After the reaction was determined complete by TLC, an internal standard of mesitylene (0.1 mmol, 13.9 μL) was added to the reaction flask. All contents of the flask were then removed and transferred to an NMR tube. Yield of **2.42b** (65%) was determined by ¹H NMR analysis, integrating against an internal standard. Contents in the NMR tube were then filtered through a plug of alumina using 3 mL of CDCl₃ and a second spectra taken. Observed ¹H NMR peaks match those reported in the literature.⁴⁰



Epoxide 2.30. Prepared according to “**General procedure for the catalytic radical-polar crossover of allylic alcohols**” The reaction was performed with 0.75 mmol (216.9 mg) of **2.29**, 12.5 μ mol (8.8 mg) of **2.32**, 0.75 mmol (103 μ L) of MePhSiH₂, and 0.25 mmol (50.5 mg) vinylcyclohexanol **2.25** producing a 4.2:1.0 ratio of **2.30** to **2.26**. The inseparable mixture was subjected to protocol 1. The crude was chromatographed (gradient elution: 100% pentane to 15% v/v CH₂Cl₂/pentane to deliver 26.3 mg (52%) of **2.30** as a colorless oil.



Epoxide 2.30

¹H NMR (500 MHz, CDCl₃, 25 °C):

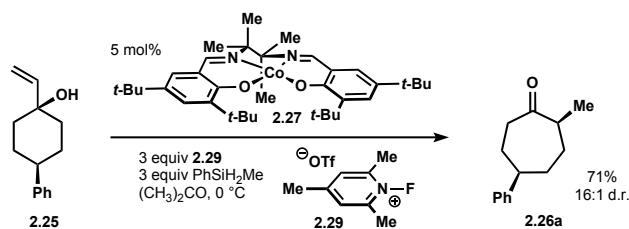
δ 7.32-7.29 (m, 2H)	2.05-1.92 (m, 2H)
7.26 (d, J = 6.3 Hz, 3H)	1.90-1.76 (m, 4H)
7.22-7.18 (m, 1H)	1.61-1.57 (m, 1H)
2.94 (q, J = 5.6 Hz, 1H)	1.34 (q, J = 2.9 Hz, 1H)
2.65-2.59 (m, 1H) 1.31	(d, J = 5.6 Hz, 3H)

¹³C NMR (126 MHz, CDCl₃, 25 °C):

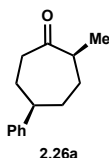
δ 146.8	44.0
128.4	34.9
126.8	31.41
126.1	31.34
61.5	28.7
59.9	13.4

HRMS (ESI) calculated for C₁₄H₁₈O [M+Na]⁺: 225.1255, found: 225.1256

TLC: R_f = 0.24 (10% Et₂O/hexanes)



Cycloheptanone 2.26a. Prepared according to “**General procedure for the catalytic radical-polar crossover of allylic alcohols**”. The reaction was performed with 0.75 mmol (216.9 mg) of **2.29**, 12.5 μmol (7.6 mg) of **2.27**, 0.75 mmol (103 μL) of MePhSiH_2 , and 0.25 mmol (50.5 mg) of vinylcyclohexanol **2.25** producing a 10.6 :1.0 ratio of **2.26a** to **2.30**. The inseparable mixture was subjected to protocol 2. The crude was chromatographed (gradient elution: 100% pentane to 15% v/v CH_2Cl_2 /pentane) to afford 30.5 mg (71%) of **11b** as a clear colorless oil.



Cycloheptanone **2.26a**

^1H NMR (500 MHz, CDCl_3 , 25 °C):

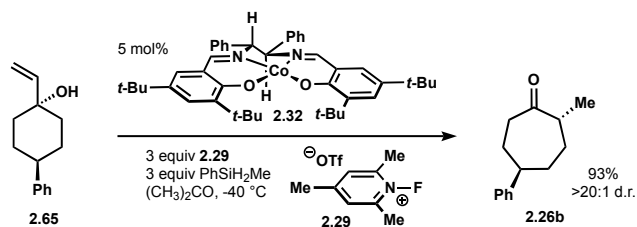
δ 7.29 (t, $J = 7.5$ Hz, 2H)	2.08-2.02 (m, 1H)
7.20-7.16 (m, 3H)	1.92-1.88 (m, 1H)
2.83-2.75 (m, 2H)	1.82 (dddd, $J = 14.7, 8.3, 3.7, 1.4$ Hz, 1H)
2.73-2.67 (m, 1H)	1.71 (dtd, $J = 14.3, 11.9, 2.4$ Hz, 1H)
2.53 (ddd, $J = 12.1, 7.1, 2.6$ Hz, 1H)	1.63 (ddd, $J = 13.6, 10.3, 1.4$ Hz, 1H)
2.20-2.13 (m, 1H)	1.17 (d, $J = 7.0$ Hz, 3H)

^{13}C NMR (126 MHz, CDCl_3 , 25 °C):

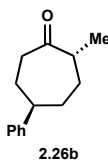
δ 215.7	48.1	30.6
147.1	45.7	15.8
128.5	41.6	
126.7	33.1	
126.2	31.9	

HRMS (ESI) calculated for $\text{C}_{14}\text{H}_{18}\text{O}$ $[\text{M}+\text{Na}]^+$: 225.1255, found: 225.1255

TLC: $R_f = 0.2$ (10% Et_2O /hexanes)



Cycloheptanone 2.26b. Prepared according to “General procedure for the catalytic radical-polar crossover of allylic alcohols”. The reaction was performed with 0.75 mmol (216.9 mg) of **2.29**, 12.5 μmol (7.6 mg) of **2.32**, 0.75 mmol (103 μL) of MePhSiH₂, and 0.25 mmol (50.5 mg) of vinylcyclohexanol **2.65**. The crude was chromatographed (gradient elution: 100% pentane to 15% v/v CH₂Cl₂/pentane) to afford 47.2 mg (93%) of **2.26b** as a clear colorless oil.



Cycloheptanone **2.26b**

¹H NMR (500 MHz, CDCl₃, 25 °C):

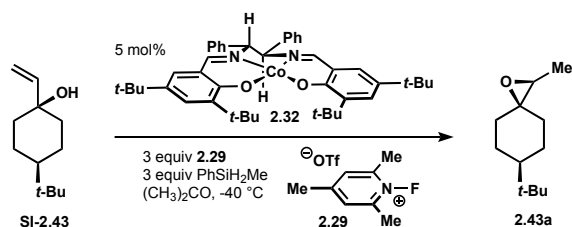
δ 7.29 (t, <i>J</i> = 7.6 Hz, 2H)	2.09-2.01 (m, 2H)
7.19 (dd, <i>J</i> = 14.8, 7.7 Hz, 3H)	1.95-1.87 (m, 2H)
2.74-2.65 (m, 2H)	1.72-1.64 (m, 1H)
2.61 (tt, <i>J</i> = 11.6, 2.5 Hz, 1H)	1.60-1.52 (m, 1H)
2.54 (ddd, <i>J</i> = 15.1, 5.7, 2.9 Hz, 1H)	1.12 (d, <i>J</i> = 7.0 Hz, 3H)

¹³C NMR (126 MHz, CDCl₃, 25 °C):

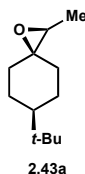
δ 216.3	126.3	37.6
147.7	48.3	33.4
128.6	47.1	32.1
126.5	41.6	17.9

HRMS (ESI) calculated for C₁₄H₁₈O [M+Na]⁺: 225.1255, found: 225.1255

TLC: R_f = 0.2 (10% Et₂O/hexanes)



Epoxide 2.43a. Prepared according to “**General procedure for the catalytic radical-polar crossover of allylic alcohols**” The reaction was performed with 3.0 mmol (867.8 mg) of **2.29**, 50 μ mol (35.1 mg) of **2.32**, 3.0 mmol (412 μ L) of MePhSiH₂, and 1.0 mmol (182.3 mg) vinylcyclohexanol **SI-2.43** producing a 2.8:1.0 ratio of **2.43a** to **2.43b**. The inseparable mixture was subjected to protocol 1. The crude was chromatographed (gradient elution: 100% hexanes to 20% v/v CH₂Cl₂/hexanes) to afford 102.8 mg (56%) of **2.43a** as a colorless oil.



Epoxide **2.43a**

¹H NMR (500 MHz, CDCl₃, 25 °C):

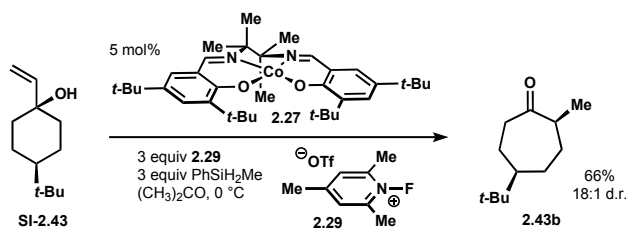
δ 2.87 (q, $J = 5.6$ Hz, 1H)	1.41-1.29 (m, 2H)
1.84-1.78 (m, 2H)	1.26 (d, $J = 5.6$ Hz, 3H)
1.77-1.72 (m, 1H)	1.24-1.20 (m, 1H)
1.62 (dt, $J = 9.1, 4.5$ Hz, 1H)	1.11-1.05 (m, 1H)
1.49 (dq, $J = 13.7, 3.2$ Hz, 1H)	0.88 (s, 9H)

¹³C NMR (126 MHz, CDCl₃, 25 °C):

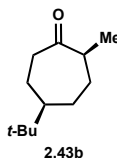
δ 62.1	28.8
59.8	27.6
47.8	24.71
35.0	24.66
32.5	13.4

HRMS (ESI) calculated for C₁₂H₂₂O [M+Na]⁺: 205.1568, found: 205.1573

TLC: R_f = 0.32 (10% Et₂O/hexanes)



Cycloheptanone 2.43b. Prepared according to “General procedure for the catalytic radical-polar crossover of allylic alcohols”. The reaction was performed with 0.75 mmol (216.9 mg) of **2.29**, 12.5 μmol (7.6 mg) of **2.27**, 0.75 mmol (103 μL) of MePhSiH₂, and 0.25 mmol (45.6 mg) of vinylcyclohexanol **SI-2.43** producing a 10.1 :1.0 ratio of **2.43b** to **2.43a**. The inseparable mixture was subjected to protocol 2. The crude was chromatographed (gradient elution: 100% pentane to 15% v/v CH₂Cl₂/pentane) to afford 30.0 mg (66%) of **2.43b** as a clear colorless oil.



Cycloheptanone **2.43b**

¹H NMR (500 MHz, CDCl₃, 25 °C):

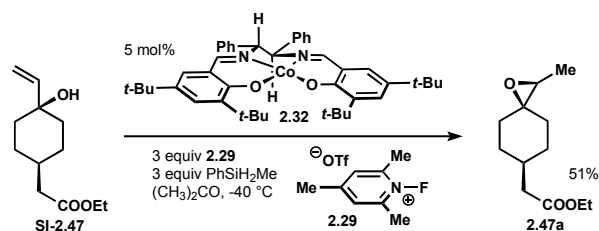
δ 2.62-2.55 (m, 2H)	1.25 (ddt, <i>J</i> = 8.8, 5.9, 2.7 Hz, 2H)
2.46 (ddd, <i>J</i> = 12.3, 6.7, 2.7 Hz, 1H)	1.08 (d, <i>J</i> = 7.0 Hz, 3H)
1.93 (ddtd, <i>J</i> = 12.1, 9.7, 4.9, 2.4 Hz, 2H)	1.05-0.99 (m, 1H)
1.87-1.82 (m, 1H)	0.86 (s, 9H)
1.71 (dddd, <i>J</i> = 14.6, 8.5, 4.4, 2.1 Hz, 1H)	

¹³C NMR (126 MHz, CDCl₃, 25 °C):

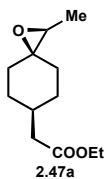
δ 216.5	30.8	16.0
51.1	27.65	
45.5	27.56	
41.7	26.4	
33.5	25.5	

HRMS (ESI) calculated for C₁₂H₂₂O [M+Na]⁺: 205.1528, found: 205.1571

TLC: R_f = 0.47 (20% Et₂O/hexanes)



Epoxide 2.47a. Prepared according to “**General procedure for the catalytic radical-polar crossover of allylic alcohols**” The reaction was performed with 0.6 mmol (173.6 mg) of **2.29**, 10 μ mol (7.0 mg) of **2.32**, 0.6 mmol (82 μ L) of MePhSiH₂, and 0.2 mmol (42.5 mg) vinylcyclohexanol **SI-2.47** producing a 4.7:1.0 ratio of **2.47a** to **2.47b**. The inseparable mixture was subjected to protocol 1. The crude was chromatographed (gradient elution: 100% pentane to 10% v/v Et₂O/pentane) to afford 21.5 mg (51%) of **2.47a** as a colorless oil.



Epoxide **2.47a**

¹H NMR (500 MHz, CDCl₃, 25 °C):

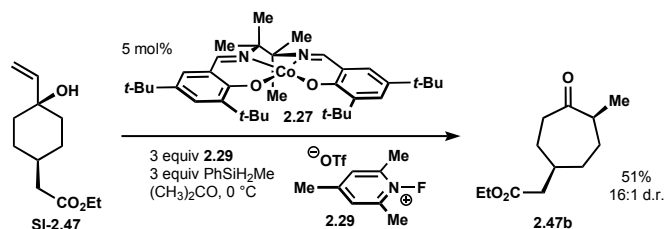
δ 4.19 (q, J = 7.1 Hz, 2H)	1.88 (ddd, J = 18.8, 12.2, 7.1 Hz, 2H)
2.93 (q, J = 5.5 Hz, 1H)	1.81-1.72 (m, 2H), 1.54-1.50 (m, 1H)
2.31 (d, J = 7.1 Hz, 2H)	1.43 (ddt, J = 24.4, 12.3, 6.2 Hz, 2H)
2.00-1.95 (m, 1H)	1.29 (dd, J = 26.6, 4.5 Hz, 8H)

¹³C NMR (126 MHz, CDCl₃, 25 °C):

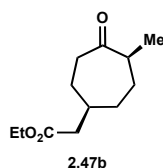
δ 172.9	34.09	14.3
61.6	34.05	13.3
60.2	29.98	
59.8	29.92	
41.3	27.9	

HRMS (ESI) calculated for C₁₂H₂₀O₃ [M+Na]⁺: 235.1310, found: 235.1313

TLC: R_f = 0.28 (30% Et₂O/Hex)



Cycloheptanone 2.47b. Prepared according to “General procedure for the catalytic radical-polar crossover of allylic alcohols”. The reaction was performed with 0.6 mmol (173.6 mg) of **2.29**, 10 μmol (6.1 mg) of **2.27**, 0.6 mmol (82 μL) of MePhSiH₂, and 0.20 mmol (42.5 mg) vinylcyclohexanol **SI-2.47** producing a 6.9:1.0 ratio of **2.47b** to **2.47a**. The crude was chromatographed (gradient elution: 100% pentane to 10% v/v Et₂O/pentane) to afford 21.8 mg of **2.47b** as a clear colorless oil.



Cycloheptanone **2.47b**

¹H NMR (500 MHz, CDCl₃, 25 °C):

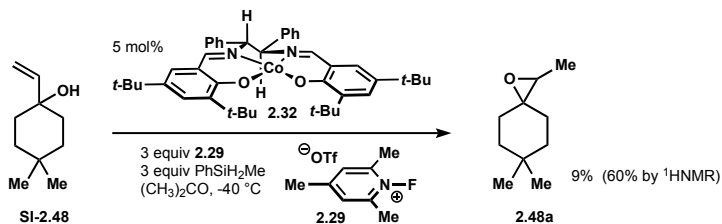
δ 4.12 (q, <i>J</i> = 7.1 Hz, 2H)	1.95-1.88 (m, 2H)	1.35-1.28 (m, 1H)
2.65-2.57 (m, 2H)	1.74-1.70 (m, 1H)	1.25 (t, <i>J</i> = 7.1 Hz, 3H)
2.45 (ddd, <i>J</i> = 13.4, 8.8, 3.0 Hz, 1H)	1.65-1.59 (m, 1H)	1.08 (d, <i>J</i> = 6.9 Hz, 3H)
2.25-2.17 (m, 3H)	1.44-1.37 (m, 1H)	

¹³C NMR (126 MHz, CDCl₃, 25 °C):

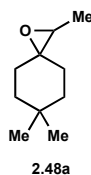
δ 215.6	36.6
172.7	31.3
60.4	30.2
45.8	29.5
40.31	16.2
40.24	14.3

HRMS (ESI) calculated for C₁₂H₂₀O₃ [M+Na]⁺: 235.1310, found: 235.1308

TLC: R_f = 0.29 (30% Et₂O/hexanes)



Epoxide 2.48a. Prepared according to “**General procedure for the catalytic radical-polar crossover of allylic alcohols**” The reaction was performed with 1.5 mmol (433.9 mg) of **2.29**, 25 μ mol (17.5 mg) of **2.32**, 1.5 mmol (41 μ L) of MePhSiH₂, and 0.5 mmol (77.1 mg) vinylcyclohexanol **SI-2.48** producing a 3.0:1.0 ratio of **2.48a** to **2.48b**. The inseparable mixture was subjected to protocol 1. The crude was chromatographed with 0.5% v/v Et₂O/pentane to deliver 7.1 mg (9.2%) of **2.48a** as a colorless, sweet smelling oil. Due to high volatility, ¹HNMR yield from the crude reaction mixture determined by internal standard of mesitylene is also reported.



Epoxide **2.48a**

¹H NMR (500 MHz, CDCl₃, 25 °C):

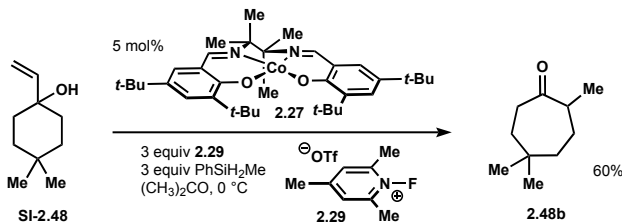
δ 2.84 (q, J = 5.6 Hz, 1H) 1.25 (s, 1H)
 1.60-1.47 (m, 7H) 0.98 (s, 3H)
 1.37-1.31 (m, 2H) 0.95 (s, 3H)
 1.28 (d, J = 5.6 Hz, 3H)

¹³C NMR (126 MHz, CDCl₃, 25 °C):

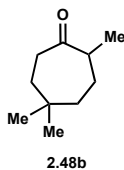
δ 62.5 30.0
 59.9 28.4
 37.46 27.6
 37.38 24.9
 31.3 13.6

HRMS (ESI) calculated for C₁₀H₁₈O [M+Na]⁺: 177.1255, found: 177.1252

TLC: R_f = 0.31 (10% Et₂O/Hex)



Cycloheptanone 2.48b. Prepared according to “General procedure for the catalytic radical-polar crossover of allylic alcohols”. The reaction was performed with 1.50 mmol (433.9 mg) of **2.29**, 25 μmol (15.1 mg) of **2.27**, 1.50 mmol (206 μL) of MePhSiH₂, and 0.50 mmol (77.1 mg) vinylcyclohexanol **SI-2.48** producing a 5.7:1.0 ratio of **2.48b** to **2.48a**. The inseparable mixture was subjected to protocol 2. The crude was chromatographed with 0.5% v/v Et₂O/pentane to afford 30.0 mg (60%) of **2.48b** as a clear colorless oil.



Cycloheptanone **2.48b**

¹H NMR (500 MHz, CDCl₃, 25 °C):

δ 2.57 (qd, <i>J</i> = 6.6, 3.5 Hz, 1H)	1.05 (d, <i>J</i> = 6.9 Hz, 3H)
2.51 (ddd, <i>J</i> = 14.4, 10.8, 3.4 Hz, 1H)	0.97 (s, 3H)
2.34 (ddd, <i>J</i> = 16.0, 6.3, 3.3 Hz, 1H)	0.88 (s, 3H)

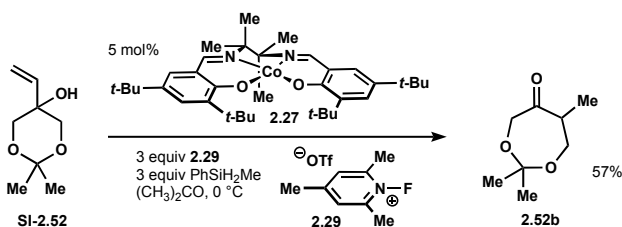
1.69-1.62 (m, 2H), 1.53-1.36 (m, 4H)

¹³C NMR (126 MHz, CDCl₃, 25 °C):

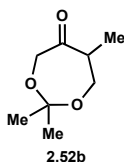
δ 216.3	33.1
46.3	32.4
41.8	28.9
38.9	25.2
36.4	17.3

HRMS (ESI) calculated for C₁₀H₁₈O [M+Na]⁺: 177.1255, found: 177.1257

TLC: R_f = 0.26 (10% Et₂O/hexanes)



Cycloheptanone 2.52b. Prepared according to “**General procedure for the catalytic radical-polar crossover of allylic alcohols**”. The reaction was performed with 0.75 mmol (216.9 mg) of **2.29**, 12.5 μmol (7.6 mg) of **2.27**, 0.75 mmol (103 μL) of MePhSiH_2 , and 0.25 mmol (39.6 mg) vinylcyclohexanol **SI-2.52**. The crude material was chromatographed with 5% v/v Et_2O /pentane to afford 22.6 mg of **2.52b** (57%) as a clear colorless oil.



Cycloheptanone **2.52b**

^1H NMR (500 MHz, CDCl_3 , 25 °C):

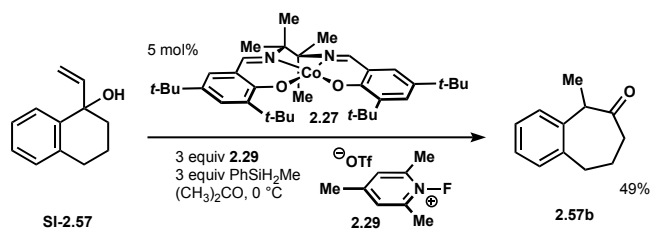
δ 4.09 (t, $J = 5.4$ Hz, 1H)	1.53 (s, 3H)
4.05 (d, $J = 17.7$ Hz, 1H)	1.36 (s, 3H)
3.95 (d, $J = 17.8$ Hz, 1H)	0.99 (d, $J = 6.3$ Hz, 3H)
3.43-3.32 (m, 2H)	

^{13}C NMR (126 MHz, CDCl_3 , 25 °C):

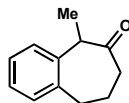
δ 213.0	43.3
101.9	24.5
68.2	23.6
64.6	11.6

HRMS (ESI) calculated for $\text{C}_8\text{H}_{14}\text{O}_3$ $[\text{M}]^+$: 159.0943, found: 159.0951

TLC: $R_f = 0.41$ (30% Et_2O /hexanes)



Cycloheptanone 2.57b. Prepared according to “General procedure for the catalytic radical-polar crossover of allylic alcohols”. The reaction was performed with 0.45 mmol (130.2 mg) of **2.29**, 7.5 μmol (4.5 mg) of **2.27**, 0.45 mmol (62 μL) of MePhSiH_2 , and 0.15 mmol (26.1 mg) vinylcyclohexanol **SI-2.57**. The crude material was chromatographed with 5% v/v Et_2O /pentane to afford 12.8 mg of **2.57b** (49%) as a clear colorless oil. Spectral data for **2.57b** matches data previously reported.⁴¹



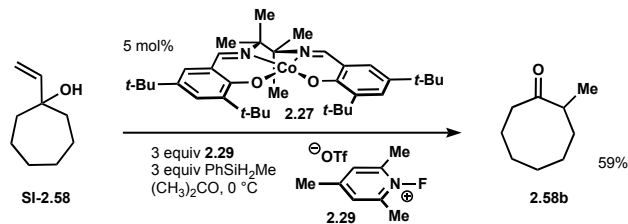
2.57b

^1H NMR (500 MHz; CDCl_3):

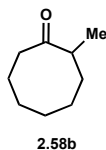
δ 7.31-7.24 (m, 4H)	2.75-2.70 (m, 1H)
7.21-7.19 (m, 1H)	2.54 (ddd, $J = 11.7, 6.2, 4.1$ Hz, 1H)
3.54 (q, $J = 7.0$ Hz, 1H)	2.17-2.10 (m, 1H)
3.06-3.00 (m, 1H)	2.03-1.95 (m, 1H)
2.93-2.87 (m, 1H)	1.51 (d, $J = 7.1$ Hz, 3H)

^{13}C NMR (126 MHz; CDCl_3):

δ 211.8	127.2	27.3
139.6	51.0	14.8
138.7	42.4	
129.4	32.5	



Cyclooctanone 2.58b. Prepared according to “General procedure for the catalytic radical-polar crossover of allylic alcohols”. The reaction was performed with 0.6 mmol (173.6 mg) of **2.29**, 10 μ mol (6.1 mg) of **2.27**, 0.6 mmol (82 μ L) of MePhSiH₂, and 0.2 mmol (28.0 mg) of vinylcyclohexanol **SI-2.58**. The crude material was chromatographed (gradient elution: 100% pentane to 15% v/v CH₂Cl₂/pentane) to afford 16.6 mg (59%) of **2.58b** as a clear colorless oil. The NMR spectra of this compound matched those reported in the literature.⁴²



Cyclooctanone **2.58b**

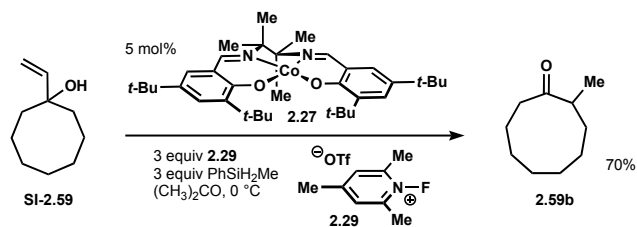
¹H NMR (500 MHz, CDCl₃, 25 °C):

δ 2.60 (dq, $J = 10.1, 6.8, 3.4$ Hz, 1H)	1.65 (dd, $J = 58.9, 3.4$ Hz, 2H)
2.44-2.36 (m, 2H)	1.58-1.37 (m, 4H)
1.96-1.85 (m, 2H)	1.27-1.17 (m, 1H)
1.78 (d, $J = 35.8$ Hz, 1H)	1.05 (d, $J = 6.9$ Hz, 3H)

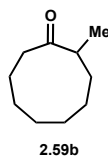
¹³C NMR (126 MHz, CDCl₃, 25 °C):

δ 220.4	26.6
45.3	25.7
40.4	24.6
33.2	16.9
27.0	

TLC: R_f = 0.38 (10% Et₂O/hexanes)



Cyclononanone 2.59b. Prepared according to “**General procedure for the catalytic radical-polar crossover of allylic alcohols**”. The reaction was performed with 3.0 mmol (868 mg) of **2.29**, 0.05 mmol (30.1 mg) of **2.27**, 0.30 mmol (0.41 mL) of MePhSiH₂, and 1.0 mmol (154.3 mg) of alcohol **SI-2.59**. The crude material was chromatographed (gradient elution: 100% hexanes to 30% v/v CH₂Cl₂/hexanes) to afford 107.4 mg (70%) of **2.59b** as a clear colorless oil. The NMR spectra of this compound matched those reported in the literature.⁴³



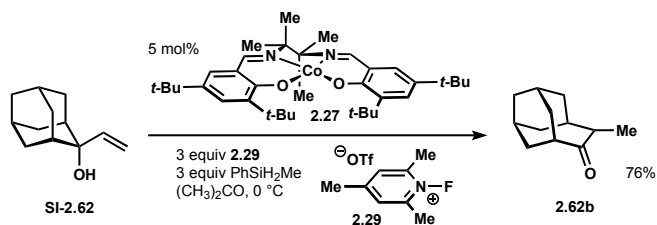
Cyclononanone **2.59b**

¹H NMR (500 MHz, CDCl₃, 25 °C):

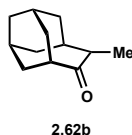
δ 2.66 (dq, <i>J</i> = 9.9, 6.7, 3.2 Hz, 1H)	1.73-1.66 (m, 1H)
2.52-2.47 (m, 1H)	1.64-1.25 (m, 10H)
2.39 (ddd, <i>J</i> = 13.2, 9.6, 3.5 Hz, 1H)	1.04 (d, <i>J</i> = 6.8 Hz, 3H)
1.90-1.75 (m, 3H)	

¹³C NMR (126 MHz, CDCl₃, 25 °C):

δ 220.1	25.1
47.4	24.76
41.1	24.58
32.0	24.4
26.1	17.2



Ketone 2.62b. Prepared according to “General procedure for the catalytic radical-polar crossover of allylic alcohols”. The reaction was performed with 0.6 mmol (173.6 mg) of **2.29**, 10 μ mol (6.1 mg) of **2.27**, 0.6 mmol (82 μ L) of MePhSiH₂, and 0.2 mmol (35.7 mg) of vinylcyclohexanol **SI-2.62**. The crude material was chromatographed (gradient elution: 100% hexanes to 10% v/v Et₂O/hexanes) to afford 27.2 mg (76%) of **2.62b** as a clear colorless oil. Spectral data match those reported in the literature.⁴⁴



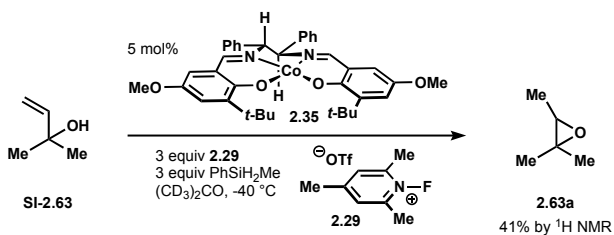
Ketone **2.62b**

¹H NMR (500 MHz, CDCl₃, 25 °C):

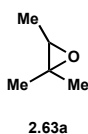
δ 2.80 (t, J = 6.1 Hz, 1H)	1.82-1.80 (m, 1H)
2.57-2.52 (m, 1H)	1.77-1.74 (m, 2H)
2.19-2.15 (m, 1H)	1.71-1.68 (m, 2H)
2.03 (dd, J = 23.1, 0.2 Hz, 2H)	1.23 (d, J = 7.2 Hz, 3H)
1.94-1.87 (m, 5H)	

¹³C NMR (126 MHz, CDCl₃, 25 °C):

δ 219.7	35.7	30.9
51.7	33.63	26.95
48.8	33.60	26.85
39.9	31.6	17.5



Epoxide 2.63a. Prepared according to “**General procedure for the catalytic radical-polar crossover of allylic alcohols**”. The reaction was performed with 0.3 mmol (86.8 mg) of **2.29**, 5 μ mol (3.2 mg) of **2.35**, 0.3 mmol (41 μ L) of MePhSiH₂, and 0.1 mmol (10.4 μ L) of 3-buten-2-ol producing a 3.4:1.0 ratio of **2.63a** to **2.63b**. 0.1 mmol (14 μ L) of mesitylene was added directly to the reaction mixture, which was transferred into an NMR tube for analysis. The NMR yield was determined by integration of relevant peaks (3 methyl multiplet 1.25-1.15, 9H) and was found to be 41%. A standard of the NMR spectrum of this compound in acetone-*d* was obtained by analysis of a sample purchased from Sigma-Aldrich, 97%.

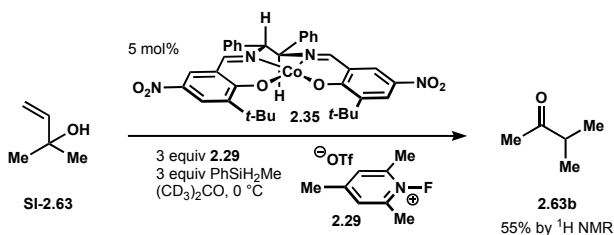


Epoxide **2.63a**

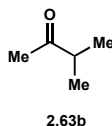
¹H NMR (500 MHz, (CD₃)₂CO, 25 °C):

δ 2.74 (q, *J* = 5.5 Hz, 1H)

1.25 – 1.15 (m, 9H)



Ketone 2.63b. Prepared according to “General procedure for the catalytic radical-polar crossover of allylic alcohols”. The reaction was performed with 0.3 mmol (86.8 mg) of **2.29**, 5 μmol (3.4 mg) of **2.33**, 0.3 mmol (41 μL) of MePhSiH₂, and 0.1 mmol (10.4 μL) of 3-buten-2-ol. 0.1 mmol (14 μL) of mesitylene was added directly to the reaction mixture, which was transferred into an NMR tube for analysis. The NMR yield was determined by integration of relevant peaks (2 methyl doublet 1.05 ppm, 6H) and was found to be 55%. A standard of the NMR spectrum of **2.63b** in acetone-*d* was obtained by analysis of a sample purchased from Sigma-Aldrich, 99%.



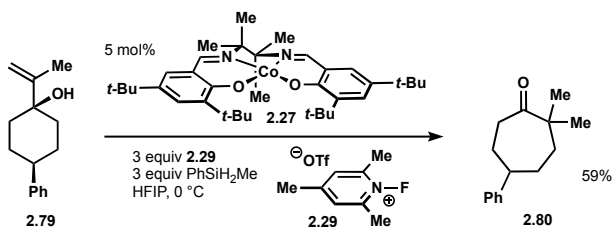
Ketone **2.63b**

¹H NMR (500 MHz, (CD₃)₂CO, 25 °C):

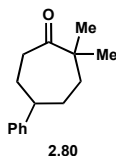
δ 2.61 (sept, *J* = 6.9 Hz, 1H)

2.09 (s, 3H)

1.05 (d, *J* = 7.1 Hz, 6H)



Ketone 2.80. Prepared according to “General procedure for the catalytic radical-polar crossover of allylic alcohols”. The reaction was performed with 0.30 mmol (86.8 mg) of **2.29**, 5.0 μmol (3.0 mg) of **2.27**, 0.30 mmol (41 μL) of MePhSiH₂, and 0.10 mmol (21.6 mg) of vinylcyclohexanol **2.79**. The crude was chromatographed (gradient elution: 100% pentane to 15% v/v CH₂Cl₂/pentane) to deliver 11.1 mg (59%) of **2.80** as a colorless oil.



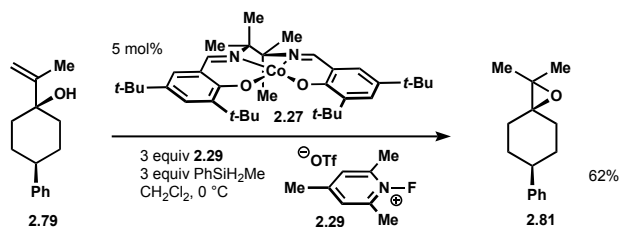
Ketone 2.80

¹H NMR (500 MHz, CDCl₃, 25 °C):

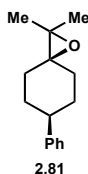
δ 7.28 (t, <i>J</i> = 7.6 Hz, 2H)	2.07 (dddt, <i>J</i> = 14.0, 6.9, 4.5, 2.3 Hz, 1H)
7.19 (t, <i>J</i> = 7.4 Hz, 1H)	1.90 (td, <i>J</i> = 14.5, 9.6 Hz, 2H)
7.16-7.14 (m, 2H)	1.80 (dd, <i>J</i> = 14.6, 8.8 Hz, 1H)
2.94 (ddd, <i>J</i> = 13.0, 11.2, 2.1 Hz, 1H)	1.67-1.49 (m, 3H)
2.71 (tt, <i>J</i> = 12.0, 3.4 Hz, 1H)	1.26 (s, 1H)
2.41 (ddd, <i>J</i> = 11.2, 7.1, 2.1 Hz, 1H)	1.16 (s, 3H)
	1.14 (s, 3H)

¹³C NMR (126 MHz, CDCl₃, 25 °C):

δ 218.0	48.9	32.5
146.9	47.8	27.8
128.5	39.2	23.5
126.7	39.0	
126.2	34.2	



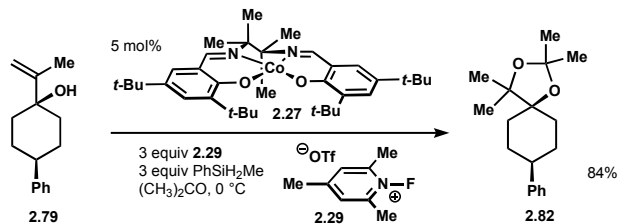
Epoxide 2.81. Prepared according to “**General procedure for the catalytic radical-polar crossover of allylic alcohols**” The reaction was performed with 0.14 mmol (40.2 mg) of **2.29**, 2.3 μmol (1.4 mg) of **2.27**, 0.14 mmol (19 μL) of MePhSiH_2 , and 0.046 mmol (10.0 mg) vinylcyclohexanol **2.79**. The crude material was chromatographed (gradient elution: 100% hexanes to 6% v/v Et_2O /hexanes) to afford 6.8 mg (62%) of **2.81** as a white film.



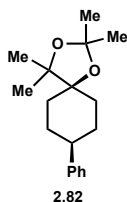
Epoxide **2.30**

^1H NMR (500 MHz, CDCl_3 , 25 °C):

δ 7.38-7.35 (m, 2H)	1.96-1.90 (m, 2H)
7.30-7.25 (m, 3H)	1.86-1.82 (m, 2H)
2.76-2.70 (m, 1H)	1.67-1.59 (m, 2H)
2.13-2.08 (m, 2H)	1.47 (s, 6H)



Epoxide 2.30. Prepared according to “**General procedure for the catalytic radical-polar crossover of allylic alcohols**” The reaction was performed with 0.15 mmol (43.4 mg) of **2.29**, 2.5 μ mol (1.5 mg) of **2.27**, 0.15 mmol (21 μ L) of MePhSiH₂, and 0.05 mmol (10.6 mg) vinylcyclohexanol **2.79**. The crude material was chromatographed (gradient elution: 100% hexanes to 6% v/v Et₂O/hexanes) to afford 11.5 mg (84%) of **2.82** as a white film.



Acetonide 2.82

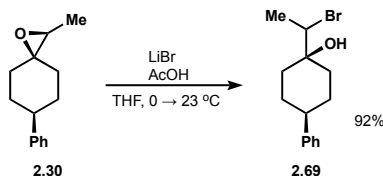
¹H NMR (500 MHz, CDCl₃, 25 °C):

δ 7.39-7.33 (m, 4H)	1.89-1.86 (m, 2H)
7.28-7.24 (m, 1H)	1.52 (s, 6H)
2.61-2.54 (m, 1H)	1.46 (ddd, $J = 15.6, 11.0, 4.4$ Hz, 3H)
2.05-1.95 (m, 4H)	1.31 (s, 6H)

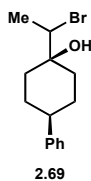
¹³C NMR (126 MHz, CDCl₃, 25 °C):

δ 147.2	106.3	32.6
128.3	82.8	30.05
127.0	82.6	29.99
126.0	44.1	24.4

Synthesis of Bromohydrins



Bromohydrin 2.69. Glacial acetic acid (66 μ L, 1.2 mmol) was added to a cooled solution of **2.30** (43.5 mg, 0.215 mmol) and LiBr (86.8 mg, 1.0 mmol) in THF (0.75 mL, 0.31M) at 0 °C in an ice bath. After stirring for 5 min at 0 °C, the reaction was allowed to warm to room temperature. After 7 h the reaction was quenched with 0.75 mL saturated aqueous NaHCO₃ and all contents transferred to a separatory funnel. The aqueous layer was extracted with Et₂O 3x in 10 mL portions (30 mL total). The combined organic layers were washed 1x with brine, dried over Na₂SO₄, and concentrated in vacuo. The crude material was purified by flash column chromatography (gradient elution: 100% hexanes to 20% v/v Et₂O/hexanes) to afford 55.8 mg (92%) of bromohydrin **2.69** as a white solid.



Bromohydrin **2.69**

¹H NMR (500 MHz, CDCl₃, 25 °C):

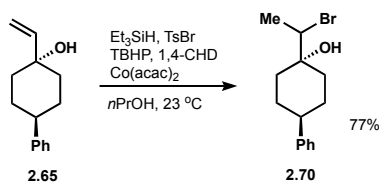
δ 7.30 (t, J = 7.5 Hz, 2H)	2.49-2.43 (m, 1H)	1.76 (s, 1H)
7.25 (d, J = 6.9 Hz, 2H)	2.00-1.86 (m, 4H)	1.61-1.52 (m, 3H)
7.21-7.18 (m, 1H)	1.81-1.79 (m, 1H)	
4.25 (q, J = 6.9 Hz, 1H)	1.77 (d, J = 6.9 Hz, 3H)	

¹³C NMR (126 MHz, CDCl₃, 25 °C):

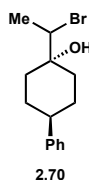
δ 146.7	72.1	32.8
128.4	65.1	29.41
126.9	43.9	29.28
126.1	36.1	20.8

HRMS (CI) calculated for C₁₄H₁₉BrO [M]⁺: 284.0600, found: 284.0574

TLC: R_f = 0.33 (20% Et₂O/hexanes)



Bromohydrin 2.70. **2.70** was prepared following the hydrobromination protocol outlined by the Herzon lab.⁴⁵ A flame dried 5 mL long necked round bottom flask containing **2.65** (101.2 mg, 0.5 mmol), tosyl bromide (293.9 mg, 1.25 mmol), and Co(acac)₂ (128.6 mg, 0.5 mmol) capped with septum was evacuated 3x via hi-vac and backfilled with a balloon of argon. The flask was then charged sequentially with *n*-PrOH (1.67 mL, 0.30 M), 1,4-cyclohexadiene (177 μ L, 1.88 mmol), *tert*-butyl hydroperoxide (90.9 μ L of a 0.5 M solution in decane, 0.5 mmol) and triethylsilane (800 μ L, 5.0 mmol). The reaction was stirred for 4 h, then diluted with 2 mL water and transferred to a separatory funnel. The aqueous layer was extracted with Et₂O 3x in 10 mL portions (30 mL total). The combined organic layers were washed 1x with brine, dried over Na₂SO₄, and concentrated in vacuo. The crude material was purified by flash column chromatography (gradient elution: 100% hexanes to 20% v/v Et₂O/hexanes) to afford 109.7 mg (77%) of bromohydrin **2.70** as a white solid.



Bromohydrin 2.70

¹H NMR (500 MHz, CDCl₃, 25 °C):

δ 7.33-7.30 (m, 2H)	2.31-2.24 (m, 1H)	1.78 (d, J = 6.8 Hz, 3H)
7.24-7.19 (m, 3H)	2.10 (s, 1H)	1.74 (td, J = 13.3, 3.7 Hz, 1H)
4.76 (q, J = 6.8 Hz, 1H)	2.05-2.01 (m, 1H)	1.68-1.59 (m, 2H)
2.69-2.63 (m, 1H)	1.94-1.91 (m, 2H)	1.53-1.44 (m, 1H) 1H)

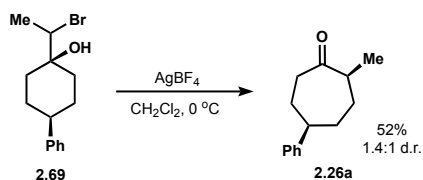
¹³C NMR (126 MHz, CDCl₃, 25 °C):

δ 145.6	126.3	42.7	30.04
128.5	72.7	38.9	29.99
126.8	59.5	33.2	20.0

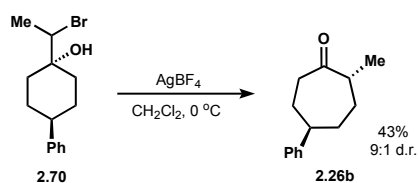
HRMS (CI) calculated for C₁₄H₁₉BrO [M+NH₄]⁺: 300.0963, found: 300.0952

TLC: R_f = 0.26 (20% Et₂O/hexanes)

Silver(I) Promoted Ring Expansions of Bromohydrins



Expansion of Bromohydrin 2.69 to cycloheptanone 2.26a. Silver(I) tetrafluoroborate (14.6 mg, 0.075 mmol) was added in a single portion to a cooled solution of **2.69** (14.2 mg, 0.05 mmol) in CH₂Cl₂ (0.50 mL, 0.1 M) at 0 °C. The reaction was stirred for 5 h at 0 °C, then diluted with H₂O (2 mL) and contents transferred to a separatory funnel. The aqueous layer was extracted with CH₂Cl₂ 3x in 10 mL portions (30 mL total). The combined organic layers were washed 1x with brine, dried over Na₂SO₄, and concentrated in vacuo. The crude material was taken up in CDCl₃ and an internal standard of mesitylene was added. Analysis by ¹HNMR determined a 52% yield of **2.26a** in 1.4:1 d.r.



Expansion of Bromohydrin 2.70 to cycloheptanone 2.26b. Silver(I) tetrafluoroborate (14.6 mg, 0.075 mmol) was added in a single portion to a cooled solution of **2.70** (14.2 mg, 0.05 mmol) in CH₂Cl₂ (0.50 mL, 0.1 M) at 0 °C. The reaction was stirred for 2 h at 0 °C, then diluted with H₂O (2 mL) and contents transferred to a separatory funnel. The aqueous layer was extracted with CH₂Cl₂ 3x in 10 mL portions (30 mL total). The combined organic layers were washed 1x with

brine, dried over Na₂SO₄, and concentrated in vacuo. The crude material was taken up in CDCl₃ and an internal standard of mesitylene was added. Analysis by ¹HNMR determined a 43% yield of **2.26b** in 9:1 d.r.

2.9 References and Notes

1. For pioneering work on relevant hydrofunctionalizations see: Mukaiyama, T.; Yamada, T. *Bull. Chem. Soc. Jpn.* **1995**, *68*, 17.
2. For an excellent review of MHAT hydrofunctionalizations see: Crossley, S. W. M.; Obradors, C.; Martinez, R. M.; Shenvi, R. A. *Chem. Rev.* **2016**, *116*, 8912.
3. For an excellent review on the chemoselectivity of metal-hydrides to engage alkenes via HAT see: Green, S. A.; Crossley, S. W. M.; Matos, J. L. M.; Vásquez-Céspedes, S.; Shevick, S. L.; Shenvi, R. A. *Acc. Chem. Res.* **2018**, *51*, 2628.
4. For selected examples see: (a) Waser, J.; Nambu, H.; Carreira, E. M. *J. Am. Chem. Soc.* **2005**, *127*, 8294. (b) Gaspar, B.; Carreira, E. M. *Angew. Chem., Int. Ed.* **2007**, *46*, 4519. (c) Gaspar, B.; Carreira, E. M. *Angew. Chem., Int. Ed.* **2008**, *47*, 5758. (d) Gaspar, B.; Carreira, E. M. *J. Am. Chem. Soc.* **2009**, *131*, 13214. (e) Girijavallabhan, V.; Alvarez, C.; Njoroge, F. G. *J. Org. Chem.* **2011**, *76*, 6442. (f) Barker, T.; Boger, D. L. *J. Am. Chem. Soc.* **2012**, *134*, 13588. (g) Leggans, E. K.; Barker, T. J.; Duncan, K. K.; Boger, D. L. *Org. Lett.* **2012**, *14*, 1428. (h) Shigehisa, H.; Nishi, E.; Fujisawa, M.; Hiroya, K. *Org. Lett.* **2013**, *15*, 5158. (i) Iwasaki, K.; Wan, K. K.; Oppedisano, A.; Crossley, S. W. M.; Shenvi, R. A. *J. Am. Chem. Soc.* **2014**, *136*, 1300. (j) King, S. M.; Ma, X.; Herzon, S. B. *J. Am. Chem. Soc.* **2014**, *136*, 6884. (k) Ma, X. S.; Herzon, S. B. *Chem. Sci.* **2015**, *6*, 6250. (l) Zheng, J.; Wang, D.; Cui, S. *Org. Lett.* **2015**, *17*, 4572. (m) Crossley, S. W. M.; Martinez, R. M.; Guevara-Zuluaga, S.; Shenvi, R. A. *Org. Lett.* **2016**, *18*, 2620. (n) Ma, X.; Herzon, S. B. *J. Am. Chem. Soc.* **2016**, *138*, 8718.
5. For selected examples, see: (a) Wang, L.-C.; Jang, H.-Y.; Roh, Y.; Lynch, V.; Schultz, A. J.; Wang, X.; Krische, M. J. *J. Am. Chem. Soc.* **2002**, *124*, 9448. (b) Waser, J.; Carreira, E. M. *J. Am. Chem. Soc.* **2004**, *126*, 5676. (c) Smith, D. M.; Pulling, M. E.; Norton, J. R. *J. Am. Chem. Soc.* **2007**, *129*, 770. (d) Lo, J. C.; Yabe, Y.; Baran, P. S. *J. Am. Chem. Soc.* **2014**, *136*, 1304. (e) Lo, J. C.; Gui, J.; Yabe, Y.; Pan, C.-M.; Baran, P. S. *Nature* **2014**, *516*, 343. (f) Crossley, S. W. M.; Barabé, F.; Shenvi, R. A. *J. Am. Chem. Soc.* **2014**, *136*, 16788. (g) Kuo, J. L.; Hartung, J.; Han, A.; Norton, J. R. *J. Am. Chem. Soc.* **2015**, *137*, 1036. (h) Gui, J.; Pan, C.-M.; Jin, Y.; Qin, T.; Lo, J. C.; Lee, B. J.; Spergel, S. H.; Mertzman, M. E.; Pitts, W. J.; La Cruz, T. E.; Schmidt, M. A.; Darvatkar, N.; Natarajan, S.; Baran, P. S. *Science* **2015**, *348*, 886. (i) Dao, H. T.; Li, C.; Michaudel, Q.; Maxwell, B. D.; Baran, P. S. *J. Am. Chem. Soc.* **2015**, *137*, 8046. (j) Zheng, J.; Qi, J.; Cui, S. *Org. Lett.* **2016**, *18*, 128. (k) Lo, J. C.; Kim, D.; Pan, C.-M.; Edwards, J. T.; Yabe, Y.; Gui, J.; Qin, T.; Gutiérrez, S.; Giacoboni, J.; Smith, M. W.; Holland, P. L.; Baran, P. S. *J. Am. Chem. Soc.* **2017**, *139*, 2484. (l) Saladrigas, M.; Bosch, C.; Saborit, G. V.; Bonjoch, J.; Bradshaw, B. *Angew. Chem., Int. Ed.* **2018**, *57*, 182. (m) Saladrigas, M.; Loren, G.; Bonjoch, J.; Bradshaw, B. *ACS Catal.* **2018**, *8*, 11699.

6. (a) Green, S. A.; Matos, J. L. M.; Yagi, A.; Shenvi, R. A. *J. Am. Chem. Soc.* **2016**, *138*, 12779. (b) Green, S.A.; Vaázquez-Céspedes, S.; Shenvi, R. A. *J. Am. Chem. Soc.* **2018**, *140*, 11317. (c) Shevick, S. L.; Obradors, C.; Shenvi, R. A. *J. Am. Chem. Soc.* **2018**, *140*, 12056.
7. Shigehisa, H.; Aoki, T.; Yamaguchi, S.; Shimizu, N.; Hiroya, K. *J. Am. Chem. Soc.* **2013**, *135*, 10306.
8. For examples of MHAT hydrofunctionalizations under catalyst control see references 5f and 6c.
9. For a review on the current mechanistic paradigm of MHAT hydrofunctionalizations see: Shevick, S. L.; Wilson, C. V.; Kotesova, S.; Kim, D.; Holland, P.; Shenvi, R. A. *Chem. Sci.* **2020**, *11*, 12401.
10. Touney, E. E.; Foy, N. J.; Pronin, S. V. *J. Am. Chem. Soc.* **2018**, *140*, 16982.
11. First suggestion of solvent caged alkylradical-metalloradical pair: Franck, J.; Rabinowitch, E. *Trans. Faraday Soc.* **1934**, *30*, 120.
12. For evidence of solvent caged alkylradical-metalloradical pair see: (a) Sweany, R.; Halpern, J. *J. Am. Chem. Soc.* **1977**, *99*, 8335. (b) Jacobsen, E. N.; Bergman, R. G. *J. Am. Chem. Soc.* **1985**, *107*, 2023. (c) Ungváry, F.; Markó, L. *J. Organomet. Chem.* **1983**, *249*, 411. (d) Matsui, Y.; Orchin, M. *J. Organomet. Chem.* **1983**, *244*, 369.
13. Shigehisa H.; Hayashi, M.; Ohkawa, H.; Suzuki, T.; Okayasu, H.; Mukai, M.; Yamazaki, A.; Kawai, R.; Kikuchi, H.; Satoh, Y.; Akane, F.; Hiroya, K. *J. Am. Chem. Soc.* **2016**, *138*, 10597.
14. Ungváry, F.; Markó, L. *Organometallics* **1982**, *1*, 1120.
15. Abley, P.; Dockal, E. R.; Halpern, J. *J. Am. Chem. Soc.* **1972**, *94*, 659.
16. (a) Halpern, J.; Chan, M. S.; Hanson, J.; Roche, T. S.; Topich, J. *J. Am. Chem. Soc.* **1975**, *97*, 1606. (b) Halpern, J.; Topich, J.; Zamaraev, K. I. *Inorg. Chim. Acta* **1976**, *20*, L21. (c) Topich, J.; Halpern, J. *Inorg. Chem.* **1979**, *18*, 1339. (d) Halpern, J.; Chan, M. S.; Roche, T. S.; Tom, G. M. *Acta Chem. Scand.* **1979**, *33a*, 141.
17. Lande, S. S.; Kochi, J. K. *J. Am. Chem. Soc.* **1968**, *90*, 5196.
18. Anderson, S. N.; Ballard, D. H.; Chrzastowski, J. Z.; Dodd, D.; Johnson, M. D. *J. Chem. Soc., Chem. Commun.* **1972**, *0*, 685.
19. Magnuson, R. H.; Halpern, J.; Levitin, I. Ya.; Vol'pin, M. E.; *J. Chem. Soc., Chem. Commun.* **1978**, *0*, 44.
20. Vol'pin, M. E.; Levitin, I. Ya.; Sigan, A. L.; Halpern, J.; Tom, G. M. *Inorg. Chim. Acta.* **1980**, *41*, 271.
21. (a) Wasserman, H. H.; Hearn, M. J.; Cochoy, R. E. *J. Org. Chem.* **1980**, *45*, 2874. For relevant expansions of allenylcyclopropanols, see: (b) Kleinbeck, F.; Toste, F. D. *J. Am. Chem. Soc.* **2009**, *131*, 9178.
22. (a) Clark, G. R.; Thiensathit, S. *Tetrahedron Lett.* **1985**, *26*, 2503. (b) Bernard, A. M.; Frongia, A.; Secci, F.; Piras, P. P. *Chem. Commun.* **2005**, *0*, 3853. (c) Masarwa, A.; Weber, M.; Sarpong, R. *J. Am. Chem. Soc.* **2015**, *137*, 6327. For relevant ring expansions of allenylcyclobutanols, see: (d) Yao, L.-F.; Wei, Y.; Shi, M. *J. Org. Chem.* **2009**, *74*, 9466.
23. For a review of relevant ring expansions, see: Mack, D. J.; Njardarson, J. T. *ACS. Catal.* **2013**, *3*, 272.
24. (a) Liu, Y.; Yeung, Y.-Y. *Org. Lett.* **2017**, *19*, 1422. (b) Song, Z. L.; Fan, C. A.; Tu, Y. Q. *Chem. Rev.* **2011**, *111*, 7523.
25. (a) Schrauzer, G. N.; Windgassen, R. J. *J. Am. Chem. Soc.* **1966**, *88*, 3738. (b) Costa, G.; Mestroni, G.; Stefani, L. *J. Organomet. Chem.* **1967**, *7*, 493. (c) Costa, G.; Mestroni, G.; Pellizer, G. *J. Organomet. Chem.* **1968**, *11*, 333. (d) McAllister, R. M.; Weber, J. H. *J.*

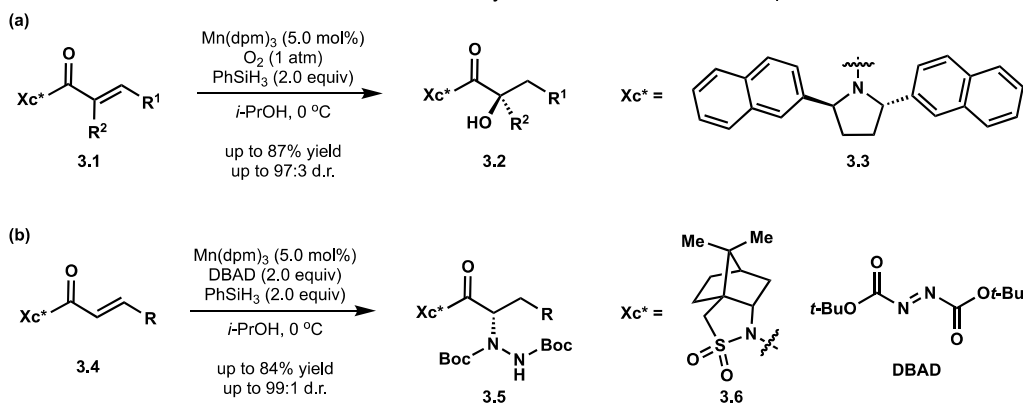
- Organomet. Chem.* **1974**, *77*, 91. (e) Li, G.; Zhang, F. F.; Chen, H.; Yin, H. F.; Chen, H. L.; Zhang, S. Y. *J. Chem. Soc., Dalton Trans.* **2002**, 105.
26. Shigehisa, H.; Koseki, N.; Shimizu, N.; Fujisawa, M.; Niitsu, M.; Hiroya, K. *J. Am. Chem. Soc.* **2014**, *136*, 13534.
 27. Shigehisa H.; Hayashi, M.; Ohkawa, H.; Suzuki, T.; Okayasu, H.; Mukai, M.; Yamazaki, A.; Kawai, R.; Kikuchi, H.; Satoh, Y.; Akane, F.; Hiroya, K. *J. Am. Chem. Soc.* **2016**, *138*, 10597.
 28. (a) Schrauzer, G. N.; Grate, J. H. *J. Am. Chem. Soc.* **1981**, *103*, 541. (b) Tsou, T.-T.; Loots, M.; Halpern, J. *J. Am. Chem. Soc.* **1982**, *104*, 623. (c) Ng, F. T. T.; Rempel, G. L.; Mancuso, C.; Halpern, J. *Organometallics* **1990**, *9*, 2762.
 29. Tsuji, N.; Kobayashi, Y.; Takemoto, Y. *Chem. Commun.* **2014**, *50*, 13691.
 30. Samsel, E. G.; Kochi, J. K. *J. Am. Chem. Soc.* **1986**, *108*, 4790.
 31. Chiang, L.; Allen, L. E. N.; Alcantara, J.; Wang, M. C. P.; Storr, T.; Shaver, M. P. *Dalton Trans.* **2014**, *43*, 4295.
 32. Zhu, L.-L.; Li, X.-X.; Zhou, W.; Li, X.; Chen, Z. *J. Org. Chem.* **2011**, *76*, 8814.
 33. Kobayashi, T.; Shimura, T.; Kurita, Y.; Katsumata, Y.; Kezuka, S. *Tetrahedron Letters* **2014**, *55*, 2818.
 34. Jayaseeli, A. M. I.; Ramdass, A.; Rajagopal, S. *Polyhedron* **2015**, *100*, 59.
 35. Ford, D. D.; Nielsen, L. P.; Zuendt, S. J.; Musgrave, C. B.; Jacobsen, E. N. *J. Am. Chem. Soc.* **2013**, *135*, 15595.
 36. Palucki, M.; Finney, N. S.; Pospisil, P. J.; Gueler, M. L.; Ishida, T.; Jacobsen, E. N. *J. Am. Chem. Soc.* **1998**, *120*, 948.
 37. Lee, Y. E.; Cao, T.; Torruellas, C.; Kozlowski, M. C. *J. Am. Chem. Soc.* **2014**, *136*, 6782.
 38. Miralles, N.; Alam, R.; Szabó, K. J.; Fernández, E. *Angew. Chem. Int. Ed.* **2016**, *55*, 4303.
 39. RajanBabu, T. V.; Nugent, W. A. *J. Am. Chem. Soc.* **1994**, *116*, 986.
 40. Van Buijtenen, J.; Van As, B. A. C.; Verbruggen, M.; Roumen, Luc.; Vekemans, J. A. J. M.; Pieterse, K.; Hilbers, P. A.; Hulsorf, L. A.; Palmans, A. R. A.; Meijer, E. W. *J. Am. Chem. Soc.* **2007**, *129*, 7373.
 41. Justik, M. W.; Koser, G. F. *Molecules*, **2005**, *10*, 217.
 42. van Buijtenen, J.; van As, B. A. C.; Verbruggen, M.; Roumen, L.; Vekemans, J. A. J. M.; Pieterse, K.; Hilbers, P. A. J.; Hulshof, L. A.; Palmans, A. R. A.; Meijer, E. W. *J. Am. Chem. Soc.* **2007**, *129*, 7393.
 43. Tomooka, K.; Ezawa, T.; Inoue, H.; Uehara, K.; Igawa, K. *J. Am. Chem. Soc.* **2011**, *133*, 1754.
 44. Krasutsky, P. A.; Kolomitsyn, I. V.; Kiprof, P.; Carlson, R. M.; Sydorenko, N. A.; Fokin, A. A. *J. Org. Chem.* **2001**, *66*, 1701.
 45. Ma, X.; Herzon, S. B. *Chem. Sci.* **2015**, *6*, 6250.

Chapter 3: Catalytic Asymmetric Radical–Polar Crossover Hydroalkoxylation

3.1 Introduction

As previously discussed, HAT-initiated radical reactions have seen a renaissance in recent decades due to the realization that metal-hydrides enable mild hydrofunctionalization of alkenes with exceptional chemo- and regioselectivity.^{1–3} Intermediate carbon-centered radicals generated by HAT have been intercepted with atom or group transfer reagents,⁴ engaged by addition into C–C multiple bonds,⁵ undergone transmetallation events,⁶ or oxidized to afford carbocationic intermediates that can capture conventional polar nucleophiles.⁷ However, due to a lack of catalyst-controlled methods, enantioselective HAT hydrofunctionalizations have remained elusive.⁸ The few instances of stereoselective MHAT alkene hydrofunctionalization represented in the literature rely on stereochemical relay from the substrate.² For example, Yamada accomplished highly stereoselective alkene hydration⁹ and hydrohydrazination¹⁰ of α,β -unsaturated carboxamides by preinstallation of C_2 -symmetric chiral auxiliaries that impart facial selectivity for radical capture (**Scheme 3.1**). The lack of stereoselective HAT hydrofunctionalizations is not surprising given the inherent challenges associated with enantiodifferentiation of prochiral alkyl radical intermediates.¹¹

Scheme 3.1 Yamada's stereoselective HAT hydrofunctionalizations of α,β -unsaturated carboxamides

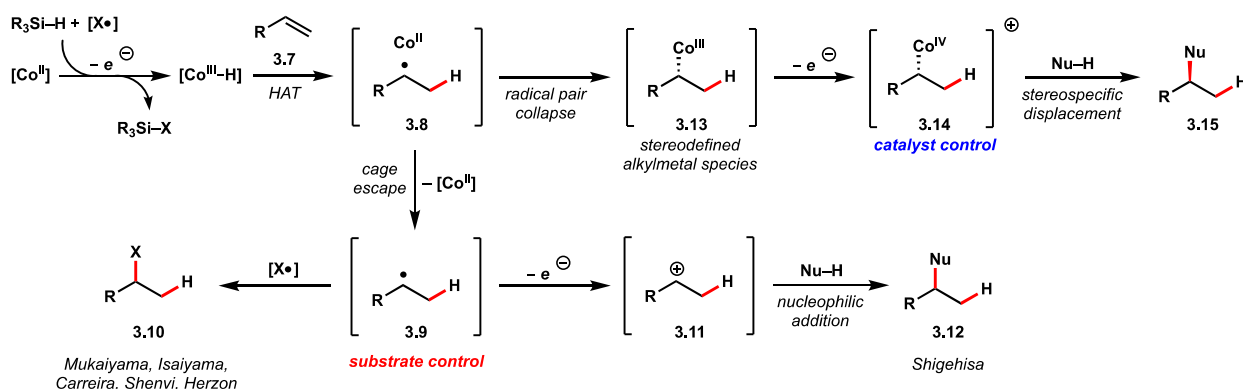


In Chapter 2 I described our discovery of a cobalt-catalyzed HAT radical–polar crossover hydrofunctionalization of tertiary alcohols that afforded corresponding epoxide and semipinacol products.¹² The reaction was under strong catalyst control which implicates the participation of electrophilic alkylcobalt(IV) intermediates.¹³ We sought to elaborate upon this methodology to accomplish enantioselective hydrofunctionalization via judicious choice of scalemic cobalt catalyst. In this chapter, I describe investigations conducted by myself and my colleague Dr. Christopher Discolo that led to the development of the first highly enantioselective method for catalytic asymmetric HAT-mediated radical–polar crossover alkene hydrofunctionalization.¹⁴

3.2 Strategy for Catalytic Asymmetric Radical–Polar Crossover Hydroalkoxylation

We sought to address the lack of catalyst-controlled stereoselective reactions by developing a catalyst system capable of enantiodifferentiation of prochiral alkyl radical intermediates to generate stereodefined alkyl metal intermediates. Accomplishing this task would require thorough understanding of the competing stereoablative processes one must contend with following the delivery of hydrogen atom to the alkene. A general proposed mechanism for our desired transformation as well as competing pathways anticipated is outlined in **Scheme 3.2**. We propose initial formation of putative cobalt(III) hydride by treatment of a scalemic cobalt(II) salen complex with a single-electron oxidant and silane.¹⁵ HAT from the cobalt(III) hydride to monosubstituted alkene **3.7** gives rise to solvent caged alkyl radical-metalloradical pair **3.8**.¹⁶ Solvent cage escape can occur to liberate alkyl radical **3.9** which is stereoablative and results in substrate control. Mukaiyama-type HAT hydrofunctionalizations as well as Shigehisa radical–polar crossover processes are proposed to proceed via free radical **3.9** which explains why highly enantioselective variants of these reaction manifolds have yet to be reported.¹⁷

Scheme 3.2 Strategy for asymmetric HAT radical–polar crossover alkene hydrofunctionalization



Conversely, a catalyst controlled pathway can be accessed if radical pair collapse occurs within the solvent caged radical pair to generate alkylcobalt(III) intermediate **3.13** containing a stereodefined alkyl–metal bond. Herein lies the first set of potential complications. In order for asymmetric induction to occur, radical pair collapse must occur faster than cage escape. Furthermore, we hope to form alkylcobalt **3.13** in a stereoselective fashion using a scalemic cobalt catalyst capable of enantiodifferentiation of prochiral alkyl radicals. If radical pair collapse is enantioselective but highly reversible, reorganization within the solvent cage may erode the stereochemical integrity of the C–Co bond, resulting in the formation of **3.13** as a racemate. However, reversible radical recombination could be advantageous if initial alkylcobalt formation is unselective and **3.13** can equilibrate to a single stereoisomer. Assuming successful production of **3.13** with high degrees of enantioinduction, single-electron oxidation would furnish electrophilic and enantioenriched alkylcobalt(IV) species **3.14**. Final stereospecific nucleophilic displacement of stereodefined **3.14** would afford enantioenriched hydrofunctionalization product **3.15** and terminate the catalytic cycle.

In summary, our scalemic cobalt catalyst must be capable of efficient HAT, undergo rapid radical pair collapse, maintain a stereodefined alkyl metal bond, and undergo stereospecific nucleophilic displacement with high efficiency. To assess our probability of success in achieving

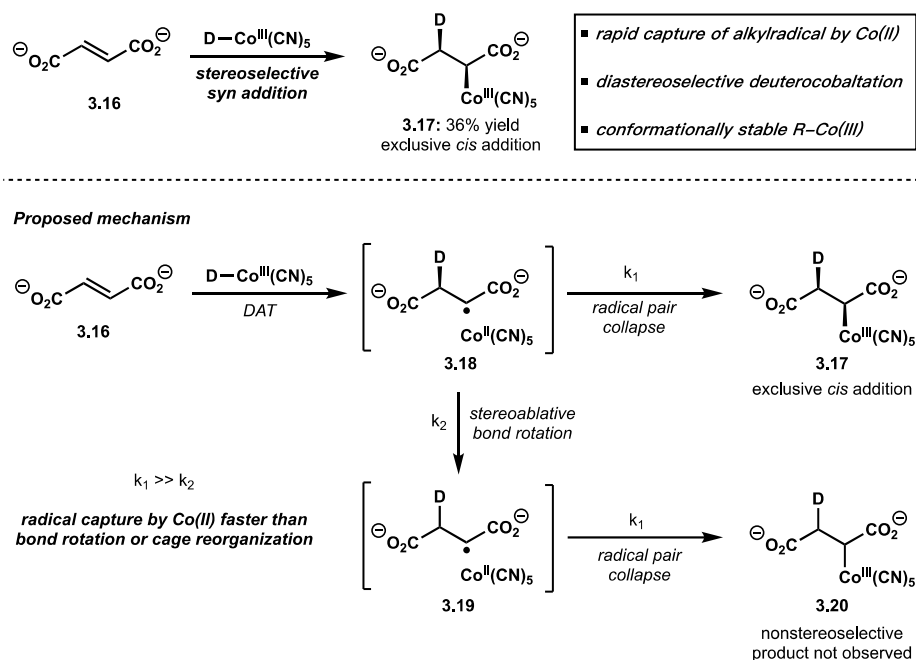
these goals, we scoured the literature not only for precedent to support the feasibility of each described elementary step that could prove problematic, but to guide our approaches towards overcoming these potential pitfalls as well.

3.3 Key Precedents for Method Development

3.3.1 Jackman's Stereoselective Deuterocobaltation

We found precedent for stereoselective radical pair collapse in a 1968 report by Jackman detailing an instance of diastereoselective deuterocobaltation (**Scheme 3.3**).¹⁸ In this early report, Jackman employed an isotope labeling strategy using pentacyanocobalt(III) deuteride prepared from hexacyanocobaltate and D₂O to assess the stereoselectivity of formal hydrometallation by ¹H NMR coupling constants. Reaction of fumarate with the pentacyanocobalt(III) deuteride complex resulted in 36% yield of alkylcobalt(III) **3.17** generated with exclusive *cis* diastereoselectivity. The remainder of the mass balance was identified as deuterogenation products formed without stereospecificity. Jackman posited a mechanism that commences with deuterium atom transfer (DAT) from (CN)₅Co(III)-D to enoate **3.16** to form solvent caged alkyl radical-metalloradical pair **3.18**. The authors proposed the observed diastereoselectivity could be attributed to rapid radical pair collapse outcompeting stereoablative bond rotation within the solvent cage. Cage escape allows free alkyl radical to abstract deuterium from a second equivalent of cobalt(III) deuteride and furnish deuterogenation products with no stereoselectivity. This seminal report of stereoselective deuterocobaltation supports our proposed strategy by offering precedent for facile radical pair collapse precluding stereoablative bond rotation and cage escape resulting in diastereoselective formation of alkylcobalt species.

Scheme 3.3 Jackman's stereoselective deutercobaltation

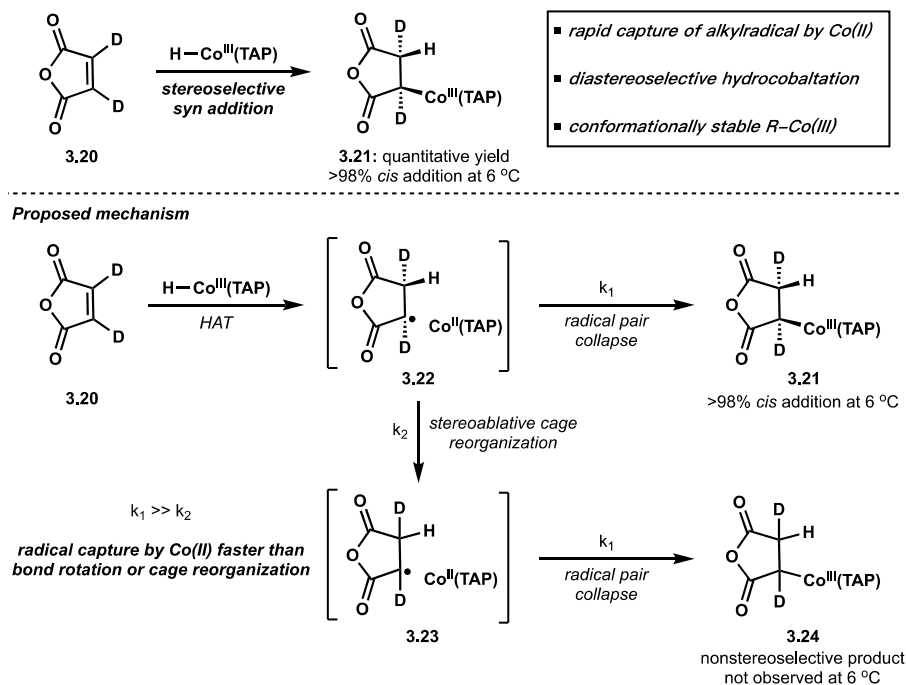


3.3.2 Gridnev's Stereoselective Hydrocobaltation

Nearly three decades after Jackman's observation of *cis* selective deutercobaltation, Gridnev disclosed a similar example of diastereoselective hydrocobaltation while investigating radical chain transfer in cobalt-catalyzed living polymerizations (**Scheme 3.4**).¹⁹ Reaction of tetraanisylporphyrin (TAP) cobalt(III) hydride with *d*₂-maleic anhydride **3.20** afforded hydrocobaltation product **3.21** in quantitative yield and nearly exclusive *cis* selectivity when performed at 6 °C. Gridnev observed reduced stereoselectivity at 23 °C and complete stereochemical erosion upon heating diastereoenriched alkylcobalt(III) **3.21** to 40 °C. The authors propose that the excellent diastereoselectivity observed at lower temperatures is a function of facile radical pair collapse of **3.18** following initial HAT. Stereochemical erosion at elevated temperatures was attributed to reversible carbon–cobalt bond homolysis increasing the opportunities for stereoablative cage reorganization to radical pair **3.19** prior to radical recombination. Gridnev's report provides further evidence for diastereoselective radical pair

collapse following HAT to alkenes. Furthermore, the fact that appreciable stereochemical erosion is not observed until heating to 40 °C is a testament to the conformational stability of the carbon–cobalt bond.

Scheme 3.4 Gridnev's stereoselective hydrocobaltation

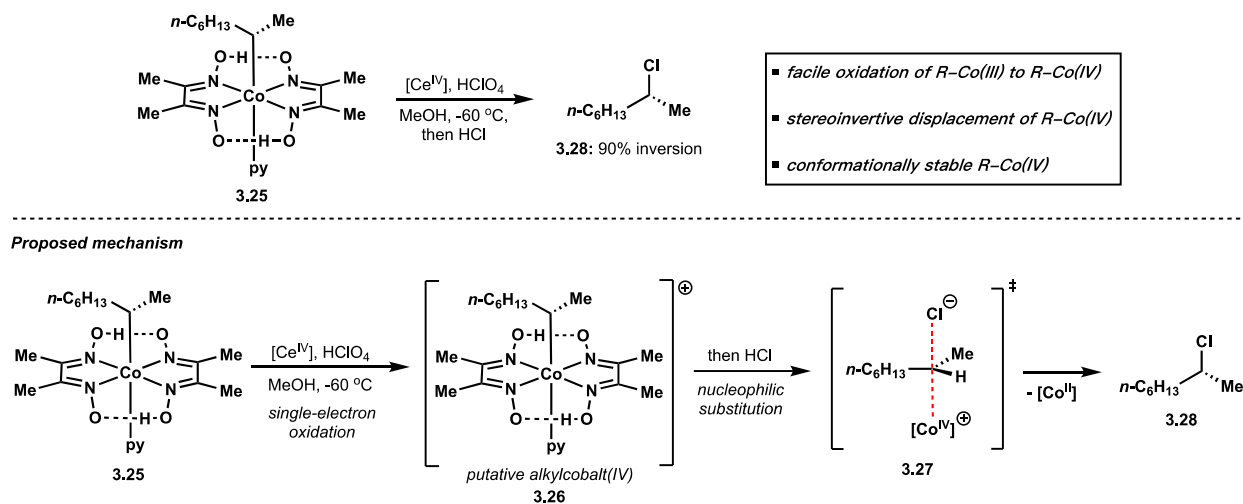


3.3.3 Halpern's Stereospecific Displacement of Alkylcobalt(IV) Complexes

The final steps of our proposed mechanistic strategy are single-electron oxidation of a stereodefined alkylcobalt(III) to a stereodefined alkylcobalt(IV) combined with concomitant nucleophilic displacement. In order for these transforms to occur, the stereodefined alkylcobalt(IV) complex must not be homolytically labile to conserve enantiopurity, yet the C–Co bond must be weak enough towards heterolytic cleavage to partake in facile stereospecific nucleophilic displacement. We found precedent for enantioenriched alkylcobalt(IV) complexes displaying these characteristics in an early report from the Halpern lab (Scheme 3.5).^{13e} In 1978 Halpern disclosed that enantioenriched *sec*-alkylcobalt(III)(dmg) complex **3.25** could undergo single-electron oxidation to corresponding cationic alkylcobalt(IV) complex **3.26** upon treatment with

cerium(IV) in the presence of perchloric acid in methanol at cryogenic temperatures. Subsequent exposure of alkylcobalt(IV) **3.26** to hydrochloric acid furnished alkyl chloride **3.28** with 90% inversion of stereochemistry. Halpern postulated that conversion of alkylcobalt(IV) **3.26** to alkyl chloride proceeds **3.28** via S_N2 type outer sphere nucleophilic substitution that proceeds through a conventional trigonal bipyramidal transition state **3.27**. This report provides precedent for conformationally stable alkylcobalt(IV) complexes undergoing facile heterolytic cleavage with a polar nucleophile with high stereoinversion, confirming that stereochemical information can be relayed from cobalt catalyst to product.

Scheme 3.5 Halpern's stereospecific nucleophilic displacement of alkylcobalt(IV) complexes

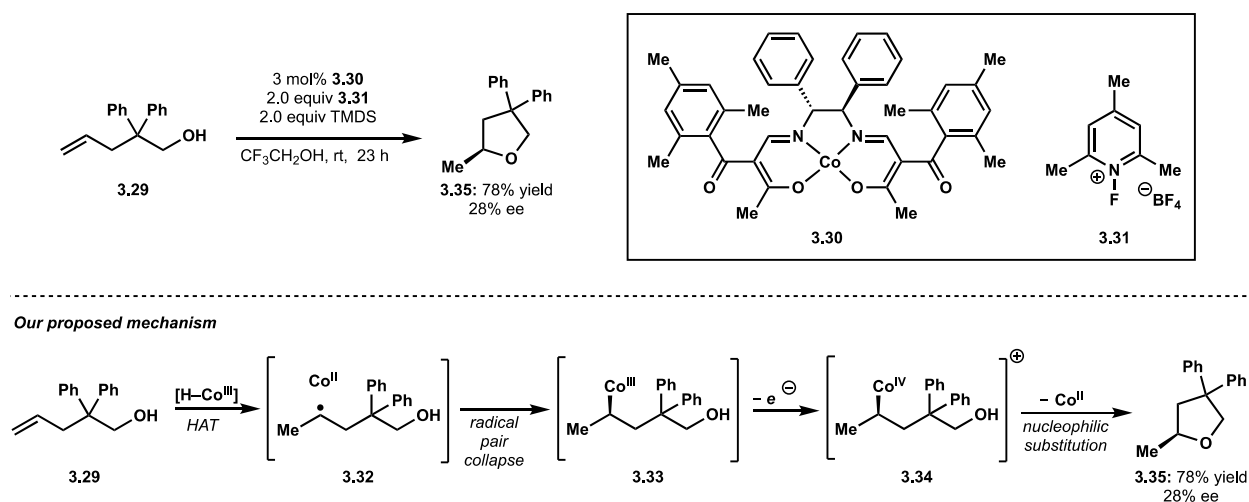


3.3.4 Shigehisa's Intramolecular HAT Radical–Polar Crossover Hydroalkoxylation

The final precedent we used to guide our proposal is a 2016 report from the Shigehisa lab describing a cobalt-catalyzed HAT radical–polar crossover method for converting alkenes bearing pendant alcohols, carboxylic acids, and esters to tetrahydrofurans, lactones, and other oxygen containing heterocycles.²⁰ Near the end of this article, Shigehisa provided a singular preliminary attempt at catalytic asymmetric intramolecular cyclization that proceeded with poor, yet appreciable enantioinduction (**Scheme 3.6**). Curiously, Shigehisa did not invoke alkylcobalt

intermediates and instead solely invoked achiral alkyl radical and carbocationic intermediates. Treatment of 2,2-diphenylpentenol **3.29** with scalemic β -diketoiminate cobalt catalyst **3.30**, *N*-fluorocollidinium tetrafluoroborate oxidant **3.31**, and tetramethyldisiloxane (TMDS) efficiently produced tetrahydrofuran **3.35** in 28% ee. Prior to our work, this lone reaction constituted the only example of enantioselective HAT hydrofunctionalization. We propose a catalyst-controlled process to account for the observed enantioinduction. HAT from cobalt(III) hydride to alkene **3.29** provides solvent caged radical pair **3.32**. Rapid radical pair collapse can then occur to form diastereomerically enriched alkylcobalt(III) **3.33**. Facile single-electron oxidation of **3.33** to conformationally stable cationic alkylcobalt(IV) **3.34** then induces stereospecific nucleophilic displacement to furnish cyclization product **3.35** in mild enantiomeric excess. Since we are also working within the purview of radical–polar crossover hydrofunctionalization using very similar reagents, Shigehisa’s report of enantioselectivity gave us hope that a highly enantioselective transformation could be achieved.

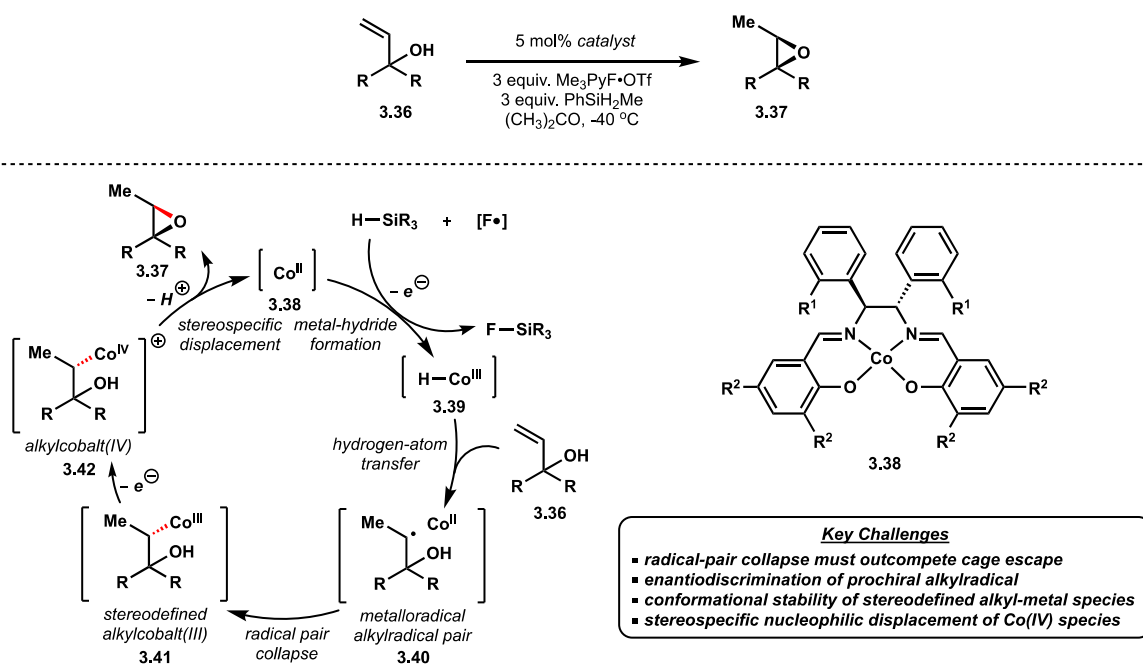
Scheme 3.6 Shigehisa’s intramolecular HAT radical–polar crossover hydroalkoxylation



3.4 Strategy Design

Building upon our catalyst controlled hydrofunctionalizations described in Chapter 2, we proposed that efficient catalyst-controlled stereochemical relay in a HAT radical–polar crossover process could be achieved by utilizing scalemic Co(II) salen complexes to afford enantioenriched epoxides from tertiary allylic alcohols (**Scheme 3.7**). Salen ligands bearing diphenyl substitution on the ethylenediamine backbone previously provided an excellent framework for exploring the reactivity of alkylcobalt complexes. We believed that investigating the chemical space around the C₂-symmetric diamine substitution (R¹) could prove essential for enantioinduction. Manipulating the electronics of the salicylaldehyde had dramatic effects on leaving group ability of the alkylcobalt(IV) in our previous report. We proposed tuning the stereoelectronics of the salicylaldehyde fragments of our salen ligands (R²) would likewise prove insightful into controlling the conformational stability of the stereodefined alkyl–metal bond as well as reactivity about the cobalt center in our enantioselective hydrofunctionalization.

Scheme 3.7 Strategy for asymmetric HAT radical–polar crossover hydroalkoxylation

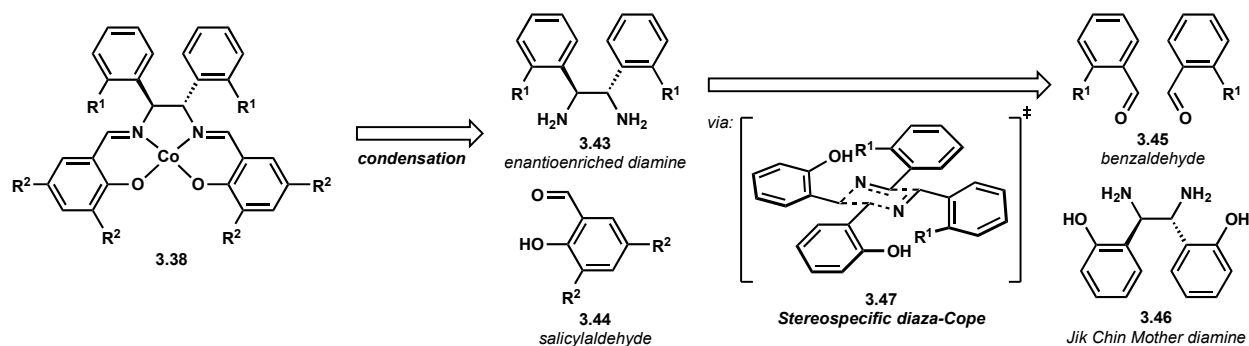


In the context of tertiary allylic alcohols, our proposed mechanism commences with HAT from our scalemic cobalt(III) hydride **3.38** to alkene **3.36** to generate a solvent caged metalloradical-alkyl radical pair **3.40**. Enantiodifferentiation of the prochiral alkyl radical by the catalyst **3.38** allows for stereoselective and facile radical pair collapse to stereodefined *sec*-alkylcobalt(III) **3.41**. Single-electron oxidation of **3.41** to the corresponding cationic alkylcobalt(IV) **3.42** with concomitant intramolecular stereospecific nucleophilic displacement by the pendant alcohol produces enantioenriched epoxide **3.37** and turns over the scalemic cobalt catalyst.

Identifying catalyst structure-activity relationships would be crucial for achieving enantioselective hydroalkoxylation. In order to quickly build a library of Co(II) salen catalysts spanning broad chemical space, we needed a concise synthetic strategy to easily and precisely introduce substitution on the diaryl ethylenediamine motif **3.43** and salicylaldehyde fragments **3.44** (**Figure 3.1**). Creating a robust collection of salicylaldehydes that vary in steric and electronic properties should be achievable through conventional Friedel-Crafts chemistry. However, constructing a diverse library of enantioenriched ethylenediamine backbones was not immediately obvious. The Jik Chin lab reported a method for preparing complex enantioenriched diaryl ethylenediamines **3.43** from two equivalents of benzaldehyde **3.45** and an enantioenriched “Mother diamine” **3.46**.²¹ Double condensation of the benzaldehyde fragments onto the “Mother diamine” promoted a highly stereospecific diaza-Cope rearrangement that was driven by hydrogen bonding interactions²² within the “Mother diamine” moiety. The diaza-Cope rearrangement ultimately generated enantioenriched diamine products embedded with substitution originating from the benzaldehyde fragments. The efficiency of stereochemical relay from “Mother diamine” to diamine product **3.43** was a function of a highly organized chair transition state **3.47**. We

ultimately decided to proceed with Jik Chin's protocol to construct our collection of enantioenriched diaryl diamines due to the extensive catalogue of commercially available benzaldehyde precursors that can be readily elaborated.²³

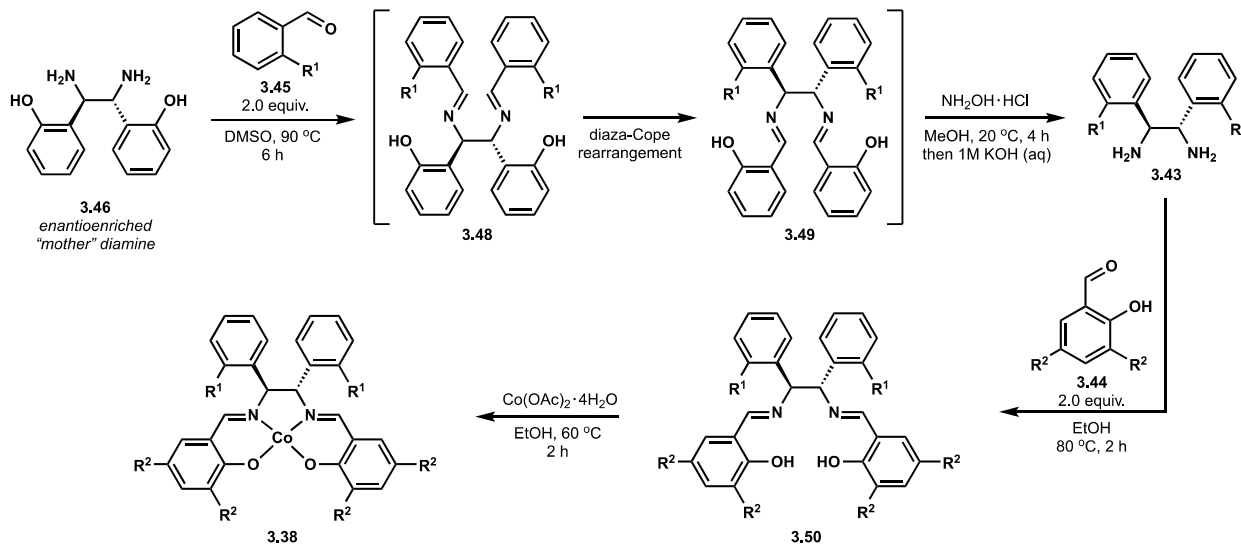
Figure 3.1 Retrosynthetic strategy for exploring Co(II) salen ligand chemical space



In the forward direction, our strategy for preparing enantioenriched salen ligands began with condensation of two equivalents of benzaldehyde **3.45** onto commercially available (*R,R*) Mother diamine to afford diamine **3.48** *in situ* (Scheme 3.8). Stereospecific diaza-Cope generated enantioenriched diimine **3.50**. Use of dimethylsulfoxide (DMSO) as solvent solvent was crucial to executing the condensation-diaza-Cope sequence in a single pot due to the superior solubility of intermediates. Condensation intermediate **3.48** precipitated out of other compatible solvents such as ethanol before diaza-Cope rearrangement could occur. Additionally, higher temperatures and longer reaction times were required to complete the condensation-diaza-Cope cascade if benzaldehyde **3.45** had bulky *ortho* substitution at R¹. Hydrolysis of **3.49** by exposure to methanolic hydroxylamine hydrochloride followed by basic aqueous workup and extraction with dichloromethane furnished freebased diamine **3.43**. Condensation of two equivalents of functionalized salicylaldehyde **3.44** onto diamine **3.43** in refluxing ethanol provided enantioenriched salen ligand **3.50**. Finally, treating salen ligand **3.50** with cobalt(II) acetate tetrahydrate in hot ethanol delivered the desired enantioenriched cobalt(II) salen complex **3.38**.

Notably, the entire synthetic sequence could be executed without chromatographic purification of intermediates with no measurable loss of catalytic efficiency or enantioinduction.

Scheme 3.8 Synthetic strategy for preparing enantioenriched Co(II) salen catalysts



3.5 Catalyst Optimization

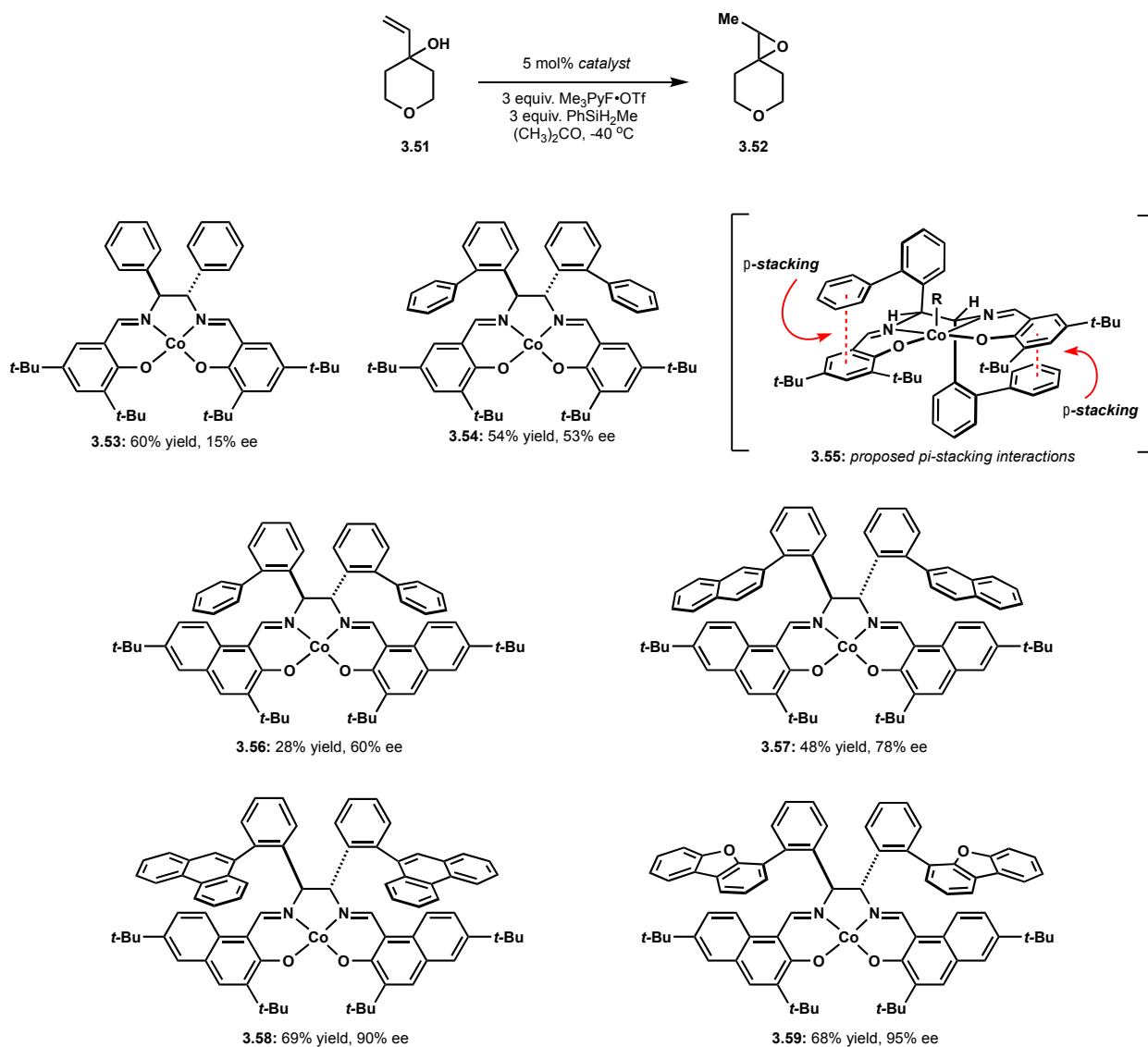
We next turned our efforts towards establishing catalyst structure-activity relationships for the asymmetric HAT-initiated radical-polar crossover hydroalkoxylation (**Table 3.1**). Subjecting pyranone-derived tertiary allylic alcohol **3.51** to the previously optimized hydroalkoxylation conditions using scalemic diphenyl catalyst **3.53** afforded epoxide **3.52** in 60% yield and 15% ee. This result was encouraging because it validated our hypothesis that asymmetric induction was possible to achieve with diaryl substituted Co(II) salen complexes. Chris and I then performed an exhaustive catalyst screen before arriving at *o*-biaryl substituted Co(II) salen complex **3.54** which delivered epoxide **3.52** in 54% yield and 53% ee, a dramatic increase in enantioinduction from previously screened catalysts. We found this result especially perplexing, as the only difference between catalyst **3.53** and **3.54** was the *o*-phenyl substitution on the diamine backbone, yet the two catalysts gave drastically different outcomes respective to enantioselectivity. Preliminary analysis with a modeling kit revealed significant steric clash between the *o*-biaryl groups when positioned

in a stepped pseudo-equatorial conformation. However, it appeared steric interactions could be relieved by twisting the ethylenediamine backbone to position the *o*-biaryl groups in a pseudo-diaxial conformation. In the modeled pseudo-diaxial conformation **3.55**, the *o*-phenyl substituents could position themselves in close proximity directly over the salicylaldehyde motifs of the salen ligand, suggesting that π -stacking interactions may be operative. We proposed that favorable π -stacking interactions within catalyst **3.54** led to increased enantioinduction by rigidifying the catalyst structure, resulting in a well-defined reaction center more capable of enantiodifferentiation of prochiral alkyl radicals. Additionally, π -stacking interactions may be stabilizing proposed alkylcobalt intermediates, leading to enhanced conformational stability during oxidation and displacement that results in superior enantioinduction.

We hypothesized that greater aromatic surface area within the catalyst would increase the proposed π -stacking interactions. Thus, we synthesized *o*-biaryl catalyst **3.55** bearing extended aromatic motifs on the salen ligand derived from 3,6-di-*tert*-butyl-2-hydroxy-1-naphthaldehyde. Subjecting **3.55** to the reaction conditions furnished epoxide **3.52** in a promising 60% ee and 28% yield. Undeterred by the loss of efficiency, we prepared catalyst **3.56** containing *o*-naphthyl substitution on the diamine backbone as well as the naphthaldehyde-derived Schiff base framework. Gratifyingly, **3.56** both increased asymmetric induction and nearly restored efficiency, affording epoxide **3.52** in 78% ee and 48% yield. Expanding arene surface area further by installing phenanthrenes on the *o*-biaryl diamine led to the best performance observed yet, as catalyst **3.57** provided epoxide **3.52** in an impressive 69% yield and 90% ee. Unfortunately, trying to capitalize on the proposed π -stacking interactions by further expansion of the *o*-arene surface area to pyrenyl and anthracenyl substitution led to diminished reactivity and erosion of enantioselectivity, likely due to steric clash with the naphthaldehyde *tert*-butyl groups.

Having apparently run out of room to expand π -surface area, we sought to evaluate the influence of ligand electronics on enantioinduction by installing a variety of aromatic heterocycles on the *o*-biaryl diamine backbone. Electron-rich heteroaromatics consistently delivered superior outcomes. Ultimately, 4-dibenzofuran substituted Co(II) salen **3.59** provided the best results, affording epoxide **3.52** in a remarkable 95% ee and 68% yield. Having developed the first highly enantioselective HAT-initiated hydrofunctionalization, Chris and I sought to assess the generality of our reaction manifold.

Table 3.1 Catalyst structure-activity relationships for asymmetric HAT radical-polar crossover hydroalkoxylation



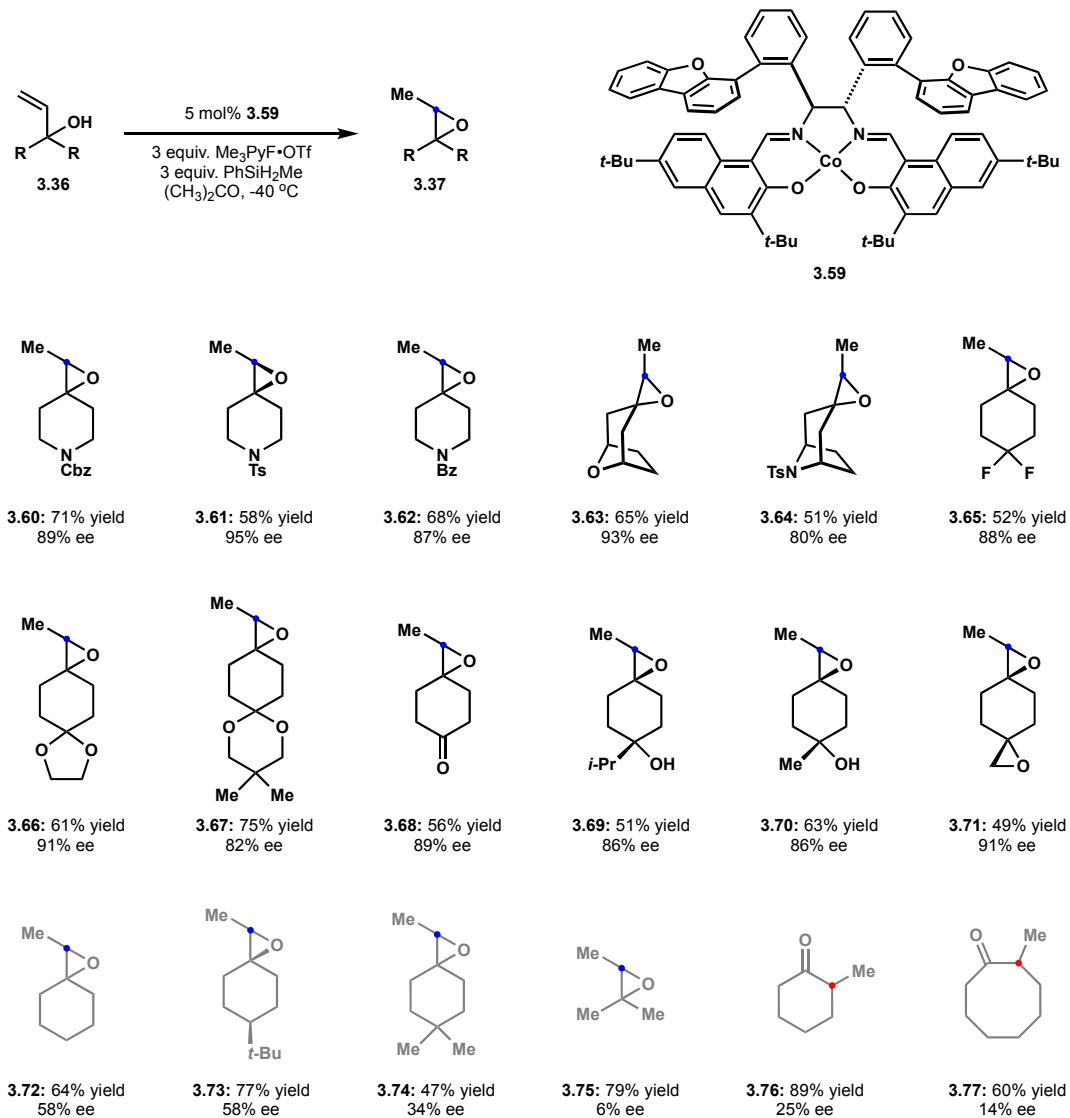
3.6 Substrate Scope

Catalyst **3.59** allowed for efficient conversion of various cyclohexane-based tertiary allylic alcohols to the corresponding epoxide products with high levels of enantioinduction (**Table 3.2**). A series of protected piperidone-derived allylic alcohols were transformed to epoxides **3.60–3.62** with high enantioselectivity and good yield. The *N*-tosyl protected piperidine epoxide **3.61** gave X-ray quality crystals which established the absolute configuration of the newly formed stereocenter as *R*. We assume the other epoxides produced by catalyst **3.59** share this assigned absolute stereochemistry. Epoxides derived from oxabicyclic frameworks (**3.63**) and *N*-tosyl protected nortropinone derivatives (**3.64**) were afforded in modest yield and good stereocontrol. Substrates bearing 4,4-diheteroatom substitution including 4,4-difluorination and ketals were converted efficiently to the requisite epoxide products **3.65–3.67** with excellent asymmetric induction. Planarizing the 4-position with ketone substitution did not erode enantioselectivity or efficiency (**3.68**). Cyclohexane substrates with tertiary heteroatoms at the axial 4-position were prepared with excellent stereocontrol regardless of the geminal equatorial alkyl substitution including methyl, isopropyl, and tethered methylene units (**3.69–3.71**).

Cyclohexyl substrates lacking heteroatom substitution at the 4-position furnished epoxides with moderate enantioselectivity (**3.72–3.74**). Similar levels of asymmetric induction were observed for all substrates bearing axial hydrogen atoms at the 4-position regardless of the equatorial substitution at the 4-position, for example products **3.72** and **3.73**. Substituting hydrogen atoms for methyl groups eroded enantioselectivity further, with 4,4-dimethyl epoxide **3.74** being formed in 34% ee. Acyclic tertiary allylic alcohols were converted to epoxides with high efficiency, but as a near racemic mixture (**3.75**). Attempted reactions of vinylcarbinols derived from five-membered and seven-membered rings solely delivered the corresponding

cyclohexanone and cyclooctanone ring expanded products **3.76** and **3.77**, respectively. Unfortunately, these semipinacol rearrangement products were formed with poor stereocontrol.

Table 3.2 Substrate scope for catalytic asymmetric HAT radical–polar crossover hydroalkoxylation



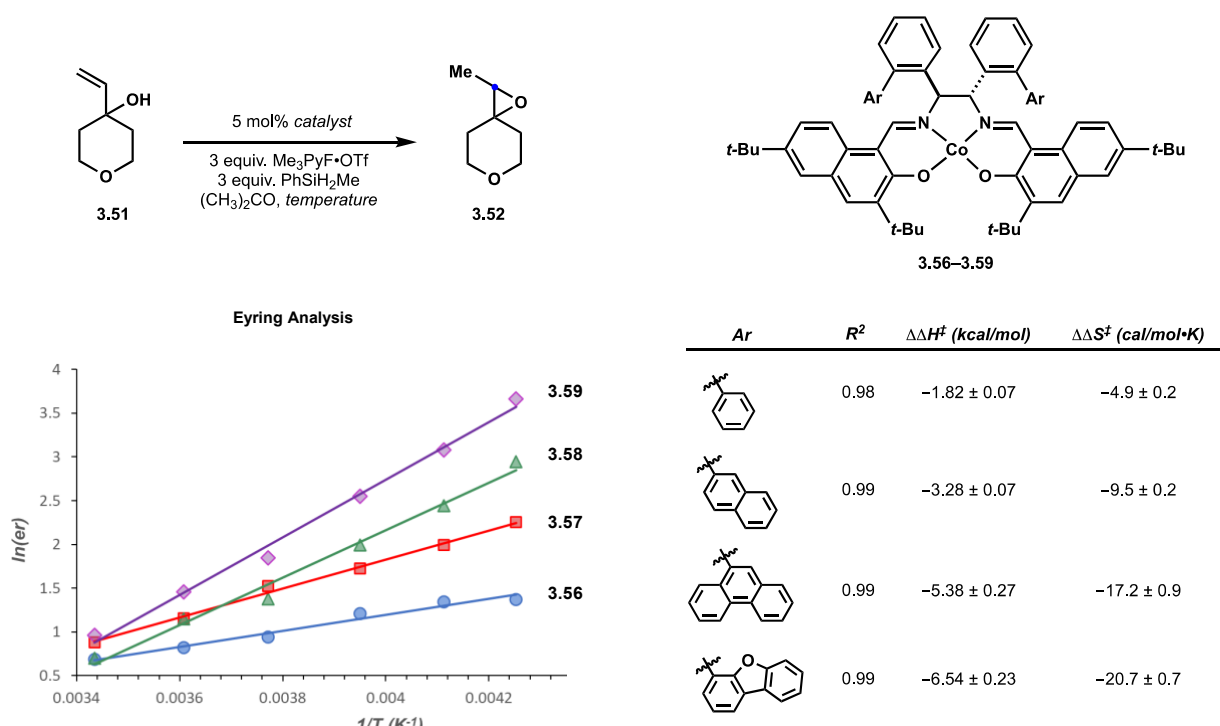
3.7 Mechanistic Studies

3.7.1 Eyring Analysis

Intrigued by the influence of catalyst arene surface area and electronics on enantioselectivity, our mechanistic investigations began by searching for methods to evaluate the proposed intra-catalyst π -stacking interactions between the *o*-biaryl diamine and naphthaldehyde

fragments. We took inspiration from a seminal report by Jacobsen, where the effect of participating cation- π interactions in enantioselective thiourea-catalyzed cationic polycyclizations were interrogated by Eyring analysis.²⁴ Thus, my colleague Dr. Chris Discolo conducted an Eyring analysis of our hydroalkoxylation protocol using allylic alcohol **3.51** to assess the differential activation parameters in the enantiodetermining step and probe the participation of stabilizing π -stacking interactions (Figure 3.2).

Figure 3.2 Eyring analysis supports pi-stacking interactions in enantiodetermining step



Chris conducted the Eyring analysis by performing the hydroalkoxylation with pyran allylic alcohol **3.51** using catalysts **3.56–3.59**. Outcomes of enantioselectivity were recorded for each catalyst at six different temperatures in ten degree increments ranging from -40 °C to 20 °C. Plotting the natural log of enantiomeric ratio (er) of product **3.52** as a function of inverse temperature provided the Eyring plot for a respective catalyst. The plotted lines allow one to calculate the differential enthalpy of activation and differential entropy of activation for the

enantiodetermining step respective to the catalyst the line correlates to. Differential enthalpy of activation was calculated from the slope of the line and differential entropy of activation was calculated from the y-intercept of the line. Eyring plots for each catalyst produced a linear correlation between $\ln(k_r)$ and inverse temperature, suggesting that all catalysts are operating through a single mechanism consistent across all temperatures tested.

Analysis of the differential activation parameters revealed that enantioselectivity was enthalpically controlled in all cases. The magnitude of differential enthalpy of activation nearly doubled with each additional arene installed on the diamine backbone. These trends are consistent with the participation of noncovalent cation- π -stacking interactions between arenes analogous to those observed by Jacobsen, the energetic benefits of which are often manifested enthalpically.²⁵ Notably, 4-dibenzofuran catalyst **3.59** displayed a markedly increased differential enthalpy of activation compared to 9-phenanthrene-substituted catalyst **3.58** despite the two sharing similar π -surface area. This result is consistent with the participation of cation- π interactions, as electron-rich aromatics should strengthen noncovalent cationic interactions to a greater extent compared to electronically neutral aromatic systems due to a greater donation of delocalized electron density into the electron-deficient cation.

The enthalpic benefits gained by expansion of the arene moieties were attenuated by a corresponding increase in the magnitude of differential entropy of activation terms across the series of catalysts. Positive correlation between arene expanse and differential entropy of activation suggests that the transition state of the enantiodetermining step is more ordered as π -surface area is increased. This is consistent with noncovalent π -interactions between the diamine and naphthaldehyde fragments strengthening as arene surface area is increased, leading to a more organized catalyst structure. 4-dibenzofuran catalyst **3.59** displayed an increased differential

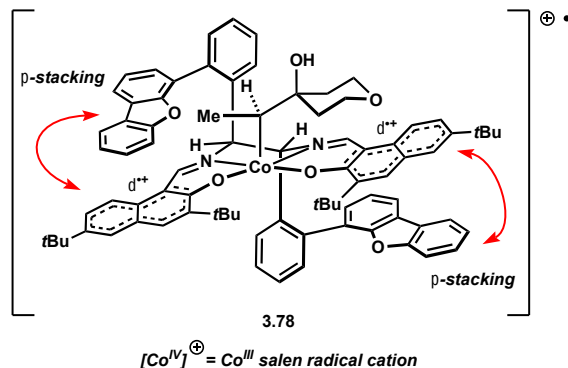
entropy of activation term compared to 9-phenanthrene substituted catalyst **3.58** despite the two sharing similar π -surface area, suggesting that extra electron density further rigidifies the catalyst structure and improves enantioselectivity, which is likewise consistent with the participation of stabilizing cation- π interactions.

Positive correlations between arene surface area and differential activation parameters suggest the participation of cation- π interactions that stabilize the major transition state assembly in the enantiodetermining step.²⁶ Spectroscopic and computational studies of cationic alkylcobalt(IV) complexes bearing redox-active ligands suggest that upon oxidation of alkylcobalt(III) complexes to the corresponding cationic alkylcobalt(IV), ligand to metal charge transfer (LMCT) can occur to reduce the cobalt center and simultaneously generate a resonance stabilized radical cation delocalized across the ligand framework.²⁷⁻²⁸ We propose a similar LMCT event is operative in our catalyst system. Thus, our colloquial alkylcobalt(IV) complex may be better represented as an alkylcobalt(III) radical cation (**Figure 3.3**). Putative radical cation intermediates are consistent with the superior performance of electron-rich catalyst **3.59**, which should better stabilize the salen-derived radical cation by greater donation of electron density into the radical-cation delocalized across the naphthaldehyde motif via cation- π interactions, as is depicted in **Figure 3.3**.

However, while positive correlations between arene surface area and differential activation parameters are consistent with stabilizing noncovalent π -stacking interactions lowering the energy of the transition state assembly leading to the major enantiomer, in principle these data are also consistent with increased arene bulk simply destabilizing the minor transition state by steric interactions. Thus, further investigation was required to clarify whether enhanced stereocontrol is

primarily a function of noncovalent stabilization or steric destabilization differentiating the major and minor transition state assemblies.

Figure 3.3 Representation of putative alkylcobalt(IV) intermediate derived from catalyst **3.59** and substrate **3.51**.

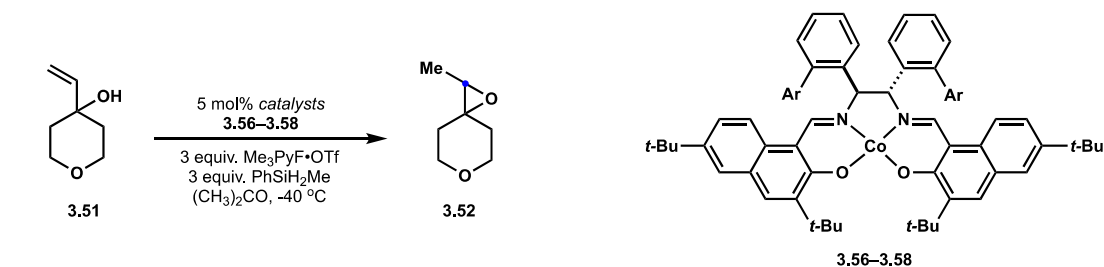


3.7.2 Arene Property Correlations

To determine whether increased asymmetric induction as a result of increasing catalyst arene substitution is a function of stabilizing the major transition state in the enantiodetermining step via cation- π interactions or destabilization of the minor transition state via greater steric interactions, correlations between arene properties and enantioselectivity were probed (**Figure 3.4**). Plotting the polarizability of benzene, naphthalene, and phenanthrene against the $\ln(er)$ of epoxide **3.52** using catalysts **3.56–3.58** revealed a positive linear correlation between arene polarizability and enantioselectivity.²⁹ Plotting the quadrupole moment of benzene, naphthalene, and phenanthrene against the $\ln(er)$ of epoxide **3.52** from reactions with catalysts **3.56–3.58** likewise displayed a linear correlation between quadrupole moment and enantioinduction.³⁰ Since the strength of cation- π interactions should primarily be a function of electrostatic³¹ and dispersion forces,³² the observed linear correlations between the physical properties of isoelectronic arenes and the degree of asymmetric induction suggest that cation- π interactions contribute to the improved stereochemical outcomes by lowering the energy of the major transition state in the enantiodetermining step. If enantioenrichment was instead driven primarily by a destabilization of

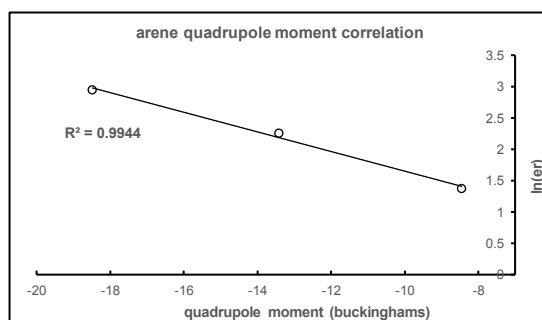
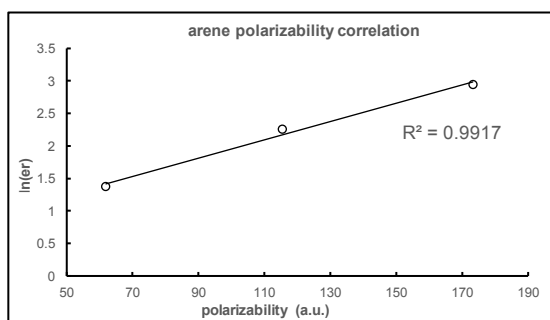
the minor transition state by sterics, the observed correlations between arene dispersion forces and enantioselectivity would not be expected.^{24,33} Additionally, these results are consistent with the observation that the introduction of electronically rich aromatics into the catalyst structure results in enhanced enantioselectivity compared to otherwise sterically similar catalysts embedded with electronically neutral arenes.

Figure 3.4 Linear correlation of arene properties with enantioselectivity



Arene property correlation

Ar	polarizability	quadrupole moment	er
	61.9	-8.45	79.8:20.2
	115.5	-13.42	90.5:9.5
	173.2	-18.48	95:5



3.7.3 Rationalizing the Influence of Substrate Structure on Enantioselectivity

Correlations between shared structural features and stereochemical outcomes observed in **Table 3.2** provide additional evidence for the participation of stabilizing cation- π interactions.

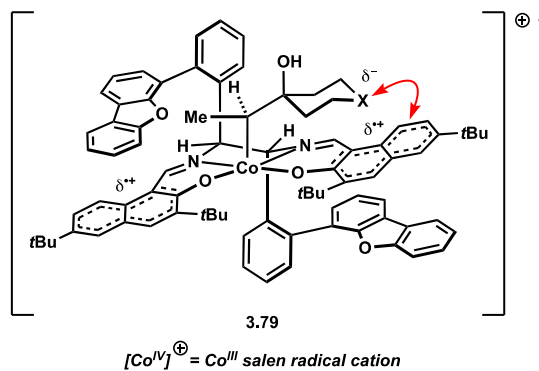
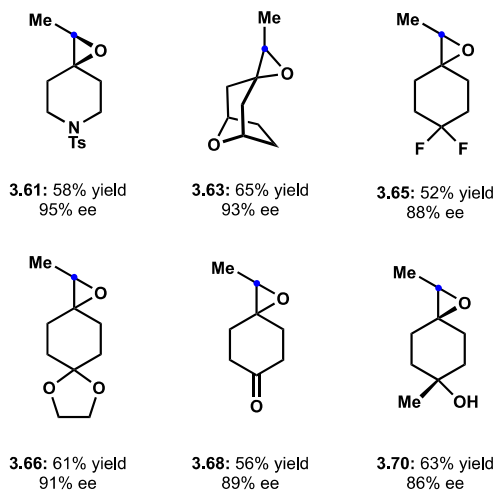
Analysis of the evaluated substrates revealed that substrates bearing heteroatom substitution embedded at the 4-position of the cyclohexyl framework were converted to epoxides with high enantioselectivity (**Figure 3.5a**). Representative examples include pyran epoxide **3.52**, piperidine epoxide **3.61**, and oxabicyclic epoxide **3.63**. Likewise, substrates with heteroatom substitution at the axial 4-position benefit from similarly enhanced enantioselectivity. Representative examples include 4,4-difluoro-epoxide **3.65**, ketal **3.66**, epoxyketone **3.68**, and tertiary carbinol **3.70**.³⁴ We attribute the superior enantioinduction for these classes of substrates to potential noncovalent dipole- π interactions between the alkylcobalt(IV) radical cation motifs and the substrate heteroatom. Building a model of the putative alkylcobalt(IV) intermediates generated following radical-pair collapse and single-electron oxidation suggest the cyclohexyl framework of the substrate may be positioned over the open face of the radical cation motif. Substrates containing heteroatom substitution might be appropriately positioned to donate electron density into the electropositive radical cation motif via lone pair donation, resulting in an overall stabilization and rigidification of the alkylcobalt(IV) intermediate. Electrostatic dipole- π interactions between substrate and catalyst could be expected to have similar effects to the proposed intra-catalyst cation- π interactions, where the major transition state is both lowered in energy and better organized, leading to increased levels of enantiodifferentiation.

Conversely, epoxides obtained from allylic alcohols lacking the capability to donate electron density from the 4-position suffered from decreased enantioselectivity (**Figure 3.5b**). Substrates substituted with axial hydrogen atoms at the 4-position were converted to epoxides with only moderate enantioinduction. For example, cyclohexanone derived epoxide **3.72** and 4-*tert*-butyl substituted epoxide **3.73** were both formed in 58% ee. Modeling the alkylcobalt(IV) intermediate derived from these substrates suggest the axial proton only serves to disrupt the

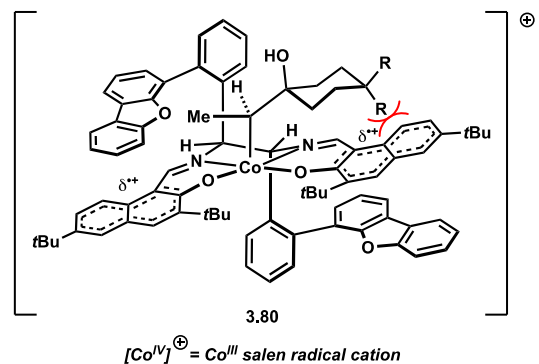
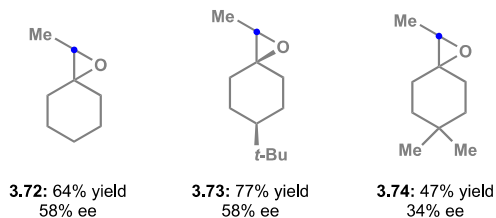
transition state assembly via steric clash with the open face of the salen. Additionally, the 4-equatorial substituent appeared to be positioned out and away from the catalyst aromatics, which may explain why both **3.72** and **3.73** were prepared with the same degree of enantioinduction despite wildly dissimilar steric profiles about the 4-position. Increased steric clash between substrate and the naphthaldehyde motif would be expected to further erode enantioselectivity. Indeed, asymmetric induction dropped significantly when the axial hydrogen was substituted for a more sterically bulky methyl group in the case of epoxide **3.74**. Poor enantioselectivity is likely a function of disrupting stabilizing cation- π interactions via steric clash from forcing the axial methyl group directly over and into the salen fragment.

Figure 3.5 Proposed influence of substrate structural features on stereochemical outcomes

(a) Lone pair donation improves enantioselectivity



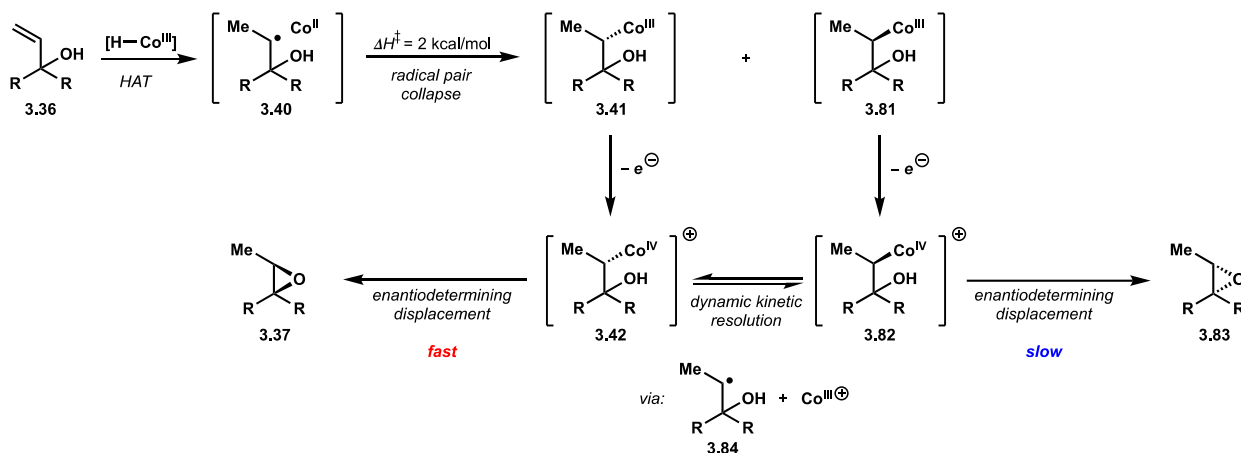
(b) Sterics erodes enantioselectivity



3.7.4 Proposed Mechanism for Catalytic Asymmetric Radical–Polar Crossover Hydroalkoxylation

Taken all together, our data support the involvement of cationic cobalt complexes in the enantiodetermining step. However, describing the precise mechanism by which these complexes exert stereocontrol is challenging as multiple pathways and opportunities for enantiodifferentiation are possible. Thus, we sought to develop a mechanistic proposal that incorporate cationic cobalt complexes in a manner consistent with both our data as well as previous reports of relevant oxidative displacements of alkyl metal complexes (**Scheme 3.9**).

Scheme 3.9 Proposed mechanism for the catalytic asymmetric radical–polar crossover hydroalkoxylation



Our proposed mechanism commences with HAT from the putative cobalt(III) hydride generated from our scalemic cobalt(II) complex to tertiary allylic alcohol **3.36** to form solvent caged alkyl radical-metalloradical pair **3.40**.¹⁶ Facile radical pair collapse provides a diastereomeric mixture of alkylcobalt(III) complexes **3.41** and **3.81**. We do not believe that radical pair collapse is the enantiodetermining step as the radical pair collapse between alkyl radicals and relevant cobalt(II) complexes is known to be a diffusion-controlled process with an enthalpy of activation lower than the calculated differential enthalpy of activation using catalyst **3.59**.³⁵ Subsequent single-electron oxidation of the mixture of diastereomeric alkylcobalt(III) complexes

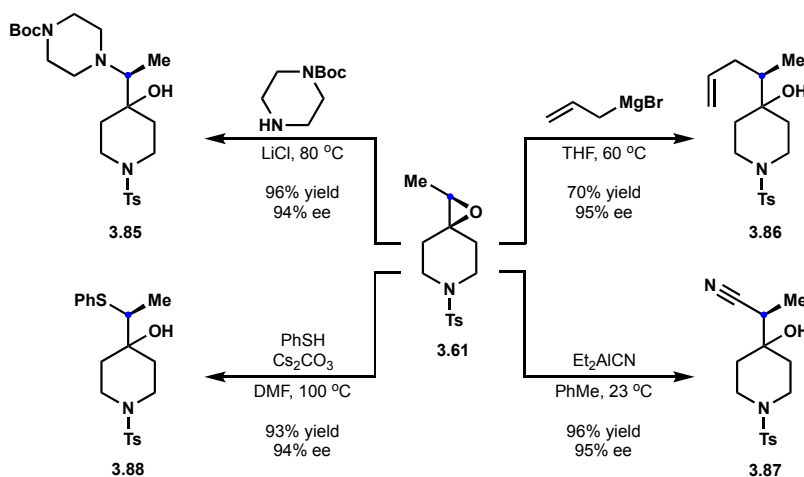
generates the corresponding mixture of cationic alkylcobalt(IV) diastereomers **3.42** and **3.82**.¹³ Studies on the mechanism of enantioselective dual photoredox/nickel-catalyzed cross-coupling reactions supported dynamic kinetic resolution via reversible homolysis of alkylnickel(III) intermediates with subsequent reductive elimination as the enantiodetermining step.³⁶ We propose a similar dynamic kinetic resolution process under Curtin-Hammett control may be operative in our asymmetric hydroalkoxylation, where alkylcobalt(IV) diastereomers **3.42** and **3.82** undergo interconversion between one another and competitive nucleophilic displacement is the enantiodetermining step.³⁷ In this scenario, an increase in cation- π interactions in the catalyst would stabilize the electrophilic alkylcobalt(IV) complexes, leading to a later transition state and enhanced enantioselectivity. The higher energy diastereomer that benefits least from stabilizing cation- π interactions would have a lower ΔG^\ddagger and react faster to produce the observed enantioenriched epoxide product **3.37** via kinetically facile nucleophilic displacement.

Kochi demonstrated that alkylcobalt(IV) salen complexes readily undergo reversible homolysis to generate cationic cobalt(III) salen and an alkyl radical via radical chain mechanism.³⁸ Alkylcobalt(IV) diastereomers **3.42** and **3.82** may likewise interconvert between one another upon epimerization via reversible homolysis of the stereodefined carbon-cobalt bond to produce alkyl radical **3.84** and a cationic cobalt(III) salen complex followed by radical pair collapse. It is unclear whether homolytic interconversion of alkylcobalt(IV) diastereomers in the context of our hydroalkoxylation occur solely by reorganization within the solvent cage or by a similar radical chain mechanism proposed by Kochi. Additionally, the possibility that radical pair collapse of alkyl radical **3.84** and a cationic cobalt(III) salen to regenerate a diastereoenriched alkylcobalt(IV) complex is the enantiodetermining step cannot be definitively ruled out.^{39,40}

3.8 Derivatization of Epoxide 3.61

To further showcase the utility of our asymmetric hydroalkoxylation, enantioenriched *N*-tosyl piperidine epoxide **3.61** was subjected to S_N2 reactions with a variety of nucleophiles to afford formal enantioenriched Markovnikov hydrofunctionalization products derived from tertiary allylic alcohols (Scheme 3.10). In all cases, complete stereoinversion of the methyl stereocenter was observed. Reaction of epoxide **3.61** with Boc-protected piperazine and lithium chloride produced aminoalcohol **3.85** in near quantitative yield. Related piperazine scaffolds previously found application in medicinal chemistry efforts.⁴¹ Efficient epoxide opening with allylmagnesium bromide provided alcohol **3.86** in good yield. Subjecting **3.61** to Nagata's reagent in toluene at ambient temperature cleanly delivered *sec*-nitrile **3.87**. Finally, sulfide **3.88** was accessed in excellent yield by careful treatment of **3.61** with thiophenolate in DMF at 100 °C.

Scheme 3.10 Derivatization of epoxide 3.61



3.9 Conclusions and Outlook

In summary, we have developed the first highly enantioselective HAT-mediated alkene hydrofunctionalization. In order to overcome this long standing challenge, catalyst structure-activity relationships were revealed that lead to the synthesis of a series of novel scalemic Co(II) salen complexes containing extended aromatic systems on the diamine and salicylaldehyde

fragments. The asymmetric hydroalkoxylation protocol proved successful for converting a variety of cyclic tertiary allylic alcohols derived from heterocycles and substituted cyclohexanones to the corresponding epoxides with high levels of enantioselectivity. Analysis of thermodynamic parameters via Eyring plots combined with correlations of arene polarizability and quadrupole moment suggest that stabilizing noncovalent cation– π interactions between the catalyst diamine *o*-biaryl substitution and naphthaldehyde motifs are essential to asymmetric induction. To our knowledge, this is the first example of harnessing intramolecular cation– π interactions within a catalyst to induce asymmetry. This methodology provides a platform to develop enantioselective variants of other intramolecular HAT hydrofunctionalizations. Additionally, we hope this work provides insight into solving the yet to be overcome challenge of catalytic asymmetric intermolecular HAT-initiated hydrofunctionalizations.

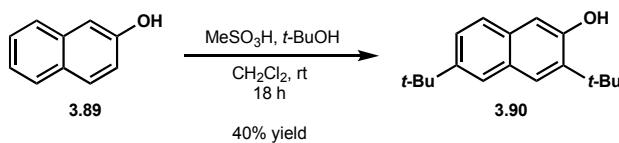
3.10 Experimental Section

3.10.1 Materials and Methods

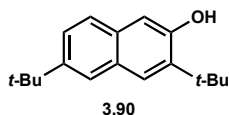
All reactions were carried out in flame-dried glassware under positive pressure of dry nitrogen unless otherwise noted. Reaction solvents including tetrahydrofuran (THF, Fisher, HPLC Grade), dichloromethane (DCM, Fisher, HPLC Grade), dimethylformamide (DMF, Fisher, HPLC Grade), and toluene (Fisher, HPLC Grade), were dried by percolation through a column packed with neutral alumina and a column packed with a supported copper catalyst for scavenging oxygen (Q5) under positive pressure of argon. Acetone was dried over anhydrous powdered CaSO₄ overnight, distilled into a two-neck round bottom, and then transferred by cannula into a storage Schlenk. Solvents for extraction, thin layer chromatography (TLC), and flash column chromatography were purchased from Fischer (ACS Grade) and VWR (ACS Grade) and used without further purification.

Chloroform-d and acetone-d₆ for ¹H and ¹³C NMR analysis were purchased from Cambridge Isotope Laboratories and used without further purification. Commercially available reagents were used without further purification unless otherwise noted. Reactions were cooled in a Thermo Scientific EK90 immersion cooler. Reactions were monitored by thin layer chromatography (TLC) using precoated silica gel plates (EMD Chemicals, Silica gel 60 F₂₅₄). Flash column chromatography was performed over silica gel (Acros Organics, 60 Å, particle size 0.04-0.063 mm). Infrared (IR) spectra were obtained on a Nicolet iS5 FT-IR spectrometer with an iD5 ATR, and are reported in terms of frequency of absorption (cm⁻¹). GC/FID analysis was performed on Agilent 7820A system with helium as carrier gas. Enantiomeric ratio for enantioselective reactions was determined by chiral SFC analysis using an Agilent Technologies HPLC (1200 series) system and Aurora A5 Fusion. Optical rotations were collected on a JASCO P-1010 polarimeter. ¹H NMR and ¹³C NMR spectra were recorded on Bruker DRX-500 (BBO probe), Bruker DRX-500 (TCI cryoprobe), Bruker AVANCE600 (TBI probe), and Bruker AVANCE600 (BBFO cryoprobe) spectrometers using residual solvent peaks as internal standards (CHCl₃ @ 7.26 ppm ¹H NMR, 77.00 ppm ¹³C NMR; C₆H₆ @ 7.16 ppm ¹H NMR, 128.00 ppm ¹³C NMR; (CD₃)₂CO @ 2.05 ppm ¹H NMR, 29.84 ppm ¹³C NMR; (CD₃)₂SO @ 2.50 ppm ¹H NMR, 39.52 ppm ¹³C NMR). High-resolution mass spectra (HRMS) were recorded on Waters LCT Premier TOF spectrometer with ESI and CI sources.

3.10.2 Experimental Procedures



3,6-di-*t*-butyl-2-naphthol. To a solution of 2-naphthol (7.2 g, 50 mmol, 1.0 equiv) and *t*BuOH (14 mL, 150 mmol, 3.0 equiv) in CH₂Cl₂ (170 mL, 0.30 M w.r.t. 2-naphthol) in a 1 L roundbottom flask was added MeSO₃H (22 mL, 350 mmol, 7.0 equiv) dropwise with external cooling by a water bath and stirred for 18 h at room temperature following addition. The reaction mixture was poured onto ice water (500 mL) with vigorous stirring and then warmed to room temperature. The aqueous layer was extracted with CH₂Cl₂ (3 x 100 mL), washed with H₂O and brine, dried over MgSO₄, filtered and concentrated under reduced pressure. The crude product was purified by flash SiO₂ chromatography (gradient elution 10% CH₂Cl₂/hexanes to 40% CH₂Cl₂/hexanes) to yield 3,6-di-*t*-butyl-2-naphthol as a white crystalline solid (5.2 g, 40% yield). The spectral data were identical to those reported in the literature.⁴²



3,6-di-*t*-butyl-2-naphthol **3.90**

¹H NMR (500 MHz, CDCl₃, 25 °C):

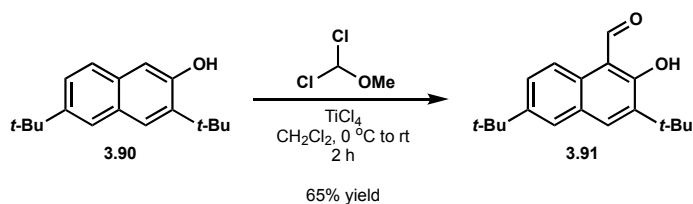
δ 7.68 (s, 2H)

7.56 (d, *J* = 8.9 Hz, 1H)

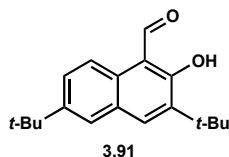
7.47 (dd, *J* = 8.6, 2.0 Hz, 1H)

6.98 (s, 1H), 4.97 (s, 1H)

1.50 (s, 9H), 1.39 (s, 9H)



To a flame-dried, N₂-purged 250 mL roundbottom flask was added **3.90** (4.4 g, 17.1 mmol, 1.0 equiv) and dichloromethylmethyl ether (1.5 mL, 17.1 mmol, 1.0 equiv) in CH₂Cl₂ (86 mL, 0.2 M w.r.t **3.90**) and the flask was cooled to 0 °C in an ice bath. TiCl₄ (3.8 mL, 34.2 mmol, 2.0 equiv) was added dropwise to the reaction mixture at 0 °C. The ice bath was warmed to room temperature and stirred for 2 h. The reaction mixture was poured onto ice water (200 mL), and the aqueous layer was extracted with CH₂Cl₂ (3 x 100 mL). The combined organic layers were washed with brine, dried over MgSO₄, filtered, and concentrated under reduced pressure. The crude material was purified by flash silica chromatography (20% CH₂Cl₂/Hexanes) to yield 3.16 g (65% yield) of salicylaldehyde **3.91**. The spectral data was identical to those reported in the literature.⁴³



Salicylaldehyde **3.91**

¹H NMR (500 MHz, CDCl₃, 25 °C):

δ 14.02 (s, 1H)

10.80 (s, 1H)

8.23 (d, J = 8.8 Hz, 1H)

7.92 (s, 1H)

7.71 (d, J = 2.1 Hz, 1H)

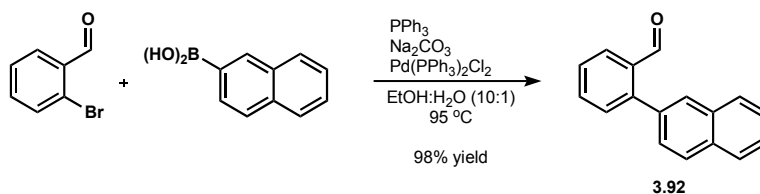
7.65 (dd, J = 8.8, 2.1 Hz, 1H)

1.51 (s, 9H)

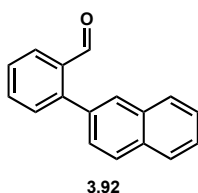
1.41 (s, 9H)

General Procedure I: Preparation of 2-arylbenzaldehydes 3.92–3.94.

To a flame dried 50 mL round bottom flask was added 2-bromobenzaldehyde (1.0 equiv), aryl boronic acid (1.2 equiv), Pd(PPh₃)₂Cl₂ (0.050 equiv), triphenylphosphine (0.10 equiv), and Na₂CO₃ (1.2 equiv). The flask was fitted with a septum and the atmosphere replaced with N₂. Degassed EtOH (0.2 M w.r.t. benzaldehyde) and degassed H₂O (2.0 M w.r.t. benzaldehyde) were added and the suspension stirred. The flask was equipped with a reflux condenser and the reaction was heated at 95 °C overnight. After allowing the reaction to cool to rt, the reaction was diluted with H₂O and the resulting mixture was extracted with Et₂O (3x). The organic layers were washed with brine and dried over MgSO₄. The crude material was purified by flash silica chromatography to yield 2-arylbenzaldehyde.



Benzaldehyde 3.92. Benzaldehyde **3.92** was prepared according to **General Procedure I** using 2-bromobenzaldehyde (0.23 mL, 2.0 mmol), 2-naphthylboronic acid (412.8 mg, 2.4 mmol), Pd(PPh₃)₂Cl₂ (70.2 mg, 0.1 mmol), triphenylphosphine (52.5 mg, 0.2 mmol), and Na₂CO₃ (254.4 mg, 2.4 mmol), and purified by flash silica chromatography (gradient elution: 100% hexanes to 5% v/v EtOAc/hexanes) to yield 455.0 mg (98% yield) of **3.92** as a white solid. The spectral data matched those reported in the literature.⁴⁴

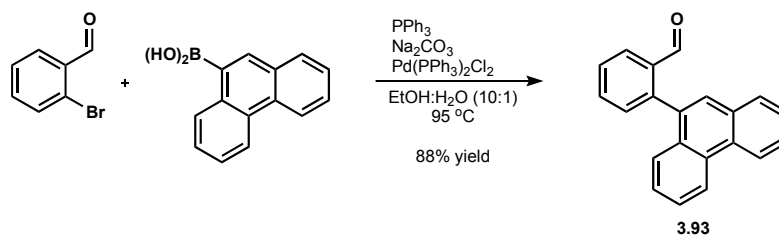


Benzaldehyde **3.92**

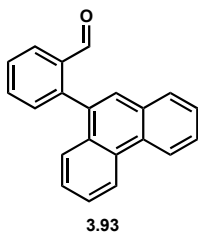
¹H NMR (500 MHz, CDCl₃, 25 °C):

δ 10.04 (d, <i>J</i> = 0.8 Hz, 1H)	7.83 (d, <i>J</i> = 1.2 Hz, 1H)
8.08 (ddd, <i>J</i> = 7.8, 1.4, 0.5 Hz, 1H)	7.68 (ddd, <i>J</i> = 7.7, 7.3, 1.4 Hz, 1H)
7.95 (d, <i>J</i> = 8.4 Hz, 1H)	7.57-7.52 (m, 5H)
7.93-7.88 (m, 2H)	

TLC: R_f = 0.46 (10% EtOAc/Hex)



Benzaldehyde 3.93. Benzaldehyde **3.93** was prepared according to **General Procedure I** using 2-bromobenzaldehyde (0.12 mL, 1.0 mmol), 9-phenanthrenylboronic acid (266.5 mg, 1.2 mmol), Pd(PPh₃)₂Cl₂ (35.1 mg, 0.05 mmol), triphenylphosphine (26.2 mg, 0.1 mmol), and Na₂CO₃ (127.2 mg, 1.2 mmol), and purified by flash silica chromatography (gradient elution: 100% hexanes to 5% v/v EtOAc/hexanes) to yield 248.5 mg (88% yield) of **3.93** as a white solid. The spectral data matched those reported in the literature.⁴⁵

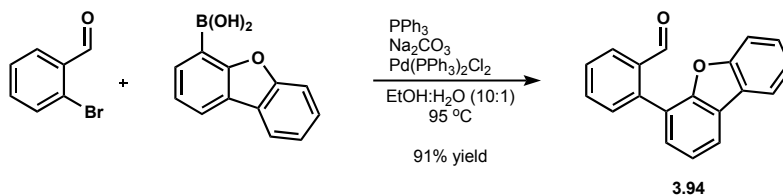


Benzaldehyde **3.93**

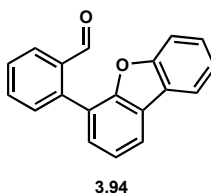
¹H NMR (500 MHz, CDCl₃, 25 °C):

δ 9.74 (d, <i>J</i> = 0.8 Hz, 1H)	7.71 (s, 1H)
8.80 (d, <i>J</i> = 8.6 Hz, 1H)	7.70-7.68 (m, 1H)
8.76 (dd, <i>J</i> = 8.3, 0.5 Hz, 1H)	7.68-7.65 (m, 1H)
8.17-8.15 (m, 1H)	7.64-7.61 (m, 1H)
7.91-7.90 (m, 1H)	7.55-7.53 (m, 2H)
7.75-7.72 (m, 2H)	7.53-7.51 (m, 1H)

TLC: R_f = 0.41 (10% EtOAc/Hex)



Benzaldehyde 3.94. Benzaldehyde **3.94** was prepared according to **General Procedure I** using 2-bromobenzaldehyde (0.58 mL, 5.0 mmol), 4-(dibenzofuranyl)boronic acid (1.2721 g, 6.0 mmol), Pd(PPh₃)₂Cl₂ (175.4 mg, 0.25 mmol), triphenylphosphine (131.1 mg, 0.5 mmol), and Na₂CO₃ (635.9 mg, 6.0 mmol), and purified by flash silica chromatography (gradient elution: 100% hexanes to 5% v/v EtOAc/hexanes) to yield 1.235 g (91% yield) of **SI-26** as a white solid.



Benzaldehyde **3.94**

¹H NMR (500 MHz, CDCl₃, 25 °C):

δ 9.91 (d, <i>J</i> = 0.7 Hz, 1H)	7.75 (td, <i>J</i> = 7.5, 1.2 Hz, 1H)	7.39-7.36 (m, 1H)
8.15 (dd, <i>J</i> = 7.8, 0.8 Hz, 1H)	7.64-7.59 (m, 2H)	
8.04 (dd, <i>J</i> = 7.4, 1.5 Hz, 1H)	7.52-7.47 (m, 2H)	
8.01 (dd, <i>J</i> = 7.7, 0.6 Hz, 1H)	7.45 (ddt, <i>J</i> = 6.7, 4.9, 1.7 Hz, 2H)	

¹³C NMR (126 MHz, CDCl₃, 25 °C):

δ 191.9	133.91	127.64	122.3
156.3	131.5	124.6	120.96
153.8	128.9	124.0	120.89
140.0	128.6	123.17	112.0
134.06	127.69	123.14	

HRMS (ESI) calculated for C₁₉H₁₂O₂ [M+Na]⁺: 295.0735, found: 295.0731

TLC: R_f = 0.43 (10% EtOAc/Hex)

General Procedure II: Preparation of Salen Ligands 3.95–3.98

A. Diaza-Cope

The procedure for the diaza-Cope was adapted from the Chin group's report on diaza-Cope transformations with sterically challenging benzaldehydes.²³ (*R,R*)-Mother diamine (0.10 mmol, 24 mg, 1.0 equiv) and 2-arylbenzaldehyde (0.24 equiv, 2.4 equiv) in DMSO (0.50 mL, 0.20 M w.r.t. mother diamine) was added to a vial and stirred at 90 °C for 6 hours. The reaction mixture was diluted with CH₂Cl₂ and transferred to a separatory funnel. The organic layer was washed with H₂O (3 x 10 mL) and brine, dried with Na₂SO₄, filtered, and concentrated under reduced pressure. The crude diaza-Cope product was taken on to the next step without purification.

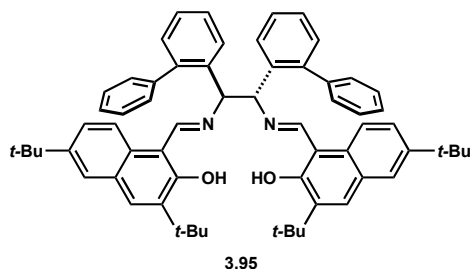
B. Salicylaldehyde deprotection

Crude diaza-Cope product (1.0 equiv) and NH₂OH•HCl (35 mg, 0.50 mmol, 5.0 equiv) in MeOH (1.0 mL, 0.10 M w.r.t. diaza-Cope product) was added to a vial and stirred at room temperature for 4 hours. 1 M NaOH (10 mL) was added to the reaction mixture and the aqueous layer was extracted with CH₂Cl₂ (5 x 10 mL), dried with Na₂SO₄, filtered, and concentrated under reduced pressure. The crude diamine was taken on to the next step without purification.

C. Salen Formation

Crude diamine (1.0 equiv) and naphthalene salicylaldehyde **SI-23** (0.20 mmol, 2.0 equiv) in EtOH (0.50 mL, 0.20 M w.r.t. diamine) was added to a vial and stirred at 60 °C for 4 hours. The reaction mixture was allowed to cool to room temperature, concentrated under reduced pressure, and purified by flash SiO₂ chromatography to afford salen as a yellow solid.

Ligand 3.95. Ligand **3.95** was prepared according to **General Procedure II** with 2-phenylbenzaldehyde (44 mg, 0.24 mmol) and purified by flash silica chromatography (20% CH₂Cl₂/Hex) to afford ligand **3.95** as a yellow solid (49 mg, 56% yield over three steps).



Ligand 3.95

¹H NMR (600 MHz, CDCl₃, 25 °C):

δ 14.90 (s, 2H)	7.25 (dtd, <i>J</i> = 14.8, 7.2, 3.5 Hz, 8H)
8.76 (s, 2H)	7.06 (dd, <i>J</i> = 6.6, 1.6 Hz, 4H)
7.55 (d, <i>J</i> = 8.8 Hz, 2H)	7.04 (d, <i>J</i> = 31.2 Hz, 6H)
7.47 (s, 2H)	5.11 (s, 2H)
7.43 (s, 2H)	1.33 (s, 20H)
7.37 (d, <i>J</i> = 1.9 Hz, 2H)	1.31 (s, 18H)
7.30 (dd, <i>J</i> = 8.8, 2.1 Hz, 2H)	

¹³C NMR (151 MHz, CDCl₃, 25 °C):

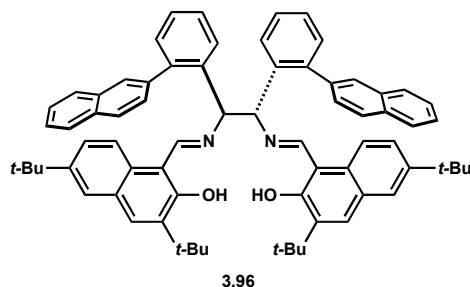
δ 169.0	131.9	125.4
160.8	130.1	124.1
145.2	128.22	117.7
142.4	128.13	107.8
140.7	127.6	72.1
140.3	127.4	31.3
135.3	126.3	29.4

LRMS (ESI) calculated for C₆₄H₆₈N₂O₂ [M+Na]⁺: 919.5, found: 919.6

TLC: R_f = 0.56 (35% v/v CH₂Cl₂ in hexanes)

[α]_D²³ = -6.6° (c = 1.8, CHCl₃)

Ligand 3.96. Ligand **3.96** was prepared according to **General Procedure II** with benzaldehyde **3.92** (56 mg, 0.24 mmol) and purified by flash silica chromatography (20% CH₂Cl₂/Hex) to afford ligand **3.96** as a yellow solid (52 mg, 51% yield over three steps).



Ligand 3.96

¹H NMR (600 MHz, CDCl₃, 25 °C):

δ 13.06 (s, 2H)	7.24 (d, <i>J</i> = 7.8 Hz, 2H)
8.16 (s, 2H)	7.20 (td, <i>J</i> = 7.7, 1.2 Hz, 2H)
7.98–7.96 (m, 2H)	7.12 (d, <i>J</i> = 7.6 Hz, 2H)
7.88 (d, <i>J</i> = 8.2 Hz, 2H)	7.10–7.02 (m, 6H)
7.80 (s, 2H)	6.80 (d, <i>J</i> = 8.2 Hz, 2H)
7.59 (dd, <i>J</i> = 6.2, 3.1 Hz, 2H)	6.76 (d, <i>J</i> = 7.4 Hz, 2H)
7.57–7.52 (m, 2H)	5.05 (s, 2H)

¹³C NMR (151 MHz, CDCl₃, 25 °C):

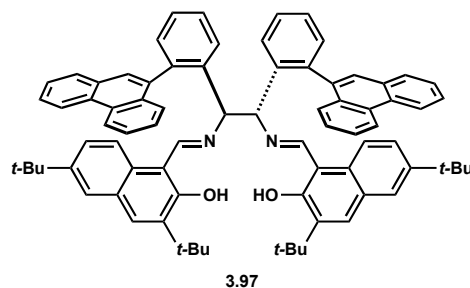
δ 165.6	131.7	126.2
160.7	130.0	118.7
141.9	128.7	118.5
138.1	127.96	116.7
136.1	127.87	74.2
132.44	127.0	
132.40	126.3	

LRMS (ESI) calculated for C₇₂H₇₂N₂O₂ [M+Na]⁺: 1019.6, found: 1019.6

TLC: R_f = 0.61 (35% v/v CH₂Cl₂ in hexanes)

[α]_D²⁵ = –130.6° (c = 1.3, CHCl₃)

Ligand 3.97. Ligand **3.97** was prepared according to **General Procedure II** with benzaldehyde **3.93** (68 mg, 0.24 mmol) and purified by flash silica chromatography (20% CH₂Cl₂/Hex) to afford ligand **3.97** as a yellow solid (51 mg, 47% yield over three steps).



Ligand 3.97

¹H NMR (600 MHz, CDCl₃, 25 °C):

δ 14.72 (s, 2H)	7.30 (s, 2H)
8.91 (t, <i>J</i> = 9.0 Hz, 4H)	7.24–7.21 (m, 4H)
8.02 (d, <i>J</i> = 3.2 Hz, 2H)	7.18–7.13 (m, 4H)
7.85–7.82 (m, 4H)	7.05–7.01 (m, 4H)
7.79–7.76 (m, 2H)	4.55 (s, 2H)
7.62 (td, <i>J</i> = 7.6, 1.2 Hz, 2H)	1.33 (s, 18H)
7.44 (td, <i>J</i> = 7.4, 1.2 Hz, 2H)	0.96 (s, 18H)
7.34 (d, <i>J</i> = 2.0 Hz, 2H)	

¹³C NMR (151 MHz, CDCl₃, 25 °C):

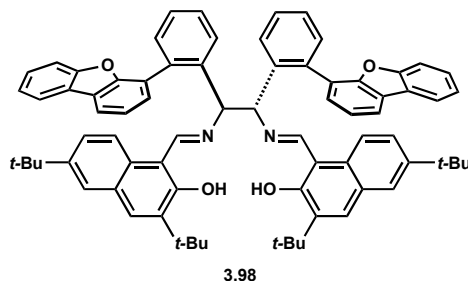
δ 167.2	136.3	130.1	127.8	123.7	34.6
161.1	131.3	129.8	127.0	123.2	34.2
145.1	131.2	129.3	126.8	122.8	31.3
139.7	131.1	129.1	126.7	118.5	28.9
139.6	130.4	128.7	126.2	107.6	
137.3	130.2	128.5	124.9	74.6	

LRMS (ESI) calculated for C₈₀H₇₆N₂O₂ [M+Na]⁺: 1119.6, found: 1119.7

TLC: R_f = 0.65 (35% v/v CH₂Cl₂ in hexanes)

[α]_D²⁵ = –62.5° (c = 0.80, CHCl₃)

Ligand 3.98. Ligand **3.98** was prepared according to **General Procedure II** with benzaldehyde **3.94** (65 mg, 0.24 mmol) and purified by flash silica chromatography (20% CH₂Cl₂/Hex) to afford ligand **3.98** as a yellow solid (45 mg, 42% yield over three steps).



Ligand 3.98

¹H NMR (600 MHz, DMSO-d₆, 100 °C):

δ 14.68 (s, 2H)	7.08 (d, <i>J</i> = 5.2, Hz, 6H)
8.56 (s, 2H)	6.87 (d, <i>J</i> = 5.3, Hz, 4H)
8.15 (dd, <i>J</i> = 25.7, 7.7 Hz, 4H)	5.15 (s, 2H)
7.44–7.37 (m, 6H)	1.31 (s, 18H)
7.32 (t, <i>J</i> = 7.3, 4H)	1.21 (s, 18H)
7.21 (d, <i>J</i> = 6.6, Hz, 4H)	

¹³C NMR (151 MHz, DMSO-d₆, 100 °C):

δ 169.1	135.5	127.41	123.31	110.8	30.4
159.8	130.8	127.40	123.20	106.5	28.7
154.8	129.9	126.9	122.4	70.66	
152.3	129.4	126.4	122.1	70.64	
144.0	128.17	125.1	120.2	53.9	
139.8	128.16	123.87	119.7	33.9	
136.1	127.7	123.75	117.2	33.2	

LRMS (ESI) calculated for C₇₆H₇₂N₂O₂ [M+Na]⁺: 1099.5, found: 1099.6

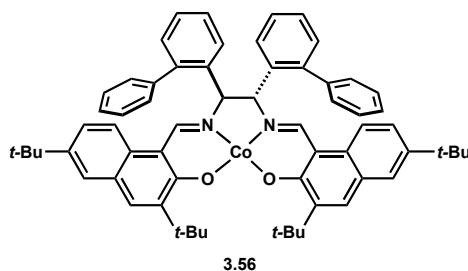
TLC: R_f = 0.52 (35% v/v CH₂Cl₂ in hexanes)

[α]_D²⁵ = −163° (c = 1.0, CHCl₃)

General Procedure III: Preparation of Co(II) Salen Complexes 3.56–3.59

A vial was charged with $\text{Co}(\text{OAc})_2 \cdot 4\text{H}_2\text{O}$ (25 mg, 0.10 mmol, 1.0 equiv) and salen (0.10 mmol, 1.0 equiv) and purged with N_2 . EtOH (500 μL , 0.20 M w.r.t. salen) was degassed by sparging with Ar under sonication for 5 minutes and then added to the reaction vial. The reaction mixture was heated to 80 $^\circ\text{C}$ with vigorous stirring for 2 hours at which point the Co(II) salen had precipitated out of solution as a bright red solid. The solid was transferred to a fine glass frit and washed with MeOH (3 x 10 mL). CH_2Cl_2 (15 mL) was then added to the fine glass frit to dissolve the red solid, filtered through into a clean flask, and then concentrated under reduced pressure to afford the Co(II) salen as a bright red powder.

Co(II) salen complex 3.56. Co(II) salen complex **3.56** was prepared according to **General Procedure III** with salen **3.95** (90 mg, 0.10 mmol) to afford Co(II) salen complex **3.56** as a bright red powder (92 mg, 96% yield).

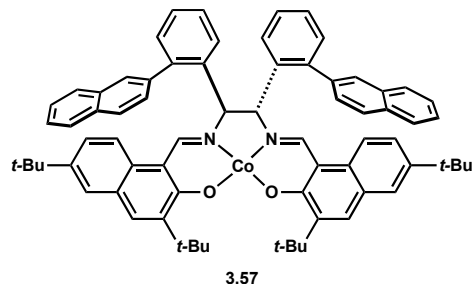


Co(II) salen complex 3.56

IR: 3057.98, 2955.83, 2860.67, 1594.55, 1569.99, 1538.49, 1497.48, 1478.37, 1409.33, 1388.18, 1380.67, 745.53, 700.62 cm^{-1}

LRMS (ESI) calculated for $\text{C}_{64}\text{H}_{66}\text{CoN}_2\text{O}_2$ $[\text{M}+\text{H}]^+$: 954.5, found: 954.5

Co(II) salen complex 3.57. Co(II) salen complex **3.57** was prepared according to **General Procedure III** with salen **3.96** (100 mg, 0.10 mmol) to afford Co(II) salen complex **3.57** as a bright red powder (103 mg, 98% yield).

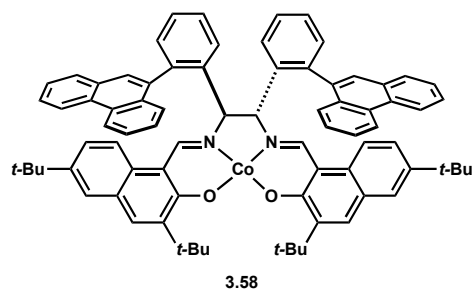


Co(II) salen complex 3.57

IR: 3052.02, 2866.92, 1595.10, 1538.75, 1496.33, 1432.16, 1381.06, 1338.43, 757.36, 742.69, 691.94 cm^{-1}

LRMS (ESI) calculated for $\text{C}_{72}\text{H}_{70}\text{CoN}_2\text{O}_2$ $[\text{M}+\text{H}]^+$: 1054.5, found: 1054.5

Co(II) salen complex 3.58. Co(II) salen complex **3.58** was prepared according to **General Procedure III** with salen **3.97** (110 mg, 0.10 mmol) to afford Co(II) salen complex **3.58** as a bright orange powder (105 mg, 91% yield).

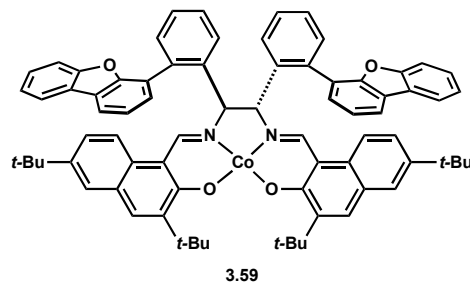


Co(II) salen complex 3.58

IR: 2955.36, 1594.44, 1537.54, 1380.48, 1338.29, 1261.84, 815.49, 746.88, 725.89 cm^{-1}

LRMS (ESI) calculated for $\text{C}_{80}\text{H}_{74}\text{CoN}_2\text{O}_2$ $[\text{M}+\text{H}]^+$: 1154.6, found: 1154.6

Co(II) salen complex 3.59. Co(II) salen complex **3.59** was prepared according to **General Procedure III** with salen **3.98** (108 mg, 0.10 mmol) to afford Co(II) salen complex **3.59** as a bright orange powder (106 mg, 93% yield).



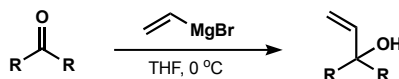
Co(II) salen complex 3.59

IR: 3705.87, 3680.15, 2966.13, 2922.03, 2864.92, 1537.86, 1380.04, 1186.19, 1055.94, 1014.08, 750.96 cm^{-1}

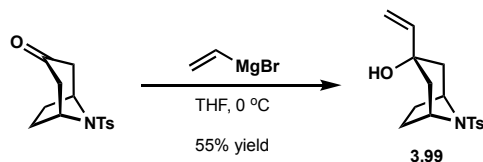
LRMS (ESI) calculated for $\text{C}_{76}\text{H}_{70}\text{CoN}_2\text{O}_2$ $[\text{M}+\text{H}]^+$: 1134.5, found: 1134.5

Preparation of starting materials:

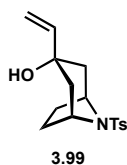
General Procedure IV: Synthesis of Allylic Alcohols



Allylic alcohols. A solution of vinylmagnesium bromide (2.0 equiv) in THF (0.6 M w.r.t. Grignard reagent) was cooled to 0 °C. A solution of ketone (1.0 equiv) in THF (0.6 M w.r.t. ketone, final reaction concentration 0.2 M) was added slowly. After 1 h, the reaction was quenched by the addition of saturated aqueous NH_4Cl (30 mL). The resulting mixture was extracted with Et_2O (3 x 30 mL). The organics were washed with brine and dried over MgSO_4 . The desired allylic alcohols were purified by flash column chromatography.



Allylic alcohol 3.99. Allylic alcohol **3.99** was prepared according to General Procedure IV with N-tosyl-nortropinone⁴⁶ (100 mg, 0.36 mmol) and vinylmagnesium bromide (720 μ L, 0.72 mmol, 1.0 M solution in THF) in THF (1.8 mL) to afford allylic alcohol **3.99** as a white crystalline solid (61 mg, 55% yield).



Allylic alcohol **3.99**

¹H NMR (600 MHz, CDCl₃, 25 °C):

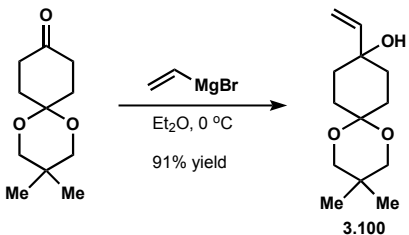
δ 7.75 (d, J = 8.2 Hz, 2H)	2.42 (s, 3H)
7.28 (s, 2H)	2.15-2.06 (m, 4H)
5.79 (dd, J = 17.2, 10.6 Hz, 1H)	1.66-1.63 (m, 2H)
5.17 (d, J = 17.2 Hz, 1H)	1.47-1.45 (m, 2H)
4.99 (d, J = 10.6 Hz, 1H)	1.14 (s, 1H).
4.25 (s, 2H)	

¹³C NMR (151 MHz, CDCl₃, 25 °C):

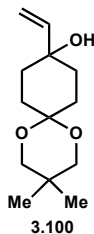
δ 158.5	129.6	56.1
147.0	127.3	44.7
143.3	111.2	27.8
137.3	71.6	21.5

LRMS (ESI) calc. for C₁₆H₂₁NO₃S [M+Na]⁺: 330.1, found: 330.1.

TLC R_f = 0.50 (50% v/v EtOAc in hexanes)



Allylic alcohol 3.100. A solution of vinylmagnesium bromide (5.0 mL, 1.0 M in THF, 5.0 mmol) in Et₂O (10 mL) was cooled to 0 °C. A solution of 1,4-cyclohexanedione mono(2,2-dimethyltrimethylene ketal) (594.8 mg, 3.0 mmol) in Et₂O (5.0 mL) was added slowly. After 1 h, the reaction was quenched by the addition of sat. aq. NH₄Cl (10 mL). The resulting mixture was extracted with Et₂O 3x 30 mL. The organics were washed with brine and dried over MgSO₄. The crude material was purified by flash silica chromatography (gradient elution: 100% hexanes to 60% v/v Et₂O/hexanes) to yield 620.5 mg (91% yield) of **3.100** as a white solid.



Allylic alcohol 3.100

¹H NMR (500 MHz, CDCl₃, 25 °C):

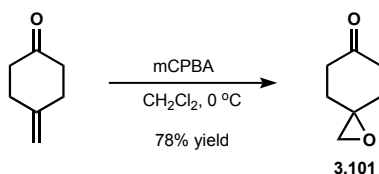
δ 5.96 (dd, J = 17.4, 10.8 Hz, 1H)	2.04-2.01 (m, 2H)
5.27 (dd, J = 17.3, 0.4 Hz, 1H)	1.87-1.81 (m, 2H)
5.05 (dd, J = 10.8, 0.2 Hz, 1H)	1.72 (td, J = 13.0, 3.8 Hz, 2H)
3.54 (s, 2H), 3.47 (s, 2H)	1.55 (d, J = 13.2 Hz, 2H)

¹³C NMR (126 MHz, CDCl₃, 25 °C):

δ 145.5	70.13	27.9
111.9	70.07	22.8
97.3	33.8	
71.4	30.3	

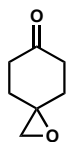
LRMS (ESI) calculated for C₁₃H₂₂O₃ [M+Na]⁺: 249.1468, found: 249.4133

TLC: R_f = 0.17 (50% Et₂O/Hex)



3.101

Epoxyketone 3.101. *m*CPBA (3.36 g, 19.46 mmol) was added in three equal portions over 15 min to a solution of 4-methylenecyclohexan-1-one⁴⁷ (1.07 g, 9.73 mmol) in CH₂Cl₂ (32.4 mL, 0.3M) cooled to 0 °C. After 2.5 h the reaction was quenched with 15 mL sat aq. Na₂S₂O₃ and the mixture was extracted with CH₂Cl₂ (3 x 25 mL). The organic layers were washed with sat aq. NaHCO₃, brine, and then dried over MgSO₄. The crude material was purified by flash silica chromatography (gradient elution: 100% pentane to 50% v/v Et₂O/pentane) to yield 962.6 mg (78% yield) of epoxyketone **3.101**.



3.101

Epoxyketone 3.101

¹H NMR (500 MHz, CDCl₃, 25 °C):

δ 2.80 (s, 2H)

2.64 (ddd, *J* = 15.3, 10.7, 5.4 Hz, 2H)

2.41 (dt, *J* = 14.0, 5.0 Hz, 2H)

2.16-2.10 (m, 2H)

1.75 (dt, *J* = 12.6, 5.8 Hz, 2H)

¹³C NMR (126 MHz, CDCl₃, 25 °C):

δ 209.9

56.9

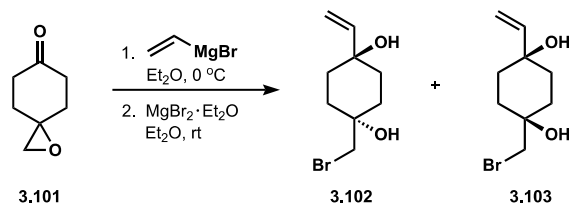
54.1

38.9

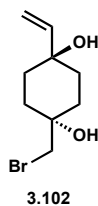
32.3

HRMS (CI) calculated for C₇H₁₀O₂ [M]⁺: 126.0681, found: 126.0680

TLC: R_f = 0.15 (50% Et₂O/Hex)



Bromohydrins 3.102 and 3.103. Vinylmagnesium bromide (1.0 M in THF, 8.0 mL, 8.0 mmol) was added slowly to a solution of **3.101** (962.6 mg, 7.69 mmol) in Et₂O (34 mL, 0.23 M) cooled to 0 °C. After 1.5 h the reaction was quenched with sat. aq. NH₄Cl and the mixture was extracted with Et₂O (3 x 50 mL). The organic layers were washed with brine and dried over Na₂SO₄. The crude material was purified by flash silica chromatography (gradient elution: 100% hexanes to 20% v/v Et₂O/hexanes) to yield 420.1 mg (35% yield) of an inseparable mixture of diastereomeric allylic alcohols. The mixture of allylic alcohols (100.0 mg, 0.648 mmol) was dissolved in THF (6.5 mL, 0.1 M) at 0 °C and MgBr₂·Et₂O (837.2 mg, 3.24 mmol) was added in a single portion.⁴⁸ After 10 min the reaction was allowed to warm to rt and then stirred for a further 18 h. The reaction was quenched with H₂O and the mixture extracted with Et₂O (3 x 25 mL). The organics were washed with brine and dried over Na₂SO₄. The crude material was purified by flash silica chromatography (gradient elution: 100% hexanes to 60% v/v EtOAc/hexanes) to yield 61.1 mg (40% yield) of **3.102** and 64.7 mg (42% yield) of **3.103** as white solids. The diastereomeric bromohydrins were distinguished on the basis of NOESY analysis and an observation that diastereomer **3.102** undergoes formation of corresponding [2.2.2]-oxabicyclic product (in addition to the expected epoxide) upon exposure to NaH in THF.



Bromohydrin **3.102**

¹H NMR (500 MHz, CDCl₃, 25 °C):

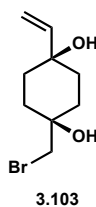
δ 5.99 (dd, J = 17.4, 10.7 Hz, 1H)	1.79 (td, J = 13.1, 3.3 Hz, 3H)
5.26 (d, J = 17.4 Hz, 1H)	1.68 (d, J = 12.9 Hz, 2H)
5.05 (d, J = 10.8 Hz, 1H)	1.49 (d, J = 13.0 Hz, 2H)
3.49 (s, 2H)	1.14 (s, 1H)
1.93-1.87 (m, 2H)	

^{13}C NMR (126 MHz, CDCl_3 , 25 °C):

δ 146.0	47.4
111.6	32.5
71.2	30.7
69.1	

HRMS (CI) calculated for $\text{C}_9\text{H}_{15}\text{BrO}_2$ $[\text{M}]^+$: 234.0255, found: 234.0248

TLC: R_f = 0.21 (30% EtOAc/Hex)



Bromohydrin **3.103**

^1H NMR (500 MHz, CDCl_3 , 25 °C):

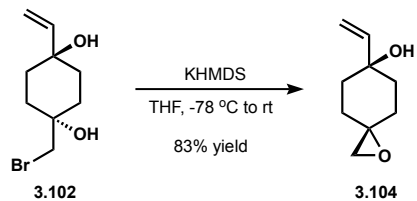
δ 5.97 (dd, J = 17.4, 10.8 Hz, 1H)	1.91 (dd, J = 10.7, 5.9 Hz, 2H)
5.31 (d, J = 17.4 Hz, 1H)	1.82 (t, J = 11.7 Hz, 2H)
5.15 (d, J = 10.7 Hz, 1H)	1.62 (dd, J = 11.6, 7.0 Hz, 4H)
3.52 (s, 2H)	1.51 (bs, 1H)
2.04 (bs, 1H)	

^{13}C NMR (126 MHz, CDCl_3 , 25 °C):

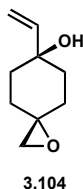
δ 143.2	44.7
113.7	34.0
71.2	32.3
69.5	

HRMS (CI) calculated for $\text{C}_9\text{H}_{15}\text{BrO}_2$ $[\text{M}]^+$: 234.0255, found: 234.0258

TLC: R_f = 0.25 (60% EtOAc/Hex)



Allylic alcohol 3.104. KHMDS (0.5 M in PhMe, 1.7 mL, 0.85 mmol) was added slowly to a solution of bromohydrin **3.102** (50.0 mg, 0.213 mmol) in THF (5.0 mL, 0.04 M) at -78 °C. After 5 min, the reaction was removed from the cooling bath and warmed to rt. After 45 min the reaction was quenched by the addition of sat. aq. NH₄Cl. The resulting mixture was extracted with Et₂O (3x 10 mL). The organics were washed with brine and dried over Na₂SO₄. The crude material was purified by flash silica chromatography (gradient elution: 100% hexanes to 30% v/v Et₂O/hexanes) to yield 27.3 mg (83% yield) of **3.104** as a clear colorless oil.



Allylic alcohol **3.104**

¹H NMR (500 MHz, CDCl₃, 25 °C):

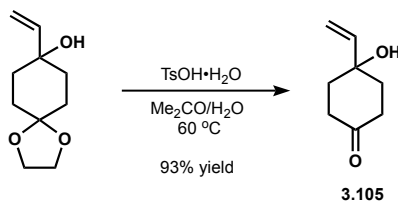
δ 5.99 (dd, J = 17.4, 10.8 Hz, 1H)	1.86 (td, J = 13.3, 4.1 Hz, 2H)
5.27 (d, J = 17.4 Hz, 1H)	1.64 (d, J = 13.5 Hz, 2H)
5.06 (d, J = 10.8 Hz, 1H)	1.50 (s, 1H)
2.66 (s, 2H)	1.19 (d, J = 13.6 Hz, 2H)
2.24 (td, J = 13.3, 4.1 Hz, 2H)	

¹³C NMR (126 MHz, CDCl₃, 25 °C):

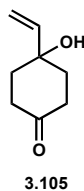
δ 145.8	54.1
111.8	34.8
71.0	28.4
58.0	

LRMS (ESI) calculated for C₉H₁₄O₂ [M+Na]⁺: 177.0892, found: 177.0894

TLC: R_f = 0.44 (50% EtOAc/Hex)



Allylic Alcohol 3.105. *p*-Toluenesulfonic acid monohydrate (361 mg, 1.92 mmol, 0.10 equiv) was added to a solution of 8-vinyl-1,4-dioxaspiro[4.5]decan-8-ol¹² (3.54 g, 19.2 mmol, 1.0 equiv) in Me₂CO/H₂O (1:1 v/v, 100 mL, 0.20 M w.r.t. allylic alcohol) and stirred for 5 minutes at 25 °C, then heated to 60 °C for 4 h. The reaction mixture was cooled to ambient temperature and the acetone was removed under reduced pressure. EtOAc (50 mL) and sat. aq. NaHCO₃ (100 mL) was added to the reaction mixture and the aqueous layer was extracted with EtOAc (3 x 50 mL). The combined organic layers were dried over MgSO₄, filtered, and concentrated under reduced pressure. The crude material was purified by flash column chromatography (40% v/v EtOAc/hexanes) to afford **3.105** as a white crystalline solid (2.50 g, 93% yield). The spectral data for **3.105** matched those reported in the literature.⁴⁹



Allylic Alcohol **3.105**

¹H NMR (600 MHz, CDCl₃, 25 °C):

δ 6.02 (dd, J = 17.4, 10.7 Hz, 1H)	2.29 (ddt, J = 14.8, 5.4, 2.4 Hz, 2H)
5.35 (dd, J = 17.4, 0.8 Hz, 1H)	1.96 (dq, J = 9.3, 3.3 Hz, 4H)
5.16 (dd, J = 10.8, 0.8 Hz, 1H)	1.68-1.54 (m, 2H).
2.79-2.74 (m, 2H)	

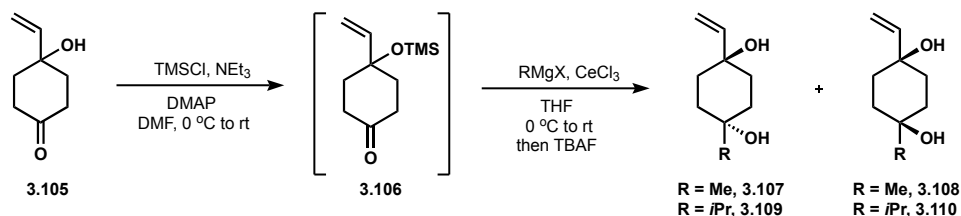
¹³C NMR (151 MHz, CDCl₃, 25 °C):

δ 211.4	70.6
144.1	37.07
113.0	36.95

LRMS (ESI) calculated for C₈H₁₂O₂ [M+Na]⁺: 163.1, found: 163.1

TLC: R_f = 0.27 (40% EtOAc/Hex)

General Procedure V: Preparation of trans-cyclohexanediols.



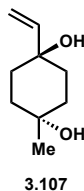
TMS Protection of 3.105. Trimethylsilyl chloride (2.5 mL, 19.7 mmol, 1.1 equiv) was added dropwise to a solution of **3.105** (2.50 g, 17.9 mmol, 1.0 equiv), triethylamine (3.7 mL, 26.9 mmol, 1.5 equiv), and DMAP (122 mg, 1.79 mmol, 0.10 equiv) in DMF (45 mL, 0.40 M w.r.t. **3.105**) at 0 °C. The reaction was stirred at 0 °C for 30 min and then allowed to warm to ambient temperature and stirred for an additional 2 h. The reaction was cooled to 0 °C and quenched by the addition of a saturated aqueous solution of NaHCO₃ (100 mL). The reaction mixture was diluted with Et₂O (150 mL) and the organic layer was washed with H₂O (3 x 100 mL). The combined aqueous layer was extracted with Et₂O (3 x 50 mL) and the organic layers were combined and washed with brine. The combined organic layer was dried over MgSO₄, filtered, and concentrated under reduced pressure. The crude product was used without further purification.

Grignard Addition into 3.106. The following procedure was adapted from a protocol developed by the Inamoto group.⁵⁰ Anhydrous CeCl₃ (579 mg, 2.35 mmol, 1.0 equiv) was added to a solution of **3.106** (500 mg, 2.35 mmol, 1.0 equiv) in anhydrous THF (10 mL, 0.25 M w.r.t. **3.106**) and sonicated under positive pressure of argon for 30 minutes at ambient temperature. The reaction mixture was cooled to 0 °C and vigorously stirred for 15 minutes. Grignard reagent (1.5 equiv) was added rapidly in a single portion to the reaction mixture with vigorous stirring. The reaction was stirred at 0 °C for 30 min and then allowed to warm to ambient temperature and stirred for 1 h. The reaction was then poured onto a vigorously stirred solution of EtOAc (50 mL) and a 15% aqueous solution of NH₄Cl (100 mL) at 0 °C. The aqueous layer was extracted with EtOAc (3 x 30 mL). The combined organic layer was washed with brine (50 mL), dried over MgSO₄, filtered, and concentrated under reduced pressure to afford crude cis- and trans-cyclohexanediols in a ca. 1:1 ratio. The crude product was used without further purification.

TMS Deprotection. Crude **3.106** was treated with TBAF (7.0 mL, 1.0 M solution in THF, 3.0 equiv) and stirred at ambient temperature for 2 h. The reaction mixture was quenched by addition

of saturated aqueous solution of NH_4Cl (25 mL). The aqueous layer was extracted with EtOAc (3 x 30 mL) and the combined organic layer was dried with Na_2SO_4 , filtered, and concentrated under reduced pressure. The crude product was purified by flash chromatography (40% v/v EtOAc/hexanes) to afford the trans-cyclohexanediol as a white crystalline solid. The relative stereochemistry was assigned by NOESY correlation.

Allylic Alcohol 3.107. General Procedure V was used to prepare **3.107** using MeMgBr (1.2 mL, 3.0 M solution in Et₂O). The crude product after TMS deprotection was purified by flash chromatography to afford **3.107** as a white crystalline solid (130 mg, 0.83 mmol, 35% yield from **3.105**).



Allylic Alcohol 3.107

¹H NMR (600 MHz, CDCl₃, 25 °C):

δ 5.98 (dd, J = 17.4, 10.8 Hz, 1H)	1.90-1.79 (m, 4H),
5.26 (dd, J = 17.4, 1.2 Hz, 1H)	1.52-1.43 (m, 4H)
5.04 (dd, J = 10.8, 1.2 Hz, 1H)	1.27 (s, 3H)

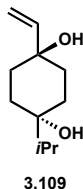
¹³C NMR (151 MHz, CDCl₃, 25 °C):

δ 146.3	34.0
111.3	32.7
71.1	31.3
68.8	

LRMS (ESI) calculated for C₉H₁₆O₂ [M+Na]⁺: 179.1, found: 179.1

TLC: R_f = 0.20 (40% EtOAc/Hex)

Allylic Alcohol 3.109. General Procedure V was used to prepare **3.109** using *i*PrMgCl (1.6 mL, 2.0 M solution in THF). The crude product after TMS deprotection was purified by flash chromatography to afford **3.109** as a white crystalline solid (150 mg, 0.81 mmol, 34% yield from **3.105**).



Allylic Alcohol 3.109

^1H NMR (600 MHz, CDCl_3 , 25 °C):

δ 5.98 (dd, $J = 17.4, 10.8$ Hz, 1H)	1.79 (td, $J = 13.6, 4.0$ Hz, 2H)
5.25 (dd, $J = 17.4, 1.2$ Hz, 1H)	1.62 (dq, $J = 13.8, 6.9$ Hz, 1H)
5.02 (dd, $J = 10.7, 1.2$ Hz, 1H)	1.45 (dt, $J = 14.7, 2.9$ Hz, 4H)
1.88 (td, $J = 13.5, 4.0$ Hz, 2H)	0.94 (d, $J = 6.9$ Hz, 6H)

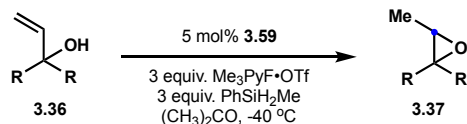
^{13}C NMR (151 MHz, CDCl_3 , 25 °C):

δ 146.6	38.5
111.1	32.5
72.5	29.0
71.3	16.8

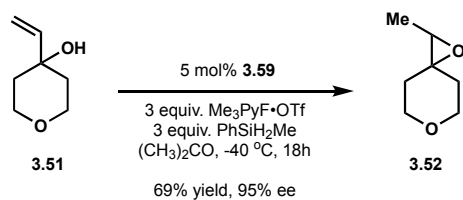
LRMS (ESI) calculated for $\text{C}_{11}\text{H}_{20}\text{O}_2$ $[\text{M}+\text{Na}]^+$: 179.1, found: 179.1

TLC: $R_f = 0.60$ (40% EtOAc/Hex)

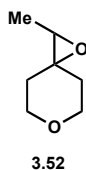
General Procedure VI. Catalytic asymmetric radical-polar crossover hydroalkoxylation of allylic alcohols.



To an oven dried 2 dram vial was added Co(II) salen catalyst **3.59** (5.7 mg, 0.005 mmol, 0.05 equiv) and $\text{Me}_3\text{PyF}\cdot\text{OTf}$ oxidant (87 mg, 0.30 mmol, 3.0 equiv). The vial was then placed under an atmosphere of nitrogen. The allylic alcohol (0.10 mmol, 1.0 equiv) was added as a solution in dry acetone (0.10 M w.r.t. allylic alcohol). The resulting solution was sparged with argon and simultaneously subjected to sonication for 5 min. After cooling to $-40\text{ }^\circ\text{C}$ in an immersion cooler, MePhSiH_2 (41 μL , 0.30 mmol, 3.0 equiv) was added at a rate of 1 drop/10 s. The reaction quickly developed a bright orange color. After 12–72 h, the reaction was quenched by the dropwise addition of pyridine as a degassed solution in dry acetone (0.1 M) and allowed to warm to ambient temperature following addition. The reaction was diluted with CH_2Cl_2 (5 mL), washed with sat. aq. NH_4Cl . The aqueous phase was extracted with CH_2Cl_2 (3 x 5 mL) and the combined organic layer was washed with brine, dried over Na_2SO_4 , filtered, and concentrated under reduced pressure. The products were isolated using flash column chromatography. NOTE: ^1H NMR yields of epoxides **2** and **15** in radical-polar crossover epoxidations were determined by using acetone- d_6 and obtaining ^1H NMR of the crude reaction mixture after quenching with pyridine.



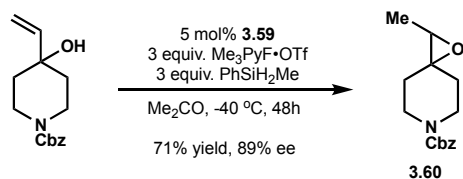
Epoxide 3.52. Epoxide **3.52** was prepared according to General Procedure VI with allylic alcohol **3.51** (13 mg, 0.10 mmol) to afford epoxide **3.52** in 69% yield by ^1H NMR with mesitylene as the internal standard. Spectral data match those reported in the literature.¹² Epoxide **3.52** is volatile and losses of 20-30% of the product are observed after purification by flash silica chromatography. NOTE: A racemic standard of epoxide **3.52** was prepared according to the previously reported procedure.¹²



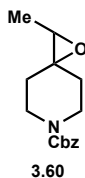
Epoxide **3.52**

Chiral GC/FID: HP – chiral – 20B column, 6.88 psi, 0.50 mL/min, 80 °C, 75 min, tR = 70.2, 74.0 min.

$[\alpha]_D^{25} = +10.8^\circ$ (c = 0.90, CHCl_3); 95% ee.



Epoxide 3.60. Epoxide **3.60** was prepared according to General Procedure VI with 1-carboxybenzyl-4-vinylpiperidin-4-ol⁵⁰ (28 mg, 0.10 mmol) and purified by flash chromatography (30% v/v EtOAc in hexanes) to afford epoxide **3.60** as a clear oil (18.5 mg, 71% yield). NOTE: A racemic standard of epoxide **3.60** was prepared according to the previously reported procedure for radical polar crossover epoxidation using racemic catalyst **3.53**.¹²



Epoxide **3.60**

¹H NMR (500 MHz, CDCl₃, 25 °C):

δ 7.35 (dd, J = 10.4, 3.2 Hz, 4H)	2.93 (q, J = 5.5 Hz, 1H)
7.32 (ddd, J = 8.5, 5.0, 3.6 Hz, 1H)	1.79 (s, 2H)
5.15 (s, 2H)	1.47 (dd, J = 59.2, 12.0 Hz, 3H)
3.83 (s, 2H)	1.30 (d, J = 5.6 Hz, 3H)
3.49-3.41 (m, 2H)	1.26 (s, 1H)

¹³C NMR (126 MHz, CDCl₃, 25 °C):

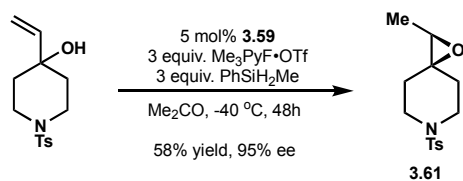
δ 155.2	128.01	60.5	42.47
136.7	127.88	59.6	13.4
128.5	67.2	42.50	

LRMS (ESI) calc. for C₁₅H₁₉NO₃ [M+Na]⁺: 284.1, found: 284.1.

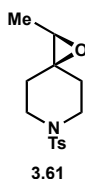
TLC R_f = 0.36 (40% v/v EtOAc in hexanes)

Chiral SFC: CHIRALCEL OD-H, 5% iPrOH, 2.0 mL/min, 210 nm, 40 °C, nozzle pressure = 200 bar CO₂, t_R = 8.6, 9.4 min.

[α]_D²⁵ = +5.35 ° (c = 0.9, CHCl₃); 89% ee.



Epoxide 3.61. Epoxide **3.61** was prepared according to General Procedure VI with 1-tosyl-4-vinylpiperidin-4-ol⁵¹ (30.4 mg, 0.10 mmol) and purified by flash chromatography (25% v/v EtOAc in hexanes) to afford epoxide **3.61** as a white crystalline solid (17.6 mg, 58% yield). X-ray quality crystals were obtained by slow evaporation of a solution of epoxide **3.61** in CH₂Cl₂. NOTE: A racemic standard of epoxide **3.61** was prepared according to the previously reported procedure for radical polar crossover epoxidation using racemic catalyst **3.53**.¹²



Epoxide **3.61**

¹H NMR (600 MHz, CDCl₃, 25 °C):

δ 7.65 (d, J = 8.3 Hz, 2H)	2.44 (s, 3H)
7.32 (d, J = 7.9 Hz, 2H)	2.05-1.95 (m, 2H)
3.54 (ddtd, J = 24.3, 11.4, 4.7, 1.6 Hz, 2H)	1.54 (dddd, J = 13.7, 4.6, 3.1, 1.7 Hz, 1H)
2.88 (q, J = 5.5 Hz, 1H)	1.37 (dddd, J = 13.6, 4.5, 3.1, 1.7 Hz, 1H)
2.78 (dtd, J = 14.3, 11.2, 3.2 Hz, 2H)	1.24 (d, J = 5.5 Hz, 3H).

¹³C NMR (151 MHz, CDCl₃, 25 °C):

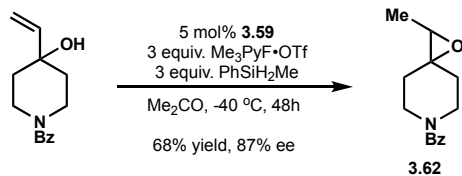
δ 143.7	127.7	44.67	28.3
133.0	59.53	44.60	21.5
129.7	59.51	33.9	13.3

LRMS (ESI) calc. for C₁₄H₁₉NO₃ [M+Na]⁺: 304.1, found: 304.1.

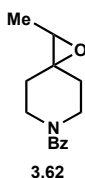
TLC R_f = 0.52 (40% v/v EtOAc in hexanes)

Chiral SFC: CHIRALPAK AD, 20% iPrOH, 2.0 mL/min, 210 nm, 40 °C, nozzle pressure = 200 bar CO₂, t_R = 4.1, 5.5 min.

[α]_D²⁵ = +1.88 ° (c = 1.13, CHCl₃); 95% ee.



Epoxide 3.62. Epoxide **3.62** was prepared according to General Procedure VI with 1-benzoyl-4-vinylpiperidin-4-ol⁵² (13 mg, 0.10 mmol) and purified by flash chromatography (60% v/v EtOAc in hexanes) to afford epoxide **3.62** as a clear oil (16.3 mg, 68% yield). NOTE: A racemic standard of epoxide **3.62** was prepared according to the previously reported procedure for radical polar crossover epoxidation using racemic catalyst **3.53**.¹²



Epoxide **3.62**

¹H NMR (600 MHz, DMSO-d₆, 100 °C):

δ 7.44 (td, J = 4.3, 2.3 Hz, 2H)	1.76 (dddd, J = 22.6, 13.6, 8.9, 4.5 Hz, 2H)
7.41-7.40 (m, 2H)	1.56-1.52 (m, 1H)
3.65 (s, 2H)	1.47-1.43 (m, 1H)
3.50 (t, J = 10.4 Hz, 2H)	1.26 (t, J = 8.4 Hz, 4H).
2.93 (q, J = 5.5 Hz, 1H)	

¹³C NMR (151 MHz, DMSO-d₆, 100 °C):

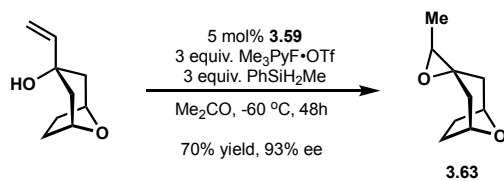
δ 168.8	59.5
136.0	58.1
128.7	33.7
127.8	28.1
126.1	12.7

LRMS (ESI) calc. for C₁₄H₁₇NO₂ [M+Na]⁺: 254.1, found: 254.1.

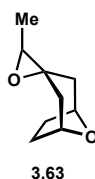
TLC R_f = 0.50 (EtOAc)

Chiral SFC: CHIRALCEL OJ-H, 1% iPrOH, 2.0 mL/min, 254 nm, 44 °C, nozzle pressure = 200 bar CO₂, t_R = 4.9, 5.3 min.

[α]_D²⁵ = -3.75 ° (c = 0.80, CHCl₃); 87% ee.



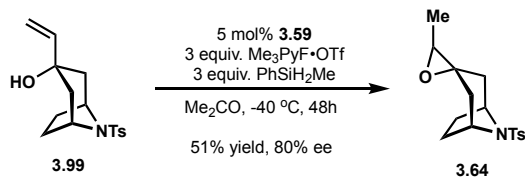
Epoxide 3.63. Epoxide **3.63** was prepared according to General Procedure VI with 3-vinyl-8-oxabicyclo[3.2.1]octan-3-ol¹² (15.4 mg, 0.10 mmol) and purified by flash chromatography to afford epoxide **3.63** as a clear oil (10.8 mg, 70% yield). Spectral data match those reported in the literature.¹²



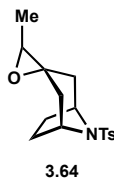
Epoxide **3.63**

Chiral GC/FID: HP – chiral – 20B column, 6.88 psi, 0.50 mL/min, 105 °C, 120 min, tR = 76.9, 78.7.

$[\alpha]_D^{25} = 6.1^\circ$ (c = 0.30, CHCl₃); 93% ee.



Epoxide 3.64. Epoxide **3.64** was prepared according to General Procedure VI with **3.99** (33 mg, 0.10 mmol) and purified by flash chromatography (25% v/v EtOAc in hexanes) to afford epoxide **3.64** as a white crystalline solid (16.8 mg, 70% yield). NOTE: A racemic standard of epoxide **3.64** was prepared according to the previously reported procedure for radical polar crossover epoxidation using racemic catalyst **3.53**.¹²



Epoxide **3.64**

¹H NMR (600 MHz, CDCl₃, 25 °C):

δ 7.75 (d, J = 8.3 Hz, 2H)	2.33 (dd, J = 14.1, 3.5 Hz, 1H)
7.28 (d, J = 8.0 Hz, 2H)	1.93 (dd, J = 8.3, 2.8 Hz, 2H)
4.32 (dt, J = 35.2, 2.9 Hz, 2H)	1.52-1.49 (m, 2H)
2.64 (q, J = 5.5 Hz, 1H)	1.42 (dt, J = 14.1, 2.2 Hz, 1H)
2.47 (d, J = 3.6 Hz, 1H)	1.23 (dt, J = 14.1, 2.2 Hz, 1H)
2.42 (s, 4H)	1.18 (s, 3H)

¹³C NMR (151 MHz, CDCl₃, 25 °C):

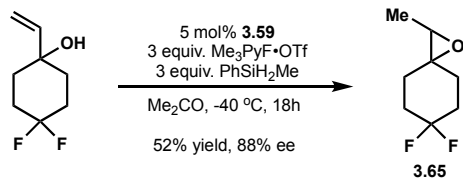
δ 143.5	57.7	42.1	21.5
137.2	56.7	37.5	12.9
129.7	56.5	27.84	
127.3	54.2	27.76	

LRMS (ESI) calc. for C₁₆H₂₁NO₃S [M+Na]⁺: 330.1, found: 330.1.

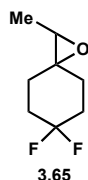
TLC R_f = 0.62 (40% v/v EtOAc in hexanes)

Chiral SFC: CHIRALCEL OJ-H, 5% iPrOH, 2.0 mL/min, 254 nm, 44 °C, nozzle pressure = 200 bar CO₂, t_R = 3.4, 3.9 min.

[α]_D²⁵ = 16.9 ° (c = 1.0, CHCl₃); 80% ee.

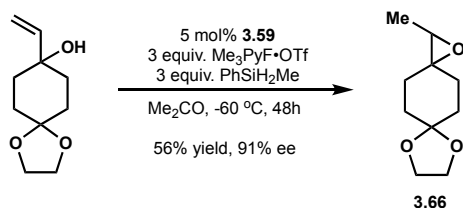


Epoxide 3.65. Epoxide **3.65** was prepared according to General Procedure VI with 4,4-difluoro-1-vinylcyclohexan-1-ol¹² (13 mg, 0.10 mmol) to afford epoxide **3.65** in 53% yield by ¹H NMR with mesitylene as the internal standard. Spectral data match those reported in the literature.¹² NOTE: Epoxide **3.65** is volatile and losses of 20-30% of the product are observed after purification by flash silica chromatography.

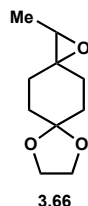


Epoxide **3.65**

Chiral GC/FID: HP – chiral – 20B column, 6.88 psi, 0.50 mL/min, 80 °C, 75 min tR = 53.0, 56.5. $[\alpha]_D^{25} = 11.2^\circ$ (c = 0.90, CHCl₃); 88% ee.

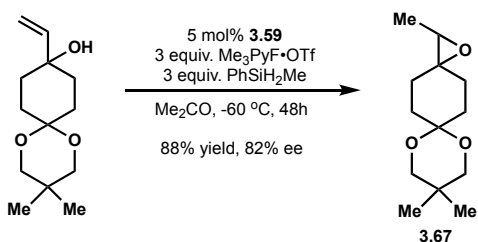


Epoxide 3.66. Epoxide **3.66** was prepared according to General Procedure VI with 8-vinyl-1,4-dioxaspiro[4.5]decan-8-ol¹² (18.4 mg, 0.10 mmol) and purified by flash chromatography to afford epoxide **3.66** as a clear oil (10.3 mg, 56% yield). Spectral data match those reported in the literature.¹²

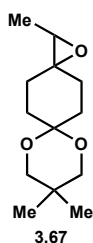


Epoxide **3.66**

Chiral GC/FID: HP – chiral – 20B column, 6.88 psi, 0.50 mL/min, 110 °C, 180 min ramp to 150 °C, 40 min tR = 179.1, 181.4. $[\alpha]_D^{25} = 7.5^\circ$ (c = 0.30, CHCl₃); 91% ee.



Epoxide 3.67. Epoxide **3.67** was prepared according to General Procedure VI with allylic alcohol **3.100** (22.6 mg, 0.10 mmol) and purified by flash chromatography (20% v/v EtOAc in hexanes) to afford epoxide **3.67** as a clear oil (19.9 mg, 88% yield). NOTE: A racemic standard of epoxide **3.67** was prepared according to the previously reported procedure for radical polar crossover epoxidation using racemic catalyst **3.53**.¹²



Epoxide 3.67

¹H NMR (600 MHz, CDCl₃, 25 °C):

δ 3.53 (s, 2H)	1.58-1.53 (m, 1H)
3.49 (s, 2H)	1.48-1.42 (m, 1H)
2.89 (q, J = 5.6 Hz, 1H)	1.28 (d, J = 5.6 Hz, 3H)
2.01-1.87 (m, 4H)	0.98 (s, 3H)
1.72 (td, J = 11.7, 4.2 Hz, 2H)	0.96 (s, 3H)

¹³C NMR (151 MHz, CDCl₃, 25 °C):

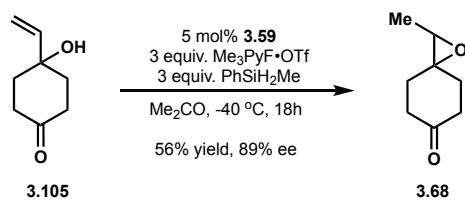
δ 97.3	61.8	30.35	24.6	13.7
70.32	59.7	30.25	22.77	
70.13	30.9	30.10	22.72	

HRMS (ESI) calc. for C₁₃H₂₂O₃ [M+Na]⁺: 249.1467, found: 249.1468

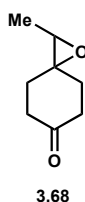
TLC R_f = 0.47 (30% EtOAc/Hex)

Chiral GC/FID: HP – chiral – 20B column, 6.88 psi, 0.50 mL/min, 130 °C, 180 min t_R = 163.4, 167.5.

[α]_D²⁵ = +8.3 ° (c = 1.0, CHCl₃); 82% ee.



Epoxide 3.68. Epoxide **3.68** was prepared according to General Procedure VI with allylic alcohol **3.105** (14.0 mg, 0.10 mmol) and purified by flash chromatography (20% v/v EtOAc in hexanes) to afford epoxide **3.68** as a clear oil (7.8 mg, 56% yield). NOTE: A racemic standard of epoxide **3.68** was prepared according to the previously reported procedure for radical polar crossover epoxidation using racemic catalyst **3.53**.¹²



Epoxide **3.68**

¹H NMR (600 MHz, CDCl₃, 25 °C):

δ 3.09 (q, J = 5.5 Hz, 1H)	1.88 (dtd, J = 13.9, 5.8, 2.3 Hz, 1H)
2.70-2.60 (m, 2H)	1.76 (dtd, J = 13.8, 5.7, 2.3 Hz, 1H)
2.47-2.40 (m, 2H)	1.37 (d, J = 5.6 Hz, 3H)
2.11-2.02 (m, 2H)	

¹³C NMR (151 MHz, CDCl₃, 25 °C):

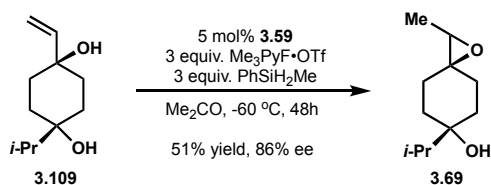
δ 210.4	38.60
60.4	33.6
60.1	27.7
38.69	14.0

LRMS (ESI) calc. for C₈H₁₂O₂ [M+Na]⁺: 140.1, found: 140.1

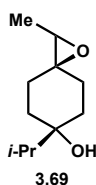
TLC R_f = 0.34 (40% EtOAc/Hex)

Chiral GC/FID: HP – chiral – 20B column, 6.88 psi, 0.50 mL/min, 100 °C, 120 min t_R = 114.7, 116.1

[α]_D²⁵ = +13.2 ° (c = 0.40, CHCl₃); 89% ee.



Epoxide 3.69. Epoxide **3.69** was prepared according to General Procedure VI with allylic alcohol **3.109** (15.6 mg, 0.10 mmol) and purified by flash chromatography (40% v/v EtOAc in hexanes) to afford epoxide **3.69** as a clear oil (9.8 mg, 51% yield). NOTE: A racemic standard of epoxide **3.69** was prepared according to the previously reported procedure for radical polar crossover epoxidation using racemic catalyst **3.53**.¹²



Epoxide **3.69**

¹H NMR (600 MHz, CDCl₃, 25 °C):

δ 2.91 (q, J = 5.6 Hz, 1H)	1.51-1.42 (m, 3H)
2.20 (td, J = 13.5, 4.6 Hz, 1H)	1.29 (d, J = 5.6 Hz, 2H)
2.05 (td, J = 13.4, 4.7 Hz, 1H)	0.95 (d, J = 6.9 Hz, 6H).
1.79-1.56 (m, 8H)	

¹³C NMR (151 MHz, CDCl₃, 25 °C):

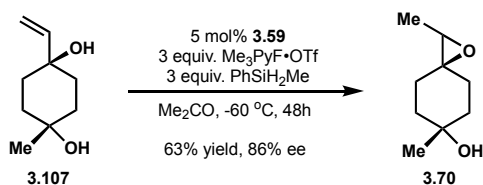
δ 73.2	31.8	29.2
70.9	31.34	23.8
59.9	31.19	16.8
38.3	30.0	

LRMS (ESI) calc. for C₁₁H₂₀O₂ [M+Na]⁺: 184.1, found: 184.1

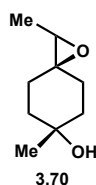
TLC R_f = 0.44 (40% EtOAc/Hex)

Chiral GC/FID: HP – chiral – 20B column, 6.88 psi, 0.50 mL/min, 110 °C, 180 min, then ramp to 200 °C at 10 °C per minute, t_R = 188.4, 188.7

[α]_D²⁵ = +8.66° (c = 0.60, CHCl₃); 86% ee.



Epoxide 3.70. Epoxide **3.70** was prepared according to General Procedure VI with allylic alcohol **3.107** (15.6 mg, 0.10 mmol) and purified by flash chromatography (40% v/v EtOAc in hexanes) to afford epoxide **3.70** as a clear oil (9.8 mg, 63% yield). NOTE: A racemic standard of epoxide **3.70** was prepared according to the previously reported procedure for radical polar crossover epoxidation using racemic catalyst **3.53**.¹²



Epoxide **3.70**

^1H NMR (600 MHz, CDCl_3 , $25\text{ }^\circ\text{C}$):

δ 2.91 (q, $J = 5.6$ Hz, 1H)	1.63 (dtd, $J = 13.6, 4.4, 2.3$ Hz, 1H)
2.09 (ddd, $J = 13.6, 12.3, 4.6$ Hz, 1H)	1.37 (dtd, $J = 13.8, 4.4, 2.1$ Hz, 1H)
1.98 (ddd, $J = 13.8, 11.9, 4.8$ Hz, 1H)	1.30 (s, 3H)
1.75 (dtd, $J = 24.7, 12.4, 4.5$ Hz, 2H)	1.29 (d, $J = 5.6$ Hz, 3H)
1.68 (dtd, $J = 13.6, 4.6, 2.4$ Hz, 1H)	

^{13}C NMR (151 MHz, CDCl_3 , $25\text{ }^\circ\text{C}$):

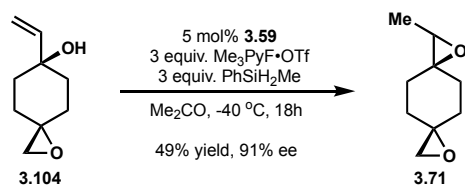
δ 69.5	30.57
61.7	30.43
59.9	24.2
36.50	13.5
36.49	

LRMS (ESI) calc. for $\text{C}_9\text{H}_{16}\text{O}_2$ $[\text{M}+\text{Na}]^+$: 156.1, found: 156.1

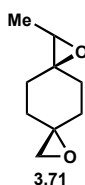
TLC $R_f = 0.24$ (40% EtOAc/Hex)

Chiral GC/FID: HP – chiral – 20B column, 6.88 psi, 0.50 mL/min, $130\text{ }^\circ\text{C}$, 30 min $t_R = 17.8, 18.9$

$[\alpha]_D^{25} = +2.1^\circ$ ($c = 0.60$, CHCl_3); 86% ee.



Epoxide 3.71. Prepared according to General Procedure VI using vinylcyclohexanol **3.104** (15.4 mg, 0.10 mmol). The crude was chromatographed (gradient elution: 100% pentane to 15% v/v Et₂O/pentane) to afford 7.5 mg (49% yield, 91% ee) of **3.71** as a clear colorless oil. NOTE: A racemic standard of epoxide **3.71** was prepared according to the previously reported procedure for radical polar crossover epoxidation using racemic catalyst **3.53**.¹²



Epoxide **3.71**

¹H NMR (500 MHz, CDCl₃, 25 °C):

δ 2.96 (q, J = 5.6 Hz, 1H)	1.62-1.57 (m, 2H)
2.71 (s, 2H)	1.50-1.46 (m, 2H)
2.13-2.01 (m, 3H)	1.33 (d, J = 5.6 Hz, 3H)
2.01-1.95 (m, 1H)	

¹³C NMR (126 MHz, CDCl₃, 25 °C):

δ 61.4	32.5
60.1	30.8
58.3	26.3
54.3	13.6

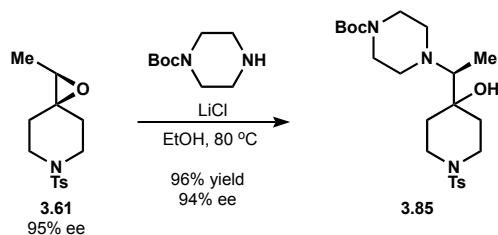
LRMS (ESI) calculated for C₉H₁₄O₂ [M+Na]⁺: 177.0892, found: 177.3611

TLC: R_f = 0.41 (40% EtOAc/Hex)

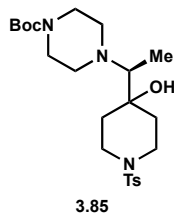
Chiral GC/FID: HP – chiral – 20B column, 6.88 psi, 0.50 mL/min, 110 °C, 90 min t_R = 61.6, 64.5.

[α]_D²⁵ = +10.3 (c = 0.5, CDCl₃); 91% ee.

Derivatization of Enriched Epoxide 3.61.



Aminoalcohol 3.85. Enriched epoxide **3.61** (5.0 mg, 0.018 mmol), 1-boc-piperazine (66.3 mg, 0.356 mmol) and LiCl (16.2 mg, 0.383 mmol) were dissolved in EtOH (0.3 mL) in a 1 dram vial. The vial was sealed with a Teflon cap and the reaction was stirred while heated to 80 °C for 20 h. After cooling to rt, the contents were diluted with CH₂Cl₂, transferred to a separatory funnel and extracted with CH₂Cl₂ (3 x 6 mL) from 10 mL of H₂O. The combined organic layers were dried over Na₂SO₄. The crude material was purified by flash silica chromatography (gradient elution: 100% hexanes to 20% v/v EtOAc/hexanes) to yield 8.0 mg (96% yield, 94% ee) of **3.85** as a tan solid. NOTE: Racemic **3.85** was prepared by subjecting racemic epoxide **3.61** to the above conditions.



Aminoalcohol **3.85**

¹H NMR (500 MHz, CDCl₃, 25 °C):

δ 7.64 (d, J = 8.2 Hz, 2H)	3.38 (d, J = 15.3 Hz, 4H)	1.83-1.73 (m, 2H)
7.30 (d, J = 7.9 Hz, 2H)	2.65-2.59 (m, 4H)	1.44 (s, 9H)
4.27 (s, 1H)	2.42 (s, 3H)	1.36 (td, J = 22.9, 9.1 Hz, 3H)
3.66-3.64 (m, 2H)	2.37 (dd, J = 14.5, 7.3 Hz, 3H)	1.01 (d, J = 7.1 Hz, 3H)

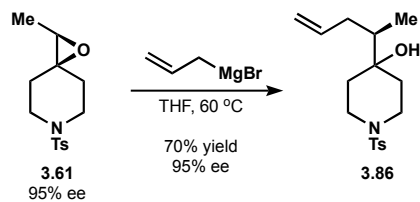
¹³C NMR (126 MHz, CDCl₃, 25 °C):

δ 154.6	129.6	69.3	42.2	21.5
143.4	127.7	68.3	35.2	8.0
133.2	79.9	42.8	28.4	

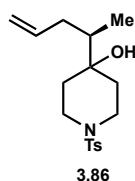
HRMS (ESI) calculated for C₂₃H₃₇N₃O₅S [M+H]⁺: 468.2532, found: 468.2534

TLC: R_f = 0.47 (50% EtOAc/Hex)

[α]_D²⁵ = +43.1 (c = 1.0, CDCl₃)



Hydroxyalkene 3.86. Allylmagnesium bromide (1.0 M in Et₂O, 0.2 mL, 0.2 mmol) was added dropwise to a solution of **3.61** (9.0 mg, 0.032 mmol) in 0.4 mL of THF at rt. The reaction was stirred for a further 5 min at rt and then heated to 60 °C in an oil bath. After 20 min the reaction was removed from heat and quenched with sat. aq. NH₄Cl. The mixture was extracted with CH₂Cl₂ (3 x 6 mL) and the organic layers dried over Na₂SO₄. The crude material was purified by flash silica chromatography (gradient elution: 100% hexanes to 15% v/v EtOAc/hexanes) to yield 7.2 mg (70% yield, 95% ee) of **3.86** as a tan solid. NOTE: Racemic **3.86** was prepared by subjecting racemic epoxide **3.61** to the above conditions.



Hydroxyalkene **3.86**

¹H NMR (500 MHz, CDCl₃, 25 °C):

δ 7.65 (d, J = 8.2 Hz, 2H)	2.32 (d, J = 13.0 Hz, 1H)
7.31 (d, J = 7.9 Hz, 2H)	1.84-1.70 (m, 3H)
5.82-5.74 (m, 1H)	1.58 (t, J = 2.2 Hz, 1H)
5.05-5.01 (m, 2H)	1.54 (d, J = 2.2 Hz, 1H)
3.64-3.60 (m, 2H)	1.48 (ddd, J = 9.6, 6.5, 3.3 Hz, 1H)
2.59 (tdd, J = 11.9, 6.3, 2.2 Hz, 2H)	0.92 (s, 1H)
2.43 (s, 3H)	0.89 (d, J = 6.9 Hz, 3H)

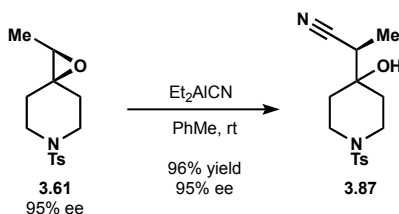
¹³C NMR (126 MHz, CDCl₃, 25 °C):

δ 143.4	116.5	35.4
137.7	71.3	34.2
133.3	43.2	33.0
129.6	42.17	21.5
127.7	42.10	13.5

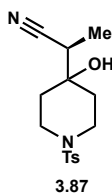
HRMS (ESI) calculated for C₁₇H₂₅NO₃S [M+Na]⁺: 346.1453, found: 346.1462

TLC: R_f = 0.41 (30% EtOAc/Hex)

[α]_D²⁵ = -3.2 (c = 1.0, CDCl₃)



Hydroxynitrile 3.87. Adapted from a procedure reported by Neef.⁵³ Et₂AlCN (1.0 M in PhMe, 90 μL, 0.09 mmol) was added dropwise to a stirred solution of **3.61** (5.0 mg, 0.018 mmol) in 0.30 mL of dry PhMe at rt. The reaction was stirred for 18 h and then quenched with sat. aq. NH₄Cl. The mixture was extracted with CH₂Cl₂ (3x 6 mL) and the organic layers dried over Na₂SO₄. The crude material was purified by flash silica chromatography (gradient elution: 100% hexanes to 40% v/v EtOAc/hexanes) to yield 5.3 mg (96% yield, 95% ee) of **3.87** as a tan solid. NOTE: Racemic **3.87** was prepared by subjecting racemic epoxide **3.61** to the above conditions.



Hydroxynitrile **3.87**

¹H NMR (500 MHz, CDCl₃, 25 °C):

δ 7.65 (d, J = 8.2 Hz, 2H)	2.44 (s, 3H)	1.41 (d, J = 0.2 Hz, 1H)
7.33 (d, J = 7.9 Hz, 2H)	1.86 (td, J = 13.0, 4.6 Hz, 1H)	1.31 (d, J = 7.2 Hz, 3H)
3.69 (d, J = 11.4 Hz, 2H)	1.79 (dd, J = 13.8, 2.1 Hz, 1H)	
2.63-2.58 (m, 3H)	1.73 (q, J = 9.2 Hz, 2H)	

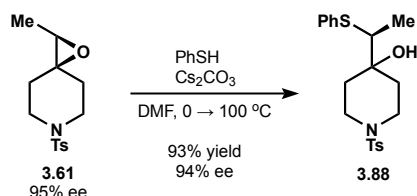
¹³C NMR (126 MHz, CDCl₃, 25 °C):

δ 143.8	120.4	34.7
133.1	69.4	33.0
129.8	41.7	21.6
127.7	38.2	12.0

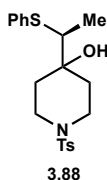
HRMS (ESI) calculated for C₁₅H₂₀N₂O₃S [M+Na]⁺: 331.1092, found: 331.1086

TLC: R_f = 0.24 (50% EtOAc/Hex)

[α]_D²⁵ = -3.9 (c = 1.0, CHCl₃)



Hydroxysulfide **3.88**. Adapted from a procedure reported by Zaimoku.⁵⁴ Enriched epoxide **3.61** (5.0 mg, 0.018 mmol) and Cs₂CO₃ (57.8 mg, 0.178 mmol) were added to a flame dried Schlenk which was then evacuated and backfilled 3x with N₂. Dry DMF was added and the suspension was degassed by freeze-pump-thaw. The mixture was cooled to 0 °C and PhSH (18.2 μL, 0.178 mmol) was added dropwise. The reaction was then transferred to an oil bath and heated to 100 °C. After 2 h the reaction was removed from heat and quenched with sat. aq. NH₄Cl. The mixture was extracted with CH₂Cl₂ (3 x 6 mL) and the organic layers dried over Na₂SO₄. The crude material was purified by flash silica chromatography (gradient elution: 100% hexanes to 15% v/v EtOAc/hexanes) to yield 6.5 mg (93% yield, 94% ee) of **3.88** as a white solid. NOTE: Racemic **3.88** was prepared by subjecting racemic epoxide **3.61** to the above conditions.



Hydroxysulfide **3.88**

¹H NMR (500 MHz, CDCl₃, 25 °C):

δ 7.64 (d, J = 7.9 Hz, 2H)	2.65-2.60 (m, 2H)
7.40 (d, J = 7.3 Hz, 2H)	2.43 (s, 3H)
7.31 (d, J = 8.3 Hz, 2H)	2.17 (s, 1H)
7.28 (d, J = 7.6 Hz, 2H)	1.85-1.77 (m, 2H)
7.24 (t, J = 7.3 Hz, 1H)	1.68 (dd, J = 13.7, 1.8 Hz, 1H)
3.65 (t, J = 14.2 Hz, 2H)	1.63 (dd, J = 13.3, 2.0 Hz, 1H)
3.18 (q, J = 7.0 Hz, 1H)	1.35 (d, J = 7.1 Hz, 3H)

¹³C NMR (126 MHz, CDCl₃, 25 °C):

δ 143.5	129.7	71.2	34.8
135.2	129.2	57.4	32.4
133.3	127.7	42.4	21.6
131.9	127.4	42.0	17.2

HRMS (ESI) calculated for C₂₀H₂₅NO₃S₂ [M+Na]⁺: 414.1174, found: 414.1167

TLC: R_f = 0.38 (30% EtOAc/Hex)

[α]_D²⁵ = -28.7 (c = 1.0, CDCl₃)

3.11 References and Notes

1. For pioneering work on relevant hydrofunctionalizations see: Mukaiyama, T.; Yamada, T. *Bull. Chem. Soc. Jpn.* **1995**, *68*, 17.
2. For an excellent review of MHAT hydrofunctionalizations see: Crossley, S. W. M.; Obradors, C.; Martinez, R. M.; Shenvi, R. A. *Chem. Rev.* **2016**, *116*, 8912.
3. For an excellent review on the chemoselectivity of metal-hydrides to engage alkenes via HAT see: Green, S. A.; Crossley, S. W. M.; Matos, J. L. M.; Vásquez-Céspedes, S.; Shevick, S. L.; Shenvi, R. A. *Acc. Chem. Res.* **2018**, *51*, 2628.
4. For selected examples see: (a) Waser, J.; Nambu, H.; Carreira, E. M. *J. Am. Chem. Soc.* **2005**, *127*, 8294. (b) Gaspar, B.; Carreira, E. M. *Angew. Chem., Int. Ed.* **2007**, *46*, 4519. (c) Gaspar, B.; Carreira, E. M. *Angew. Chem., Int. Ed.* **2008**, *47*, 5758. (d) Gaspar, B.; Carreira, E. M. *J. Am. Chem. Soc.* **2009**, *131*, 13214. (e) Girijavallabhan, V.; Alvarez, C.; Njoroge, F. G. *J. Org. Chem.* **2011**, *76*, 6442. (f) Barker, T.; Boger, D. L. *J. Am. Chem. Soc.* **2012**, *134*, 13588. (g) Leggans, E. K.; Barker, T. J.; Duncan, K. K.; Boger, D. L. *Org. Lett.* **2012**, *14*, 1428. (h) Shigehisa, H.; Nishi, E.; Fujisawa, M.; Hiroya, K. *Org. Lett.* **2013**, *15*, 5158. (i) Iwasaki, K.; Wan, K. K.; Oppedisano, A.; Crossley, S. W. M.; Shenvi, R. A. *J. Am. Chem. Soc.* **2014**, *136*, 1300. (j) King, S. M.; Ma, X.; Herzon, S. B. *J. Am. Chem. Soc.* **2014**, *136*, 6884. (k) Ma, X. S.; Herzon, S. B. *Chem. Sci.* **2015**, *6*, 6250. (l) Zheng, J.; Wang, D.; Cui, S. *Org. Lett.* **2015**, *17*, 4572. (m) Crossley, S. W. M.; Martinez, R. M.; Guevara-Zuluaga, S.; Shenvi, R. A. *Org. Lett.* **2016**, *18*, 2620. (n) Ma, X.; Herzon, S. B. *J. Am. Chem. Soc.* **2016**, *138*, 8718. (o) Ma, X.; Dang, H.; Rose, J. A.; Rablen, P.; Herzon, S. B. *J. Am. Chem. Soc.* **2017**, *139*, 5998. (p) Qi, J.; Zheng, J.; Cui, S. *Org. Lett.* **2018**, *20*, 1355. (q) Yang, L.; Ji, W.-W.; Lin, E.; Li, J.-L.; Fan, W.-X.; Li, Q.; Wang, H. *Org. Lett.* **2018**, *20*, 1924. (r) Zhang, Y.; Huang, C.; Lin, X.; Hu, Q.; Hu, B.; Zhou, Y.; Zhu, G. *Org. Lett.* **2019**, *21*, 2261. (s) Zhou, X.-L.; Yang, F.; Sun, H.-L.; Yin, Y.-N.; Ye, W.-T.; Zhu, R. *J. Am. Chem. Soc.* **2019**, *141*, 7250.
5. For selected examples, see: (a) Wang, L.-C.; Jang, H.-Y.; Roh, Y.; Lynch, V.; Schultz, A. J.; Wang, X.; Krische, M. J. *J. Am. Chem. Soc.* **2002**, *124*, 9448. (b) Waser, J.; Carreira, E. M. *J. Am. Chem. Soc.* **2004**, *126*, 5676. (c) Smith, D. M.; Pulling, M. E.; Norton, J. R. *J. Am. Chem. Soc.* **2007**, *129*, 770. (d) Lo, J. C.; Yabe, Y.; Baran, P. S. *J. Am. Chem. Soc.* **2014**, *136*, 1304.

- (e) Lo, J. C.; Gui, J.; Yabe, Y.; Pan, C.-M.; Baran, P. S. *Nature* **2014**, *516*, 343. (f) Crossley, S. W. M.; Barabé, F.; Shenvi, R. A. *J. Am. Chem. Soc.* **2014**, *136*, 16788. (g) Kuo, J. L.; Hartung, J.; Han, A.; Norton, J. R. *J. Am. Chem. Soc.* **2015**, *137*, 1036. (h) Gui, J.; Pan, C.-M.; Jin, Y.; Qin, T.; Lo, J. C.; Lee, B. J.; Spergel, S. H.; Mertzman, M. E.; Pitts, W. J.; La Cruz, T. E.; Schmidt, M. A.; Darvatkar, N.; Natarajan, S.; Baran, P. S. *Science* **2015**, *348*, 886. (i) Dao, H. T.; Li, C.; Michaudel, Q.; Maxwell, B. D.; Baran, P. S. *J. Am. Chem. Soc.* **2015**, *137*, 8046. (j) Zheng, J.; Qi, J.; Cui, S. *Org. Lett.* **2016**, *18*, 128. (k) Lo, J. C.; Kim, D.; Pan, C.-M.; Edwards, J. T.; Yabe, Y.; Gui, J.; Qin, T.; Gutiérrez, S.; Giacoboni, J.; Smith, M. W.; Holland, P. L.; Baran, P. S. *J. Am. Chem. Soc.* **2017**, *139*, 2484. (l) Saladrigas, M.; Bosch, C.; Saborit, G. V.; Bonjoch, J.; Bradshaw, B. *Angew. Chem., Int. Ed.* **2018**, *57*, 182. (m) Saladrigas, M.; Loren, G.; Bonjoch, J.; Bradshaw, B. *ACS Catal.* **2018**, *8*, 11699. (n) Matos, J. L. M.; Vásquez-Céspedes, S.; Gu, J.; Oguma, T.; Shenvi, R. A. *J. Am. Chem. Soc.* **2018**, *140*, 16976.
6. (a) Green, S. A.; Matos, J. L. M.; Yagi, A.; Shenvi, R. A. *J. Am. Chem. Soc.* **2016**, *138*, 12779. (b) Green, S. A.; Vásquez-Céspedes, S.; Shenvi, R. A. *J. Am. Chem. Soc.* **2018**, *140*, 11317. (c) Shevick, S. L.; Obradors, C.; Shenvi, R. A. *J. Am. Chem. Soc.* **2018**, *140*, 12056. (d) Green, S. A.; Huffman, T. R.; McCourt, R. O.; van der Puyl, V.; Shenvi, R. A. *J. Am. Chem. Soc.* **2019**, *141*, 7709.
7. (a) Shigehisa, H.; Aoki, T.; Yamaguchi, S.; Shimizu, N.; Hiroya, K. *J. Am. Chem. Soc.* **2013**, *135*, 10306. (b) Shigehisa, H.; Koseki, N.; Shimizu, N.; Fujisawa, M.; Niitsu, M.; Hiroya, K. *J. Am. Chem. Soc.* **2014**, *136*, 13534. (c) Shigehisa, H.; Ano, T.; Honma, H.; Ebisawa, K.; Hiroya, K. *Org. Lett.* **2016**, *18*, 3622.
8. For examples of MHAT hydrofunctionalizations under catalyst control see references 5f and 6c.
9. Sato, M.; Gunji, Y.; Ikeno, T.; Yamada, T. *Chem. Lett.* **2004**, *33*, 1304.
10. Sato, M.; Gunji, Y.; Ikeno, T.; Yamada, T. *Chem. Lett.* **2005**, *34*, 316.
11. For relevant discussion, see: (a) Sibi, M. P.; Manyem, S.; Zimmerman, J. *Chem. Rev.* **2003**, *103*, 3263. (b) Studer, A.; Curran, D. P. *Angew. Chem., Int. Ed.* **2016**, *55*, 58. (c) Yan, M.; Lo, J. C.; Edwards, J. T.; Baran, P. S. *J. Am. Chem. Soc.* **2016**, *138*, 12692. (d) Lu, Q.; Glorius, F. *Angew. Chem., Int. Ed.* **2017**, *56*, 49.
12. Touney, E. E.; Foy, N. J.; Pronin, S. V. *J. Am. Chem. Soc.* **2018**, *140*, 16982.
13. (a) Abley, P.; Dockal, E. R.; Halpern, J. *J. Am. Chem. Soc.* **1972**, *94*, 659. (b) Anderson, S. N.; Ballard, D. H.; Chrzastowski, J. Z.; Dodd, D.; Johnson, M. D. *J. Chem. Soc., Chem. Commun.* **1972**, *0*, 685. (c) Halpern, J.; Chan, M. S.; Hanson, J.; Roche, T. S.; Topich, J. A. *J. Am. Chem. Soc.* **1975**, *97*, 1606. (d) Halpern, J.; Topich, J.; Zamaraev, K. I. *Inorg. Chim. Acta* **1976**, *20*, L21. (e) Magnuson, R. H.; Halpern, J.; Levitin, I. Ya.; Vol'pin, M. E. *J. Chem. Soc., Chem. Commun.* **1978**, *0*, 44. (f) Topich, J.; Halpern, J. *Inorg. Chem.* **1979**, *18*, 1339. (g) Halpern, J.; Chan, M. S.; Roche, T. S.; Tom, G. M.; Hoyer, E.; Spiridonov, V. P.; Strand, T. G. *Acta Chem. Scand.* **1979**, *33*, 141.
14. Discolo, C. A.; Touney, E. E.; Pronin, S. V. *J. Am. Chem. Soc.* **2019**, *141*, 17527.
15. Lacy, D. C.; Roberts, G. M.; Peters, J. C. *J. Am. Chem. Soc.* **2015**, *137*, 4860.
16. For evidence of solvent caged alkylradical-metalloradical pair see: (a) Sweany, R.; Halpern, J. *J. Am. Chem. Soc.* **1977**, *99*, 8335. (b) Jacobsen, E. N.; Bergman, R. G. *J. Am. Chem. Soc.* **1985**, *107*, 2023. (c) Ungváry, F.; Markó, L. *J. Organomet. Chem.* **1983**, *249*, 411. (d) Matsui, Y.; Orchin, M. *J. Organomet. Chem.* **1983**, *244*, 369.
17. Shigehisa and Lu have since reported enantioselective MHAT reactions: (a) Ebisawa, K.; Izumi, K.; Ooka, Y.; Kato, H.; Kanazawa, S.; Komatsu, S.; Nishi, E.; Shigehisa, H. *J. Am.*

- Chem. Soc.* **2020**, *142*, 13481. (b) Shen, X.; Chen, X.; Chen, J.; Sun, Y.; Cheng, Z.; Lu, Z. *Nat. Comm.* **2020**, *11*, 783.
18. Jackman, L. M.; Hamilton, J. A.; Lawlor, J. M. *J. Am. Chem. Soc.* **1968**, *90*, 1914.
 19. Gridnev, A. A.; Ittel, S. D.; Wayland, B. B.; Fryd, M. *Organometallics* **1996**, *15*, 5116.
 20. Shigehisa, H.; Hayashi, M.; Ohkawa, H.; Suzuki, T.; Okayasu, H.; Mukai, M.; Yamazaki, A.; Kawai, R.; Kikuchi, H.; Satoh, Y.; Fukuyama, A.; Hiroya, K. *J. Am. Chem. Soc.* **2016**, *138*, 10597.
 21. Kim, H.; Nguyen, Y.; Pai-Hui, C.; Chagal, L.; Lough, A. J.; Kim, B. M.; Chin, J. *J. Am. Chem. Soc.* **2008**, *130*, 12184.
 22. Chin, J.; Mancin, F.; Thavarajah, N.; Lee, D.; Lough, A.; Chung, D. S. *J. Am. Chem. Soc.* **2003**, *125*, 15276.
 23. Kim, H.; Nguyen, Y.; Lough, A.; Chin, J. *Angew. Chem. Int. Ed.* **2008**, *47*, 8678.
 24. Knowles, R. R.; Lin, S.; Jacobsen, E. N. *J. Am. Chem. Soc.* **2010**, *132*, 5030.
 25. (a) Williams, D. H.; Calderone, C. T. *J. Am. Chem. Soc.* **2001**, *123*, 6262. (b) Dunitz, J. D. *Chem. Biol.* **1995**, *2*, 709. (c) Westwell, M. S.; Searle, M. S.; Klein, J.; Williams, D. H. *J. Phys. Chem.* **1996**, *100*, 16000.
 26. For selected reviews of cation– π interactions in chemical catalysis, see: (a) Pluth, M. D.; Bergman, R. G.; Raymond, K. N. *Acc. Chem. Res.* **2009**, *42*, 1650. (b) Brown, C. J.; Toste, F. D.; Bergman, R. G.; Raymond, K. N. *Chem. Rev.* **2015**, *115*, 3012. (c) Kennedy, C. R.; Lin, S.; Jacobsen, E. N. *Angew. Chem., Int. Ed.* **2016**, *55*, 12596. (d) Neel, A. J.; Hilton, M. J.; Sigman, M. S.; Toste, F. D. *Nature* **2017**, *543*, 637. (e) Yamada, S. *Chem. Rev.* **2018**, *118*, 11353.
 27. For examples of relevant alkylcobalt(IV) complexes that point to diversity of electronic structures, see: (a) Ref 13f. (b) Fukuzumi, S.; Miyamoto, K.; Suenobu, T.; Van Caemelbecke, E.; Kadish, K. M. *J. Am. Chem. Soc.* **1998**, *120*, 2880. (c) Harmer, J.; Van Doorslaer, S.; Gromov, I.; Bröring, M.; Jeschke, G.; Schweiger, A. *J. Phys. Chem. B* **2002**, *106*, 2801. (d) Kumar, N.; Kuta, J.; Galezowski, W.; Kozlowski, P. M. *Inorg. Chem.* **2013**, *52*, 1762.
 28. For studies of relevant cobalt(III) salen complexes, see: (a) Bar-Nahum, I.; Cohen, H.; Neumann, R. *Inorg. Chem.* **2003**, *42*, 3677. (b) Kochem, A.; Kanso, H.; Baptiste, B.; Arora, H.; Philouze, C.; Jarjays, O.; Vezin, H.; Luneau, D.; Orio, M.; Thomas, F. *Inorg. Chem.* **2012**, *51*, 10557.
 29. For polarizabilities, see: Waite, J.; Papadopoulos, M. G.; Nicolaidis, C. A. *J. Chem. Phys.* **1982**, *77*, 2536.
 30. For quadrupole moments, see: Heard, G. L.; Boyd, R. J. *J. Phys. Chem. A* **1997**, *101*, 5374.
 31. For a discussion of the role of electrostatics in cation– π interactions, see: Mecozzi, S.; West, A. P.; Dougherty, D. A. *J. Am. Chem. Soc.* **1996**, *118*, 2307.
 32. For a discussion of the role of dispersion forces in cation– π interactions, see: Tsuzuki, S.; Mikami, M.; Yamada, S. *J. Am. Chem. Soc.* **2007**, *129*, 8656.
 33. For additional examples of tuning cation– π interactions with extended aromatic motifs in enantioselective catalysis, see: (a) Lin, S.; Jacobsen, E. N. *Nat. Chem.* **2012**, *4*, 817. (b) Bendelsmith, A. J.; Kim, S. C.; Wasa, M.; Roche, S. P.; Jacobsen, E. N. *J. Am. Chem. Soc.* **2019**, *141*, 11414.
 34. For discussion of alkyl fluoride–cation interactions relevant to the case of product **3.65**, see: Ferraris, D.; Cox, C.; Anand, R.; Lectka, T. *J. Am. Chem. Soc.* **1997**, *119*, 4319.
 35. For more on kinetics of radical pair collapse, see: Tsou, T.-T.; Loots, M.; Halpern, J. *J. Am. Chem. Soc.* **1982**, *104*, 623.

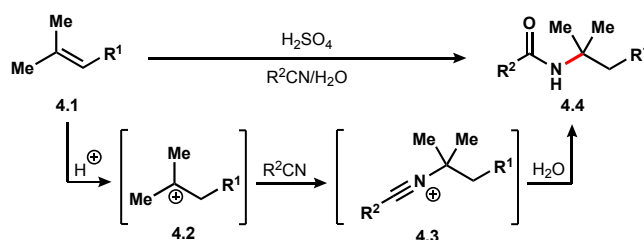
36. For a relevant dynamic kinetic resolution: Gutierrez, O.; Tellis, J. C.; Primer, D. N.; Molander, G. A.; Kozlowski, M. C. *J. Am. Chem. Soc.* **2015**, *137*, 4896.
37. Palucki, M.; Finney, N. S.; Pospisil, P. J.; Güler, M. L.; Ishida, T.; Jacobsen, E. N. *J. Am. Chem. Soc.* **1998**, *120*, 948.
38. (a) Samsel, E. G.; Kochi, J. K. *J. Am. Chem. Soc.* **1986**, *108*, 4790. For a relevant radical chain mechanism in nickel-catalyzed cross-coupling reactions, see: (b) Schley, N. D.; Fu, G. C. *J. Am. Chem. Soc.* **2014**, *136*, 16588.
39. Lande, S. S.; Kochi, J. K. *J. Am. Chem. Soc.* **1968**, *90*, 5196.
40. For an excellent discussion of the activation parameters of the capture of diffusing alkyl radicals with metal complexes, see: Koenig, T. W.; Hay, B. P.; Finke, R. G. *Polyhedron* **1988**, *7*, 1499.
41. (a) Clark, R. D.; Caroon, J. M.; Repke, D. B.; Strosberg, A. M.; Bitter, S. M.; Okada, M. S.; Michel, A. D.; Whiting, R. L. *J. Med. Chem.* **1983**, *26*, 855. (b) Hewitt, P.; McFarland, M. M.; Rountree, J. S. S.; Burkamp, F.; Bell, C.; Proctor, L.; Helm, M. D.; O'Dowd, C.; Harrison, T. Preparation of oxoheterocyclalkyl hydroxypiperidinyketones as ubiquitin-specific protease USP19 inhibitors useful in treatment of diseases. PCT Int. Appl. WO 2018/020242 A1, Feb 1, 2018.
42. Arnold, D. A.; Natrajan, L. S.; Hall, J. L.; Bird, S. J.; Wilson, C. *J. Organomet. Chem.* **2002**, *647*, 205.
43. Damavandi, S.; Samadieh, M.; Ahmadjo, S.; Etemadinia, Z.; Zohuri, G. H. *Eur. Polym. J.* **2016**, *64*, 118.
44. Tummatorn, J.; Krajangsri, S.; Norseeda, K.; Thongsornkleeb, C.; Ruchirawat, S. *Org. Biomol. Chem.* **2008**, *106*, 1059.
45. Xu, D.; Duan, Y.; Blair, I. A.; Pennig, T. M.; Harvey, R. G. *Org. Lett.* **2008**, *10*, 1059.
46. Niu, J.; Willis, M. C. *Org. Chem. Front.* **2016**, *3*, 625.
47. Kabalka, G. W.; Wu, Z.; Yao, M.-L. *Appl. Organometal. Chem.* **2008**, *22*, 516.
48. Zipfel, H. F.; Carreira, E. M. *Chem. Eur. J.* **2015**, *21*, 12475.
49. Carreaux, F.; Posseme, F.; Carboni, B.; Arrieta, A.; Lecea, B.; Cossia, F. P. *J. Org. Chem.* **2002**, *67*, 9153.
50. Zheng, H.; Lejkowski, M.; Hall, D. G. *Chem. Sci.* **2011**, *2*, 1305.
51. Salomon, P.; Zard, S. Z. *Org. Lett.* **2014**, *16*, 2926.
52. Finkelstein, J. A.; Perchonock, C. D. *Tetrahedron Lett.* **1980**, *21*, 3323.
53. Neef, G.; Eckle, E.; Müller-Fahrnow, A. *Tetrahedron* **1993**, *49*, 833.
54. Zaimoku, H.; Taniguchi, T. *Chem. Eur. J.* **2014**, *20*, 9613.

Chapter 4: Catalytic Radical–Polar Crossover Ritter Reactions of Trisubstituted and Tetrasubstituted Alkenes

4.1 Introduction

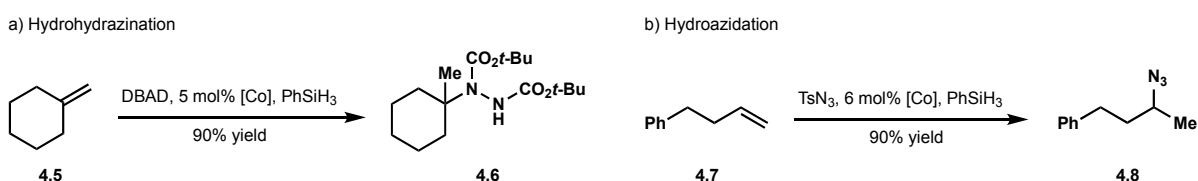
Discovered by Ritter in 1948, hydroamidation of alkenes with nitriles in the presence of strong Brønsted acid and water is a straightforward approach to access sterically demanding *tert*-alkyl carboxamides and their derivatives (**Scheme 4.1**).^{1,2} A general mechanism commences with initial rate-determining protonation of alkene **4.1** to tertiary carbocation **4.2**. Nucleophilic attack of carbocation **4.2** with a nitrile source results in formation of nitrilium ion **4.3**. Subsequent hydrolysis of **4.3** furnishes the functionalized *N*-alkyl amide product **4.4**. The Ritter reaction has seen widespread application in industrial and academic settings for installation of nitrogen-based functional groups.³ For example, the Ritter reaction is used to produce feedstock chemicals such as *tert*-octylamine and its higher molecular weight homologs annually on metric ton scale.⁴ Pharmaceutical companies and academic research labs have applied the Ritter reaction towards the synthesis of drug candidates and other biologically active molecules with therapeutic potential across a broad range of disease classes.^{5–11} However, the power of Ritter's methodology is undermined by the need for strong Brønsted acid to generate high energy carbocation intermediates via rate-limiting alkene protonation, which greatly restricts functional group compatibility. Given the utility of the canonical Ritter reaction, an acid-free variant would be a powerful transformation.

Scheme 4.1 The Ritter reaction and a general mechanism



Metal hydride-initiated hydrogen atom transfer (MHAT) reactions enable mild and chemoselective hydrofunctionalization of unactivated alkenes without the need for harsh Brønsted acids.^{12,13} Intermediate carbon-centered radicals generated by HAT can be intercepted with radicalophiles atom and group transfer agents¹⁴ to obtain hydrofunctionalization products with excellent Markovnikov regioselectivity, making MHAT radical reactions a complementary method to traditional Brønsted acid-catalysis. Thus, the Ritter reaction seems like an ideal candidate to develop into a MHAT manifold. A diverse array of metal-hydride-mediated C–N bond forming reactions have been developed that benefit from expanded functional group tolerance thanks to the mild nature of HAT.^{13,15–20} Prominent examples relevant to our labs research include Carreira’s cobalt-catalyzed hydrohydrazination^{15,17} and hydroazidation (**Scheme 4.2**).^{16,17} However, a method for Mukaiyama-type HAT radical hydroamidation has failed to materialize, likely due to the lack of a compatible group transfer agent capable of directly installing amide functionality.

Scheme 4.2 Select examples from Carreira's cobalt-catalyzed hydrohydrazination and hydroazidation

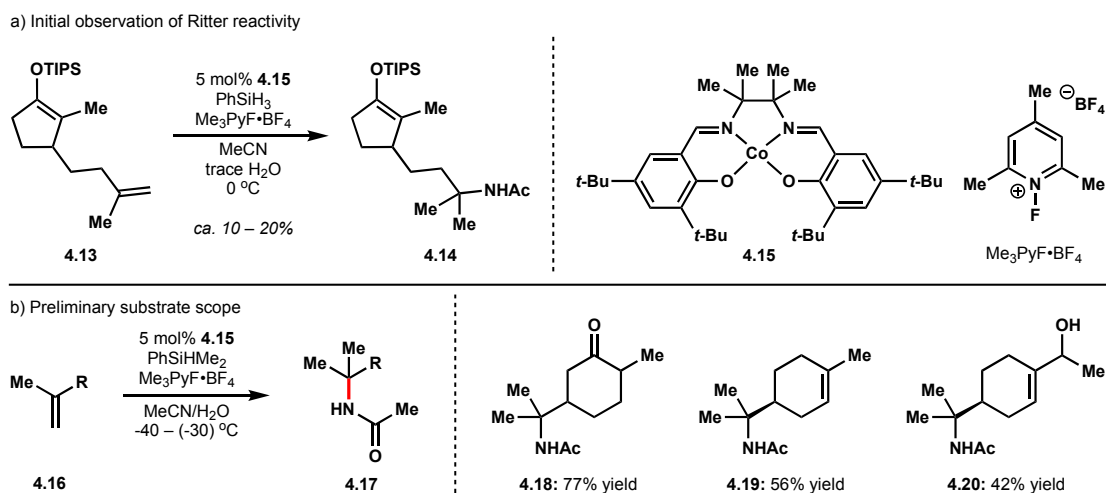


Discussed in detail in Chapter 2 and Chapter 3, our lab has capitalized on the ability for cobalt-catalyzed HAT radical–polar crossover reactions to generate electrophilic intermediates from unactivated alkenes.^{21,22} Radical–polar crossover alkene hydrofunctionalizations are an increasingly rich field of chemistry that offer a strategy to access carbocations from alkenes via mild single-electron oxidation of carbon-centered radicals following chemoselective HAT from a metal-hydride.²³ Capture of the transient carbocation with a polar nucleophile delivers Markovnikov alkene hydrofunctionalization products traditionally obtained by Brønsted acid-

catalysis.^{23a,24} Because canonical Ritter reactions proceed through carbocationic intermediates that are captured by two-electron nucleophiles, we proposed an acid-free Ritter reaction might be achievable through a HAT radical–polar crossover manifold.

During his investigations into HAT-initiated radical–polar crossover cationic polyene cyclizations of silyl enol ether **4.13**, Dr. David George serendipitously observed that application of wet acetonitrile as solvent resulted in formation of small amounts of acetamide byproduct **4.14** arising from apparent Markovnikov addition of acetamide to the C–C double bond (**Scheme 4.3a**).²⁵ Further optimization allowed for efficient conversion of a series of 1,1-disubstituted alkenes to the corresponding hydroamidation products using cobalt(II) salen catalyst **4.15** (**Scheme 4.3b**). However, while David successfully developed a preliminary HAT-initiated radical–polar crossover Ritter reaction, he observed significant limitations in the substrate scope with respect to alkene substitution. Despite continued optimization efforts, only 1,1-disubstituted alkenes could be reliably engaged, while trisubstituted alkenes remained untouched. This shortfall is perhaps best exemplified by acetamide **4.19**, derived from (–)-limonene.

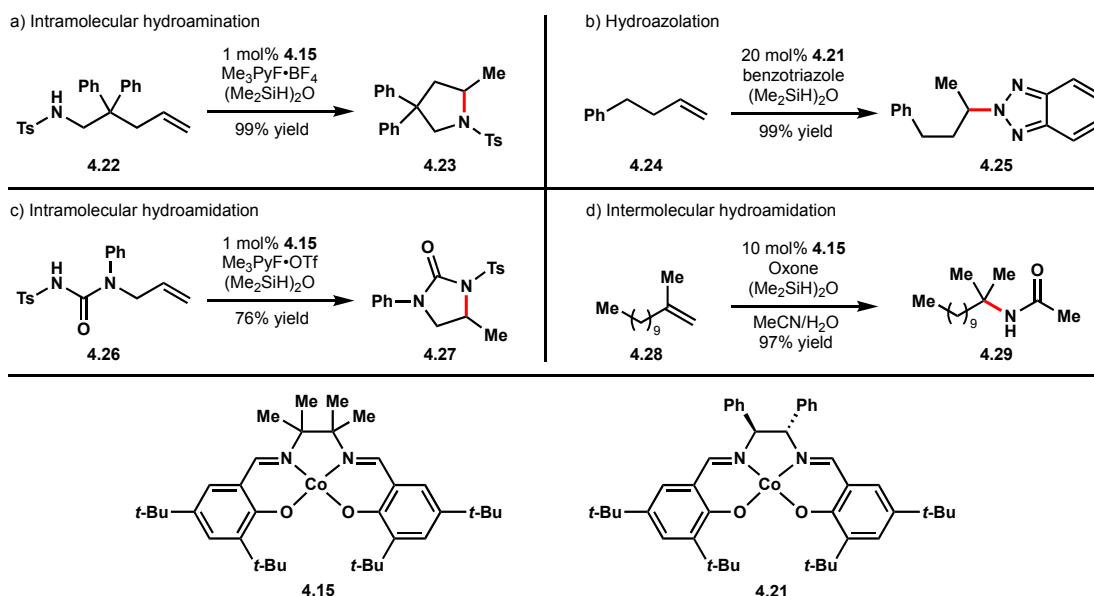
Scheme 4.3 Initial studies of the catalytic radical–polar crossover Ritter reaction



A survey of the literature revealed that related hydrofunctionalizations to install nitrogen-based functionalities suffer from similar restrictions in the scope of amenable alkene partners

(**Scheme 4.4**). The seminal report of cobalt-catalyzed radical–polar crossover hydroamination was published by Shigehisa in 2014 (**Scheme 4.4a**).^{24b} The reaction was mostly restricted to intramolecular cyclizations of pendant amines onto monosubstituted alkenes, for example conversion of alkene **4.22** to pyrrolidine **4.23**, although a handful of 1,1-disubstituted alkenes were engaged. Akai expanded the breadth of reactivity to encompass intermolecular installation of nitrogen functionality by effectively converting 4-phenylbutene **4.24** to *N*²-alkylated benzotriazole **4.25** (**Scheme 4.4b**).²⁶ However, Akai’s conditions were again limited to monosubstituted and a handful of 1,2-disubstituted alkene partners. An intramolecular radical–polar crossover hydroamidation catalyzed by cobalt(II) salen complexes was reported by Shigehisa in 2020, but the optimized conditions were not amenable to engaging alkenes with substitution patterns other than monosubstituted or 1,1-disubstituted (**Scheme 4.4c**).²⁷ While preparing this dissertation, the first report of intermolecular radical–polar crossover hydroamidation was reported by the Zhu lab (**Scheme 4.4d**).²⁸ Although they managed to develop an impressive acid-free variant of the Ritter reaction using Oxone as oxidant and a conventional cobalt (II) salen catalyst, Zhu’s protocol suffered from similar pitfalls as previous reports with respect to substrate scope. Most reaction

Scheme 4.4 Select examples from relevant radical–polar crossover hydrofunctionalizations



partners resemble the conversion of 1,1-disubstituted alkene **4.28** to the requisite *tert*-alkyl acetamide product **4.29**. Admittedly, Zhu was able to engage strained endocyclic trisubstituted alkenes in moderate yield, but the protocol failed during attempts to hydrofunctionalize acyclic trisubstituted alkenes such as prenyl groups. In fact, the intolerance of HAT radical–polar crossover reactions towards substrates containing heavily substituted alkene patterns is not limited to C–N bond forming events, but is endemic across all modes of radical–polar crossover reactivity.²⁹

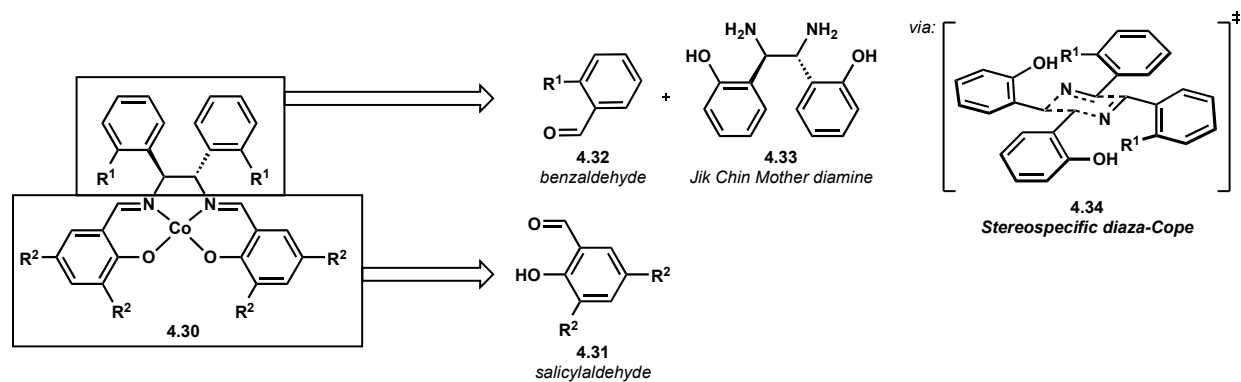
In this chapter, I describe investigations conducted by myself and my colleagues, Riley Cooper and Sarah Bredenkamp, that led to the development of a HAT-mediated radical–polar crossover hydroamidation protocol that can efficiently engage alkene substitutions previously inaccessible by conventional cobalt(II) salen complexes.

4.2 Strategy for a Catalytic Radical–Polar Crossover Ritter Reaction

We sought to overcome the existing limits of compatible alkene partners for HAT radical–polar crossover hydrofunctionalizations by developing a catalyst system capable of engaging challenging alkene substitution patterns in HAT. We suspect that cobalt(III) hydrides derived from commonly employed cobalt(II) salen catalysts, such as **4.15** and **4.21**, are not reactive enough to deliver a hydrogen atom to more thermodynamically stable and sterically demanding alkenes. Given our previous success establishing structure activity relationships between ligand structure and reactivity in the context of catalyst-controlled asymmetric induction, we thought we could likewise engineer salen ligands to produce a cobalt(II) complex capable of HAT towards heavily substituted alkenes.²²

Having identified the need to rapidly construct a library of cobalt(II) salen complexes with steric and stereoelectronic character spanning a broad chemical space, we opted to adapt the retrosynthetic strategy described in Chapter 3 (**Figure 4.1**). Disconnecting general catalyst **4.30** through a condensation transform brought us back to salicylaldehyde **4.31** and an ethylenediamine fragment. The ethylenediamine motif can be further disconnected via stereospecific diaza-Cope transform **4.34** to reveal benzaldehyde **4.32** and commercially available Jik Chin Mother diamine **4.33**.³⁰ Manipulating the sterics and electronics of the salicylaldehyde should allow us to control reactivity about the cobalt center.^{31,32} The ethylenediamine should allow us to regulate the steric environment around the backbone. Additionally, the ethylenediamine backbone could potentially provide another entry to influencing reactivity about the cobalt center depending on whether R¹ substitution promotes the participation of cation- π interactions.³³⁻³⁵

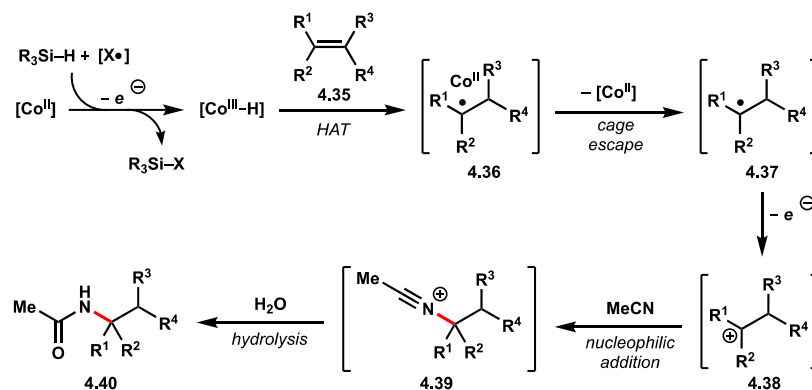
Figure 4.1 Retrosynthetic strategy for exploring Co(II) salen ligand chemical space



A general proposed mechanism for our desired hydroamidation is outlined in **Scheme 4.5**. We propose initial formation of putative cobalt(III) hydride by treatment of a modified cobalt(II) salen complex with a single-electron oxidant and silane.³⁶ HAT from the cobalt(III) hydride to substituted alkene **4.35** gives rise to solvent caged alkyl radical-metalloradical pair **4.36**.³⁷ We anticipate facile solvent cage escape to liberate tertiary alkyl radical **4.37** outcompeting radical pair collapse due to the steric encumbrance of alkyl radical **4.37**.^{38,39} Single-electron oxidation of

alkyl radical **4.37** would furnish electrophilic carbocation **4.38** and intersects our mechanism with that of the canonical Ritter reaction. Subsequent nucleophilic addition of acetonitrile into carbocation **4.38** to generate nitrilium ion **4.39** followed by hydrolysis is expected to furnish the desired *tert*-alkyl acetamide **4.40**.

Scheme 4.5 Strategy for a HAT radical–polar crossover Ritter reaction

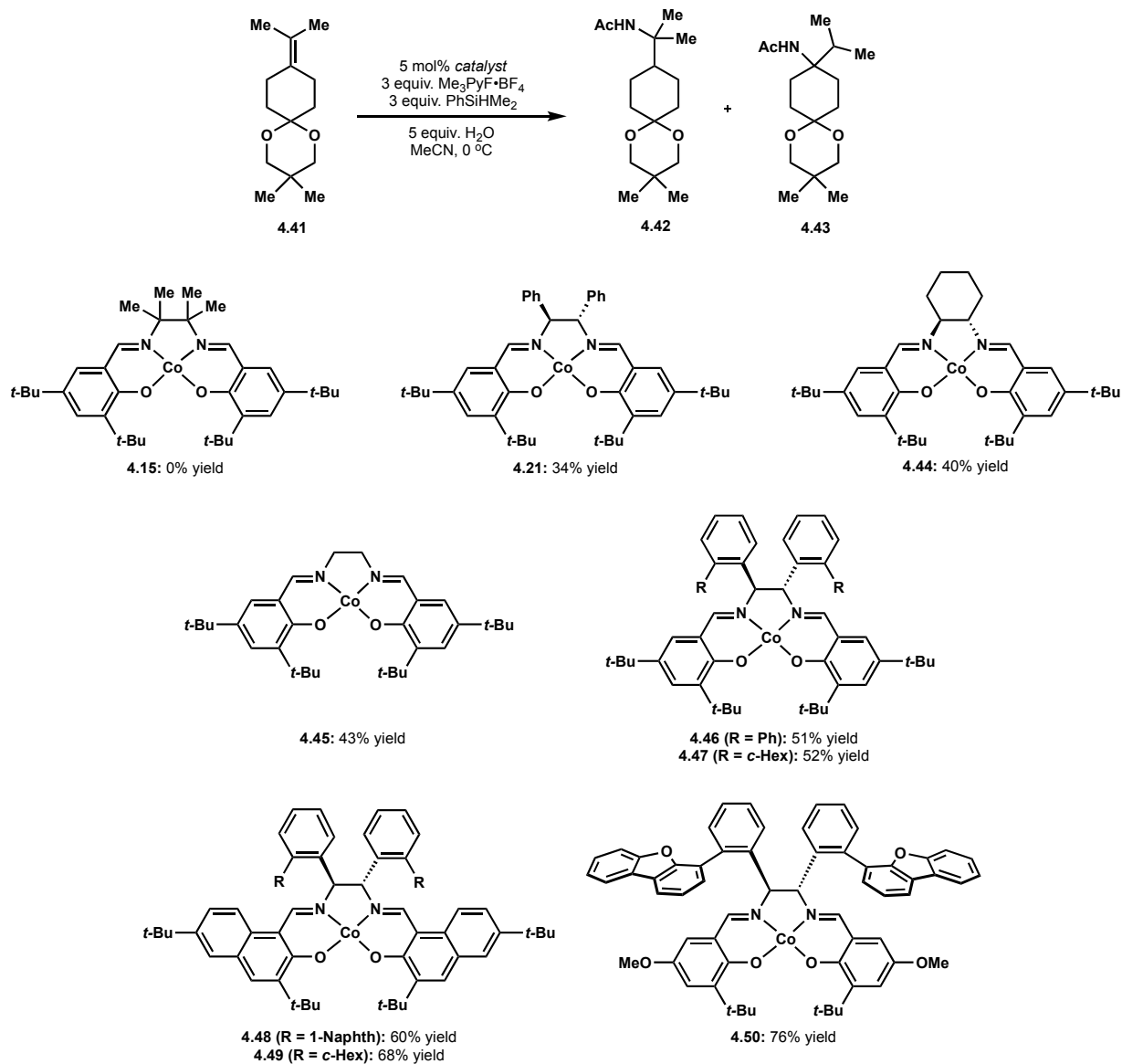


4.3 Catalyst Optimization

4.3.1 Catalyst Optimization for Hydroamidation of Tetrasubstituted Alkene **4.41**

We next turned our efforts towards probing the effects of catalyst structure on the HAT-initiated radical–polar crossover Ritter reaction using tetrasubstituted alkene **4.41** (Table 4.1). Reoptimized reaction conditions were similar to those initially developed by David George with the exception of temperature. Conventional cobalt(II) salen catalyst **4.15** failed to engage fully substituted alkene **4.41** when the optimized protocol was applied. This result was consistent with previous limitations observed in HAT-initiated radical–polar crossover reactions.²⁹ Gain of reactivity was achieved using diphenyl complex **4.21**, but mostly returned starting alkene. Similarly low yields of acetamides **4.42** and **4.43** were obtained with 1,2-cyclohexanediamine complex **4.44** and unsubstituted ethylenediamine complex **4.45**. Increased reaction times, additional amounts of oxidant and reductant, and changes in the order of addition did not lead to improved outcomes. Notably, it was critical that silane was added slowly dropwise as a solution

Table 4.1 Effect of catalyst structure on the HAT radical–polar crossover Ritter reaction of tetrasubstituted alkene **4.41**^a



^aYields and ratios were determined by ^1H NMR analysis using an internal standard of mesitylene. Work performed with REC.

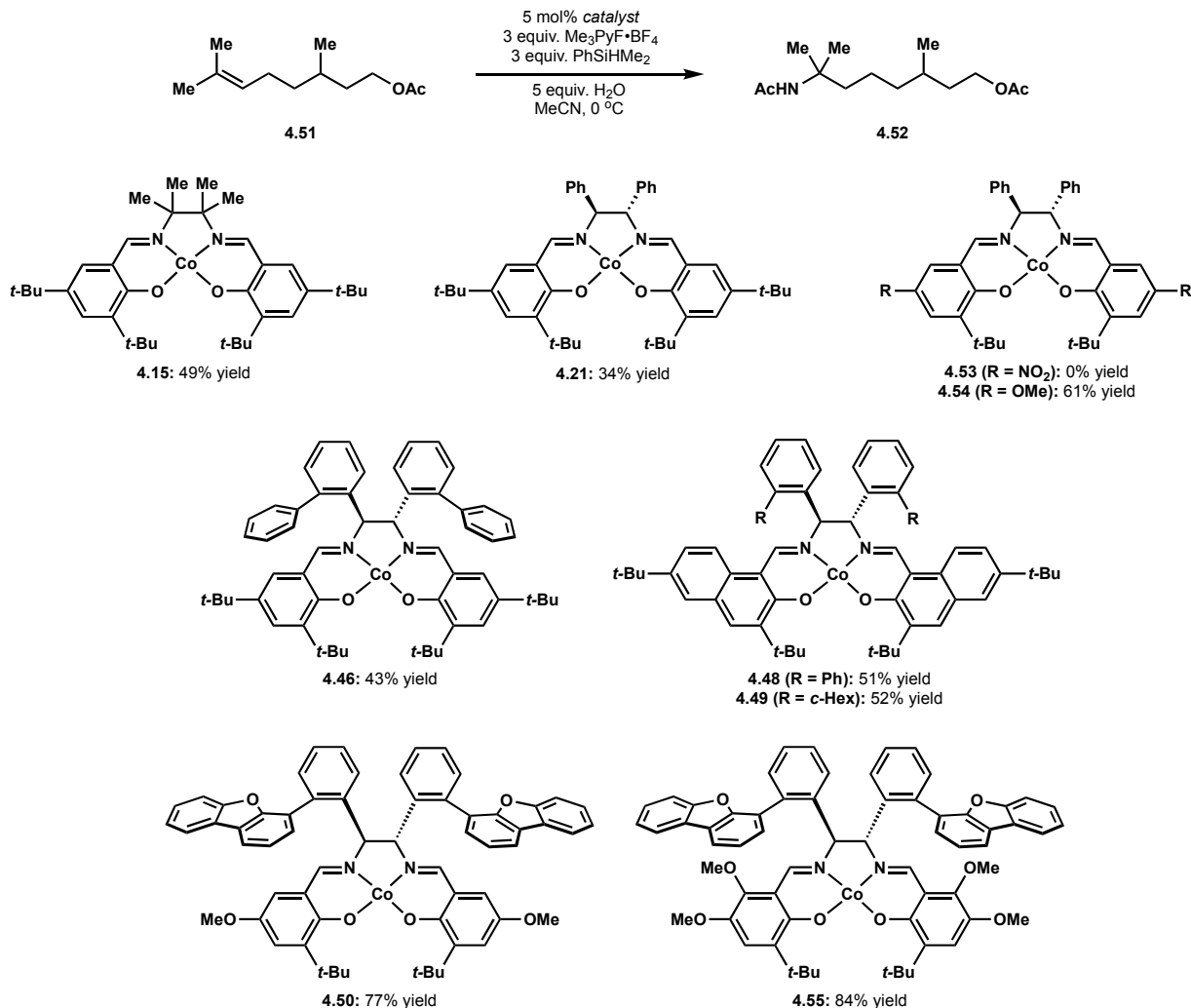
in acetonitrile using a syringe pump. Addition of neat silane quickly (<1 min) resulted in incomplete conversion of starting material and a greater degree of parasitic alkene hydrogenation.⁴⁰ To probe the potential influence of cation– π interactions, *o*-biaryl substituted cobalt(II) salen complex **4.46** was applied, and alkene **4.41** was converted to acetamides **4.42** and **4.43** in a combined yield of 51%. A virtually identical yield of amide products was achieved with *o*-cyclohexyl substituted complex **4.47**, suggesting that the improvement in yield was primarily a

function of sterics rather than cation– π interactions. Extending the salen aromatics to naphthaldehyde-derived motifs further improved performance, and good yields of acetamides were obtained with catalysts **4.48** and **4.49**. Ultimately, alkene **4.41** was most efficiently engaged using electron-rich cobalt(II) salen complex **4.50**, which delivered amides **4.42** and **4.43** in a combined 76% yield. Interestingly, amides **4.42** and **4.43** were consistently produced as a 4:1 mixture of regioisomers regardless of catalyst employed, perhaps suggesting that the corresponding carbocationic intermediates undergo rapid and reversible 1,2-hydride shift and are in equilibrium with each other. In all cases the majority of the remaining mass balance could be attributed to hydrogenation and hydration products.⁴⁰

4.3.1 Catalyst Optimization for Hydroamidation of Trisubstituted Alkene **4.51**

Similar trends in catalyst performance were observed when trisubstituted alkene **4.51** was subjected to the hydroamidation protocol (**Table 4.2**). Tetramethylethylenediamine catalyst **4.15** converted citronellyl acetate to the corresponding acetamide **4.52** in moderate yield. Efficiency decreased when diphenyl catalyst **4.21** was applied. Notably, installation of electron-withdrawing nitro groups on the salen ligand (catalyst **4.53**) shut down reactivity entirely while electron-donating motifs on the salicylaldehyde fragment (catalyst **4.54**) improved performance compared to the native catalyst **4.21**. This trend was consistent with the superior performance demonstrated by electron-rich catalyst **4.50** in the context of engaging tetrasubstituted alkene **4.41**. Application of *o*-biaryl catalyst **4.46** did not offer any advantages, and furnished acetamide **4.51** in a middling 43% yield. Naphthaldehyde-derived catalysts **4.48** and **4.49** likewise delivered moderate yields of amide **4.51** in essentially equal amounts, suggesting that the effect was largely steric in nature. Dibenzofuran substituted catalyst **4.50** offered a significant increase in efficiency, converting

Table 4.2 Effect of catalyst structure on the HAT radical–polar crossover Ritter reaction of trisubstituted alkene **4.51**^a



^aYields correspond to isolated, analytically pure material. Work performed with REC.

alkene **4.41** to acetamide **4.51** in good yield. Further addition of electron density to the salicylaldehyde moiety resulted in enhanced performance, and acetamide **4.51** was obtained in an impressive 84% yield using catalyst **4.55**.

Similar to our optimization efforts conducted with alkene **4.41**, increased reaction times, additional amounts of oxidant and reductant, and changes in the order of addition did not lead to improved outcomes. Generally, the *N*-fluorocollidinium triflate (Me₃PyF•OTf) oxidant provided superior outcomes compared to the tetrafluoroborate salt (Me₃PyF•BF₄). Riley made a key

observation that slow addition of Me₃PyF•OTF as a solution in acetonitrile using a syringe pump significantly improved yields. Unfortunately, a seemingly global shortage of Me₃PyF•OTF occurred during optimization efforts and we were forced to use Me₃PyF•BF₄ exclusively. However, we were pleased to realize that the slow addition of silane procedure used during optimization of tetrasubstituted alkene **4.41** could be applied to trisubstituted alkenes to achieve yields comparable to those obtained with Me₃PyF•OTF. For all catalysts the majority of the remaining mass balance could be attributed to hydration. Curiously, across all catalysts evaluated during optimization of both alkene **4.41** and alkene **4.51**, full consumption of silane and oxidant was observed regardless of how much starting material remained.

4.4 Substrate Scope

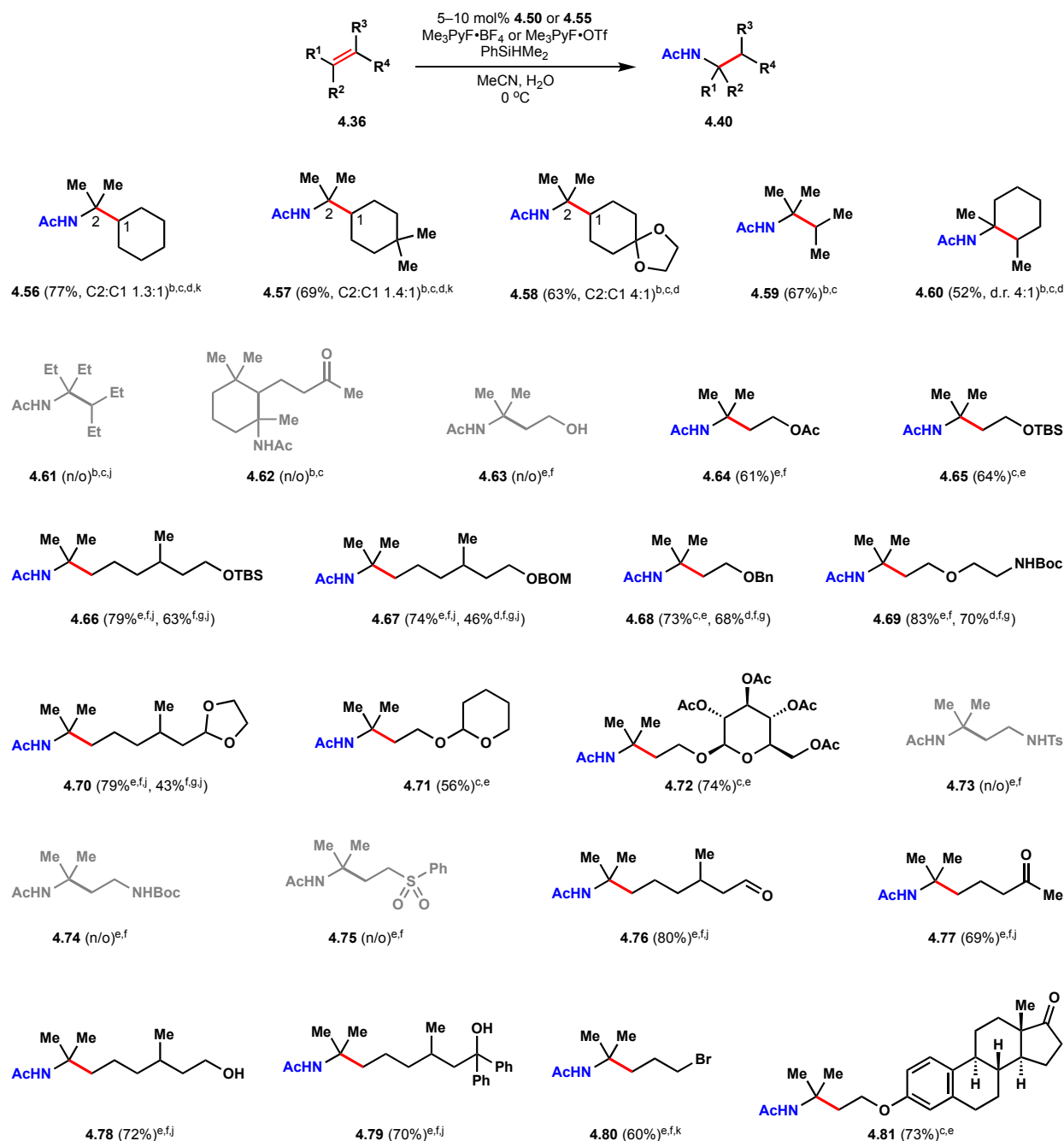
Catalysts **4.50** and **4.55** allowed for efficient conversion of various tetrasubstituted and trisubstituted alkenes to the corresponding *tert*-alkyl acetamide products (**Table 4.3**). It should be clarified that this collection of substrates was a function of work performed by myself, Riley Cooper, and Sarah Bredenkamp, and their contributions to **Table 4.3** are denoted within. A series of exocyclic tetrasubstituted alkenes underwent hydroamidation in similar yields and produced mixtures of regioisomeric amides (**4.56–4.58**). Simple acyclic alkene tetramethylethylene underwent hydroamidation to product **4.59** in good yield. 1,2-Dimethylcyclohexene was converted to acetamide **4.60** as a 4:1 mixture of diastereomers with moderate efficiency. Unfortunately, increasing steric encumbrance around the tetrasubstituted alkene motif shut down reactivity entirely, as the amide products derived from reactions conducted using tetraethylethylene (**4.61**) and dihydro- β -ionone (**4.62**) were never observed.

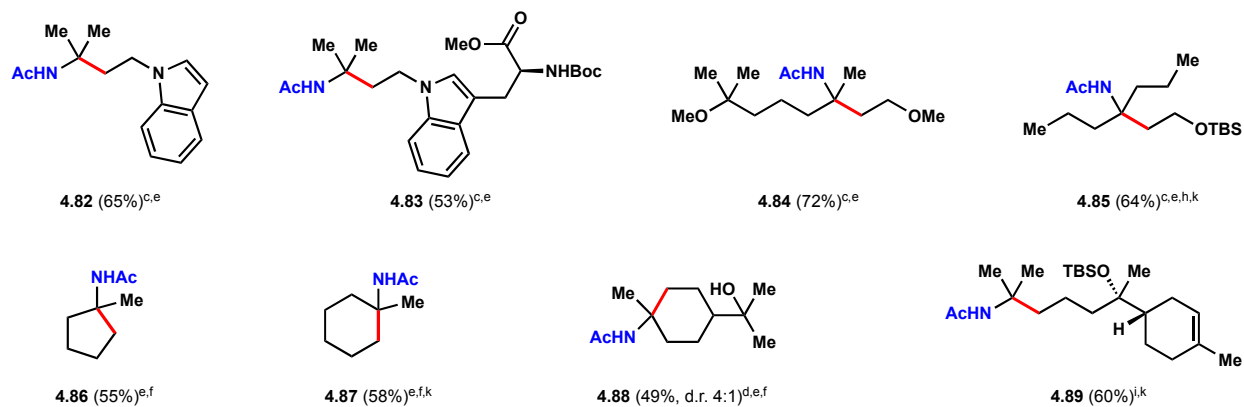
We next turned our attention towards reactions of trisubstituted alkenes. Attempts to hydrofunctionalize prenyl alcohol to acetamide **4.63** failed, likely due to intramolecular cyclization outcompeting intermolecular nucleophilic addition of acetonitrile. However, prenyl acetate was amenable to our acid-free Ritter protocol, and amide **4.64** was obtained in synthetically useful yields. Hydroamidation of several citronellol and prenyl derivatives revealed remarkable compatibility with acid-sensitive functional groups including silyl ethers (**4.65** and **4.66**), alkyl ethers (**4.67** and **4.68**), *N*-Boc-protected amines (**4.69**), and acetals (**4.70** and **4.71**), including protected glycosides (**4.72**). *N*-Tosyl and *N*-Boc-protected prenyl amines were not compatible with our hydroamidation procedure (**4.73** and **4.74**) presumably due to competing intramolecular capture of the intermediate carbocation by the internal nitrogen functionality. Electron-poor alkenes were not engaged, and the reaction of a prenylated sulfone did not deliver amide **4.75**, but only returned starting material.

Aliphatic aldehydes (**4.76**), ketones (**4.77**), alcohols (**4.78** and **4.79**), and halides (**4.80**) were also found to be suitable substrates. The compatibility of labile tertiary benzhydryl derivative **4.79** with the reaction conditions is a testament to the mild and chemoselective nature of HAT radical–polar crossover hydrofunctionalizations. Prenylated motifs containing nucleophilic functionalities properly positioned for intramolecular capture of the transient carbocationic intermediates also underwent efficient hydroamidation, including aryl ethers derived from estrone (**4.81**) as well as indoles (**4.82** and **4.83**).⁴¹ More sterically demanding trisubstituted alkenes were likewise efficiently engaged (**4.84** and **4.85**). Cyclic trisubstituted alkenes derived from five- and six-membered rings acquiesced to our hydroamidation conditions to afford *tert*-alkyl acetamides **4.86** and **4.87** in respectable yields. However, in the context of more complex cyclic substrate α -terpineol, performance was diminished and amide **4.88** was obtained in 49% yield as a 4:1 mixture

of diastereomers. A silylated bisabolol derivative was selectively functionalized at the terminal prenyl unit while the cyclic alkene remained intact (**4.89**). This was not dissimilar to the reactivity pattern observed by Dr. David George during his initial studies of the radical–polar crossover hydroamidation and underscores the limitations to our methodology that still remain.

Table 4.3 Preliminary substrate scope of the HAT radical–polar crossover Ritter reaction^a





^aUnless otherwise noted, reactions were conducted with 5 mol % of catalyst, 3 equiv. of oxidant and silane, and 5 equiv. of water. Yields in parentheses correspond to isolated, analytically pure material. n/o: not observed. ^bWith catalyst **4.50**. ^cWith Me₃PyF•BF₄. ^dYield and ratios were determined by ¹H NMR analysis using an internal standard of mesitylene. ^eWith catalyst **4.55**. ^fWith Me₃PyF•OTf. ^gWith catalyst **4.15**. ^hWith 3 equiv. of water. ⁱWith 10 mol % of catalyst, 6 equiv. of silane and oxidant, and 10 equiv. of water. ^jWork performed by REC. ^kWork performed by SEB.

4.5 Mechanistic Studies

4.5.1 Elucidating the Origin of Hydration Products

In all cases, formation of the desired acetamides was accompanied by varying amounts of the corresponding alcohols. However, it was not clear whether hydration products arose from polar nucleophilic addition of water into the proposed carbocations, or were rather a result of adventitious trapping of oxygen by alkyl radical intermediates. To clarify the mechanism of this parasitic pathway, we performed the hydroamidation of citronellyl acetate **4.51** using isotopically enriched H₂¹⁸O (Scheme 4.6). GC-MS analysis of the isolated alcohol **4.90** revealed near complete incorporation of H₂¹⁸O, suggesting that the source of alcohol by-products was trapping by water rather than Mukaiyama hydration.^{42,12} Isolated acetamide **4.52** displayed an identically high amount of ¹⁸O incorporation when analyzed by GC-MS.

Scheme 4.6 Isotope labelling experiments using H₂¹⁸O

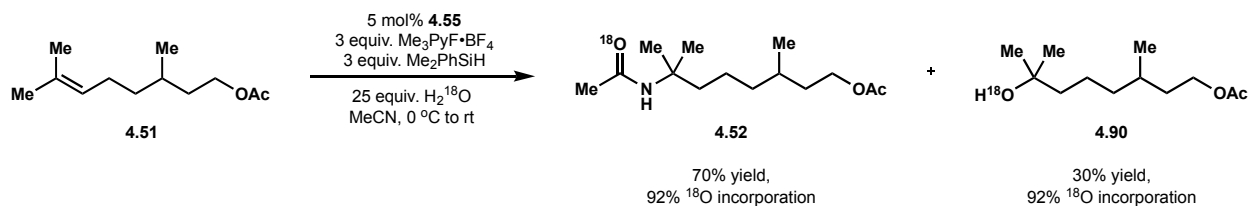
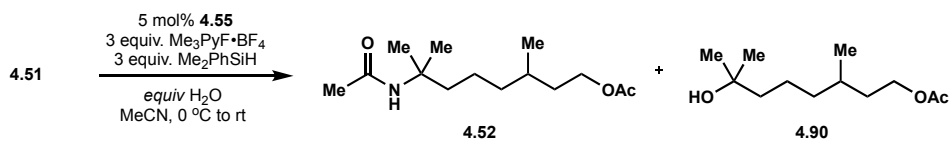
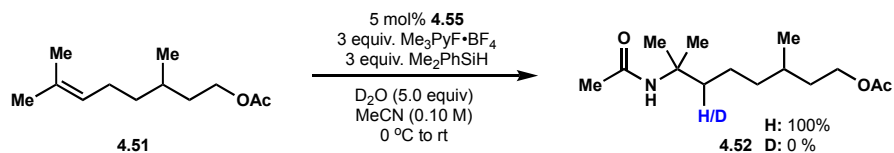


Table 4.4 Excess water experiments^a

entry	equivalents of H ₂ O	4.52 (% yield)	4.90 (% yield)
1	3.0	78	7
2	5.0	81	11
3	15.0	73	22
4	45.0	60	36

^aYields correspond to isolated, analytically pure material.

Excess water experiments provided further evidence that hydration products arose from nucleophilic capture of water (**Table 4.4**). Riley ran a series of experiments gradually increasing the equivalents of water added to the reaction using citronellyl acetate **4.51**. A positive correlation was observed between equivalents of water added and the portion of the mass balance taken up by alcohol **4.90**. Additionally, to probe the source of the newly introduced proton in acetamide product **4.52**, Riley performed deuterium labeling experiments with alkene **4.51** using heavy water (**Scheme 4.7**). Analysis of amide **4.52** by ¹H NMR and GC-MS did not indicate any deuterium incorporation, which confirmed that the newly introduced proton was derived from dimethylphenylsilane as a function of HAT rather than protonation of the alkene by hydronium or some other Brønsted acidic species.

Scheme 4.7 Deuterium labelling experiments using D₂O

4.5.2 Hydrogen Evolution Studies

As discussed previously, we observed dramatic differences in reactivity between the evaluated cobalt(II) salen complexes during optimization efforts. However, we were perplexed by

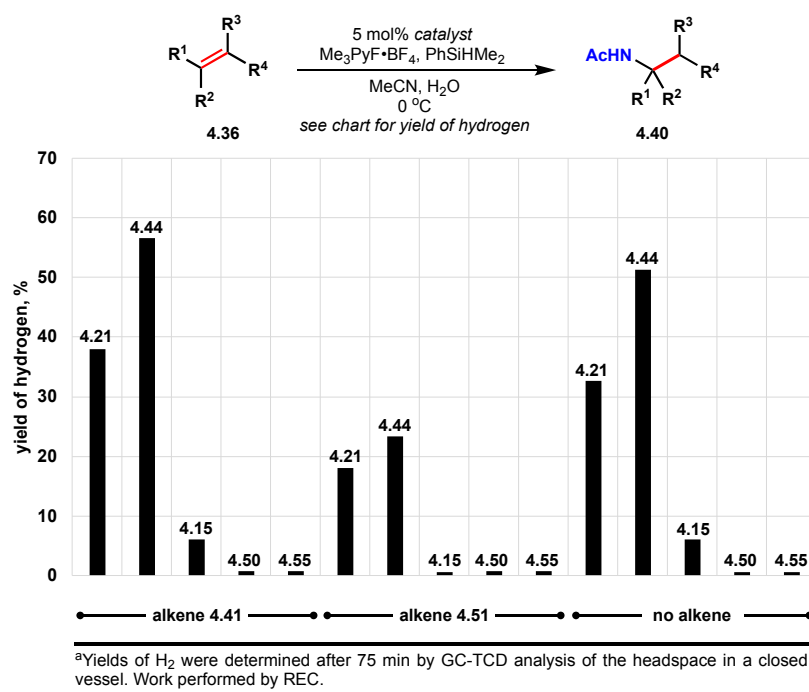
the fact that silane and oxidant were always fully consumed independent of the amount of starting material converted. This puzzling observation prompted us to investigate reaction pathways that do not lead to apparent engagement of the alkene via HAT but consume reactants all the same. We reasoned that formation of molecular hydrogen from disproportionation between putative cobalt(III) hydrides could be responsible for the background reactivity.^{36,43} The generation of hydrogen gas has long been invoked as a source of catalyst inefficiency in the context of MHAT alkene hydrofunctionalizations, likely due to anecdotal evidence that suggests observation of effervescence upon addition of silane to the reaction mixture is relatively common.^{44–46} However, to our knowledge no reports exist that confirm this hypothesis experimentally.

We sought to confirm and quantify the production of hydrogen gas generated over the course of our radical–polar crossover hydroamidations by analysis of the reaction headspace. This was accomplished by hydrogen evolution studies performed by my colleague Riley Cooper. To detect and quantify the production of hydrogen gas, Riley conducted hydroamidations of alkenes **4.41** and **4.51** across a series of catalysts. Reactions were also ran in the absence of alkene substrate to establish a baseline production of hydrogen gas for each catalyst. Samples of the headspace were collected at four separate timepoints per reaction using a gastight syringe. The gas aliquots were then injected into a gas chromatogram and the area of hydrogen calculated experimentally by GC-TCD analysis was directly correlated to the percent yield of hydrogen gas produced.

Analysis of the headspace hydrogen revealed instructive trends (**Table 4.5**). Diphenyl catalyst **4.21** and 1,2-cyclohexyldiamine catalyst **4.44** rapidly produced large quantities of molecular hydrogen both in the presence and absence of substrate, suggesting that the formation of hydrogen gas contributes significantly to consumption of the silane in these cases.⁴⁷ This data may explain why super-stoichiometric amounts of silane and oxidant are typically required to

achieve synthetically useful yields when using these catalysts for relevant alkene hydrofunctionalizations.²⁹ Tetramethyl complex **4.15** displayed an informative reactivity profile. Production of hydrogen by complex **4.15** was virtually identical both in the presence of alkene **4.41** and in the absence of substrate entirely. This was consistent with the optimization data in Table 4.1, which demonstrated that complex **4.15** was incapable of engaging tetrasubstituted alkene **4.41** in HAT. However, an appreciably lower amount of hydrogen gas was generated by catalyst **4.15** in the presence of alkene **4.51**, suggesting that productive HAT to the alkene is competitive with production of hydrogen gas.

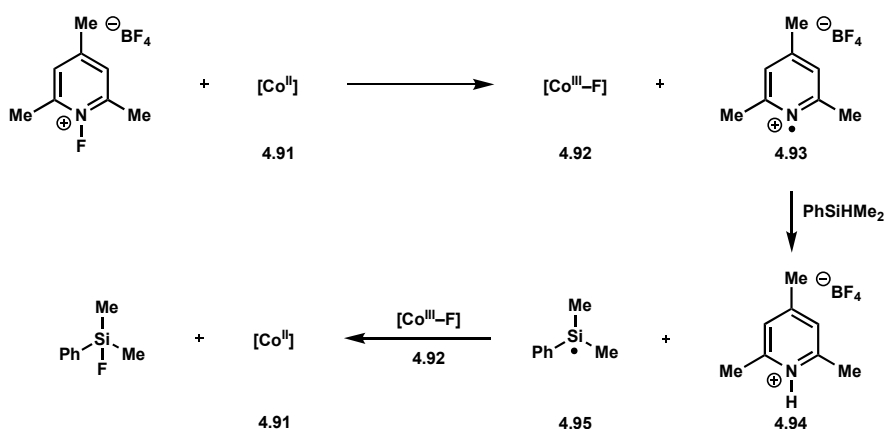
Table 4.5 Hydrogen evolution studies^a



In contrast, only trace amounts of hydrogen were ever detected upon application of designer catalysts **4.50** and **4.55** both in the presence and absence of alkene substrates.⁴⁸ This observation seemed consistent with the superior performance of catalysts **4.50** and **4.55** towards engaging alkenes **4.41** and **4.51** in HAT. However, we still observed complete consumption of silane nonetheless. The lack of hydrogen production by both catalysts in the absence of substrate

despite the full consumption of silane suggests that a pathway other than hydrogen evolution contributes to the background wasting of oxidant and silane. Moreover, the absence of hydrogen gas raises the possibility of catalytic processes that are not dependent on generation of putative cobalt(III) hydrides. Speculation of the mechanism for one of these potential processes is outlined in **Scheme 4.8**. For example, oxidation of cobalt(II) complex **4.91** upon exposure to $\text{Me}_3\text{PyF}\cdot\text{BF}_4$ may generate cobalt(III) fluoride **4.92** along with radical-cation **4.93**.⁴⁹ Abstraction of a hydrogen atom from dimethylphenylsilane by radical-cation **4.93** would deliver the protonated collidinium salt **4.94** and silyl radical **4.95**.⁵⁰ Driven by the thermodynamically favorable formation of a strong Si–F bond, subsequent fluorine atom abstraction from cobalt(III) fluoride **4.92** by silyl radical **4.95** would furnish dimethylphenylfluorosilane and regenerate cobalt(II) complex **4.91** to turn over the catalytic cycle.^{51,52} Irrespective of the finer mechanistic details, the superior performance in the hydroamidation combined with minimal production of molecular hydrogen suggest that catalysts **4.50** and **4.55** offer improved partitioning of reaction pathways available to the putative cobalt(III) hydride intermediates in favor of HAT to alkenes.

Scheme 4.8 Proposed mechanism for background consumption of silane and oxidant without formation of hydrogen gas



4.6 Conclusions and Outlook

In summary, we have developed a cobalt-catalyzed HAT-mediated radical–polar crossover variant of the Ritter reaction. Investigating the effects of electronic and structural manipulations to salen ligands facilitated the development of specialized cobalt(II) salen complexes capable of efficiently engaging a broad range of trisubstituted and tetrasubstituted alkenes to afford *tert*-alkyl acetamide products that are otherwise challenging to access. Isotope labeling and excess water experiments identified that nucleophilic capture of electrophilic intermediates by water was competitive with the desired hydroamidation. Deuterium labeling experiments confirmed that alkene hydrofunctionalization occurred via HAT rather than protonation with a Brønsted acid. Hydrogen evolution studies confirmed the long proposed notion that formation of hydrogen gas is a competitive pathway that contributes to background consumption of oxidant and silane, suggesting a mechanistic link between MHAT reactions and hydrogen evolution catalysis.^{53,54} However, some catalysts fully consumed silane and oxidant without producing hydrogen gas. This perplexing observation points to a still unidentified background reaction that likely does not involve the formation of cobalt(III) hydrides. These studies facilitate a better understanding of intermediates involved over the course of the hydroamidation reaction and provides a new metric to identify novel catalysts with improved reactivity towards alkenes in other relevant hydrofunctionalizations.

4.7 Experimental Section

4.7.1 Materials and Methods

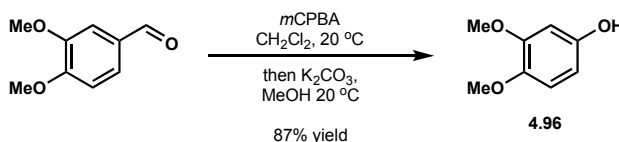
All reactions were carried out in flame-dried glassware under positive pressure of dry nitrogen unless otherwise noted. Reaction solvents including acetonitrile (MeCN, Fisher, HPLC Grade),

tetrahydrofuran (THF, Fisher, HPLC Grade), dichloromethane (DCM, Fisher, HPLC Grade), dimethylformamide (DMF, Fisher, HPLC Grade), and toluene (Fisher, HPLC Grade), were dried by percolation through a column packed with neutral alumina and a column packed with a supported copper catalyst for scavenging oxygen (Q5) under positive pressure of argon. Solvents for extraction, thin layer chromatography (TLC), and flash column chromatography were purchased from Fischer (ACS Grade) and VWR (ACS Grade) and used without further purification. Chloroform-d and DMSO-d₆ for ¹H and ¹³C NMR analysis were purchased from Cambridge Isotope Laboratories and used without further purification. Commercially available reagents were used without further purification unless otherwise noted. Reactions were monitored by thin layer chromatography (TLC) using precoated silica gel plates (EMD Chemicals, Silica gel 60 F₂₅₄). Flash column chromatography was performed over silica gel (Acros Organics, 60 Å, particle size 0.04-0.063 mm). Infrared (IR) spectra were obtained on a Nicolet iS5 FT-IR spectrometer with an iD5 ATR, and are reported in terms of frequency of absorption (cm⁻¹). GC-MS analysis was performed on Agilent 7820A system with helium as carrier gas. ¹H NMR and ¹³C NMR spectra were recorded on Bruker DRX-500 (BBO probe), Bruker DRX-500 (TCI cryoprobe), Bruker AVANCE600 (TBI probe), and Bruker AVANCE600 (BBFO cryoprobe) spectrometers using residual solvent peaks as internal standards (CHCl₃ @ 7.26 ppm ¹H NMR, 77.00 ppm ¹³C NMR; C₆H₆ @ 7.16 ppm ¹H NMR, 128.00 ppm ¹³C NMR; (CD₃)₂CO @ 2.05 ppm ¹H NMR, 29.84 ppm ¹³C NMR; (CD₃)₂SO @ 2.50 ppm ¹H NMR, 39.52 ppm ¹³C NMR). High-resolution mass spectra (HRMS) were recorded on Waters LCT Premier TOF spectrometer with ESI and CI sources.

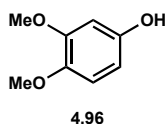
4.7.2 Experimental Procedures

General Procedure I: Preparation of Salicylaldehydes

Preparation of 3,5-dimethoxyphenol **4.96**.



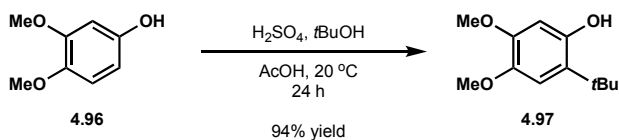
To a solution of 3,4-dimethoxybenzaldehyde (3.32 g, 20 mmol, 1.0 equiv) in CH₂Cl₂ (53 mL, 0.38 M w.r.t. 3,4-dimethoxybenzaldehyde) in a 200 mL roundbottom flask was added 75-70% *m*CPBA (5.42 g, 22 mmol, 1.1 equiv) in a single portion and stirred for 15 h at room temperature. The reaction was quenched with dimethyl sulfide (1.7 mL) and following further stirring for 10 min the reaction mixture was filtered through celite to remove precipitated benzoic acid and flushed with CH₂Cl₂ (100 mL). The organics were transferred to a separatory funnel, washed successively with sat. aq. Na₂SO₃ (3 x 100 mL), dried over Na₂SO₄, filtered and concentrated under reduced pressure in a 500 mL evaporation flask. The crude formate was then dissolved in MeOH (50 mL, 0.40 M) followed by addition of a magnetic stir bar and K₂CO₃ (5.53 g, 40 mmol, 2.0 equiv) in a single portion. Following stirring for 30 min at room temperature the reaction was concentrated under reduced pressure. The crude phenol was transferred to a separatory funnel with 100 mL CH₂Cl₂ and 100 mL H₂O. The aqueous layer was extracted with CH₂Cl₂ (3 x 100 mL), the combined organics were washed with brine, dried over Na₂SO₄, filtered and concentrated under reduced pressure. The crude product was purified by flash silica chromatography (gradient elution: 100% hexanes to 50% v/v EtOAc/hexanes) to yield 3,5-dimethoxyphenol **4.96** as a tan solid (2.67 g, 87% yield). The spectral data were identical to those reported in the literature.⁵⁵



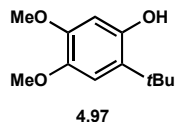
¹H NMR (500 MHz, CDCl₃, 25 °C):

δ 6.71 (d, <i>J</i> = 8.6 Hz, 1H)	5.73 (bs, 1H)
6.46 (d, <i>J</i> = 2.8 Hz, 1H)	3.80 (s, 3H)
6.35 (dd, <i>J</i> = 8.6, 2.8 Hz, 1H)	3.77 (s, 3H)

Preparation of 2-*tert*-butyl-4,5-dimethoxyphenol **4.97**.



To a solution of phenol **4.96** (463 mg, 3.0 mmol, 1.0 equiv) in glacial acetic acid (6.0 mL, 0.5 M w.r.t. **4.96**) in a 25 mL roundbottom flask was added *tert*-butanol (0.86 mL, 9.0 mmol, 3.0 equiv) and concentrated H_2SO_4 (0.2 mL, 3.6 mmol, 1.2 equiv). The reaction was stirred for 24 h at room temperature, and once conversion was determined complete by GC-MS, the reaction mixture was poured onto ice water (75 mL), and the aqueous layer was extracted with CH_2Cl_2 (3 x 25 mL). The combined organic layers were washed with brine, dried over Na_2SO_4 , filtered and concentrated under reduced pressure. The crude material was purified by flash silica chromatography (gradient elution: 100% hexanes to 30% v/v EtOAc/hexanes) to yield 595 mg (94% yield) of 2-*tert*-butyl-4,5-dimethoxyphenol **4.97** as a white solid.



2-*tert*-butyl-4,5-dimethoxyphenol **4.97**

^1H NMR (500 MHz, CDCl_3 , 25 °C):

δ 6.84 (s, 1H)	3.83 (s, 3H)
6.31 (s, 1H)	3.73 (s, 3H)
5.11 (bs, 1H)	1.40 (s, 9H)

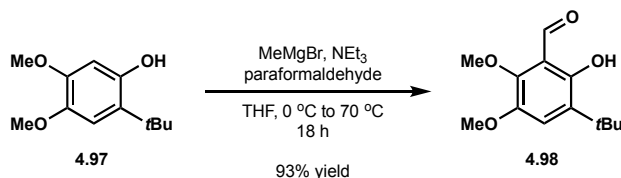
^{13}C NMR (126 MHz, CDCl_3 , 25 °C):

δ 148.4	112.3	34.1
147.5	102.2	29.8
142.0	57.0	
127.5	55.8	

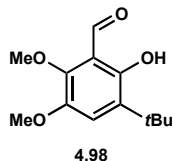
HRMS (ESI) calculated for $\text{C}_{12}\text{H}_{18}\text{O}_3$ $[\text{M}+\text{Na}]^+$: 233.1154, found: 233.1154

TLC: R_f = 0.33 (30% v/v EtOAc/Hex)

Preparation of dimethoxysalicylaldehyde **4.98**.



To a solution of phenol **4.97** (841 mg, 4.0 mmol, 1.0 equiv) in THF (7.3 mL, 0.55 M w.r.t. **4.97**) stirred at 0 °C in an ice bath was added MeMgBr (3.0 M in Et₂O, 1.7 mL, 5.0 mmol, 1.25 equiv) slowly dropwise. After stirring for 5 min at 0 °C the ice bath was removed and the reaction was allowed to warm to room temperature over 30 min after which dry NEt₃ (0.89 mL, 6.4 mmol, 1.6 equiv) and paraformaldehyde (360 mg, 12.0 mmol, 3.0 equiv) were added sequentially. The flask was equipped with a reflux condenser and the reaction was refluxed at 70 °C for 18 h. The flask was cooled to 0 °C in an ice bath and quenched by addition of 1.0 M aq. HCl (7.3 mL). The contents were transferred to a separatory funnel, diluted with water (50 mL) and Et₂O (50 mL) and the organic layer was washed with water (3 x 50 mL). The combined organic layers were washed with brine, dried over Na₂SO₄, filtered and concentrated under reduced pressure. The crude material was purified by flash silica chromatography (gradient elution: 100% hexanes to 10% v/v EtOAc/hexanes) to yield 888 mg (93% yield) of salicylaldehyde **4.98** as a bright yellow oil. This formylation procedure was adapted from a protocol reported by the Coates lab.⁵⁶



Salicylaldehyde **4.98**

¹H NMR (500 MHz, CDCl₃, 25 °C):

δ 12.01 (s, 1H)	7.21 (s, 1H)	3.84 (s, 3H)
10.30 (s, 1H)	3.97 (s, 3H)	1.38 (s, 9H)

¹³C NMR (126 MHz, CDCl₃, 25 °C):

δ 195.5	142.8	114.2	34.7
156.1	132.9	62.0	29.2
150.1	123.8	57.8	

HRMS (CI) calculated for C₁₃H₁₈O₄ [M+H]⁺: 239.1283, found: 239.1273

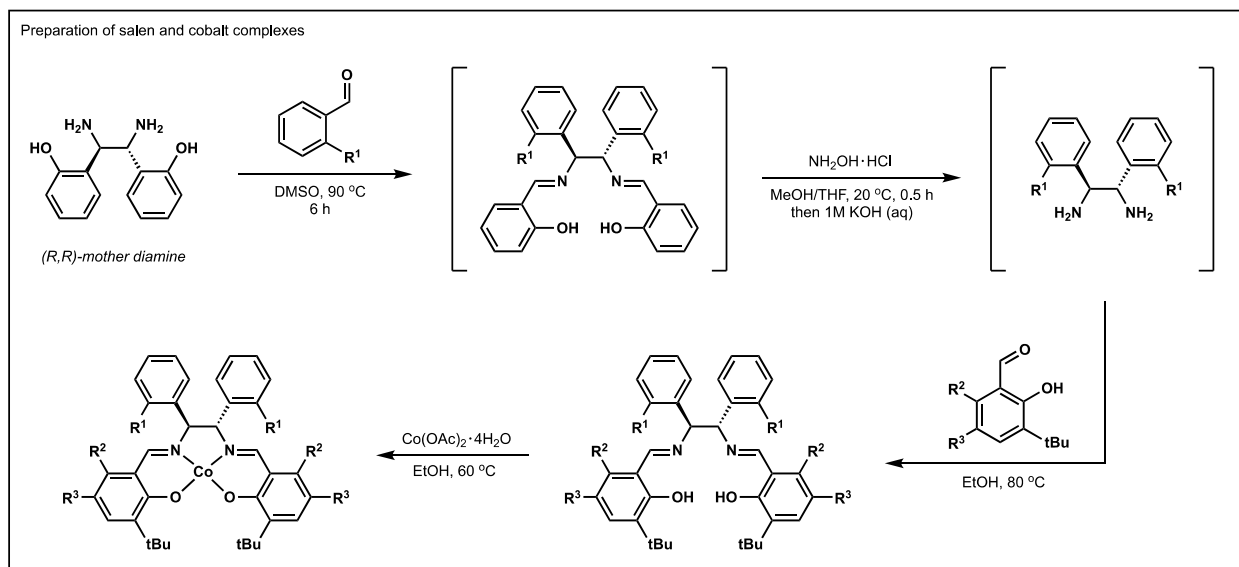
TLC: R_f = 0.39 (10% v/v EtOAc/Hex)

General Procedure II: Preparation of Salen Ligands

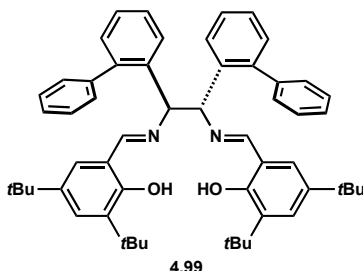
A. Diaza-Cope The procedure for the diaza-Cope was adapted from the Chin group's report on diaza-Cope transformations with sterically challenging benzaldehydes.³⁰ (*R,R*)-Mother diamine (0.10 mmol, 24 mg, 1.0 equiv) and 2-arylbenzaldehyde (0.24 equiv, 2.4 equiv) in DMSO (0.50 mL, 0.20 M w.r.t. mother diamine) was added to a vial and stirred at 90 °C for 6 hours. The reaction mixture was diluted with CH₂Cl₂ and transferred to a separatory funnel. The organic layer was washed with H₂O (3 x 10 mL) and brine, dried with Na₂SO₄, filtered, and concentrated under reduced pressure. The crude diaza-Cope product was taken on to the next step without purification.

B. Salicylaldehyde deprotection Crude diaza-Cope product (1.0 equiv) and NH₂OH·HCl (35 mg, 0.50 mmol, 5.0 equiv) in MeOH (1.0 mL, 0.10 M w.r.t. diaza-Cope product) was added to a vial and stirred at room temperature for 4 hours. 1 M NaOH (10 mL) was added to the reaction mixture and the aqueous layer was extracted with CH₂Cl₂ (5 x 10 mL), dried with Na₂SO₄, filtered, and concentrated under reduced pressure. The crude diamine was taken on to the next step without purification.

C. Salen Formation Crude diamine (1.0 equiv) and salicylaldehyde (2.0 equiv) in EtOH (0.20 M w.r.t. diamine) was added to a vial and stirred at 60 °C for 4 hours. The reaction mixture was allowed to cool to room temperature, concentrated under reduced pressure, and purified by flash SiO₂ chromatography to afford salen as a yellow solid.



Ligand 4.99. Ligand **4.99** was prepared according to the General Procedure II with 3,5-di-tert-butyl-2-hydroxybenzaldehyde (72 mg, 0.31 mmol) and purified by flash silica chromatography (gradient elution: 100% hexanes to 2% v/v EtOAc/Hexanes) to afford ligand **4.99** as a yellow solid (74 mg, 61% yield)



Salen 4.99

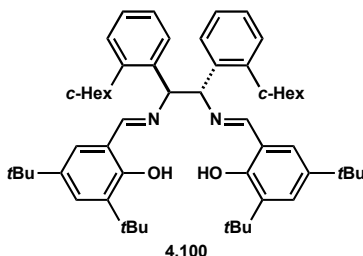
^1H NMR (500 MHz, CDCl_3 , 25 °C):

δ 13.47 (s, 2H)	6.96 (d, $J = 1.6$ Hz, 2H)
8.22 (s, 2H)	6.89 (s, 2H)
7.42 (q, $J = 6.7$ Hz, 6H)	5.07 (s, 2H)
7.32-7.29 (m, 6H)	1.39 (d, $J = 2.1$ Hz, 18H)
7.28 (s, 2H)	1.27 (d, $J = 2.1$ Hz, 18H)
7.05 (d, $J = 7.2$ Hz, 2H)	

^{13}C NMR (126 MHz, CDCl_3 , 25 °C):

δ 166.7	129.8	126.2
157.8	129.6	117.9
142.1	128.9	74.0
140.8	128.04	34.9
140.0	127.95	34.0
136.31	127.0	31.4
136.24	126.7	29.4

Ligand 4.100. Ligand **4.100** was prepared according to the General Procedure II with 3,5-di-tert-butyl-2-hydroxybenzaldehyde (117 mg, 0.50 mmol) and purified by flash silica chromatography (gradient elution: 100% hexanes to 10% v/v CH₂Cl₂/Hexanes) to afford ligand **4.100** as a yellow solid (181 mg, 89% yield).



Salen 4.100

¹H NMR (500 MHz, CDCl₃, 25 °C):

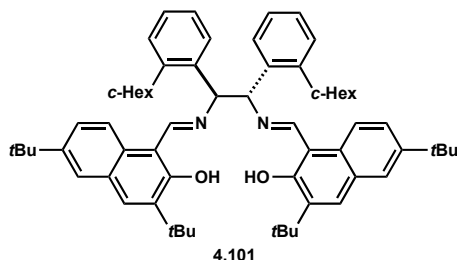
δ 13.72 (s, 2H)	7.03 (dd, <i>J</i> = 5.1, 1.7 Hz, 4H)	1.60 (d, <i>J</i> = 10.4 Hz, 2H)
8.43 (s, 2H)	5.24 (s, 2H)	1.45 (dd, <i>J</i> = 9.4, 3.3 Hz, 2H)
7.85 (d, <i>J</i> = 7.8 Hz, 2H)	2.51-2.46 (m, 2H)	1.41 (d, <i>J</i> = 13.5 Hz, 18H)
7.31 (d, <i>J</i> = 2.5 Hz, 2H)	1.81 (d, <i>J</i> = 13.2 Hz, 2H)	1.26 (s, 18H)
7.29-7.26 (m, 2H)	1.72 (d, <i>J</i> = 11.8 Hz, 2H)	1.19-1.07 (m, 8H)
7.17-7.13 (m, 2H)	1.64 (d, <i>J</i> = 13.0 Hz, 2H)	0.32 (d, <i>J</i> = 9.6 Hz, 2H)

¹³C NMR (126 MHz, CDCl₃, 25 °C):

δ 166.7	127.0	34.9
157.9	126.3	34.0
145.4	126.07	32.3
140.0	125.93	31.4
136.7	118.0	29.4
136.2	74.4	27.2
128.9	39.0	26.9
127.2	35.9	26.2

HRMS (ESI) calc. for C₅₆H₇₆N₂O₈ [M+H]⁺: 809.5985, found: 809.5991
TLC R_f = 0.46 (10% v/v CH₂Cl₂/hexanes)

Ligand 4.101. Ligand **4.101** was prepared according to General Procedure II with 3,6-di-*tert*-butyl-2-hydroxy-1-naphthaldehyde (57 mg, 0.20 mmol) and purified by flash silica chromatography (gradient elution: 100% hexanes to 20% v/v CH₂Cl₂/Hexanes) to afford ligand **4.101** as an orange solid (78 mg, 86% yield)



Salen 4.101

¹H NMR (500 MHz, CDCl₃, 25 °C):

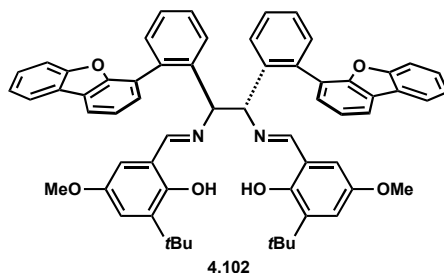
δ 9.14-9.10 (m, 2H)	5.39 (s, 2H)
7.96 (d, <i>J</i> = 7.8 Hz, 2H)	2.59 (d, <i>J</i> = 8.9 Hz, 2H)
7.77 (d, <i>J</i> = 8.9 Hz, 2H)	1.84-1.67 (m, 10H)
7.53 (s, 2H)	1.40 (s, 18H)
7.45 (d, <i>J</i> = 1.9 Hz, 2H)	1.37 (s, 18H)
7.39-7.36 (m, 4H)	1.24-1.16 (m, 8H)
7.22 (t, <i>J</i> = 7.1 Hz, 2H)	0.74 (s, 2H)
7.10 (d, <i>J</i> = 7.5 Hz, 2H)	0.47 (d, <i>J</i> = 5.8 Hz, 2H)

¹³C NMR (126 MHz, CDCl₃, 25 °C):

δ 167.8	128.4	108.0	31.3
161.4	127.7	72.4	29.5
145.7	126.39	39.2	27.2
145.1	126.30	36.0	26.9
140.0	126.20	35.0	26.1
135.7	125.4	34.3	
131.5	124.0	32.4	
129.9	117.8	31.9	

HRMS (ESI) calc. for C₆₄H₈₀N₂O₂ [M+H]⁺: 909.6298, found: 909.6306
TLC R_f = 0.35 (30% v/v CH₂Cl₂/hexanes)

Ligand 4.102. Ligand **4.102** was prepared according to General Procedure II with 3-(*tert*-butyl)-2-hydroxy-5-methoxybenzaldehyde (62 mg, 0.30 mmol) and purified by flash silica chromatography (gradient elution: 100% hexanes to 5% v/v EtOAc/Hexanes) to afford ligand **4.102** as a yellow solid (119 mg, 85% yield).



Salen 4.102

^1H NMR (600 MHz, $\text{DMSO-}d_6$, 125 °C):

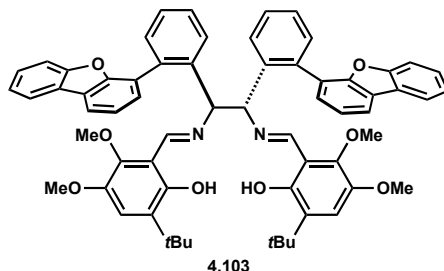
δ 12.90 (s, 2H)	7.39 (d, $J = 7.6$ Hz, 2H)	6.77 (d, $J = 3.0$ Hz, 2H)
8.17-8.16 (m, 2H)	7.24 (s, 2H)	6.27 (s, 2H)
8.14 (dd, $J = 7.7, 0.9$ Hz, 2H)	7.17 (d, $J = 9.2$ Hz, 6H)	4.89 (s, 2H)
7.92 (s, 2H)	7.09 (s, 2H)	3.58 (s, 6H)
7.41 (dt, $J = 4.4, 2.2$ Hz, 4H)	6.84 (d, $J = 2.9$ Hz, 2H)	1.23 (s, 18H)

^{13}C NMR (151 MHz, $\text{DMSO-}d_6$, 125 °C):

δ 196.7	137.3	123.4	112.0
165.9	136.6	122.3	110.8
154.8	135.2	122.1	74.2
154.0	129.6	120.5	54.9
153.2	128.1	119.5	33.7
152.2	126.55	117.4	28.5
151.5	126.45	117.1	
150.4	123.9	112.9	

HRMS (ESI) calc. for $\text{C}_{62}\text{H}_{56}\text{N}_2\text{O}_6$ $[\text{M}+\text{H}]^+$: 925.4217, found: 925.4199
 TLC $R_f = 0.24$ (5% v/v EtOAc/hexanes)

Ligand 4.103. Ligand **4.103** was prepared according to the General Procedure II with salicylaldehyde **4.98** (72 mg, 0.30 mmol) and purified by flash silica chromatography (gradient elution: 100% hexanes to 10% v/v EtOAc/Hexanes) to afford ligand **4.103** as a yellow solid (105 mg, 71% yield)



Salen **4.103**

^1H NMR (600 MHz, $\text{DMSO-}d_6$, 125 °C):

δ 13.48 (s, 2H)	7.09 (s, 2H)
8.27 (s, 2H)	6.89 (s, 2H)
8.15-8.13 (m, 2H)	6.82 (d, $J = 6.0$ Hz, 2H)
8.12 (dd, $J = 7.7, 0.9$ Hz, 2H)	4.91 (s, 2H)
7.42-7.38 (m, 4H)	3.66 (s, 6H)
7.35 (t, $J = 7.6$ Hz, 2H)	3.34 (s, 6H)
7.27 (s, 2H)	2.87 (s, 2H)
7.22-7.16 (m, 6H)	1.22 (s, 18H)

^{13}C NMR (151 MHz, $\text{DMSO-}d_6$, 125 °C):

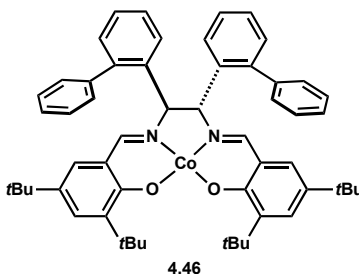
δ 162.0	135.2	126.50	110.84
154.9	130.8	123.9	74.4
154.2	129.8	123.2	59.9
152.2	128.0	120.3	57.2
147.1	127.60	119.6	33.5
141.7	127.41	118.8	28.6
136.6	126.59	110.99	

HRMS (ESI) calc. for $\text{C}_{64}\text{H}_{60}\text{N}_2\text{O}_8$ $[\text{M}+\text{Na}]^+$: 1007.4247, found: 1007.4252
 TLC $R_f = 0.29$ (10% v/v EtOAc/hexanes)

General Procedure III: Preparation of Co(II) Salen Complexes

A vial was charged with $\text{Co}(\text{OAc})_2 \cdot 4\text{H}_2\text{O}$ (1.0 equiv) and salen (1.0 equiv) and purged with N_2 . EtOH (0.05 M w.r.t. salen) was degassed by sparging with Ar under sonication for 5 minutes and then added to the reaction vial. The reaction mixture was heated to 60 °C with vigorous stirring for 4 hours at which point the Co(II) salen had precipitated out of solution as a bright red solid. The solid transferred to a fine glass frit and washed with MeOH (3 x 10 mL). CH_2Cl_2 (15 mL) was then added to the fine glass frit to dissolve the bright red solid, filtered through into a clean flask, and then concentrated under reduced pressure to afford the Co(II) salen as a bright red powder. Characterization data for Co(II) salen complexes **4.15**,^{23a} **4.21**,⁵⁷ **4.44**,⁵⁸ **4.45**,⁵⁸ **4.48**,²² **4.53**,²¹ and **4.54**²¹ has been previously reported.

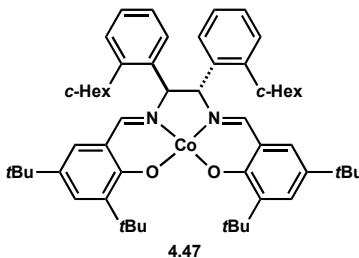
Co(II) salen complex 4.46. Co(II) salen complex **4.46** was prepared according to General Procedure III with salen **4.99** (901 mg, 1.13 mmol) to afford Co(II) salen complex **4.46** as a red-orange powder (615 mg, 64% yield).



Co(II) salen complex 4.46

HRMS (ES) calculated for $\text{C}_{56}\text{H}_{62}\text{CoN}_2\text{O}_2$ $[\text{M}]^+$ calc: 853.4143, found: 853.4158

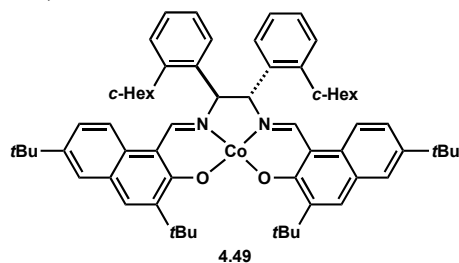
Co(II) salen complex 4.47. Co(II) salen complex **4.47** was prepared according to General Procedure III with salen **4.100** (74 mg, 0.091 mmol) to afford Co(II) salen complex **4.47** as a bright orange powder (60 mg, 76% yield).



Co(II) salen complex 4.47

HRMS (ES) calculated for $\text{C}_{56}\text{H}_{74}\text{CoN}_2\text{O}_2$ $[\text{M}]^+$ calc: 865.5082, found: 865.5096.

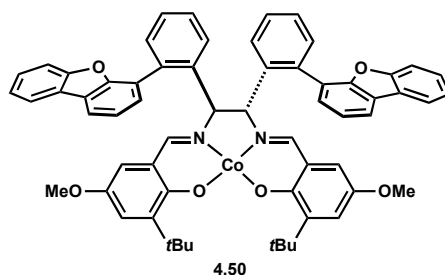
Co(II) salen complex 4.49. Co(II) salen complex **4.49** was prepared according to General Procedure III with salen **4.101** (84 mg, 0.093 mmol) to afford Co(II) salen complex **4.49** as a dull orange powder (60 mg, 67% yield).



Co(II) salen complex 4.49

HRMS (ES) calculated for $C_{64}H_{78}CoN_2O_2 [M]^+$ calc: 965.5396, found: 965.5415.

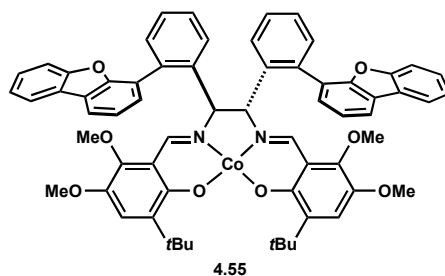
Co(II) salen complex 4.50. Co(II) salen complex **4.50** was prepared according to General Procedure III with salen **4.102** (110 mg, 0.10 mmol) to afford Co(II) salen complex **4.50** as a dull purple powder (105 mg, 91% yield).



Co(II) salen complex 4.50

HRMS (ES) calculated for $C_{62}H_{54}CoN_2O_2 [M]^+$ calc: 981.3314.6, found: 981.3294.

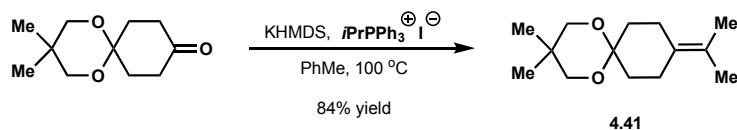
Co(II) salen complex 4.55. Co(II) salen complex **4.55** was prepared according to General Procedure III with salen **4.103** (108 mg, 0.10 mmol) to afford Co(II) salen complex **4.55** as a shiny black powder (106 mg, 93% yield).



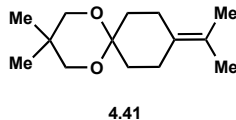
Co(II) salen complex 4.55.

HRMS (ES) calculated for $C_{64}H_{58}CoN_2O_2 [M]^+$ calc: 1041.3525, found: 1041.3531.

Preparation of starting materials.



Tetrasubstituted alkene 4.41. Prepared using a procedure reported by Pronin.⁵⁹ A suspension of *i*-PrPPh₃ (692 mg, 1.6 mmol, 1.6 equiv) in toluene (5.0 mL) was cooled to 0 °C and treated with dropwise addition of KHMDS (0.5 M in toluene, 3.1 mL, 1.55 mmol, 1.55 equiv). After stirring at 0 °C for a further 20 min, a solution of ketone (198 mg, 1.0 mmol, 1.0 equiv) in toluene (5.0 mL, final concentration w.r.t. ketone 0.1 M) was added slowly. The reaction flask was then equipped with a reflux condenser and heated to 100 °C overnight. After cooling to rt the reaction was quenched by addition of sat. aq. NH₄Cl (5.0 mL). The reaction was diluted with Et₂O (25 mL) and the contents transferred to a separatory funnel. The organic layer was washed successively with water (2 x 25 mL) and brine (25 mL). The organics were dried over MgSO₄, filtered and concentrated under reduced pressure. The crude material was purified by flash silica chromatography (gradient elution: 100% hexanes to 10% v/v EtOAc/hexanes) to yield 188 mg (84% yield) of alkene **4.41** as a white solid.



Tetrasubstituted alkene **4.41**

¹H NMR (500 MHz, CDCl₃, 25 °C):

δ 3.52 (s, 4H) 1.66 (s, 6H)
2.22 (t, *J* = 6.4 Hz, 4H) 0.97 (s, 6H)
1.79 (t, *J* = 6.6 Hz, 4H)

¹³C NMR (126 MHz, CDCl₃, 25 °C):

δ 129.8 70.1 30.2
121.5 33.0 22.8
97.7 25.4 20.1

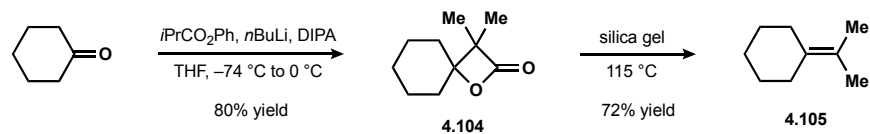
HRMS (ESI) calculated for C₁₄H₂₄O₂ [M+H]⁺: 225.1855, found: 225.1853

TLC: R_f = 0.38 (10% v/v EtOAc/Hexanes)

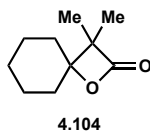
General procedure IV: Preparation of 1-isopropylidenecycloalkanes **4.105** and **4.107**

A. β -Lactone formation. Prepared according to a procedure reported by Schick.⁶⁰ To a solution of diisopropylamine (1.3 equiv) in THF (0.33 M w.r.t. diisopropylamine) cooled to $-5\text{ }^{\circ}\text{C}$ in an ice brine bath was added *n*BuLi (2.35 M in hexanes, 1.2 equiv) slowly dropwise over 3 min. After stirring for 10 min at $-5\text{ }^{\circ}\text{C}$, the ice brine bath was removed and the reaction was warmed to rt over 10 min, then cooled to $-74\text{ }^{\circ}\text{C}$ in a dry ice isopropanol bath. A solution of phenyl isobutyrate (1.2 equiv), prepared by esterification of phenol with isobutyryl chloride,⁶¹ in THF (1.2 M w.r.t. phenyl isobutyrate) was added slowly dropwise over 6 min. After stirring for 45 min at $-74\text{ }^{\circ}\text{C}$, a solution of the ketone (1.0 equiv) in THF (1.0 M w.r.t. ketone) was added slowly dropwise over 6 min. After stirring at $-74\text{ }^{\circ}\text{C}$ for 30 min, the reaction was warmed to $0\text{ }^{\circ}\text{C}$ in an ice bath. After stirring for 2 h at $0\text{ }^{\circ}\text{C}$, the reaction was quenched by addition of 1 M aq. NaOH (15 mL), diluted with water (30 mL) and Et₂O (10 mL), and the contents were transferred to a separatory funnel. The aqueous layer was extracted with Et₂O (3 x 25 mL), then the combined organics washed with brine (1 x 25 mL) and were dried over MgSO₄, filtered and concentrated under reduced pressure. The crude material was purified by flash silica chromatography (gradient elution: 100% hexanes to 8% v/v EtOAc/hexanes).

B. Decarboxylation. 1-Isopropylidenecycloalkanes were prepared according to a procedure reported by Danheiser.⁸ To a flame-dried round bottom flask was added the β -lactone and silica gel (10 wt%). The flask was equipped with a Hickman and the apparatus was evacuated (60 Torr). The flask was heated in an oil bath and the mixture was stirred at $110\text{--}120\text{ }^{\circ}\text{C}$ for 30 min, then the apparatus was filled with air and allowed to cool to rt. The crude distillate was purified by flash silica chromatography (100% pentane).



3,3-Dimethyl-1-oxaspiro[3.5]nonan-2-one 4.104. Prepared according to General Procedure IV with 5.0 mmol cyclohexanone (0.52 mL), 6.6 mmol diisopropylamine (0.93 mL), 6.1 mmol $n\text{BuLi}$ (2.6 mL), 6.0 mmol phenyl isobutyrate (986 mg), and 30 mL THF to afford β -lactone **4.104** as a white solid (672 mg, 80% yield). The spectral data for 3,3-dimethyl-1-oxaspiro[3.5]nonan-2-one matched those reported in the literature.⁶⁰



3,3-Dimethyl-1-oxaspiro[3.5]nonan-2-one **4.104**

^1H NMR (500 MHz, CDCl_3 , $25\text{ }^\circ\text{C}$):

δ 2.02–1.89 (m, 2H)

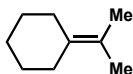
1.70–1.56 (s, 7H)

1.35–1.25 (m, 1H)

1.30 (s, 6H)

TLC: R_f = 0.30 (10% v/v EtOAc/hexanes)

Isopropylidenecyclohexane 4.105. Prepared according to General Procedure IV with 3.9 mmol 3,3-dimethyl-1-oxaspiro[3.5]nonan-2-one (651 mg) and 65 mg silica gel to afford **4.105** as a colorless oil (347 mg, 72% yield). The spectral data for **4.105** matched those reported in the literature.⁶²



4.105

Isopropylidenecyclohexane **4.105**

¹H NMR (600 MHz, CDCl₃, 25 °C):

δ 2.18–2.11 (m, 4H)

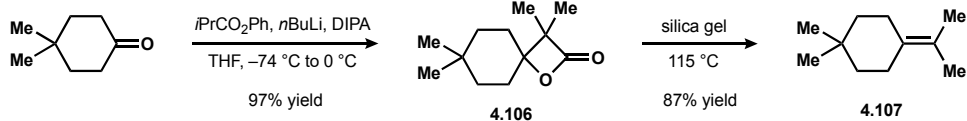
1.66 (s, 6H)

1.56–1.51 (m, 2H)

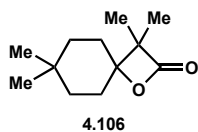
1.51–1.45 (m, 4H)

HRMS (CI) calculated for C₉H₁₆ [M]⁺: 124.1252, found: 124.1254

TLC: R_f = 0.78 (100% hexanes)



3,3,7,7-Tetramethyl-1-oxaspiro[3.5]nonan-2-one 4.106. Prepared according to General Procedure IV with 2.2 mmol 4,4-dimethylcyclohexanone (275 mg), 2.9 mmol diisopropylamine (0.40 mL), 2.7 mmol *n*BuLi (1.1 mL), 2.6 mmol phenyl isobutyrate (432 mg), and 13 mL THF to afford β -lactone **4.106** as a white solid (417 mg, 97% yield).



3,3,7,7-Tetramethyl-1-oxaspiro[3.5]nonan-2-one **4.106**

^1H NMR (600 MHz, CDCl_3 , 25 °C):

δ 1.92–1.85 (m, 2H)	1.31 (s, 6H)
1.72 (td, $J = 13.2, 3.8$ Hz, 2H)	0.96 (s, 3H)
1.54 (td, $J = 12.9, 3.8$ Hz, 2H)	0.91 (s, 3H)
1.38–1.32 (m, 2H)	

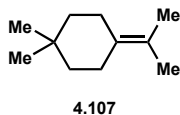
^{13}C NMR (151 MHz, CDCl_3 , 25 °C):

δ 176.1	35.0
85.0	29.0
54.2	28.4
40.4	18.1

HRMS (ESI) calculated for $\text{C}_{12}\text{H}_{20}\text{O}_2$ $[\text{M}+\text{Na}]^+$: 219.1361, found: 219.1360

TLC: $R_f = 0.33$ (10% v/v EtOAc/hexanes)

4-Isopropylidene-1,1-dimethylcyclohexane 4.107. Prepared according to General Procedure IV with 2.0 mmol 3,3,7,7-tetramethyl-1-oxaspiro[3.5]nonan-2-one (400 mg) and 40 mg silica gel to afford **4.107** as a colorless oil (270 mg, 87% yield). The spectral data for **4.107** matched those reported in the literature.⁶³



4-Isopropylidene-1,1-dimethylcyclohexane **4.107**

¹H NMR (600 MHz, CDCl₃, 25 °C):

δ 2.16 (dd, *J* = 7.3, 5.1 Hz, 4H)

1.66 (s, 6H)

1.28 (dd, *J* = 7.3, 5.4 Hz, 4H)

0.93 (s, 6H)

¹³C NMR (151 MHz, CDCl₃, 25 °C):

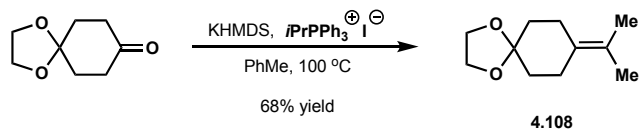
δ 131.8 28.3

120.2 26.0

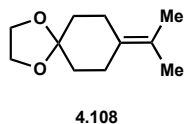
40.4 19.9

30.2

TLC: R_f = 0.82 (100% hexanes)



Tetrasubstituted alkene 4.108. Prepared using a procedure reported by Pronin.⁵⁹ A suspension of *i*-PrPPh₃ (2.08 g, 4.8 mmol, 1.6 equiv) in toluene (15.0 mL) was cooled to 0 °C and treated with dropwise addition of KHMDS (0.5 M in toluene, 9.0 mL, 4.5 mmol, 1.5 equiv). After stirring at 0 °C for a further 20 min, a solution of ketone (469 mg, 3.0 mmol, 1.0 equiv) in toluene (15.0 mL, final concentration w.r.t. ketone 0.1 M) was added slowly. The reaction flask was then equipped with a reflux condenser and heated to 100 °C overnight. After cooling to rt the reaction was quenched by addition of sat. aq. NH₄Cl (15.0 mL). The reaction was diluted with Et₂O (100 mL) and the contents transferred to a separatory funnel. The organic layer was washed successively with water (2 x 100 mL) and brine (100 mL). The organics were dried over MgSO₄, filtered and concentrated under reduced pressure. The crude material was purified by flash silica chromatography (gradient elution: 100% hexanes to 5% v/v EtOAc/hexanes) to yield 321 mg (68% yield) of alkene **4.108** as a clear colorless oil. The spectral data for **4.108** matched those reported in the literature.⁶⁴



Tetrasubstituted alkene **4.108**

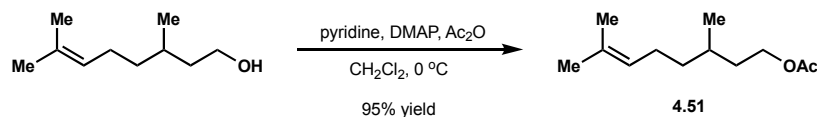
¹H NMR (500 MHz, CDCl₃, 25 °C):

δ 3.96 (s, 4H)

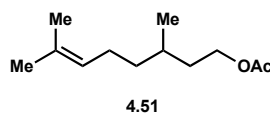
2.29 (t, *J* = 6.3 Hz, 4H)

1.67 (s, 6H)

1.64 (t, *J* = 6.5 Hz, 4H)



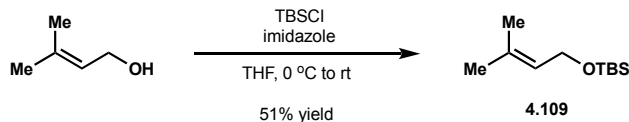
Citronellyl acetate 4.51. To a solution of citronellol (5.5 mL, 30 mmol, 1.0 equiv) in CH₂Cl₂ (150 mL, 0.2 M w.r.t. citronellol) stirred at 0 °C in an ice bath was added pyridine (10.5 mL, 130 mmol, 4.3 equiv), 4-(dimethylamino)pyridine (390 mg, 3.0 mmol, 0.10 equiv), and acetic anhydride (9.5 mL, 100 mmol, 3.3 equiv). After stirring for 5 min at 0 °C the ice bath was removed and the reaction was allowed to warm to room temperature over 2 h. The reaction was then quenched by addition of 1.0 M aq. HCl (100 mL) and the contents were transferred to a separatory funnel. The organic layer was washed successively with 1.0 M aq. HCl, water (100 mL), sat. aq. NaHCO₃ (100 mL), and brine (100 mL). The organics were dried over MgSO₄, filtered and concentrated under reduced pressure. The crude material was purified by flash silica chromatography (gradient elution: 100% hexanes to 10% v/v EtOAc/hexanes) to yield 5.63 g (95% yield) of citronellyl acetate **4.51** as a clear colorless oil. The spectral data for **4.51** matched those reported in the literature.⁶⁵



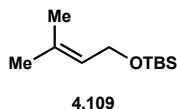
Citronellyl acetate 4.51

¹H NMR (500 MHz, CDCl₃, 25 °C):

δ 5.08 (t, J = 7.1 Hz, 1H)	1.53 (dq, J = 13.1, 6.6 Hz, 1H)
4.13-4.05 (m, 2H)	1.46-1.39 (m, 1H)
2.03 (s, 3H)	1.34 (ddt, J = 13.4, 9.5, 5.9 Hz, 1H)
2.01-1.90 (m, 2H)	1.18 (dddd, J = 13.5, 9.4, 7.7, 5.9 Hz, 1H)
1.70-1.63 (m, 4H)	0.91 (d, J = 6.7 Hz, 3H)
1.60 (s, 3H)	



TBS Prenyl ether 4.109. To a solution of 3-methyl-2-buten-1-ol (0.51 mL, 5.0 mmol, 1.0 equiv) in THF (14.3 mL, 0.35 M w.r.t. alcohol) stirred at rt was added imidazole (817 mg, 12 mmol, 2.4 equiv) in a single portion. After stirring for 5 min at rt the solution was cooled to 0 °C in an ice bath and TBSCl (904 mg, 6.0 mmol, 1.2 equiv) was added in a single portion, resulting in immediate precipitation. After stirring at 0 °C for 15 min the ice bath was removed and the reaction was allowed to warm to rt overnight. The reaction was then quenched by addition of sat. aq. NH₄Cl (5.0 mL), diluted with Et₂O and water, and the contents transferred to a separatory funnel. The organic layer was washed successively with water (2 x 25 mL) and brine (1 x 25 mL). The organics were then dried over MgSO₄, filtered and concentrated under reduced pressure. The crude material was purified by flash silica chromatography (100% hexanes) to yield 515 mg (51% yield) of TBS prenyl ether **4.109** as a clear colorless oil. The spectral data for **4.109** matched those reported in the literature.⁶⁶



TBS Prenyl ether **4.109**

¹H NMR (500 MHz, CDCl₃, 25 °C):

δ 5.30 (t, *J* = 6.4 Hz, 1H)

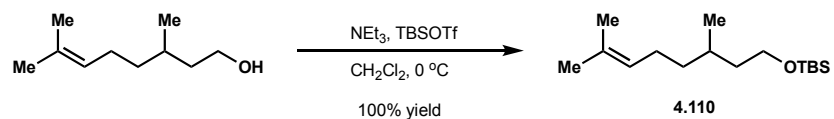
4.17 (d, *J* = 6.6 Hz, 2H)

1.72 (s, 3H)

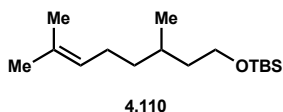
1.63 (s, 3H)

0.91 (s, 9H)

0.07 (s, 6H)



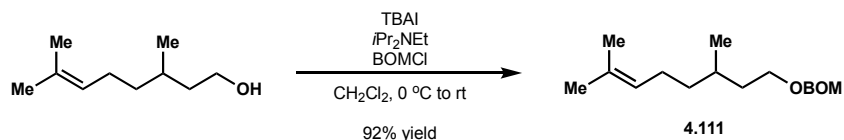
Citronellyl TBS ether 4.110. To a solution of citronellol (0.55 mL, 3.0 mmol, 1.0 equiv) in CH₂Cl₂ (15 mL, 0.2 M w.r.t. citronellol) stirred at 0 °C in an ice bath was added NEt₃ (1.25 mL, 9.0 mmol, 3.0 equiv). After stirring for 10 min at 0 °C, TBSOTf (1.03 mL, 4.5 mmol, 1.5 equiv) was added slowly dropwise. After stirring for 1.5 h at 0 °C the reaction was quenched by addition of sat. aq. NaHCO₃ (10 mL), diluted further with CH₂Cl₂ and water, and the contents were transferred to a separatory funnel. The aqueous layer was extracted with CH₂Cl₂ (3 x 50 mL) and the organics were dried over MgSO₄, filtered and concentrated under reduced pressure. The crude material was purified by flash silica chromatography (gradient elution: 100% hexanes to 5% v/v EtOAc/hexanes) to yield 812 mg (100% yield) of **4.110** as a clear colorless oil. The spectral data for **4.110** matched those reported in the literature.⁶⁷



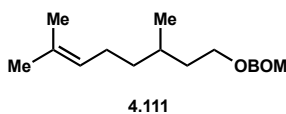
Citronellyl TBS ether **4.110**

¹H NMR (500 MHz, CDCl₃, 25 °C):

δ 5.10 (t, <i>J</i> = 7.1 Hz, 1H)	1.37-1.29 (m, 2H)
3.68-3.59 (m, 2H)	1.19-1.11 (m, 1H)
1.98 (qq, <i>J</i> = 14.6, 7.3 Hz, 2H)	0.90 (s, 9H)
1.68 (s, 3H)	0.88 (d, <i>J</i> = 6.6 Hz, 3H)
1.60 (s, 3H)	0.05 (s, 6H)
1.58-1.52 (m, 2H)	



BOM Ether 4.111. To a solution of citronellol (0.27 mL, 1.5 mmol, 1.0 equiv) in CH₂Cl₂ (15 mL, 0.1 M w.r.t. citronellol) stirred at 0 °C in an ice bath was added *i*Pr₂NEt (0.52 mL, 3.0 mmol, 2.0 equiv). After stirring for 10 min at 0 °C, BOMCl (0.31 mL, 2.2 mmol, 1.5 equiv) was added slowly dropwise. After stirring for 15 min h at 0 °C the ice bath was removed and the reaction was allowed to warm overnight to rt. After 18 h tetrabutylammonium iodide (2.1 mg, 0.006 mmol, 0.5 mol %) and BOMCl (0.15 mL, 1.1 mmol, 0.75 equiv) were added sequentially at rt. After an additional 3 h of stirring, the reaction was quenched by addition of water (15 mL). The contents were transferred to a separatory funnel, diluted with more water, and the aqueous layer was extracted with CH₂Cl₂ (3 x 25 mL). The organics were dried over Na₂SO₄, filtered and concentrated under reduced pressure. The crude material was purified by flash silica chromatography (gradient elution: 100% hexanes to 5% v/v EtOAc/hexanes) to yield 379 mg (92% yield) of **4.111** as a clear colorless oil.



BOM Ether **4.111**

¹H NMR (500 MHz, CDCl₃, 25 °C):

δ 7.37-7.35 (m, 4H)	1.67-1.63 (m, 1H)
7.32-7.28 (m, 1H)	1.61 (s, 3H)
5.11 (dddt, <i>J</i> = 7.1, 5.7, 2.8, 1.4 Hz, 1H)	1.59-1.54 (m, 1H)
4.76 (d, <i>J</i> = 1.0 Hz, 2H)	1.46-1.40 (m, 1H)
4.61 (d, <i>J</i> = 0.9 Hz, 2H)	1.39-1.33 (m, 1H)
3.67-3.58 (m, 2H)	1.22-1.14 (m, 1H)
1.99 (quintetd, <i>J</i> = 15.7, 7.4 Hz, 2H)	0.92 (dd, <i>J</i> = 6.6, 1.4 Hz, 3H)
1.69 (s, 3H)	

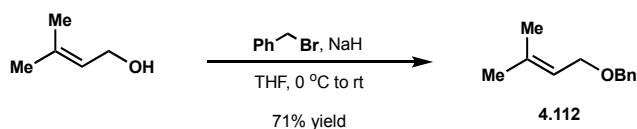
¹³C NMR (126 MHz, CDCl₃, 25 °C):

δ 138.0	127.6	66.3	25.7
131.2	124.8	37.2	25.5

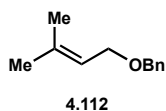
128.4	94.6	36.7	19.5
127.9	69.3	29.6	17.6

HRMS (CI) calculated for C₁₈H₂₈O₂ [M]⁺: 276.2089, found: 276.2086

TLC: R_f = 0.45 (10% v/v EtOAc/Hex)



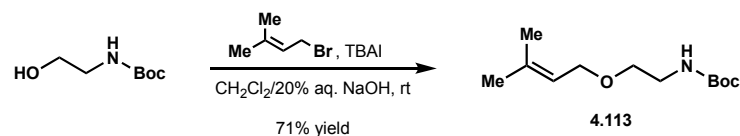
Benzyl prenyl ether 4.112. To a suspension of NaH (60% dispersion in mineral oil, 300 mg, 7.5 mmol, 1.5 equiv) in THF (10 mL, 0.5 M w.r.t. alcohol) stirred at 0 °C in an ice bath was added 3-methyl-2-buten-1-ol (0.51 mL, 5.0 mmol, 1.0 equiv) slowly dropwise. After stirring for 15 min at 0 °C, benzyl bromide (0.89 mL, 7.5 mmol, 1.5 equiv) was added slowly dropwise and the reaction was left to warm to rt overnight. The reaction was then quenched by addition of sat. aq. NH₄Cl (5 mL), diluted with Et₂O and water, and the contents were transferred to a separatory funnel. The organic layer was washed with water (2 x 25 mL), brine (1 x 25 mL) and the organics were dried over MgSO₄, filtered and concentrated under reduced pressure. The crude material was purified by flash silica chromatography (gradient elution: 100% hexanes to 5% v/v EtOAc/hexanes) to yield 623 mg (71% yield) of benzyl prenyl ether **4.112** as a clear pale yellow oil. The spectral data for **4.112** matched those reported in the literature.⁶⁸



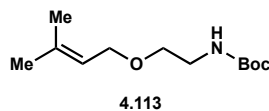
Benzyl prenyl ether **4.112**.

¹H NMR (500 MHz, CDCl₃, 25 °C):

δ 7.37-7.33 (m, 4H)	4.01 (d, <i>J</i> = 6.9 Hz, 2H)
7.29 (td, <i>J</i> = 6.2, 3.5 Hz, 1H)	1.76 (s, 3H)
5.41 (t, <i>J</i> = 6.9 Hz, 1H)	1.66 (s, 3H)
4.51 (s, 2H)	



***N*-Boc prenyl ether 4.113.** To a vigorously stirred solution of *tert*-butyl(2-hydroxyethyl)carbamate⁶⁹ (161 mg, 1.0 mmol, 1.0 equiv) and tetrabutylammonium iodide (1.11 g, 3.0 mmol, 3.0 equiv) in CH₂Cl₂ (2.0 mL, 0.5 M w.r.t. carbamate) and 20% v/v aq. NaOH (2.0 mL, 0.5 M w.r.t. carbamate) was added prenyl bromide (0.35 mL, 3.0 mmol, 3.0 equiv) slowly dropwise at rt. After 21 hours of stirring, the reaction was quenched by addition of sat. aq. NH₄Cl (5.0 mL). The contents were transferred to a separatory funnel, diluted with water (25 mL) and CH₂Cl₂ (25 mL), and the aqueous layer was extracted with CH₂Cl₂ (3 x 25 mL). The organics were dried over Na₂SO₄, filtered and concentrated under reduced pressure. The crude material was purified by flash silica chromatography (gradient elution: 100% hexanes to 10% v/v EtOAc/hexanes) to yield 163 mg (71% yield) of **4.113** as a clear tan oil.



***N*-Boc prenyl ether 4.113**

¹H NMR (500 MHz, CDCl₃, 25 °C):

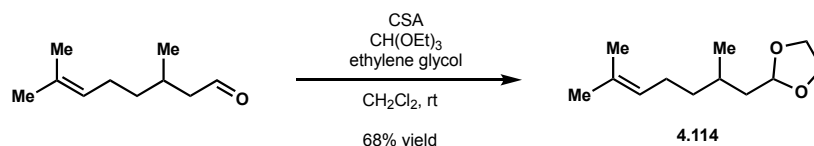
δ 5.34-5.31 (m, 1H)	3.30 (d, <i>J</i> = 4.8 Hz, 2H)
4.89 (s, 1H)	1.74 (s, 3H)
3.96 (d, <i>J</i> = 6.9 Hz, 2H)	1.67 (s, 3H)
3.47 (t, <i>J</i> = 5.0 Hz, 2H)	1.44 (s, 9H)

¹³C NMR (126 MHz, CDCl₃, 25 °C):

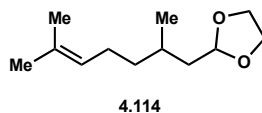
δ 156.0	79.1	40.5	18.0
137.3	68.9	28.4	
120.8	67.4	25.8	

HRMS (ESI) calculated for C₁₂H₂₃NO₃ [M+Na]⁺: 252.1576, found: 252.1576

TLC: R_f = 0.46 (10% v/v EtOAc/Hex)



Dioxolane 4.114. To a solution of camphorsulfonic acid (11.6 mg, 0.05 mmol, 5 mol%) in CH₂Cl₂ (7.1 mL, 0.15 M w.r.t. citronellal) was added (EtO)₃CH (0.50 mL, 3.0 mmol, 3.0 equiv) and ethylene glycol (0.84 mL, 15.0 mmol, 15.0 equiv). After brief stirring, citronellal (0.18 mL, 1.0 mmol, 1.0 equiv) was added slowly dropwise to the reaction flask. After 4 hours of stirring at rt, the reaction was quenched by addition of sat. aq. NaHCO₃ (3.0 mL). The contents were transferred to a separatory funnel, diluted with water (25 mL) and CH₂Cl₂ (25 mL), and the aqueous layer was extracted with CH₂Cl₂ (3 x 25 mL). The organics were dried over MgSO₄, filtered and concentrated under reduced pressure. The crude material was purified by flash silica chromatography (gradient elution: 100% hexanes to 5% v/v EtOAc/hexanes) to yield 136 mg (68% yield) of **4.114** as a clear colorless oil.



Dioxolane **4.114**

¹H NMR (500 MHz, CDCl₃, 25 °C):

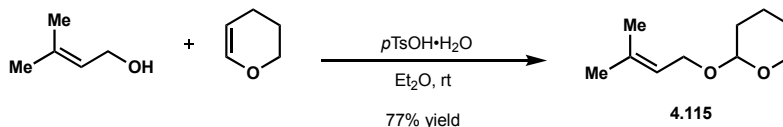
δ 5.11-5.09 (m, 1H)	1.60 (s, 3H)
4.90 (t, <i>J</i> = 4.9 Hz, 1H)	1.52-1.47 (m, 1H)
4.00-3.92 (m, 2H)	1.42-1.35 (m, 1H)
3.87-3.80 (m, 2H)	1.20 (ddt, <i>J</i> = 13.1, 9.6, 6.6 Hz, 1H)
1.98 (qq, <i>J</i> = 14.8, 7.4 Hz, 2H)	0.96 (d, <i>J</i> = 6.5 Hz, 3H)
1.67 (q, <i>J</i> = 10.0 Hz, 5H)	

¹³C NMR (126 MHz, CDCl₃, 25 °C):

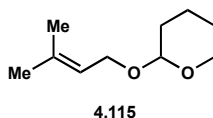
δ 131.2	64.72	29.1	19.8
124.7	64.64	25.7	17.6
103.8	40.9	25.4	

HRMS (CI) calculated for C₁₂H₂₂O₂ [M]⁺: 198.1620, found: 196.1611

TLC: R_f = 0.36 (10% v/v EtOAc/Hex)



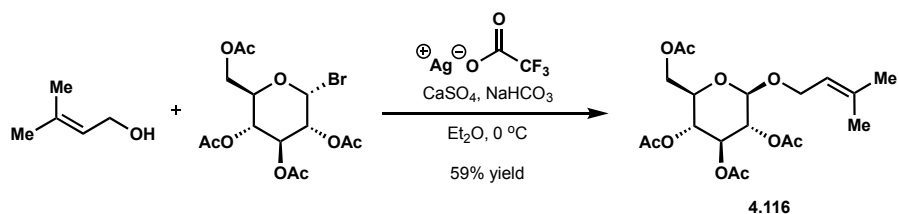
THP prenyl ether 4.115. To a solution of *p*-toluenesulfonic acid monohydrate (19 mg, 0.10 mmol, 2.0 mol%) in Et₂O (10 mL, 0.5 M w.r.t. alcohol) stirred at rt was added 3-methyl-2-buten-1-ol (0.51 mL, 5.0 mmol, 1.0 equiv) and 3,4-dihydro-2*H*-pyran (0.82 mL, 9.0 mmol, 1.8 equiv). Once determined complete by TLC, the reaction was diluted with Et₂O (50 mL) and the contents transferred to a separatory funnel. The organic layer was washed successively with water (3 x 25 mL) and brine (25 mL). The organics were dried over MgSO₄, filtered and concentrated under reduced pressure. The crude material was purified by flash silica chromatography (gradient elution: 100% hexanes to 5% v/v EtOAc/hexanes) to yield 659 mg (77% yield) of THP prenyl ether **4.115** as a clear colorless oil. The spectral data for **4.115** matched those reported in the literature.⁷⁰



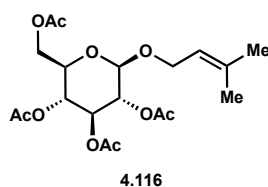
THP Prenyl ether **4.115**

¹H NMR (500 MHz, CDCl₃, 25 °C):

δ 5.37-5.35 (m, 1H)	1.87-1.80 (m, 1H)
4.62 (t, <i>J</i> = 3.2 Hz, 1H)	1.75 (s, 3H)
4.22 (dd, <i>J</i> = 11.4, 6.8 Hz, 1H)	1.71 (t, <i>J</i> = 3.3 Hz, 1H)
3.99 (dd, <i>J</i> = 11.4, 7.8 Hz, 1H)	1.68 (s, 3H)
3.91-3.87 (m, 1H)	1.58 (ddd, <i>J</i> = 15.3, 8.4, 3.3 Hz, 2H)
3.52-3.49 (m, 1H)	1.54-1.51 (m, 2H)



Prenyl glucopyranoside 4.116. Prepared using a procedure reported by Ackermann.⁷¹ A flame dried 100 mL RBF was charged with acetobromo- α -D-glucose (822 mg, 2.0 mmol, 1.0 equiv), CaSO_4 (286 mg, 2.1 mmol, 1.05 equiv), NaHCO_3 (168 mg, 2.0 mmol, 1.0 equiv), silver trifluoroacetate (442 mg, 2.0 mmol, 1.0 equiv) and then capped with a septum and placed under an inert atmosphere of N_2 . The flask of solids was cooled to 0 °C in an ice bath before a solution of 3-methyl-2-buten-1-ol (0.55 mL, 5.4 mmol, 2.7 equiv) in Et_2O (5.4 mL, 0.5 M w.r.t. alcohol) was added. The reaction was stirred at 0 °C for 0.5 h before 21 mL of Et_2O was added via syringe and stirred for a further 0.5 h at 0 °C. The reaction was diluted with Et_2O (50 mL) and the contents transferred to a separatory funnel. The organic layer was washed successively with water (2 x 50 mL), sat. aq. NaHCO_3 (2 x 50 mL) and brine (50 mL). The organics were dried over MgSO_4 , filtered and concentrated under reduced pressure. The crude material was purified by flash silica chromatography (gradient elution: 100% hexanes to 30% v/v EtOAc /hexanes) to yield 493 mg (59% yield) of prenyl glucopyranoside **4.116** as a white solid. The spectral data for **4.116** matched those reported in the literature.⁷²



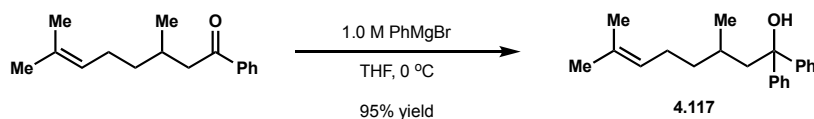
Prenyl glucopyranoside **4.116**

^1H NMR (500 MHz, CDCl_3 , 25 °C):

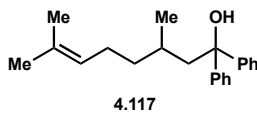
δ 5.24 (ddt, $J = 7.9, 6.5, 1.4$ Hz, 1H)	3.65 (ddd, $J = 10.0, 5.0, 2.5$ Hz, 1H)
5.19 (t, $J = 9.5$ Hz, 1H)	2.06 (s, 3H)
5.06 (t, $J = 9.7$ Hz, 1H)	2.02 (s, 3H)
4.96 (dd, $J = 9.6, 8.0$ Hz, 1H)	2.00 (s, 3H)
4.52 (d, $J = 8.0$ Hz, 1H)	1.98 (s, 3H)
4.24-4.16 (m, 3H)	1.75 (s, 3H)
4.13 (dd, $J = 12.2, 2.4$ Hz, 1H)	1.65 (s, 3H)

^{13}C NMR (126 MHz, CDCl_3 , 25 °C):

δ 170.6	119.4	68.5	20.64
170.3	98.7	65.2	20.57
169.33	72.9	62.1	20.55
169.26	71.8	25.7	17.9
138.8	71.3	20.67	



Diphenyl tertiary alcohol 4.117. A solution of phenylmagnesium bromide (1.0 M in THF, 2.8 mL, 2.8 mmol, 1.2 equiv) in THF (3.1 mL, 0.9 M w.r.t. Grignard reagent) was cooled to 0 °C. A solution of 3,7-dimethyl-1-phenyloct-6-en-1-one⁷³ (426 mg, 1.85 mmol, 1.0 equiv) in THF (3.1 mL, 0.6 M w.r.t. ketone, final reaction concentration 0.3 M). After 1 h, the reaction was quenched by addition of sat. aq. NH_4Cl (5 mL) and further diluted with water and Et_2O . The resulting mixture was extracted with Et_2O (3 x 25). The combined organics were washed with brine, dried over MgSO_4 , filtered and concentrated under reduced pressure. The crude material was purified by flash silica chromatography (gradient elution: 100% hexanes to 5% v/v EtOAc /hexanes) to yield 544 mg (95% yield) of **4.117** as a clear colorless oil.



Diphenyl tertiary alcohol **4.117**

^1H NMR (500 MHz, CDCl_3 , 25 °C):

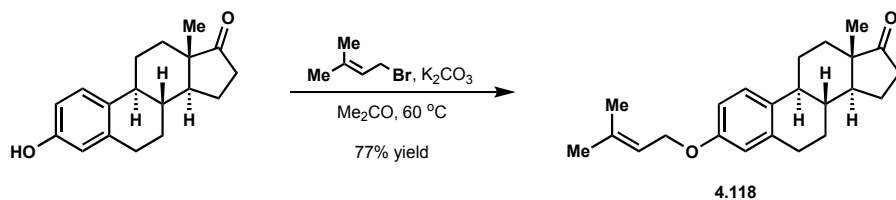
δ 7.43 (d, $J = 7.6$ Hz, 4H)	1.89 (qq, $J = 13.8, 6.9$ Hz, 2H)
7.31 (td, $J = 7.7, 1.9$ Hz, 4H)	1.66 (s, 3H)
7.22 (t, $J = 7.3$ Hz, 2H)	1.60 (dd, $J = 12.5, 6.9$ Hz, 1H)
4.99 (t, $J = 7.0$ Hz, 1H)	1.56 (s, 3H)
2.36 (dd, $J = 14.3, 4.2$ Hz, 1H)	1.37-1.30 (m, 1H)
2.17 (dd, $J = 14.3, 6.6$ Hz, 1H)	1.22-1.15 (m, 1H)
2.04 (s, 1H)	0.85 (d, $J = 6.7$ Hz, 3H)

^{13}C NMR (126 MHz, CDCl_3 , 25 °C):

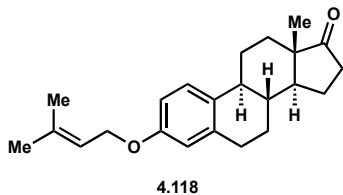
δ 147.8	126.64	38.8
147.4	126.09	28.4
131.2	126.06	25.7
128.03	124.7	25.3
128.01	78.8	21.6
126.70	48.7	17.6

HRMS (CI) calculated for $\text{C}_{22}\text{H}_{28}\text{O}$ $[\text{M}-\text{H}_2\text{O}]^+$: 290.2035 found: 290.2026

TLC: $R_f = 0.38$ (10% v/v EtOAc/Hex)



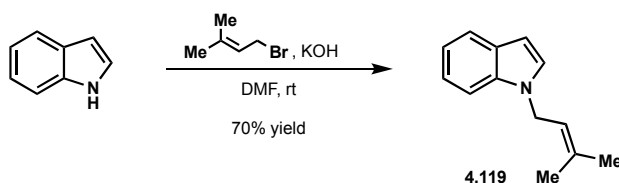
Estrone prenyl ether 4.118. Prepared using a procedure reported by Jefferson.⁷⁴ To a stirred suspension of estrone (541 mg, 2.0 mmol, 1.0 equiv) and K_2CO_3 (542 mg, 3.92 mmol, 1.96 equiv) in acetone (67 mL, 0.03 M w.r.t. estrone) at rt was added prenyl bromide (0.51 mL, 4.4 mmol, 2.2 equiv). The flask was then fitted with a reflux condenser and heated to 60 °C in an oil bath for 36 hours. The reaction was then concentrated under reduced pressure, diluted with CH_2Cl_2 (100 mL) and water (100 mL), and the contents were transferred to a separatory funnel. The aqueous layer was extracted with CH_2Cl_2 (3 x 100 mL), the combined organics were washed with brine (1 x 100 mL), dried over MgSO_4 , filtered and concentrated under reduced pressure. The crude material was purified by flash silica chromatography (gradient elution: 100% hexanes to 30% v/v EtOAc/hexanes) to yield 516 mg (76% yield) of estrone prenyl ether **4.118** as a white solid. The spectral data for **4.118** matched those reported in the literature.^{29b}



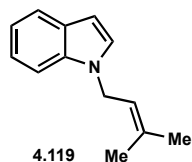
Estrone prenyl ether **4.118**

^1H NMR (500 MHz, CDCl_3 , 25 °C):

δ 7.20 (d, $J = 8.6$ Hz, 1H)	2.25 (dd, $J = 13.7, 6.8$ Hz, 1H)
6.74 (d, $J = 8.6$ Hz, 1H)	2.14 (dt, $J = 18.7, 9.2$ Hz, 1H)
6.67 (s, 1H)	2.08-1.99 (m, 2H)
5.51-5.49 (m, 1H)	1.94 (dd, $J = 16.8, 7.5$ Hz, 1H)
4.48 (d, $J = 6.8$ Hz, 2H)	1.80 (s, 3H)
2.95-2.86 (m, 2H)	1.74 (s, 3H)
2.50 (dd, $J = 19.0, 8.7$ Hz, 1H)	1.67-1.40 (m, 6H)
2.41-2.39 (m, 1H)	0.91 (s, 3H)



***N*-Prenyl indole 4.119.** Prepared using an adapted procedure reported by Sridhar.⁷⁵ To a flame dried 25 mL RBF charged with KOH (505 mg, 9.0 mmol, 3.0 equiv) under an inert atmosphere of N_2 was added DMF (3.6 mL, 2.5 M w.r.t. KOH). The solution was stirred vigorously for 15 min at rt before indole (352 mg, 3.0 mmol, 1.0 equiv) was added in a single portion and stirred for a further 30 min at rt. A solution of prenyl bromide (0.35 mL, 3.0 mmol, 1.0 equiv) in DMF (1.8 mL, 1.67 M w.r.t. bromide, final reaction concentration 0.57 M) was added over 5 min. The reaction was left to stir overnight, then quenched by addition of water (15 ml). The reaction was diluted with Et_2O (50 mL) and the contents transferred to a separatory funnel. The organic layer was washed successively with water (3 x 50 mL) and brine (1 x 50 mL). The organics were dried over MgSO_4 , filtered and concentrated under reduced pressure. The crude material was purified by flash silica chromatography (gradient elution: 100% hexanes to 30% v/v CH_2Cl_2 /hexanes) to yield 389 mg (70% yield) of *N*-prenyl indole **4.119** as a clear tan oil.



N-Prenyl indole **4.119**

^1H NMR (500 MHz, CDCl_3 , 25 °C):

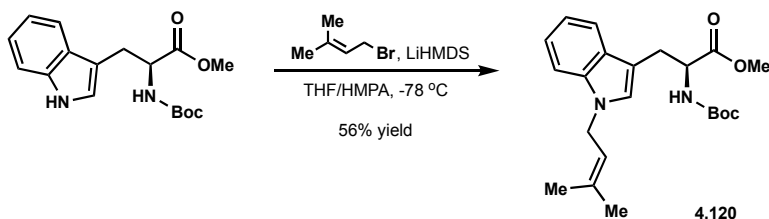
δ 7.67 (dt, $J = 7.9, 0.9$ Hz, 1H)	5.42 (tdt, $J = 6.9, 2.8, 1.4$ Hz, 1H)
7.37 (dd, $J = 8.2, 0.8$ Hz, 1H)	4.72 (d, $J = 6.9$ Hz, 2H)
7.24 (ddd, $J = 8.2, 7.0, 1.2$ Hz, 1H)	1.86 (s, 3H)
7.15-7.12 (m, 2H)	1.80 (s, 3H)
6.52 (dd, $J = 3.1, 0.8$ Hz, 1H)	

^{13}C NMR (126 MHz, CDCl_3 , 25 °C):

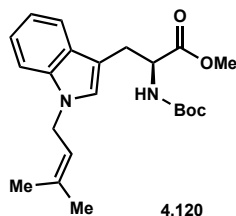
δ 136.13	120.9	44.1
135.94	120.0	25.6
128.7	119.2	18.0
127.3	109.5	
121.3	100.9	

HRMS (ESI) calculated for $\text{C}_{13}\text{H}_{15}\text{N}$ $[\text{M}]^+$: 185.1205, found: 185.1198

TLC: $R_f = 0.42$ (30% v/v $\text{CH}_2\text{Cl}_2/\text{Hex}$)



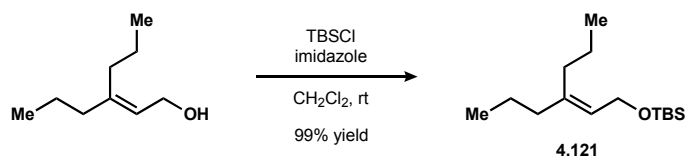
***N*-Prenyl tryptophan 4.120.** To a solution of *N*-Boc-L-tryptophan methyl ester (955 mg, 3.0 mmol, 1.0 equiv) in THF (38 mL, 0.08 M w.r.t. tryptophan) stirred at -78 °C in a dry ice acetone bath was added LiHMDS (1.0 M in THF, 3.6 mL, 3.6 mmol, 1.2 equiv) slowly dropwise. The reaction was stirred at -78 °C for 40 min followed by dropwise addition of HMPA (0.57 mL, 3.3 mmol, 1.1 equiv) and prenyl bromide (0.36 mL, 3.15 mmol, 1.05 equiv) sequentially. The reaction was further stirred at -78 °C for 1 h then the dry ice bath was removed and the reaction was allowed to warm to rt. Once determined complete by TLC, the reaction was quenched by addition of sat. aq. NH₄Cl, diluted with Et₂O (150 mL), water (150 mL), and the contents transferred to a separatory funnel. The organic layer was washed successively with water (3 x 100 mL) and brine (100 mL). The organics were dried over Na₂SO₄, filtered and concentrated under reduced pressure. The crude material was purified by flash silica chromatography (gradient elution: 100% hexanes to 30% v/v EtOAc/hexanes) to yield 652 mg (56% yield) of *N*-prenyl tryptophan **4.120** as an off white solid. The spectral data for **4.120** matched those reported in the literature.⁷⁶



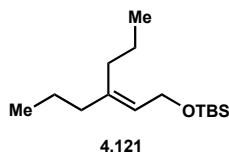
***N*-Prenyl tryptophan 4.120**

¹H NMR (500 MHz, CDCl₃, 25 °C):

δ 7.54 (d, <i>J</i> = 7.9 Hz, 1H)	4.63 (dd, <i>J</i> = 13.2, 6.3 Hz, 3H)
7.29 (d, <i>J</i> = 8.2 Hz, 1H)	3.68 (s, 3H)
7.20 (td, <i>J</i> = 7.6, 1.0 Hz, 1H)	3.31-3.23 (m, 2H)
7.10 (t, <i>J</i> = 7.5 Hz, 1H)	1.82 (s, 3H)
6.90 (s, 1H)	1.77 (s, 3H)
5.37-5.34 (m, 1H)	1.44 (s, 9H)
5.06 (d, <i>J</i> = 7.6 Hz, 1H)	



TBS Ether 4.121. To a solution of imidazole (354 mg, 5.2 mmol, 2.4 equiv) in CH₂Cl₂ (8 mL, 0.65 M w.r.t. imidazole) stirred at rt was added a solution of 3-propylhex-2-en-1-ol⁷⁷ (307 mg, 2.2 mmol, 1.0 equiv) in CH₂Cl₂ (4 mL, 0.55 M w.r.t. alcohol), followed by TBSCl (417 mg, 2.8 mmol, 1.3 equiv) in a single portion. After stirring at rt for 2.5 h, the reaction was quenched by addition of H₂O (12 mL), diluted with CH₂Cl₂ and water, and the contents were transferred to a separatory funnel. The aqueous layer was extracted with CH₂Cl₂ (3 x 10 mL), then the combined organics washed with brine (1 x 10 mL) and were dried over MgSO₄, filtered and concentrated under reduced pressure. The crude material was purified by flash silica chromatography (1% v/v EtOAc in pentane) to yield 546 mg (99% yield) of **4.121** as a clear colorless oil.



TBS Ether 4.121

¹H NMR (600 MHz, CDCl₃, 25 °C):

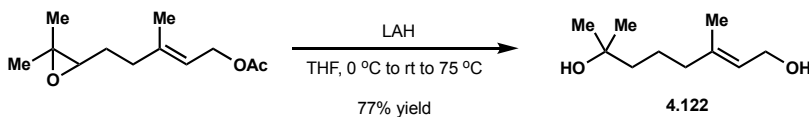
δ 5.29 (t, <i>J</i> = 6.3 Hz, 1H)	1.42 (sextet, <i>J</i> = 7.4 Hz, 2H)	0.89 (t, <i>J</i> = 7.3 Hz, 3H)
4.19 (d, <i>J</i> = 6.3 Hz, 2H)	1.37 (sextet, <i>J</i> = 7.4 Hz, 2H)	0.88 (t, <i>J</i> = 7.3 Hz, 3H)
1.97 (q, <i>J</i> = 8.1 Hz, 4H)	0.90 (s, 9H)	0.07 (s, 6H)

¹³C NMR (151 MHz, CDCl₃, 25 °C):

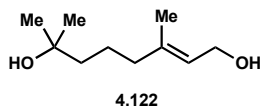
δ 141.2	32.6	18.4
124.7	26.0	14.1
60.1	21.7	13.9
38.9	21.0	-5.0

HRMS (CI) calculated for C₁₅H₃₂OSi [M]⁺: 256.2222, found: 256.2223

TLC: R_f = 0.21 (100% hexanes)



Diol 4.122. To a suspension of LiAlH_4 (569 mg, 15.0 mmol, 5.0 equiv) in THF (7.5 mL, 2.0 M w.r.t. LiAlH_4) stirred at 0 °C in an ice bath was added a solution of (*E*)-5-(3,3-dimethyloxiran-2-yl)-3-methylpent-2-en-1-yl-acetate⁷⁸ (0.65 mL, 3.0 mmol, 1.0 equiv) in THF (7.5 mL, 0.4 M, w.r.t. epoxide) via syringe pump over 20 min. After stirring for 30 min at 0 °C, the ice bath was removed and reaction was left to warm to rt over 2 h. The reaction flask was then fitted with a reflux condenser and the reaction was heated to 75 °C overnight in an oil bath. Once determined complete by TLC, the reaction was cooled to rt and quenched by addition of sat. aq. NH_4Cl (5 mL), diluted with Et_2O and water, and the contents were transferred to a separatory funnel. The organic layer was washed with water (3 x 50 mL), brine (1 x 25 mL) and the organics were dried over MgSO_4 , filtered and concentrated under reduced pressure. The crude material was purified by flash silica chromatography (gradient elution: 100% hexanes to 80% v/v EtOAc /hexanes) to yield 399 mg (77% yield) of diol **4.122** as a thick clear colorless oil.



Diol 4.122.

^1H NMR (500 MHz, CDCl_3 , 25 °C):

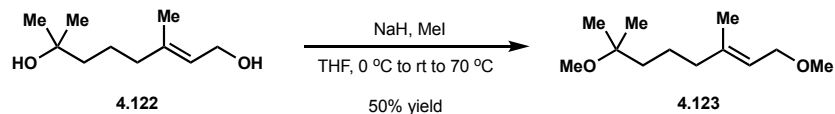
δ 5.41 (t, $J = 6.9$ Hz, 1H)	1.66 (s, 3H)
4.14 (d, $J = 6.9$ Hz, 2H)	1.52-1.41 (m, 6H)
2.02 (t, $J = 7.1$ Hz, 2H)	1.20 (s, 6H)

^{13}C NMR (126 MHz, CDCl_3 , 25 °C):

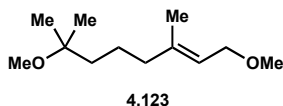
δ 139.5	59.3	29.2
123.6	43.3	22.3
70.9	39.8	16.1

HRMS (ESI) calculated for $\text{C}_{10}\text{H}_{20}\text{O}_2$ $[\text{M}+\text{Na}]^+$: 195.1361, found: 195.1351

TLC: $R_f = 0.42$ (100% v/v EtOAc)



2,8-Dimethoxy octene ether 4.123. To a cooled suspension of NaH (60% dispersion in mineral oil, 200 mg, 5.0 mmol, 5.0 equiv) in THF (1.7 mL, 2.95 M w.r.t. NaH) stirred at 0 °C in an ice bath was added a solution of diol **4.122** (172 mg, 1.0 mmol, 1.0 equiv) in THF (1.7 mL, 0.6 M w.r.t diol) slowly dropwise. After stirring for 1 h at 0 °C, the ice bath was removed and the reaction was allowed to warm to rt. A solution of MeI (0.31 mL, 5.0 mmol, 5.0 equiv) in THF (1.7 mL, 2.95 M w.r.t. MeI) was added slowly and the reaction was left to stir overnight at rt. TLC showed clean monoalkylation but sluggish dialkylation. The flask was then fitted with a reflux condenser and the reaction heated to 70 °C in an oil bath. After 12 h the reaction was cooled to rt, quenched by addition of sat. aq. NH₄Cl (5 mL), diluted with Et₂O and water, and the contents were transferred to a separatory funnel. The aqueous layer was extracted with Et₂O (3 x 25 mL), then the combined organics washed with brine (1 x 25 mL) and were dried over MgSO₄, filtered and concentrated under reduced pressure. The crude material was purified by flash silica chromatography (gradient elution: 100% hexanes to 50% v/v EtOAc/hexanes) to yield 100 mg (50% yield) of 2,8-dimethoxy octene ether **4.123** as a clear colorless oil. Most of the remaining mass balance was monoalkylated product.



2,8-Dimethoxy octene ether **4.123**

¹H NMR (500 MHz, CDCl₃, 25 °C):

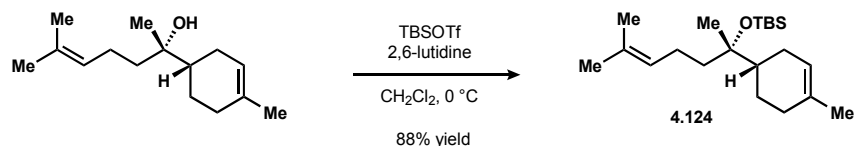
δ 5.36-5.33 (m, 1H)	3.16 (s, 3H)	1.48-1.40 (m, 4H)
3.93 (d, <i>J</i> = 6.7 Hz, 2H)	2.02 (t, <i>J</i> = 6.5 Hz, 2H)	1.13 (s, 6H)
3.32 (s, 3H)	1.66 (s, 3H)	

¹³C NMR (126 MHz, CDCl₃, 25 °C):

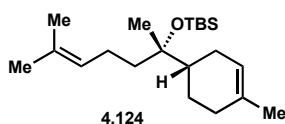
δ 140.4	69.0	40.0	21.9
120.8	57.8	39.4	16.3
74.5	49.1	25.0	

HRMS (ESI) calculated for C₁₂H₂₄O₂ [M+Na]⁺: 223.1674, found: 223.1684

TLC: R_f = 0.25 (10% v/v EtOAc/Hex)



Bisabolol TBS ether 4.124. To a solution of (–)- α -bisabolol (0.48 mL, 2.0 mmol, 1.0 equiv) in CH_2Cl_2 (6 mL, 0.34 M w.r.t. alcohol) stirred at 0 °C was added 2,6-lutidine (0.56 mL, 4.8 mmol, 2.4 equiv) slowly dropwise, followed by TBSOTf (0.55 mL, 2.4 mmol, 1.2 equiv). After stirring at 0 °C for 4 h, the reaction was quenched by addition of dry MeOH (5 mL). After stirring at 0 °C for 20 min, the solution was warmed to rt, then concentrated under vacuum. The crude material was purified by flash silica chromatography (gradient elution: 100% hexanes to 4% v/v EtOAc in hexanes) to yield 596 mg (88% yield) of **4.124** as a clear colorless oil.



Bisabolol TBS ether **4.124**

^1H NMR (600 MHz, CDCl_3 , 25 °C):

δ 5.40–5.36 (m, 1H)	1.59 (m, 2H)
5.11–5.05 (m, 1H)	1.45 (ddd, $J = 13.2, 12.4, 5.6$ Hz, 1H)
2.05–1.90 (m, 5H)	1.28 (qd, $J = 12.2, 5.6$ Hz, 1H)
1.88–1.79 (m, 2H)	1.15 (s, 3H)
1.69 (s, 1H)	0.87 (s, 9H)
1.65 (s, 1H)	0.08 (d, $J = 4.5$ Hz, 6H)
1.61 (s, 1H)	

^{13}C NMR (151 MHz, CDCl_3 , 25 °C):

δ 133.1	42.4	26.0	23.4	–1.8
131.1	40.9	25.7	22.6	–1.9
124.8	31.2	24.7	18.5	
121.1	26.6	23.5	17.6	

HRMS (CI) calculated for $\text{C}_{21}\text{H}_{40}\text{OSi}$ $[\text{M}+\text{H}]^+$: 337.2927, found: 337.2935

TLC: $R_f = 0.72$ (100% hexanes)

Catalytic Radical-Polar Crossover Ritter Reaction Protocols

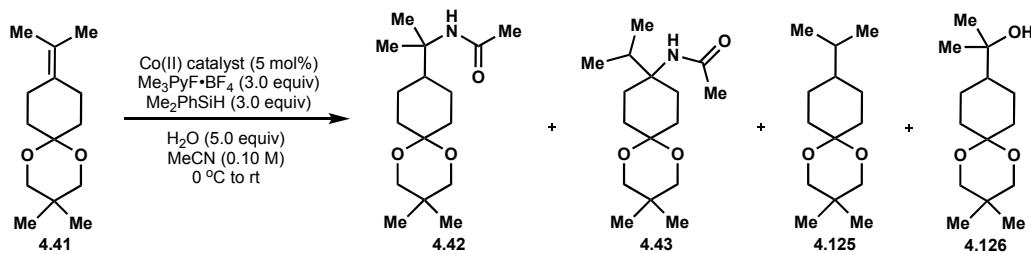
General Procedure V: Slow-Addition of Oxidant For Hydroamidation of Trisubstituted Alkenes

To a flame dried 5-mL RBF charged with a magnetic stir bar was added Co-salen catalyst **4.55** (0.005 mmol, 0.05 equiv) and alkene (0.10 mmol, 1.0 equiv). The RBF was then capped with a septum, placed under an atmosphere of nitrogen, and acetonitrile (0.5 mL, 0.2 M w.r.t. alkene) was added via syringe. To a separate flame dried 5-mL pear flask was added oxidant Me₃PyF•OTf (87 mg, 0.30 mmol, 3.0 equiv). The pear flask was then capped with a septum, placed under an atmosphere of nitrogen, and acetonitrile (0.5 mL, 0.2 M w.r.t. oxidant) was added via syringe. To a separate oven dried 1-dram vial, under an atmosphere of nitrogen, was added water (1 mL) via syringe. All three solutions were then degassed by sparging with balloons of argon while simultaneously subjected to sonication for 5 min. Once degassed, all three solutions were placed under an atmosphere of nitrogen. The stirred Co-salen/alkene solution was then cooled to 0 °C in an ice bath and degassed water (9 μL, 0.50 mmol, 5.0 equiv) was added, followed by the addition of PhMe₂SiH (46 μL, 0.30 mmol, 3.0 equiv) at a rate of 1 drop/10 s. The oxidant solution was then added to the reaction over 20 min via syringe pump. Upon complete addition of oxidant, the syringe was removed, and the reaction was left to stir at 0 °C. After 15 min, the reaction was quenched by addition of sat. aq. NH₄Cl and further diluted with CH₂Cl₂ and water. The aqueous phase was extracted with CH₂Cl₂ (3 x 5 mL) and the combined organic layers were washed with brine, dried over Na₂SO₄, filtered, and concentrated under reduced pressure. The crude material was purified by flash silica chromatography.

General Procedure VI: Slow-Addition of Silane For Hydroamidation of Trisubstituted and Tetrasubstituted Alkenes

To a flame dried 5-mL RBF charged with a magnetic stir bar was added Co-salen catalyst **4.50** (0.005 mmol, 0.05 equiv), Me₃PyF •BF₄ (68 mg, 0.30 mmol, 3.0 equiv), and alkene (0.10 mmol, 1.0 equiv). The RBF was then capped with a septum, placed under an atmosphere of nitrogen, and acetonitrile (0.5 mL, 0.2 M w.r.t. alkene) was added via syringe. To a separate flame dried 5-mL pear flask was added PhMe₂SiH (46 μL, 0.30 mmol, 3.0 equiv). The pear flask was then capped with a septum, placed under an atmosphere of nitrogen, and acetonitrile (0.5 mL, 0.2 M w.r.t. silane) was added via syringe. To a separate oven dried 1-dram vial, under an atmosphere of nitrogen, was added water (1 mL) via syringe. All three solutions were then degassed by sparging with balloons of argon while simultaneously subjected to sonication for 5 min. Once degassed, all three solutions were placed under an atmosphere of nitrogen. The stirred Co-salen/alkene solution was then cooled to 0 °C in an ice bath and degassed water (9 μL, 0.50 mmol, 5.0 equiv) was added. The silane solution was then added to the reaction via syringe pump (addition over 20 min for trisubstituted alkenes, addition over 1 h for tetrasubstituted alkenes). Upon complete addition of silane, the syringe was removed, and the reaction was left to stir at 0 °C. After 15 min, the reaction was quenched by addition of sat. aq. NH₄Cl and further diluted with CH₂Cl₂ and water. The aqueous phase was extracted with CH₂Cl₂ (3 x 5 mL) and the combined organic layers were washed with brine, dried over Na₂SO₄, filtered, and concentrated under reduced pressure. The crude material was purified by flash silica chromatography.

General procedure for optimization of catalytic radical-polar crossover Ritter reaction of tetrasubstituted alkenes



catalyst	4.41 (% yield)	4.42 + 4.43 (% yield)	4.125 (% yield)	4.126 (% yield)
4.15	100	0	0	0
4.21	62	34	1	3
4.44	47	40	6	5
4.45	45	43	4	3
4.46	32	51	7	6
4.47	34	52	6	6
4.48	17	60	9	7
4.49	15	68	3	7
4.50	10	76	7	5
4.55	30	52	6	5

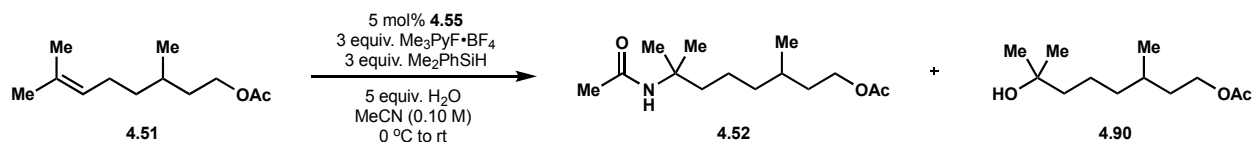
^aYields determined by ¹H NMR using an internal standard of meystylene.

Experimental Procedure: To a flame dried 5-mL RBF charged with a magnetic stir bar was added Co-salen catalyst (0.005 mmol, 0.05 equiv), Me₃PyF•BF₄ (68 mg, 0.30 mmol, 3.0 equiv), and alkene **4.41** (22.4 mg, 0.10 mmol, 1.0 equiv). The RBF was then capped with a septum, placed under an atmosphere of nitrogen, and acetonitrile (0.5 mL, 0.2 M w.r.t. alkene) was added via syringe. To a separate flame dried 5-mL pear flask was added PhMe₂SiH (46 μL, 0.30 mmol, 3.0 equiv). The pear flask was then capped with a septum, placed under an atmosphere of nitrogen, and acetonitrile (0.5 mL, 0.2 M w.r.t. silane) was added via syringe. To a separate oven dried 1-dram vial, under an atmosphere of nitrogen, was added water (1 mL) via syringe. All three solutions were then degassed by sparging with balloons of argon while simultaneously subjected to sonication for 5 min. Once degassed, all three solutions were placed under an atmosphere of nitrogen. The stirred Co-salen/alkene solution was then cooled to 0 °C in an ice bath and degassed water (9 μL, 0.50 mmol, 5.0 equiv) was added. The silane solution was then added to the reaction via syringe pump over 20 min. Upon complete addition of silane, the syringe was removed, and the reaction was left to stir at 0 °C. After 15 min, the reaction was quenched by addition of sat. aq. NH₄Cl and further diluted with CH₂Cl₂ and water. The aqueous phase was extracted with CH₂Cl₂

(3 x 5 mL) and the combined organic layers were washed with brine, dried over Na₂SO₄, filtered, and concentrated under reduced pressure. The crude material was filtered through a plug of silica gel into a scint vial first using 10 mL of 20% v/v EtOAc/hexanes as eluent until all starting alkene **4.41**, hydrogenation **4.125**, and hydration **4.126** had eluted, determined by TLC. The silica plug was moved to a new scint vial and 10 mL of 100% v/v EtOAc was passed through the plug until acetamides **7** and **8** had fully eluted, determined by TLC. The collected filtrates were concentrated under reduced pressure. To each of the resulting dark-brown residues were added CDCl₃ (0.6 mL) and mesitylene (14 uL, 0.10 mmol, 1.0 equiv).

Determination of conversion and product ratios by ¹H NMR analysis: The entirety of the samples were transferred to separate NMR tubes and spectra collected. The mesitylene singlet at 6.80 ppm was integrated to 3.0. In the ¹H NMR sample containing starting alkene **4.41**, hydrogenation product **4.125**, and hydration product **4.126**, quantification of the remaining alkene **6** was accomplished by integration of the allylic methyl proton singlet at 1.66 ppm, quantification of the hydrogenation product **4.125** was accomplished by integration of the methyl proton doublet at 0.86 ppm, and quantification of hydration product **4.126** was accomplished by integration of the methyl singlet at 1.18 ppm. In the ¹H NMR sample containing acetamides **4.42** and **4.43**, quantification of acetamide products **4.42** and **4.43** was accomplished by integration of the methylene singlets from 3.45 ppm to 3.52 ppm.

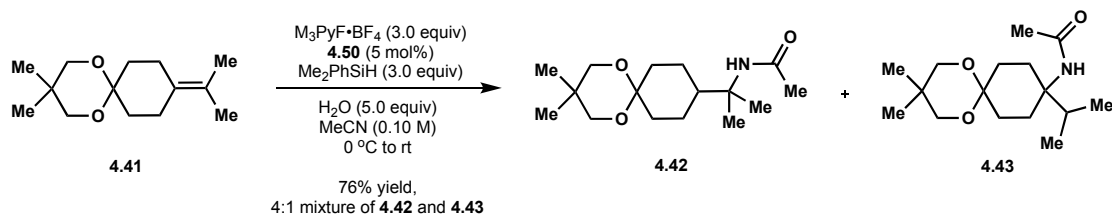
General procedure for optimization of catalytic radical-polar crossover Ritter reaction of trisubstituted alkenes



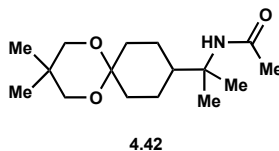
Experimental Procedure: To a flame dried 5-mL RBF charged with a magnetic stir bar was added Co-salen catalyst (0.005 mmol, 0.05 equiv), $\text{Me}_3\text{PyF}\cdot\text{BF}_4$ (68 mg, 0.30 mmol, 3.0 equiv), and alkene **4.51** (23.3 μL , 0.10 mmol, 1.0 equiv). The RBF was then capped with a septum, placed under an atmosphere of nitrogen, and acetonitrile (0.5 mL, 0.2 M w.r.t. alkene) was added via syringe. To a separate flame dried 5-mL pear flask was added PhMe_2SiH (46 μL , 0.30 mmol, 3.0 equiv). The pear flask was then capped with a septum, placed under an atmosphere of nitrogen, and acetonitrile (0.5 mL, 0.2 M w.r.t. silane) was added via syringe. To a separate oven dried 1-dram vial, under an atmosphere of nitrogen, was added water (1 mL) via syringe. All three solutions were then degassed by sparging with balloons of argon while simultaneously subjected to sonication for 5 min. Once degassed, all three solutions were placed under an atmosphere of nitrogen. The stirred Co-salen/alkene solution was then cooled to $0\text{ }^\circ\text{C}$ in an ice bath and degassed water (9 μL , 0.50 mmol, 5.0 equiv) was added. The silane solution was then added to the reaction via syringe pump over 20 min. Upon complete addition of silane, the syringe was removed, and the reaction was left to stir at $0\text{ }^\circ\text{C}$. After 15 min, the reaction was quenched by addition of sat. aq. NH_4Cl and further diluted with CH_2Cl_2 and water. The aqueous phase was extracted with CH_2Cl_2 (3 x 5 mL) and the combined organic layers were washed with brine, dried over Na_2SO_4 , filtered, and concentrated under reduced pressure. The crude material was filtered through a plug of silica gel using 5% v/v $\text{MeOH}/\text{CH}_2\text{Cl}_2$ as eluent and the collected filtrate was concentrated under reduced pressure. To the resulting dark-brown residue was added CDCl_3 (0.6 mL) and mesitylene (14 μL , 0.10 mmol, 1.0 equiv).

Determination of conversion and product ratios by ^1H NMR analysis: The entirety of the sample was transferred to an NMR tube and a spectrum collected. The mesitylene singlet at 6.80 ppm was integrated to 3.0. Quantification of the remaining alkene **4.51** was accomplished by integration of the vinyl proton at 5.08 ppm. Quantification of the acetamide product **4.52** was accomplished by integration of the acetamide methyl proton at 1.91 ppm. The extent of hydration **4.90** could only be determined quantitatively following purification by flash silica chromatography.

Experimental data.



Acetamides 4.42 and 4.43. Acetamides **4.42** and **4.43** were prepared according to General Procedure VI with alkene **4.41** (22.4 mg, 0.10 mmol) and purified by flash chromatography (gradient elution: 100% hexanes to 80% v/v EtOAc in hexanes) to afford a 4:1 mixture of acetamides **4.42** and **4.43** as a white solid (18.6 mg, 76% yield). The two regioisomers were separated by prep TLC (100% EtOAc).



Acetamide **4.42**

1H NMR (500 MHz, $CDCl_3$, $25^\circ C$):

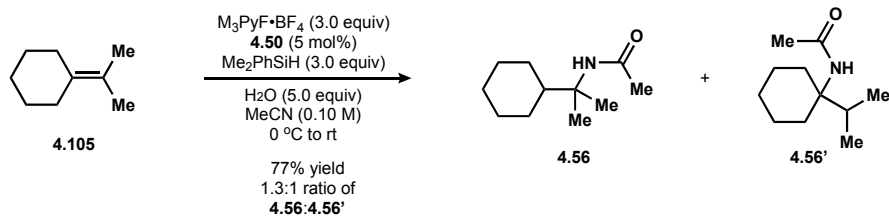
δ 5.16 (s, 1H)	1.59 (d, $J = 12.0$ Hz, 2H)
3.51 (s, 2H)	1.34 (dd, $J = 13.4, 3.3$ Hz, 2H)
3.45 (s, 2H)	1.27 (s, 6H)
2.29 (dd, $J = 13.5, 2.2$ Hz, 2H)	1.21 (dd, $J = 13.0, 2.5$ Hz, 2H)
2.06 (tt, $J = 12.1, 3.2$ Hz, 1H)	0.95 (s, 6H)
1.92 (s, 3H)	

^{13}C NMR (126 MHz, $CDCl_3$, $25^\circ C$):

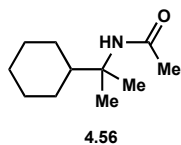
δ 169.2	69.9	32.2	24.47
97.5	56.3	30.2	23.2
70.1	43.7	24.58	22.7

HRMS (ESI) calculated for $C_{16}H_{29}NO_3$ $[M+Na]^+$: 306.2045, found: 306.2051

TLC: $R_f = 0.31$ (100% v/v EtOAc)



Acetamides 4.56 and 4.56'. Acetamides **4.56** and **4.56'** were prepared according to General Procedure VI with 0.30 mmol **4.105** (44 μL), 0.015 mmol Co-salen catalyst **4.50** (14.7 mg), 0.90 mmol oxidant $\text{Me}_3\text{PyF}\cdot\text{BF}_4$ (204 mg), 0.91 mmol PhMe_2SiH (0.14 mL), and 1.5 mmol water (27 μL). The crude material was purified by flash chromatography (gradient elution: 100% hexanes to 28% v/v EtOAc in hexanes) to afford a 1.3:1 mixture of acetamides **4.56** and **4.56'** as a tan solid (41.8 mg, 77% yield).



Acetamide **4.56**

^1H NMR (600 MHz, CDCl_3 , 25 °C):

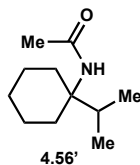
δ 5.15 (s, 1H)	1.68–1.63 (m, 1H)
1.910 (s, 3H)	1.26 (s, 6H)
1.908 (tt, $J = 12.1, 3.1$ Hz, 3H)	1.25 (qt, $J = 13.0, 3.6$ Hz, 2H)
1.79–1.73 (m, 2H)	1.09 (qt, $J = 13.0, 3.6$ Hz, 1H)
1.73–1.68 (m, 2H)	0.94 (qd, $J = 12.5, 3.1$ Hz, 2H)

^{13}C NMR (151 MHz, CDCl_3 , 25 °C):

δ 169.2	26.6
56.6	26.5
44.7	24.6
27.5	24.2

HRMS (CI) calculated for $\text{C}_{11}\text{H}_{21}\text{NO}$ $[\text{M}+\text{H}]^+$: 184.1701, found: 184.1707

TLC: $R_f = 0.31$ (60% v/v EtOAc/hexanes)



Acetamide **4.56'**

¹H NMR (600 MHz, CDCl₃, 25 °C):

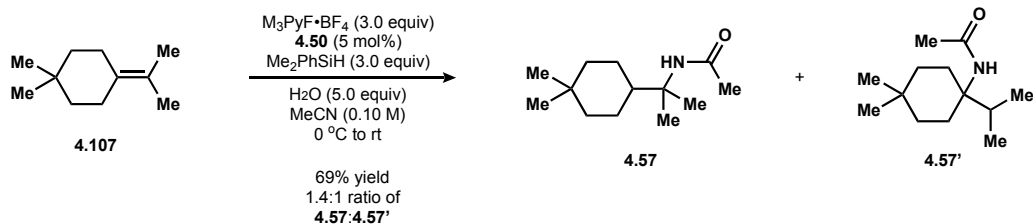
δ 4.95 (s, 1H)	1.61–1.52 (m, 2H)
2.40 (septet, <i>J</i> = 7.0 Hz, 1H)	1.40–1.28 (m, 4H)
2.07–2.00 (m, 2H)	1.20–1.10 (m, 1H)
1.98 (s, 3H)	0.86 (d, <i>J</i> = 7.0 Hz, 6H)
1.67–1.61 (m, 1H)	

¹³C NMR (151 MHz, CDCl₃, 25 °C):

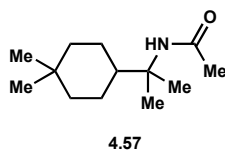
δ 169.4	25.8
59.4	24.6
33.5	21.8
30.1	17.1

HRMS (CI) calculated for C₁₁H₂₁NO [M+H]⁺: 184.1701, found: 184.1704

TLC: R_f = 0.39 (60% v/v EtOAc/hexanes)



Acetamides 4.57 and 4.57'. Acetamides **4.57** and **4.57'** were prepared according to General Procedure VI with 0.30 mmol **4.107** (56 μL), 0.015 mmol Co-salen catalyst **4.50** (14.7 mg), 0.90 mmol oxidant $\text{Me}_3\text{PyF}\cdot\text{BF}_4$ (204 mg), 0.91 mmol PhMe_2SiH (0.14 mL), and 1.5 mmol water (27 μL). The crude material was purified by flash chromatography (gradient elution: 100% hexanes to 26% v/v EtOAc in hexanes) to afford a 1.4:1 mixture of acetamides **4.57** and **4.57'** as a tan solid (43.5 mg, 69% yield).



Acetamide **4.57**

^1H NMR (600 MHz, CDCl_3 , 25 °C):

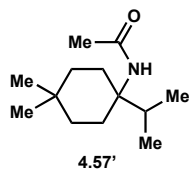
δ 5.19 (s, 1H)	1.27 (s, 6H)
1.89 (s, 3H)	1.25–1.11 (m, 4H)
1.84 (tt, $J = 11.8, 3.2$ Hz, 1H)	0.89 (s, 3H)
1.51–1.46 (m, 2H)	0.85 (s, 3H)
1.43–1.37 (m, 2H)	

^{13}C NMR (151 MHz, CDCl_3 , 25 °C):

δ 169.3	29.8
56.5	24.3
44.7	24.0
39.4	23.0
32.9	

HRMS (CI) calculated for $\text{C}_{13}\text{H}_{25}\text{NO}$ $[\text{M}+\text{H}]^+$: 212.2014, found: 212.2006

TLC: $R_f = 0.36$ (60% v/v EtOAc/hexanes)



Acetamide **4.57'**

^1H NMR (600 MHz, CDCl_3 , 25 °C):

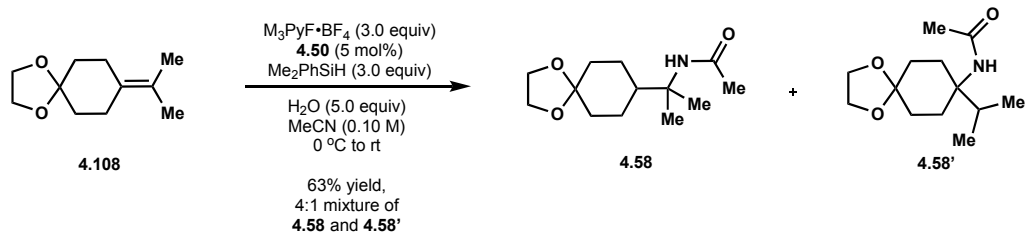
δ 4.91 (s, 1H)	1.32–1.20 (m, 4H)
2.41 (septet, $J = 6.8$ Hz, 1H)	0.91 (s, 3H)
1.97 (s, 3H)	0.874 (s, 3H)
1.92–1.86 (m, 2H)	0.872 (d, $J = 6.8$ Hz, 6H)
1.52 (td, $J = 13.4, 4.4$ Hz, 2H)	

^{13}C NMR (151 MHz, CDCl_3 , 25 °C):

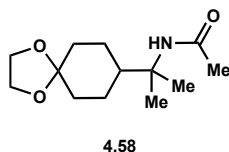
δ 169.5	29.5
59.1	25.9
34.6	24.6
33.3	24.1
32.5	17.2

HRMS (CI) calculated for $\text{C}_{13}\text{H}_{25}\text{NO}$ $[\text{M}+\text{H}]^+$: 212.2014, found: 212.2016

TLC: $R_f = 0.47$ (60% v/v EtOAc/hexanes)



Acetamides 4.58 and 4.58'. Acetamides **4.58** and **4.58'** were prepared according to General Procedure VI with alkene **4.108** (54.6 mg, 0.30 mmol) and purified by flash chromatography (gradient elution: 100% hexanes to 80% v/v EtOAc in hexanes) to afford a 4:1 mixture of acetamides **4.58** and **4.58'** as a white solid (45.2 mg, 63% yield). The two regioisomers were separated by prep TLC (100% EtOAc).



Acetamide 4.58.

1H NMR (500 MHz, $CDCl_3$, 25 °C):

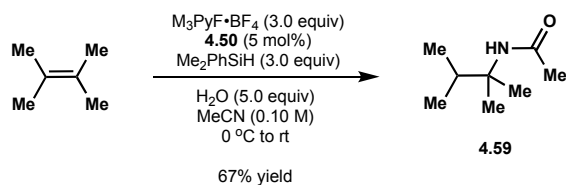
δ 5.22 (s, 1H)	1.68 (dt, $J = 8.7, 2.8$ Hz, 2H)
3.91 (t, $J = 2.7$ Hz, 4H)	1.53 (td, $J = 13.3, 4.1$ Hz, 2H)
2.08 (tt, $J = 12.4, 3.1$ Hz, 1H)	1.33-1.28 (m, 2H)
1.90 (s, 3H)	1.26 (s, 6H)
1.75 (dt, $J = 14.4, 2.8$ Hz, 2H)	

^{13}C NMR (126 MHz, $CDCl_3$, 25 °C):

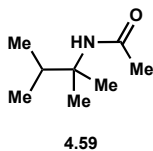
δ 169.2	56.3	24.69
108.8	43.0	24.60
64.2	34.8	24.50

HRMS (CI) calculated for $C_{13}H_{23}NO_3$ $[M+H]^+$: 242.1756, found: 242.1745

TLC: $R_f = 0.40$ (100% EtOAc)



Acetamide 4.59. Acetamide **4.59** was prepared according to General Procedure VI with 2,3-dimethyl-2-butene (59 μL , 0.50 mmol) and purified by flash chromatography (gradient elution: 100% hexanes to 40% v/v EtOAc in hexanes) to afford acetamide **4.59** as a tan solid (48.3 mg, 67% yield).



Acetamide 4.59

^1H NMR (500 MHz, CDCl_3 , 25 °C):

δ 5.28 (s, 1H)

2.29 (7, $J = 6.9$ Hz, 1H)

1.90 (s, 3H)

1.24 (s, 6H)

0.85 (d, $J = 7.4$ Hz, 6H)

^{13}C NMR (126 MHz, CDCl_3 , 25 °C):

δ 169.3

56.7

34.3

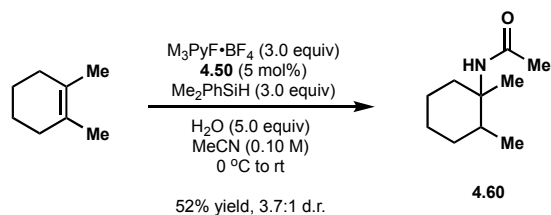
24.5

23.4

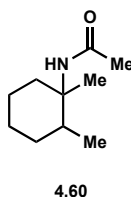
17.3

HRMS (CI) calculated for $\text{C}_8\text{H}_{17}\text{NO}$ $[\text{M}+\text{H}]^+$: 144.1388, found: 144.1383

TLC: $R_f = 0.24$ (60% v/v EtOAc/hexanes)



Acetamide 4.60. Acetamide **4.60** was prepared according to General Procedure VI (with the modification that silane was added over 6 h) with 1,2-dimethylcyclohexene¹⁷ (40 μL , 0.30 mmol) and purified by flash chromatography (gradient elution: 100% hexanes to 20% v/v EtOAc in hexanes) to afford acetamide **4.60** as a 3.7:1 mixture of diastereomers (26.2 mg, 52% yield).



Acetamide **4.60**

¹H NMR (500 MHz, CDCl_3 , 25 °C):

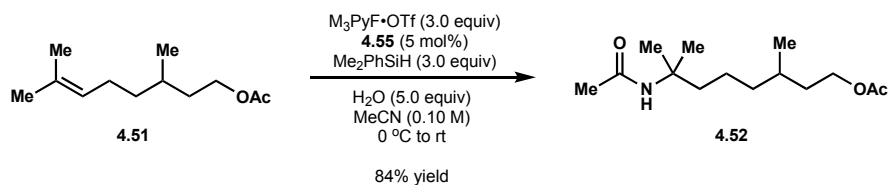
δ 5.04 (s, 1H)	1.42 (s, 3H)
2.57-2.54 (m, 1H)	1.36-1.22 (m, 2H)
1.95 (s, 3H)	1.20-1.13 (m, 1H)
1.64-1.61 (m, 1H)	1.11-1.05 (m, 1H)
1.54-1.47 (m, 3H)	0.91 (d, $J = 6.8$ Hz, 3H)

¹³C NMR (126 MHz, CDCl_3 , 25 °C):

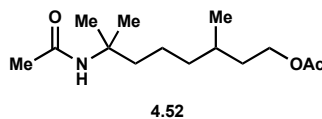
δ 169.5	25.3
55.5	25.0
40.8	24.6
34.9	22.0
30.4	15.3

HRMS (CI) calculated for $\text{C}_{10}\text{H}_{19}\text{NO}$ $[\text{M}+\text{H}]^+$: 170.1545, found: 170.1541

TLC: $R_f = 0.50$ (60% v/v EtOAc/hexanes)



Acetamide 4.52. Acetamide **4.52** was prepared according to General Procedure V with citronellyl acetate **4.51** (23 μL , 0.10 mmol) and purified by flash chromatography (gradient elution: 40% v/v EtOAc in hexanes to 20% v/v EtOAc in hexanes) to afford acetamide **4.52** as a tan oil (21.6mg, 84% yield).



Acetamide **4.52**

^1H NMR (500 MHz, CDCl_3 , 25 °C):

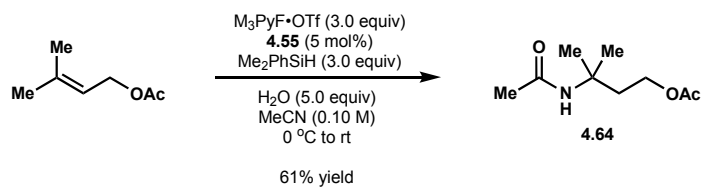
δ 5.19 (br s, 1H)	1.56-1.50 (m, 1H)
4.12-4.04 (m, 2H)	1.45-1.38 (m 2H)
2.03 (s, 3H)	1.29 (s, 6H)
1.91 (s, 3H)	1.24-1.11 (m, 3H)
1.67-1.60 (m, 3H)	0.89 (d, $J = 6.6$ Hz, 3H)

^{13}C NMR (125 MHz, CDCl_3 , 25 °C):

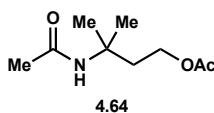
δ 171.2	27.8
169.4	27.0
63.0	24.5
53.7	21.4
40.3	21.0
37.1	19.4
35.4	

HRMS (ESI) calculated for $\text{C}_{14}\text{H}_{24}\text{N}_2\text{O}_4$ $[\text{M}+\text{H}]^+$: 258.2069, found: 258.2

TLC: $R_f = 0.45$ (60% v/v EtOAc in hexanes)



Acetamide 4.64. Acetamide **4.64** was prepared according to General Procedure V with prenyl acetate (12.8 mg, 0.10 mmol) and purified by flash chromatography (gradient elution: 100% hexanes to 40% v/v EtOAc in hexanes) to afford acetamide **4.64** as a tan oil (11.5 mg, 61% yield). Spectral data match those reported in the literature.⁷⁹



Acetamide **4.64**

¹H NMR (500 MHz, CDCl₃, 25 °C):

δ 5.45 (s, 1H)

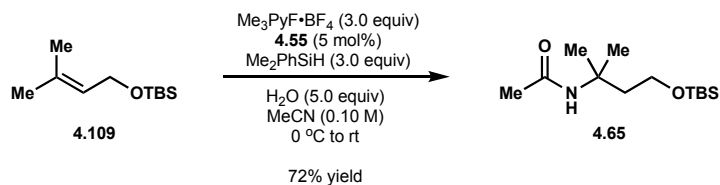
4.12 (t, *J* = 6.9 Hz, 2H)

2.09 (t, *J* = 6.9 Hz, 2H)

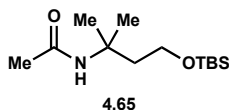
2.03 (s, 3H)

1.91 (s, 3H)

1.34 (s, 6H)



Acetamide 4.65. Acetamide **4.65** was prepared according to General Procedure VI with alkene **4.109** (20.0 mg, 0.10 mmol) and purified by flash chromatography (gradient elution: 100% hexanes to 50% v/v EtOAc in hexanes) to afford acetamide **4.655** as a tan oil (18.7 mg, 72% yield).



Acetamide **4.65**

^1H NMR (500 MHz, CDCl_3 , 25 °C):

δ 6.75 (s, 1H)

3.81 (t, $J = 5.4$ Hz, 2H)

1.86 (s, 3H)

1.70 (t, $J = 5.3$ Hz, 2H)

1.41 (s, 6H)

0.91 (s, 9H)

0.08 (s, 6H)

^{13}C NMR (126 MHz, CDCl_3 , 25 °C):

δ 169.3 25.9

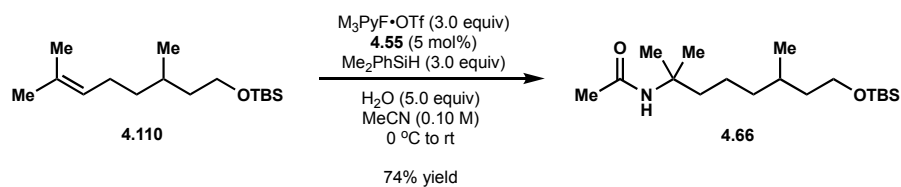
60.2 24.7

44.0 18.2

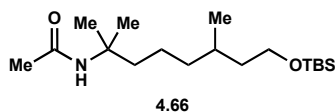
29.7 -5.5

26.2

HRMS (ESI) calculated for $\text{C}_{13}\text{H}_{29}\text{NO}_2\text{Si}$ $[\text{M}+\text{Na}]^+$: 282.1865, found: 282.1855



Acetamide 4.66. Acetamide **4.66** was prepared according to General Procedure V with alkene **4.110** (33 μ L, 0.10 mmol) and purified by flash chromatography (gradient elution: 10% v/v EtOAc in hexanes to 30% v/v EtOAc in hexanes) to afford acetamide **4.66** as a tan oil (26.1 mg, 79% yield).



Acetamide **4.66**

1H NMR (500 MHz, $CDCl_3$, 25 °C):

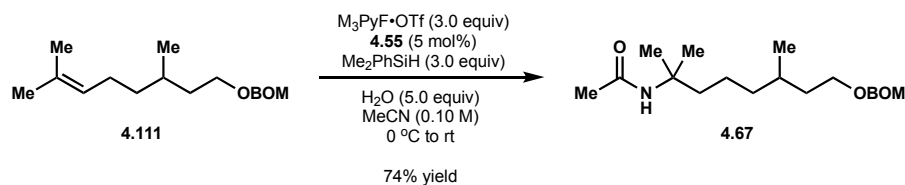
δ 5.17 (br s, 1H)	1.32-1.08 (m, 5H)
3.67-3.58 (m, 2H)	1.29 (s, 6H)
1.90 (s, 3H)	0.89 (s, 9H)
1.65-1.61 (m, 2H)	0.86 (d, $J = 6.3$ Hz, 3H)
1.57-1.53 (m, 2H)	0.04 (s, 6H)

^{13}C NMR (125 MHz, $CDCl_3$, 25 °C):

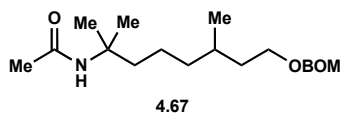
δ 169.3	26.9
61.4	26.0
53.7	24.5
40.5	21.5
39.9	19.7
37.4	18.3
29.5	-5.27
-5.28	

HRMS (ESI) calculated for $C_{14}H_{24}N_2O_4$ $[M+H]^+$: 330.2828, found: 330.3

TLC: $R_f = 0.44$ (40% v/v EtOAc in hexanes)



Acetamide 4.67. Acetamide **4.67** was prepared according to General Procedure VII with alkene **4.111** (29 μL , 0.10 mmol) and purified by flash chromatography (gradient elution: 10% v/v EtOAc in hexanes to 40% v/v EtOAc in hexanes) to afford acetamide **4.67** as a tan oil (25.0 mg, 74% yield).



Acetamide **4.67**

^1H NMR (500 MHz, CDCl_3 , 25 °C):

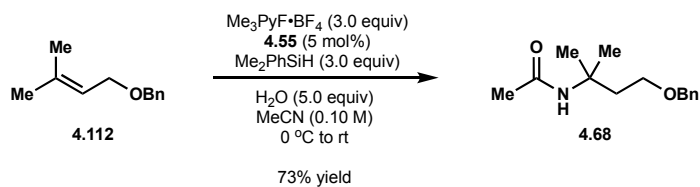
δ 7.36-7.33 (m, 4H)	1.90 (s, 3H)
7.31-7.28 (m, 1H)	1.66-1.61 (m, 3H)
5.12 (br s, 1H)	1.43-1.36 (m, 2H)
4.76 (s, 2H)	1.29 (s, 6H)
4.60 (s, 2H)	1.22-1.12 (m, 6H)
3.65-3.58 (m, 2H)	0.89 (d, $J = 6.6\text{Hz}$, 3H)

^{13}C NMR (125 MHz, CDCl_3 , 25 °C):

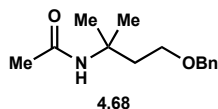
δ 169.3	94.6	37.4	24.6
138.0	69.3	36.7	21.5
128.4	66.3	29.8	19.5
127.85	53.7	26.93	
127.66	40.4	26.90	

HRMS (ESI) calculated for $\text{C}_{14}\text{H}_{24}\text{N}_2\text{O}_4$ $[\text{M}+\text{H}]^+$: 358.2358, found: 358.2

TLC: $R_f = 0.36$ (40% v/v EtOAc in hexanes)



Acetamide 4.68. Acetamide **4.68** was prepared according to General Procedure VI with alkene **4.112** (17.6 mg, 0.10 mmol) and purified by flash chromatography (gradient elution: 100% hexanes to 40% v/v EtOAc in hexanes) to afford acetamide **4.68** as a tan solid (17.2 mg, 73% yield).



Acetamide **4.68**

^1H NMR (500 MHz, CDCl_3 , 25 °C):

δ 7.37-7.28 (m, 5H)

6.45 (s, 1H)

4.49 (s, 2H)

3.66 (t, $J = 5.6$ Hz, 2H)

1.84 (t, $J = 5.6$ Hz, 2H)

1.78 (s, 3H)

1.39 (s, 6H)

^{13}C NMR (126 MHz, CDCl_3 , 25 °C):

δ 169.5 67.3

137.9 53.3

128.4 41.1

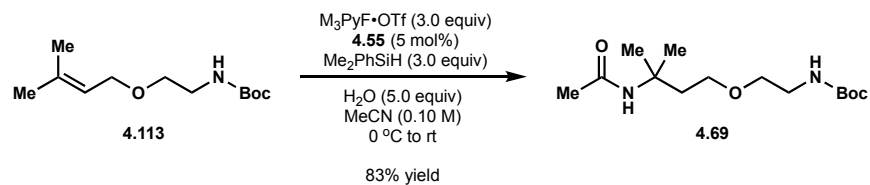
127.80 26.4

127.65 24.5

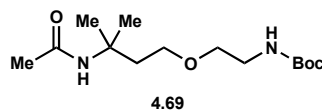
73.3

HRMS (CI) calculated for $\text{C}_{14}\text{H}_{21}\text{NO}_2$ $[\text{M}+\text{H}]^+$: 236.1651, found: 236.1649

TLC: $R_f = 0.28$ (60% v/v EtOAc/hexanes)



Acetamide 4.69. Acetamide **4.69** was prepared according to General Procedure V with alkene **4.113** (22.9 mg, 0.10 mmol) and purified by flash chromatography (gradient elution: 100% hexanes to 80% v/v EtOAc in hexanes) to afford acetamide **4.69** as a tan solid (24.0 mg, 83% yield).



Acetamide **4.69**

1H NMR (500 MHz, $CDCl_3$, 25 °C):

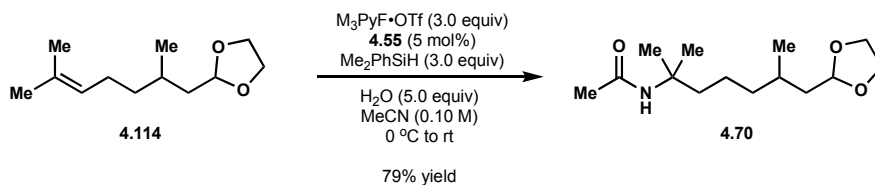
δ 6.18 (s, 1H)	1.89 (s, 3H)
4.80 (s, 1H)	1.85 (t, $J = 5.8$ Hz, 2H)
3.57 (t, $J = 5.8$ Hz, 2H)	1.43 (s, 9H)
3.47 (t, $J = 5.2$ Hz, 2H)	1.37 (s, 6H)
3.30 (d, $J = 4.9$ Hz, 2H)	

^{13}C NMR (126 MHz, $CDCl_3$, 25 °C):

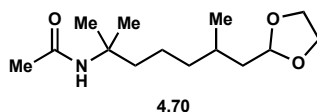
δ 169.6	40.6
155.9	40.3
79.4	28.4
70.0	26.7
67.8	24.5
53.1	

HRMS (ESI) calculated for $C_{14}H_{24}N_2O_4$ $[M+Na]^+$: 311.1947, found: 311.1954

TLC: $R_f = 0.21$ (100% v/v EtOAc)



Acetamide 4.70. Acetamide **4.70** was prepared according to General Procedure V with alkene **4.114** (22 μL , 0.10 mmol) and purified by flash chromatography (gradient elution: 40% v/v EtOAc in hexanes to 80% v/v EtOAc in hexanes) to afford acetamide **4.70** as a tan solid (20.3 mg, 79% yield).



Acetamide **4.70**

^1H NMR (500 MHz, CDCl_3 , 25 °C):

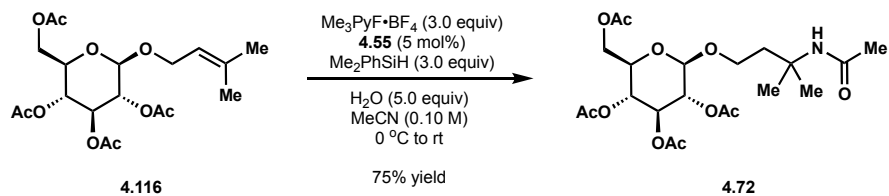
δ 5.15 (br s, 1H)	1.69-1.61 (m, 4H)
4.88 (t, $J = 5.0$ Hz, 1H)	1.51-1.46 (m, 1H)
4.00-3.92 (m, 2H)	1.37-1.14 (m, 4H)
3.87-3.80 (m, 2H)	1.29 (s, 6H)
1.90 (s, 3H)	0.94 (d, $J = 6.6$ Hz, 3H)

^{13}C NMR (125 MHz, CDCl_3 , 25 °C):

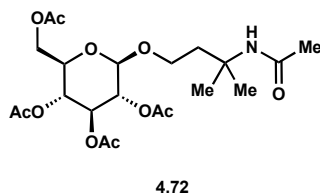
δ 169.3	37.5
103.7	29.3
64.69	26.90
64.61	26.84
53.7	24.5
40.9	21.3
40.4	19.9

HRMS (ESI) calculated for $\text{C}_{14}\text{H}_{24}\text{N}_2\text{O}_4$ $[\text{M}+\text{Na}]^+$: 280.1889, found: 280.2

TLC: $R_f = 0.32$ (60% v/v EtOAc in hexanes)



Acetamide 4.72. Acetamide **4.72** was prepared according to General Procedure VI with alkene **4.116** (124.9 mg, 0.30 mmol) and purified by flash chromatography (gradient elution: 100% hexanes to 90% v/v EtOAc in hexanes) to afford acetamide **4.72** as a tan solid (105.2 mg, 74% yield).



Acetamide **4.72**

^1H NMR (500 MHz, CDCl_3 , 25 °C):

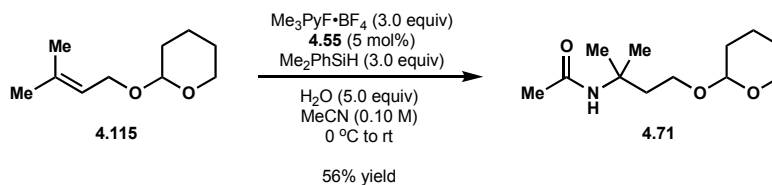
δ 5.81 (s, 1H)	4.14 (d, $J = 11.5$ Hz, 1H)	1.99 (s, 3H)
5.16 (t, $J = 9.5$ Hz, 1H)	3.95 (dt, $J = 9.3, 6.3$ Hz, 1H)	1.96 (s, 3H)
5.04 (t, $J = 9.7$ Hz, 1H)	3.68-3.66 (m, 1H)	1.92 (dd, $J = 12.9, 8.4$ Hz, 1H)
4.92 (t, $J = 8.8$ Hz, 1H)	3.58 (dt, $J = 9.6, 5.3$ Hz, 1H)	1.88 (s, 3H)
4.45 (d, $J = 8.0$ Hz, 1H)	2.05 (s, 3H)	1.86-1.80 (m, 1H)
4.21 (dd, $J = 12.2, 4.5$ Hz, 1H)	2.00 (s, 3H)	1.32 (s, 3H)
		1.30 (s, 3H)

^{13}C NMR (126 MHz, CDCl_3 , 25 °C):

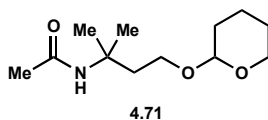
δ 170.6	100.7	66.9	26.6
170.2	72.7	61.8	24.4
169.8	71.9	52.9	20.74
169.41	71.3	39.8	20.69
169.39	68.4	27.2	20.59

HRMS (ESI) calculated for $\text{C}_{21}\text{H}_{33}\text{NO}_{11}$ $[\text{M}+\text{Na}]^+$: 498.1951, found: 498.1972

TLC: $R_f = 0.27$ (100% v/v EtOAc)



Acetamide 4.71. Acetamide **4.71** was prepared according to General Procedure VI with alkene **4.115** (51.1 mg, 0.30 mmol) and purified by flash chromatography (gradient elution: 100% hexanes to 80% v/v EtOAc in hexanes) to afford acetamide **4.71** as a tan solid (38.7 mg, 56% yield).



Acetamide **4.71**

^1H NMR (500 MHz, CDCl_3 , 25 °C):

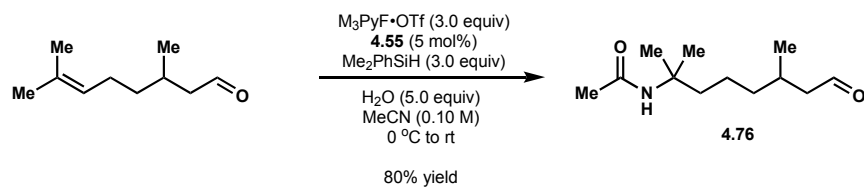
δ 6.40 (s, 1H)	1.83-1.80 (m, 2H)
4.55 (t, J = 3.5 Hz, 1H)	1.79-1.74 (m, 1H)
3.91 (ddd, J = 10.3, 6.9, 4.8 Hz, 1H)	1.70 (ddd, J = 13.3, 7.5, 2.6 Hz, 1H)
3.82 (ddd, J = 11.4, 8.2, 3.2 Hz, 1H)	1.61-1.53 (m, 2H)
3.50 (ddd, J = 10.4, 6.6, 4.8 Hz, 2H)	1.52-1.46 (m, 2H)
1.85 (s, 3H)	1.38 (s, 6H)

^{13}C NMR (126 MHz, CDCl_3 , 25 °C):

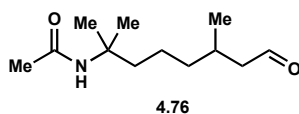
δ 169.3	30.7
99.0	26.44
64.4	26.31
62.3	25.3
53.2	24.5
41.0	19.5

HRMS (ESI) calculated for $\text{C}_{12}\text{H}_{23}\text{NO}_3$ $[\text{M}+\text{Na}]^+$: 252.1576, found: 252.1582

TLC: R_f = 0.10 (60% v/v EtOAc/hexanes)



Acetamide 4.76. Acetamide **4.76** was prepared according to General Procedure V with citronellal (54 μ L, 0.30 mmol) and purified by flash chromatography (gradient elution: 40% v/v EtOAc in hexanes to 80% v/v EtOAc in hexanes) to afford acetamide **4.76** as a tan oil (51.2 mg, 80% yield).



Acetamide **4.76**

^1H NMR (500 MHz, CDCl_3 , 25 $^\circ\text{C}$):

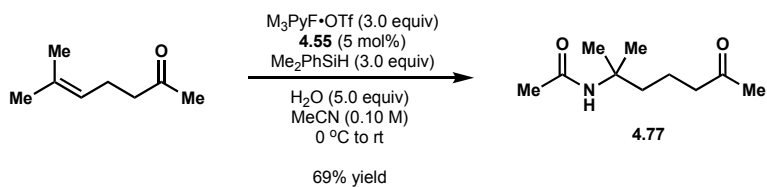
δ 9.72 (t, $J = 2.1$ Hz, 1H)	1.89 (s, 3H)
5.29 (br s, 1H)	1.66 (dd, $J = 10.3, 6.4$ Hz, 2H)
2.36 (ddd, $J = 16.2, 5.6, 1.7$ Hz, 1H)	1.31-1.15 (m, 4H)
2.20 (ddd, $J = 16.3, 7.9, 2.5$ Hz, 1H)	1.26 (s, 6H)
2.08-1.99 (m, 1H)	0.93 (d, $J = 6.7$ Hz, 3H)

^{13}C NMR (125 MHz, CDCl_3 , 25 $^\circ\text{C}$):

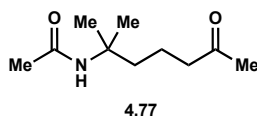
δ 203.0	28.0
169.4	26.97
53.6	26.92
51.0	24.4
39.8	21.4
37.0	19.9

HRMS (CI) calculated for $\text{C}_{14}\text{H}_{24}\text{N}_2\text{O}_4$ $[\text{M}+\text{H}]^+$: 213.2039, found: 213.2

TLC: $R_f = 0.24$ (60% v/v EtOAc in hexanes)



Acetamide 4.77. Acetamide **4.77** was prepared according to General Procedure V with 6-methyl-5-hepten-2-one (15 μ L, 0.10 mmol) and purified by flash chromatography (gradient elution: 50% v/v EtOAc in hexanes to 100% v/v EtOAc) to afford acetamide **4.77** as a tan solid (12.8 mg, 69% yield).



Acetamide 4.77

^1H NMR (500 MHz, CDCl_3 , 25 $^\circ\text{C}$):

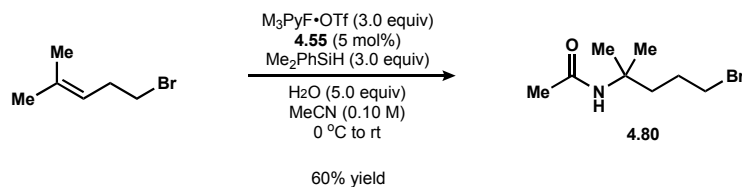
δ 5.50 (br s, 1H)	1.65-1.62 (m, 2H)
2.45 (t, J = 7.0 Hz, 2H)	1.55-1.49 (m, 2H)
2.13 (s, 3H)	1.30 (s, 6H)
1.92 (s, 3H)	

^{13}C NMR (125 MHz, CDCl_3 , 25 $^\circ\text{C}$):

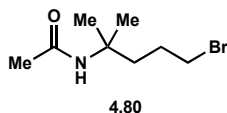
δ 209.2	30.0
169.6	26.8
53.6	24.5
43.5	18.0
39.4	

HRMS (ESI) calculated for $\text{C}_{14}\text{H}_{24}\text{N}_2\text{O}_4$ $[\text{M}+\text{Na}]^+$: 208.1313, found: 208.6

TLC: R_f = 0.38 (70% v/v EtOAc in hexanes)



Acetamide 4.80. Acetamide **4.80** was prepared according to General Procedure VII with homoprenyl bromide⁸⁰ (13 μL , 0.10 mmol) and purified by flash chromatography (gradient elution: 100% hexanes to 30% v/v EtOAc in hexanes) to afford acetamide **4.80** as a tan solid (13.3 mg, 60% yield).



Acetamide **4.80**

^1H NMR (600 MHz, CDCl_3 , 25 °C):

δ 5.21 (s, 1H)

3.39 (t, J = 6.5 Hz, 2H)

1.92 (s, 3H)

1.89–1.79 (m, 4H)

1.30 (s, 6H)

^{13}C NMR (151 MHz, CDCl_3 , 25 °C):

δ 169.5 28.1

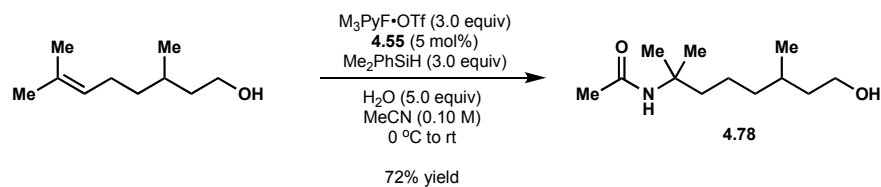
53.3 27.1

38.3 24.4

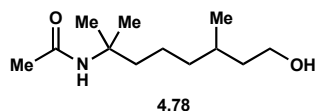
33.9

HRMS (ESI) calculated for $\text{C}_{22}\text{H}_{42}\text{NO}_2\text{Si}$ $[\text{M}+\text{Na}]^+$: 244.0313, found: 244.0320

TLC: R_f = 0.18 (60% v/v EtOAc/hexanes)



Acetamide 4.78. Acetamide **4.78** was prepared according to General Procedure V with β -citronellol (54 μ L, 0.30mmol) and purified by flash chromatography (gradient elution: 50% v/v EtOAc in hexanes to 100% v/v EtOAc) to afford acetamide **4.78** as a tan oil (46.5 mg, 72% yield).



Acetamide **4.78**

^1H NMR (500 MHz, CDCl_3 , 25 $^\circ\text{C}$):

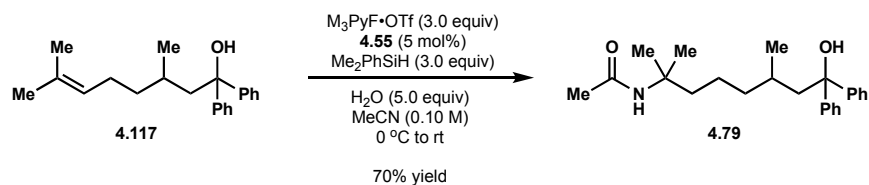
δ 5.18 (br s, 1H)	1.38-1.12 (m, 5H)
3.72-3.62 (m, 2H)	1.29 (s, 3H)
1.91 (s, 3H)	1.28 (s, 3H)
1.72-1.54 (m, 5H)	0.87 (d, $J = 6.5$ Hz, 3H)

^{13}C NMR (125 MHz, CDCl_3 , 25 $^\circ\text{C}$):

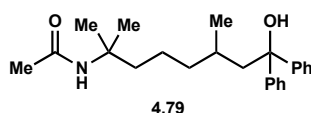
δ 169.5	29.2
61.1	27.04
53.8	26.99
40.05	24.5
39.76	21.4
37.2	19.7

HRMS (ESI) calculated for $\text{C}_{14}\text{H}_{24}\text{N}_2\text{O}_4$ $[\text{M}+\text{Na}]^+$: 238.1783, found: 238.1846

TLC: $R_f = 0.15$ (70% v/v EtOAc in hexanes)



Acetamide 4.79. Acetamide **4.79** was prepared according to General Procedure V with alkene **4.117** (30.8 mg, 0.10 mmol) and purified by flash chromatography (gradient elution: 10% v/v EtOAc in hexanes to 50% v/v EtOAc in hexanes) to afford acetamide **4.79** as a tan solid (25.8 mg, 70% yield).



Acetamide 4.79

^1H NMR (500 MHz, CDCl_3 , 25 °C):

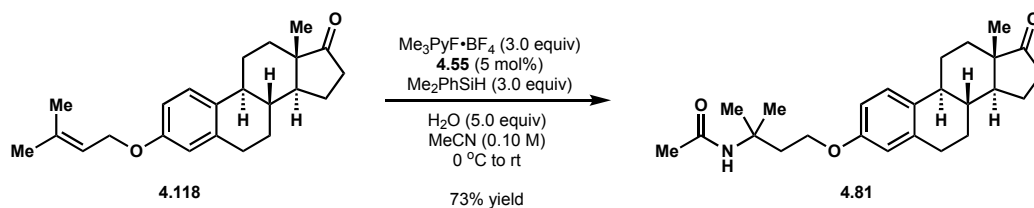
δ 7.45-7.42 (m, 4H)	1.67-1.61 (m, 2H)
7.31-7.27 (td, $J = 7.8, 3.5$ Hz, 4H)	1.47-1.41 (m, 1H)
7.20 (t, $J = 7.4$ Hz, 2H)	1.26 (s, 3H)
5.12 (br s, 1H)	1.22 (s, 3H)
2.38 (br s, 1H)	1.17-1.12 (m, 3H)
2.30 (dd, $J = 14.2, 3.7$ Hz, 1H)	0.88 (t, $J = 7.2$ Hz, 1H)
2.14 (dd, $J = 14.3, 7.6$ Hz, 1H)	0.75 (d, $J = 6.7$ Hz, 3H)
1.82 (s, 3H)	

^{13}C NMR (125 MHz, CDCl_3 , 25 °C):

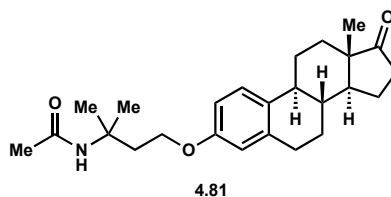
δ 169.4	126.59	48.3	26.89
147.94	126.08	39.9	24.4
147.75	126.03	38.6	21.8
128.00	78.4	28.2	21.0
126.61	57.3	26.96	

HRMS (ESI) calculated for $\text{C}_{14}\text{H}_{24}\text{N}_2\text{O}_4$ $[\text{M}+\text{Na}]^+$: 390.2409, found: 390.2

TLC: $R_f = 0.375$ (40% v/v EtOAc in hexanes)



Acetamide 4.81. Acetamide **4.81** was prepared according to General Procedure VI with alkene **4.118** (101.5 mg, 0.30 mmol) and purified by flash chromatography (gradient elution: 100% hexanes to 50% v/v EtOAc in hexanes) to afford acetamide **4.81** as a tan solid (87.4 mg, 73% yield).



Acetamide **4.81**

^1H NMR (500 MHz, CDCl_3 , 25 °C):

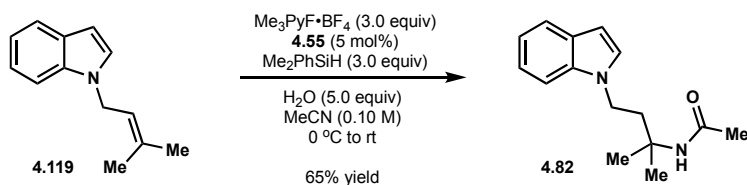
δ 7.18 (d, $J = 8.6$ Hz, 1H)	2.21 (dd, $J = 13.7, 6.9$ Hz, 1H)
6.69-6.67 (m, 1H)	2.15-2.08 (m, 3H)
6.62 (s, 1H)	2.06-1.96 (m, 2H)
6.10 (s, 1H)	1.94 (s, 1H)
4.04 (t, $J = 5.7$ Hz, 2H)	1.90 (s, 3H)
2.93-2.84 (m, 2H)	1.65-1.45 (m, 6H)
2.48 (dd, $J = 19.0, 8.7$ Hz, 1H)	1.41 (s, 6H)
2.36 (d, $J = 11.3$ Hz, 1H)	0.88 (s, 3H)

^{13}C NMR (126 MHz, CDCl_3 , 25 °C):

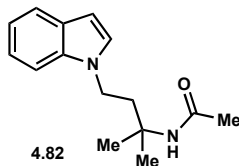
δ 220.7	126.4	50.3	35.8	26.4
169.5	114.2	47.9	31.5	25.8
156.4	112.0	43.9	29.6	24.5
137.8	64.7	39.5	27.01	21.5
132.3	53.1	38.3	26.99	13.8

HRMS (ESI) calculated for $\text{C}_{25}\text{H}_{35}\text{NO}_3$ $[\text{M}+\text{H}]^+$: 398.2695, found: 398.2690

TLC: $R_f = 0.27$ (60% v/v EtOAc/hexanes)



Acetamide 4.82. Acetamide **4.82** was prepared according to General Procedure VI with alkene **4.119** (18.5 mg, 0.10 mmol) and purified by flash chromatography (gradient elution: 100% hexanes to 40% v/v EtOAc/hexanes) to afford acetamide **4.82** as a tan solid (15.9 mg, 65% yield).



Acetamide **4.82**

^1H NMR (500 MHz, CDCl_3 , 25 °C):

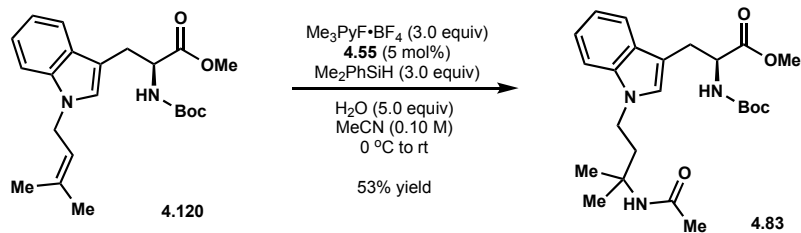
δ 7.62 (d, $J = 7.9$ Hz, 1H)	5.11 (s, 1H)
7.36 (dd, $J = 8.3, 0.6$ Hz, 1H)	4.17-4.14 (m, 2H)
7.23-7.20 (m, 1H)	2.33 (t, $J = 7.7$ Hz, 2H)
7.11-7.08 (m, 2H)	1.84 (s, 3H)
6.49 (dd, $J = 3.1, 0.7$ Hz, 1H)	1.35 (s, 6H)

^{13}C NMR (126 MHz, CDCl_3 , 25 °C):

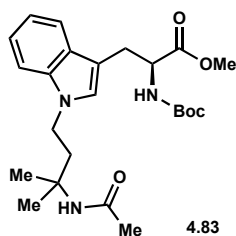
δ 169.7	109.3
135.8	101.3
128.6	52.7
127.6	42.4
121.5	39.0
121.0	27.5
119.2	24.2

HRMS (ESI) calculated for $\text{C}_{15}\text{H}_{20}\text{N}_2\text{O}$ $[\text{M}+\text{H}]^+$: 245.1654, found: 245.1664

TLC: $R_f = 0.27$ (60% v/v EtOAc/hexanes)



Acetamide 4.83. Acetamide **4.83** was prepared according to General Procedure VI with alkene **4.120** (115.9 mg, 0.30 mmol) and purified by flash chromatography (gradient elution: 100% hexanes to 80% v/v EtOAc in hexanes) to afford acetamide **4.83** as a tan solid (70.8 mg, 53% yield).



Acetamide **4.83**

^1H NMR (500 MHz, CDCl_3 , $25\text{ }^\circ\text{C}$):

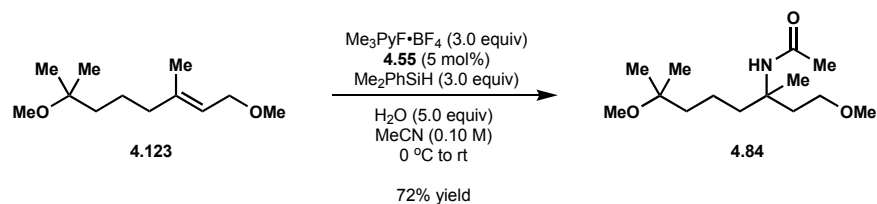
δ 7.57 (d, $J = 7.9$ Hz, 1H)	5.41 (d, $J = 55.2$ Hz, 1H)	3.35-3.26 (m, 2H)
7.37 (d, $J = 8.2$ Hz, 1H)	5.16-4.90 (m, 1H)	2.42-2.29 (m, 2H)
7.27-7.24 (bs, 1H)	4.68-4.49 (m, 1H)	1.86 (s, 3H)
7.16-7.13 (bs, 1H)	4.15 (t, $J = 7.6$ Hz, 2H)	1.48 (s, 9H)
6.95 (bs, 1H)	3.74 (s, 3H)	1.35 (s, 6H)

^{13}C NMR (126 MHz, CDCl_3 , $25\text{ }^\circ\text{C}$):

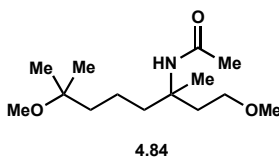
δ 172.7	121.7	54.2	27.8
169.7	119.1	52.6	27.53
155.2	118.8	52.1	27.49
136.0	109.5	42.4	24.0
128.2	108.7	38.6	
126.3	79.7	28.3	

HRMS (ESI) calculated for $\text{C}_{24}\text{H}_{35}\text{N}_3\text{O}_5$ $[\text{M}+\text{H}]^+$: 446.2655, found: 446.2659

TLC: $R_f = 0.25$ (80% v/v EtOAc/hexanes)



Acetamide 4.84. Acetamide **4.84** was prepared according to General Procedure VI with alkene **4.123** (20.0 mg, 0.10 mmol) and purified by flash chromatography (gradient elution: 100% hexanes to 90% v/v EtOAc in hexanes) to afford acetamide **41** as a tan solid (18.6 mg, 72% yield).



Acetamide **4.84**

^1H NMR (500 MHz, CDCl_3 , 25 °C):

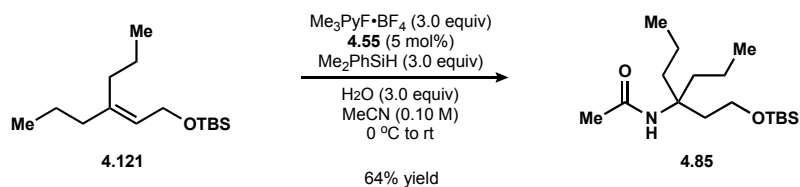
δ 6.15 (s, 1H)	1.78 (qt, $J = 11.8, 5.7$ Hz, 2H)
3.50 (dt, $J = 13.0, 8.8, 4.4$ Hz, 2H)	1.65 (ddd, $J = 14.6, 5.9, 4.8$ Hz, 1H)
3.32 (s, 3H)	1.43 (t, $J = 8.3$ Hz, 2H)
3.15 (s, 3H)	1.35 (s, 3H)
2.01 (ddd, $J = 14.1, 8.0, 5.5$ Hz, 1H)	1.30-1.19 (m, 3H)
1.88 (s, 3H)	1.12 (s, 6H)

^{13}C NMR (126 MHz, CDCl_3 , 25 °C):

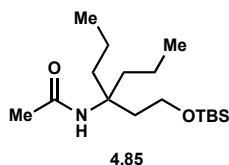
δ 169.4	38.9
74.5	38.1
69.4	25.10
58.7	25.08
55.9	24.6
49.1	24.2
39.8	18.0

HRMS (ESI) calculated for $\text{C}_{14}\text{H}_{29}\text{NO}_3$ $[\text{M}+\text{Na}]^+$: 282.2045, found: 282.2032

TLC: $R_f = 0.26$ (100% v/v EtOAc)



Acetamide 4.85. Acetamide **4.85** was prepared according to General Procedure VI with 0.30 mmol **4.121** (77.0 mg), 0.015 mmol Co-salen catalyst **23** (15.6 mg), 0.90 mmol oxidant $\text{Me}_3\text{PyF}\cdot\text{BF}_4$ (204 mg), 0.91 mmol PhMe_2SiH (0.14 mL), and 0.89 mmol water (16 μL). The crude material was purified by flash chromatography (gradient elution: 100% hexanes to 16% v/v EtOAc in hexanes) to afford acetamide **42** as a tan solid (61.0 mg, 64% yield).



Acetamide **4.85**

^1H NMR (600 MHz, CDCl_3 , 25 $^\circ\text{C}$):

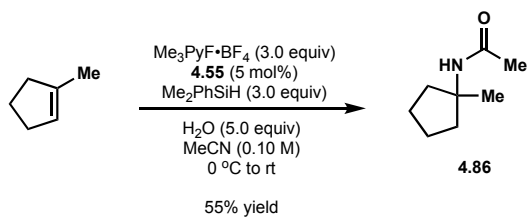
δ 6.28 (s, 1H)	1.69 (ddd, $J = 13.2, 12.7, 4.8$ Hz, 2H)
3.75 (t, $J = 5.7$ Hz, 2H)	1.31–1.15 (m, 4H)
1.88 (s, 3H)	0.91 (s, 9H)
1.86 (ddd, $J = 13.7, 12.7, 4.8$ Hz, 2H)	0.89 (t, $J = 7.3$ Hz, 6H)
1.75 (t, $J = 5.7$ Hz, 2H)	0.07 (s, 6H)

^{13}C NMR (151 MHz, CDCl_3 , 25 $^\circ\text{C}$):

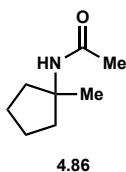
δ 169.0	24.6
60.0	18.2
58.8	16.9
38.5	14.5
37.3	−5.5
25.9	

HRMS (ESI) calculated for $\text{C}_{17}\text{H}_{37}\text{NO}_2\text{Si}$ $[\text{M}+\text{H}]^+$: 316.2672, found: 316.2661

TLC: Rf = 0.26 (20% v/v EtOAc/hexanes)



Acetamide 4.86. Acetamide **4.86** was prepared according to General Procedure VI using 1-methylcyclopentene (40 μL , 0.30 mmol, 1.0 equiv) and with the modification that silane was added over 6 h. The crude material was purified by flash silica chromatography (gradient elution: 100% hexanes to 20% v/v EtOAc in hexanes) to afford acetamide **4.86** as a white solid (26.2 mg, 52% yield). Spectral data match those reported in the literature.⁷⁹



Acetamide 4.86

$^1\text{H NMR}$ (500 MHz, CDCl_3 , 25 $^\circ\text{C}$):

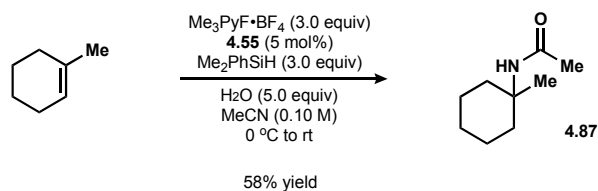
δ 5.45 (s, 1H)

1.96-1.90 (m, 2H)

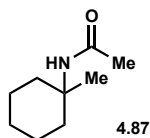
1.89 (s, 3H)

1.72-1.59 (m, 6H)

1.38 (s, 3H)



Acetamide 4.87. Acetamide **4.87** was prepared according to General Procedure VI with 0.30 mmol 1-methylcyclohexene (36 μL), 0.015 mmol Co-salen catalyst **4.55** (15.6 mg), 0.90 mmol oxidant $\text{Me}_3\text{PyF}\cdot\text{BF}_4$ (204 mg), 0.91 mmol PhMe_2SiH (0.14 mL), and 1.5 mmol water (27 μL). The crude material was purified by flash chromatography (gradient elution: 100% hexanes to 32% v/v EtOAc in hexanes) to afford acetamide **4.87** as a tan solid (27.2 mg, 58% yield). Spectral data match those reported in the literature.⁷⁹

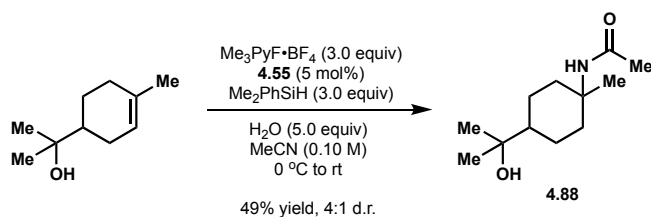


Acetamide 4.87

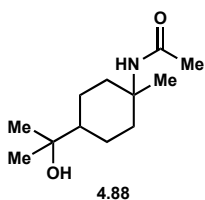
^1H NMR (500 MHz, CDCl_3 , 25 °C):

δ 5.17 (s, 1H)	1.44–1.36 (m, 4H)
2.00–1.94 (m, 2H)	1.34 (s, 3H)
1.92 (s, 3H)	1.31–1.25 (m, 1H)
1.54–1.45 (m, 3H)	

TLC: R_f = 0.26 (40% v/v EtOAc/hexanes)



Acetamide 4.88. Acetamide **4.88** was prepared according to General Procedure VI (with the modification that silane was added over 6 h) with α -terpineol (49.8 μL , 0.30 mmol) and purified by flash chromatography (gradient elution: 100% hexanes to 90% v/v EtOAc/hexanes) to afford acetamide **4.88** as a colorless oil comprised of a 4:1 mixture of inseparable diastereomers (31.2 mg, 49% yield).



Acetamide 4.88

^1H NMR (500 MHz, CDCl_3 , 25 $^\circ\text{C}$):

δ 5.07 (s, 1H)

2.26 (d, $J = 12.2$ Hz, 2H)

1.94 (s, 3H)

1.68-1.65 (m, 2H)

1.35 (s, 3H)

1.26-1.15 (m, 12H)

^{13}C NMR (126 MHz, CDCl_3 , 25 $^\circ\text{C}$):

δ 169.6 27.6

72.5 27.2

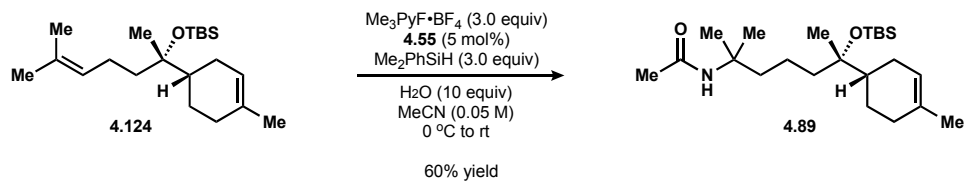
52.8 24.6

48.2 22.6

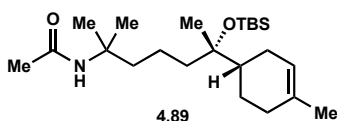
36.5

HRMS (ESI) calculated for $\text{C}_{12}\text{H}_{23}\text{NO}_2$ $[\text{M}+\text{Na}]^+$: 236.1626, found: 236.1632

TLC: $R_f = 0.13$ (100% v/v EtOAc)



Acetamide 4.89. Acetamide **4.89** was prepared according to General Procedure VI with 0.048 mmol **4.124** (16.2 mg, 1.0 equiv), Co-salen catalyst **4.55** (5.2 mg, 0.005 mmol, 0.1 equiv), 0.30 mmol oxidant $\text{Me}_3\text{PyF}\cdot\text{BF}_4$ (68 mg, 6.3 equiv), 0.30 mmol PhMe_2SiH (46 μL , 6.3 equiv), and 0.5 mmol water (9 μL , 10 equiv). The crude material was purified by flash chromatography (gradient elution: 100% hexanes to 15% v/v EtOAc in hexanes) to afford acetamide **4.89** as a tan oil (11.4 mg, 60% yield).



Acetamide **4.89**

^1H NMR (600 MHz, CDCl_3 , 25 $^\circ\text{C}$):

δ 5.37 (m, 1H)	1.70–1.65 (m, 1H)	1.29 (s, 6H)
5.16 (s, 1H)	1.64 (s, 3H)	1.28–1.20 (m, 3H)
2.03–1.93 (m, 2H)	1.63–1.58 (m, 1H)	1.11 (s, 3H)
1.90 (s, 3H)	1.56–1.48 (m, 1H)	0.86 (s, 9H)
1.89–1.73 (m, 3H)	1.47–1.38 (m, 2H)	0.06 (s, 6H)

^{13}C NMR (151 MHz, CDCl_3 , 25 $^\circ\text{C}$):

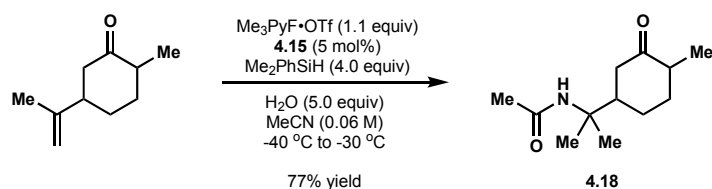
δ 169.3	41.1	26.7	23.4
134.0	40.7	26.0	18.5
121.0	31.2	24.55	18.2
53.8	26.94	24.51	-1.89
42.6	26.91	23.5	-1.92

HRMS (CI) calculated for $\text{C}_{22}\text{H}_{42}\text{NO}_2\text{Si}$ $[\text{M}-\text{CH}_3]^+$: 380.2985, found: 380.2978

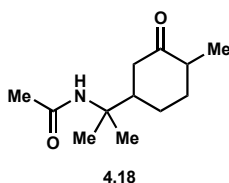
TLC: R_f = 0.46 (40% v/v EtOAc/hexanes)

Initially developed procedure for catalytic radical–polar crossover Ritter reaction of 1,1-disubstituted alkenes

An appropriately sized vessel was charged with cobalt(II) salen complex **5** (0.05 equiv) and acetonitrile (1/5 of total volume, 0.06M overall), water (5.0 equiv), substrate (1.0 equiv), and dimethylphenylsilane (4.0 equiv). The resulting solution was vigorously stirred and cooled to approximately -30 °C. A solution of Me₃PyF•OTf (1.1 equiv) in acetonitrile (4/5 of total volume, 0.06 M overall) was added in a slow steady stream. The temperature was maintained between -40 °C and -30 °C. The reaction was monitored by TLC and upon completion the volatiles were removed under reduced pressure. Purification by flash chromatography afforded *tert*-alkyl acetamide products.



Acetamide 4.18. Acetamide **4.18** was prepared using (D)-dihydrocarvone (24.6 μ L, 0.15 mmol). The crude material was purified by flash chromatography to afford acetamide **4.18** (24.3 mg, 77% yield).



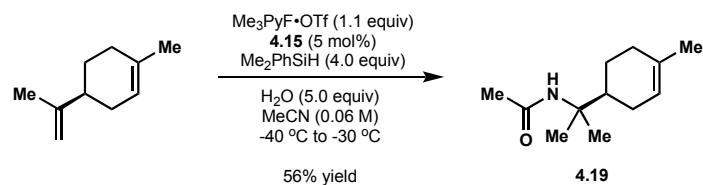
Acetamide **4.18**

¹H NMR (600 MHz, CDCl₃, 25 °C):

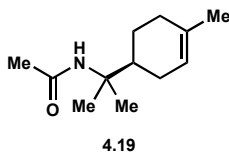
δ 5.32 (br s, 1H)	2.08 (td, $J = 8.9, 4.0$ Hz, 2H)	1.26 (s, 3H)
2.53–2.48 (m, 1H)	1.90 (s, 4H)	0.99 (d, $J = 6.5$ Hz, 3H)
2.39 (d, $J = 13.0$ Hz, 1H)	1.44 (qd, $J = 12.7, 3.1$ Hz, 1H)	
2.27 (dt, $J = 12.7, 6.3$ Hz, 1H)	1.34–1.31 (m, 4H)	

¹³C NMR (151 MHz, CDCl₃, 25 °C):

δ 212.6	45.8	34.3	24.54
169.6	44.9	26.7	24.1
56.0	43.3	24.57	14.4



Acetamide 4.19. Acetamide **4.19** was prepared using (*S*)-(-)-limonene (24.2 μL , 0.15 mmol). The crude material was purified by flash chromatography (gradient elution: 100% hexanes to 30% v/v EtOAc in hexanes) to afford acetamide **4.19** (16.3 mg, 56% yield). Spectral data match those reported in the literature.⁸¹

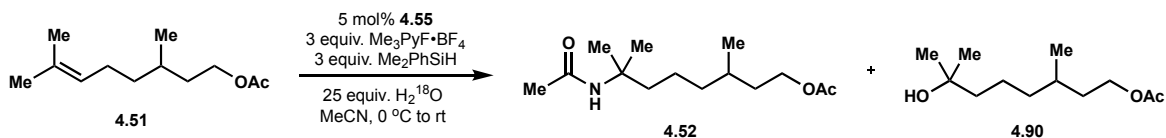


Acetamide **4.19**

^1H NMR (500 MHz, CDCl_3 , 25 $^\circ\text{C}$):

δ 5.35 (br s, 1H)	1.75 (tdd, $J = 8.7, 3.9, 2.6$ Hz, 2H)
5.24 (s, 1H)	1.62 (s, 3H)
2.14–2.09 (m, 1H)	1.29 (s, 3H)
2.03–1.95 (m, 3H)	1.27 (s, 3H)
1.91 (s, 3H)	

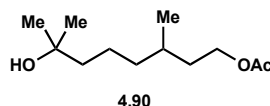
Excess Water Experiments.



entry	equivalents of H_2O	4.52 (% yield)	4.90 (% yield)
1	3.0	78	7
2	5.0	81	11
3	15.0	73	22
4	45.0	60	36

^aYields correspond to isolated, analytically pure material.

Excess water protocol: Amount of hydration was assessed by subjecting alkene **4.51** (23.3 μL , 0.10 mmol, 1.0 equiv) to General Procedure VI using catalyst **4.55** (5.2 mg, 0.005 mmol, 5.0 mol%) and varying equivalents of H_2O as described in the table above. Crude reaction mixtures were analyzed by GC-MS. Reported yields correspond to isolated, analytically pure compounds. Product distribution is displayed in the table above.



Alcohol **4.90**

^1H NMR (500 MHz, CDCl_3 , 25 °C):

δ 4.14–4.06 (m, 2H)	1.36–1.28 (m, 3H)
2.04 (s, 3H)	1.26 (s, 1H)
1.67 (dq, $J = 13.1, 6.5$ Hz, 1H)	1.22 (s, 6H)
1.56 (dq, $J = 12.6, 6.3$ Hz, 1H)	1.17 (td, $J = 7.7, 3.7$ Hz, 1H)
1.46–1.40 (m, 3H)	0.92 (d, $J = 6.6$ Hz, 3H)

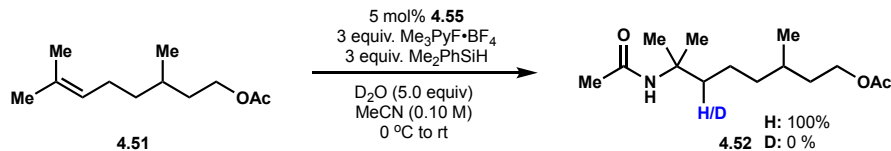
^{13}C NMR (126 MHz, CDCl_3 , 25 °C):

δ 171.2	37.4	29.25
71.0	35.5	21.6
63.0	29.8	21.0
44.1	29.32	19.5

HRMS (ESI) calculated for $\text{C}_{12}\text{H}_{24}\text{O}_3$ $[\text{M}+\text{Na}]^+$: 239.1623, found: 239.1615

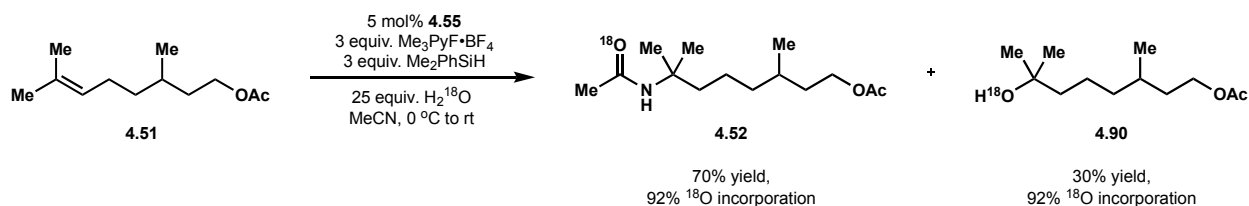
TLC: $R_f = 0.36$ (40% v/v EtOAc/hexanes)

Deuterium Labeling Study.

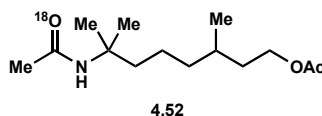


Deuterium labeling protocol: Deuterium incorporation was determined by subjecting alkene **4.51** (23.3 μL , 0.10 mmol, 1.0 equiv) to General Procedure VI using D_2O (9.0 μL , 0.50 mmol, 5.0 equiv). The crude material was purified by flash chromatography (gradient elution: 100% hexanes to 40% v/v EtOAc in hexanes) to afford acetamide **4.52** as a tan solid (18.1 mg, 70% yield). No deuterium incorporation was observed by analysis of the pure material by ^1H NMR and GC-MS.

H₂¹⁸O Labeling Studies.



H₂¹⁸O labeling protocol: ¹⁸O labeled products were prepared according to General Procedure VI using alkene **4.51** (23.3 μL, 0.10 mmol, 1.0 equiv) and H₂¹⁸O (45 μL, 2.5 mmol, 25.0 equiv). NOTE: H₂¹⁸O was not degassed prior to use. The crude material was purified by flash chromatography (gradient elution: 100% hexanes to 40% v/v EtOAc in hexanes) to afford acetamide **4.52** as a tan solid (18.1 mg, 70% yield) and alcohol **4.90** as a clear colorless oil (6.5 mg, 30% yield). ¹⁸O incorporation was determined by collecting GC-MS spectra of the analytically pure ¹⁸O product, integrating the extracted ion chromatograms (EIC) of the masses that correspond to ¹⁸O and ¹⁶O incorporation, and calculating percent composition of ¹⁸O from the total area. Masses reported correspond to [M-CH₃]⁺.



Acetamide **4.52**

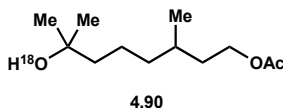
GC-MS EIC:

244.2 m/z, Area: 80454.09

242.2 m/z, Area: 6542.68

HRMS (ESI) calculated for C₁₄H₂₇NO₂¹⁸O [M+Na]⁺: 282.1931, found: 282.1924

TLC: R_f = 0.30 (60% v/v EtOAc/hexanes)



Alcohol **4.90**

GC-MS EIC:

203.2 m/z, Area: 41400.01

201.2 m/z, Area: 3382.58

HRMS (ESI) calculated for C₁₂H₂₄O₂¹⁸O [M+Na]⁺: 241.1666, found: 241.1663

TLC: R_f = 0.36 (40% v/v EtOAc/hexanes)

Hydrogen Evolution Studies.

A. Calibration Curves

Procedure for generating calibration curves: A flame dried 5-mL RBF charged with a magnetic stir bar was capped with a septum, placed under an atmosphere of nitrogen, and dry acetonitrile (1 mL) was added via syringe. To a separate oven dried 1-dram vial, under an atmosphere of nitrogen, was added water (1 mL) via syringe. Both solutions were then degassed by sparging with balloons of argon while simultaneously subjected to sonication for 5 min. Once degassed, both solutions were placed under an atmosphere of nitrogen. Degassed water (9 μ L) was added and the headspace was purged of oxygen via a nitrogen line for twenty minutes. A separate 5-mL RBF was capped with a septum and the headspace was purged of oxygen via a hydrogen balloon for twenty minutes. A separate 5-mL RBF was capped with a septum and the headspace was purged of oxygen via a nitrogen line for twenty minutes. Afterward, the nitrogen line and venting needle were removed from the 5-mL RBF containing the acetonitrile/water solution. The venting needles were removed from the other two 5-mL RBF's as well. A specified volume was then removed from the hydrogen-filled RBF via a gas-tight syringe and transferred to the acetonitrile/water containing RBF. The gas-tight syringe was cycled four times with nitrogen by removing headspace from the nitrogen-filled RBF and expelling it outside the RBF. After cycling, 0.6 mL of headspace were removed from the 5-mL RBF containing the acetonitrile/water solution. A total of three samples were analyzed via GC-TCD. This process was repeated to generate the two calibration curves provided in this SI.

B. Time Studies

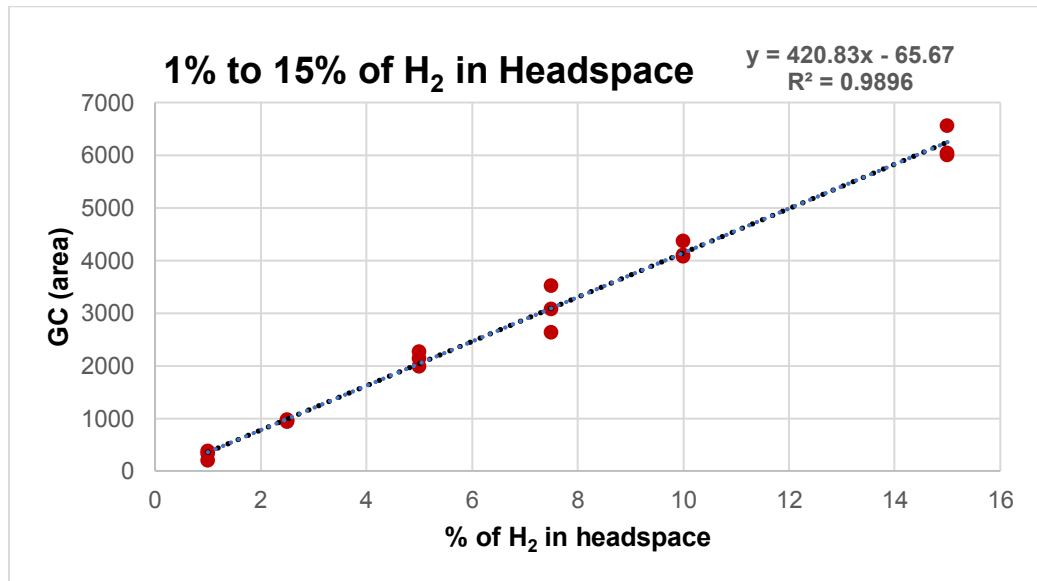
Procedure for conducting time studies: To a flame dried 5-mL RBF charged with a magnetic stir bar was added Co-salen catalyst (0.005 mmol, 0.05 equiv), Me₃PyF•BF₄ (68 mg, 0.30 mmol, 3.0 equiv), and alkene (0.10 mmol, 1.0 equiv). *It should be noted that no alkene was added in the case of the control experiments.* The RBF was then capped with a septum, placed under an atmosphere of nitrogen, and acetonitrile (1 mL mL, 0.1 M w.r.t. alkene) was added via syringe. To a separate oven dried 1-dram vial, under an atmosphere of nitrogen, was added water (1 mL) via syringe. Both solutions were then degassed by sparging with balloons of argon while simultaneously subjected to sonication for 5 min. Once degassed, both solutions were placed under an atmosphere of nitrogen. The stirred Co-salen/alkene solution was then cooled to 0 °C in an ice bath and degassed water (9 μL, 0.50 mmol, 5.0 equiv) was added. The headspace was then purged of oxygen via a nitrogen line for twenty minutes. Afterward, the nitrogen line and venting needle were removed from the 5-mL RBF containing the acetonitrile/water solution. Then, Me₂PhSiH (46 μL, 0.3 mmol, 3.0 equiv) was added at a rate of 1 drop/10 s. At the specified time intervals, 0.6 mL of headspace were removed via a gas-tight syringe. A total of three samples were analyzed via GC-TCD.

Calibration Curves

Calibration Curve A: 1%-15% of H₂ in Headspace

H2 (mL)	GC (area)	H2% of headspace	H2 (mL)	GC (area)	H2% of headspace
0.09	385.2	1	0.638	3081	7.5
0.09	327.4	1	0.638	3517.6	7.5
0.09	206.3	1	0.638	2630.3	7.5
0.213	958.9	2.5	0.85	4080.1	10
0.213	977.2	2.5	0.85	4373	10
0.213	934	2.5	0.85	4106.5	10
0.425	2139.3	5	1.275	6008.9	15
0.425	2270.4	5	1.275	6557.8	15
0.425	1988.7	5	1.275	6037.7	15

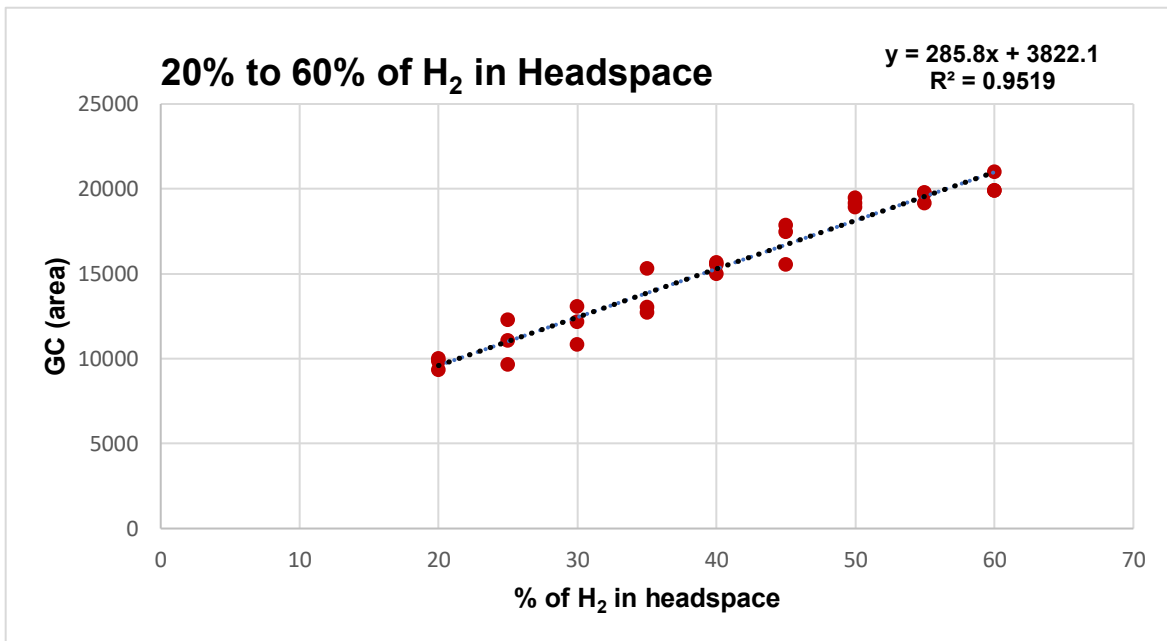
total headspace volume: 8.5 mL



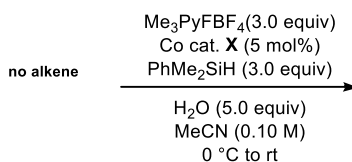
Calibration Curve B: 20%-60% of H₂ in Headspace

H2 (mL)	GC (area)	H2% of headspace	H2 (mL)	GC (area)	H2% of headspace
1.7	9818.6	20	3.83	17461.1	45
1.7	9327.6	20	3.83	17839	45
1.7	9992.1	20	3.83	15515.1	45
2.13	11051.8	25	4.25	18912.8	50
2.13	12258.6	25	4.25	19136.5	50
2.13	9631.1	25	4.25	19450	50
2.55	13040.2	30	4.68	19743.3	55
2.55	12156.8	30	4.68	19711.9	55
2.55	10810.7	30	4.68	19123.3	55
2.98	12993.8	35	5.1	19892	60
2.98	15278.6	35	5.1	20980.9	60
2.98	12709.2	35	5.1	19888.1	60
3.4	15530.6	40			
3.4	15622.8	40			
3.4	14983.6	40			

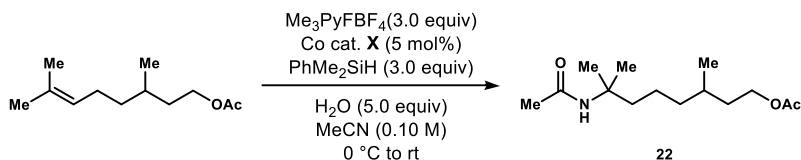
total headspace volume: 8.5 mL



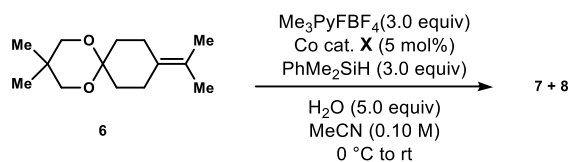
Hydrogen Evolution Time Studies



	T= 0 °C	T= 0 °C	T= 5 °C
no alkene	10 min	45 min	1 hr 15 min
Co-cat. 3	8,629.1	9557.6	6607.4
	10,332.6	10209.3	8357.5
	9,227.9	9331.6	7818.3
Ave:	9396.5	9699.5	7594.4
% H2:	19.5	20.6	13.2
moles H2:	0.0000740	0.0000780	0.0000492
mmoles H2:	0.0740	0.0780	0.0492
Co-cat. 9	8077.3	10365.2	8616.3
	6573.6	11346.7	8729.3
	4885.3	9979	11754.1
Ave:	6512.1	10563.6	9699.9
% H2:	9.4	23.6	20.6
moles H2:	0.0000357	0.0000895	0.0000766
mmoles H2:	0.0357	0.0895	0.0766
Co-cat. 5	11.2	N/A	948.6
	27.8	691	993
	30.8	507.3	932.1
Ave:	23.3	599.2	957.9
% H2:	0.211	1.58	2.43
moles H2:	0.000000802	0.00000599	0.00000906
mmoles H2:	0.000802	0.00599	0.00906
Co-cat. 23	19.9	24.6	20
	21.1	32.6	24.7
	22.4	31.4	24.8
Ave:	21.1	29.5	23.2
% H2:	0.206	0.23	0.21
moles H2:	0.000000783	0.000000858	0.000000787
mmoles H2:	0.000783	0.000858	0.000787
Co-cat. 15	13.2	17	24.8
	10.2	24.6	28.2
	12	22.2	32
Ave:	11.8	21.3	28.3
% H2:	0.184	0.21	0.22
moles H2:	0.000000699	0.000000784	0.000000832
mmoles H2:	0.000699	0.000784	0.000832



	T= 0°C	T= 0°C	T= 5°C
with alkene 21	10 min	45 min	1 hr 15 min
Co-cat. 3	6,327.7	N/A	N/A
	7,146.6	6769.3	3992.4
	6,634.3	5416.6	7818.3
Ave:	6702.9	6093.0	5905.4
% H2:	10.1	7.9	7.3
moles H2:	0.0000382	0.0000302	0.0000272
mmoles H2:	0.0382	0.0302	0.0272
Co-cat. 9	6875.3	6802.2	7599.2
	6687	7080.2	6347.3
	5458.5	6363.5	5525.4
Ave:	6340.3	6748.6	6490.6
% H2:	8.8	10.2	9.3
moles H2:	0.0000334	0.0000389	0.0000348
mmoles H2:	0.0334	0.0389	0.0348
Co-cat. 5	4.4	15.8	24.9
	6.3	17.5	43.3
	7	19.2	39.6
Ave:	5.9	17.5	35.9
% H2:	0.170	0.20	0.24
moles H2:	0.00000645	0.00000750	0.00000900
mmoles H2:	0.000645	0.000750	0.000900
Co-cat. 23	69.3	67.1	76.3
	67.9	73.2	75.5
	59.2	51.3	68.2
Ave:	65.5	63.9	73.3
% H2:	0.312	0.31	0.33
moles H2:	0.00000118	0.00000117	0.00000123
mmoles H2:	0.00118	0.00117	0.00123
Co-cat. 15	27.8	36.7	67.9
	30.5	34	84.8
	24.3	35.8	68.2
Ave:	27.5	35.5	73.6
% H2:	0.221	0.24	0.33
moles H2:	0.000000840	0.000000912	0.000001233
mmoles H2:	0.000840	0.000912	0.00123



	T= 0 °C	T= 0 °C	T= 5 °C
with alkene 6	10 min	45 min	1 hr 15 min
Co-cat. 3	7,403.8	N/A	8463.9
	10,152.6	7363.3	7880.2
	7,834.5	7277.8	8232.7
Ave:	8463.6	7320.6	8192.3
% H2:	16.2	12.2	15.3
moles H2:	0.0000616	0.0000464	0.0000570
mmoles H2:	0.0616	0.0464	0.0570
Co-cat. 9	11419.6	10872	10285
	12316.8	11344.9	10349.2
	10451.6	9283.6	10399.5
Ave:	11396.0	10500.2	10344.6
% H2:	26.5	23.4	22.8
moles H2:	0.000101	0.0000887	0.0000850
mmoles H2:	0.101	0.0887	0.0850
Co-cat. 5	38.3	520.3	1066.4
	38.6	588.7	1017.3
	39.8	532	912.4
Ave:	38.9	547.0	998.7
% H2:	0.248	1.46	2.53
moles H2:	0.00000094	0.00000552	0.00000942
mmoles H2:	0.000943	0.00552	0.00942
Co-cat. 23	25	48.2	49.6
	27.8	49.5	66.5
	22.4	42.1	38.9
Ave:	25.1	46.6	51.7
% H2:	0.216	0.267	0.279
moles H2:	0.00000082	0.00000101	0.00000104
mmoles H2:	0.000818	0.00101	0.00104
Co-cat. 15	5.6	26.9	61.5
	7	31.1	68.1
	6.8	30.1	61.5
Ave:	6.5	29.4	63.7
% H2:	0.171	0.226	0.307
moles H2:	0.000000650	0.000000857	0.00000115
mmoles H2:	0.000650	0.000857	0.00115

4.8 References and Notes

1. Ritter, J. J.; Kalish, J. *J. Am. Chem. Soc.* **1948**, *70*, 4048.
2. Ritter, J. J.; Minieri, P. P. *J. Am. Chem. Soc.* **1948**, *70*, 4045.
3. For reviews on applications and variants of the Ritter reaction, see: (a) Ziarani, G. H.; Hasankiadeh, F. S.; Mohajer, F. *ChemistrySelect*, **2020**, *5*, 14349. (b) Bolsakova, J.; Jirgensons, A. *Chemistry of Heterocyclic Compounds* **2017**, *53*, 1167. (c) Jiang, D.; He, T.; Ma, L.; Wang, Z. *RSC Adv.* **2014**, *4*, 64936. (d) Guérinot, A.; Reymond, S.; Cossy, J. *Eur. J. Org. Chem.* **2012**, *2012*, 19.
4. Roose, P.; Eller, K.; Henkes, E.; Rossbacher, R.; Höke, H. Amines, aliphatic. *Ullmann's Encyclopedia of Industrial Chemistry* **2015**, 1-55.
5. Reider, P. J. *Chimia* **1997**, *51*, 306.
6. Nair, V.; Rajan, R.; Rath, N. P. *Org. Lett.* **2002**, *4*, 1575–1577.
7. Nakaya, T.; Matsuda, A.; Ichikawa, S. *Org. Biomol. Chem.* **2015**, *13*, 7720.
8. Leiva, R.; Gazzarrini, S.; Esplugas, R.; Moroni, A.; Naesens, L.; Sureda, F. X.; Vázquez, S. *Tetrahedron Lett.* **2015**, *56*, 1272.
9. Huber, J.; Wölfling, J.; Schneider, G.; Ocsovszki, I.; Varga, M.; Zupkó, I.; Mernyák, E. *Steroids* **2015**, *102*, 76.
10. Stepanovs, D.; Posevins, D.; Turks, M. *Acta Crystallogr.* **2015**, *71*, 1117.
11. Ji, M.; Feng, C.; Yan, B.; Yin, G.; Chen, J. *Synlett* **2018**, *29*, 2257.
12. For pioneering work on relevant hydrofunctionalizations see: Mukaiyama, T.; Yamada, T. *Bull. Chem. Soc. Jpn.* **1995**, *68*, 17.
13. For an excellent review of MHAT hydrofunctionalizations see: Crossley, S. W. M.; Obradors, C.; Martinez, R. M.; Shenvi, R. A. *Chem. Rev.* **2016**, *116*, 8912.
14. For selected examples see: (a) Waser, J.; Nambu, H.; Carreira, E. M. *J. Am. Chem. Soc.* **2005**, *127*, 8294. (b) Gaspar, B.; Carreira, E. M. *Angew. Chem., Int. Ed.* **2007**, *46*, 4519. (c) Gaspar, B.; Carreira, E. M. *Angew. Chem., Int. Ed.* **2008**, *47*, 5758. (d) Gaspar, B.; Carreira, E. M. *J. Am. Chem. Soc.* **2009**, *131*, 13214. (e) Girijavallabhan, V.; Alvarez, C.; Njoroge, F. G. *J. Org. Chem.* **2011**, *76*, 6442. (f) Barker, T.; Boger, D. L. *J. Am. Chem. Soc.* **2012**, *134*, 13588. (g) Leggans, E. K.; Barker, T. J.; Duncan, K. K.; Boger, D. L. *Org. Lett.* **2012**, *14*, 1428. (h) Shigehisa, H.; Nishi, E.; Fujisawa, M.; Hiroya, K. *Org. Lett.* **2013**, *15*, 5158. (i) Iwasaki, K.; Wan, K. K.; Oppedisano, A.; Crossley, S. W. M.; Shenvi, R. A. *J. Am. Chem. Soc.* **2014**, *136*, 1300. (j) King, S. M.; Ma, X.; Herzon, S. B. *J. Am. Chem. Soc.* **2014**, *136*, 6884. (k) Ma, X. S.; Herzon, S. B. *Chem. Sci.* **2015**, *6*, 6250. (l) Zheng, J.; Wang, D.; Cui, S. *Org. Lett.* **2015**, *17*, 4572. (m) Crossley, S. W. M.; Martinez, R. M.; Guevara-Zuluaga, S.; Shenvi, R. A. *Org. Lett.* **2016**, *18*, 2620. (n) Ma, X.; Herzon, S. B. *J. Am. Chem. Soc.* **2016**, *138*, 8718. (o) Ma, X.; Dang, H.; Rose, J. A.; Rablen, P.; Herzon, S. B. *J. Am. Chem. Soc.* **2017**, *139*, 5998. (p) Qi, J.; Zheng, J.; Cui, S. *Org. Lett.* **2018**, *20*, 1355. (q) Yang, L.; Ji, W.-W.; Lin, E.; Li, J.-L.; Fan, W.-X.; Li, Q.; Wang, H. *Org. Lett.* **2018**, *20*, 1924. (r) Zhang, Y.; Huang, C.; Lin, X.; Hu, Q.; Hu, B.; Zhou, Y.; Zhu, G. *Org. Lett.* **2019**, *21*, 2261. (s) Zhou, X.-L.; Yang, F.; Sun, H.-L.; Yin, Y.-N.; Ye, W.-T.; Zhu, R. *J. Am. Chem. Soc.* **2019**, *141*, 7250.
15. Waser, J.; Carreira, E. M. *J. Am. Chem. Soc.* **2004**, *126*, 5676.
16. Waser, J.; Nambu, H.; Carreira, E. M. *J. Am. Chem. Soc.* **2005**, *127*, 8294.
17. Waser, J.; Gaspar, B.; Nambu, H.; Carreira, E. M. *J. Am. Chem. Soc.* **2006**, *128*, 11693.
18. Leggans, E. K.; Barker, T. J.; Duncan, K. K.; Boger, D. L. *Org. Lett.* **2012**, *14*, 1428.
19. Zheng, J.; Qi, J.; Cui, S. *Org. Lett.* **2016**, *18*, 128.

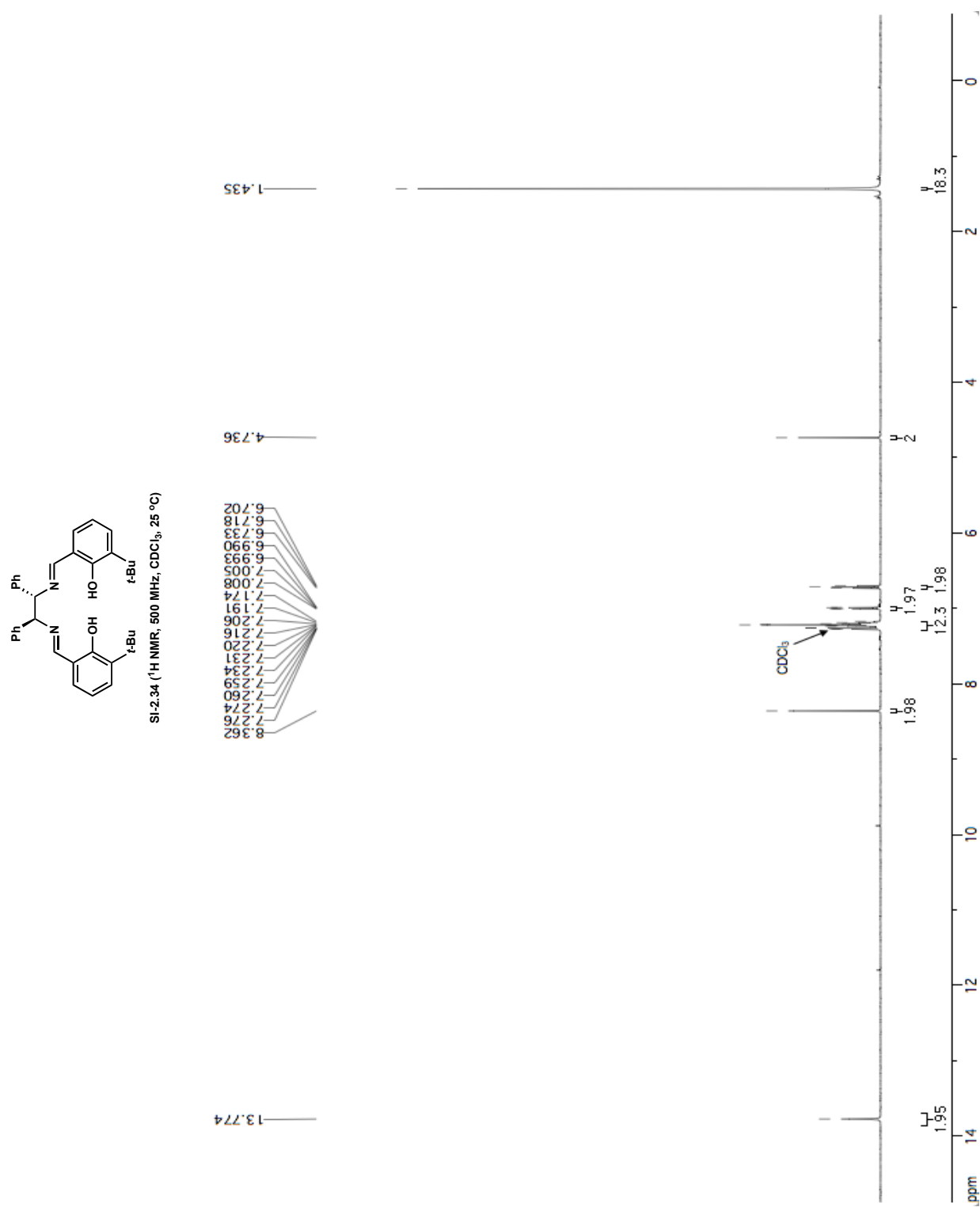
20. Gui, J.; Pan, C.-M.; Jin, Y.; Qin, T.; Lo, J. C.; Lee, B. J.; Spergel, S. H.; Mertzman, M. E.; Pitts, W. J.; La Cruz, T. E.; Schmidt, M. A.; Darvatkar, N.; Natarajan, S. R.; Baran, P. S. *Science* **2015**, *348*, 886.
21. Touney, E. E.; Foy, N. J.; Pronin, S. V. *J. Am. Chem. Soc.* **2018**, *140*, 16982.
22. Discolo, C. A.; Touney, E. E.; Pronin, S. V. *J. Am. Chem. Soc.* **2019**, *141*, 17527.
23. (a) Shigehisa, H.; Aoki, T.; Yamaguchi, S.; Shimizu, N.; Hiroya, K. *J. Am. Chem. Soc.* **2013**, *135*, 10306. (b) Lande, S. S.; Kochi, J. K. *J. Am. Chem. Soc.* **1968**, *90*, 5196.
24. For selected examples, see: (a) Shigehisa, H.; Koseki, N.; Shimizu, N.; Fujisawa, M.; Niitsu, M.; Hiroya, K. *J. Am. Chem. Soc.* **2014**, *136*, 13534. (b) Shigehisa H.; Hayashi, M.; Ohkawa, H.; Suzuki, T.; Okayasu, H.; Mukai, M.; Yamazaki, A.; Kawai, R.; Kikuchi, H.; Satoh, Y.; Akane, F.; Hiroya, K. *J. Am. Chem. Soc.* **2016**, *138*, 10597.
25. George, D. T. Total synthesis of paxilline indole diterpenes and development of new chemical methods utilizing cobalt catalysis. Ph.D. Thesis. *UC Irvine*. **2018**.
26. Yahata, K.; Kaneko, Y.; Akai, S. *Org. Lett.* **2020**, *22*, 598.
27. Nagai, T.; Mimata, N.; Terada, Y.; Sebe, C.; Shigehisa, H. *Org. Lett.* **2020**, *22*, 5522.
28. Yin, Y.-N.; Ding, R.-Q.; Ouyang, D.-C.; Zhang, Q.; Zhu, R. *Nature Communications* **2021**, *12*, 2552.
29. For selected examples, see: (a) References 21, 22, 23a, 24b, and 24c. (b) Shigehisa, H.; Ano, T.; Honma, H.; Ebisawa, K.; Hiroya, K. *Org. Lett.* **2016**, *18*, 3622. (c) Date, S.; Hamasaki, K.; Sunagawa, K.; Koyama, H.; Sebe, C.; Hiroya, K.; Shigehisa, H. *ACS Catal.* **2020**, *10*, 2039. (d) Ebisawa, K.; Izumi, K.; Ooka, Y.; Kato, H.; Kanazawa, S.; Komatsu, S.; Nishi, E.; Shigehisa, H. *J. Am. Chem. Soc.* **2020**, *142*, 13481. (e) Ohuchi, S.; Koyama, H.; Shigehisa, H. *ACS Catal.* **2021**, *11*, 900. (f) Zhou, X.-L.; Yang, F.; Sun, H.-L.; Yin, Y.-N.; Ye, W.-T.; Zhu, R. *J. Am. Chem. Soc.* **2019**, *141*, 7250. (g) Sun, H.-L.; Yang, F.; Ye, W.-T.; Wang, J.-J.; Zhu, R. *ACS Catal.* **2020**, *10*, 4983. (h) Vrubliauskas, D.; Vanderwal, C. D. *Angew. Chem. Int. Ed.* **2020**, *59*, 6115. (i) Vrubliauskas, D.; Gross, B. M.; Vanderwal, C. D. *J. Am. Chem. Soc.* **2021**, *143*, 2944.
30. Kim, H.; Nguyen, Y.; Lough, A.; Chin, J. *Angew. Chem. Int. Ed.* **2008**, *47*, 8678.
31. For examples of MHAT hydrofunctionalizations under catalyst control, see: (a) Crossley, S. W. M.; Barabé, F.; Shenvi, R. A. *J. Am. Chem. Soc.* **2014**, *136*, 16788. (b) Shevick, S. L.; Obradors, C.; Shenvi, R. A. *J. Am. Chem. Soc.* **2018**, *140*, 12056.
32. Chiang, L.; Allen, L. E. N.; Alcantara, J.; Wang, M. C. P.; Storr, T.; Shaver, M. P. *Dalton Trans.* **2014**, *43*, 4295.
33. Knowles, R. R.; Lin, S.; Jacobsen, E. N. *J. Am. Chem. Soc.* **2010**, *132*, 5030.
34. For selected reviews of cation- π interactions in chemical catalysis, see: (a) Pluth, M. D.; Bergman, R. G.; Raymond, K. N. *Acc. Chem. Res.* **2009**, *42*, 1650. (b) Brown, C. J.; Toste, F. D.; Bergman, R. G.; Raymond, K. N. *Chem. Rev.* **2015**, *115*, 3012. (c) Kennedy, C. R.; Lin, S.; Jacobsen, E. N. *Angew. Chem., Int. Ed.* **2016**, *55*, 12596. (d) Neel, A. J.; Hilton, M. J.; Sigman, M. S.; Toste, F. D. *Nature* **2017**, *543*, 637. (e) Yamada, S. *Chem. Rev.* **2018**, *118*, 11353.
35. For additional examples of tuning cation- π interactions with extended aromatic motifs in enantioselective catalysis, see: (a) Lin, S.; Jacobsen, E. N. *Nat. Chem.* **2012**, *4*, 817. (b) Bendel-Smith, A. J.; Kim, S. C.; Wasa, M.; Roche, S. P.; Jacobsen, E. N. *J. Am. Chem. Soc.* **2019**, *141*, 11414.
36. Lacy, D. C.; Roberts, G. M.; Peters, J. C. *J. Am. Chem. Soc.* **2015**, *137*, 4860.

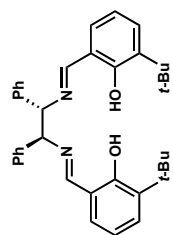
37. For evidence of solvent caged alkylradical-metalloradical pair see: (a) Sweany, R.; Halpern, J. *J. Am. Chem. Soc.* **1977**, *99*, 8335. (b) Jacobsen, E. N.; Bergman, R. G. *J. Am. Chem. Soc.* **1985**, *107*, 2023. (c) Ungváry, F.; Markó, L. *J. Organomet. Chem.* **1983**, *249*, 411. (d) Matsui, Y.; Orchin, M. *J. Organomet. Chem.* **1983**, *244*, 369.
38. For preparations of alkylcobalt complexes, see: (a) Schrauzer, G. N.; Windgassen, R. J. *J. Am. Chem. Soc.* **1966**, *88*, 3738. (b) Costa, G.; Mestroni, G.; Stefani, L. *J. Organomet. Chem.* **1967**, *7*, 493. (c) Costa, G.; Mestroni, G.; Pellizer, G. *J. Organomet. Chem.* **1968**, *11*, 333. (d) McAllister, R. M.; Weber, J. H. *J. Organomet. Chem.* **1974**, *77*, 91. (e) Li, G.; Zhang, F. F.; Chen, H.; Yin, H. F.; Chen, H. L.; Zhang, S. Y. *J. Chem. Soc., Dalton Trans.* **2002**, 105.
39. For relevant studies on the sensitivity of alkylcobalts to steric encumbrance, see: (a) Schrauzer, G. N.; Grate, J. H. *J. Am. Chem. Soc.* **1981**, *103*, 541. (b) Tsou, T.-T.; Loots, M.; Halpern, J. *J. Am. Chem. Soc.* **1982**, *104*, 623. (c) Ng, F. T. T.; Rempel, G. L.; Mancuso, C.; Halpern, J. *Organometallics* **1990**, *9*, 2762.
40. For relevant hydrogenation, see: References 14i and 14j.
41. For relevant cyclizations, see: References 29a, 29h, 29i, and 31a.
42. Isayama, S.; Mukaiyama, T. *Chem. Lett.* **1989**, *18*, 1071.
43. (a) Bhattacharjee, A.; Chavarot-Kerlidou, M.; Andreiadis, E. S.; Fontecave, M.; Field, M. J.; Artero, V. *Inorg. Chem.* **2012**, *51*, 7087. (b) Estes, D. P.; Grills, D. C.; Norton, J. R. *J. Am. Chem. Soc.* **2014**, *136*, 17362.
44. Formation of H₂ was previously proposed to accompany relevant HAT-initiated reactions: (a) Reference 31b. (b) Matos, J. L. M.; Green, S. A.; Chun, Y.; Dang, V. Q.; Dushin, R. G.; Richardson, P.; Chen, J. S.; Piotrowski, D. W.; Paegel, B. M.; Shenvi, R. A. *Angew. Chem. Int. Ed.* **2020**, *59*, 12998.
45. For relevant discussion see: (a) Green, S. A.; Crossley, S. W. M.; Matos, J. L. M.; Vásquez-Céspedes, S.; Shevick, S. L.; Shenvi, R. A. *Acc. Chem. Res.* **2018**, *51*, 2628. (b) Shevick, S. L.; Wilson, C. V.; Kotesova, S.; Kim, D.; Holland, P. L.; Shenvi, R. A. *Chem. Sci.* **2020**, *11*, 12401.
46. For selected examples of leveraging a reverse reaction for generation of putative cobalt hydrides in HAT-initiated processes see: (a) Li, G.; Han, A.; Pulling, M. E.; Estes, D. P.; Norton, J. R. *J. Am. Chem. Soc.* **2012**, *134*, 14662. (b) Li, G.; Kuo, J. L.; Han, A.; Abuyuan, J. M.; Young, L. C.; Norton, J. R.; Palmer, J. H. *J. Am. Chem. Soc.* **2016**, *138*, 7698.
47. Sampling of the headspace at different time points indicated comparable hydrogen content as early as 10 min after addition of silane.
48. No hydrogen was detected in the absence of catalysts.
49. For relevant considerations regarding generation of collidinium radical cation see: Shigehisa, H.; Nishi, E.; Fujisawa, M.; Hiroya, K. *Org. Lett.* **2013**, *15*, 5158.
50. Formation of silyl radicals was previously proposed in a relevant HAT-initiated hydrosilylation: Obradors, C.; Martinez, R. M.; Shenvi, R. *J. Am. Chem. Soc.* **2016**, *138*, 4962.
51. Fluorine transfer from a cobalt fluoride complex to an alkyl radical intermediate was recently proposed: Guo, P.; Li, Y.; Zhang, X.-G.; Han, J.-F.; Yu, Y.; Zhu, J.; Ye, K.-Y. *Org. Lett.* **2020**, *22*, 3601.
52. Formation of dimethylphenylfluorosilane was observed by GCMSD analysis in all cases.
53. For examples of relevant studies in hydrogen evolution catalysis, see: (a) Dempsey, J. L.; Brunenschwig, B. S.; Winkler, J. R.; Gray, H. B. *Acc. Chem. Res.* **2009**, *42*, 1995. (b) Jacques, P.-A.; Altero, V.; Pécaut, J.; Fontecave, M. *Proc. Natl. Acad. Sci. USA* **2009**, *106*, 20627.

54. For examples of hydrogen evolution catalysis by relevant cobalt salen complexes, see: Li, C.-B.; Gong, P.; Yang, Y.; Wang, H.-Y. *Catal. Lett.* **2018**, *148*, 3158.
55. Tummatorn, J.; Khorphueng, P.; Petsom, A.; Muangsin, N.; Chaichit, N.; Roengsumran, S. *Tetrahedron* **2007**, *63*, 11878.
56. Abel, B. A.; Lidston, C. A. L.; Coates, G. W. *J. Am. Chem. Soc.* **2019**, *141*, 12760.
57. Kobayashi, T.; Shimura, T.; Kurita, Y.; Katsumata, Y.; Kezuka, S. *Tetrahedron Letters* **2014**, *55*, 2818.
58. Jayaseeli, A. M. I.; Ramdass, A.; Rajagopal, S. *Polyhedron* **2015**, *100*, 59.
59. George, D. T.; Kuenstner, E. J.; Pronin, S. V. *J. Am. Chem. Soc.* **2015**, *137*, 15410.
60. Wedler, C.; Kunath, A.; Schick, H. *J. Org. Chem.* **1995**, *60*, 758–760.
61. Oesterreicher, A.; Meinhart, R.; Hennen, D.; Mostegel, F. H.; Edler, M.; Kappaun, S.; Griesser, T. *Eur. Polym. J.* **2017**, *88*, 393–402.
62. Danheiser, R. L.; Nowick, J. S. *J. Org. Chem.* **1991**, *56*, 1176–1185.
63. Masuyama, A.; Sugawara, T.; Nojima, M.; McCullough, K. J. *Tetrahedron* **2003**, *59*, 353–366.
64. Greb, A.; Poh, J.-S.; Greed, S.; Battilocchio, C.; Pasau, P.; Blakemore, D. C.; Ley, S. V. *Angew. Chem. Int. Ed.* **2017**, *56*, 16602.
65. Chapman, R. S. L.; Francis, M.; Lawrence, R.; Tibbets, J. D.; Bull, S. D. *Tetrahedron* **2018**, *74*, 6442.
66. Nasrallah, A.; Grelier, G.; Lapuh, M. I.; Duran, F. J.; Darses, B.; Dauban, P. *Eur. J. Org. Chem.* **2018**, 5836.
67. Green, S. A.; Vásquez-Céspedes, S.; Shenvi, R. A. *J. Am. Chem. Soc.* **2018**, *140*, 11317.
68. Fu, N.; Sauer, G. S.; Saha, A.; Loo, A.; Lin, S. *Science* **2017**, *357*, 575.
69. Kim, I.-H.; Kanayama, Y.; Nishiwaki, H.; Sugahara, T.; Nishi, K. *J. Med. Chem.* **2019**, *62*, 9576.
70. Turek, T. C.; Gaon, I.; Distefano, M. D.; Strickland, C. L. *J. Org. Chem.* **2001**, *66*, 3253.
71. Ackermann, I. E.; Banthorpe, D. V.; Fordham, W. D.; Kinder, J. P.; Poots, I. *Liebigs Ann. Chem.* **1989**, 79.
72. Akita, H.; Kurashima, K.; Nakamura, T.; Kato, K. *Tetrahedron: Asymmetry* **1999**, *10*, 2429.
73. Ludwig, J. R.; Watson, R. B.; Nasrallah, D. J.; Gianino, J. B.; Zimmerman, P. M.; Wiscons, R. A.; Schindler, C. S. *Science* **2018**, *361*, 1363.
74. Jefferson, A.; Scheinmann, F. *J. Chem. Soc. C* **1969**, 243.
75. Sridhar, S. N. C.; Palawat, S.; Paul, A. T. *New. J. Chem.* **2020**, *44*, 12355.
76. Yu, H.; Zong, Y.; Xu, T. *Chem. Sci.* **2020**, *11*, 656.
77. Nguyen, T. N. T.; Thiel, N. O.; Pape, F.; Teichert, J. F. *Org. Lett.* **2016**, *18*, 2455.
78. Surendra, K.; Rajendar, G.; Corey, E. J. *J. Am. Chem. Soc.* **2014**, *136*, 642.
79. Kiyokawa, K.; Takemoto, K.; Minakata, S. *Chem. Commun.* **2016**, *52*, 13082.
80. Biernacki, W.; Gdula, A. *Synthesis* **1979**, 37.
81. Darbre, T.; Nussbaumer, C.; Borschberg, H.-J. *Helv. Chim. Acta* **1984**, *67*, 1040.

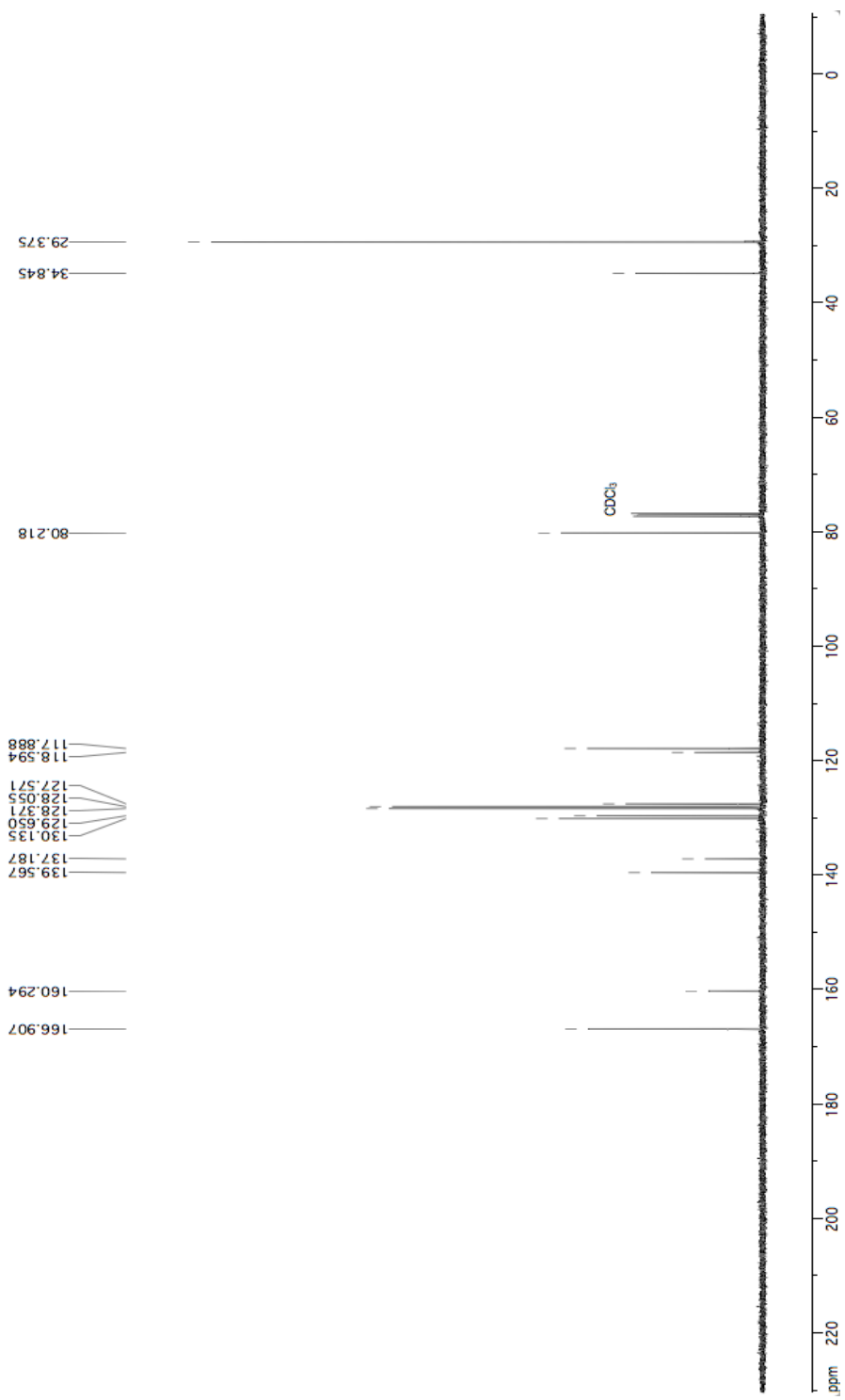
Appendix A: NMR Spectra for Chapter 2

NMR Spectra of Ligands

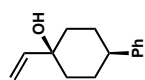




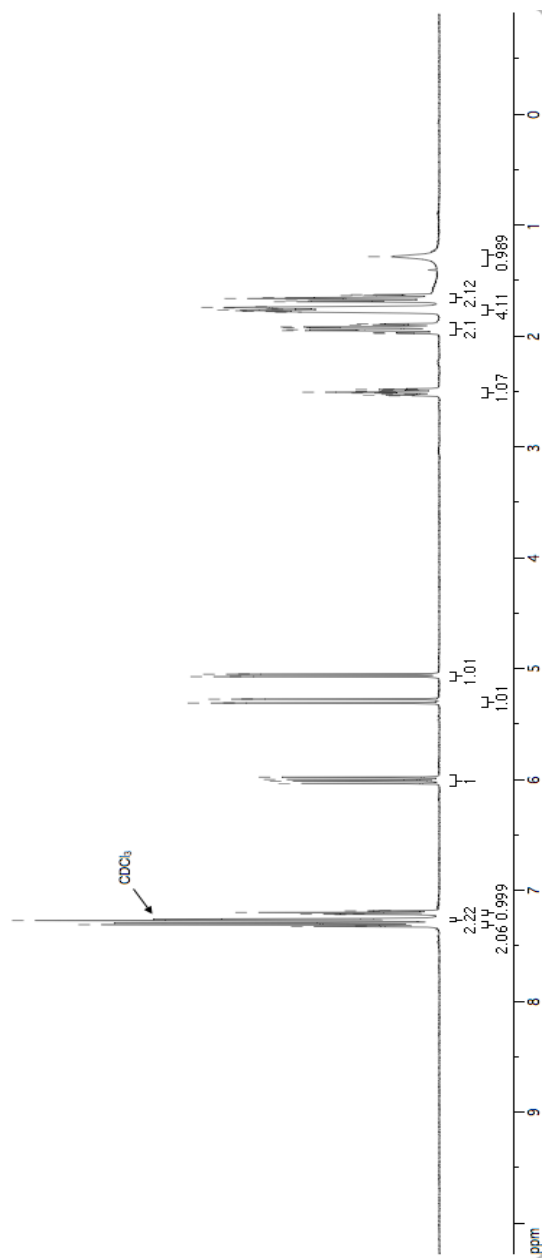
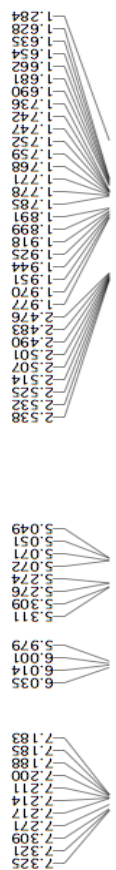
SI-2.34 (^{13}C NMR, 126 MHz, CDCl_3 , 25 $^\circ\text{C}$)

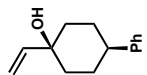


NMR Spectra of Starting Materials

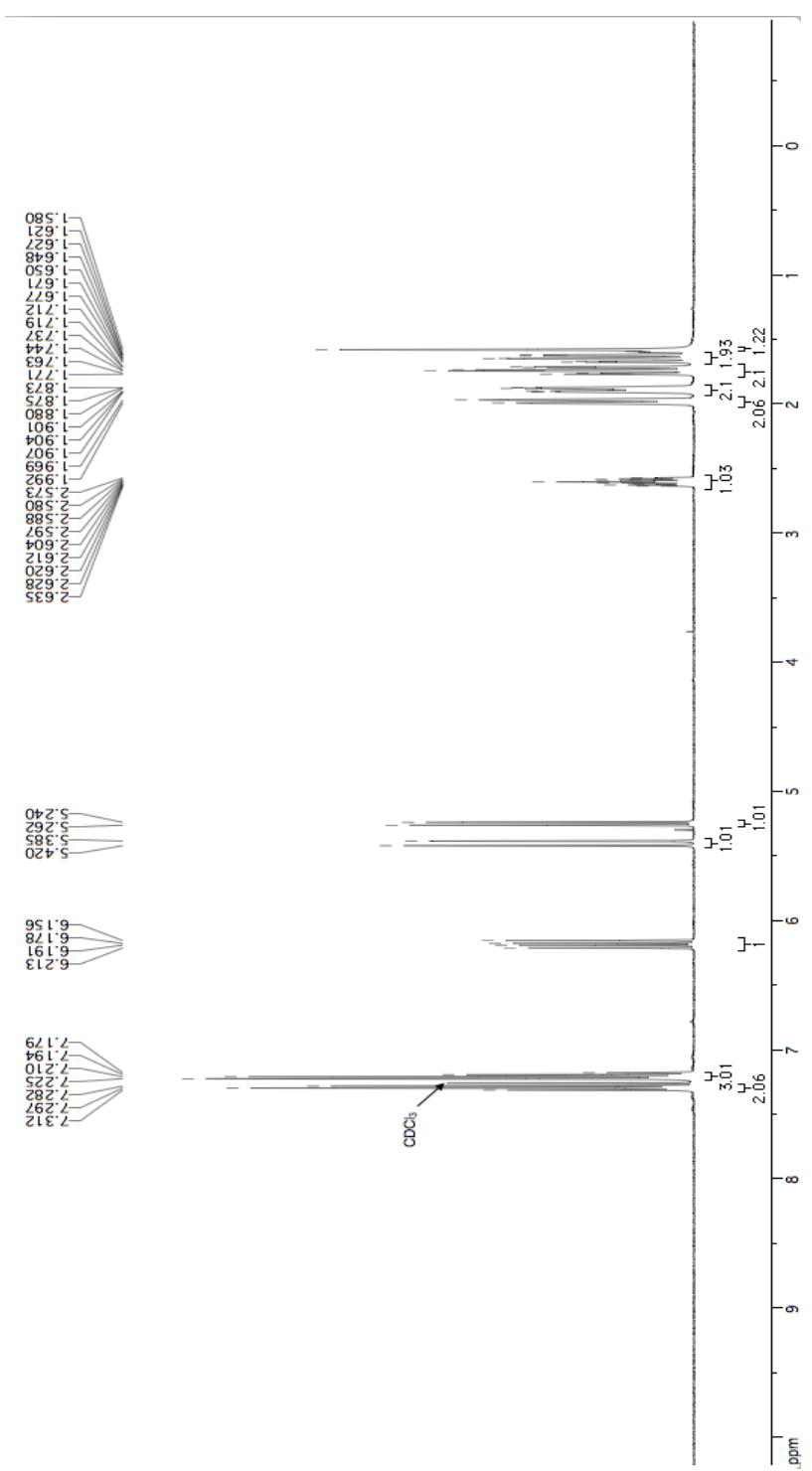


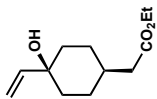
2.25 (1H NMR, 500 MHz, CDCl₃, 25 °C)



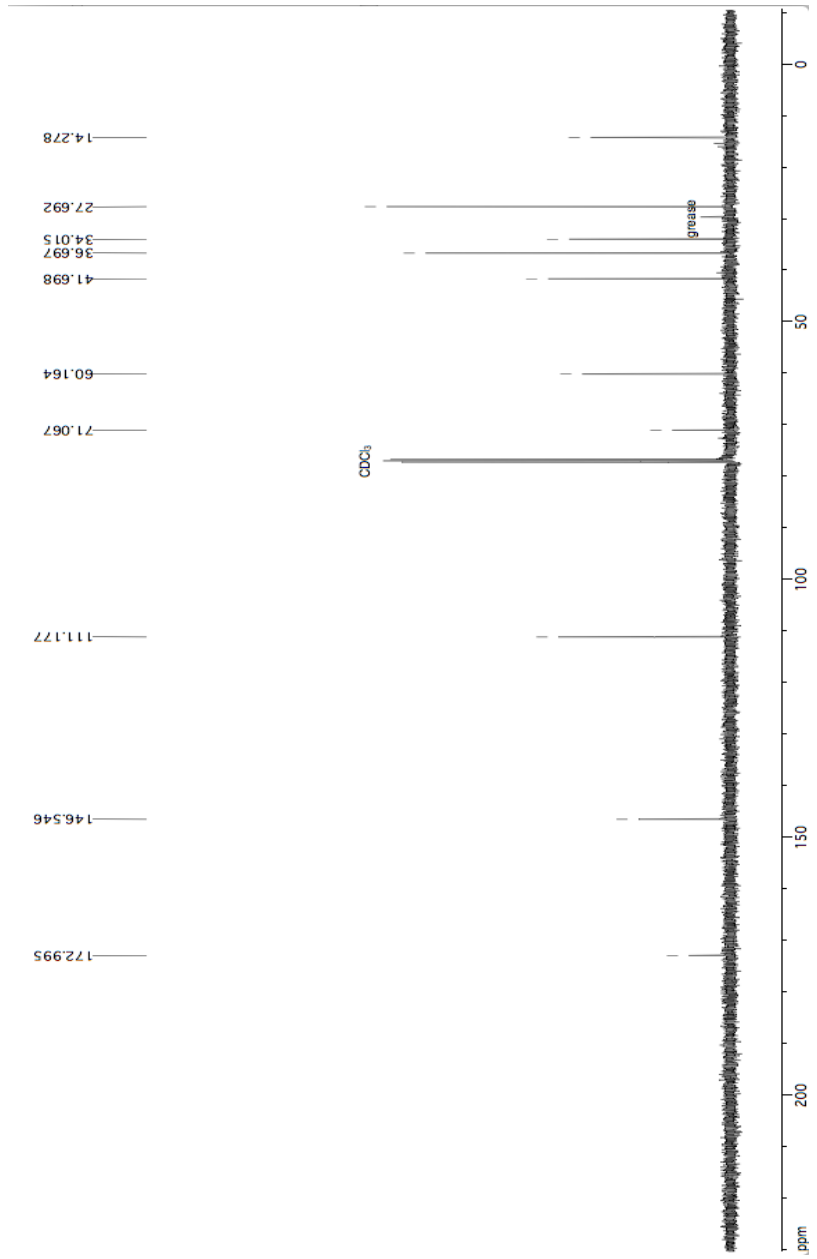


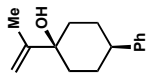
2.25 (¹H NMR, 500 MHz, CDCl₃, 25 °C)



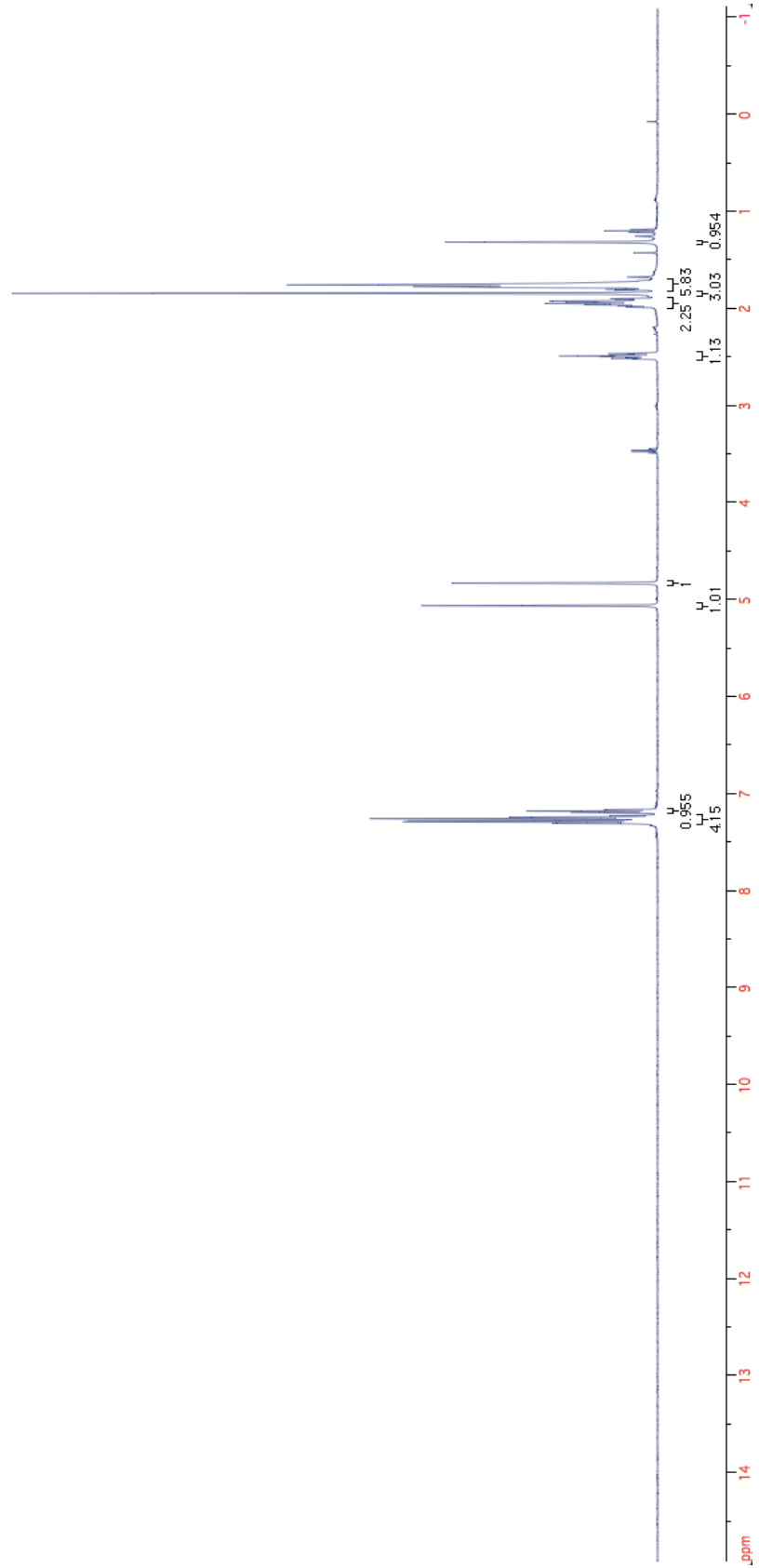


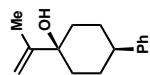
SI-2.47 (¹³C NMR, 126 MHz, CDCl₃, 25 °C)



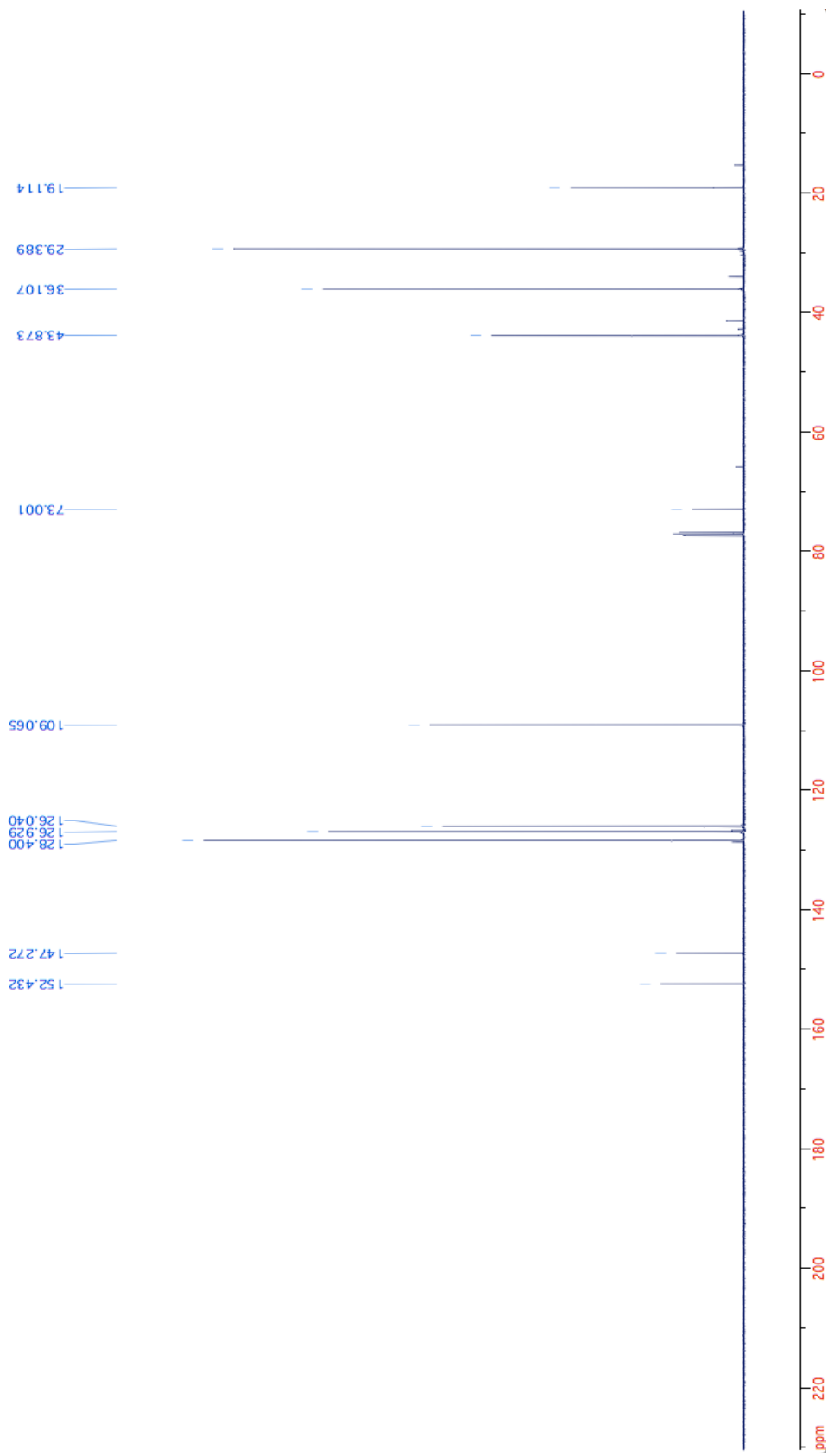


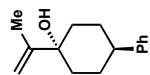
2.79 (¹H NMR, 500 MHz, CDCl₃, 25 °C)



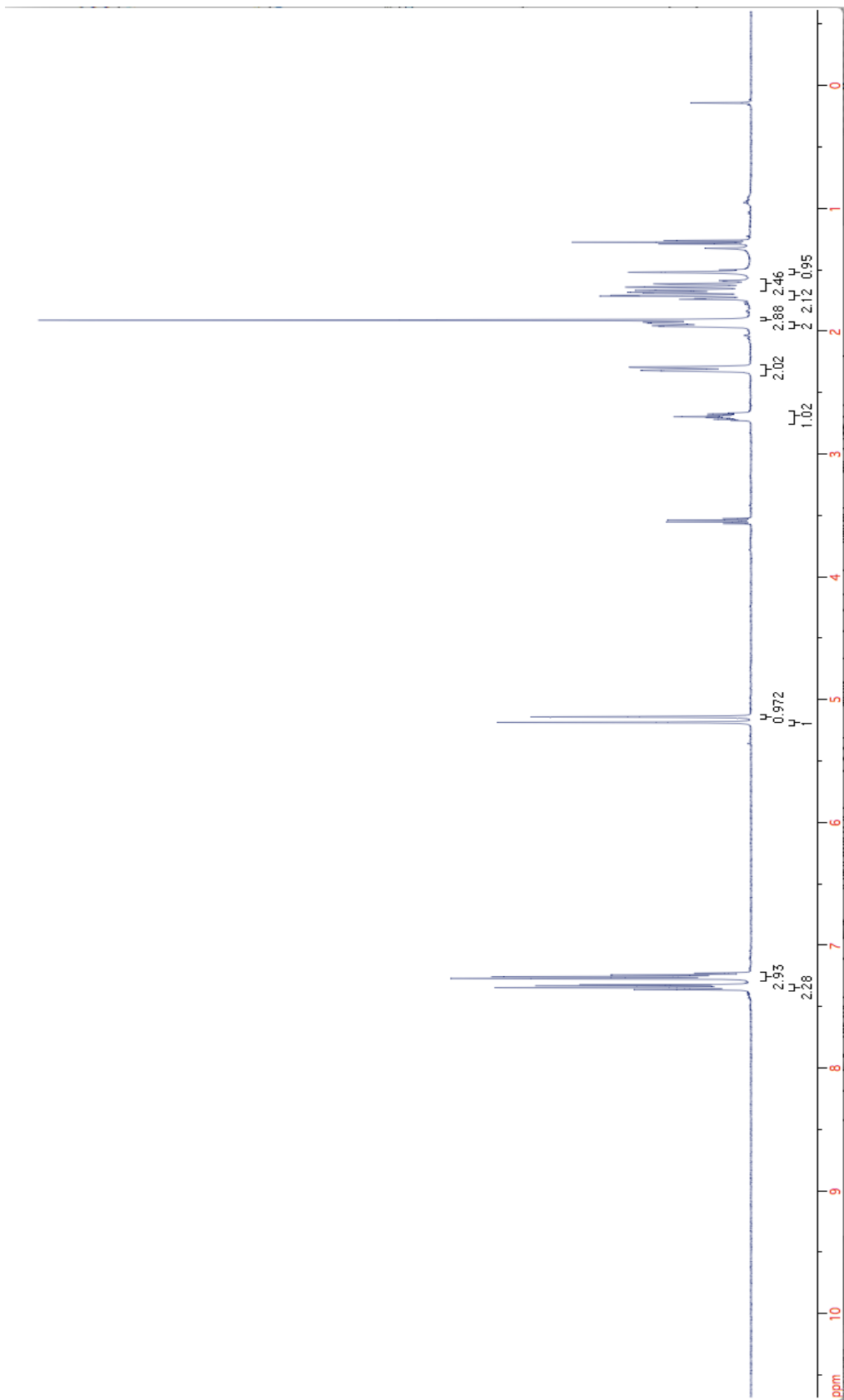


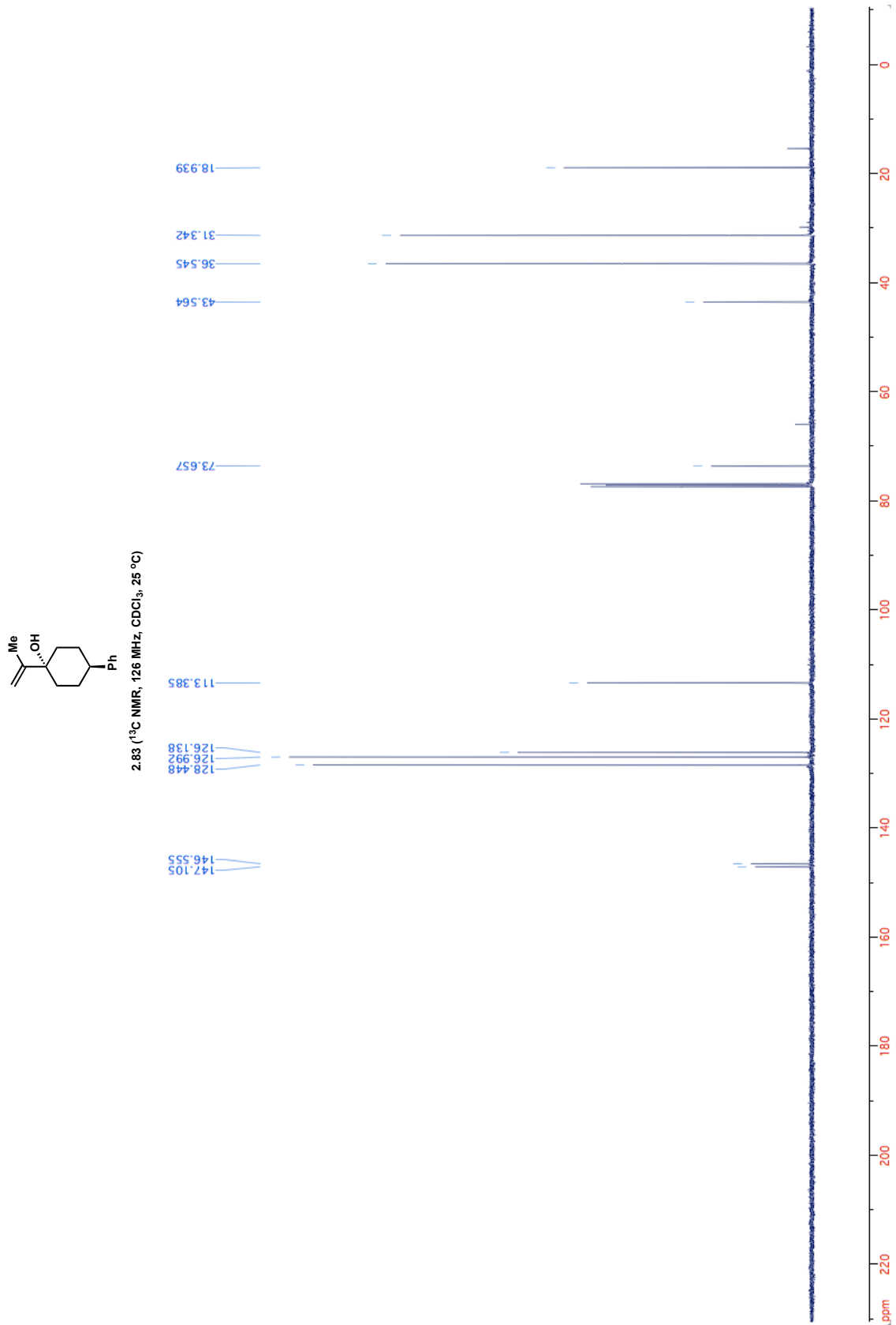
2.79 (¹³C NMR, 126 MHz, CDCl₃, 25 °C)



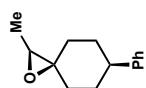


2.83 (1H NMR, 500 MHz, CDCl₃, 25 °C)

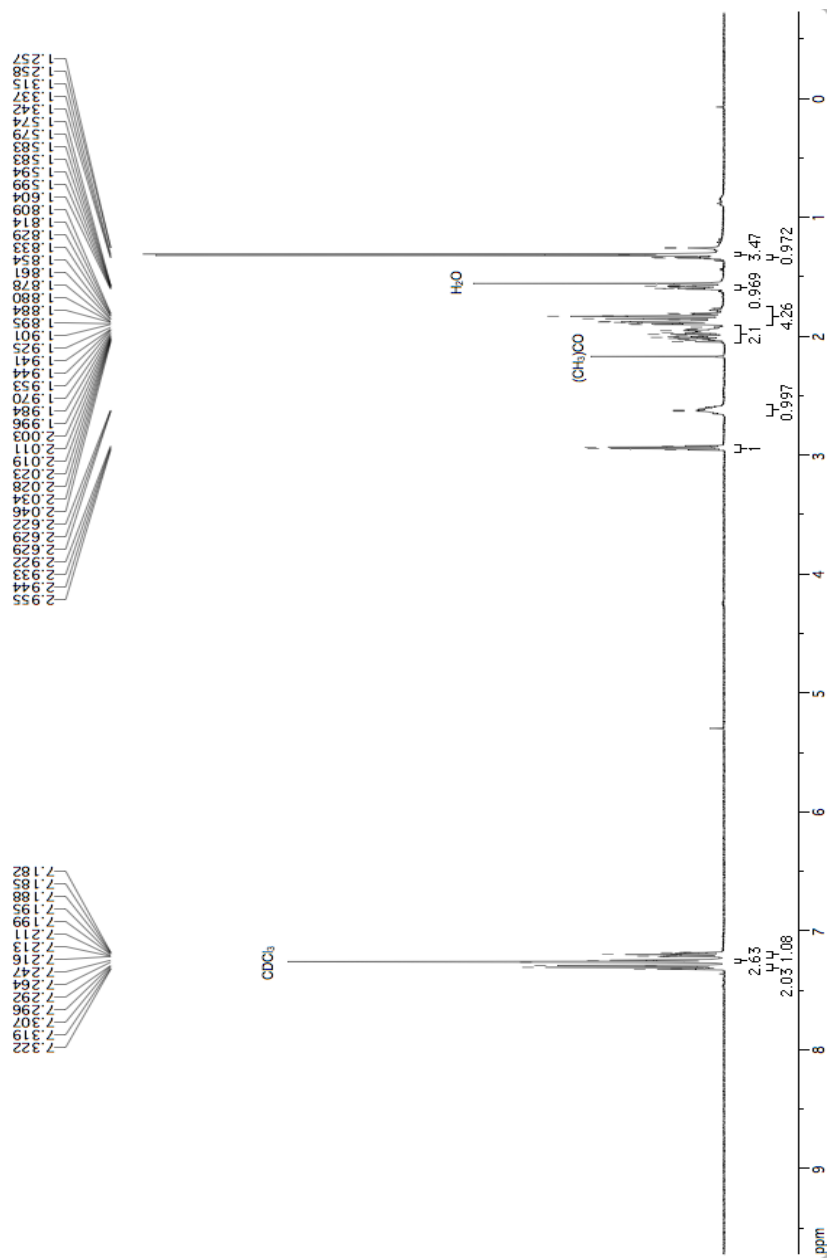


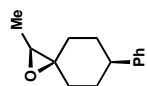


NMR Spectra of Radical–Polar Crossover Products

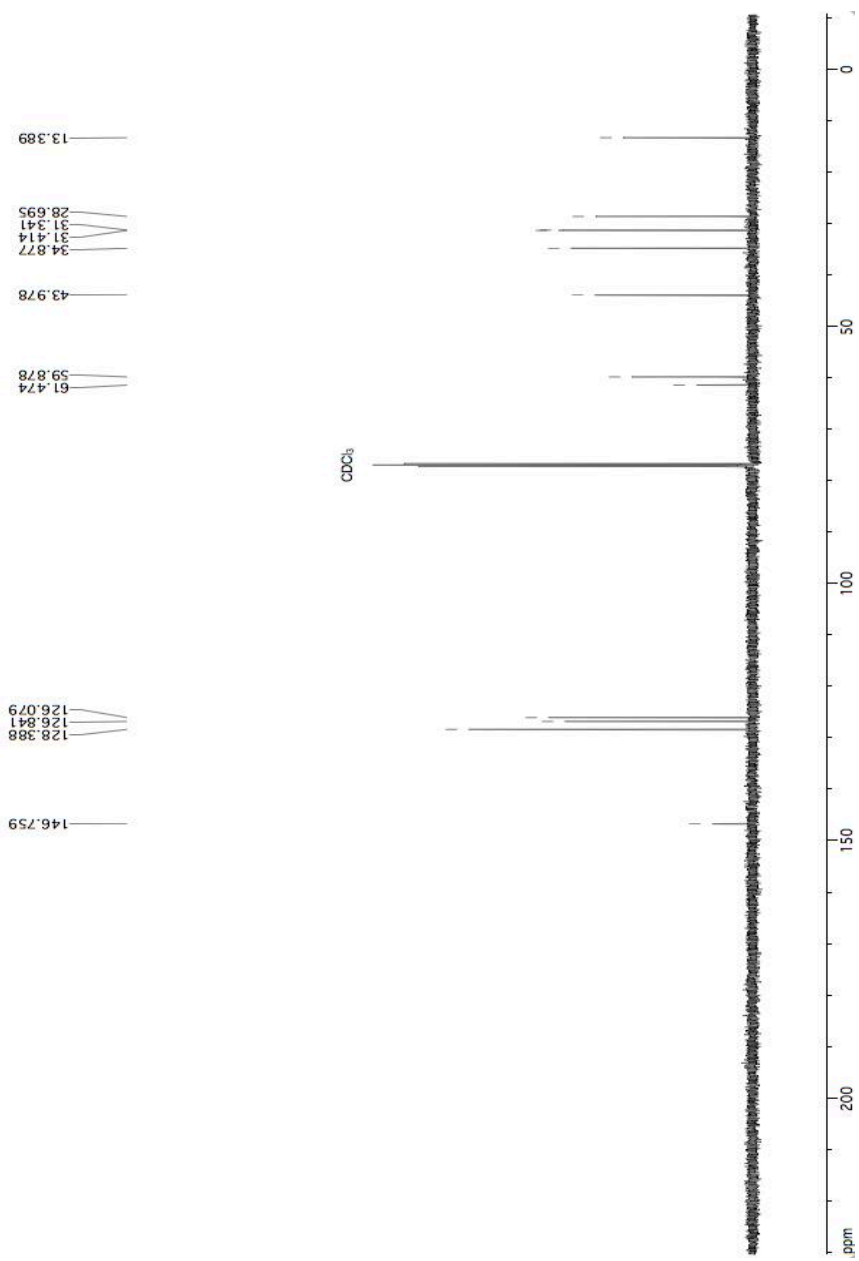


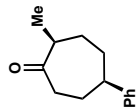
2.30 (^1H NMR, 500 MHz, CDCl_3 , 25 $^\circ\text{C}$)



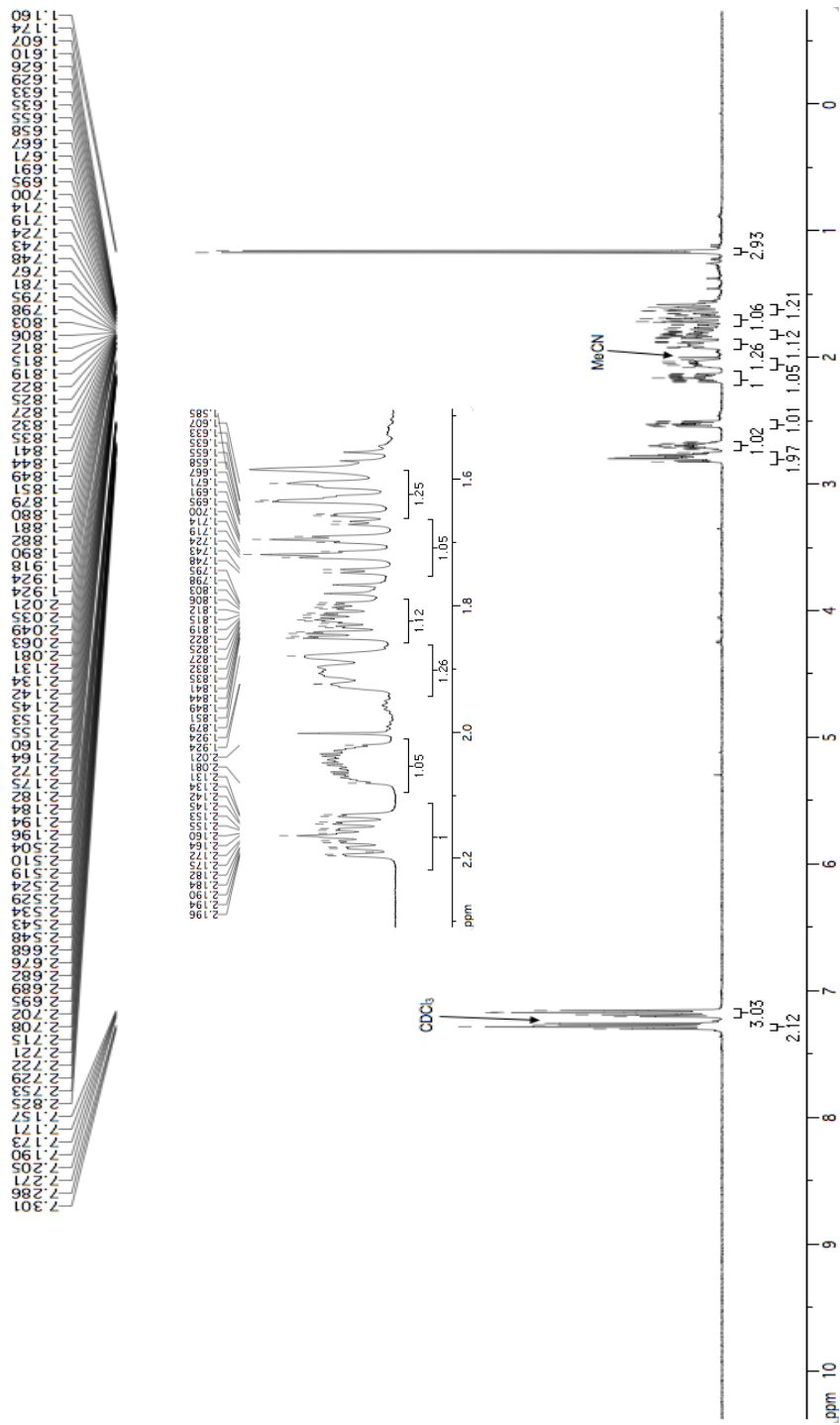


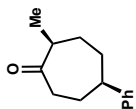
2.30 (¹³C NMR, 126 MHz, CDCl₃, 25 °C)



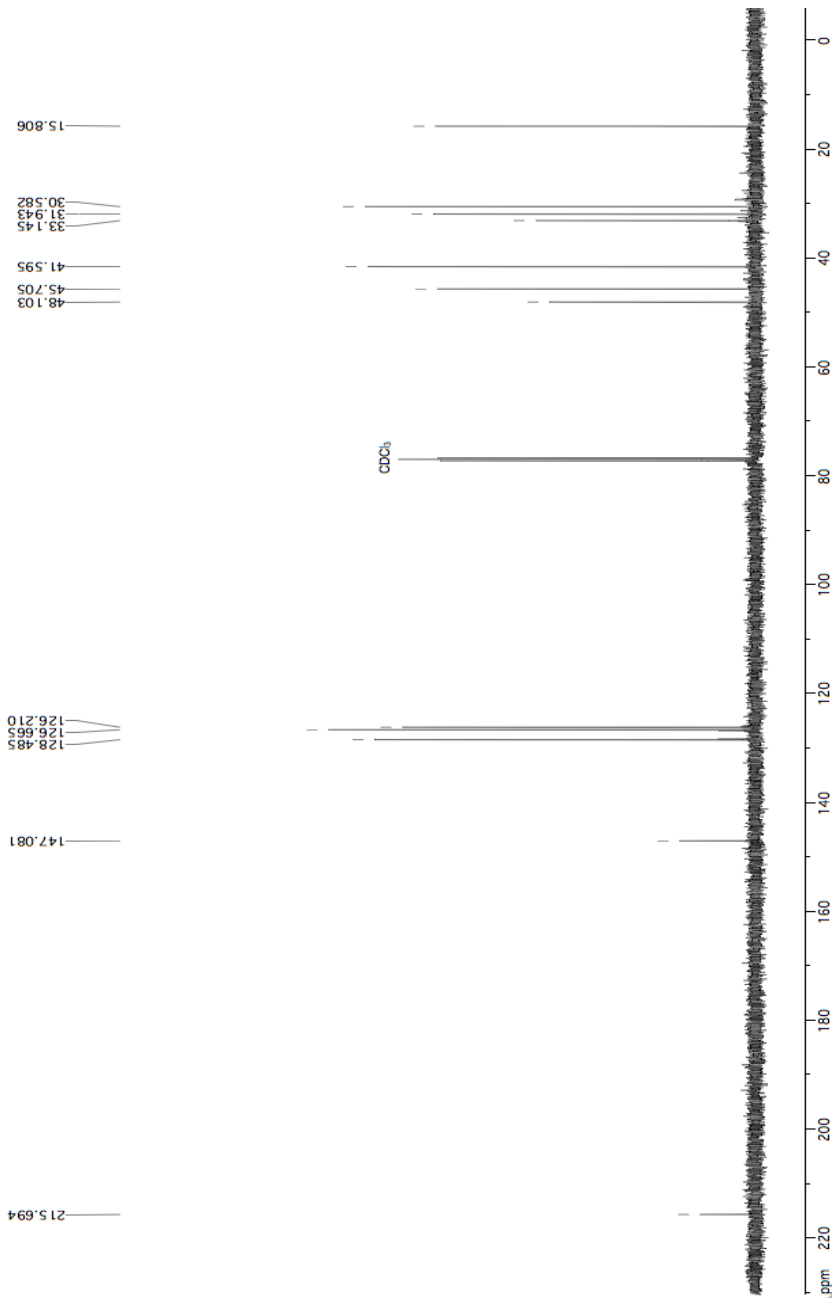


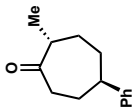
2.26a (¹H NMR, 500 MHz, CDCl₃, 25 °C)



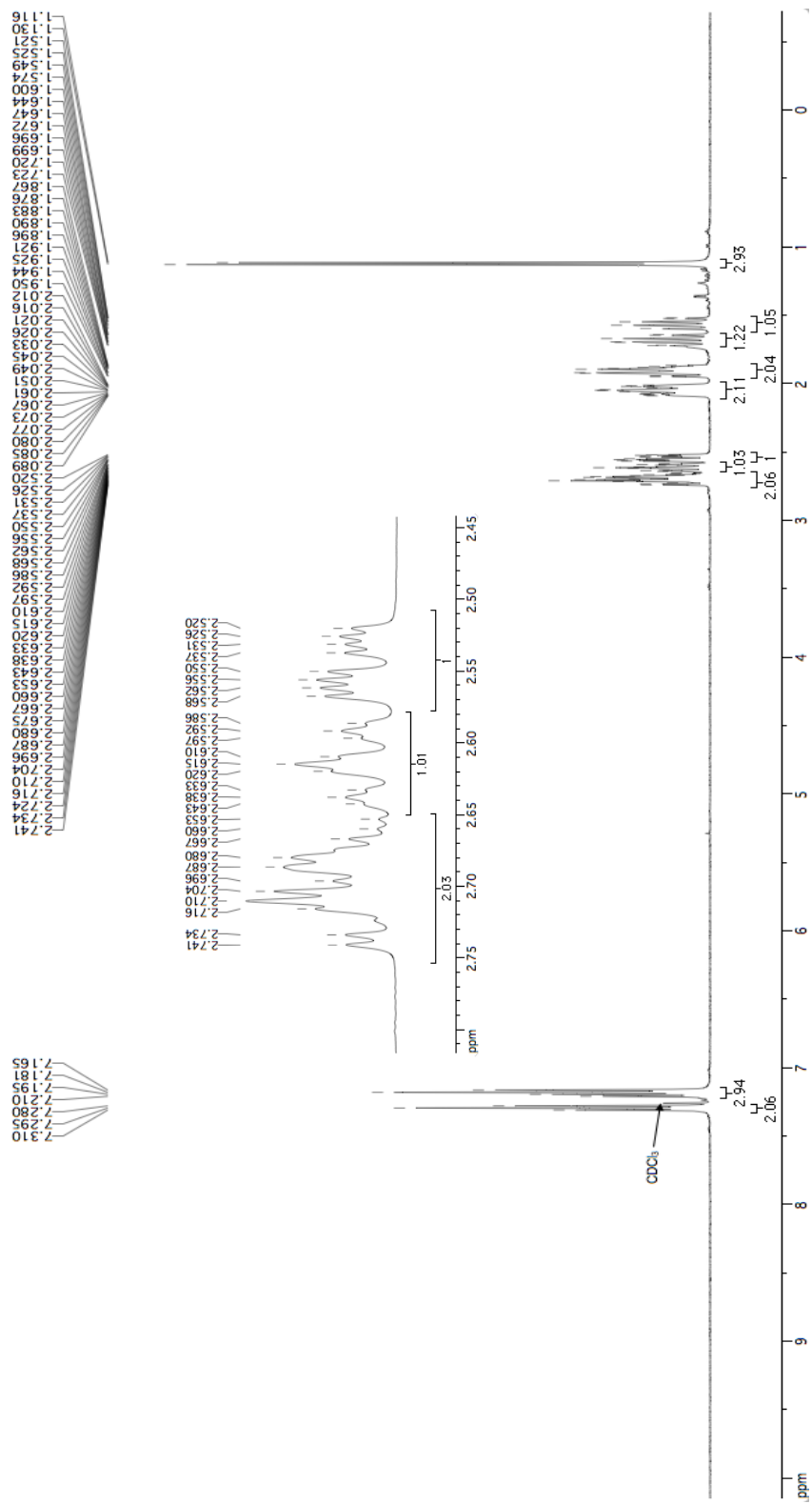


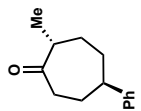
2.26a (¹³C NMR, 126 MHz, CDCl₃, 25 °C)



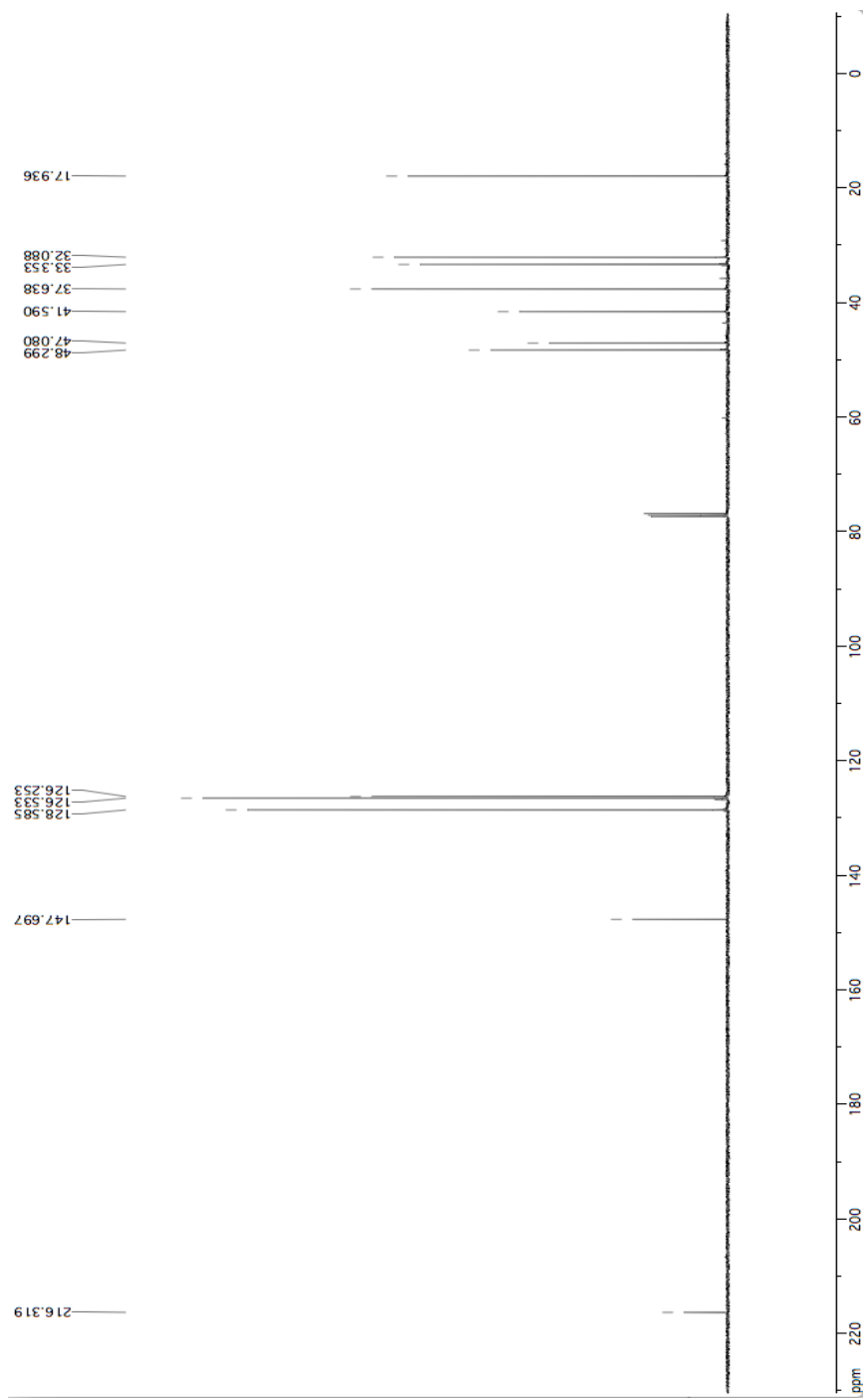


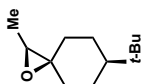
2.26b (¹H NMR, 500 MHz, CDCl₃, 25 °C)



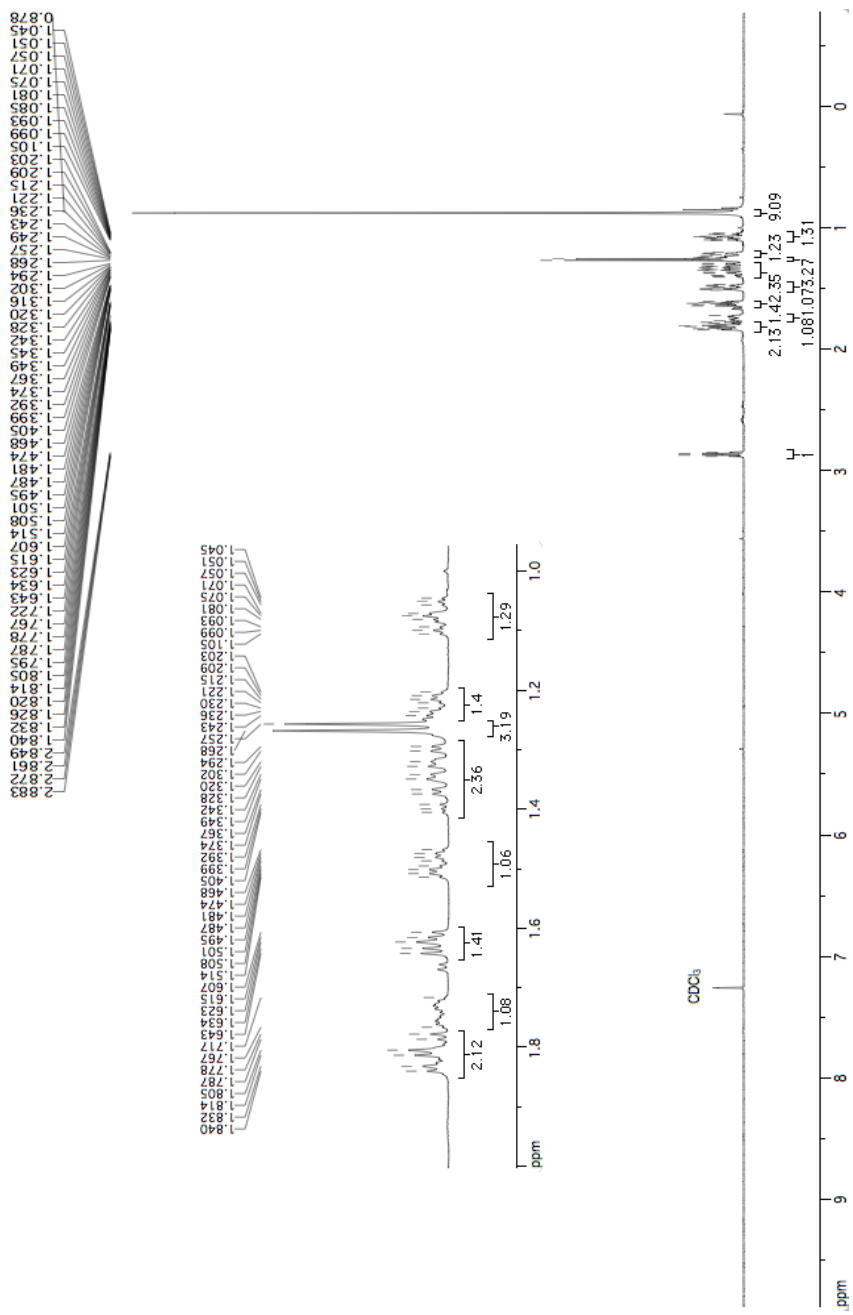


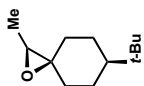
2.26b (¹³C NMR, 126 MHz, CDCl₃, 25 °C)



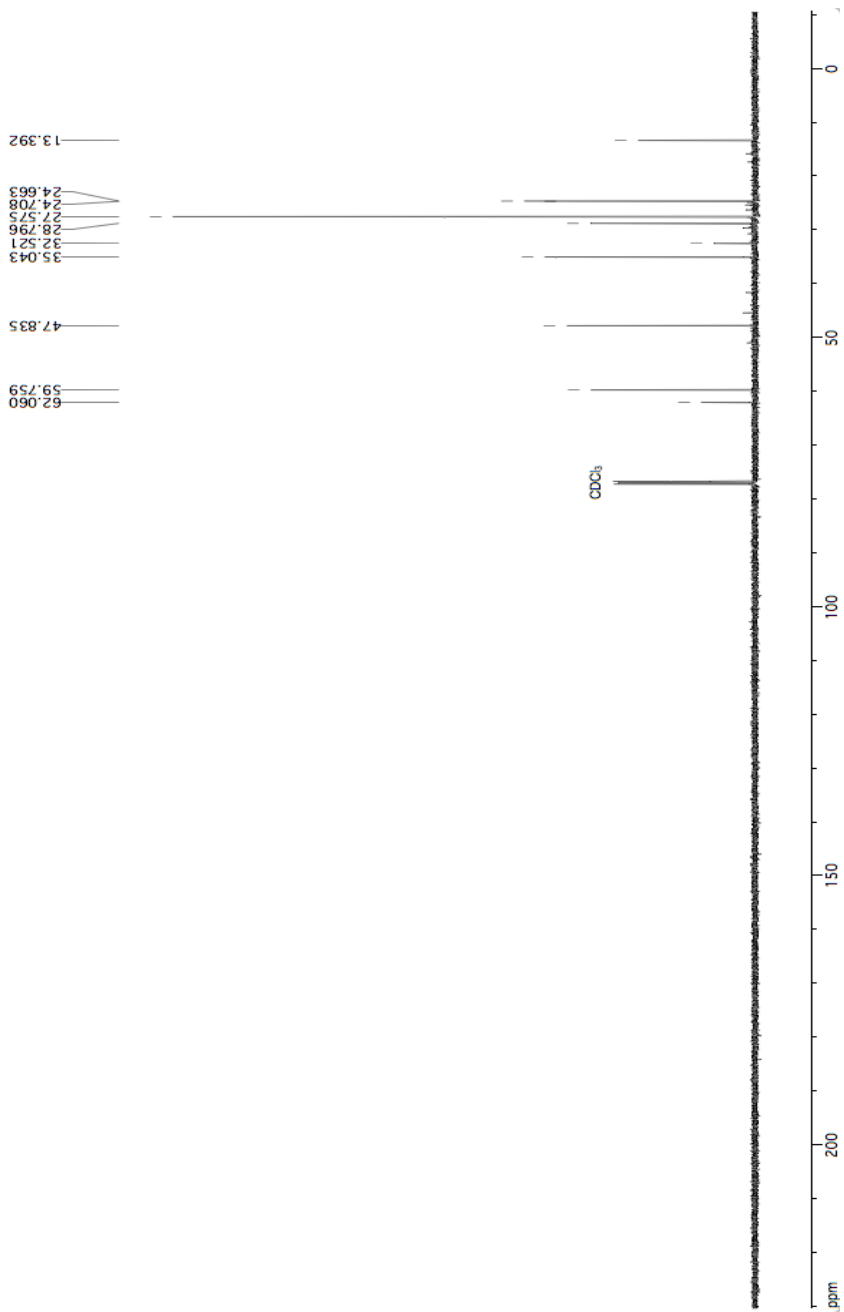


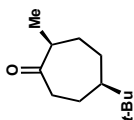
2.43a (¹H NMR, 500 MHz, CDCl₃, 25 °C)



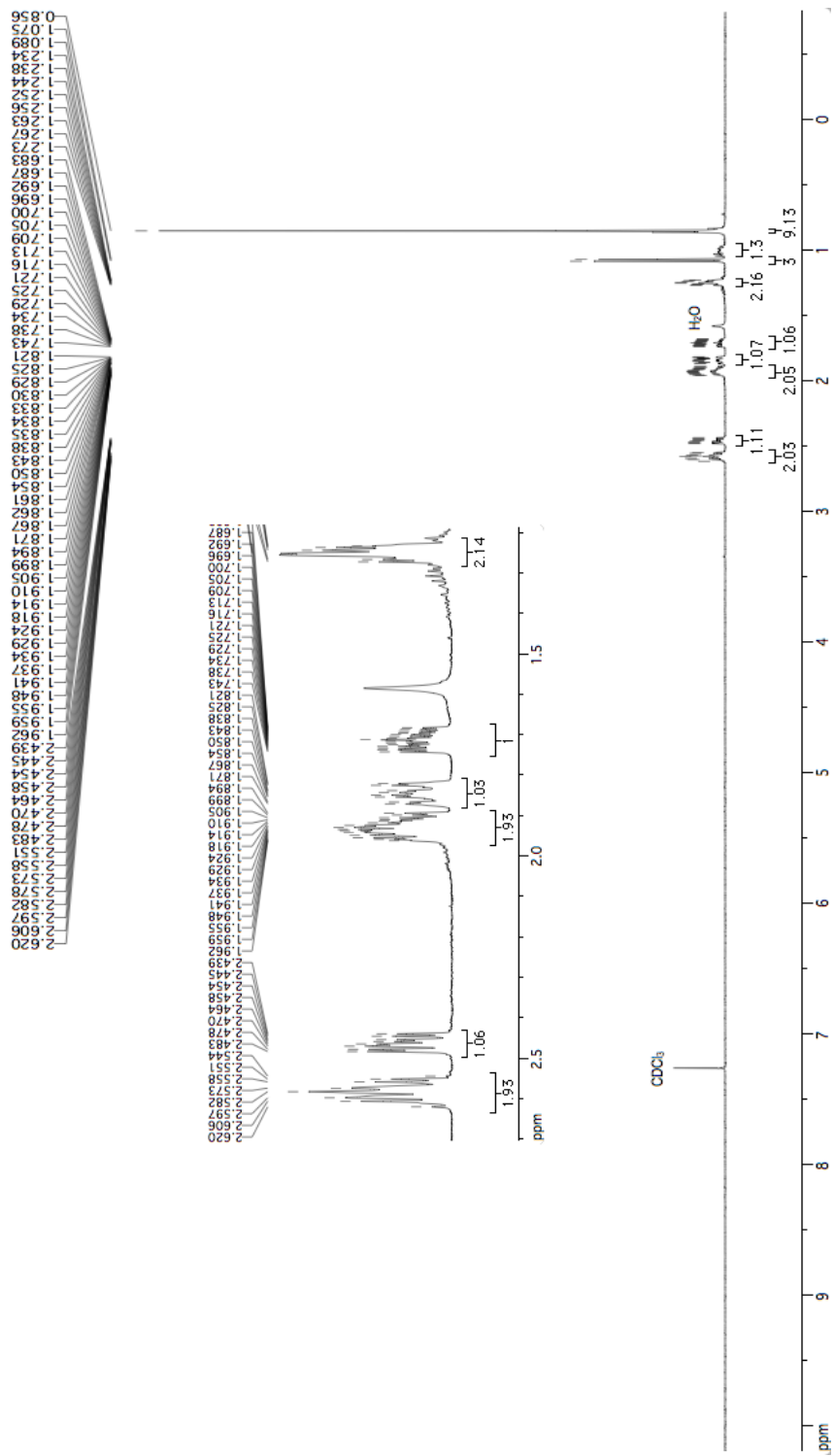


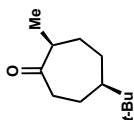
2.43a (¹³C NMR, 126 MHz, CDCl₃, 25 °C)



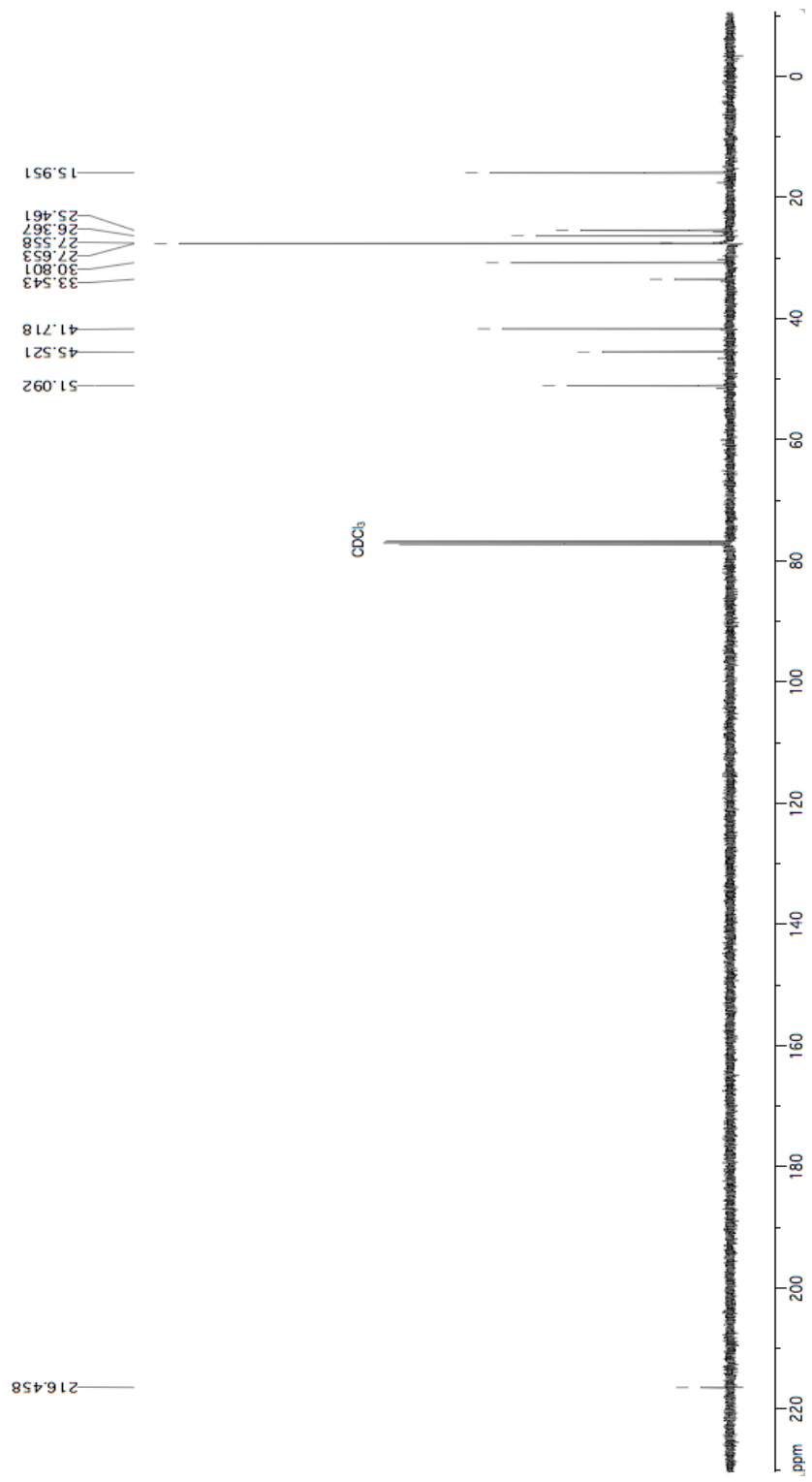


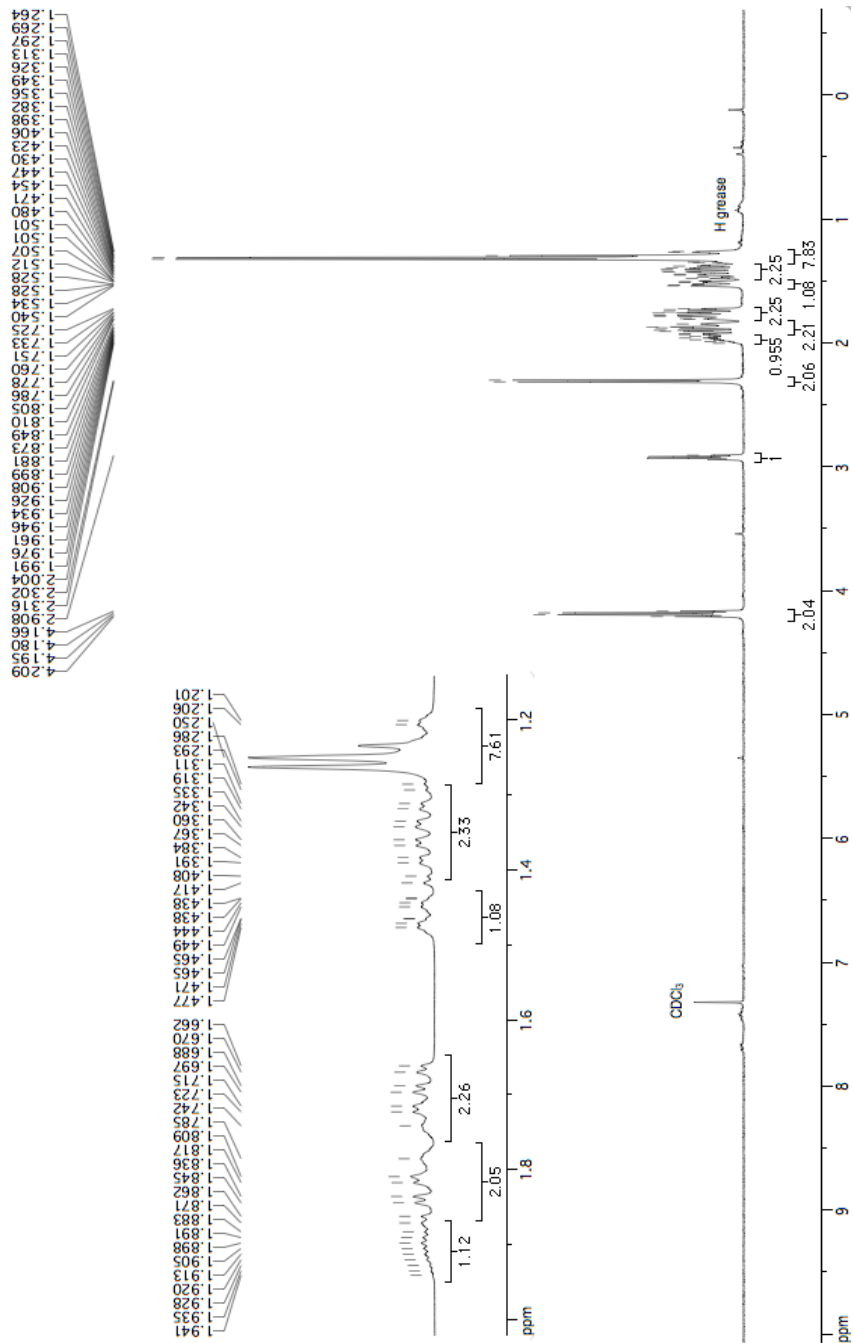
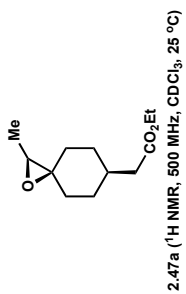
2.43b (¹H NMR, 500 MHz, CDCl₃, 25 °C)

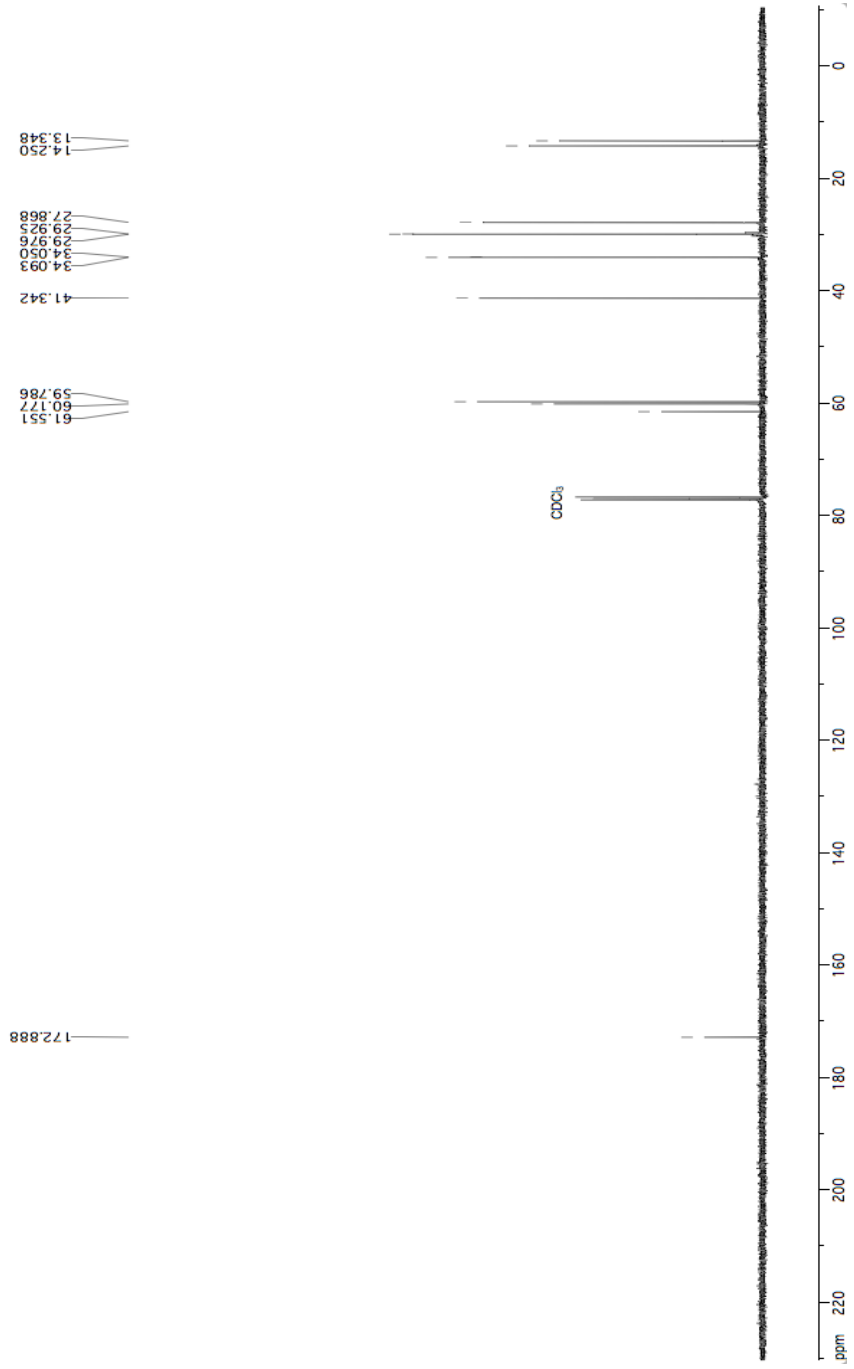
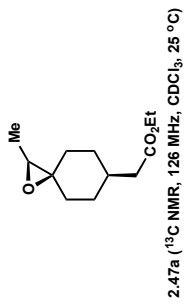


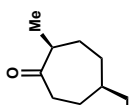


2.43b (¹³C NMR, 126 MHz, CDCl₃, 25 °C)

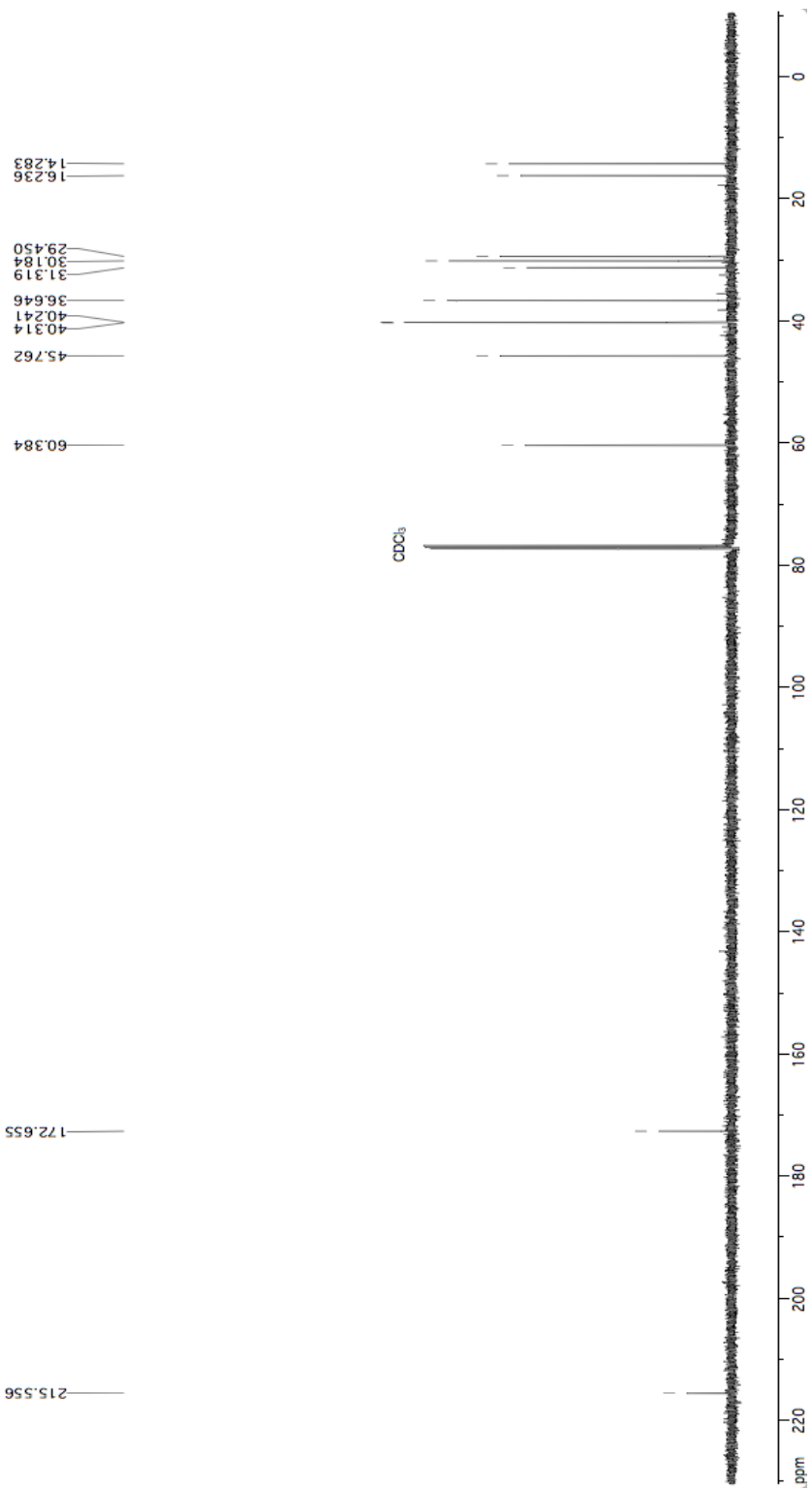


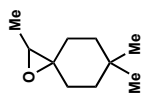




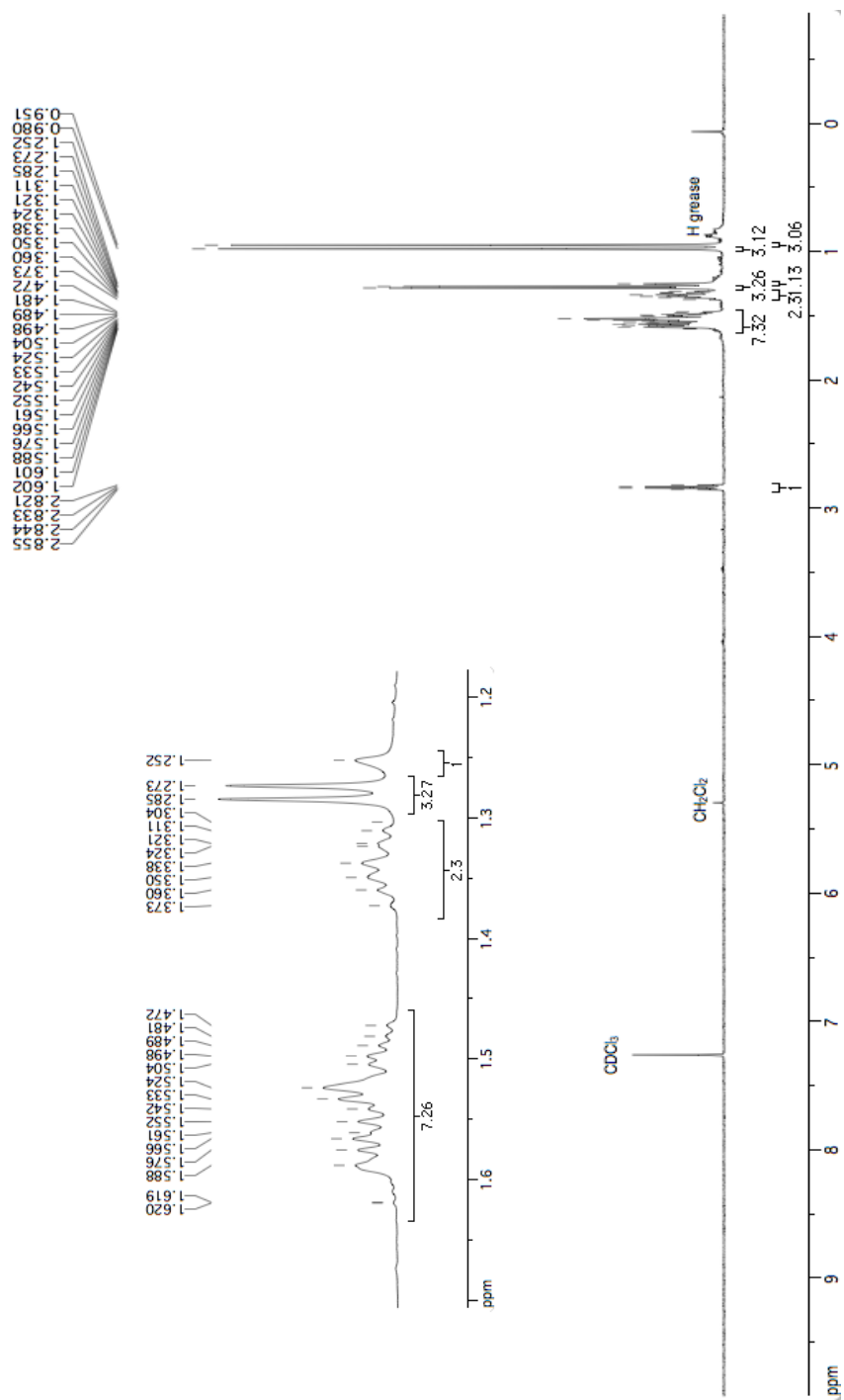


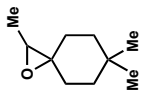
2.47b (¹³C NMR, 126 MHz, CDCl₃, 25 °C)



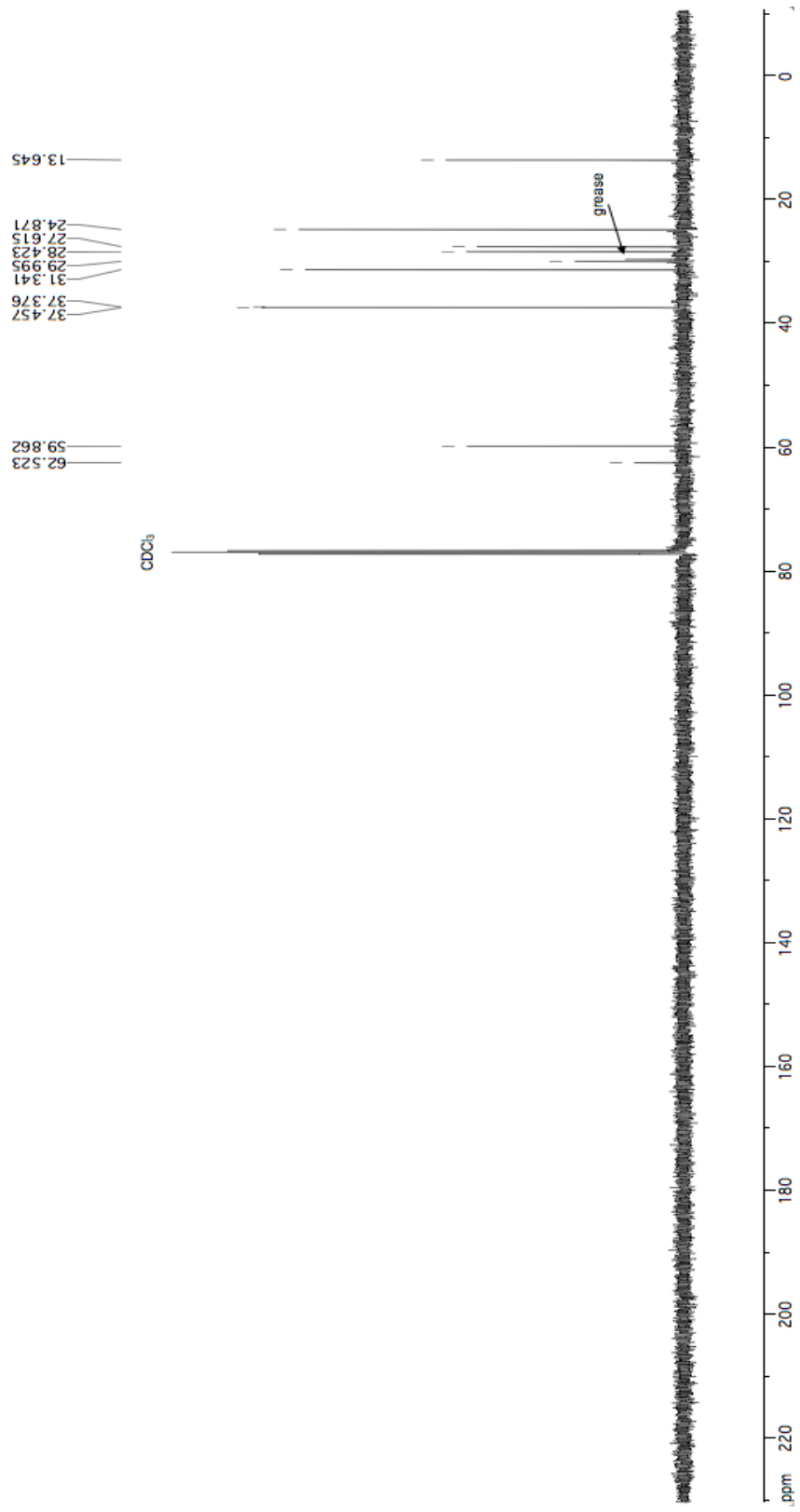


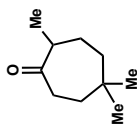
2.48a ($^1\text{H NMR}$, 500 MHz, CDCl_3 , 25 $^\circ\text{C}$)



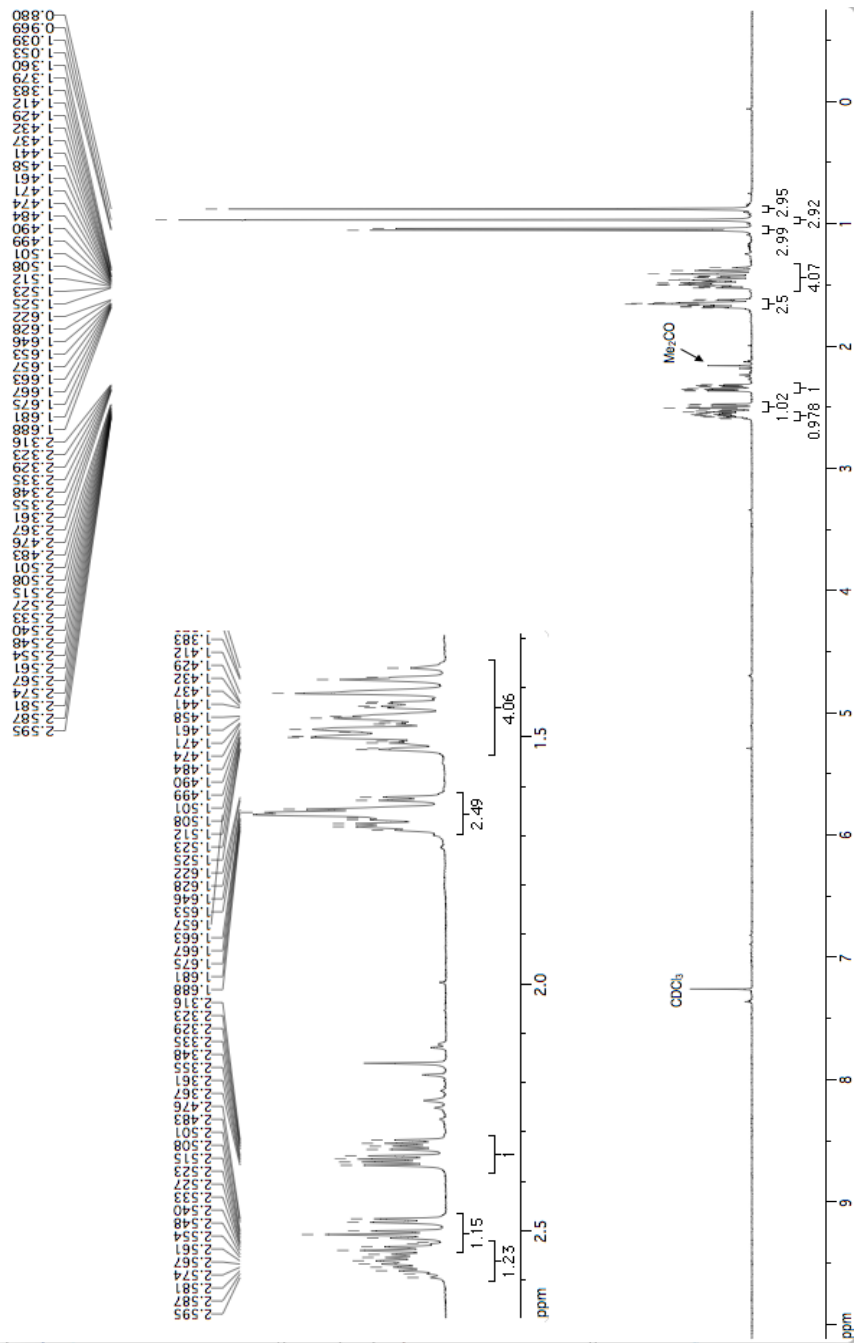


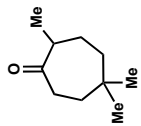
2.48a (^{13}C NMR, 126 MHz, CDCl_3 , 25 $^\circ\text{C}$)



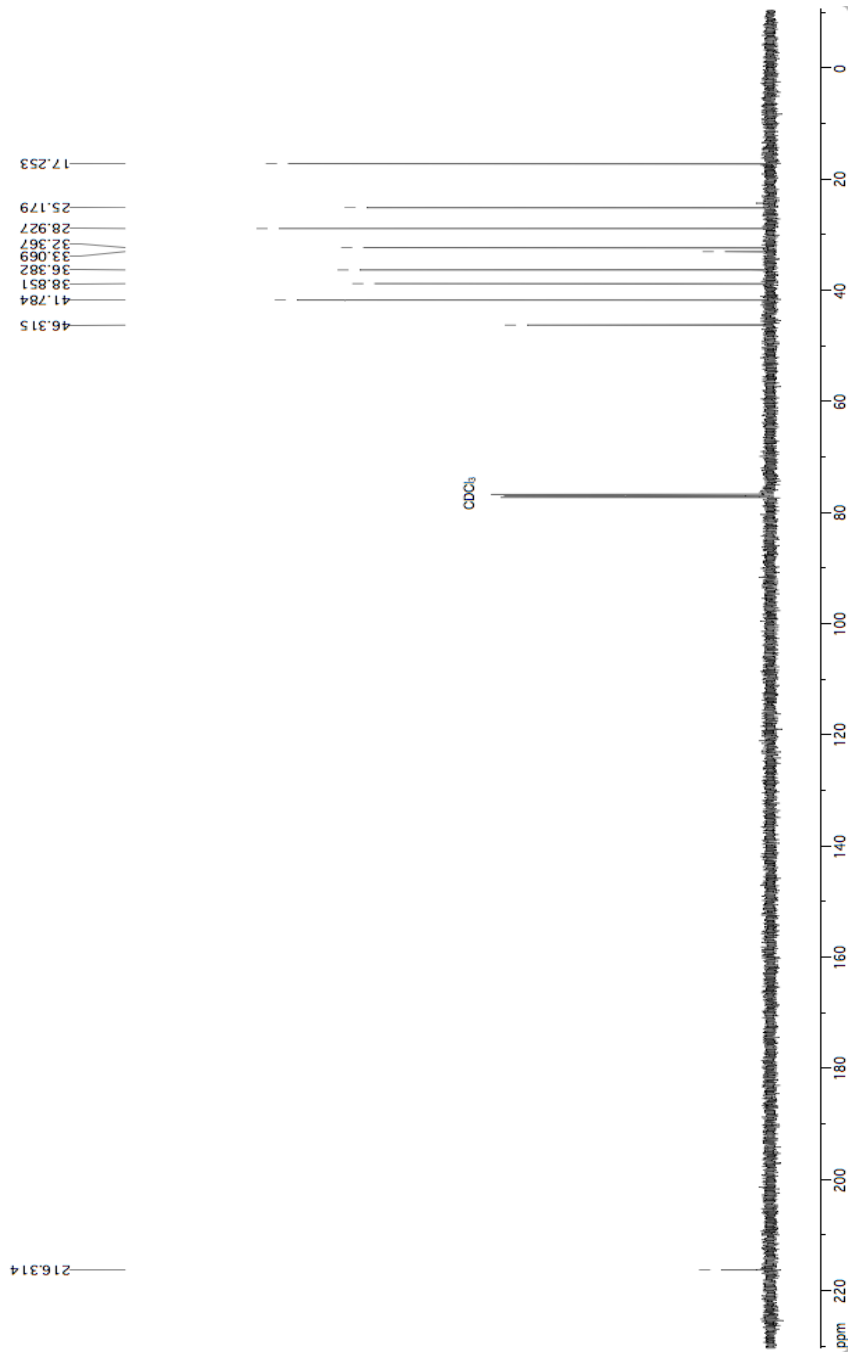


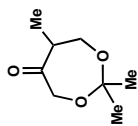
2.48b (¹H NMR, 500 MHz, CDCl₃, 25 °C)



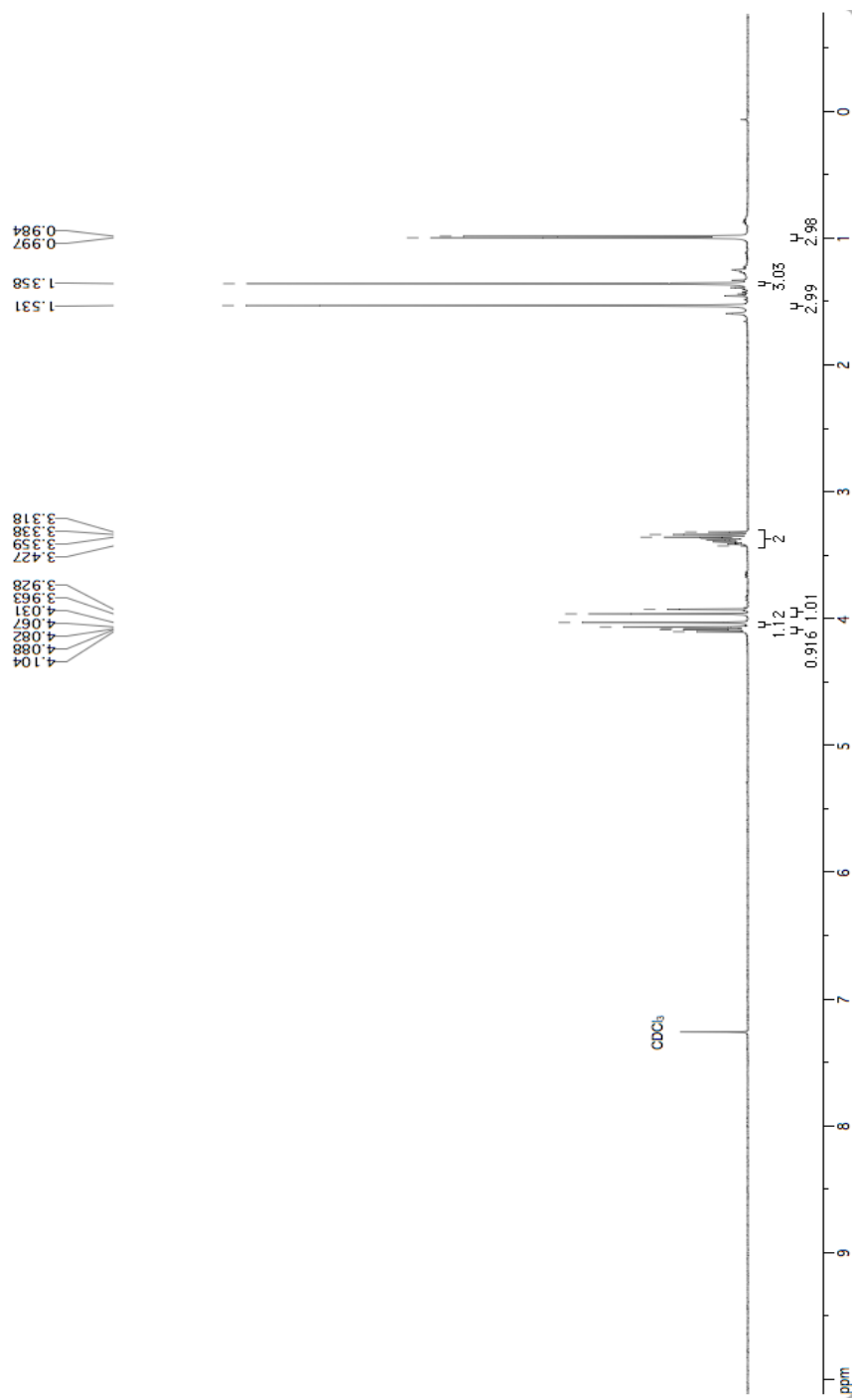


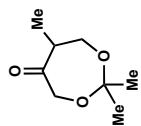
2.48b (¹³C NMR, 126 MHz, CDCl₃, 25 °C)



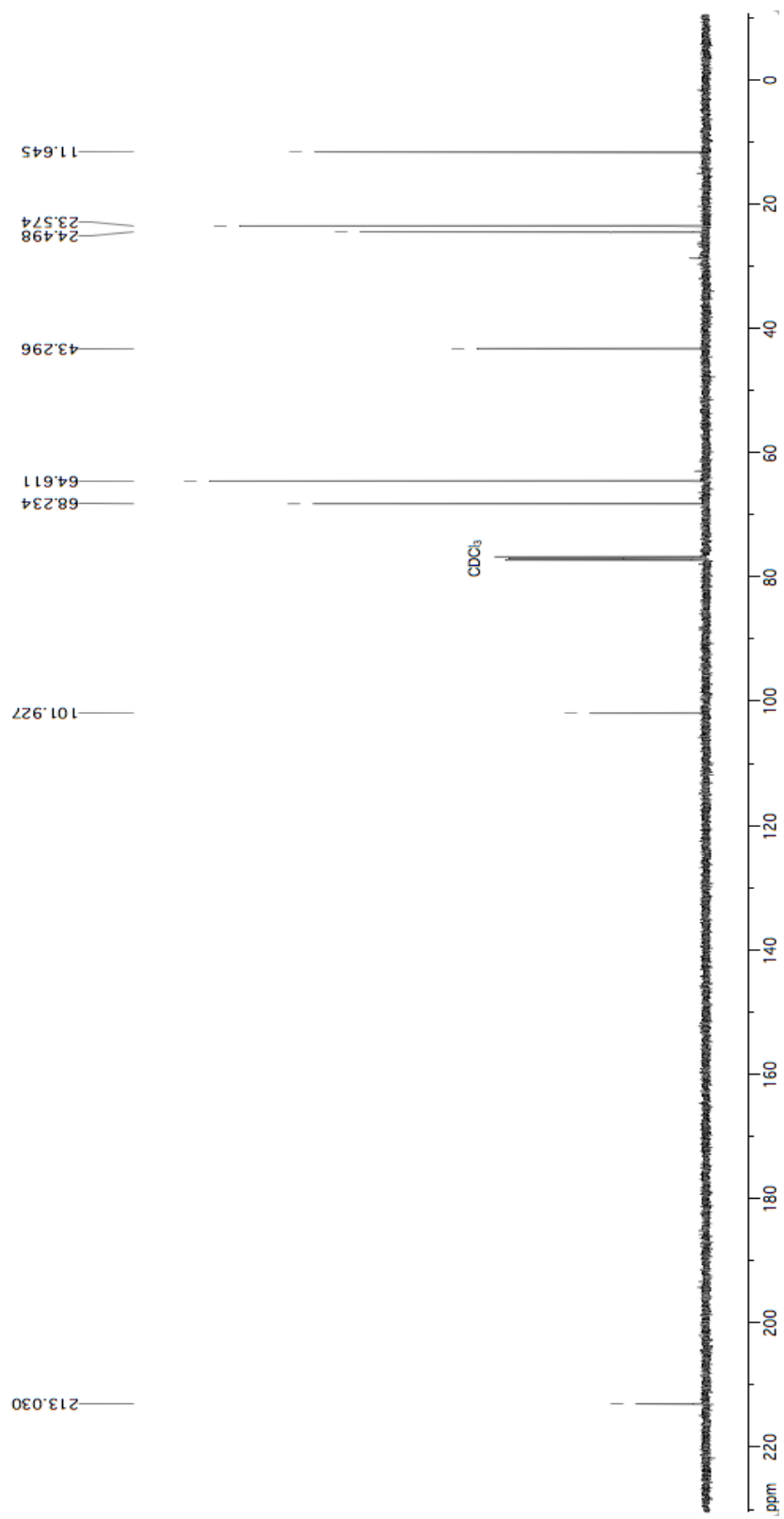


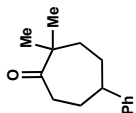
2.52b (¹H NMR, 500 MHz, CDCl₃, 25 °C)



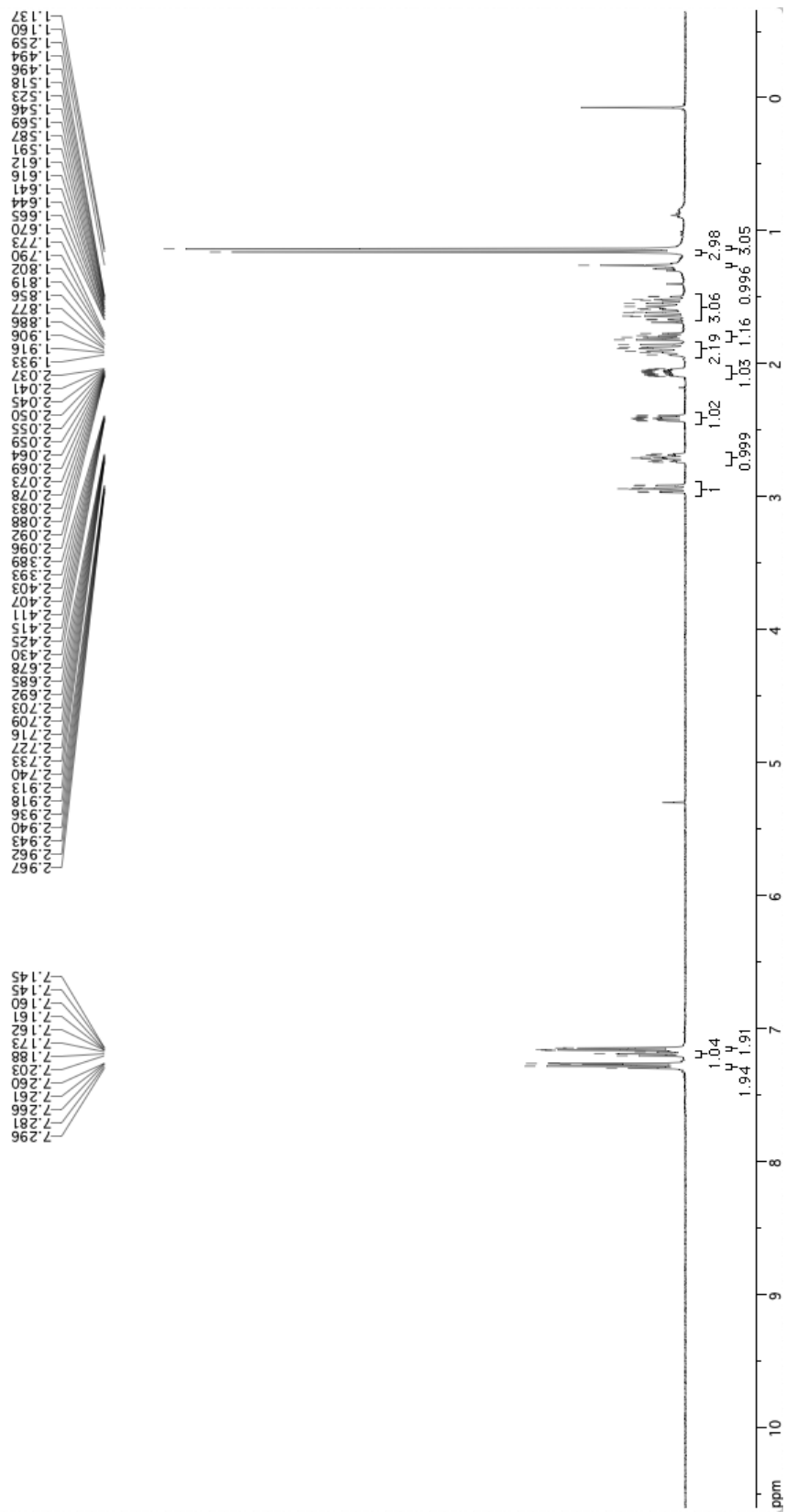


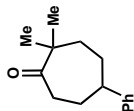
2.52b (¹³C NMR, 126 MHz, CDCl₃, 25 °C)



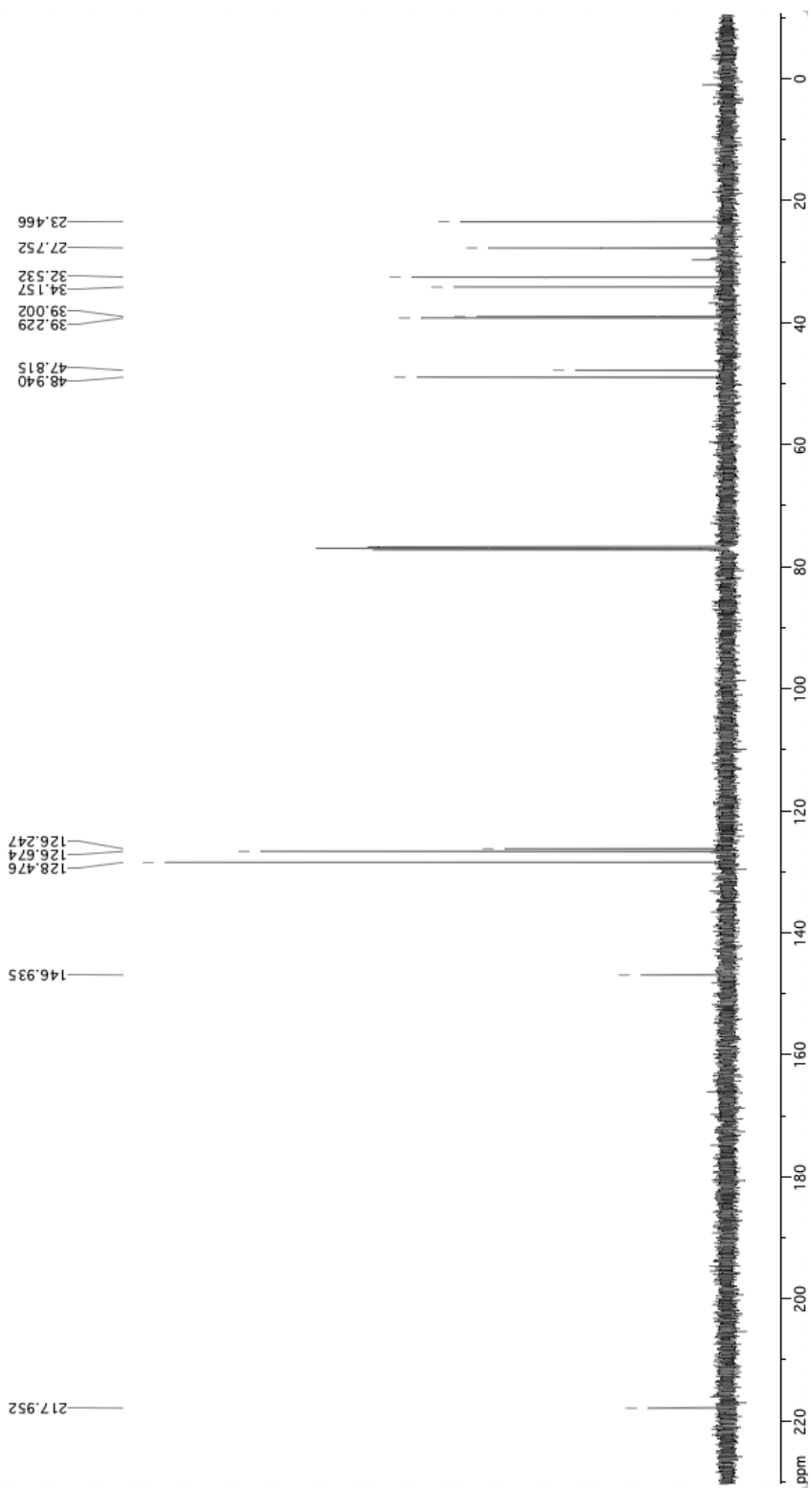


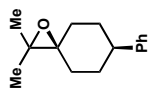
2.80 (1H NMR, 500 MHz, CDCl₃, 25 °C)



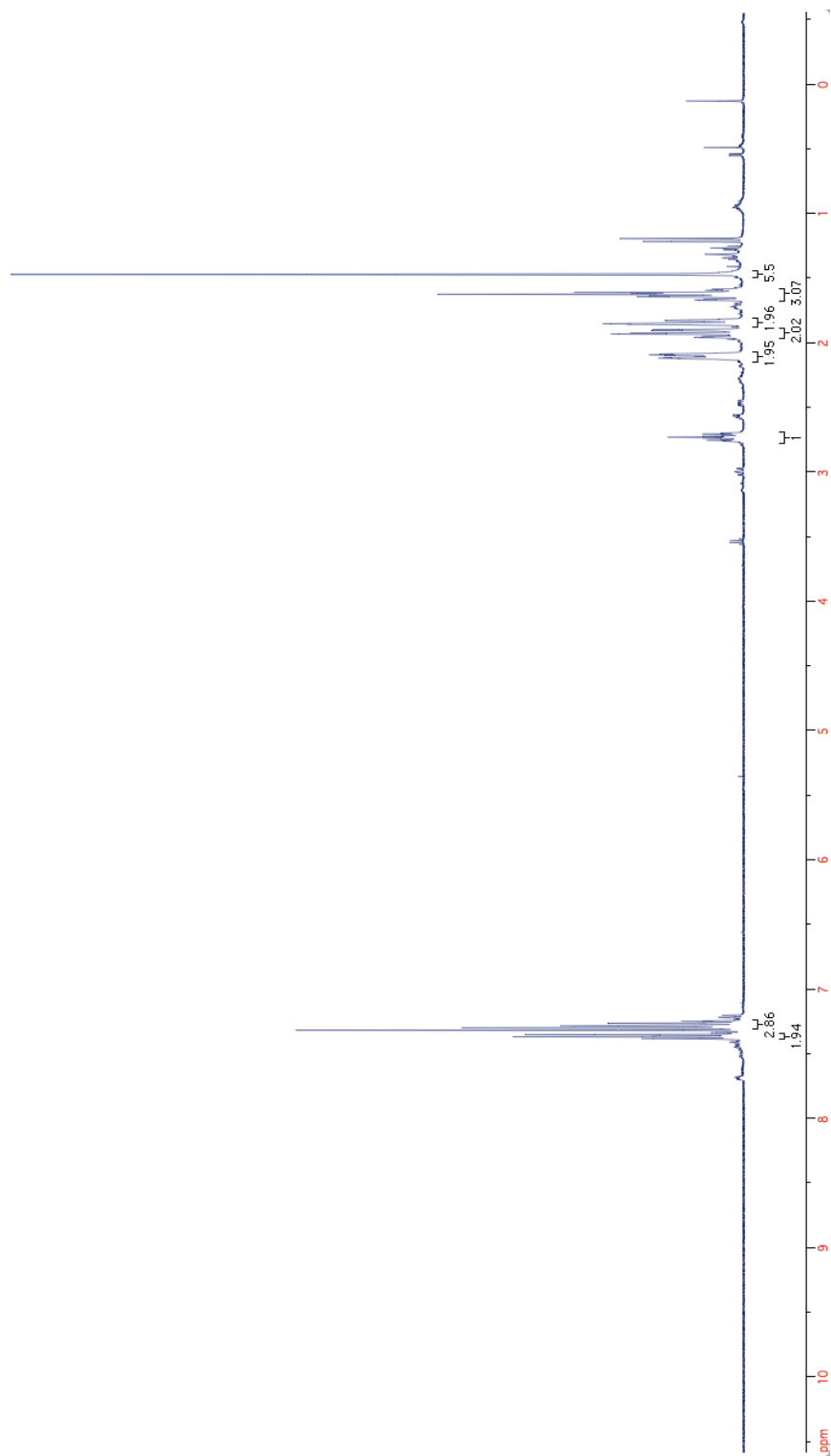


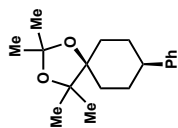
2.80 (¹³C NMR, 126 MHz, CDCl₃, 25 °C)



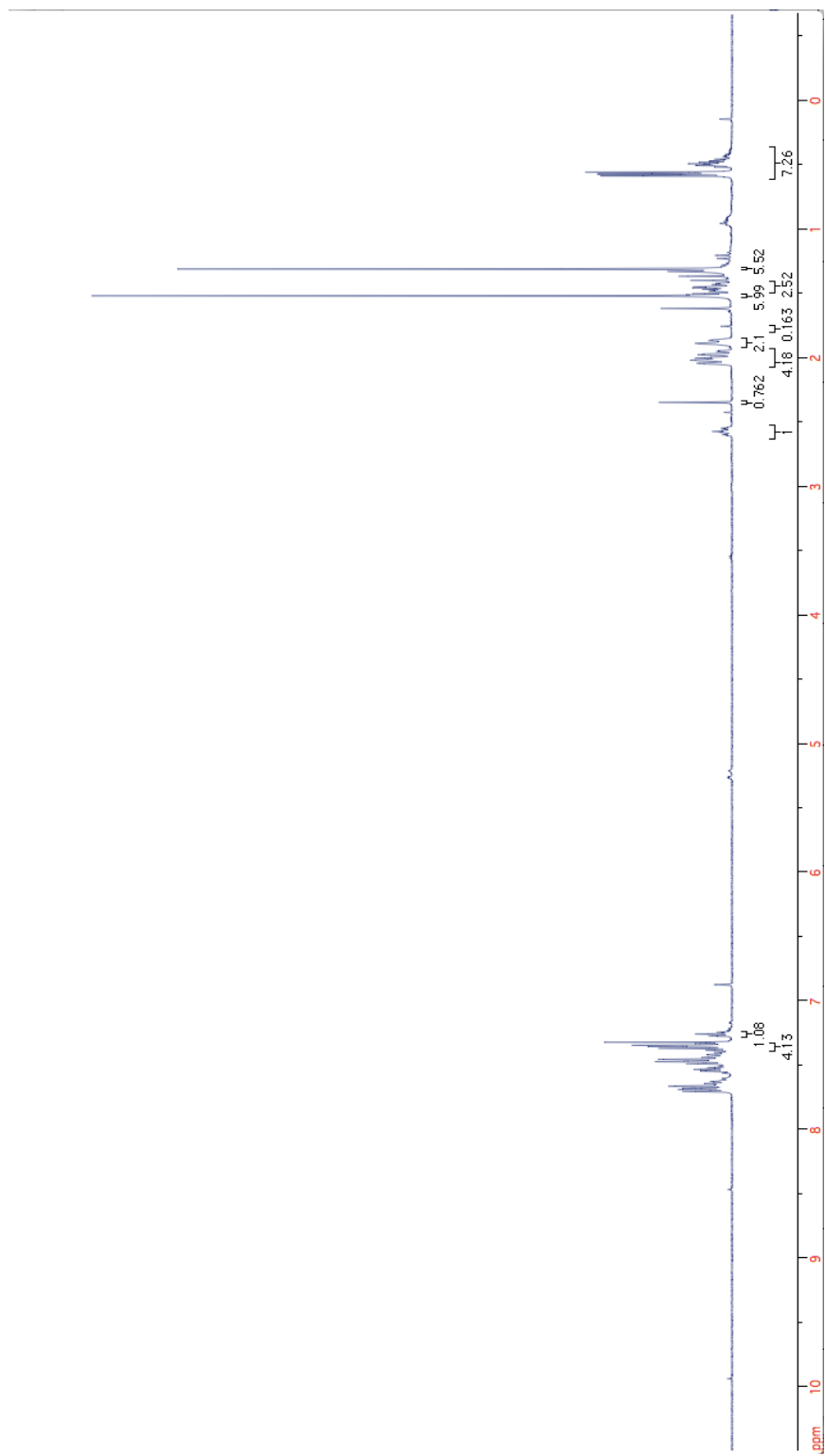


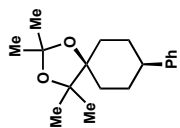
2.81 (¹H NMR, 500 MHz, CDCl₃, 25 °C)



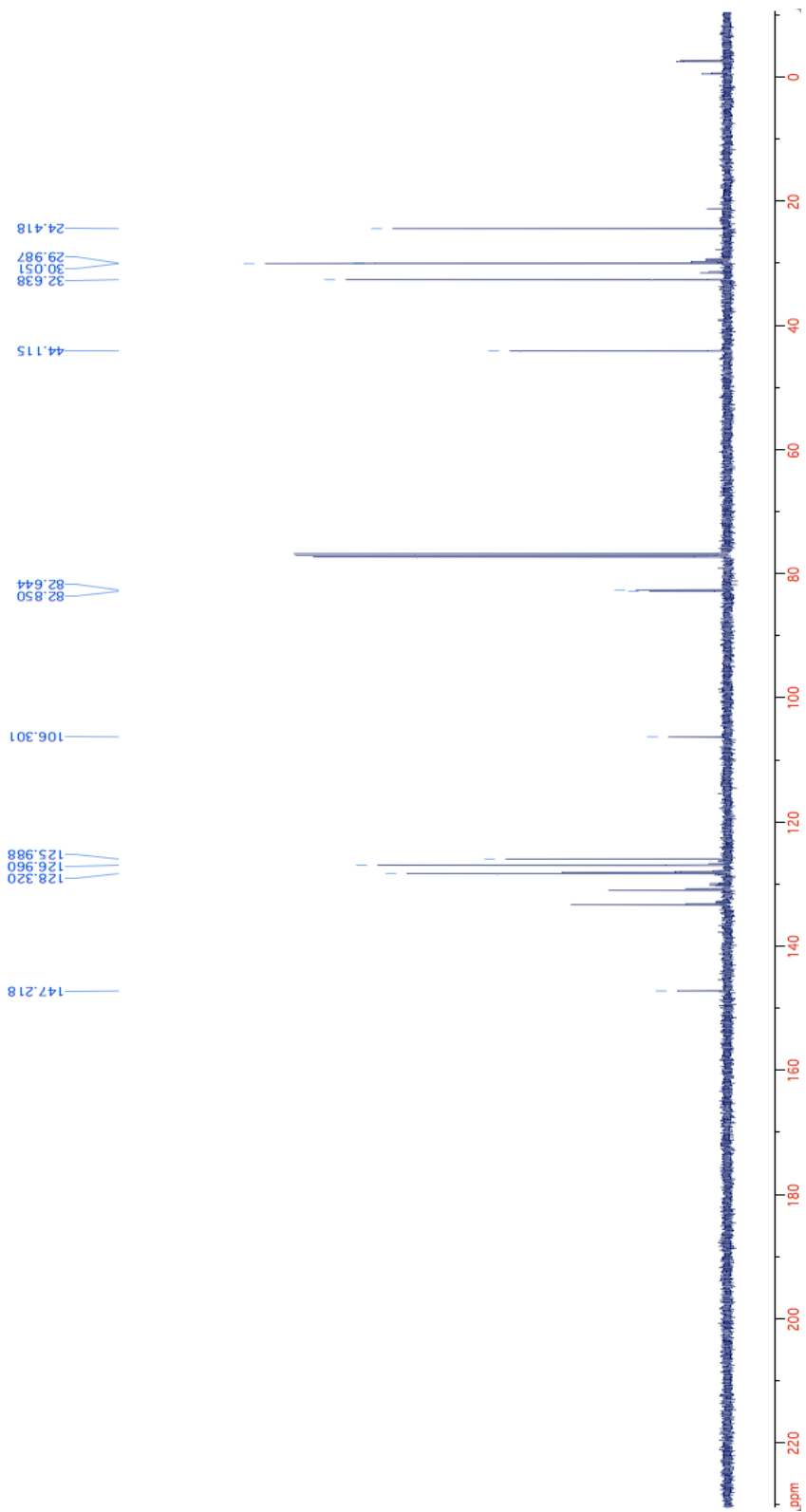


2.83 (¹H NMR, 500 MHz, CDCl₃, 25 °C)

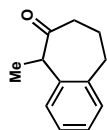




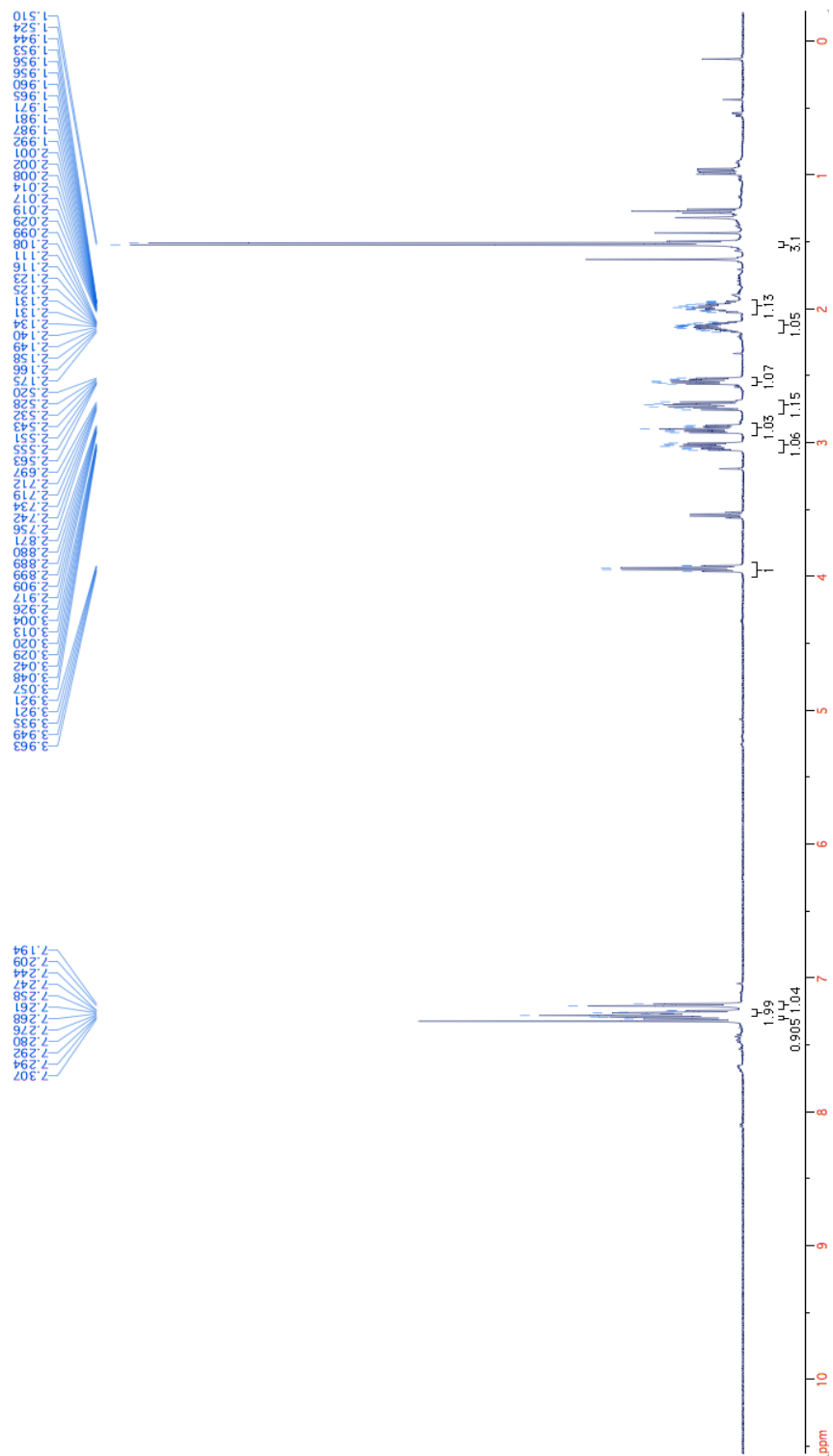
2.82 (¹³C NMR, 126 MHz, CDCl₃, 25 °C)

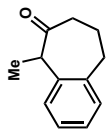


NMR spectra of known compounds reported in Table 2.4

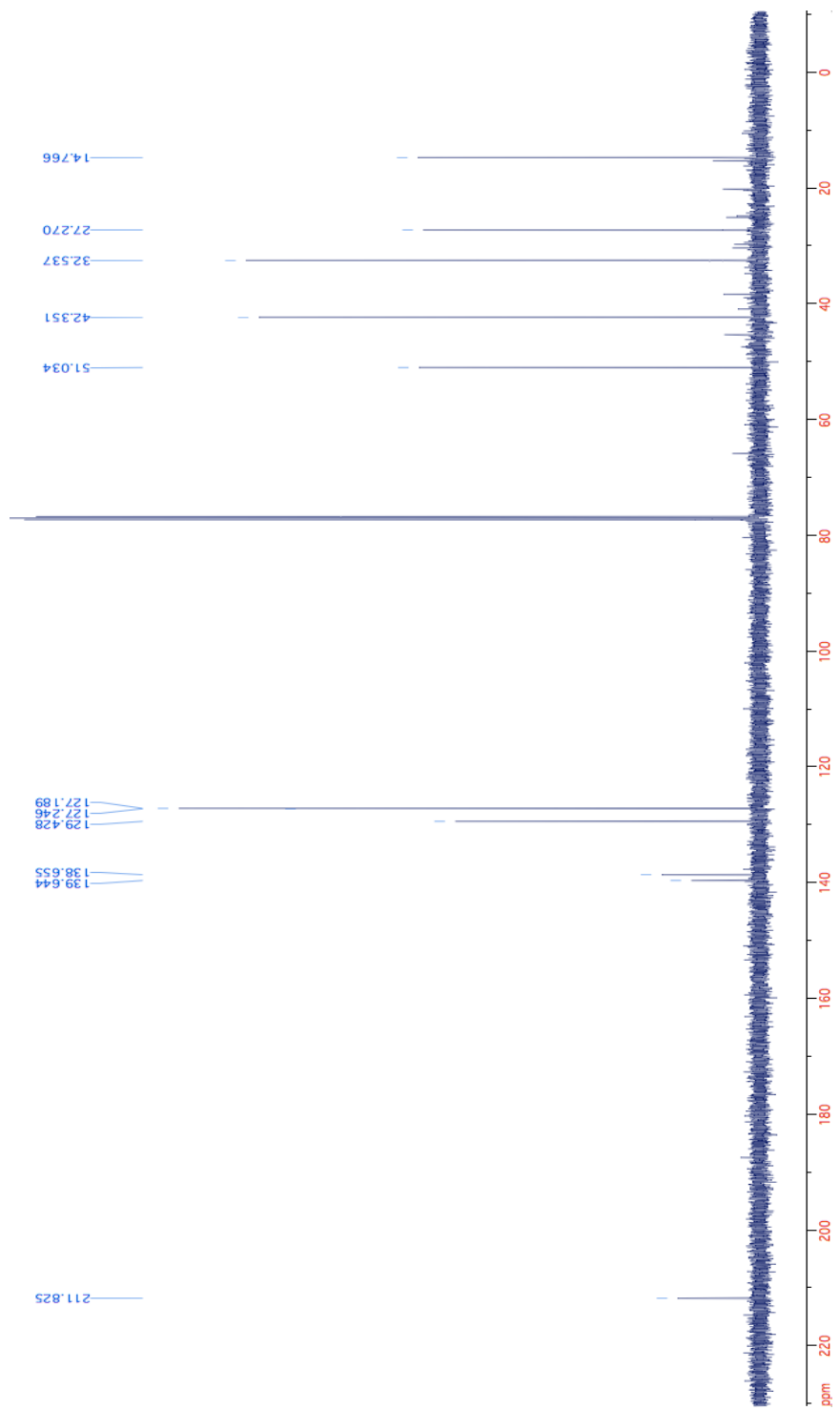


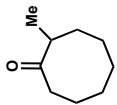
2.57b (¹H NMR, 500 MHz, CDCl₃, 25 °C)



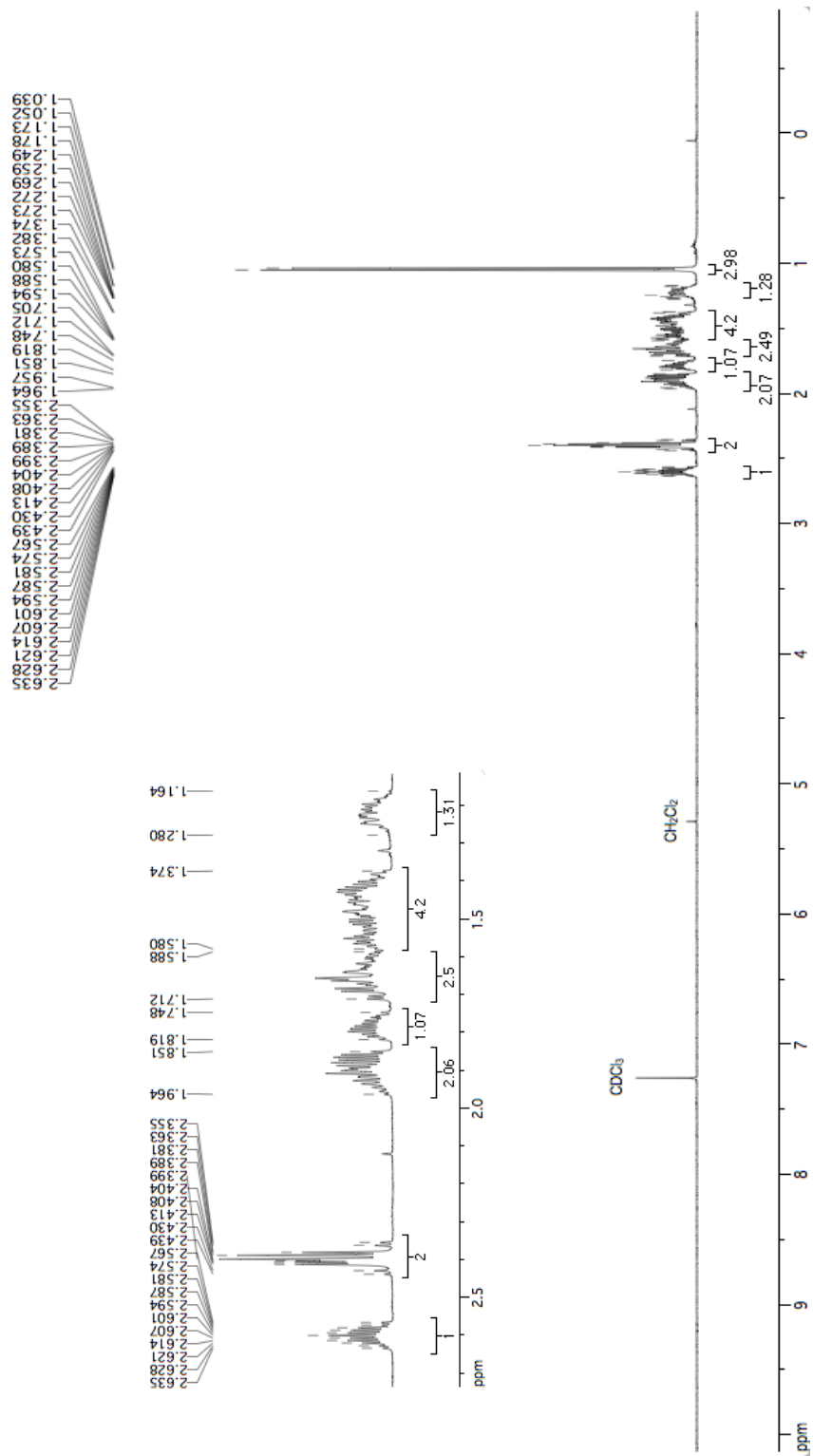


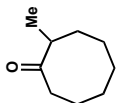
2.57b (¹³C NMR, 126 MHz, CDCl₃, 25 °C)



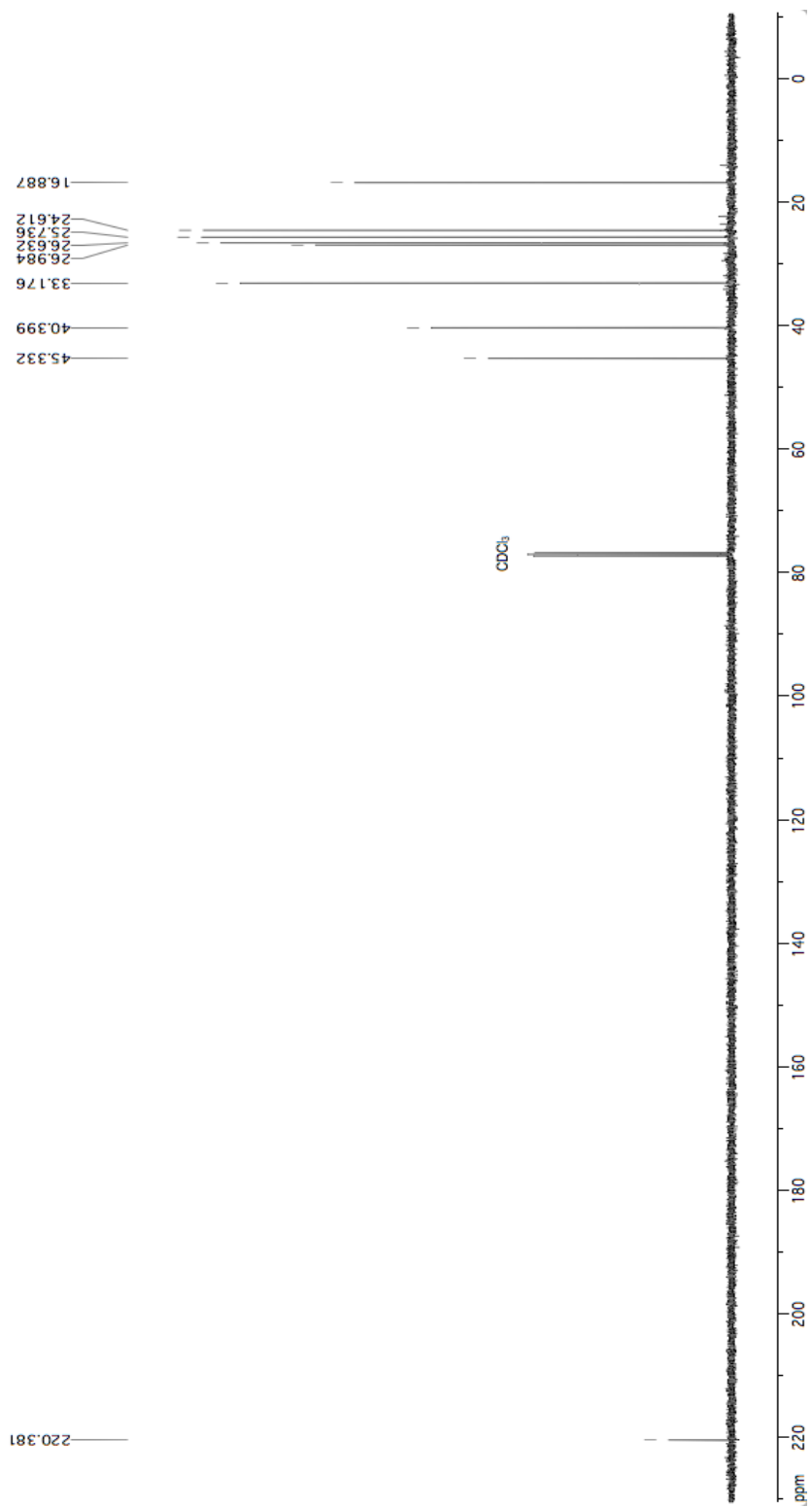


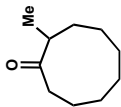
2.58b (¹H NMR, 500 MHz, CDCl₃, 25 °C)



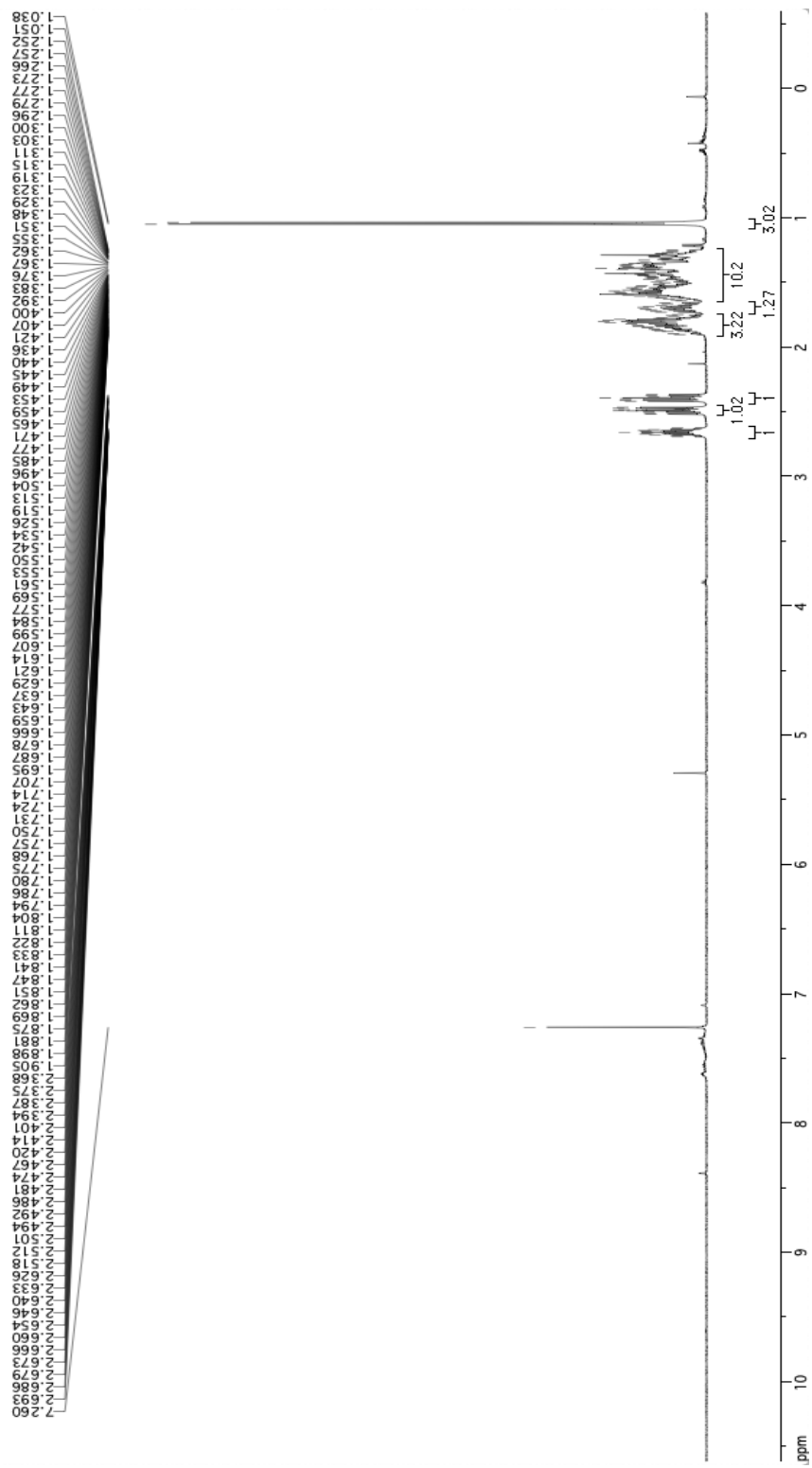


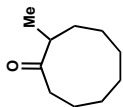
2.68b (^{13}C NMR, 126 MHz, CDCl_3 , 25 $^\circ\text{C}$)



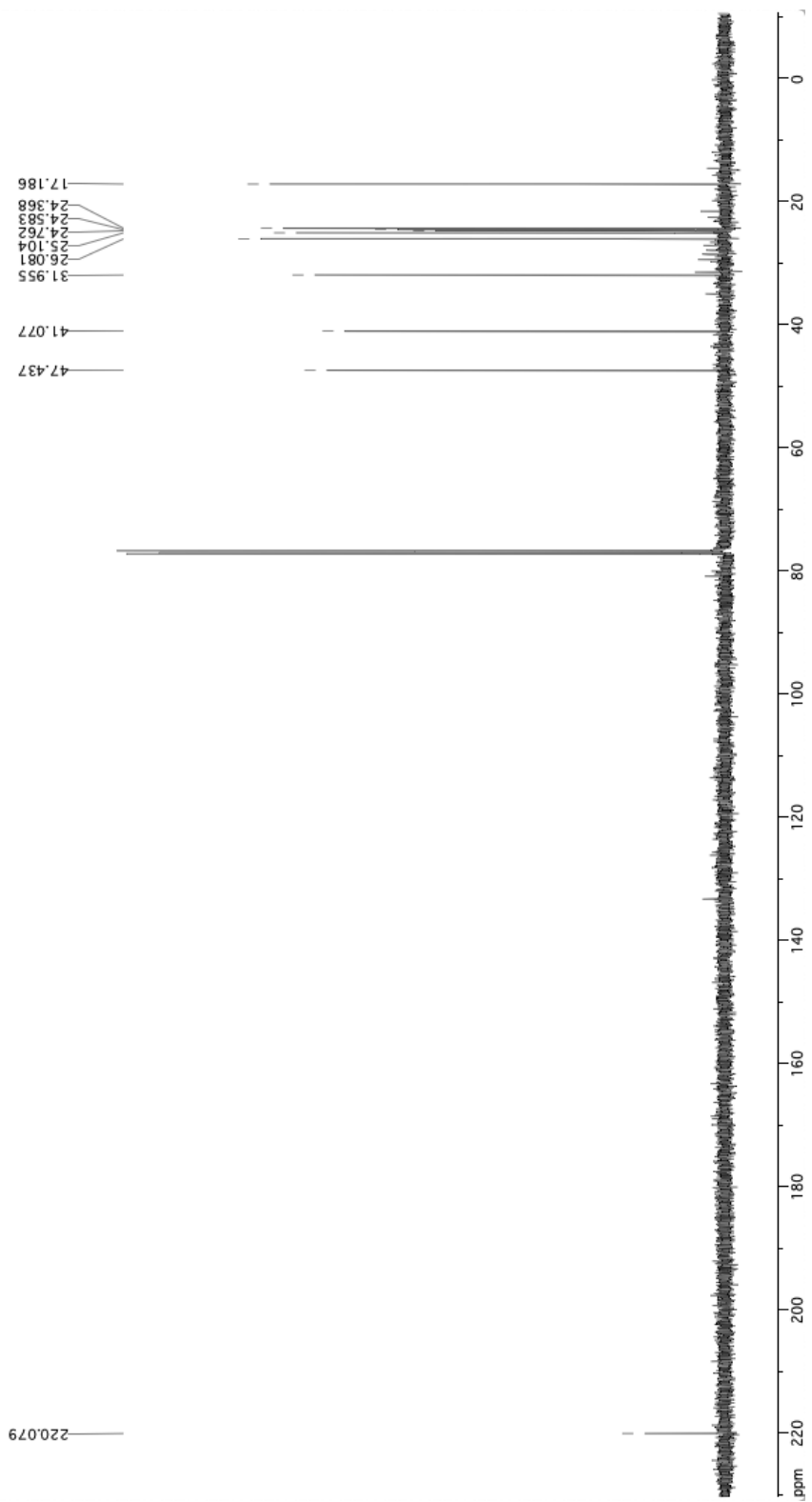


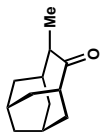
2.59b (¹H NMR, 500 MHz, CDCl₃, 25 °C)



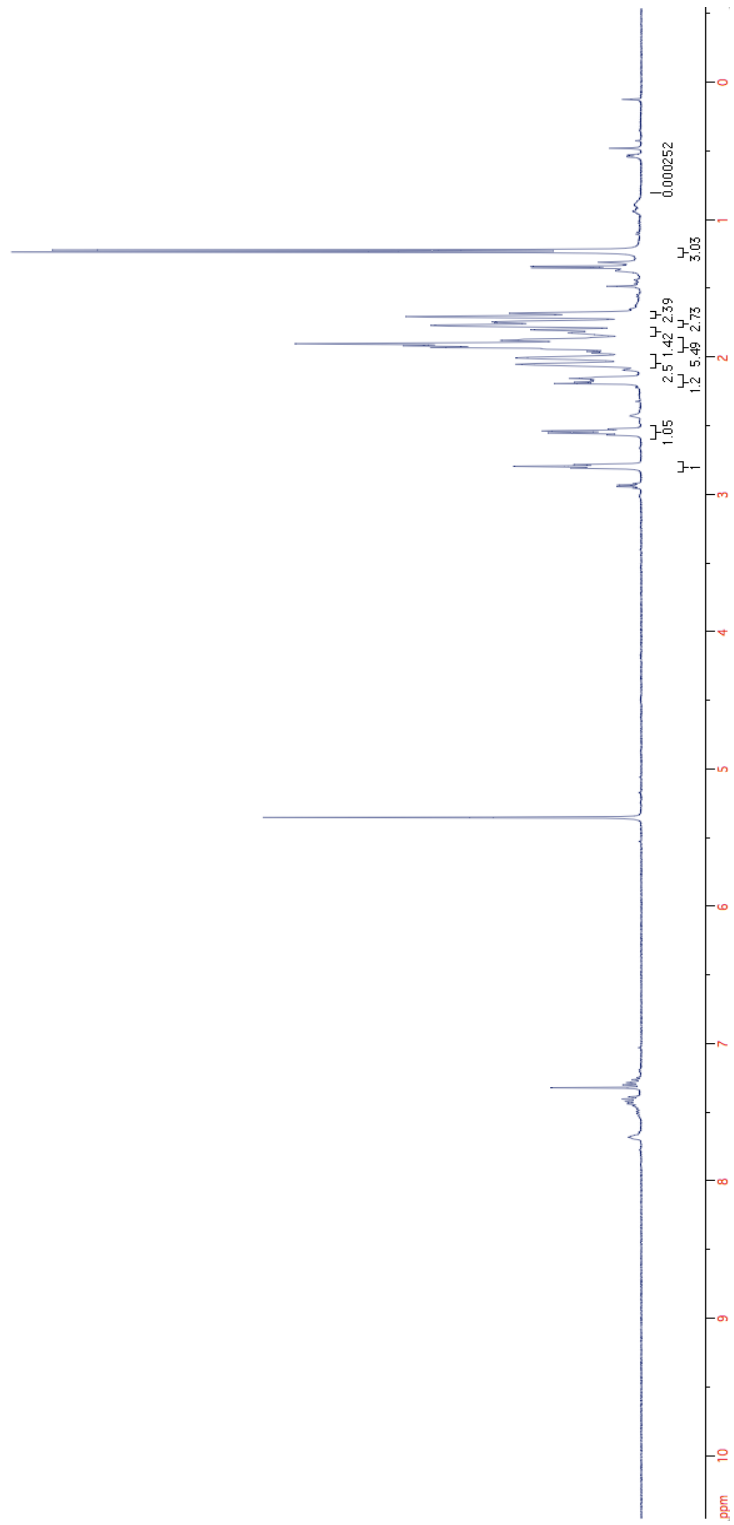


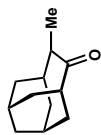
2.59b (^{13}C NMR, 126 MHz, CDCl_3 , 25 $^\circ\text{C}$)



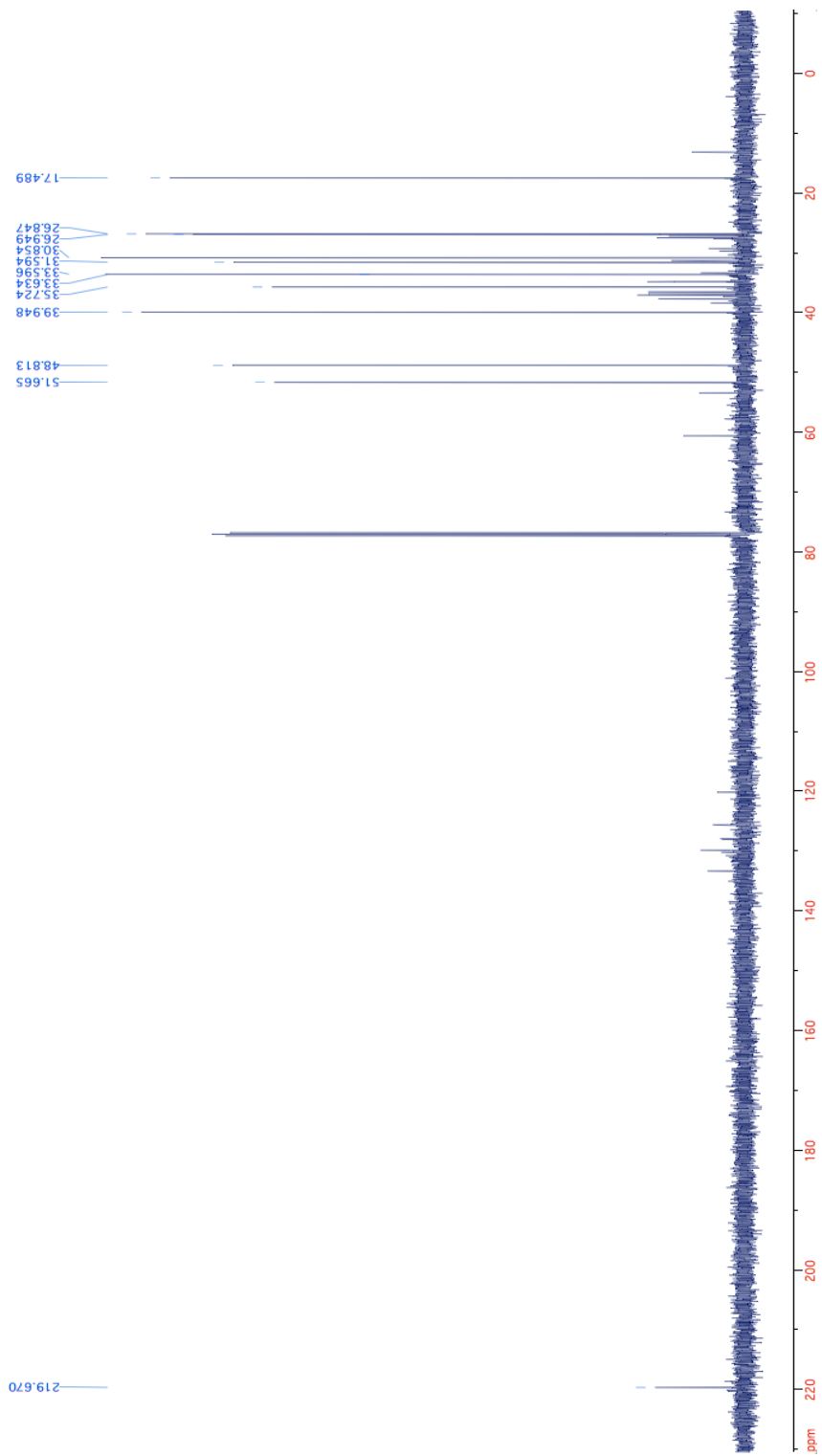


2.62b (¹H NMR, 500 MHz, CDCl₃, 25 °C)

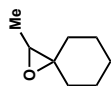




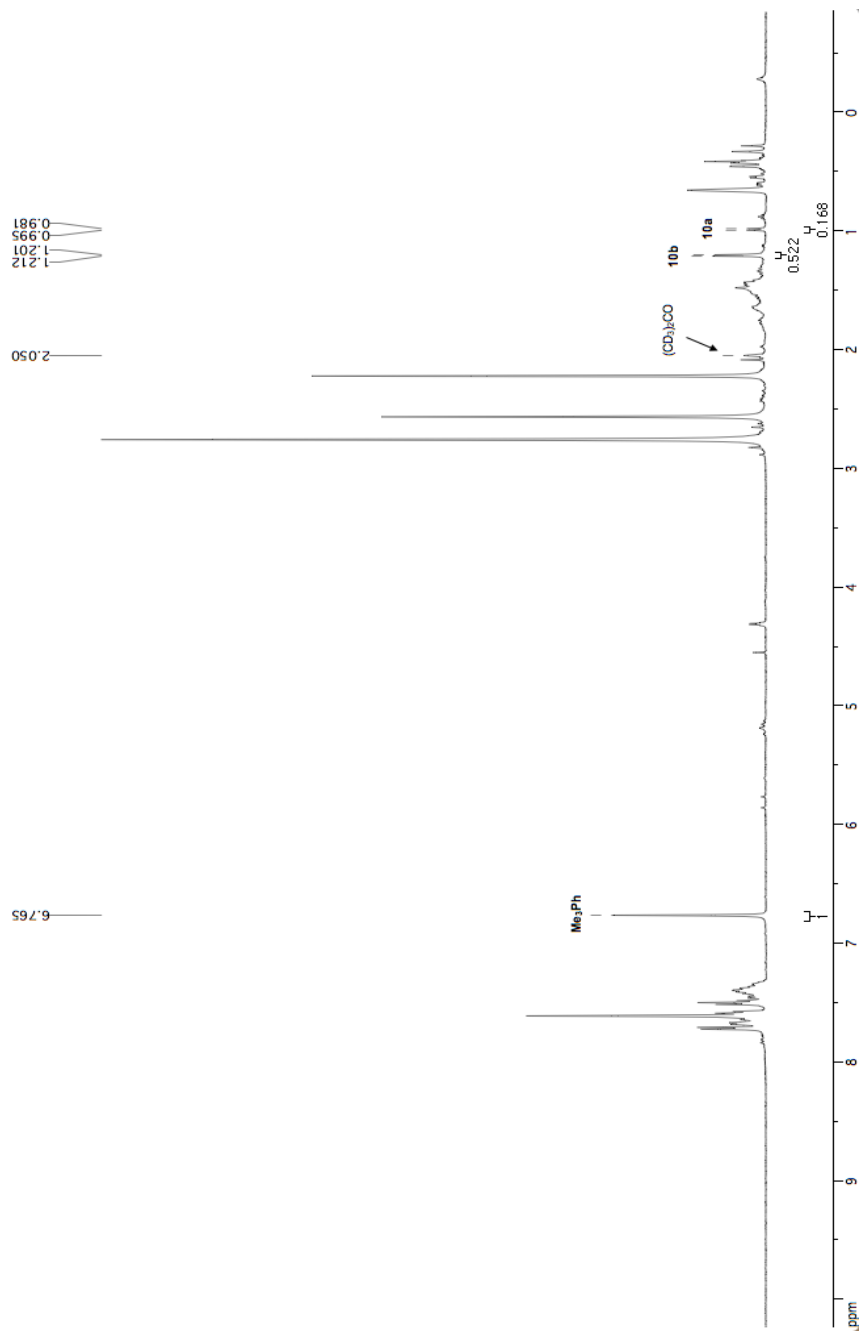
2.62b (¹³C NMR, 126 MHz, CDCl₃, 25 °C)

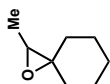


NMR spectra for NMR yields of compounds in Table 2.4



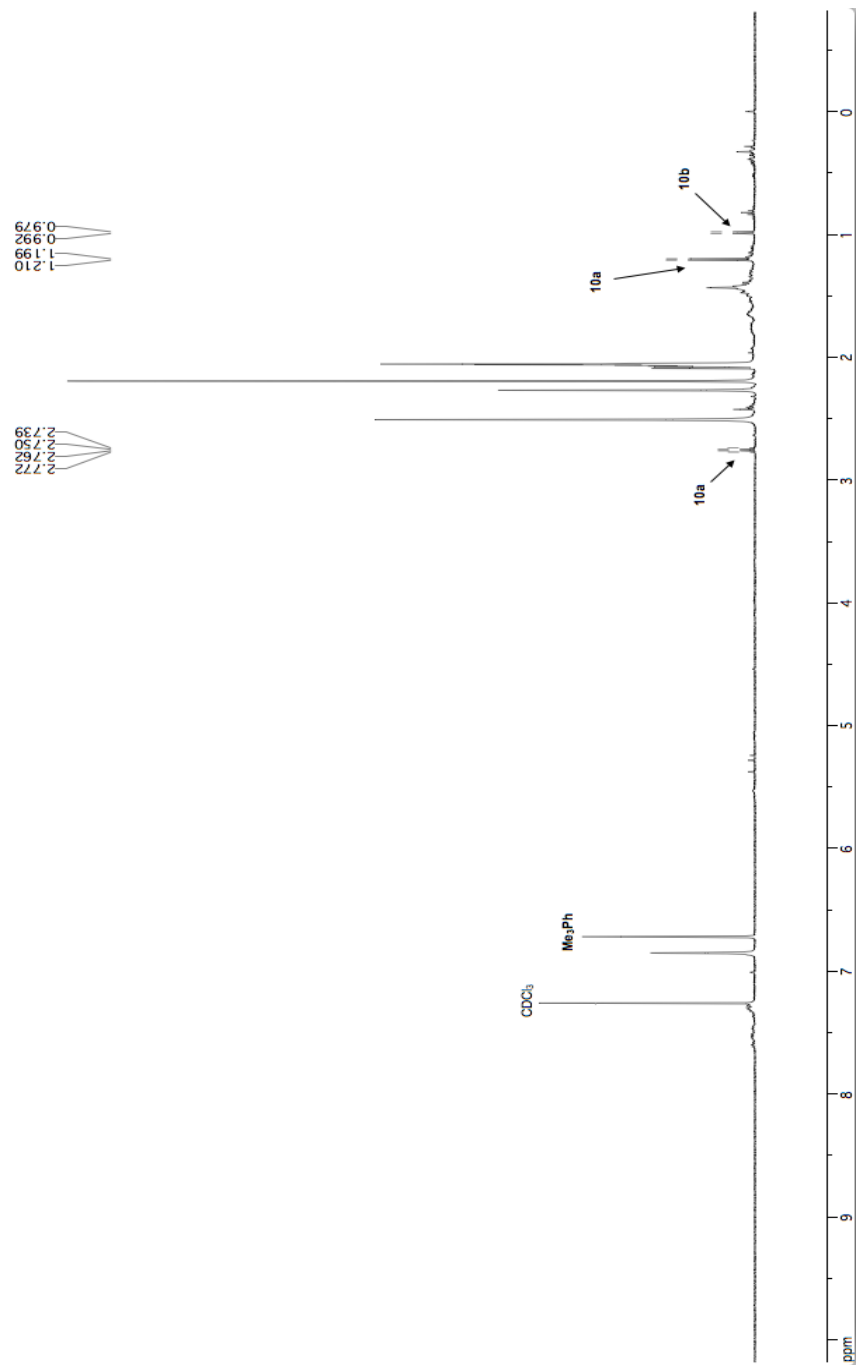
2.42a (¹H NMR, 500 MHz, (CD₃)₂CO, 25 °C)
Crude reaction mixture with mesitylene internal standard

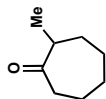




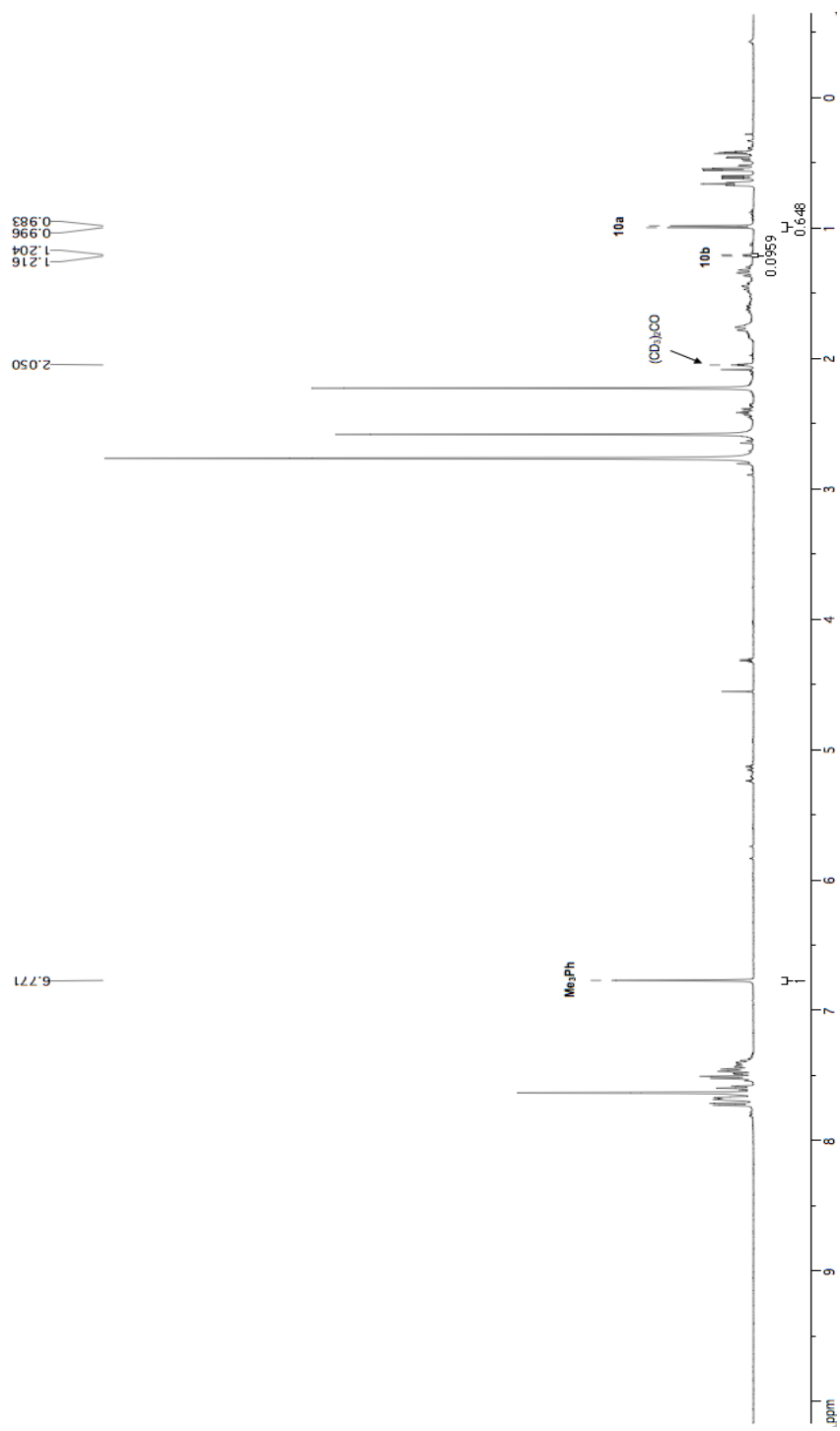
2.42a (¹H NMR, 500 MHz, CDCl₃, 25 °C)

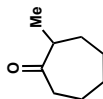
Crude reaction mixture with mesitylene internal standard





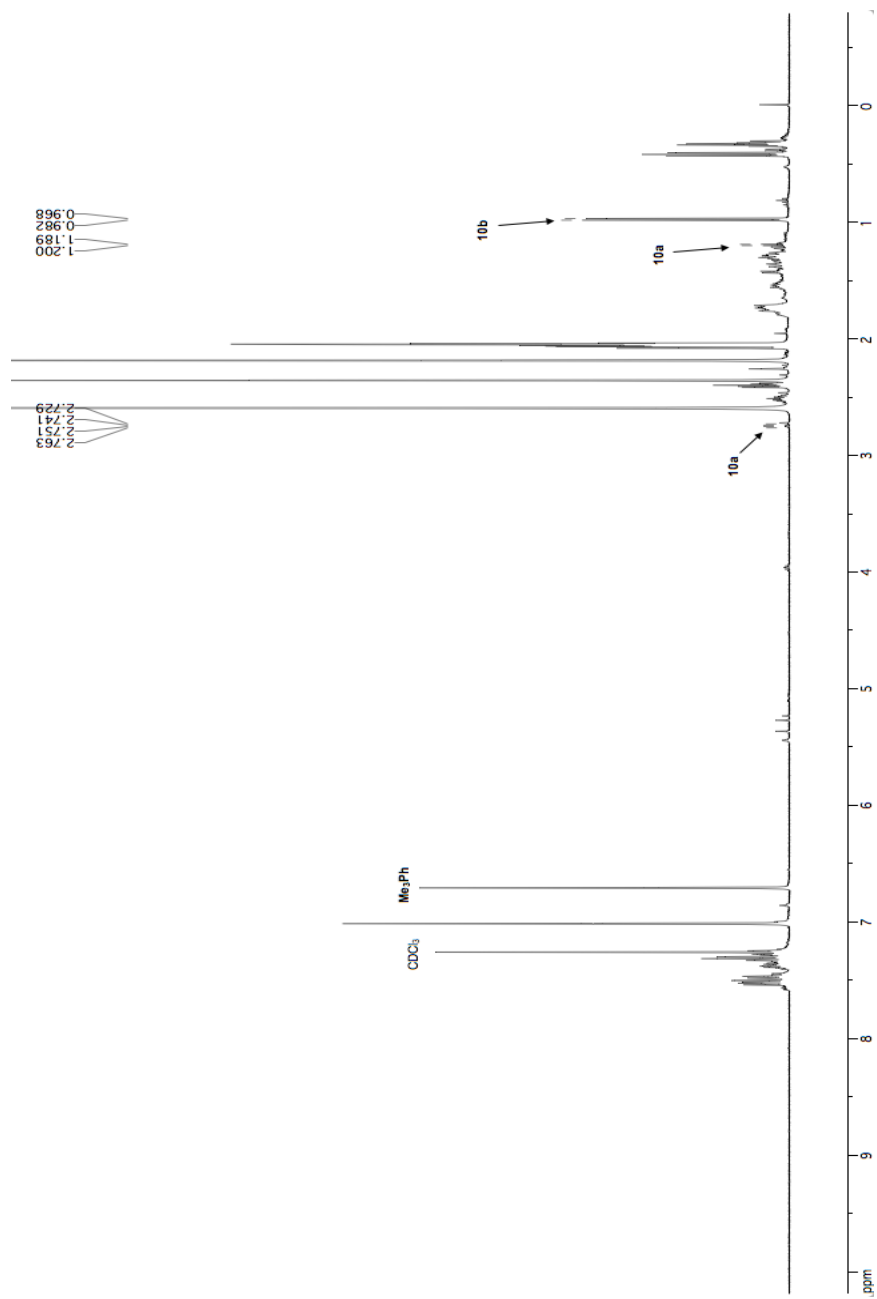
2.42b (¹H NMR, 500 MHz, (CD₃)₂CO, 25 °C)
Crude reaction mixture with mesitylene internal standard

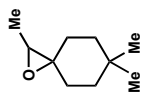




2.42b (¹H NMR, 500 MHz, CDCl₃, 25 °C)

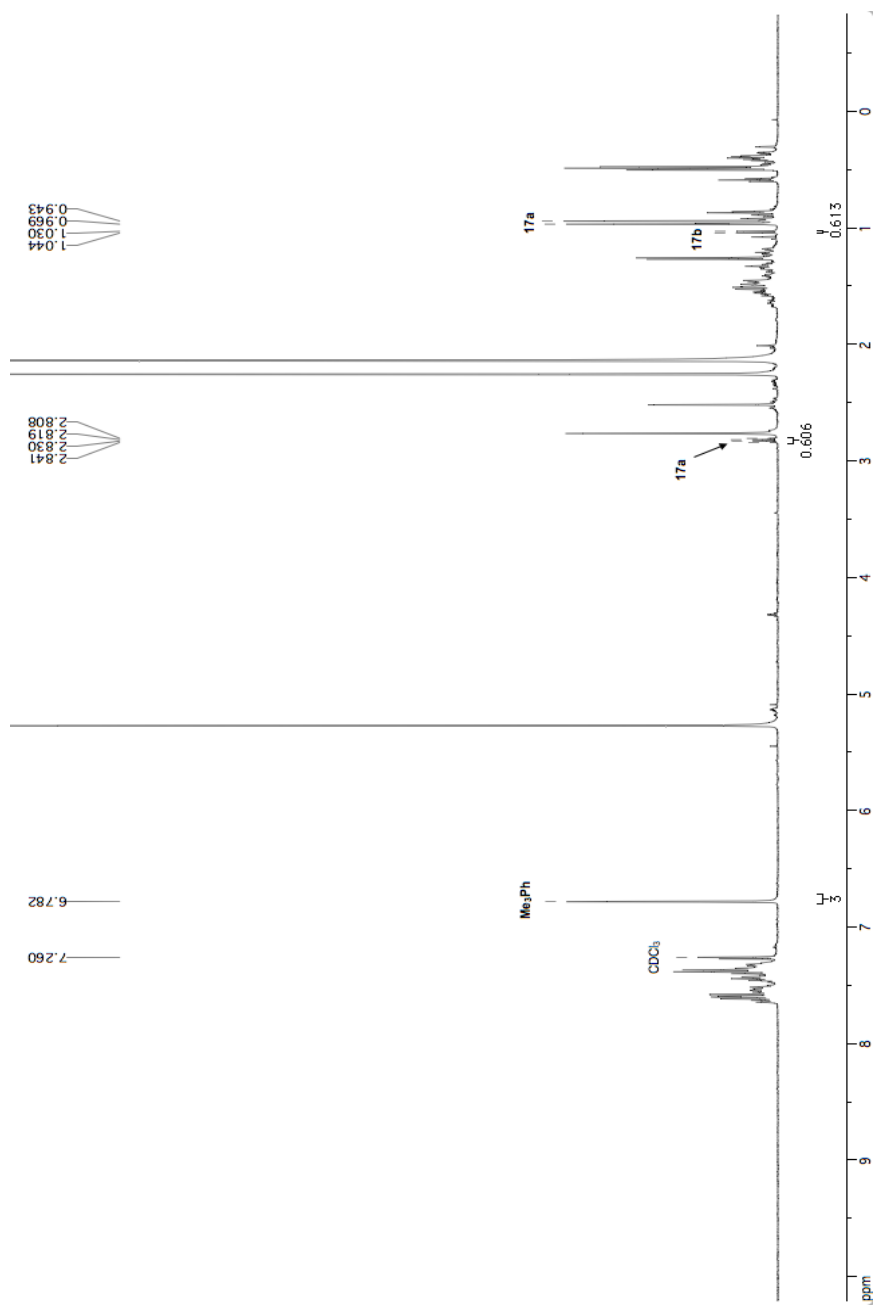
Crude reaction mixture with mesitylene internal standard

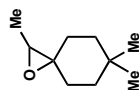




2.48a (¹H NMR, 500 MHz, CDCl₃, 25 °C)

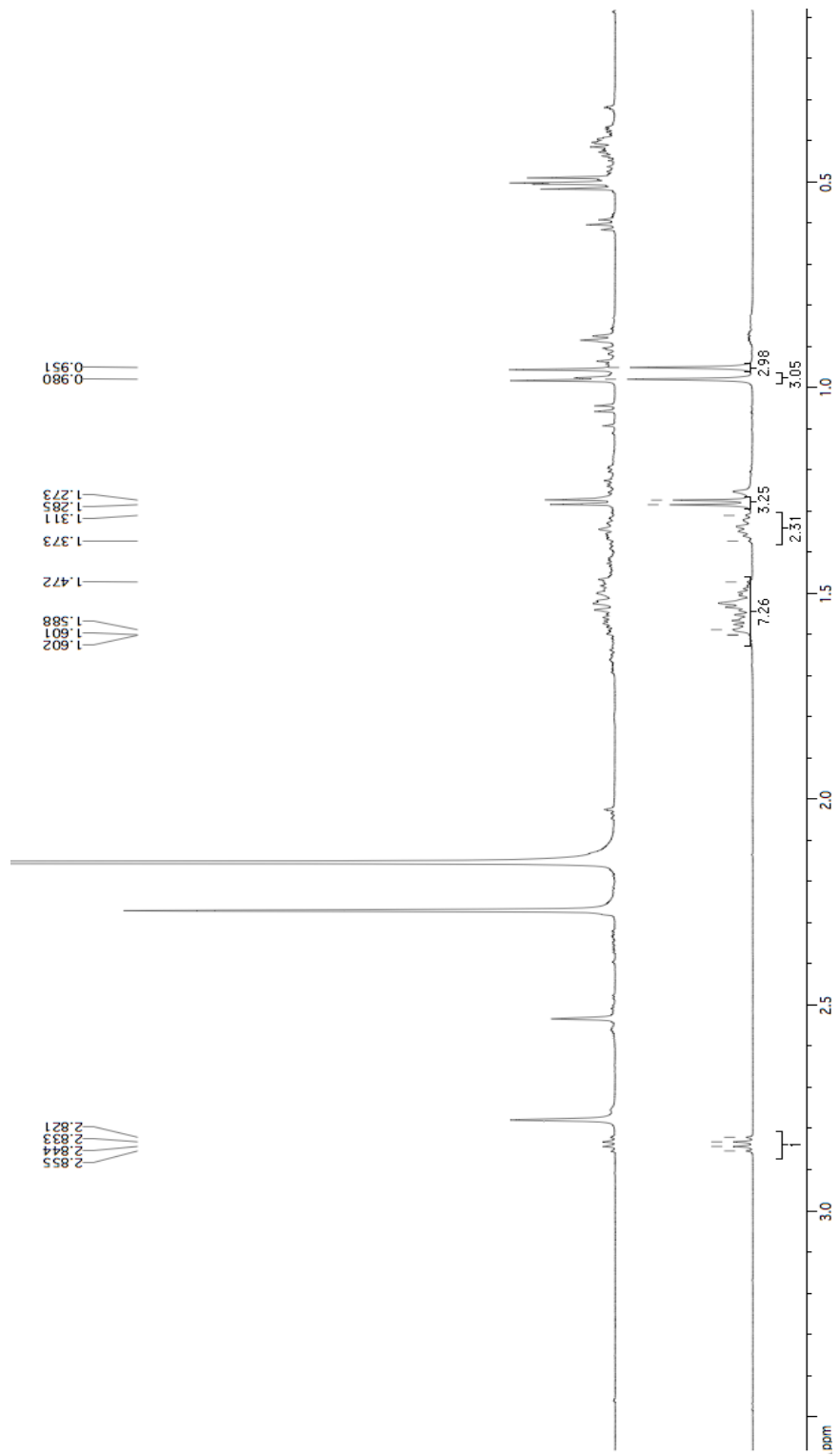
Crude reaction mixture with mesitylene internal standard





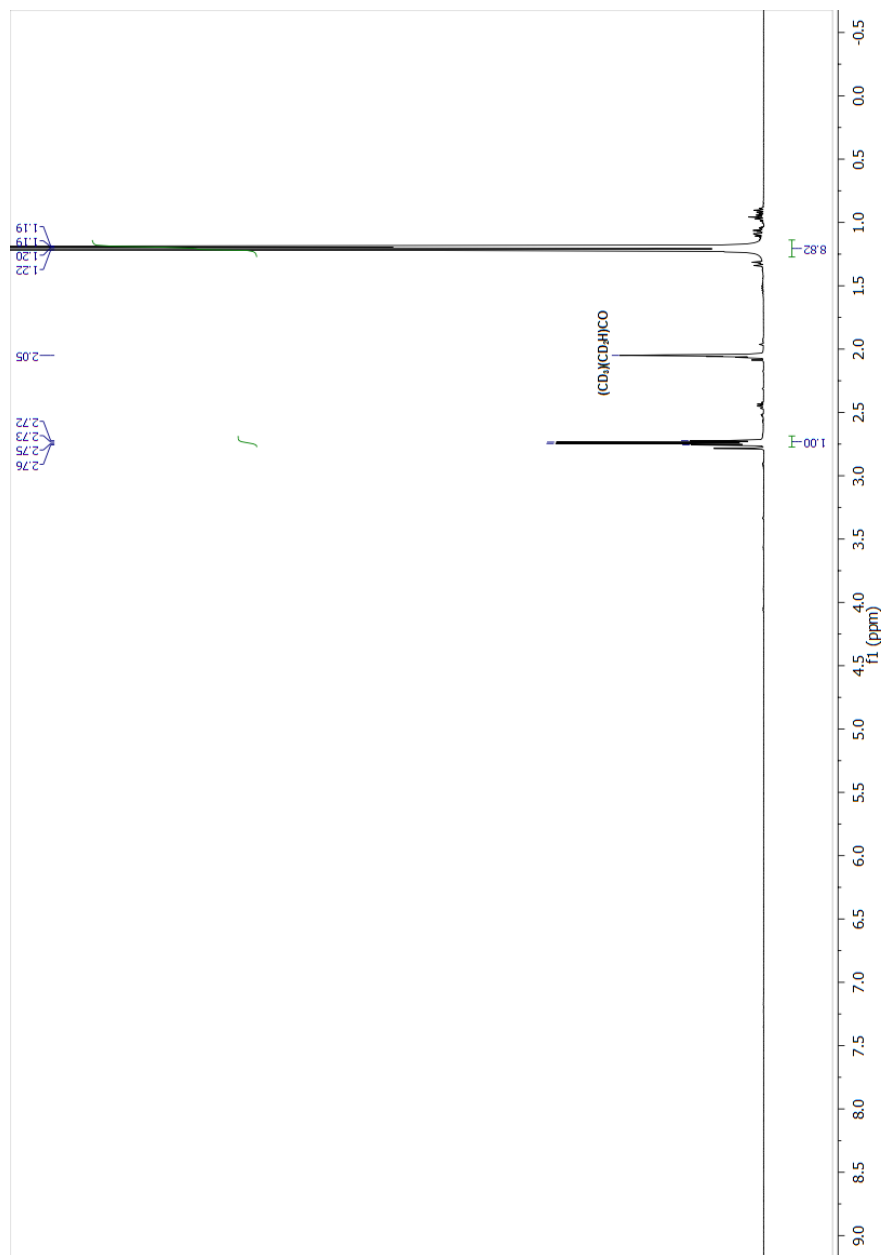
2.48a (¹H NMR, 500 MHz, CDCl₃, 25 °C)

Overlay of analytical standard with crude reaction mixture



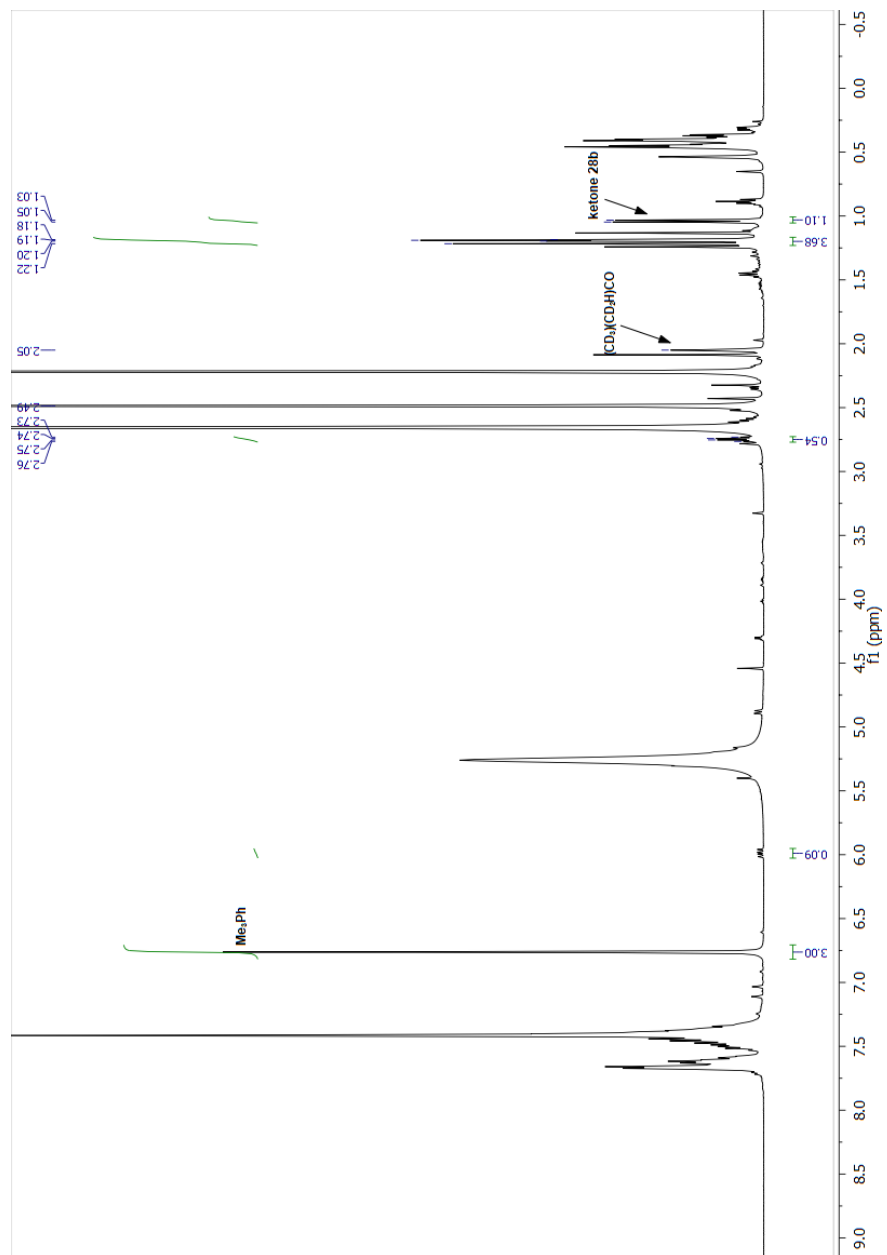


2.63a (¹H NMR, 500 MHz, (CD₃)₂CO, 25 °C)
Analytical standard, 97% from Sigma-Aldrich





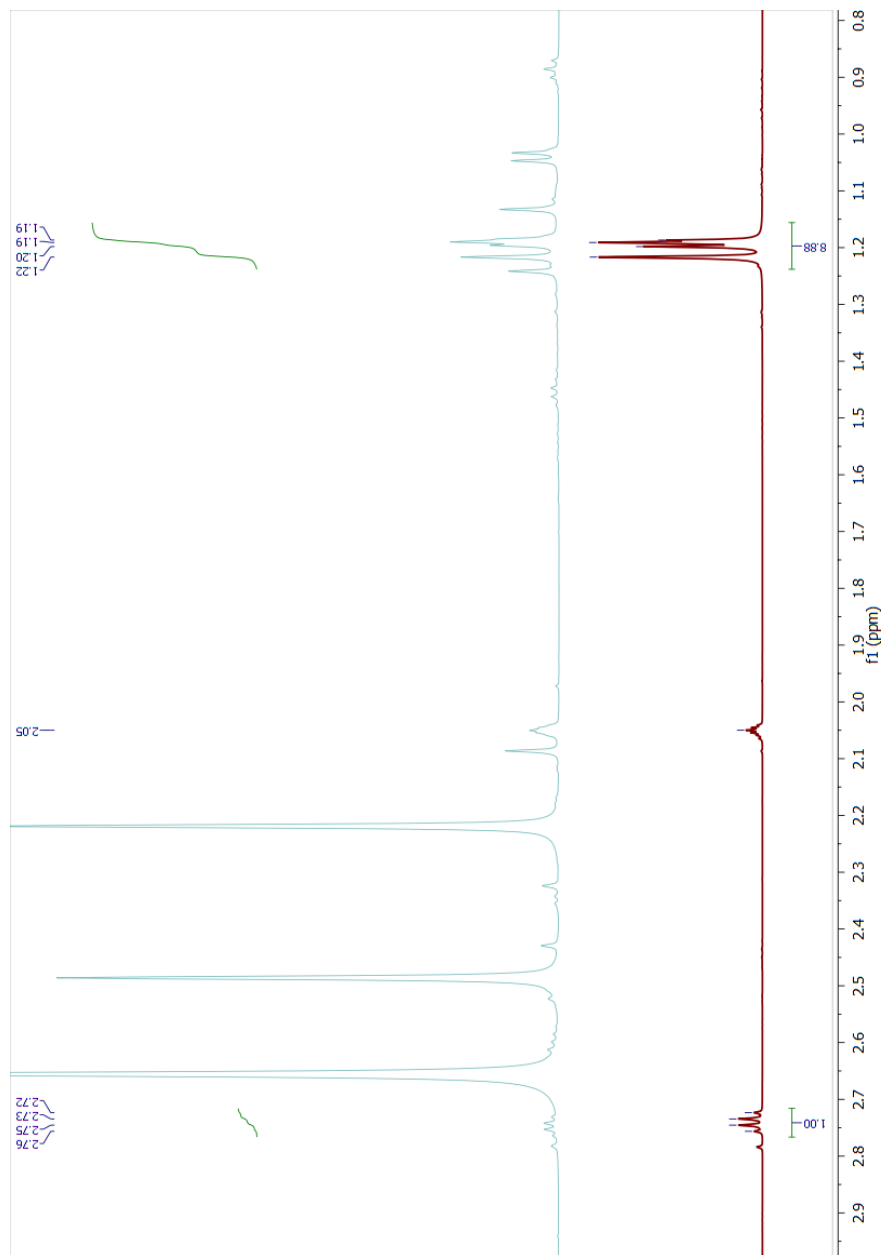
2.63a (^1H NMR, 500 MHz, $(\text{CD}_3)_2\text{CO}$, 25 $^\circ\text{C}$)
 Crude reaction mixture with mesitylene internal standard

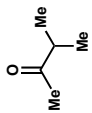




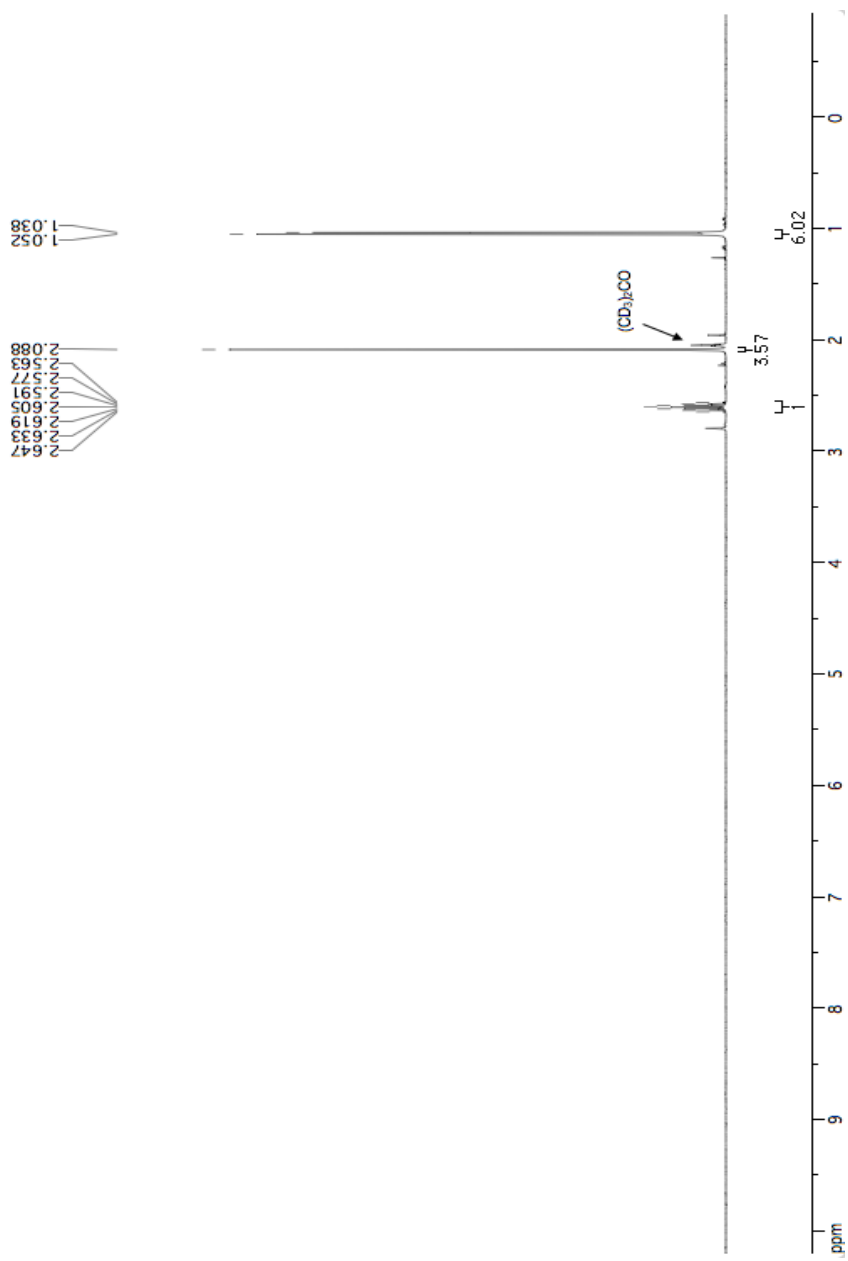
2.63a (¹H NMR, 500 MHz, (CD₃)₂CO, 25 °C)

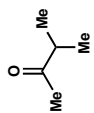
Overlay of analytical standard and crude reaction mixture





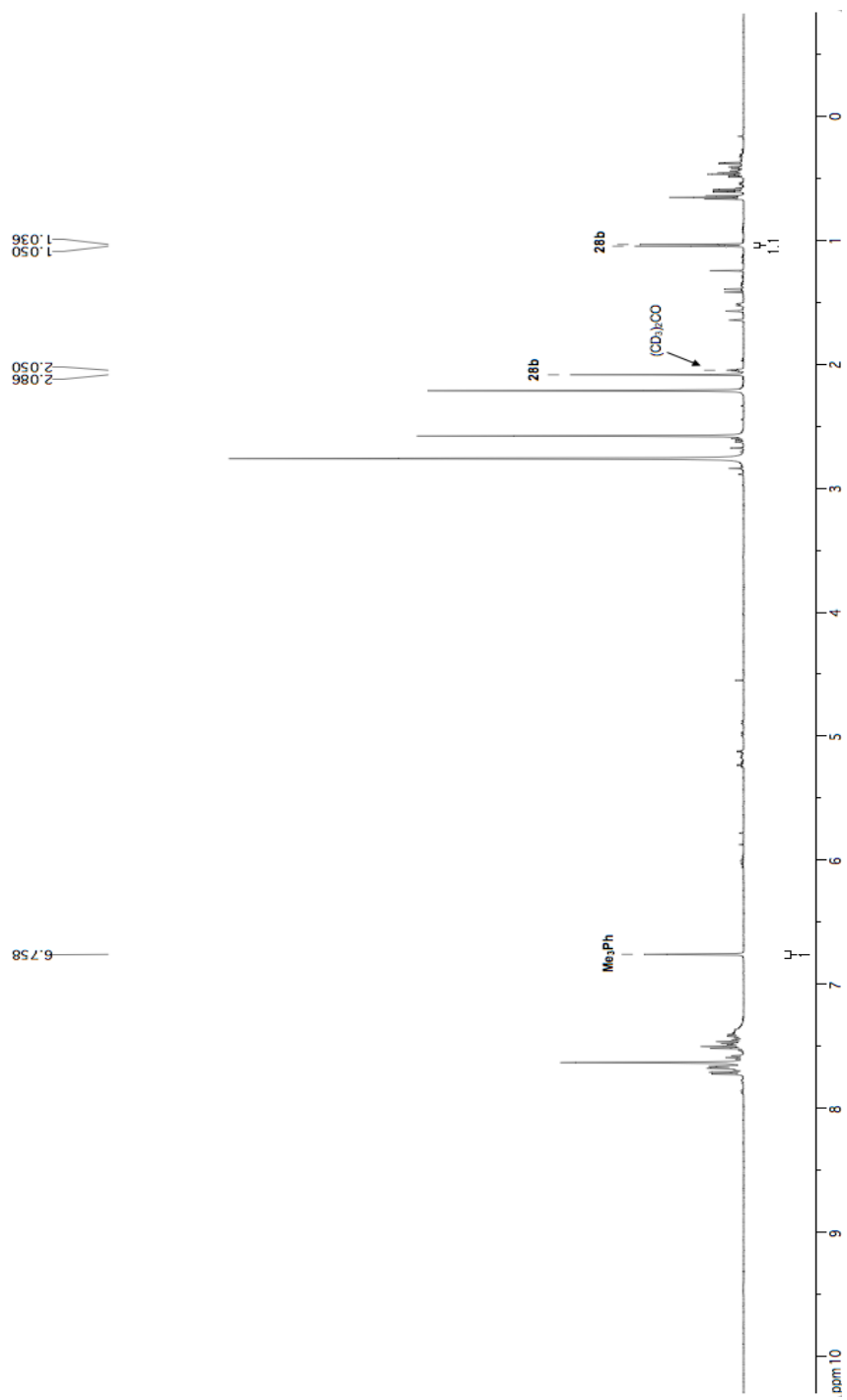
2.63b (¹H NMR, 500 MHz, (CD₃)₂CO, 25 °C)
Analytical standard, 99% from Sigma-Aldrich

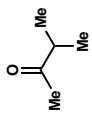




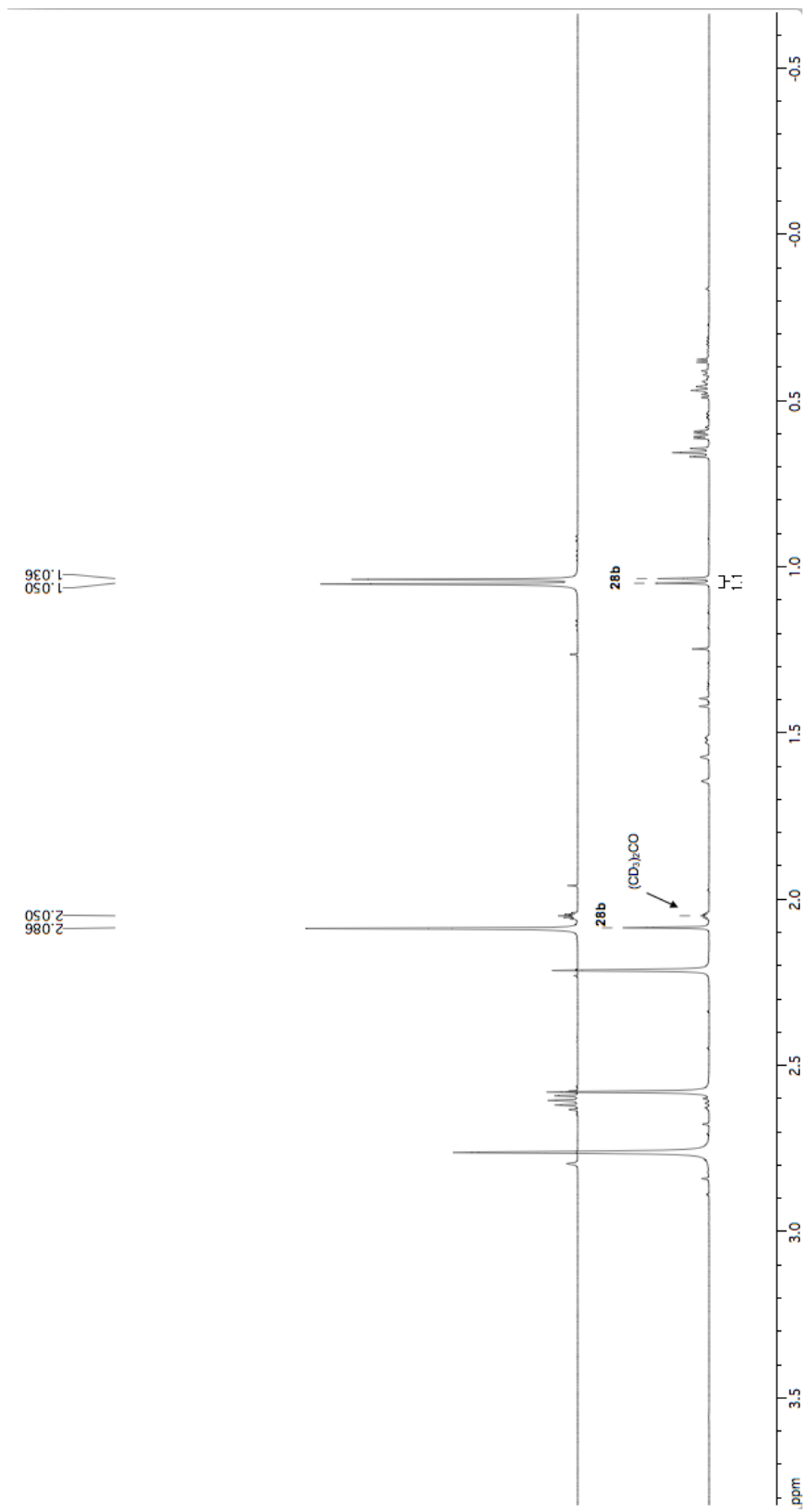
2.63b (¹H NMR, 500 MHz, (CD₃)₂CO, 25 °C)

Crude reaction mixture with mesitylene internal standard

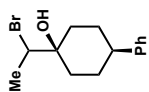




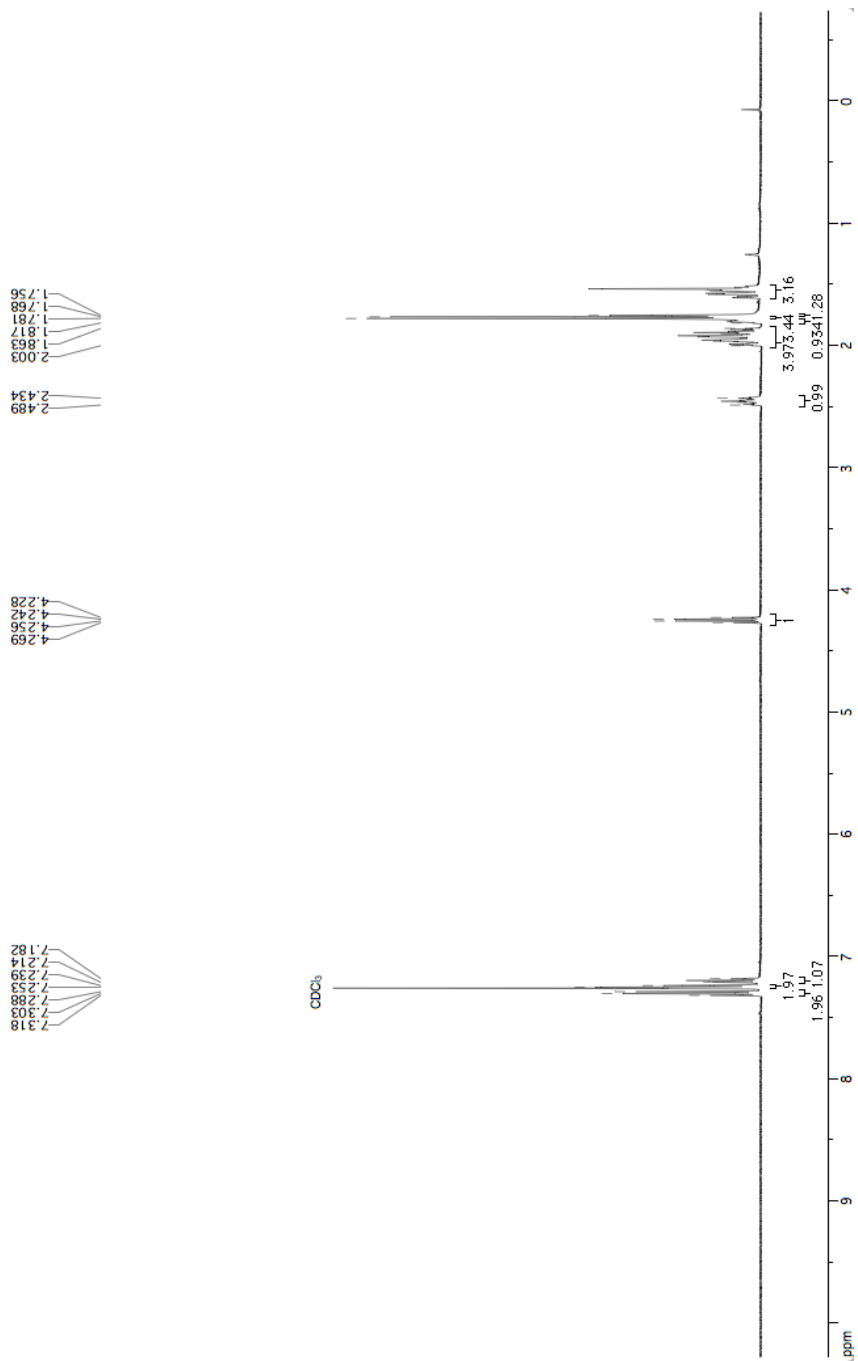
2.63b (¹H NMR, 500 MHz, (CD₃)₂CO, 25 °C)
Overlay of analytical standard with crude reaction mixture

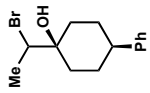


NMR Spectra of bromohydrins

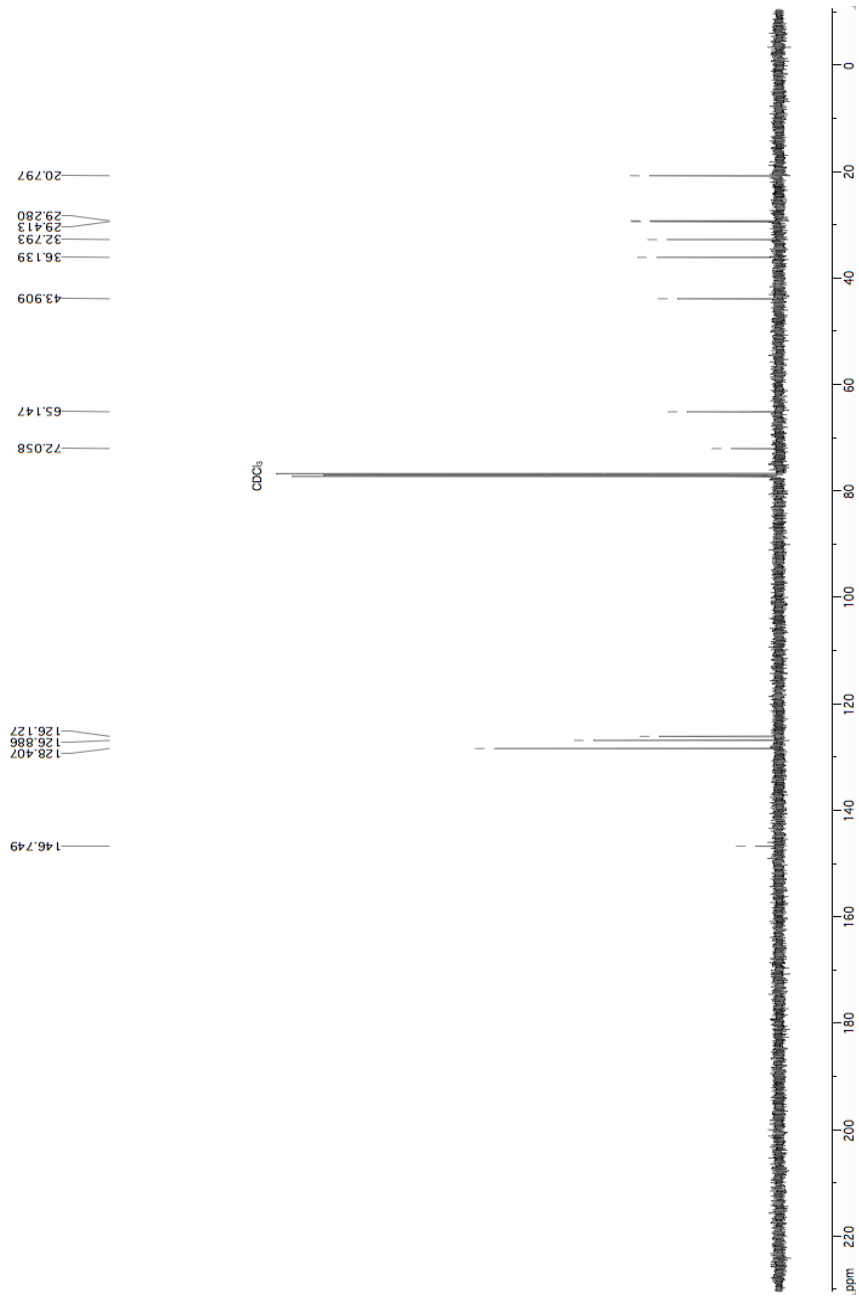


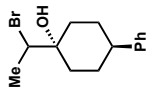
2.69 (¹H NMR, 500 MHz, CDCl₃, 25 °C)



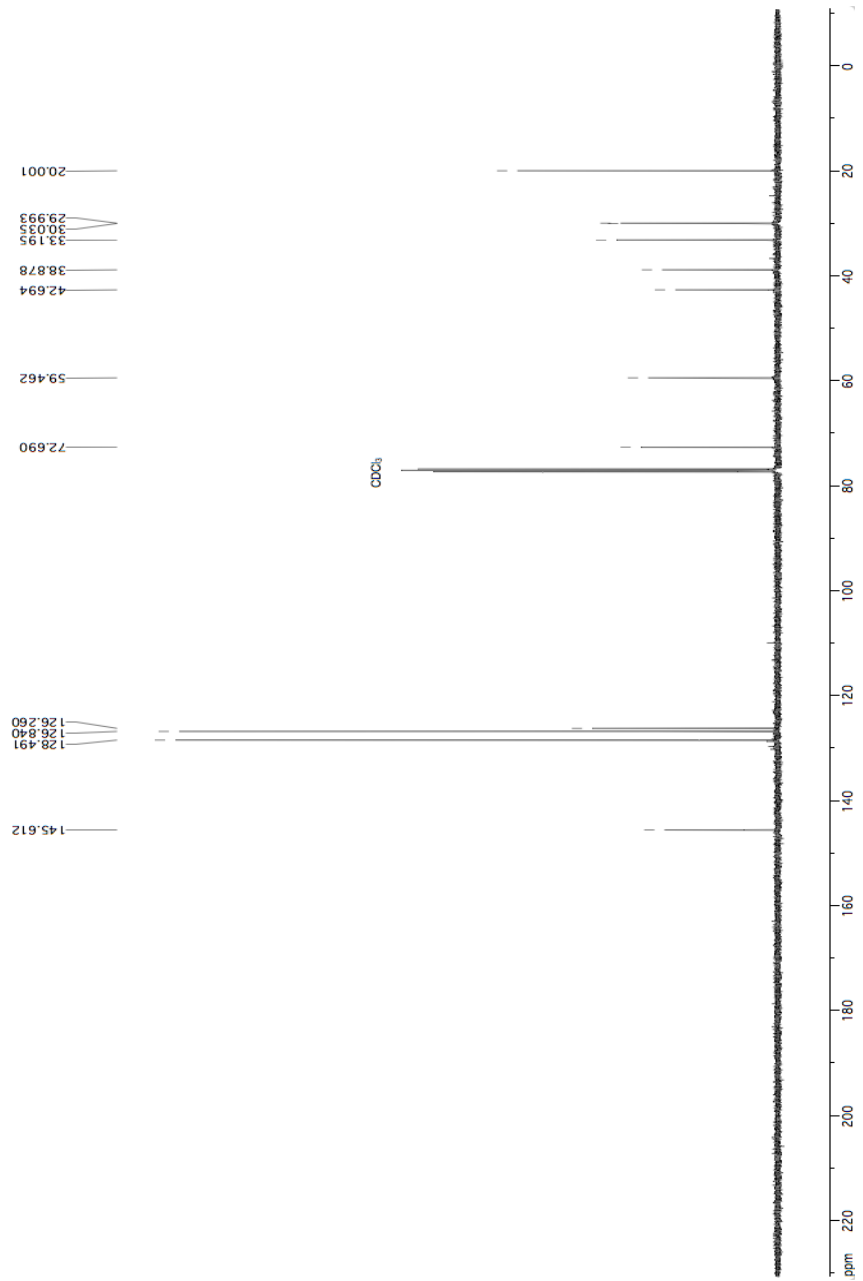


2.68 (¹³C NMR, 126 MHz, CDCl₃, 25 °C)



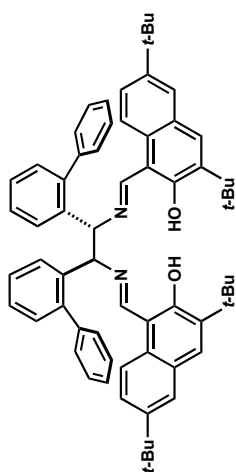


2.70 (¹³C NMR, 126 MHz, CDCl₃, 25 °C)

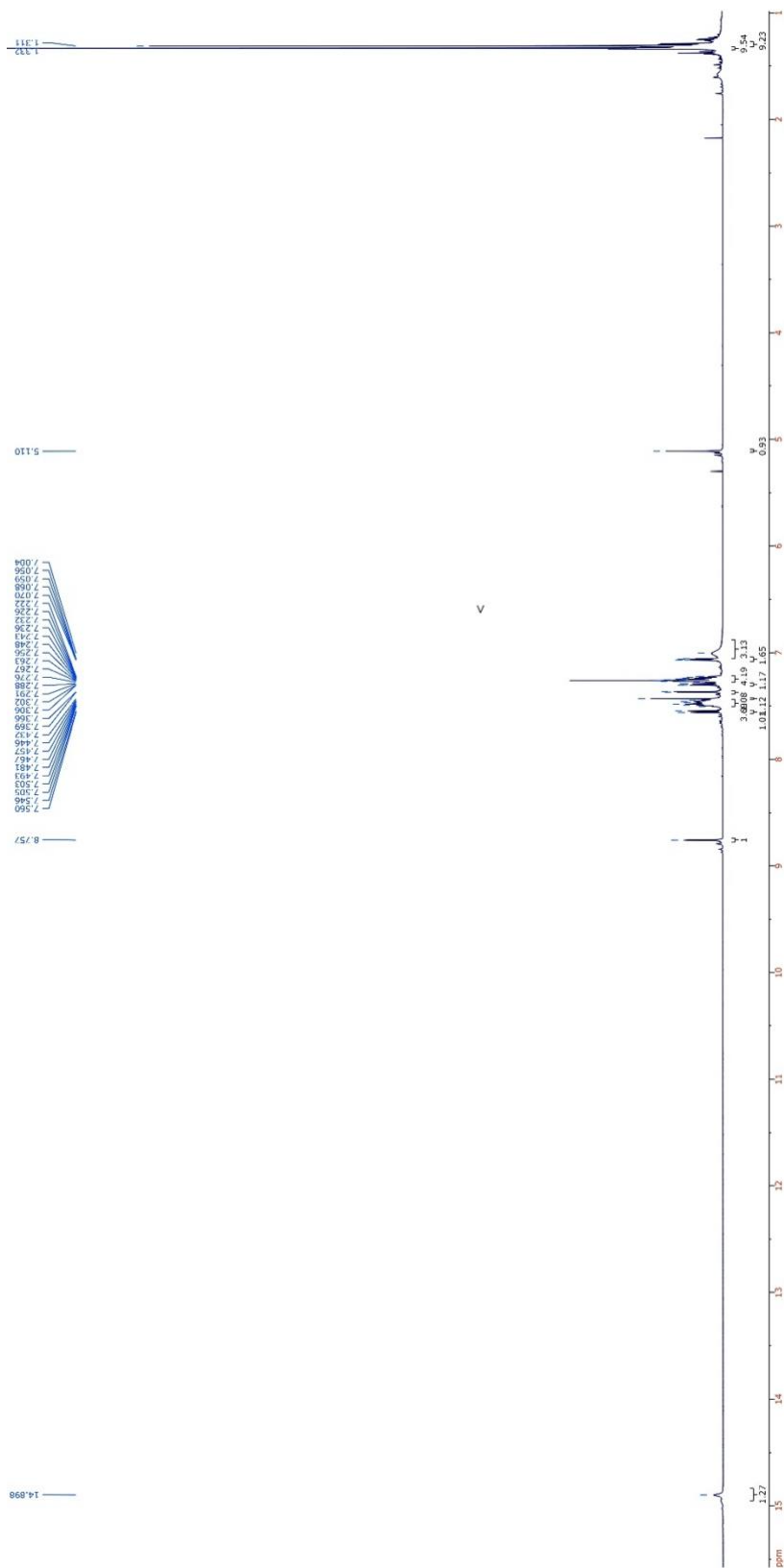


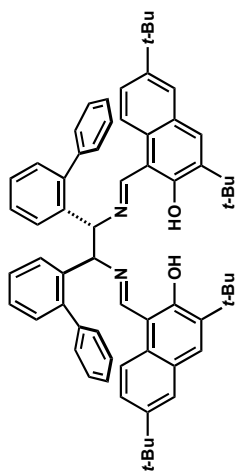
Appendix B: NMR Spectra for Chapter 3

NMR Spectra

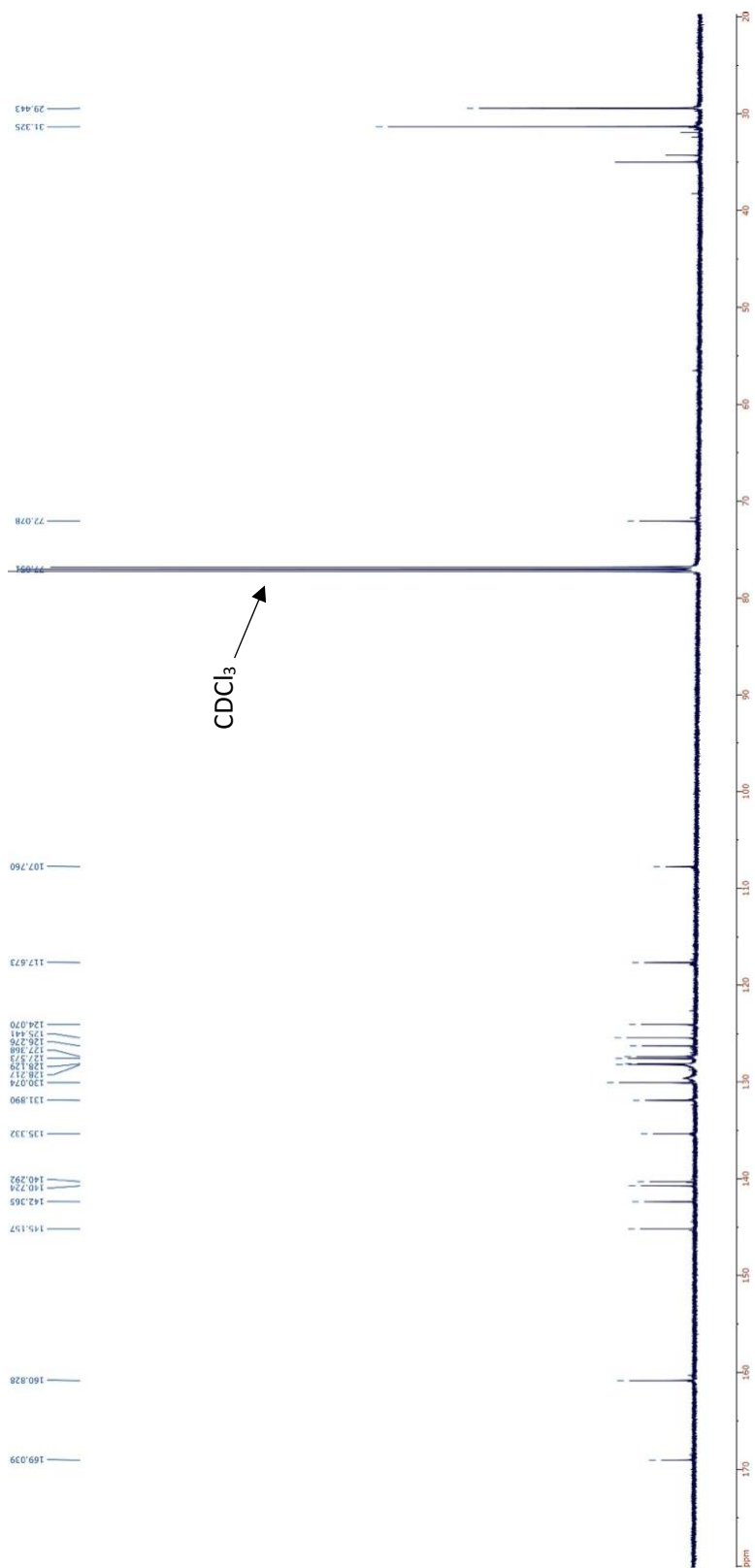


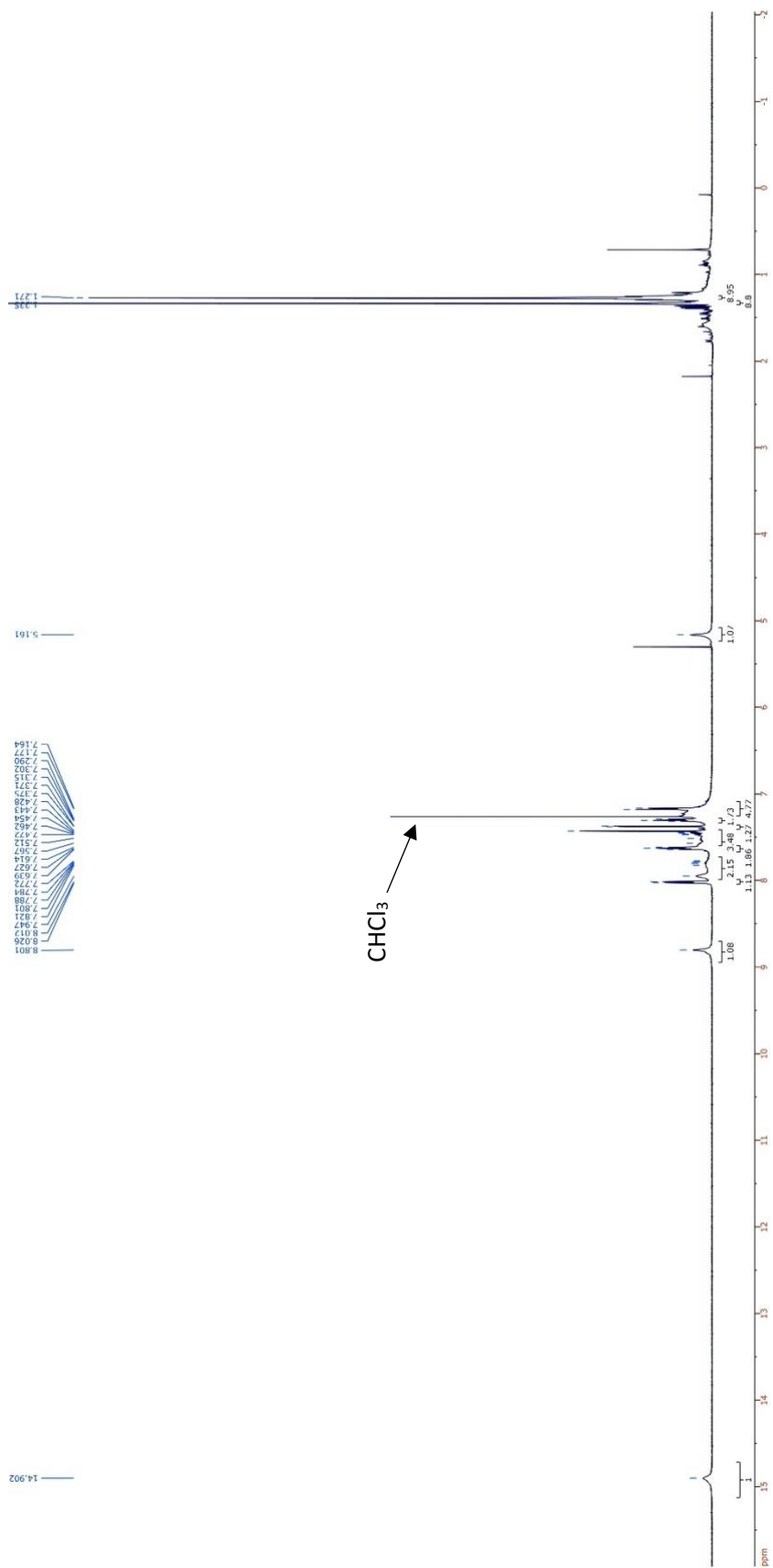
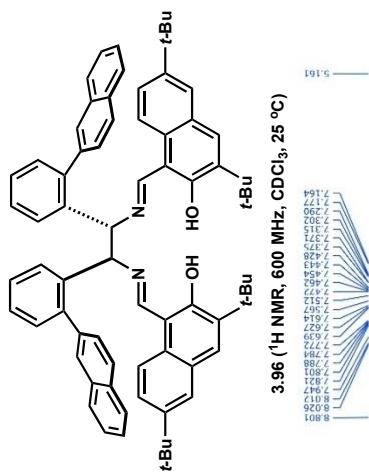
3.95 (1H NMR, 600 MHz, CDCl₃, 25 °C)

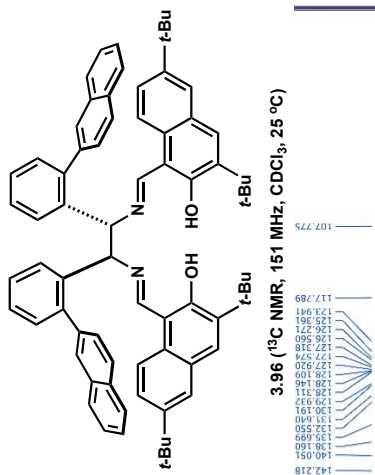




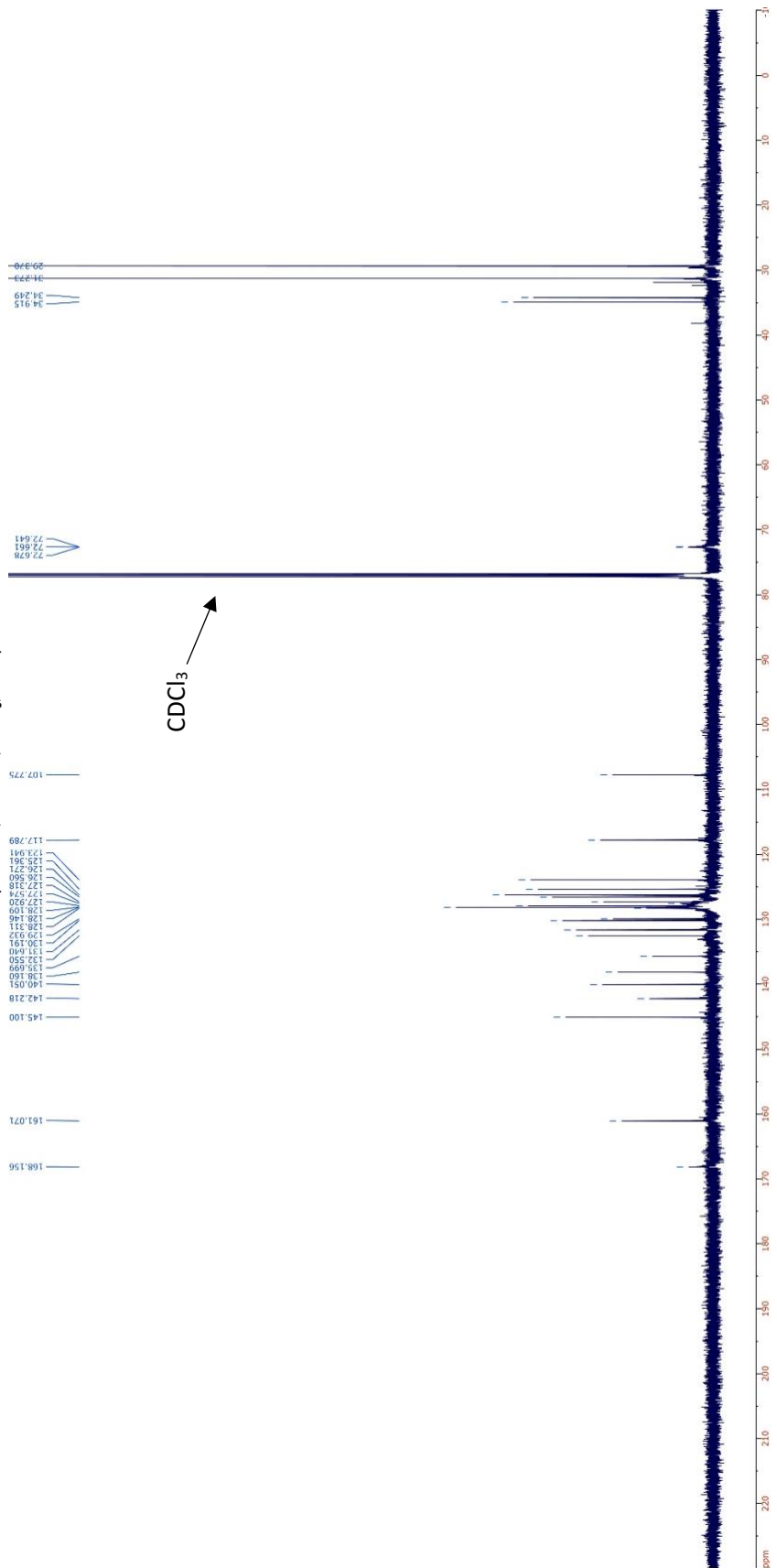
3.95 (^{13}C NMR, 151 MHz, CDCl_3 , 25 $^\circ\text{C}$)

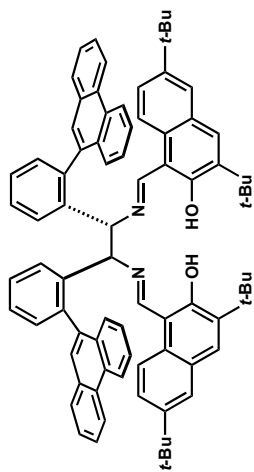






3.96 (¹³C NMR, 151 MHz, CDCl₃, 25 °C)





3.97 (¹³C NMR, 151 MHz, CDCl₃, 25 °C)

28.961
31.287
34.249

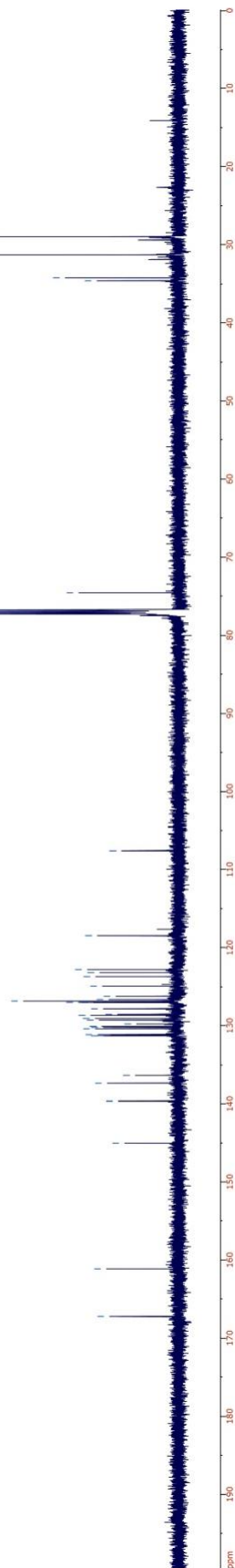
74.573

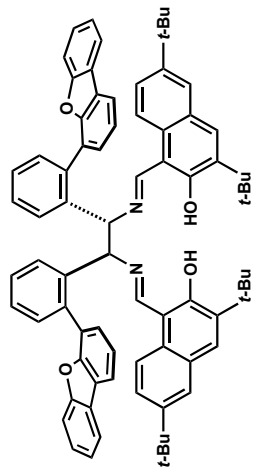
107.594
118.489
122.804
122.804
122.697
122.697
125.225
125.225
126.656
126.656
127.003
127.003
127.824
127.824
128.536
128.536
129.090
129.090
129.795
129.795
130.025
130.025
130.409
130.409
131.147
131.147
131.251
131.251
131.302
131.302
137.347
137.347
139.647
139.647
145.063

161.131

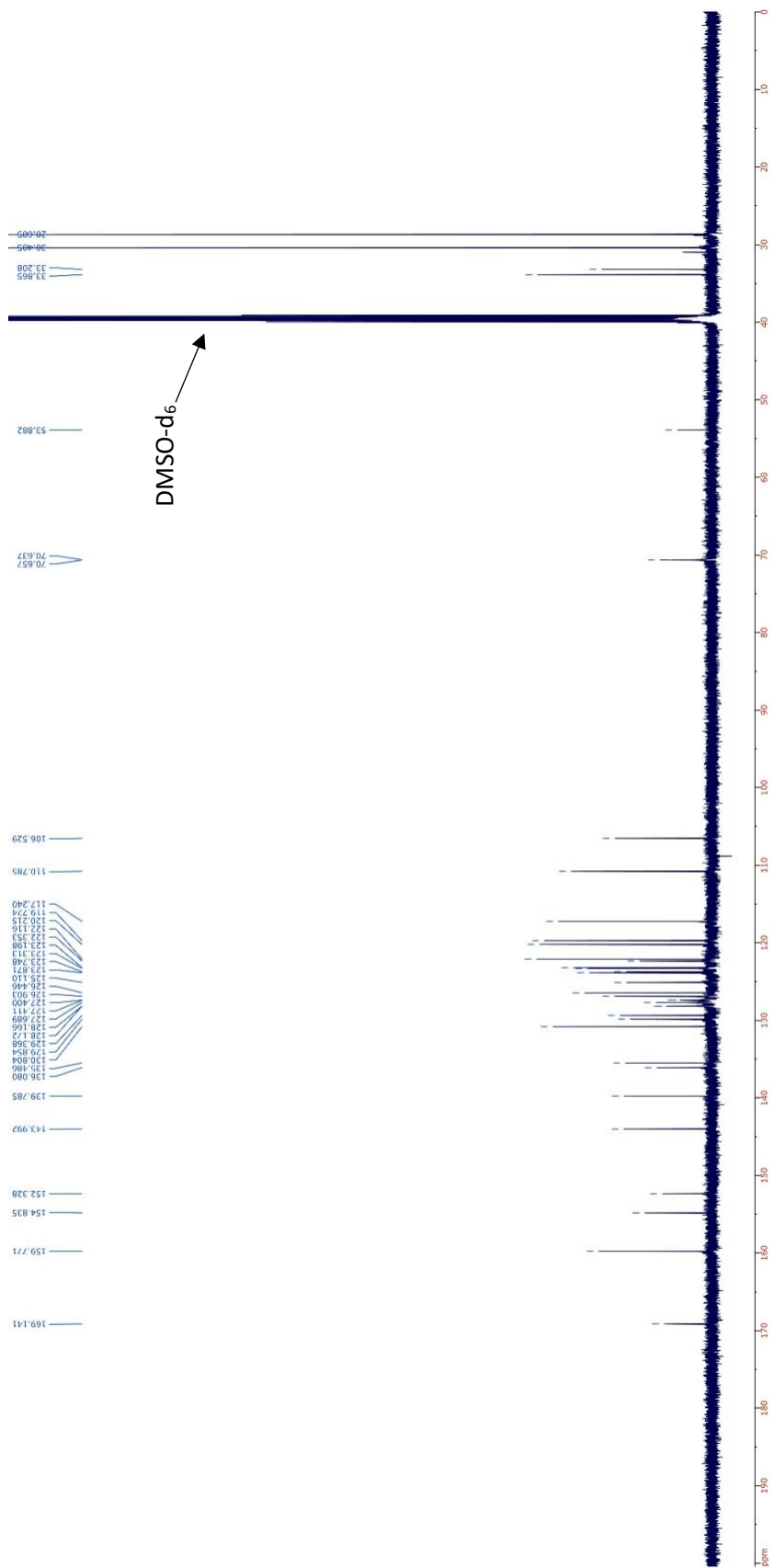
167.238

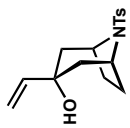
CDCl₃



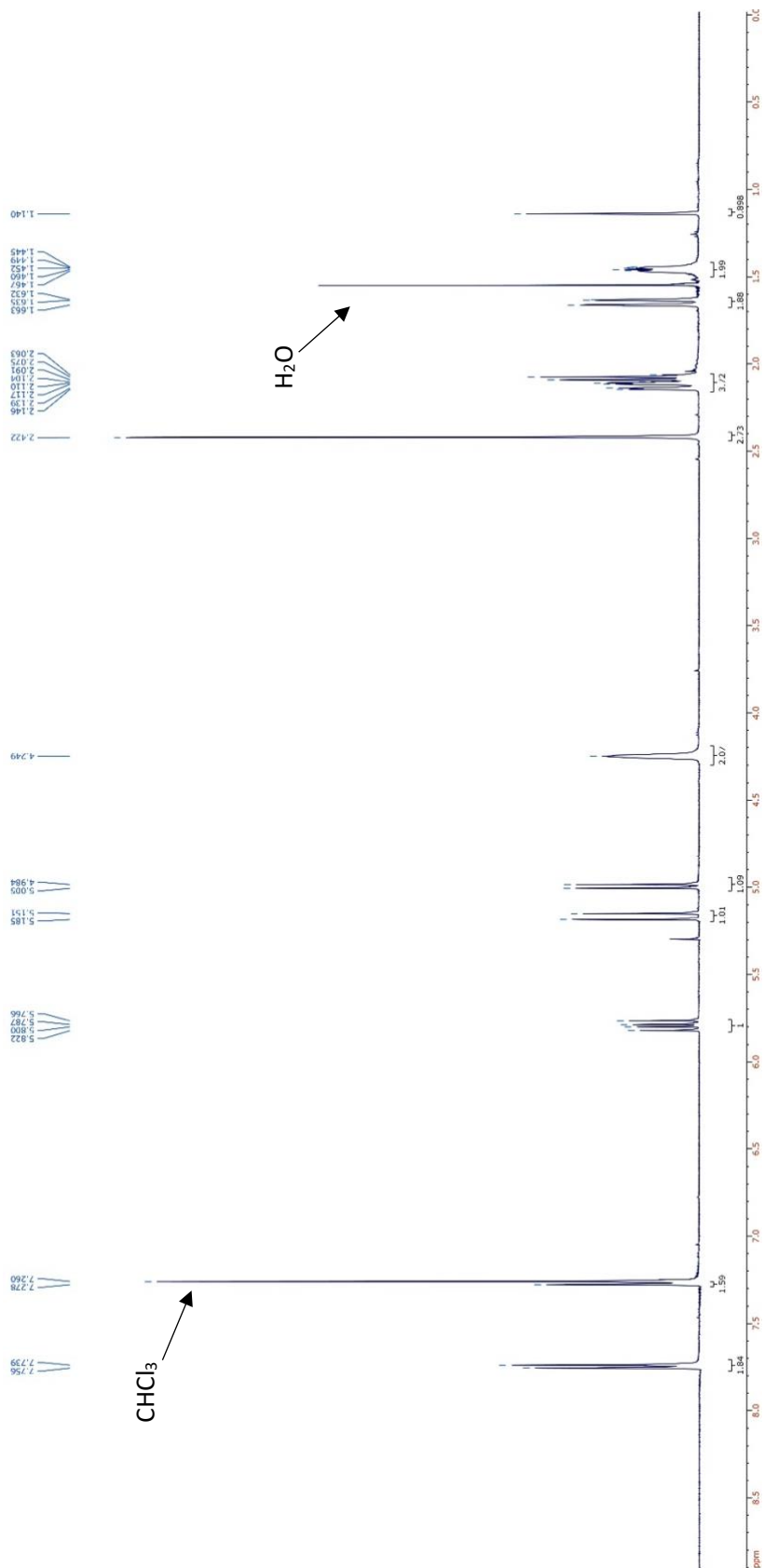


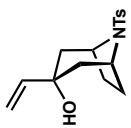
3.98 (^{13}C NMR, 151 MHz, DMSO-d_6 , 25 °C)



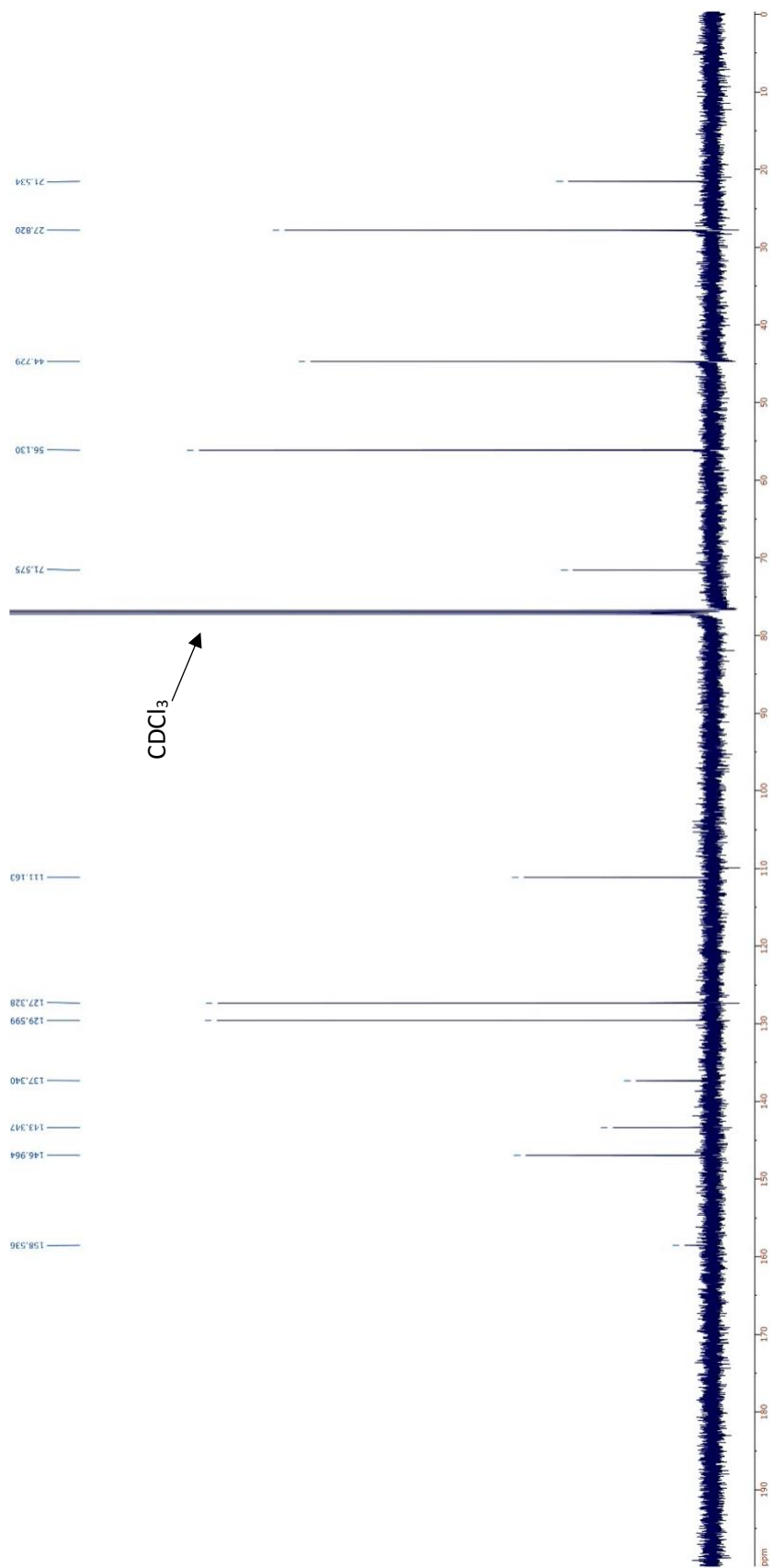


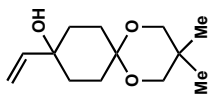
3.99 (¹H NMR, 600 MHz, CDCl₃, 25 °C)



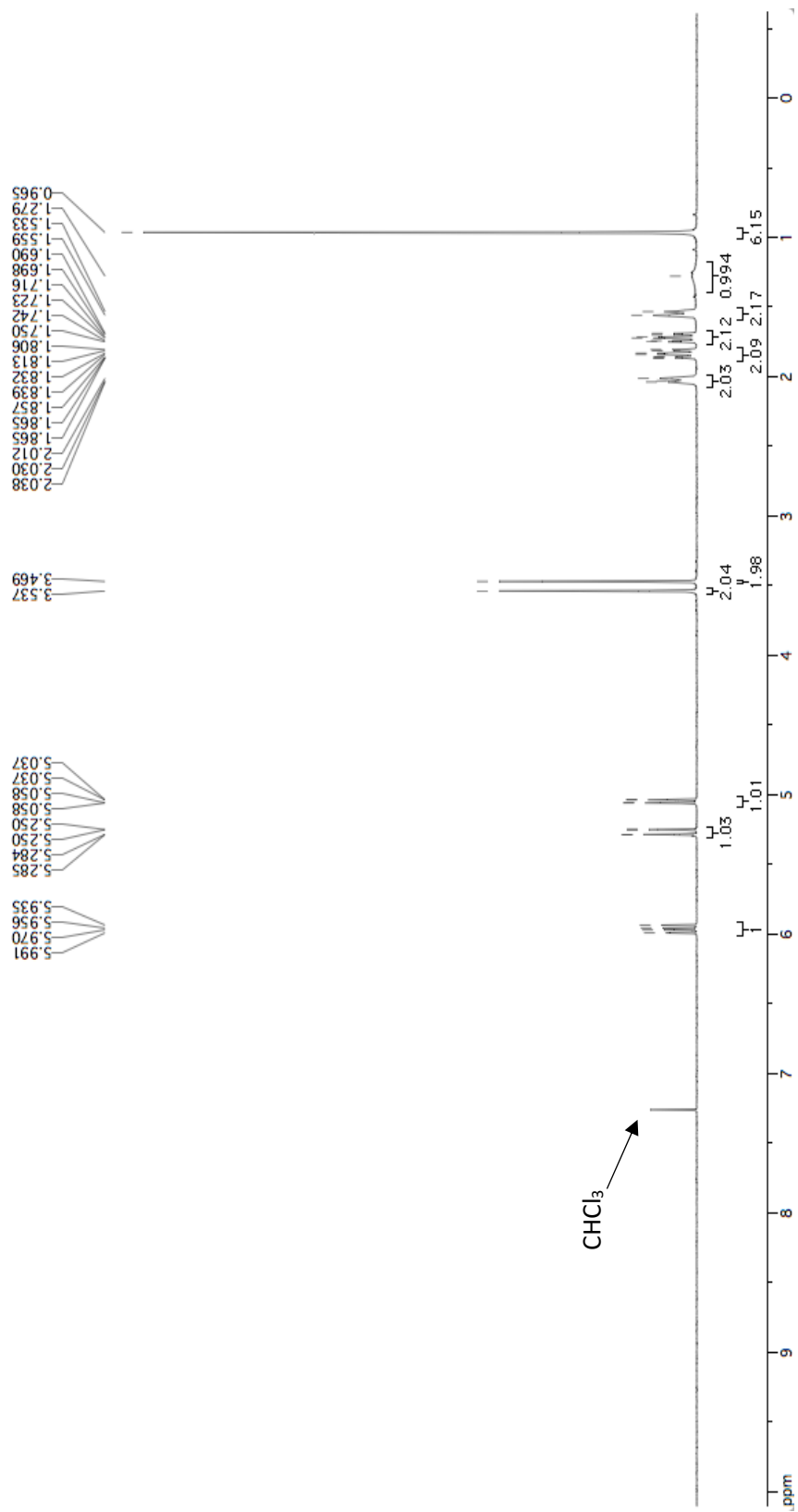


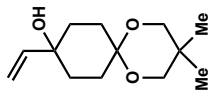
3.99 (¹³C NMR, 151 MHz, CDCl₃, 25 °C)



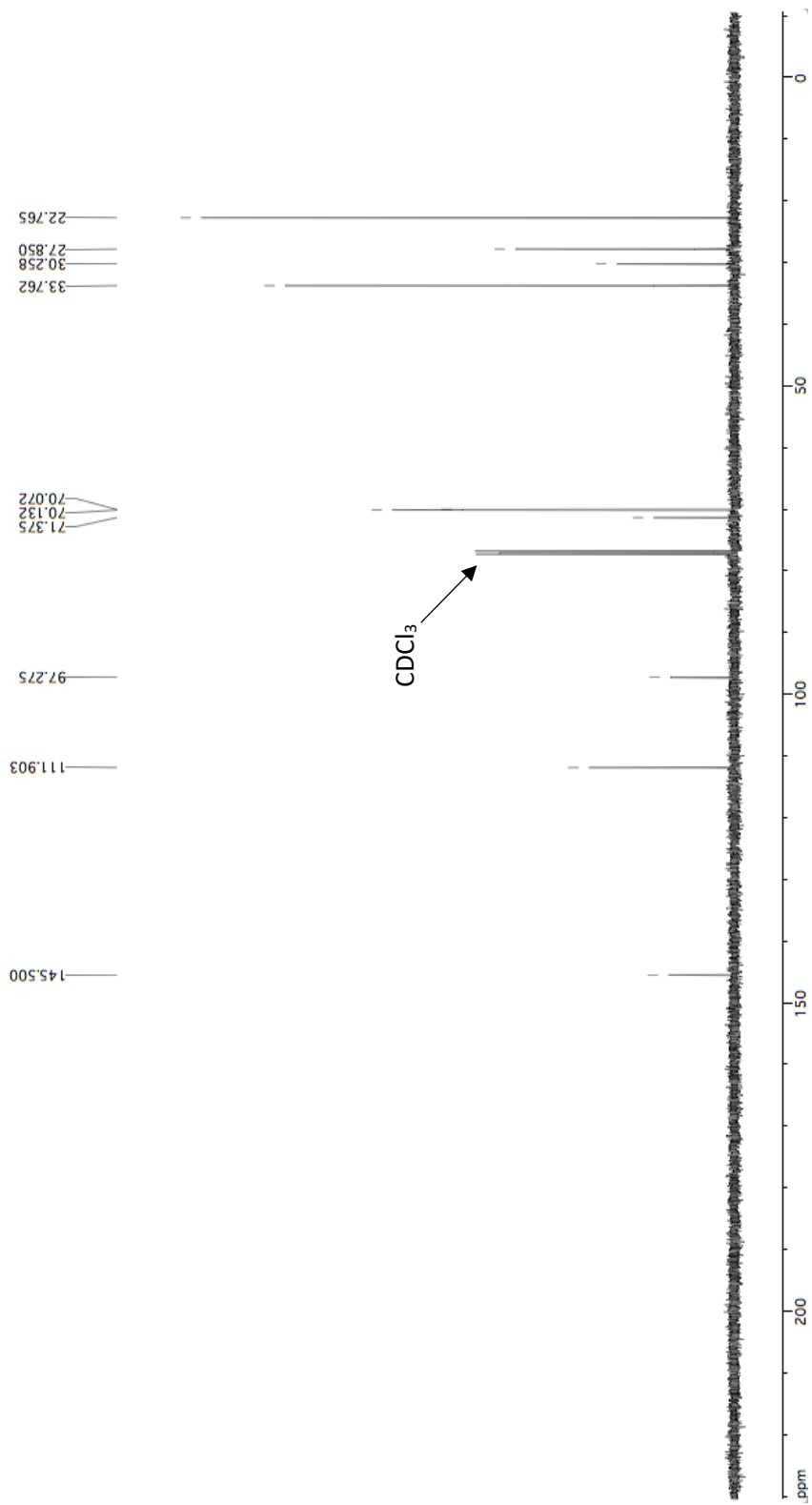


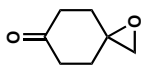
3.100 (¹H NMR, 500 MHz, CDCl₃, 25 °C)





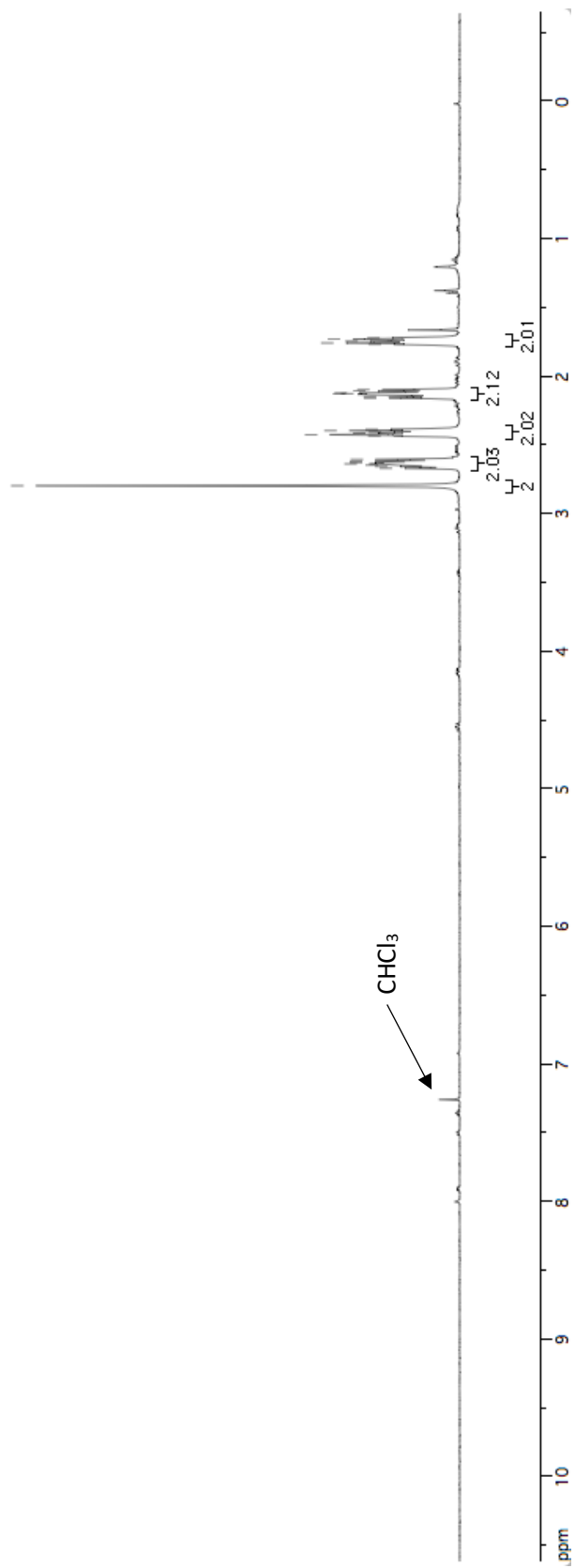
3.100 (¹³C NMR, 126 MHz, CDCl₃, 25 °C)

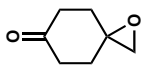




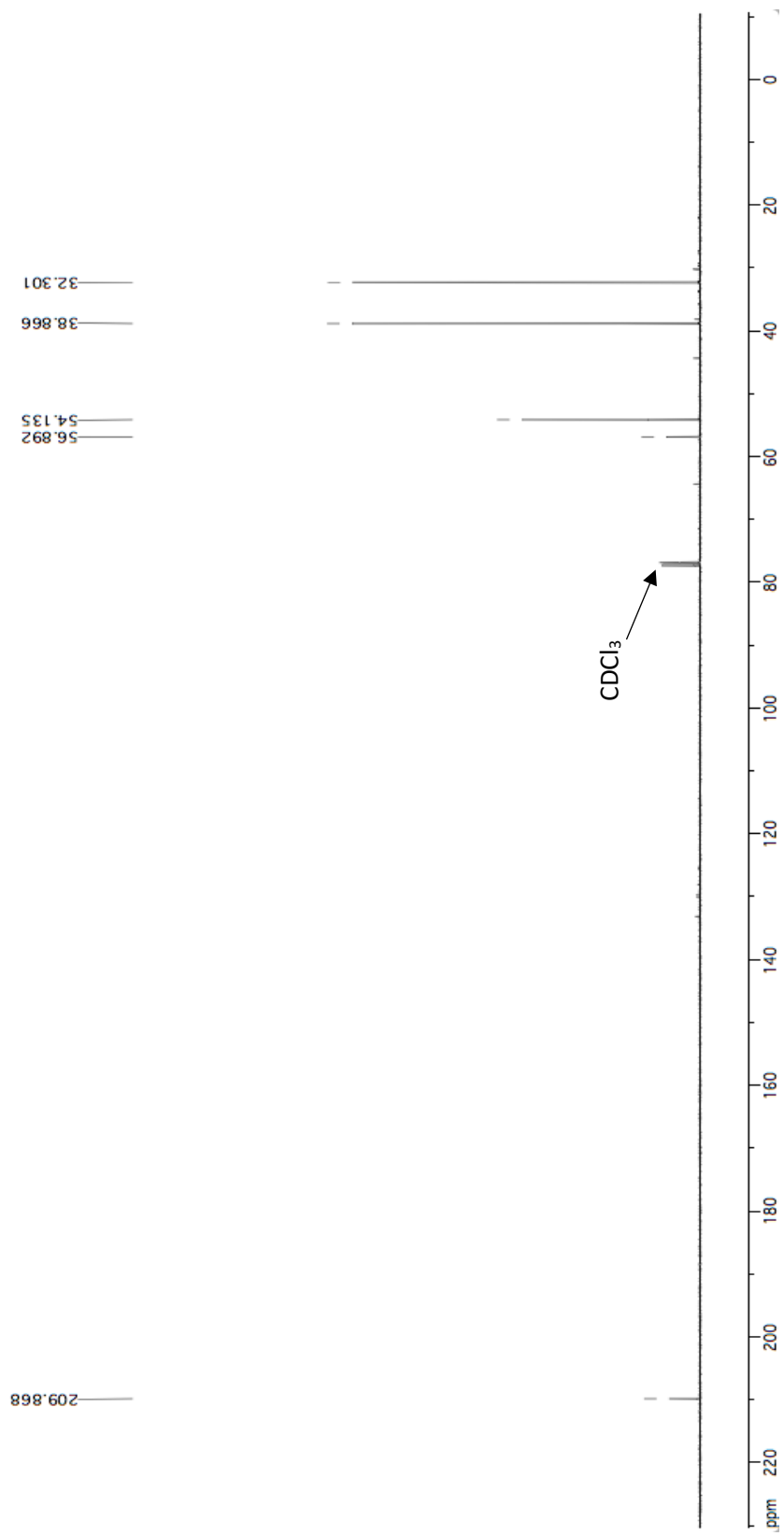
3.101 (¹H NMR, 500 MHz, CDCl₃, 25 °C)

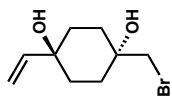
2.798
2.671
2.659
2.648
2.639
2.630
2.619
2.607
2.436
2.427
2.416
2.409
2.398
2.389
2.161
2.150
2.133
2.129
2.124
2.111
2.100
1.770
1.760
1.747
1.733
1.724



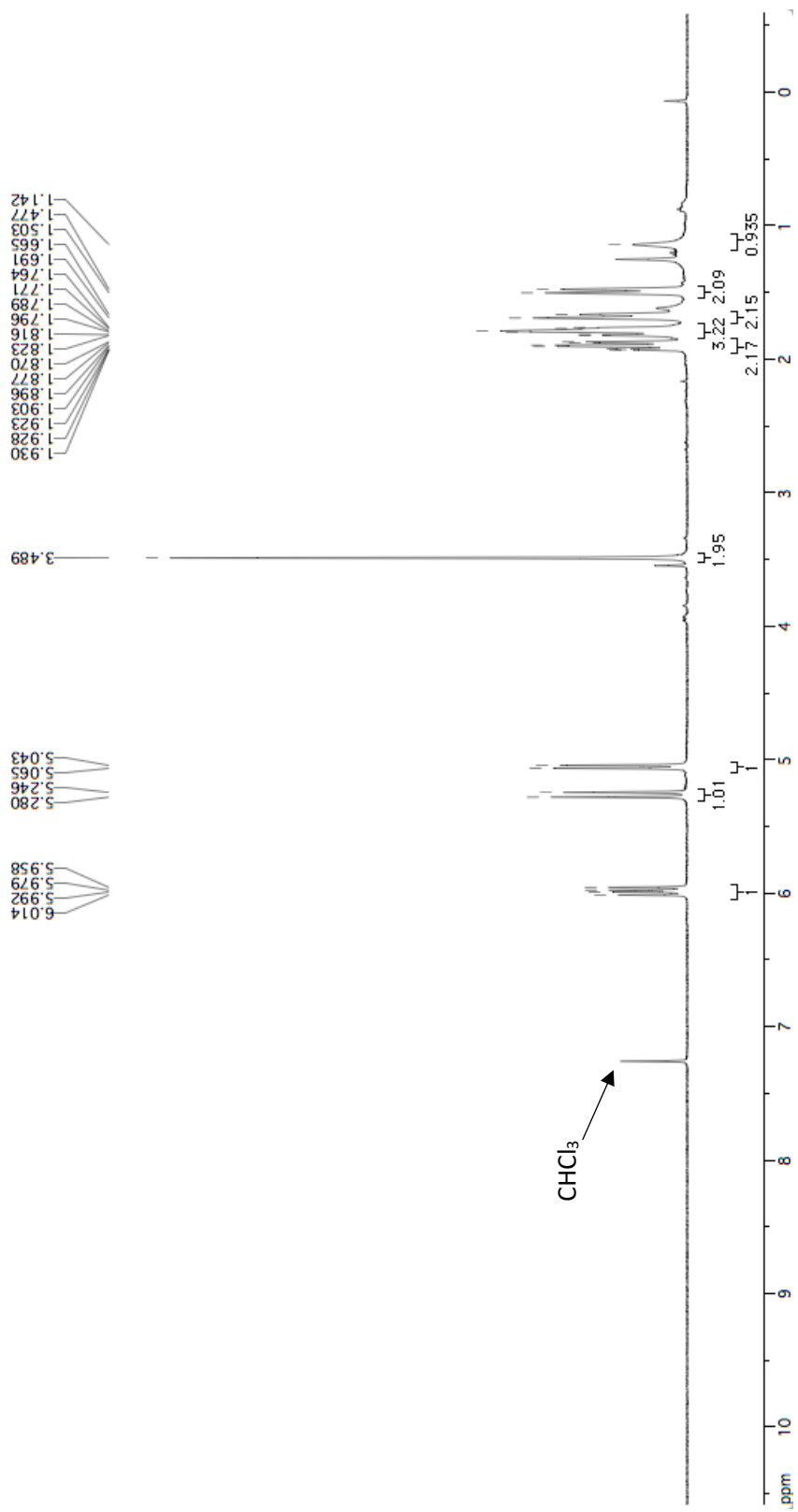


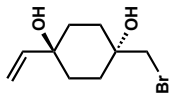
3.101 (¹³C NMR, 126 MHz, CDCl₃, 25 °C)



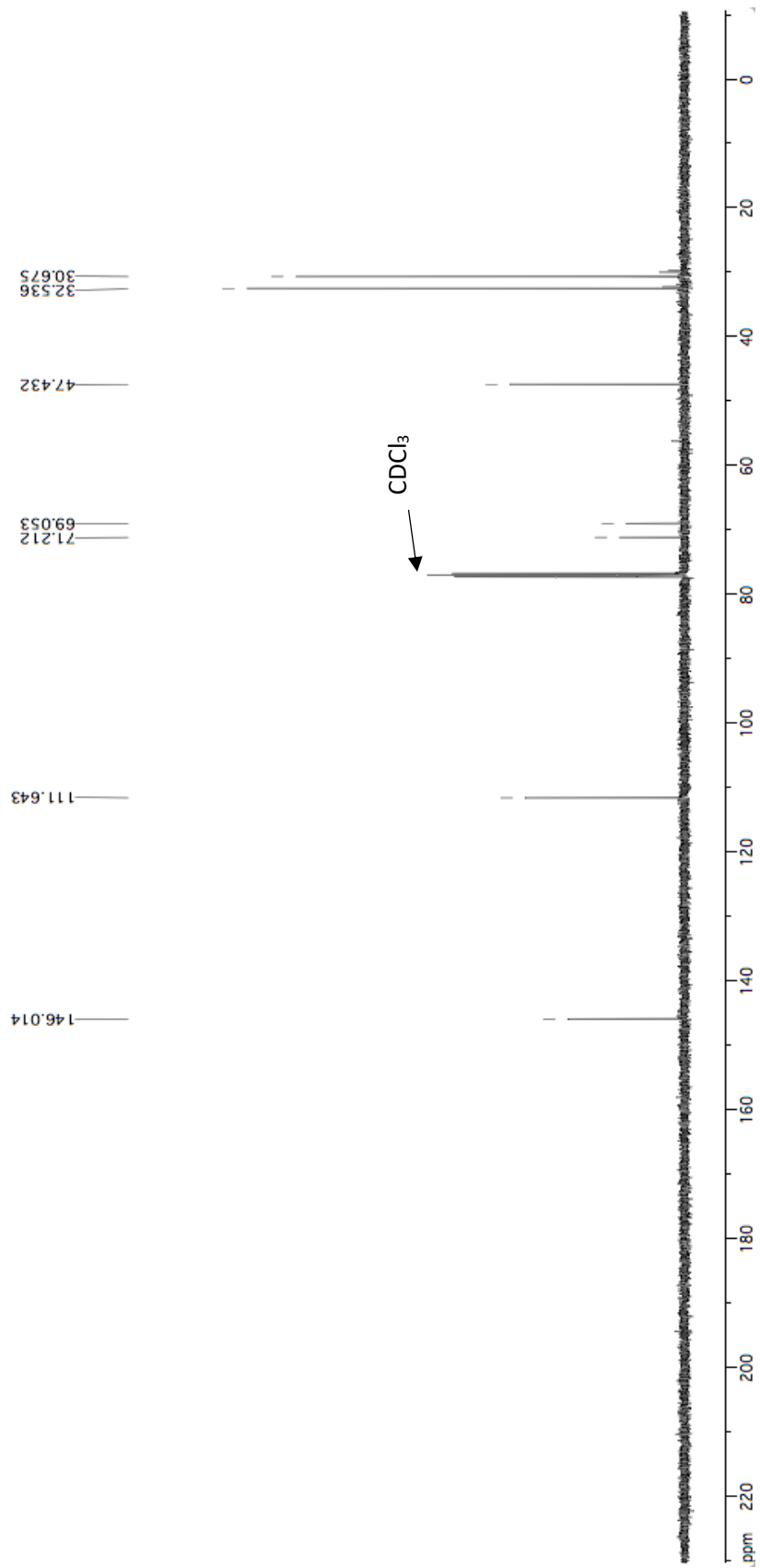


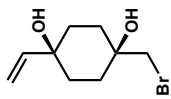
3.102 (¹H NMR, 500 MHz, CDCl₃, 25 °C)



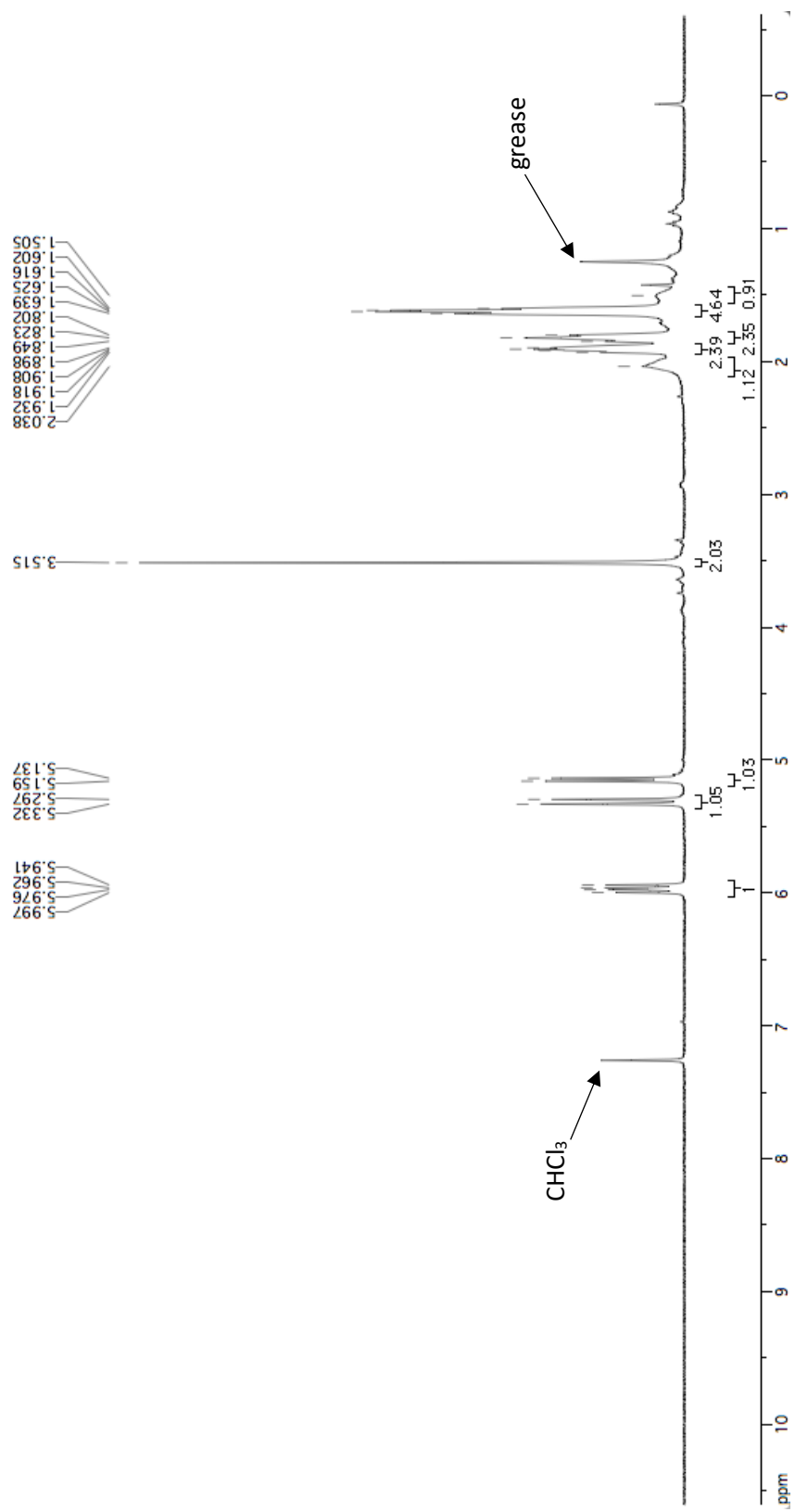


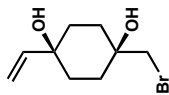
3.102 (¹³C NMR, 126 MHz, CDCl₃, 25 °C)



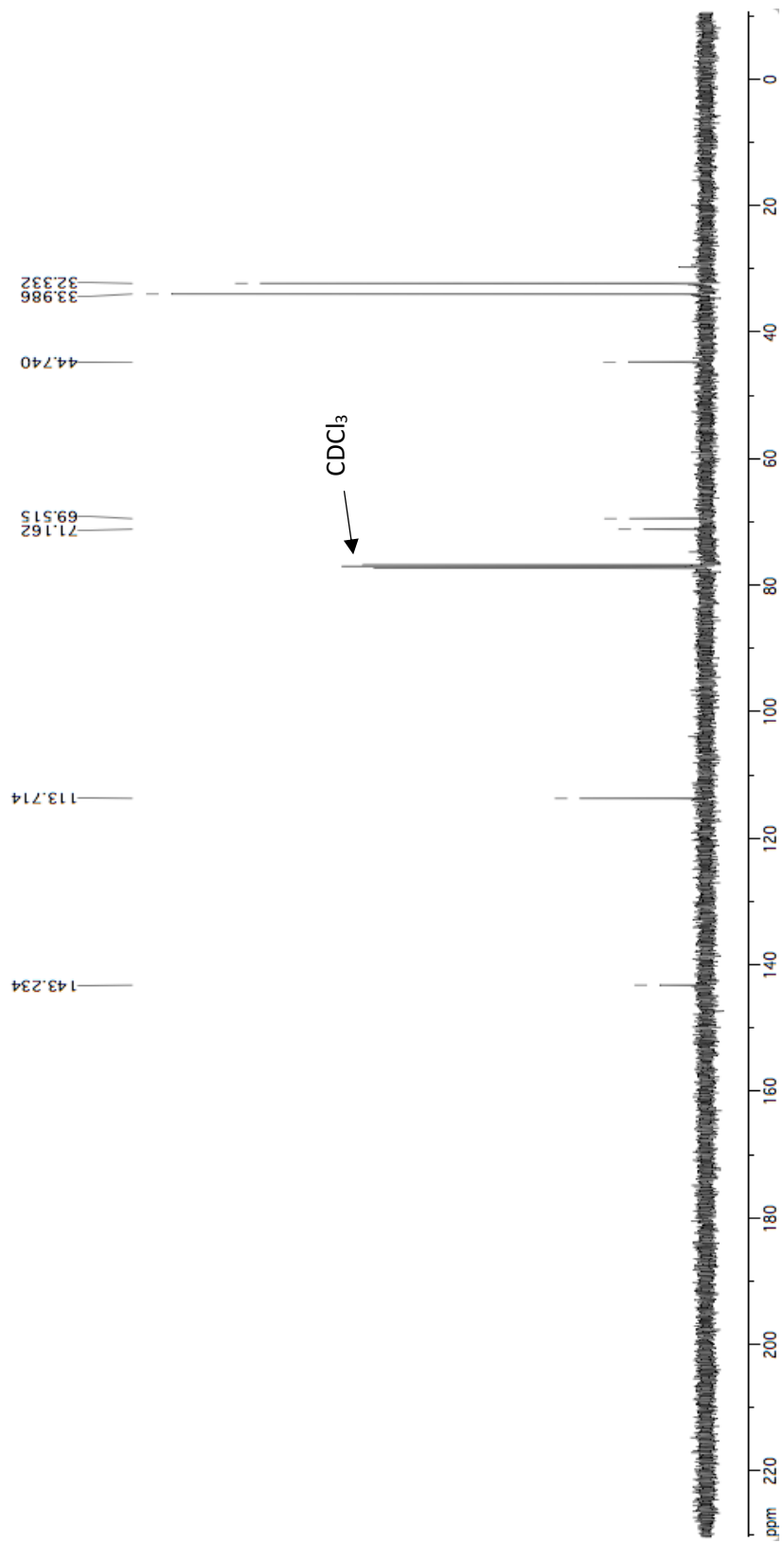


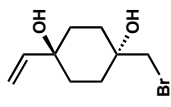
3.103 (¹H NMR, 500 MHz, CDCl₃, 25 °C)



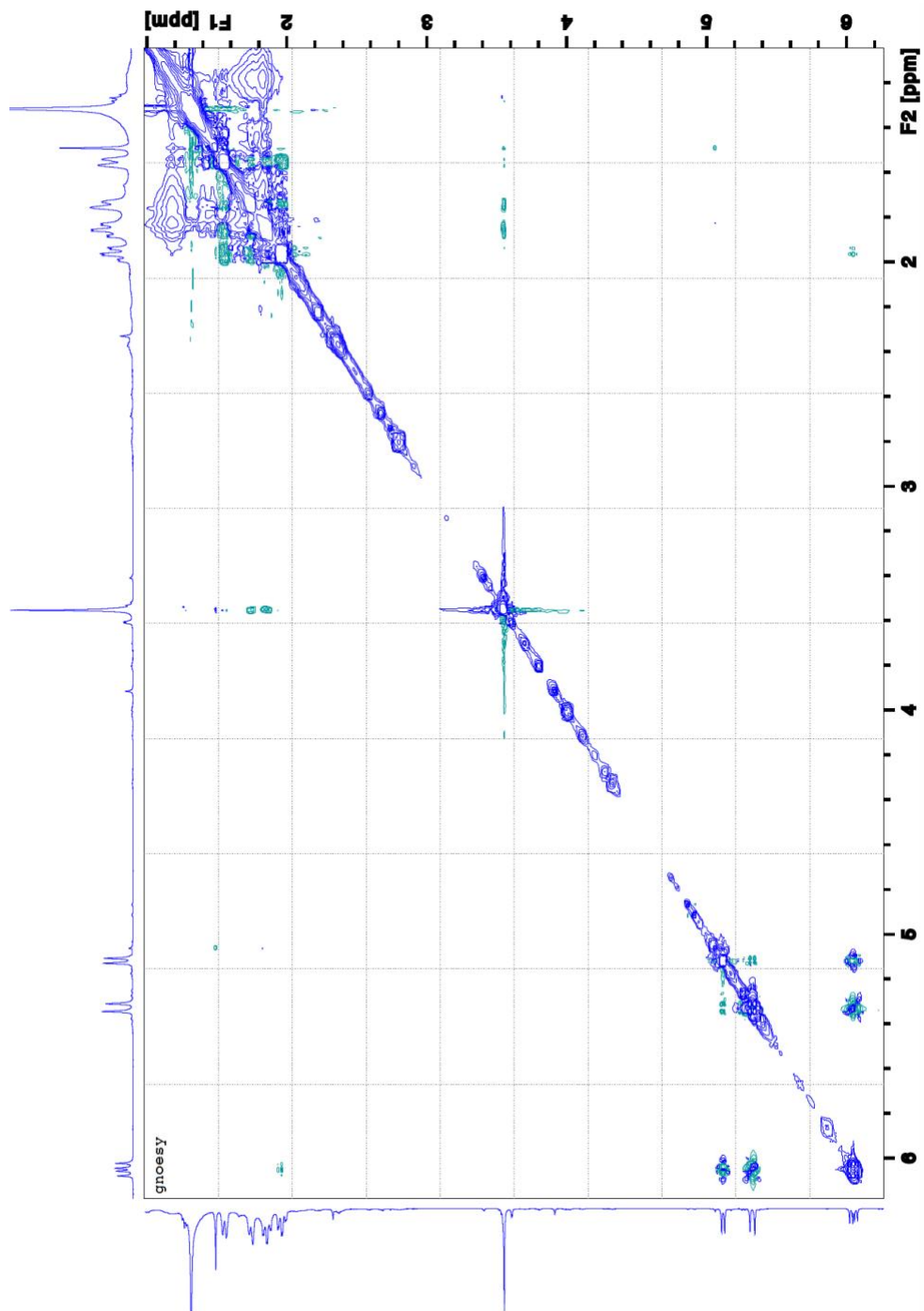


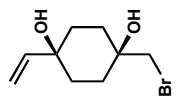
3.103 (¹³C NMR, 126 MHz, CDCl₃, 25 °C)



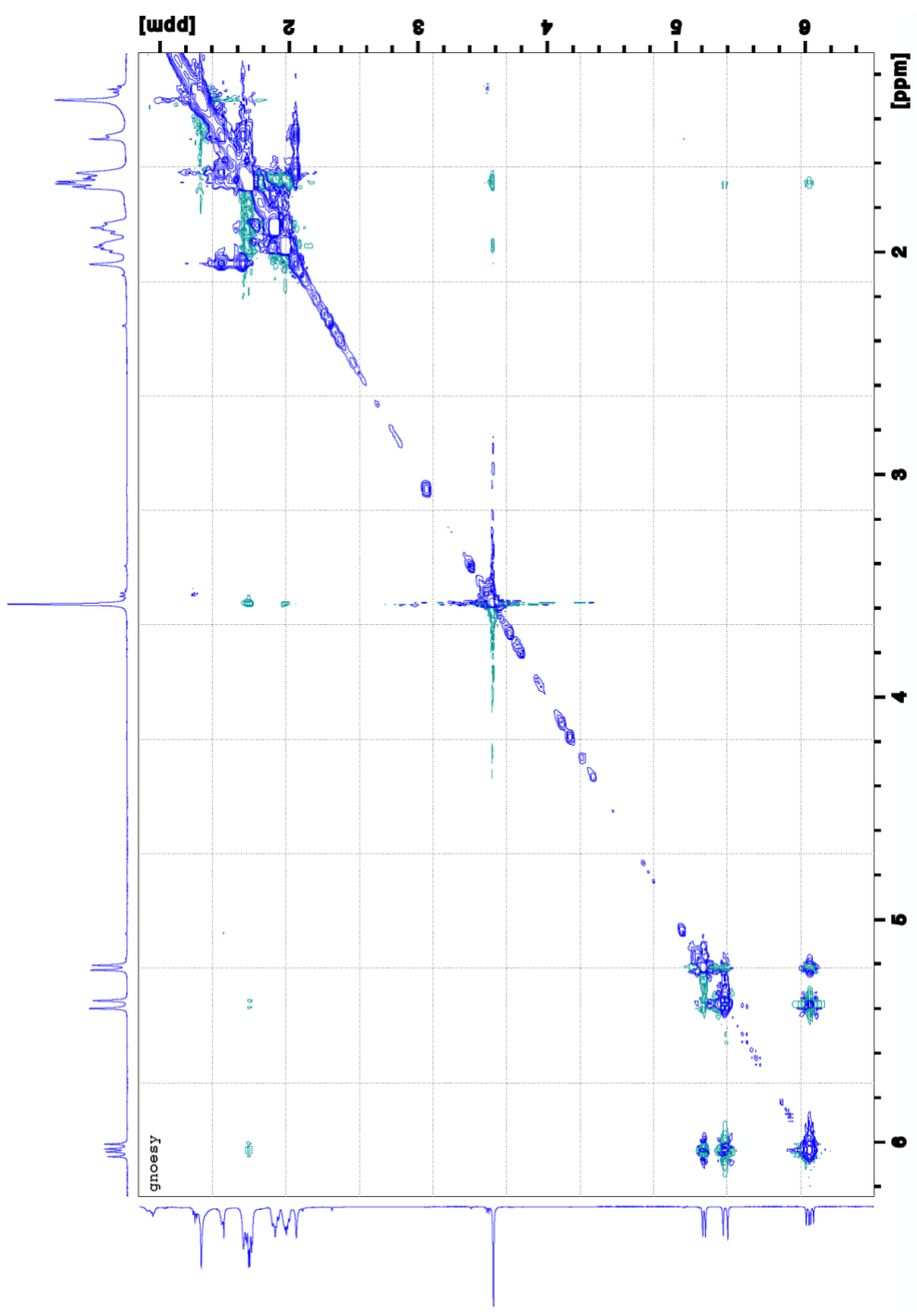


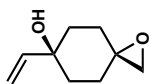
3.102 (NOESY, CDCl₃, 25 °C)



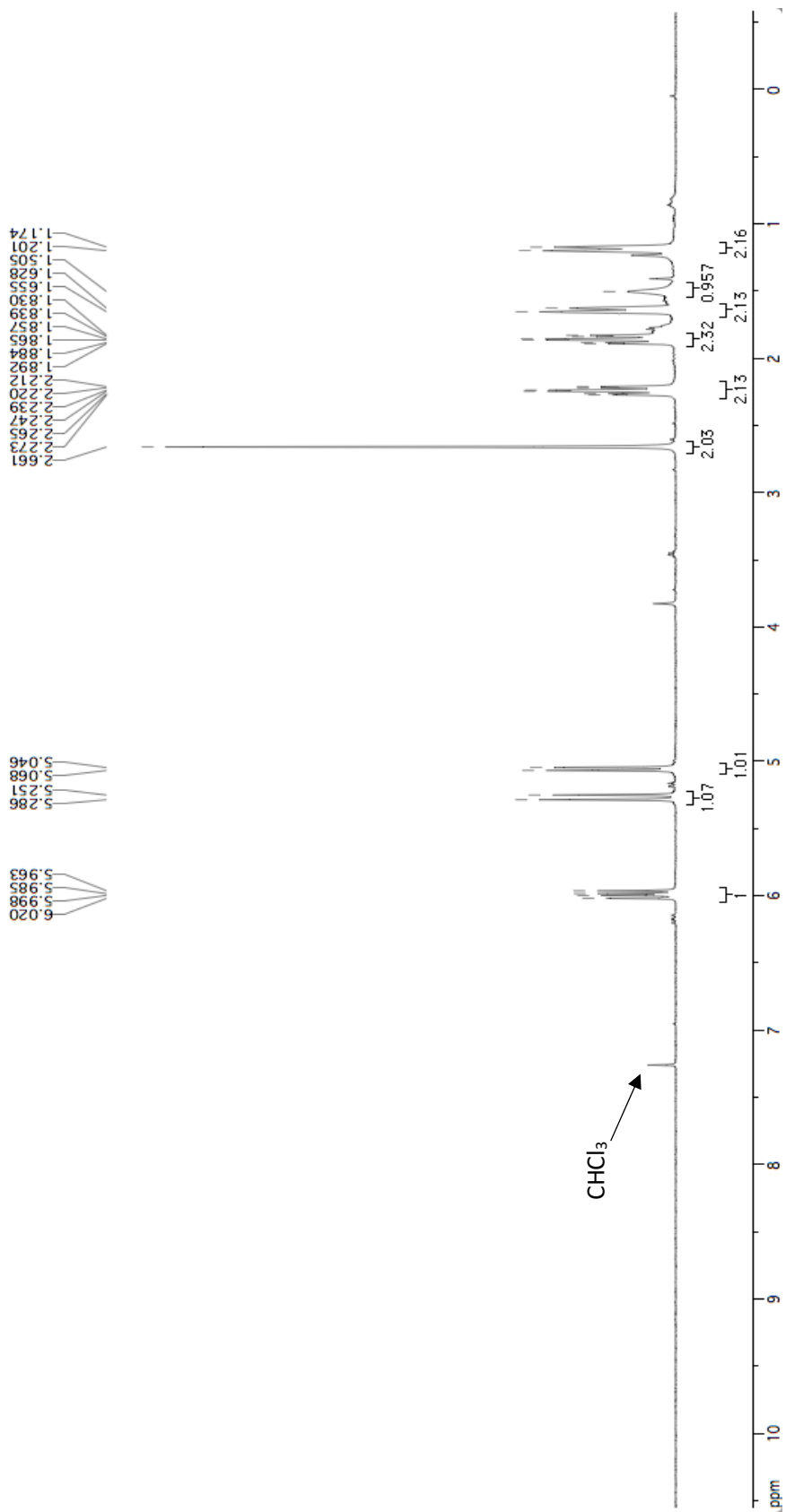


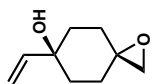
3.103 (NOESY, CDCl₃, 25 °C)



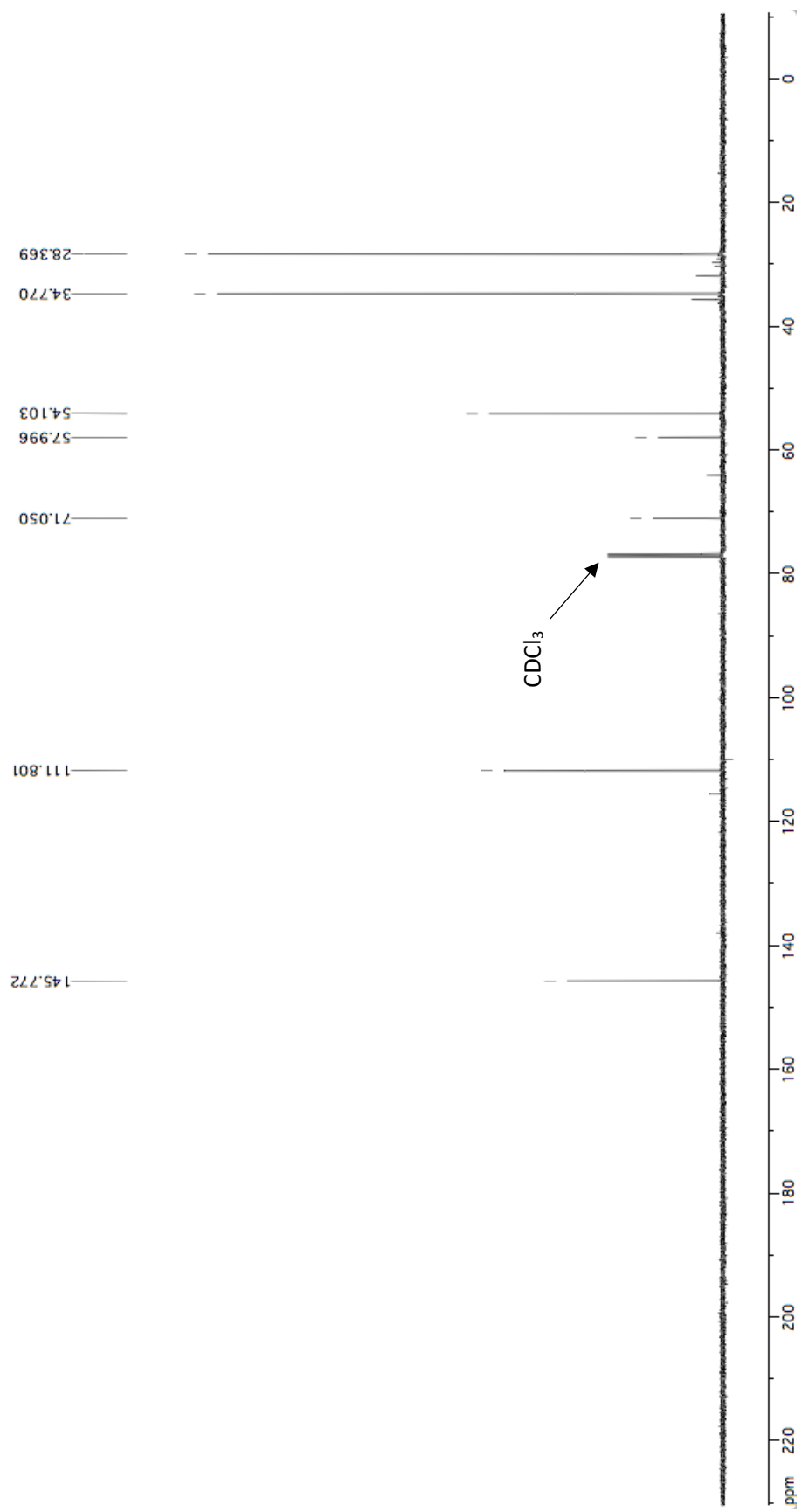


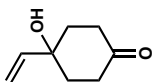
3.104 (¹H NMR, 500 MHz, CDCl₃, 25 °C)





3.104 (¹³C NMR, 126 MHz, CDCl₃, 25 °C)





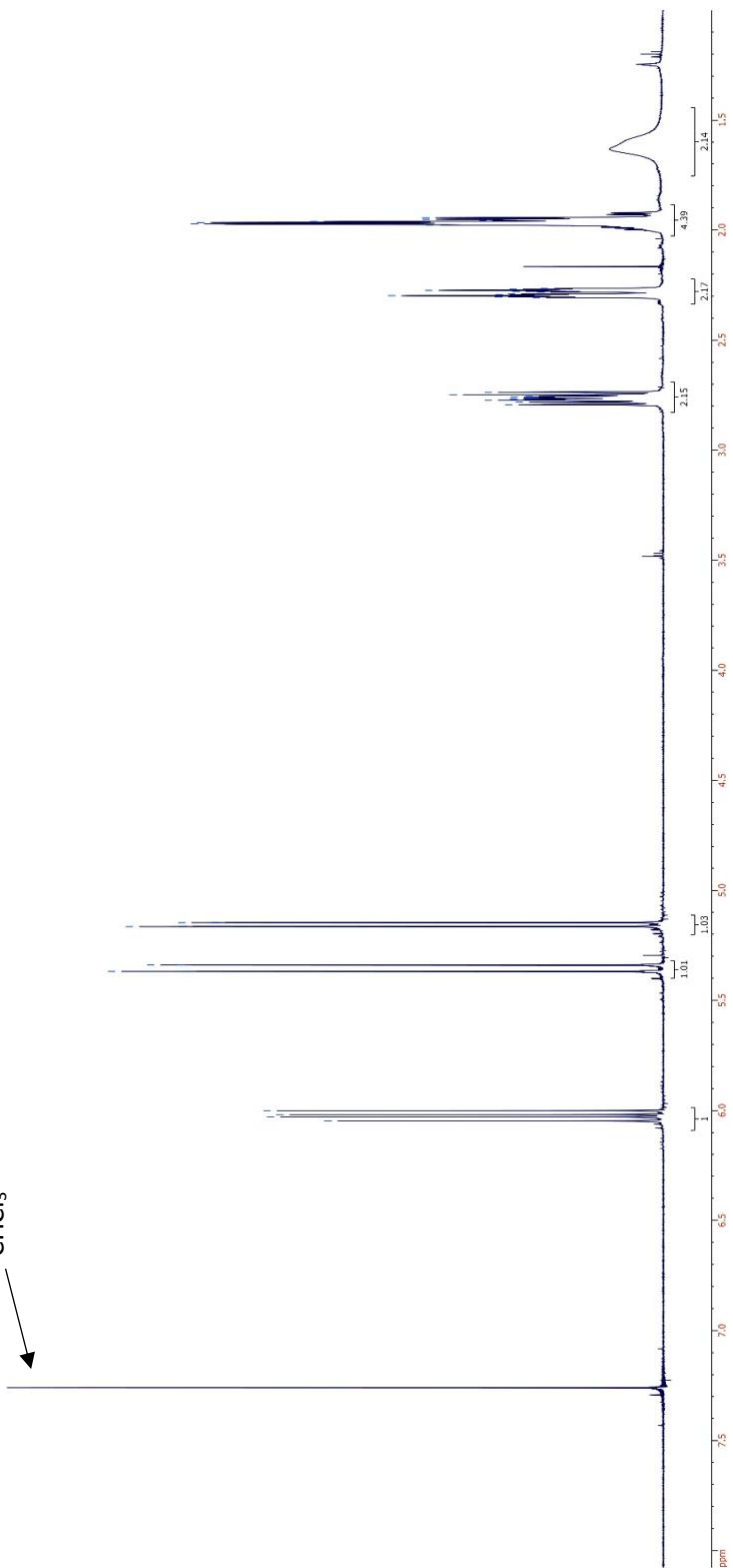
3.105 (¹H NMR, 600 MHz, CDCl₃, 25 °C)

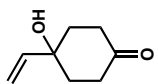
7.294
7.178
7.171
7.166
7.164
7.160
7.150
7.140
7.137
7.137
2.307
2.299
2.294
2.290
2.282
2.279
2.269
2.266
1.978
1.972
1.965
1.962
1.957
1.952
1.944

5.369
5.368
5.368
5.339
5.314
5.177
5.165
5.146

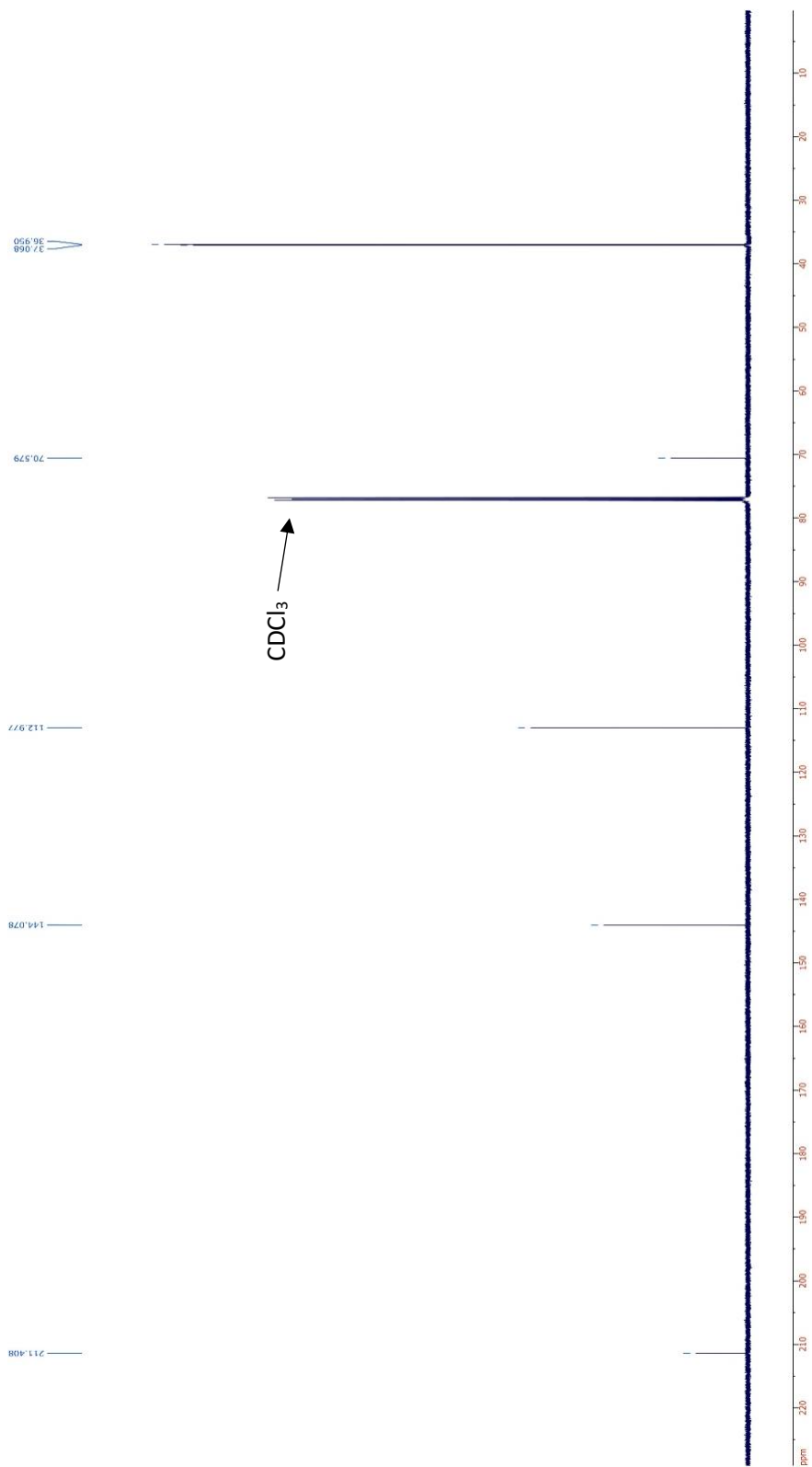
6.018
6.010
6.001

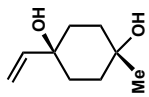
CHCl₃



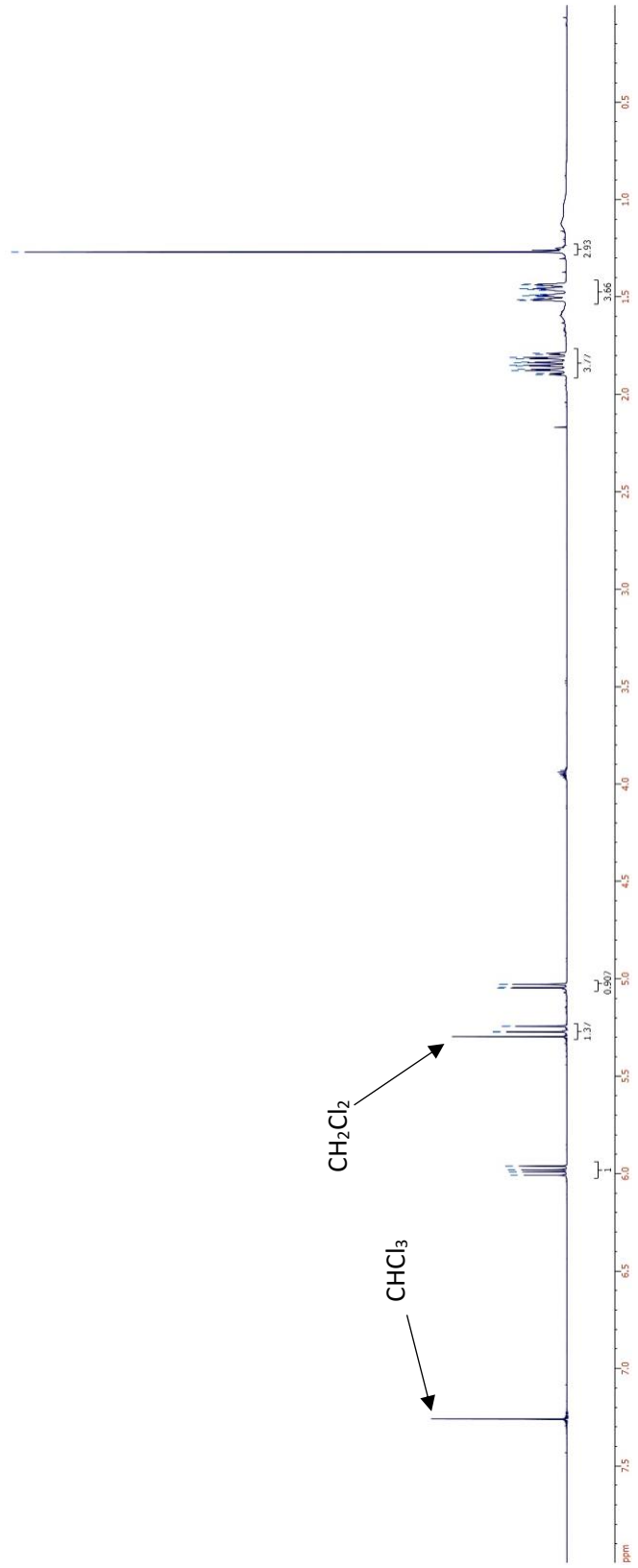
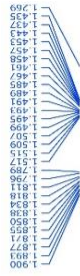


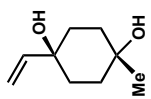
3.105 (¹³C NMR, 151 MHz, CDCl₃, 25 °C)



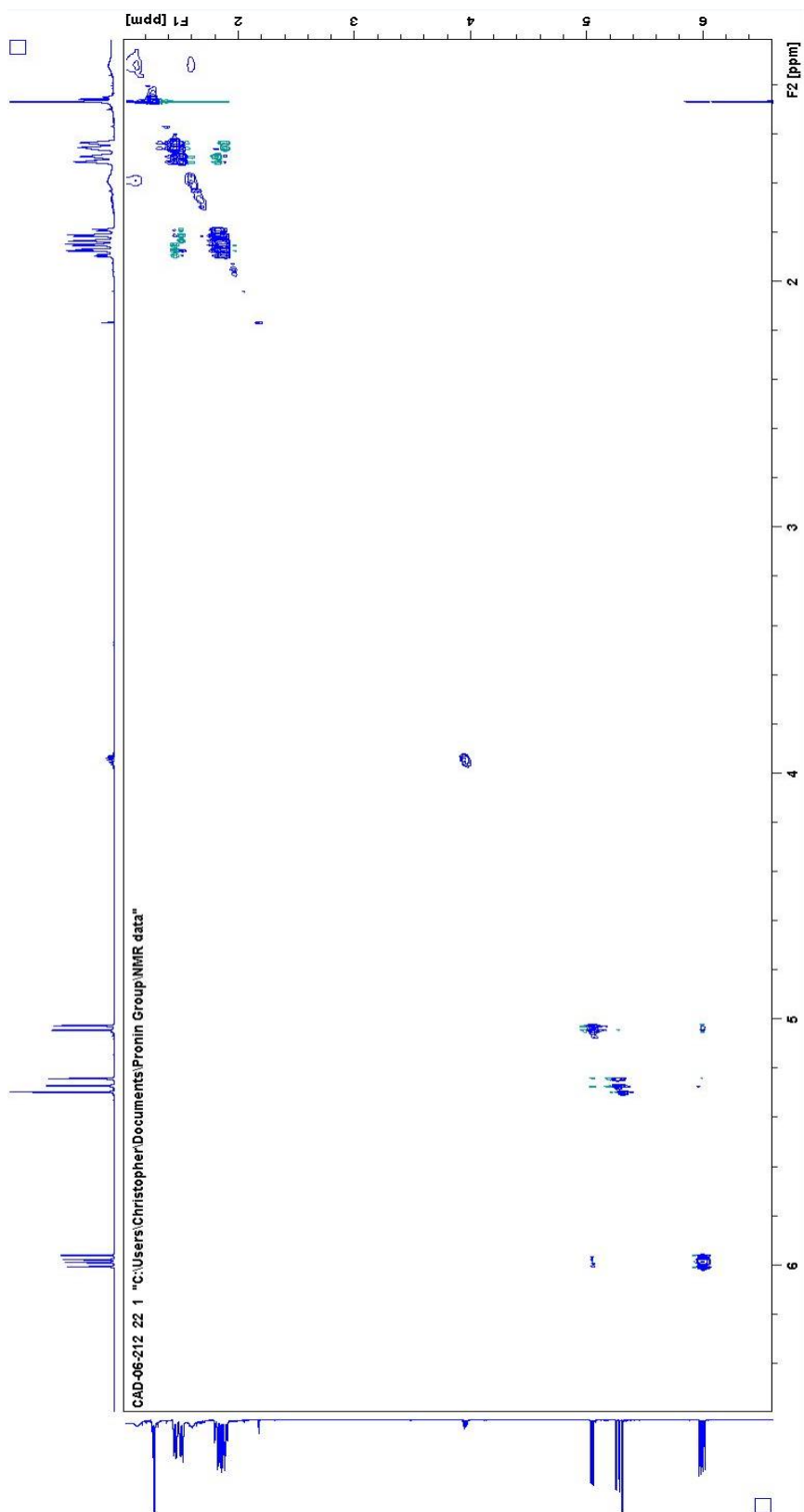


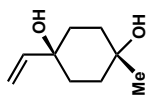
3.107 (¹H NMR, 600 MHz, CDCl₃, 25 °C)



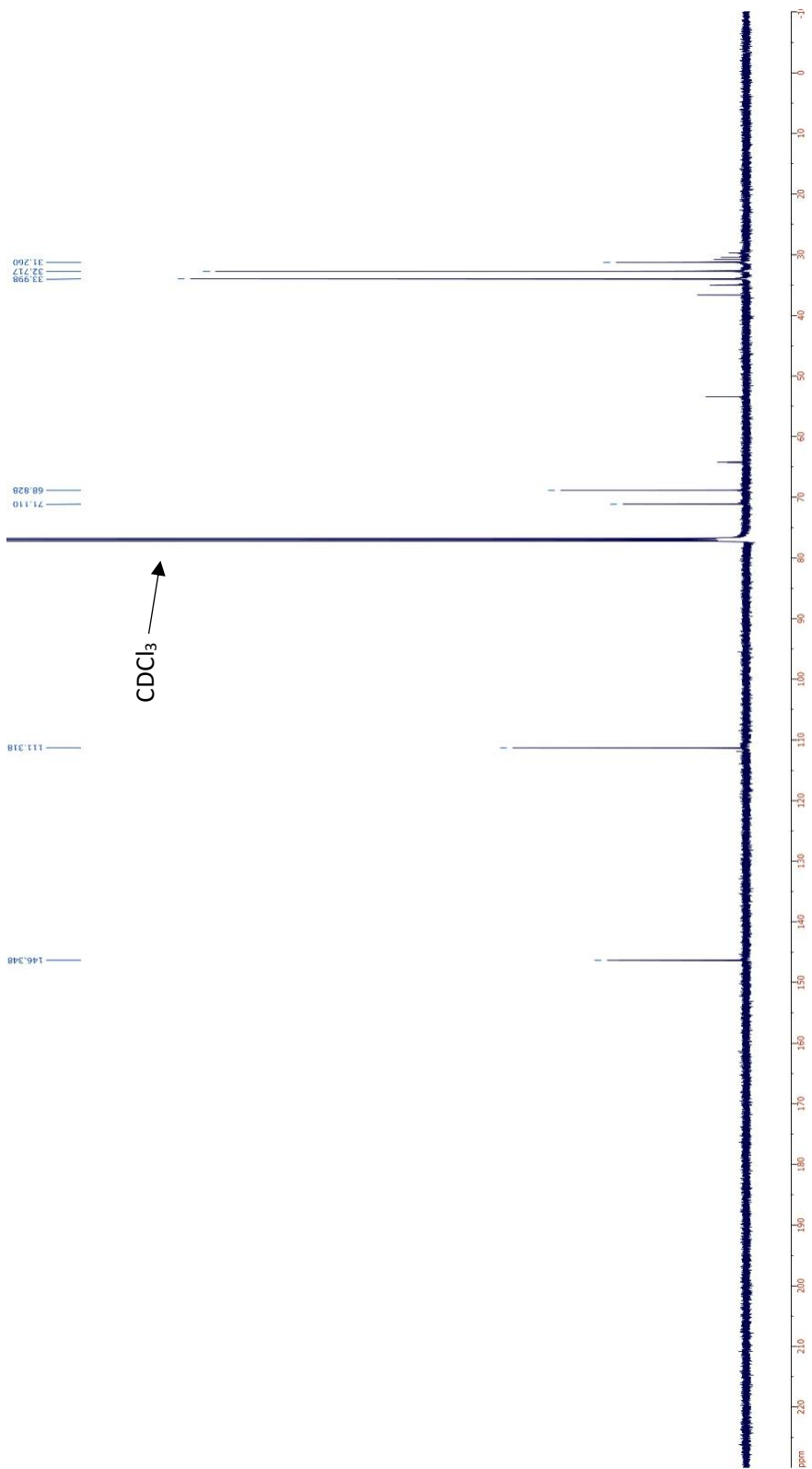


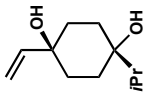
3.107 (NOESY, CDCl₃, 25 °C)



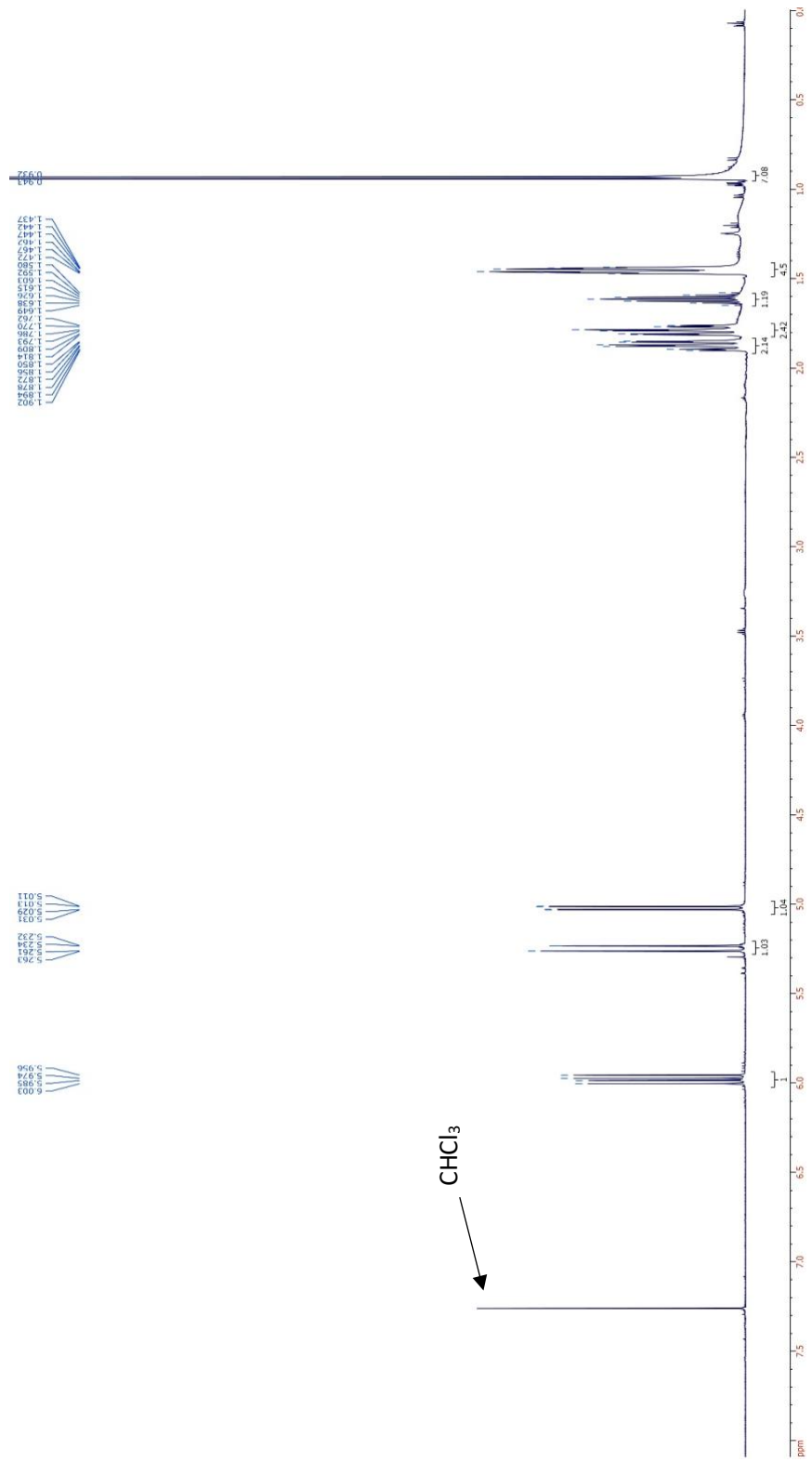


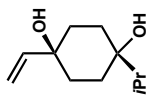
3.107 (¹³C NMR, 151 MHz, CDCl₃, 25 °C)



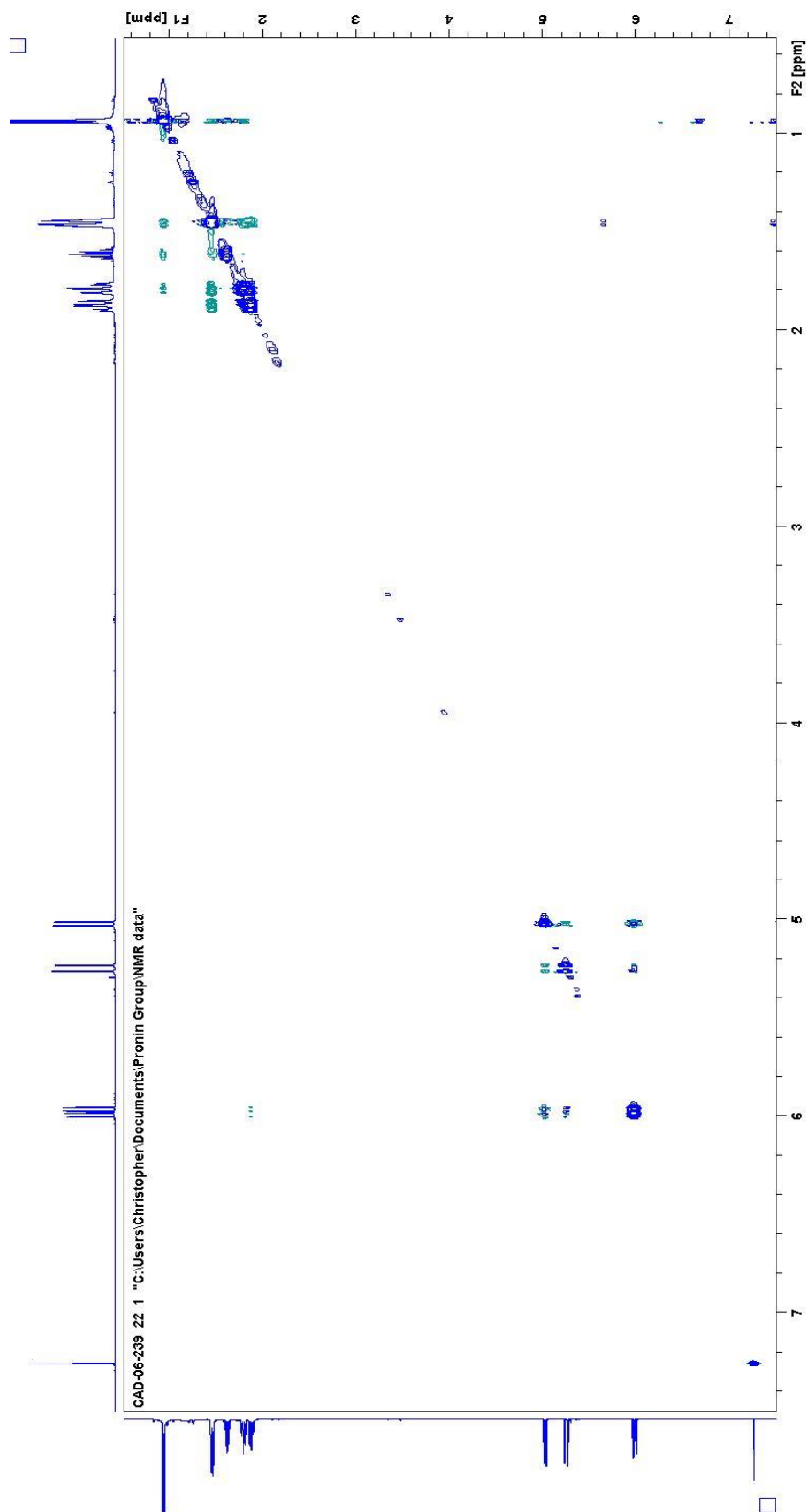


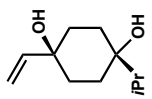
3.109 (¹H NMR, 600 MHz, CDCl₃, 25 °C)



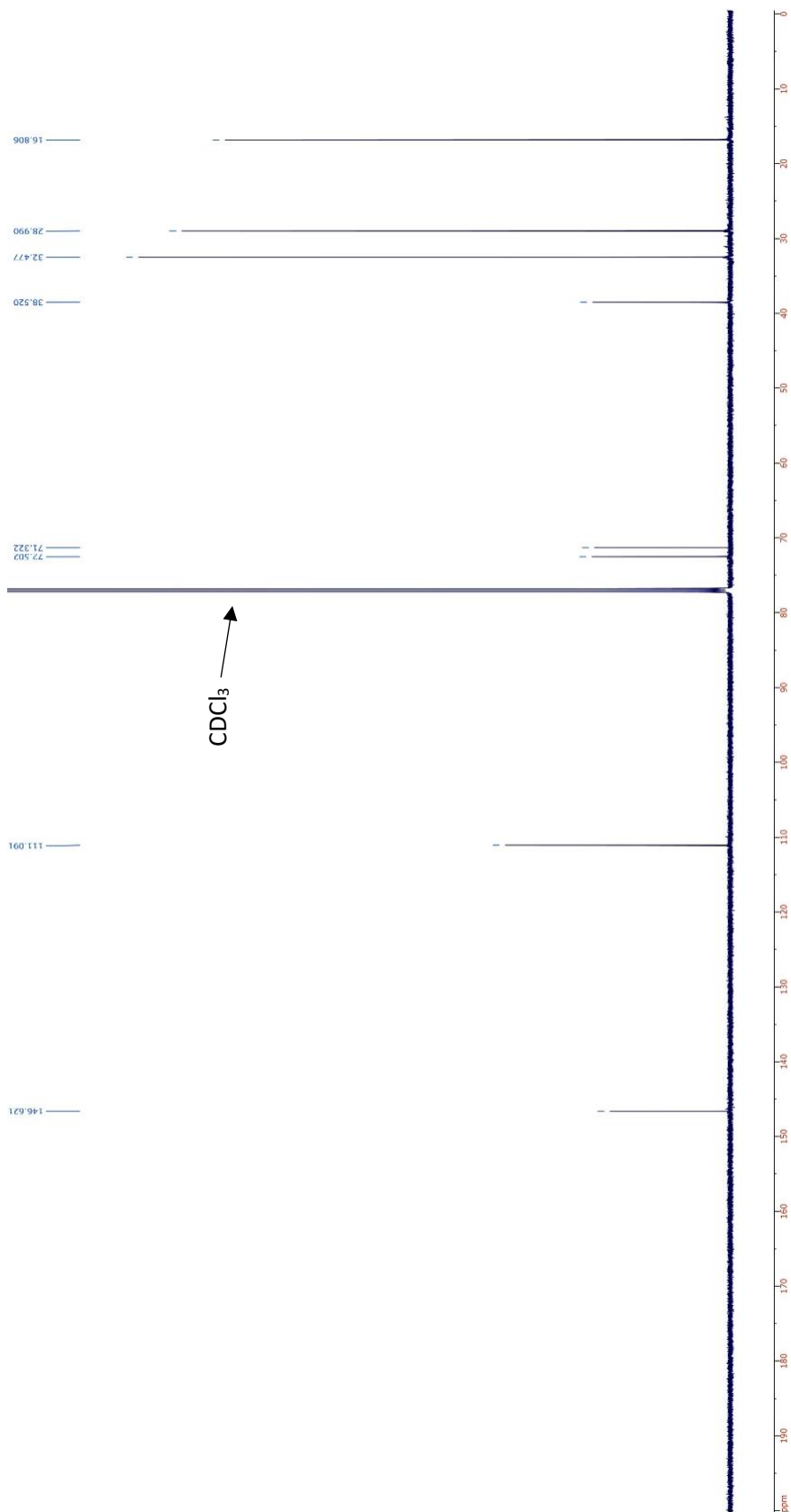


3.109 (NOESY, CDCl₃, 25 °C)

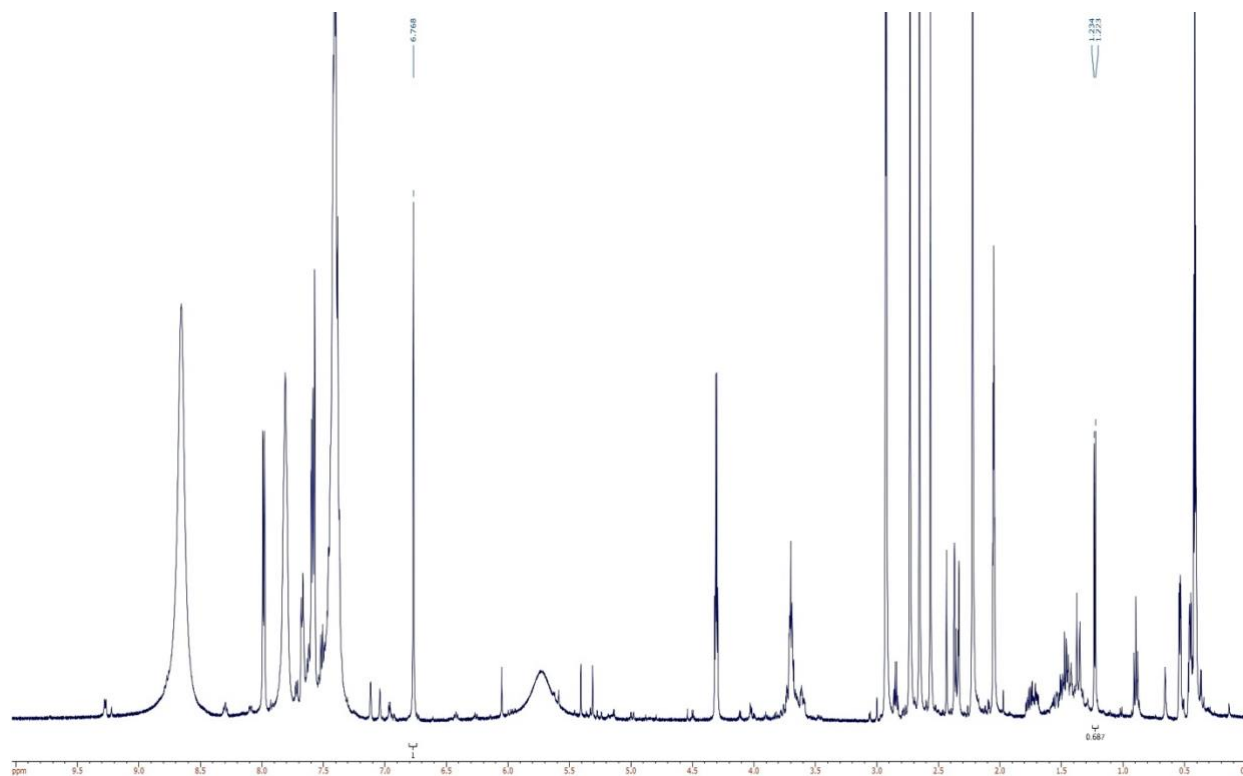
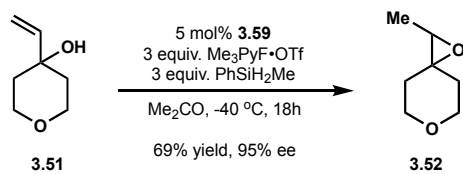




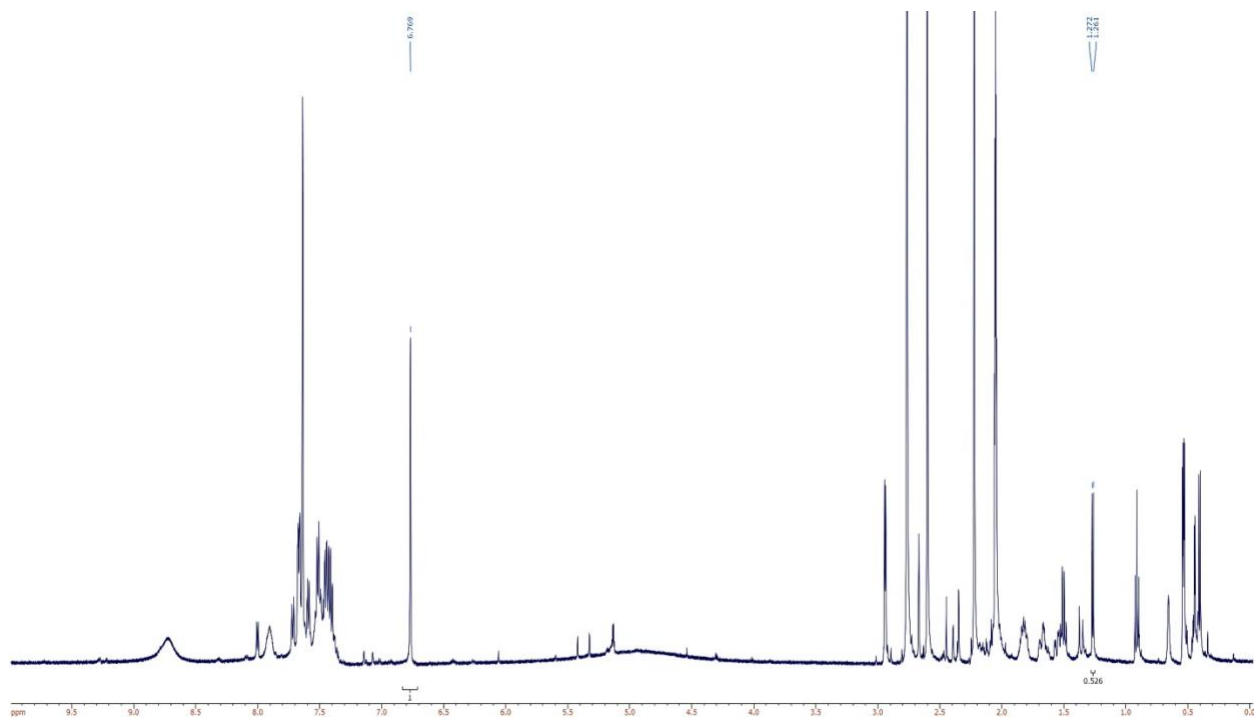
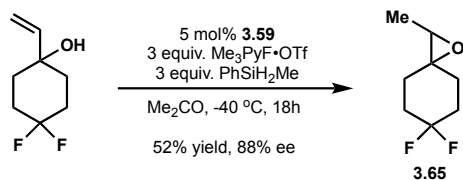
3.109 (^{13}C NMR, 151 MHz, CDCl_3 , 25 °C)

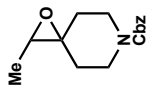


^1H NMR of crude radical-polar crossover epoxidation using allylic alcohol **3.51** (12.8 mg, 0.10 mmol) and catalyst **3.59** with mesitylene (12 mg, 0.10 mmol) as the internal standard to determine ^1H NMR yield. The methyl doublet of the epoxide **3.52** (1.23 ppm, d, $J = 5.5$ Hz, 3H) is integrated against the aromatic C–H resonance of mesitylene (6.77 ppm, s, 3H) indicating 69% ^1H NMR yield.

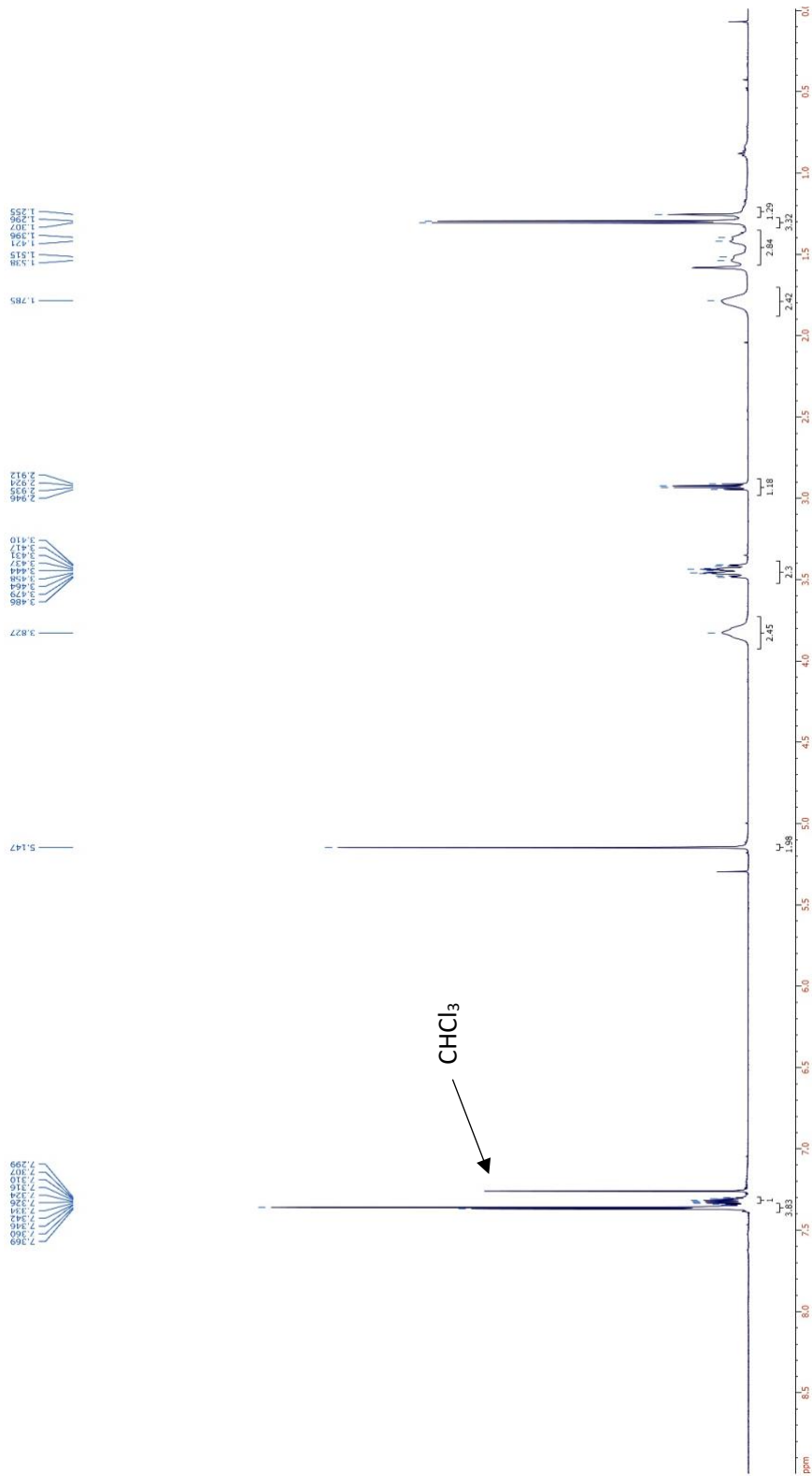


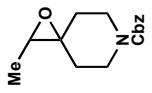
^1H NMR of crude radical-polar crossover epoxidation using 4,4-difluoro-1-vinylcyclohexan-1-ol (16.2 mg, 0.10 mmol) and catalyst **3.59** with mesitylene (12 mg, 0.10 mmol) as the internal standard to determine ^1H NMR yield. The methyl doublet of epoxide **3.65** (1.27 ppm, d, $J = 5.5$ Hz, 3H) is integrated against the aromatic C–H resonance of mesitylene (6.77 ppm, s, 3H) indicating 53% ^1H NMR yield.



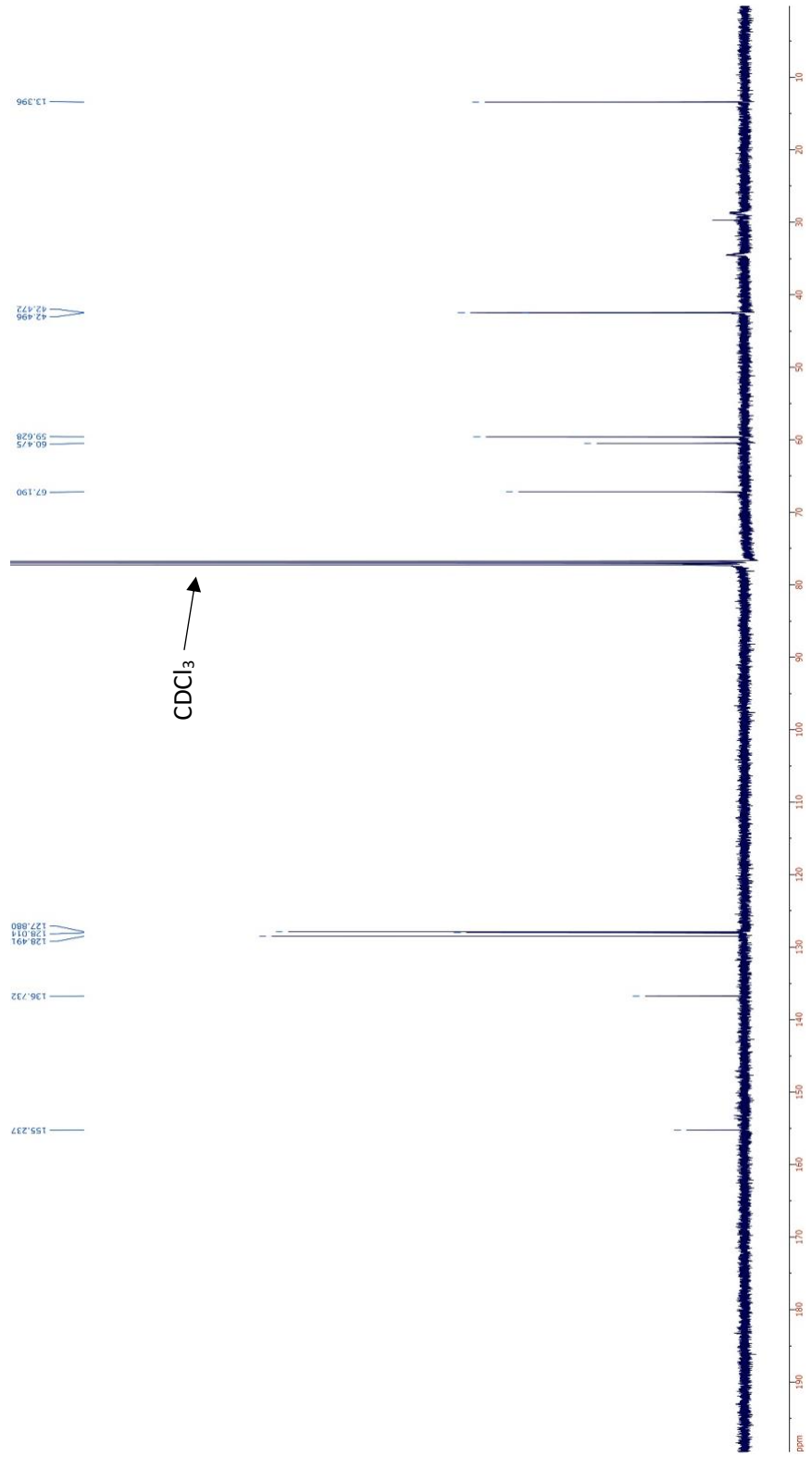


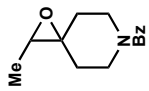
3.60 (¹H NMR, 600 MHz, CDCl₃, 25 °C)



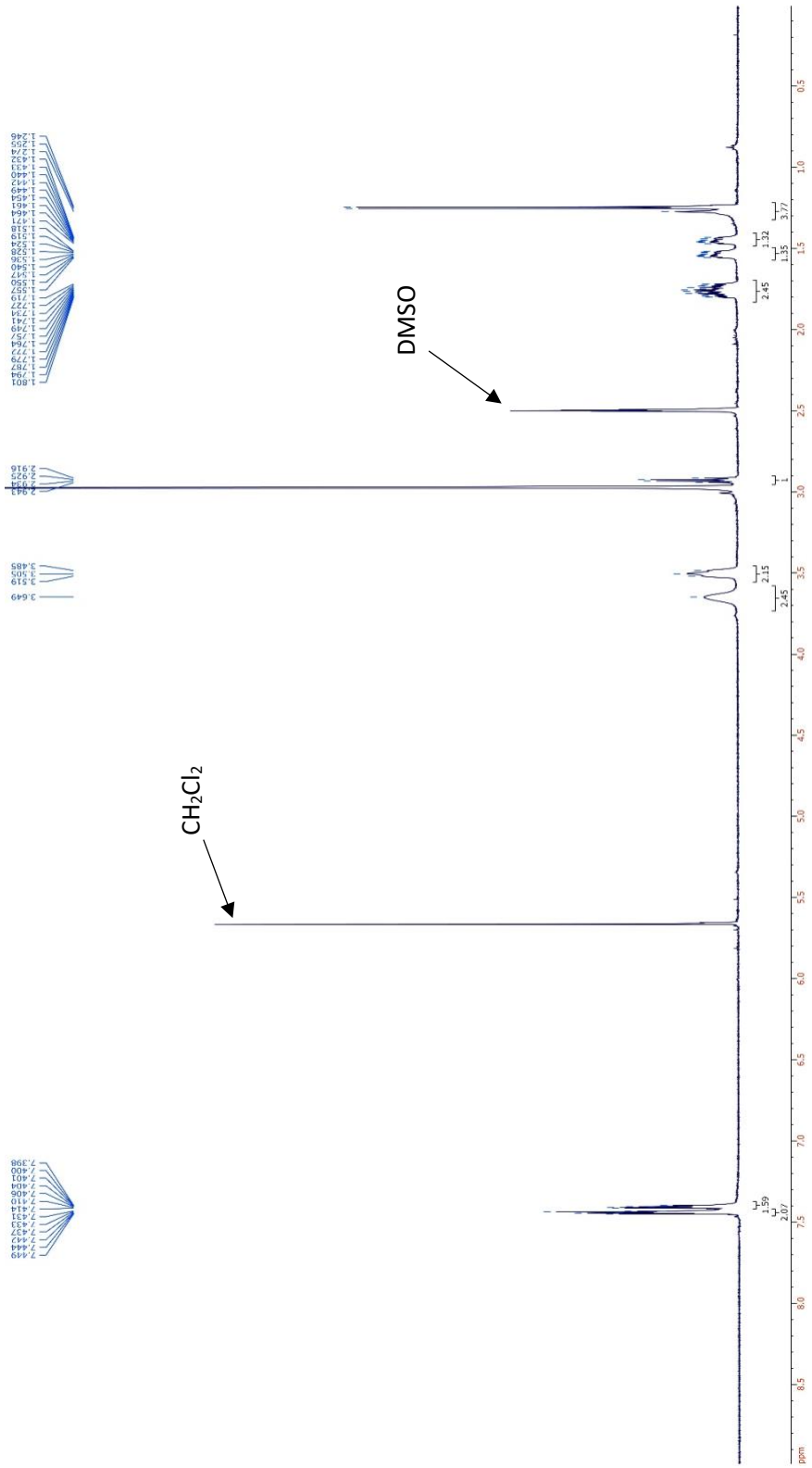


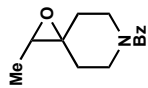
3.60 (¹³C NMR, 151 MHz, CDCl₃, 25 °C)



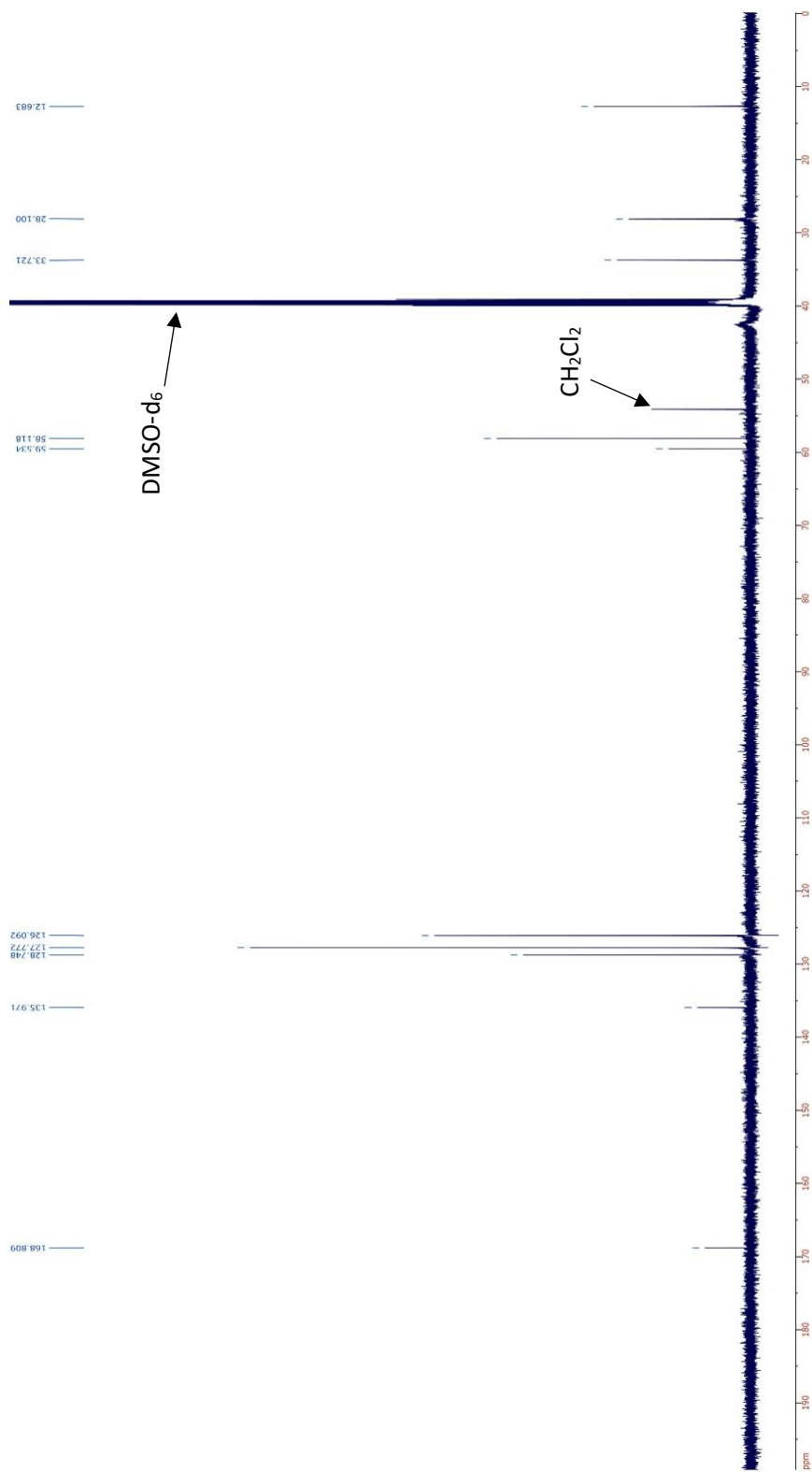


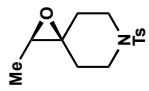
3.62 (¹H NMR, 600 MHz, DMSO-d₆, 100 °C)



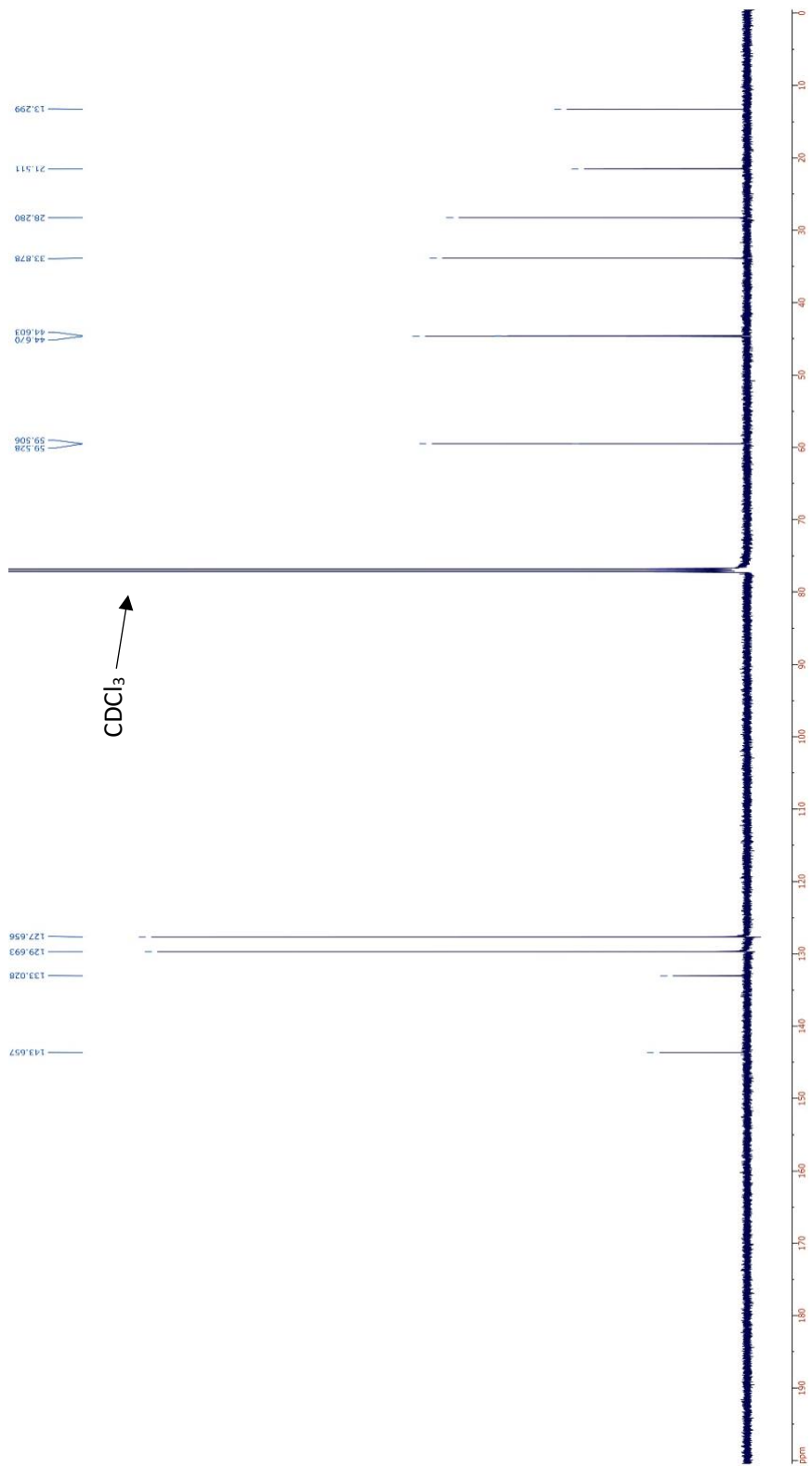


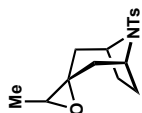
3.62 (^{13}C NMR, 151 MHz, DMSO-d_6 , 100 °C)



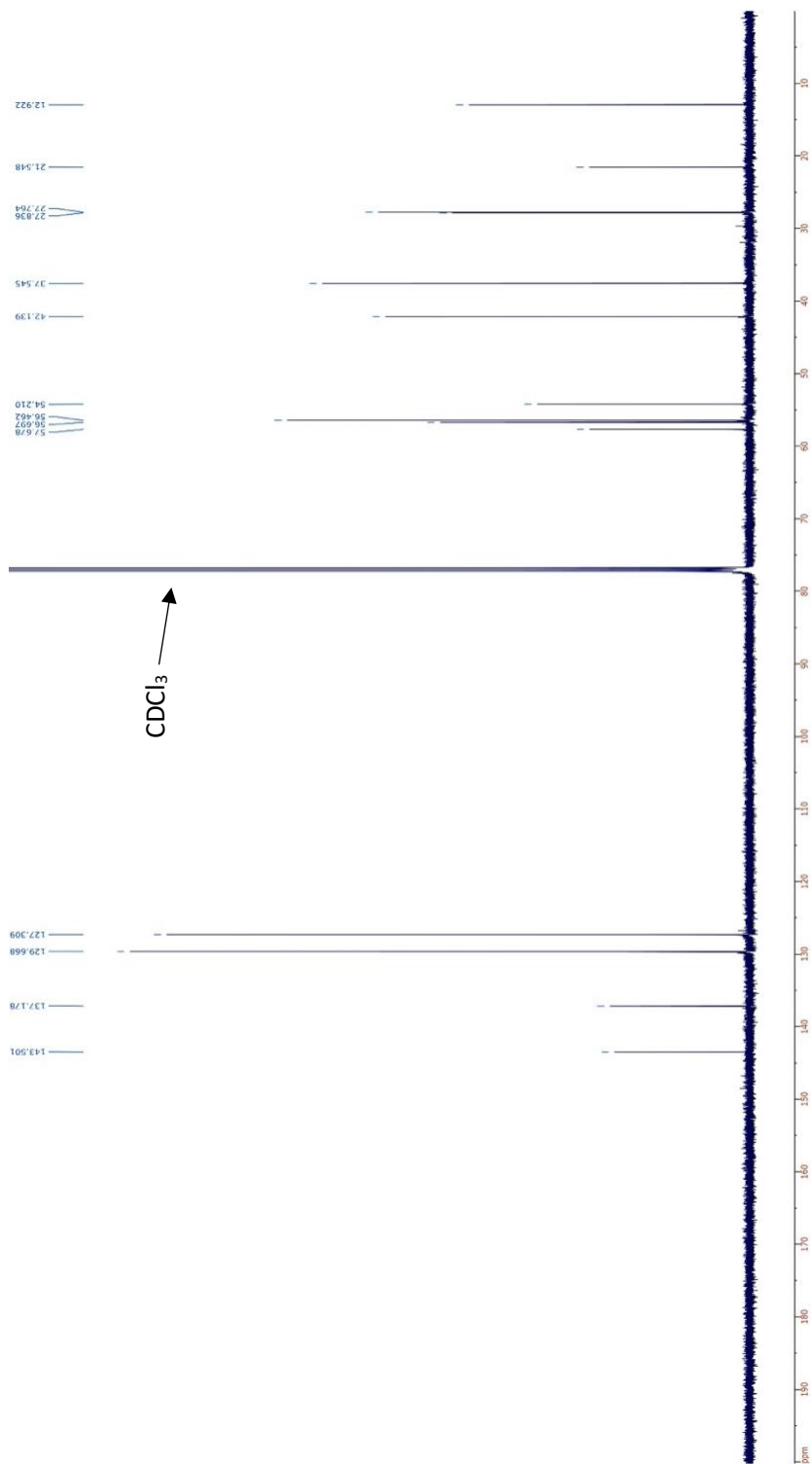


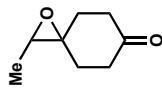
3.61 (¹³C NMR, 151 MHz, CDCl₃, 25 °C)



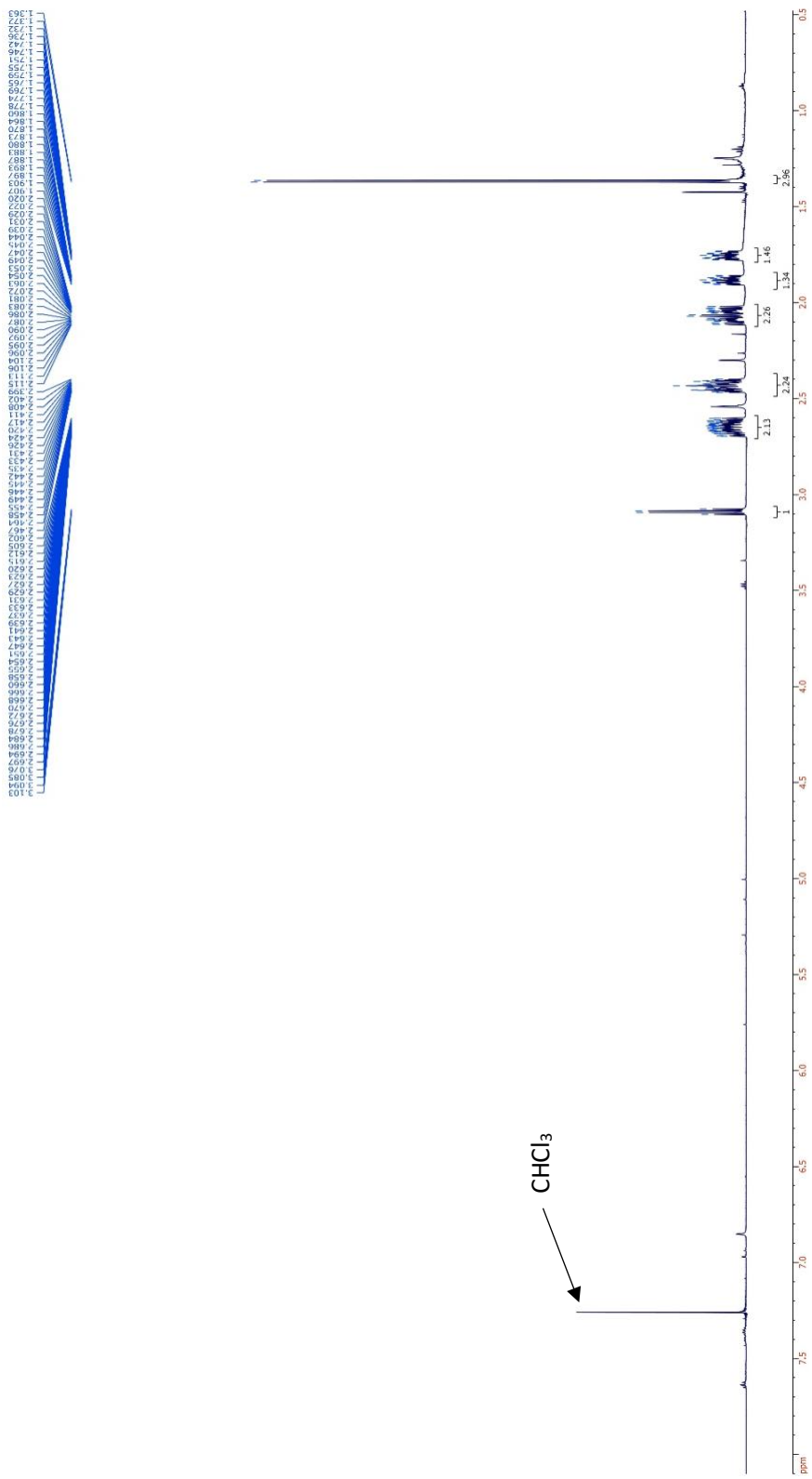


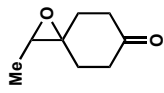
3.64 (¹³C NMR, 151 MHz, CDCl₃, 25 °C)



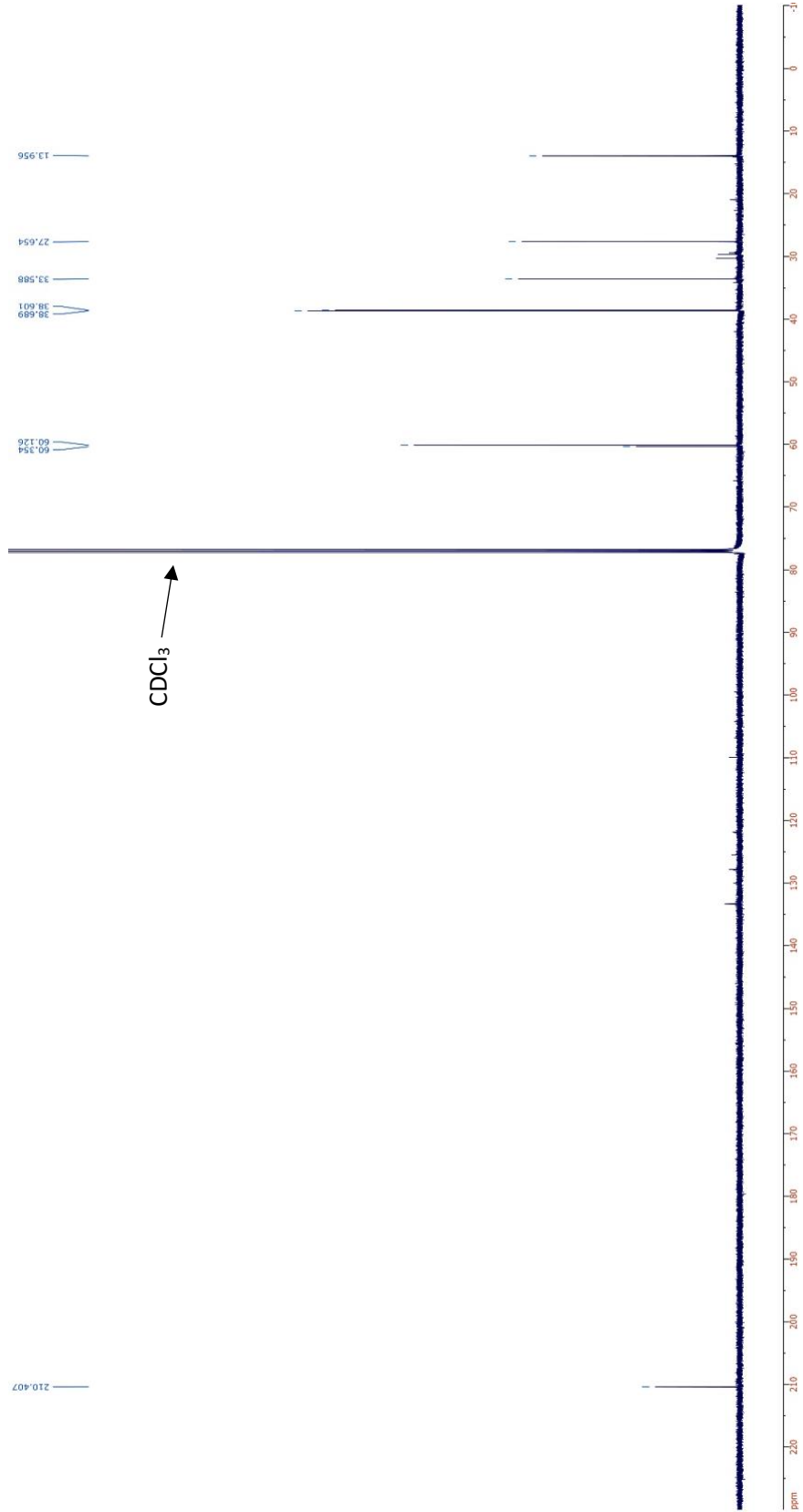


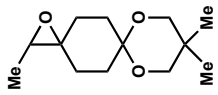
3.68 (¹H NMR, 600 MHz, CDCl₃, 25 °C)



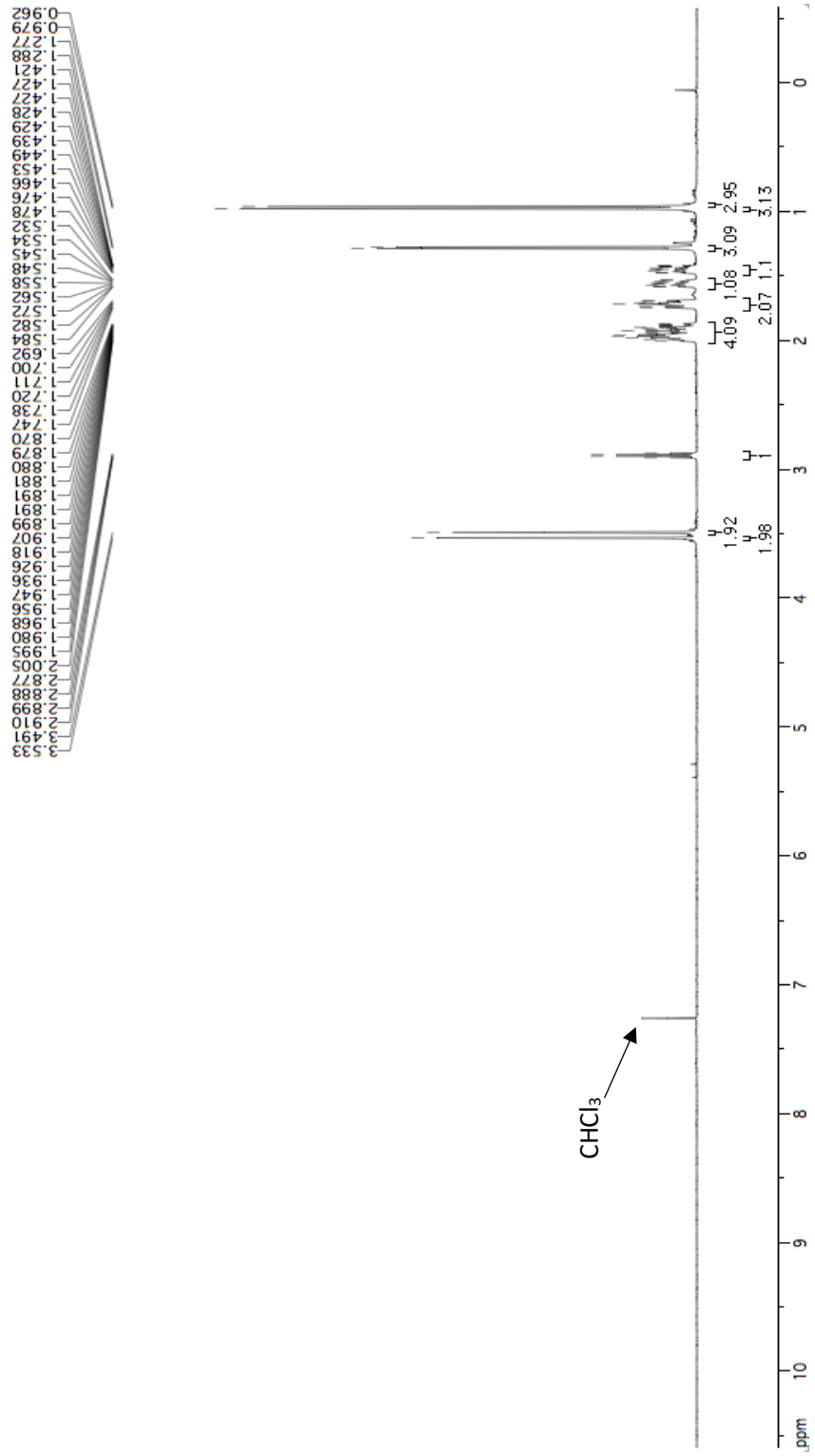


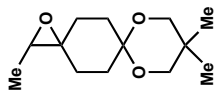
3.68 (¹³C NMR, 151 MHz, CDCl₃, 25 °C)



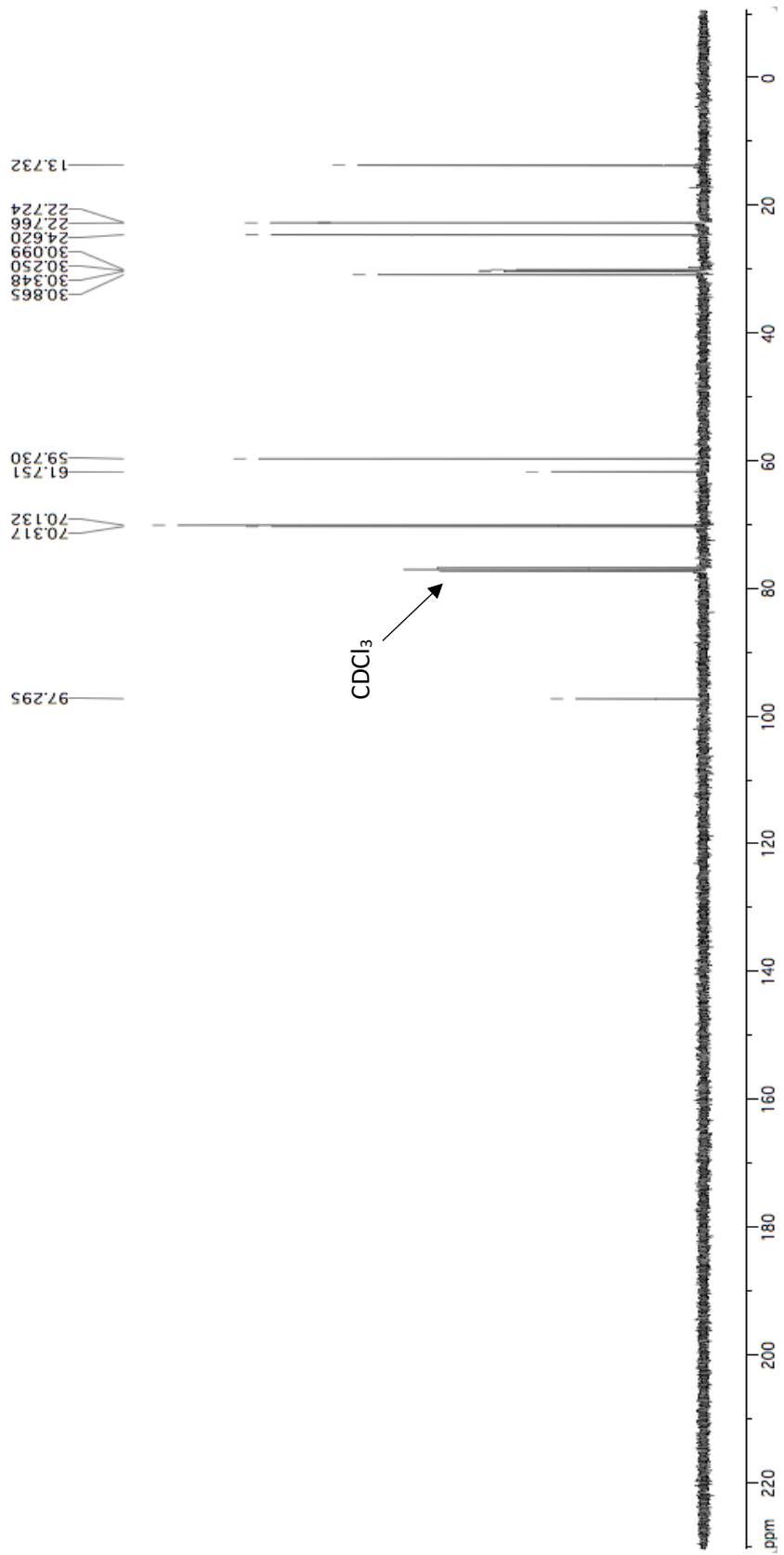


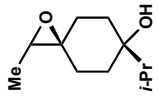
3.67 (¹H NMR, 500 MHz, CDCl₃, 25 °C)



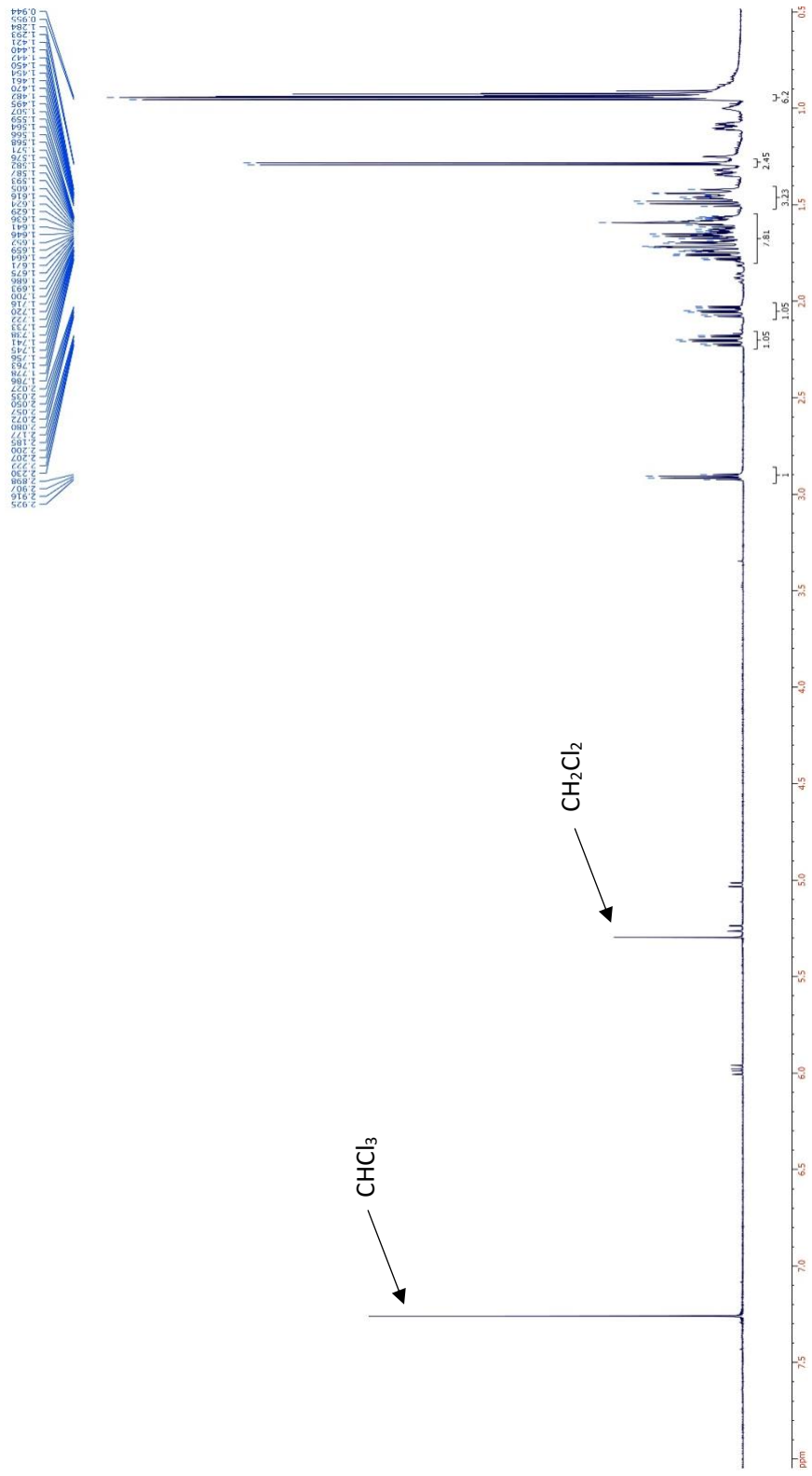


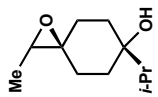
3.67 (¹³C NMR, 126 MHz, CDCl₃, 25 °C)



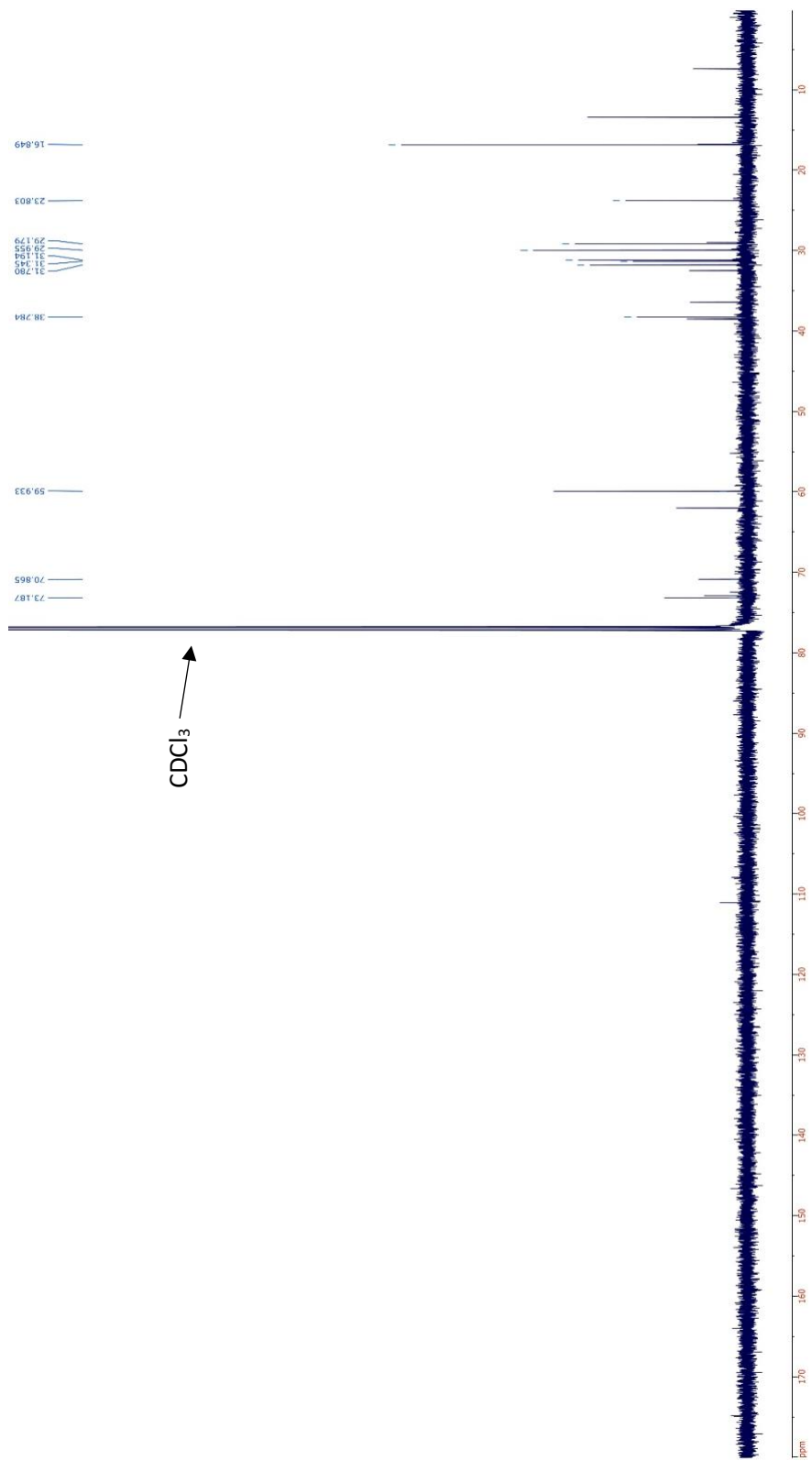


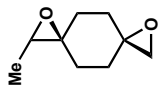
3.69 (¹H NMR, 600 MHz, CDCl₃, 25 °C)





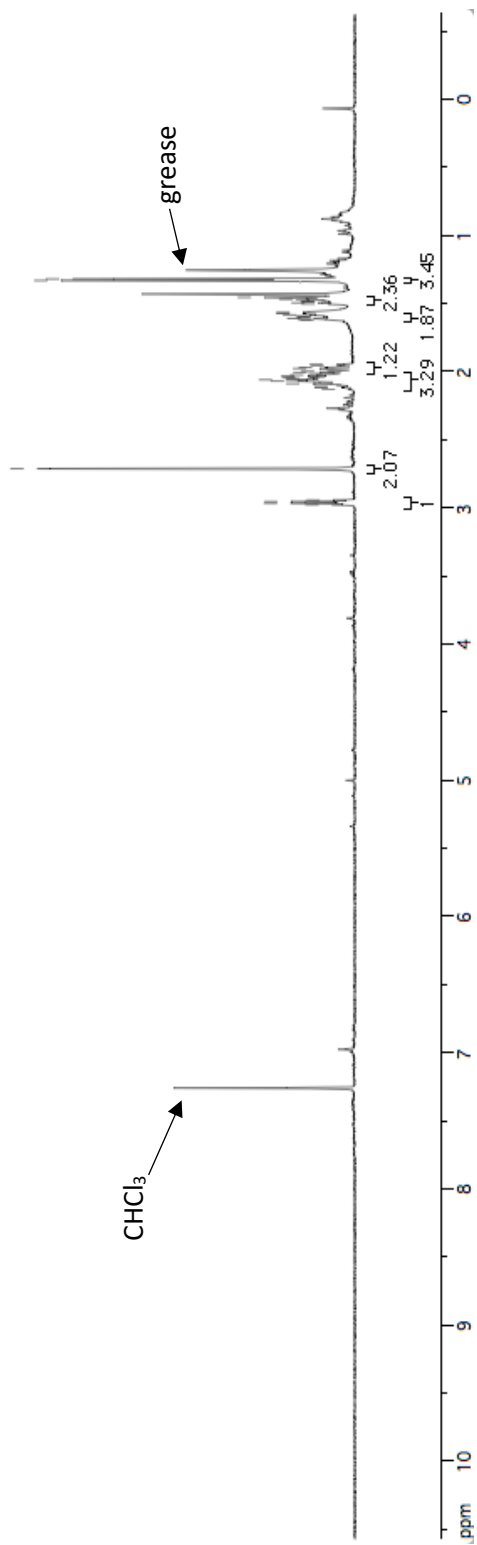
3.69 (¹³C NMR, 151 MHz, CDCl₃, 25 °C)

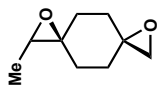




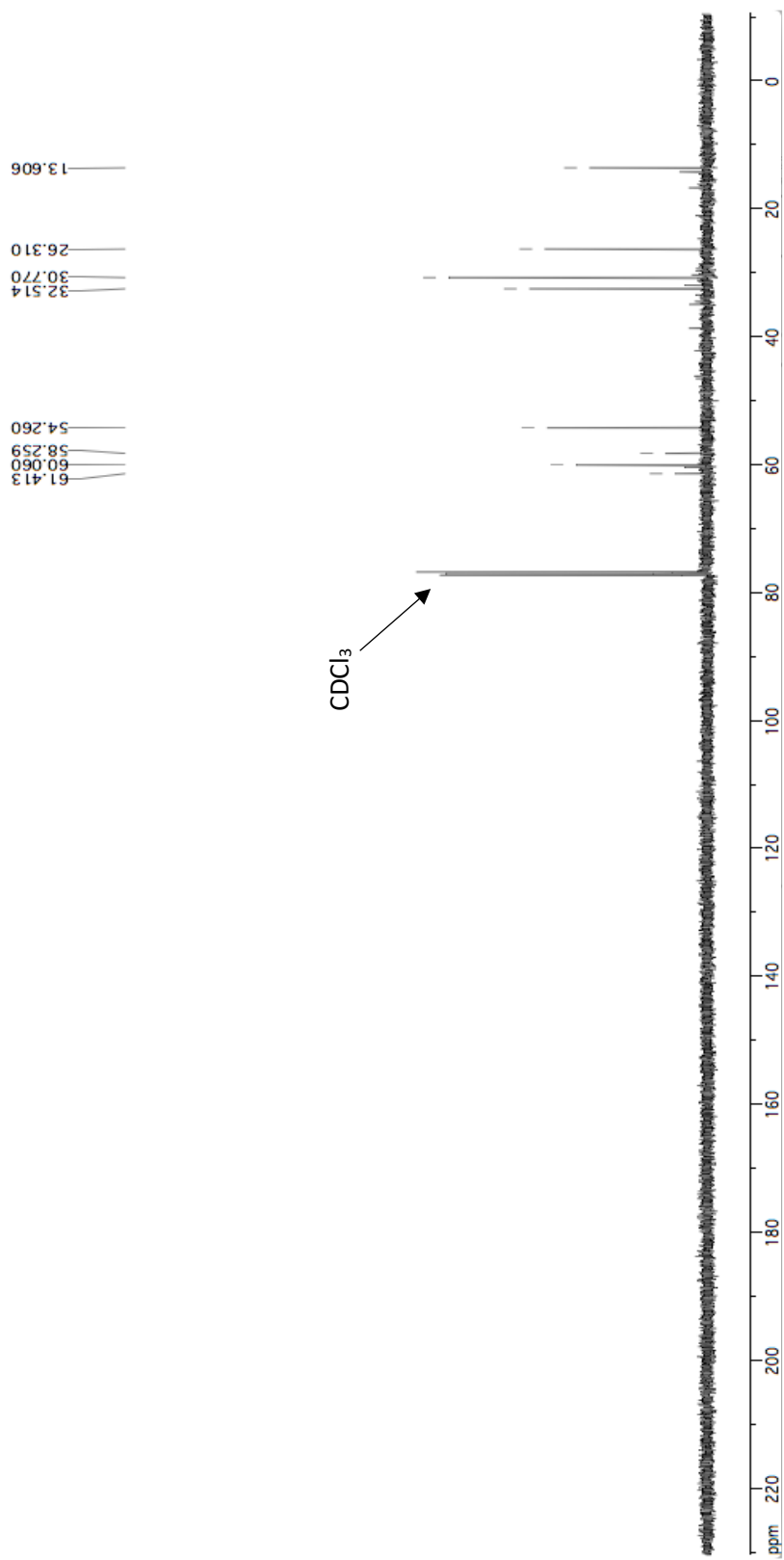
3.71 (¹H NMR, 500 MHz, CDCl₃, 25 °C)

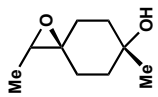
2.978
2.967
2.956
2.945
2.714
2.129
2.118
2.112
2.089
2.070
2.070
2.060
2.051
2.043
2.032
2.025
2.015
2.005
1.998
1.978
1.971
1.956
1.948
1.621
1.618
1.611
1.603
1.600
1.592
1.584
1.573
1.566
1.503
1.495
1.488
1.484
1.477
1.470
1.456
1.332
1.321



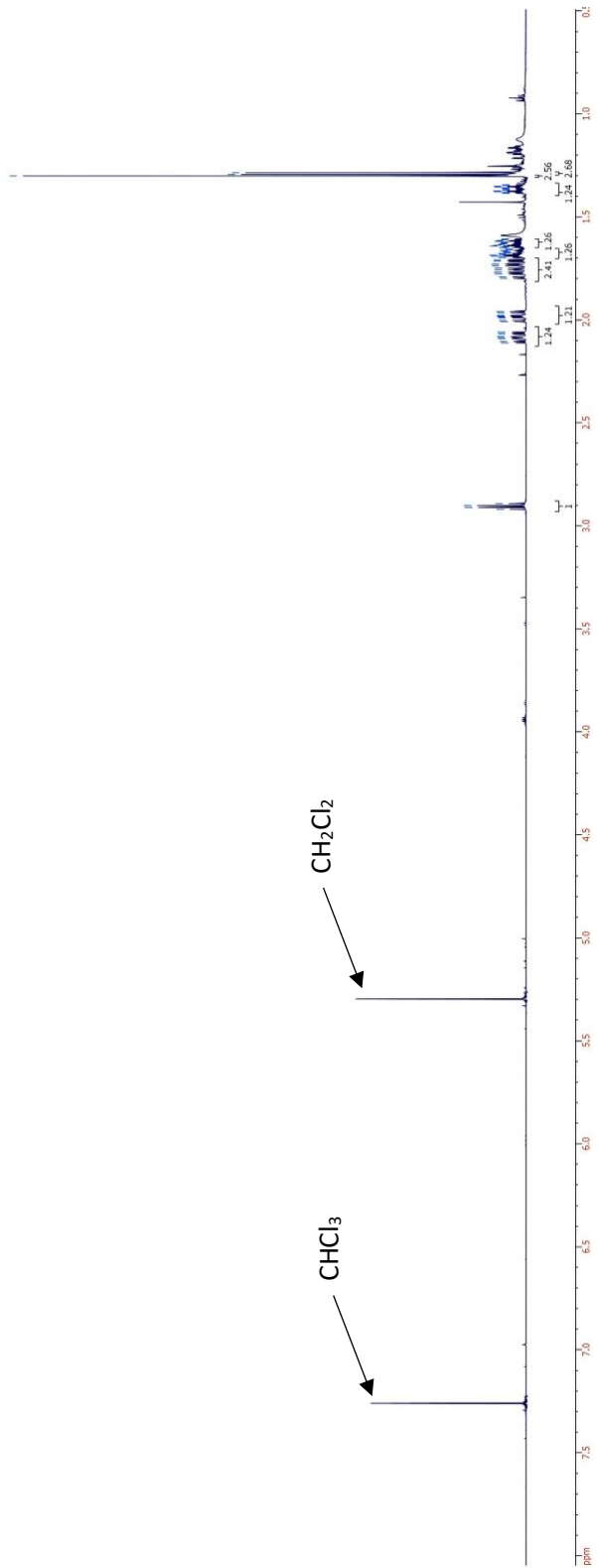


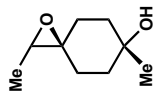
3.71 (¹³C NMR, 126 MHz, CDCl₃, 25 °C)



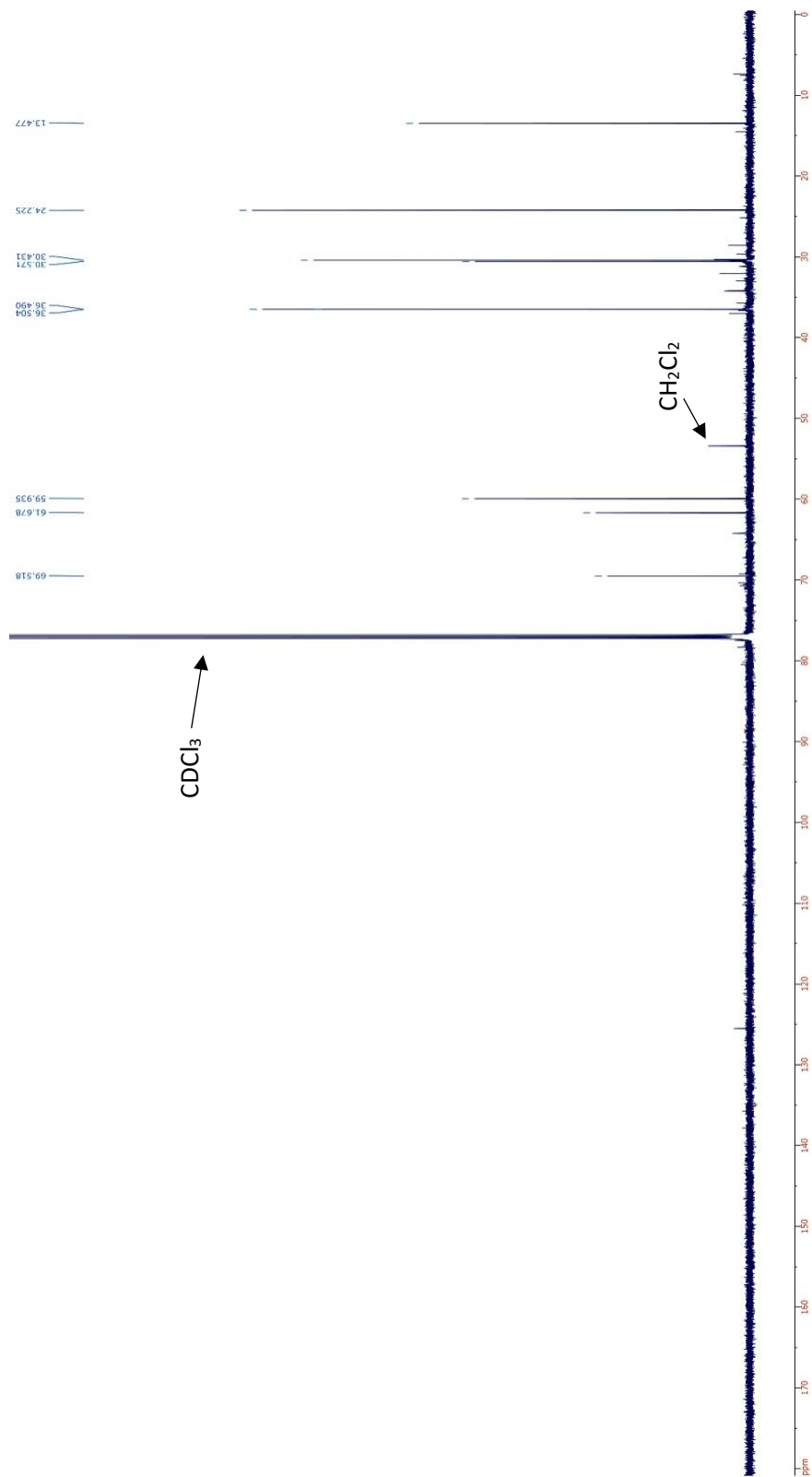


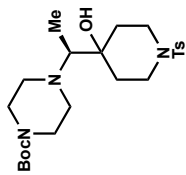
3.70 (¹H NMR, 500 MHz, CDCl₃, 25 °C)



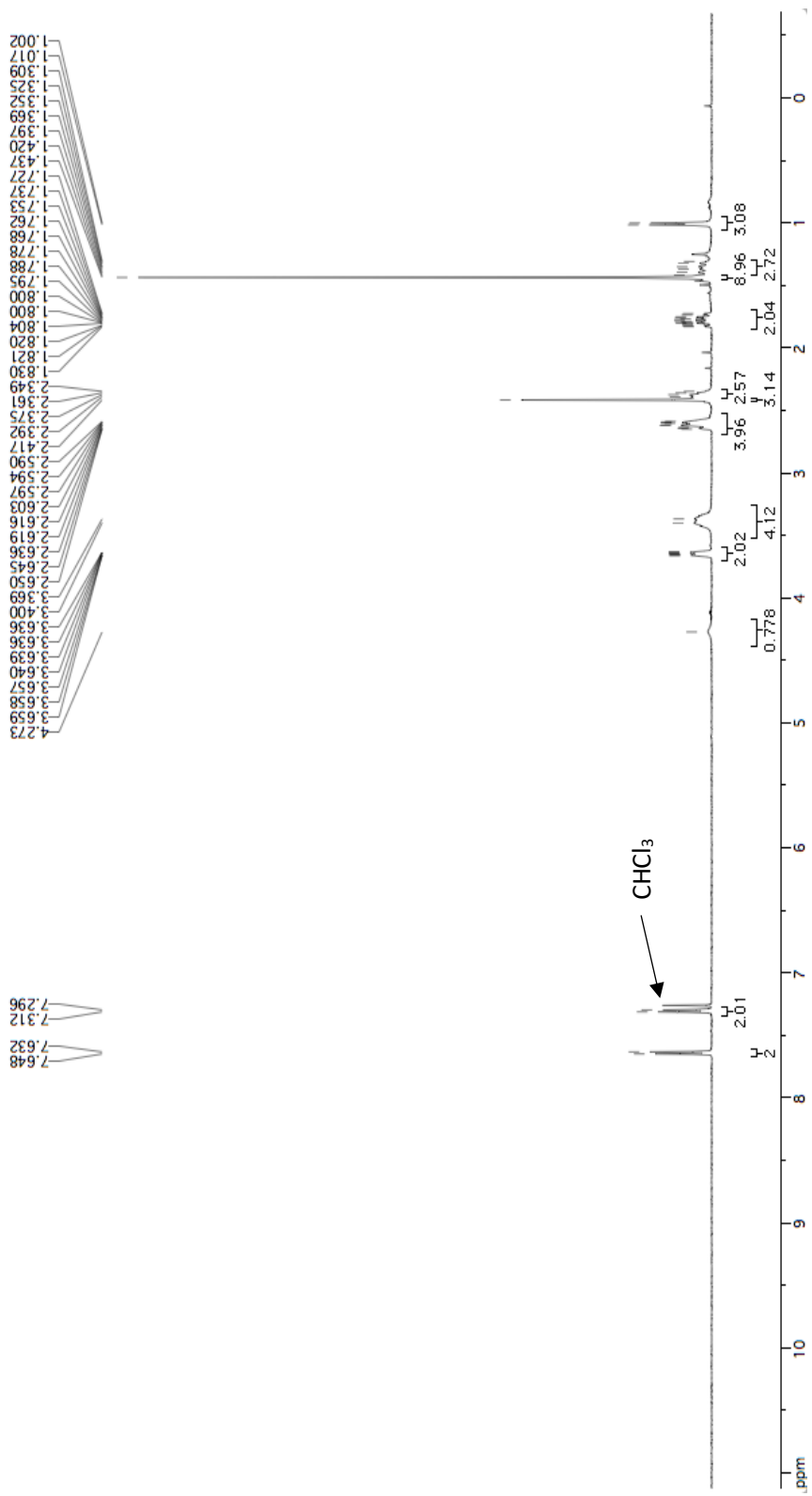


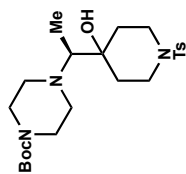
3.70 (¹³C NMR, 126 MHz, CDCl₃, 25 °C)



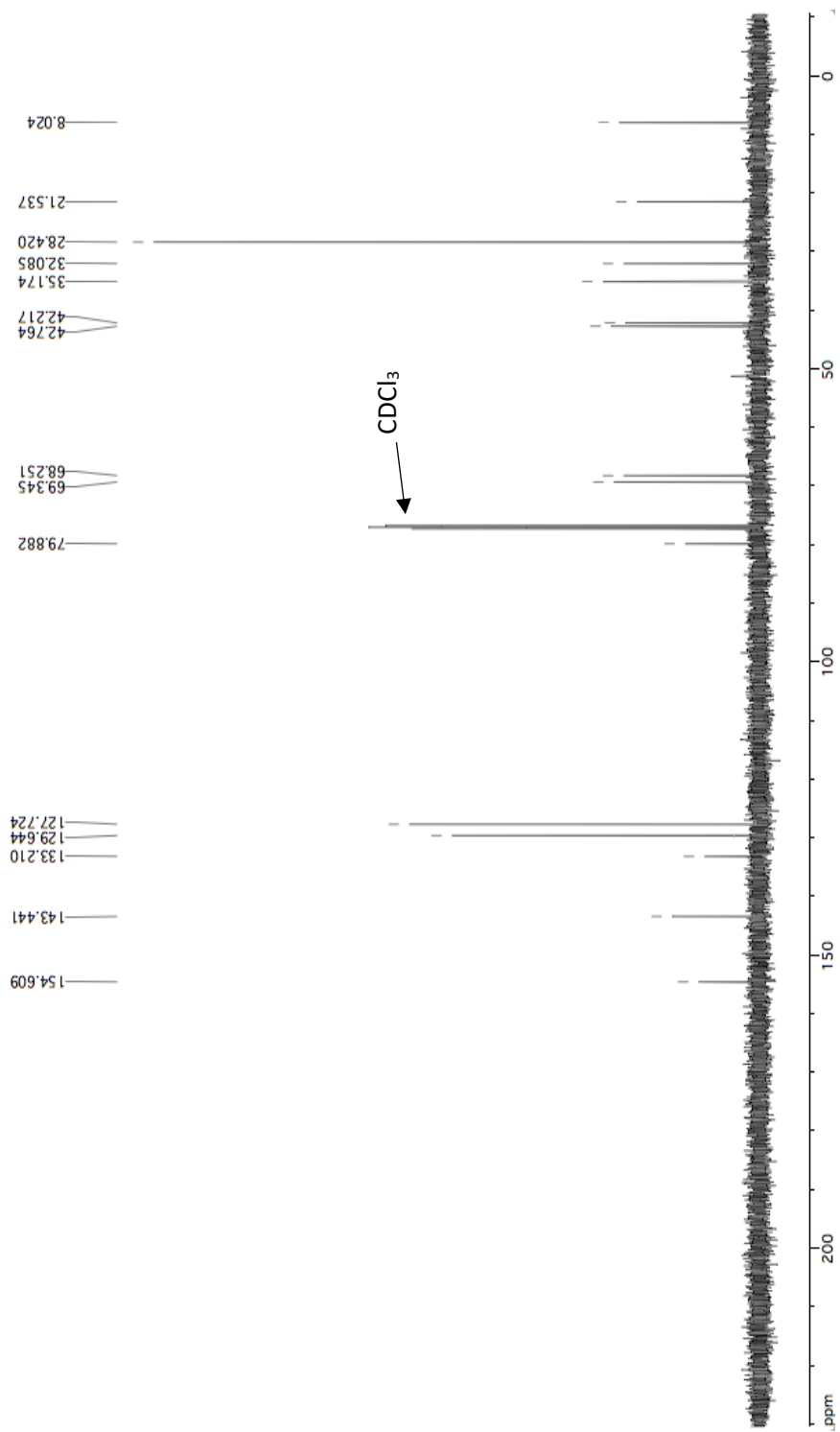


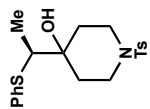
3.85 (¹H NMR, 500 MHz, CDCl₃, 25 °C)



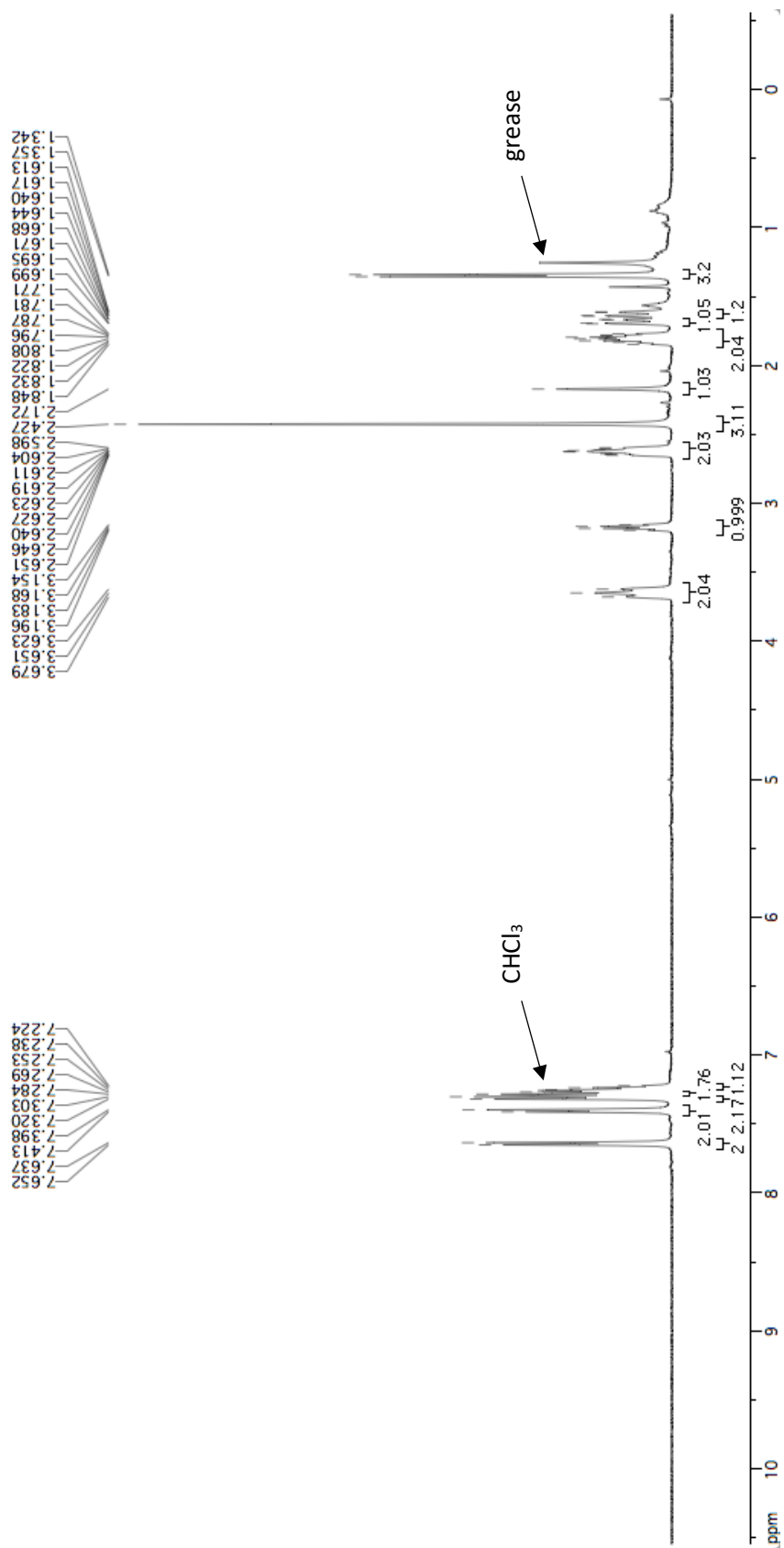


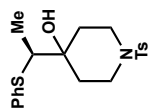
3.85 (¹³C NMR, 126 MHz, CDCl₃, 25 °C)



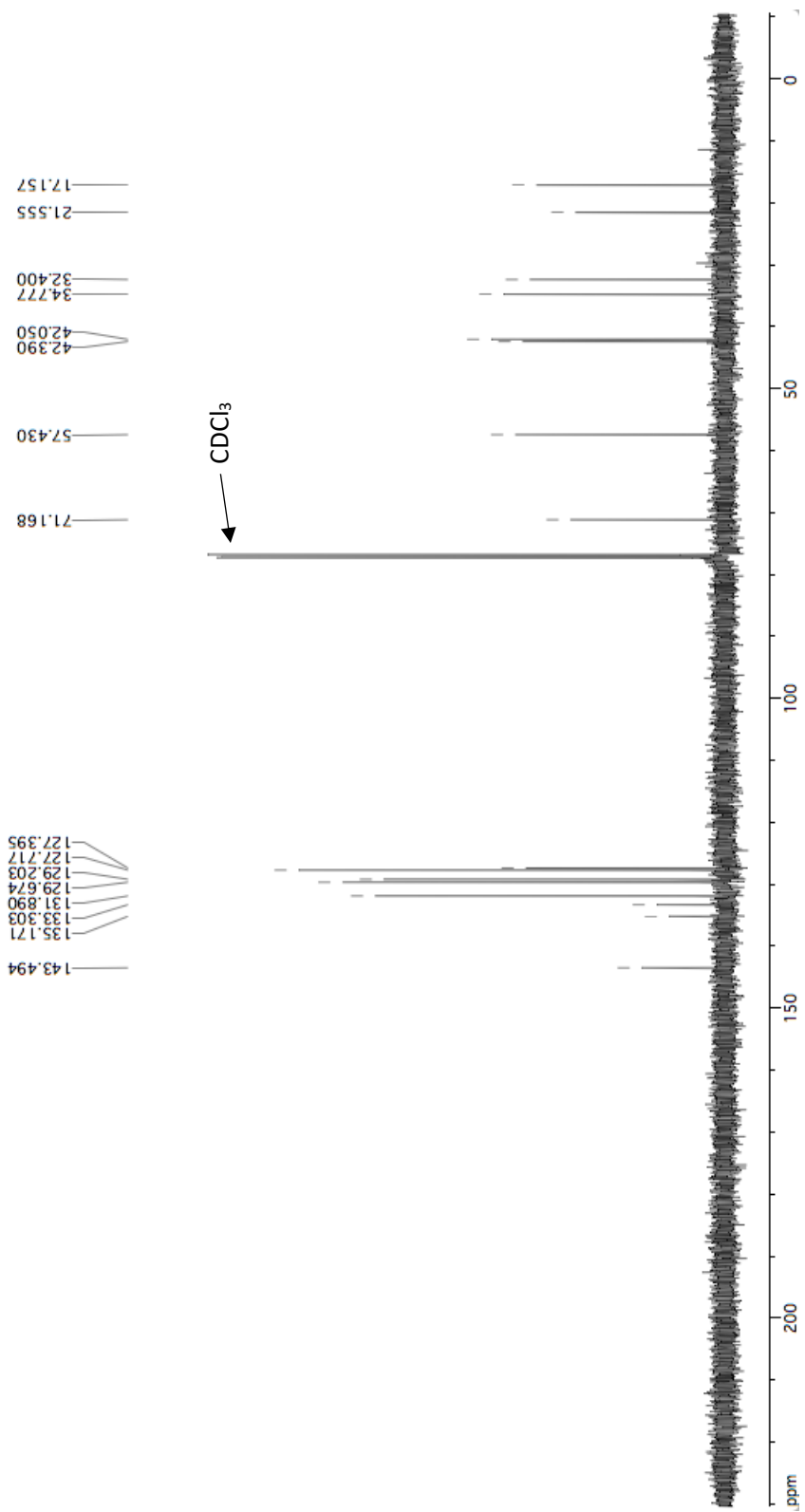


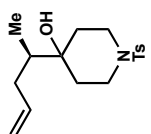
3.88 (¹H NMR, 500 MHz, CDCl₃, 25 °C)



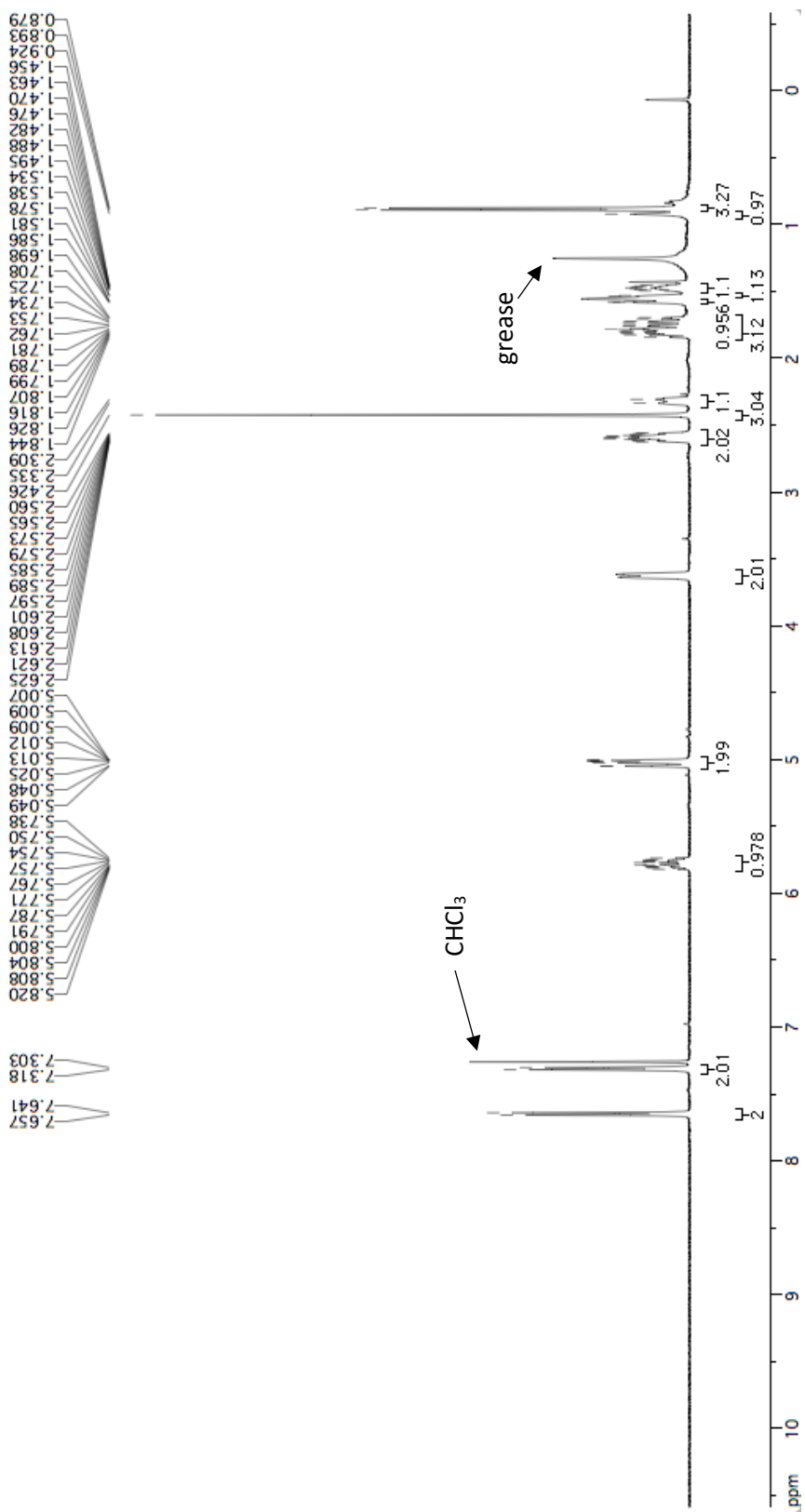


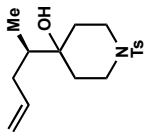
3.88 (¹³C NMR, 126 MHz, CDCl₃, 25 °C)



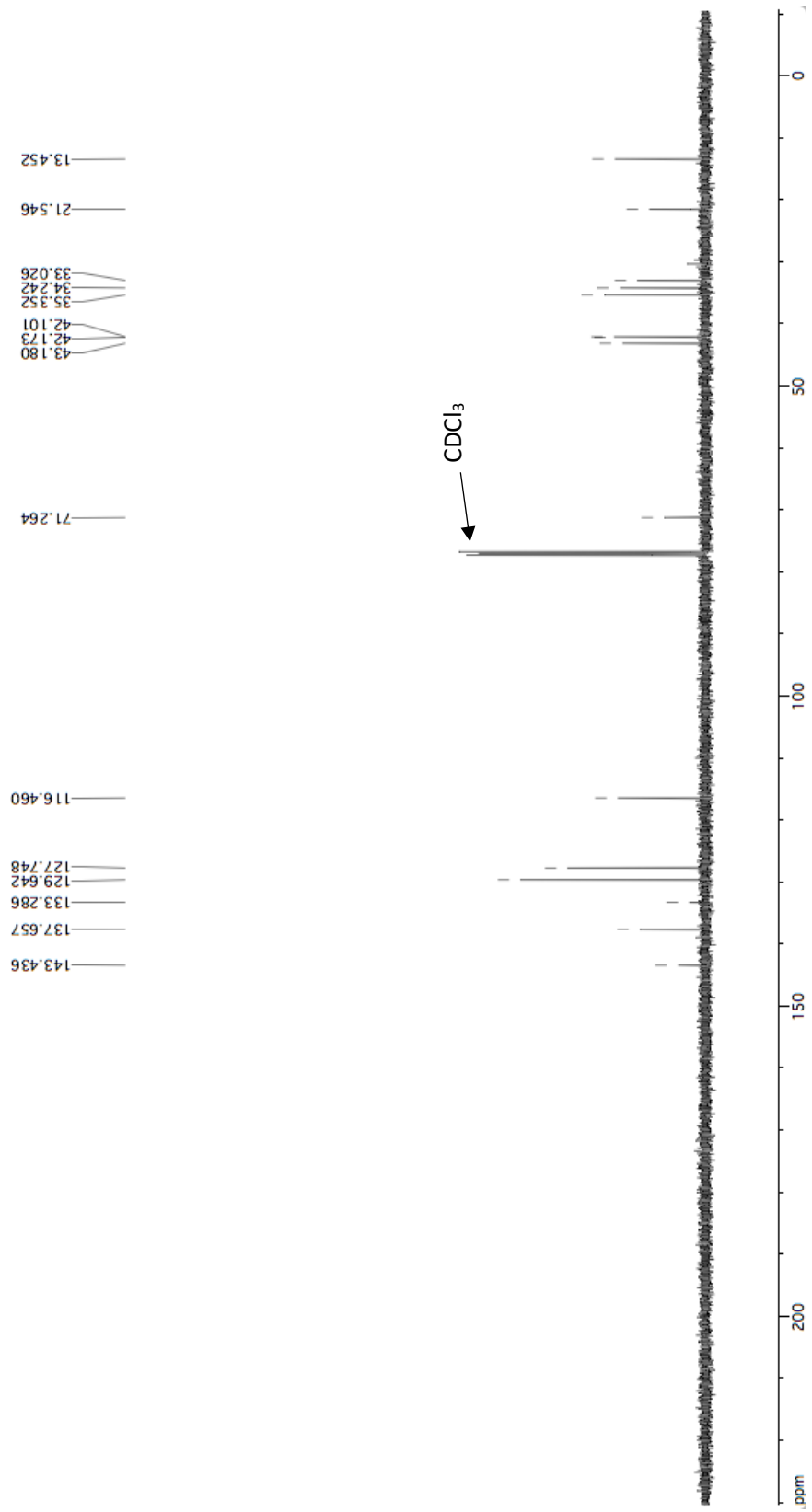


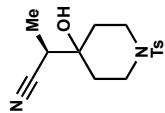
3.86 ($^1\text{H NMR}$, 500 MHz, CDCl_3 , 25 $^\circ\text{C}$)



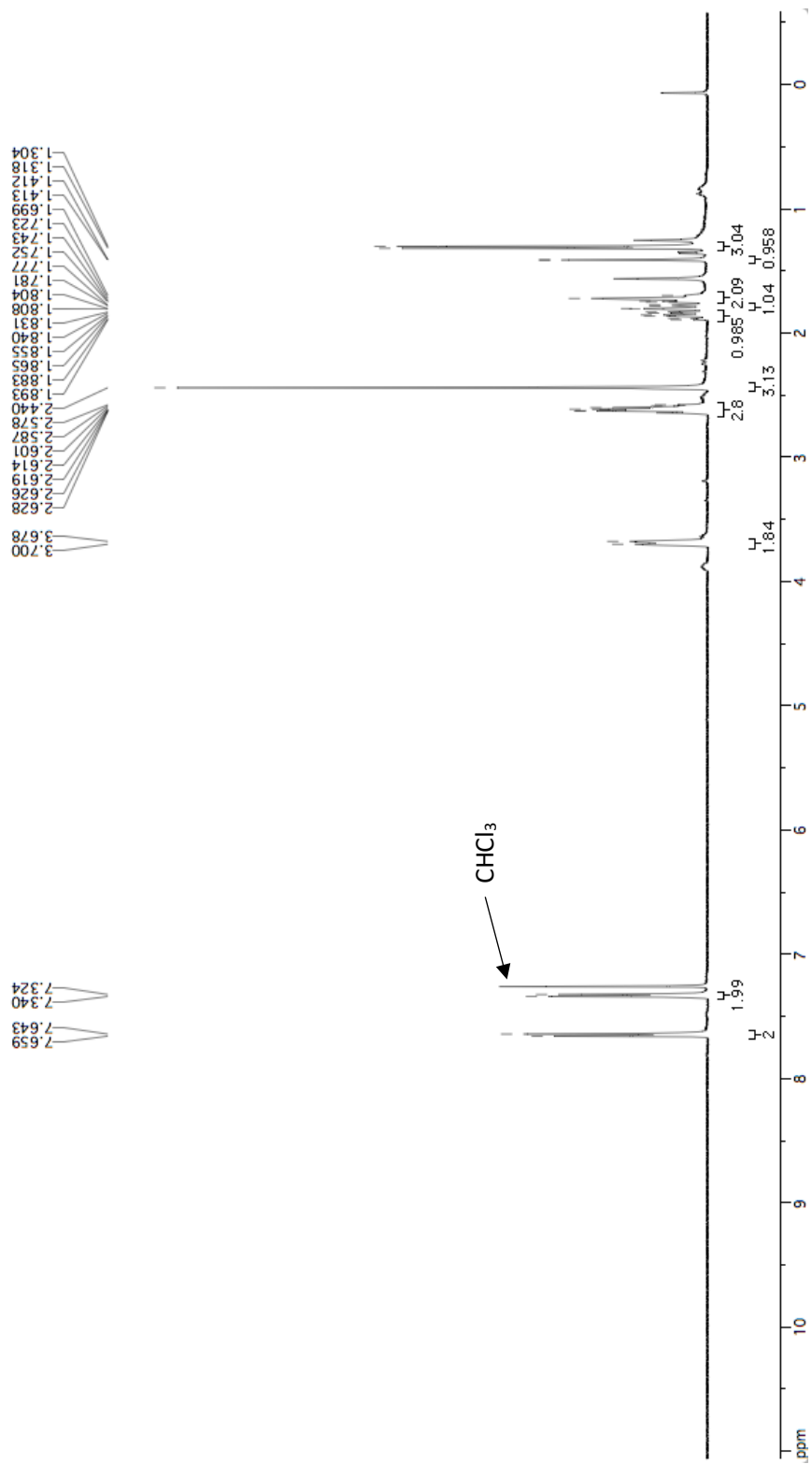


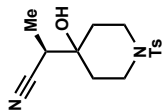
3.86 (¹³C NMR, 126 MHz, CDCl₃, 25 °C)



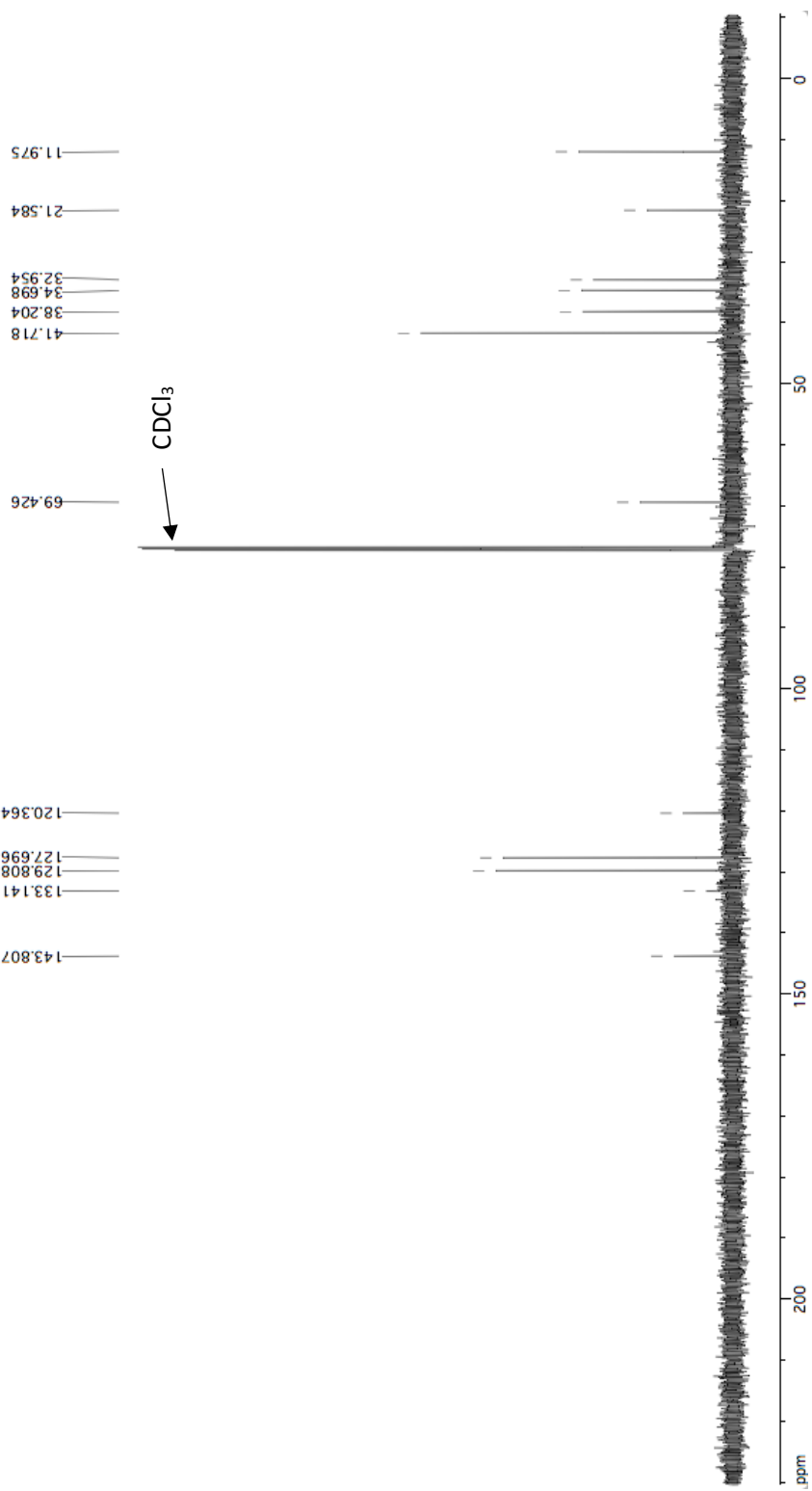


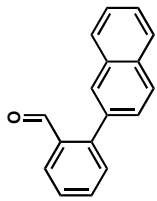
3.87 (¹H NMR, 500 MHz, CDCl₃, 25 °C)



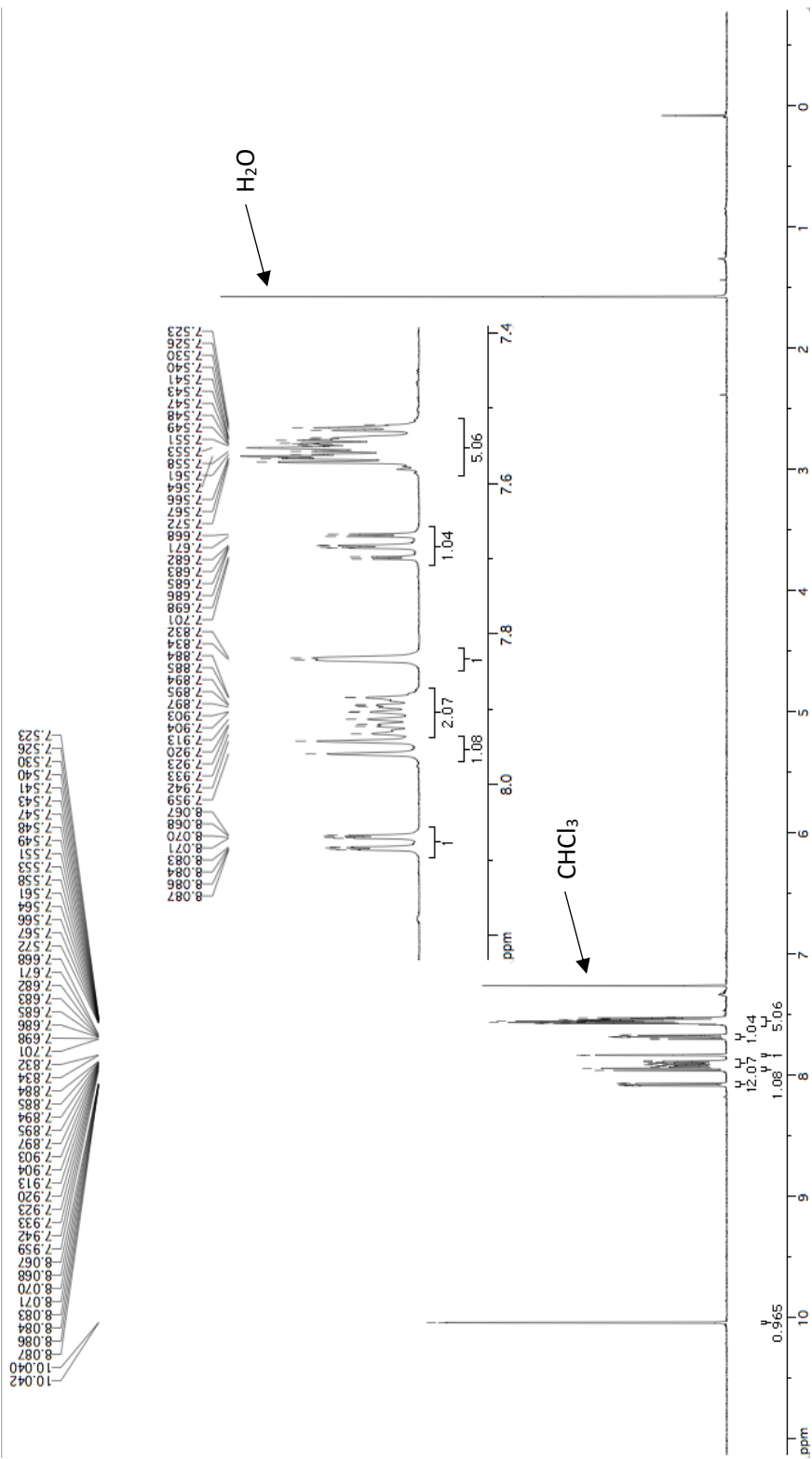


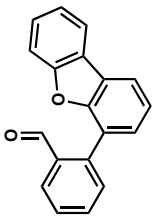
3.87 (¹³C NMR, 126 MHz, CDCl₃, 25 °C)



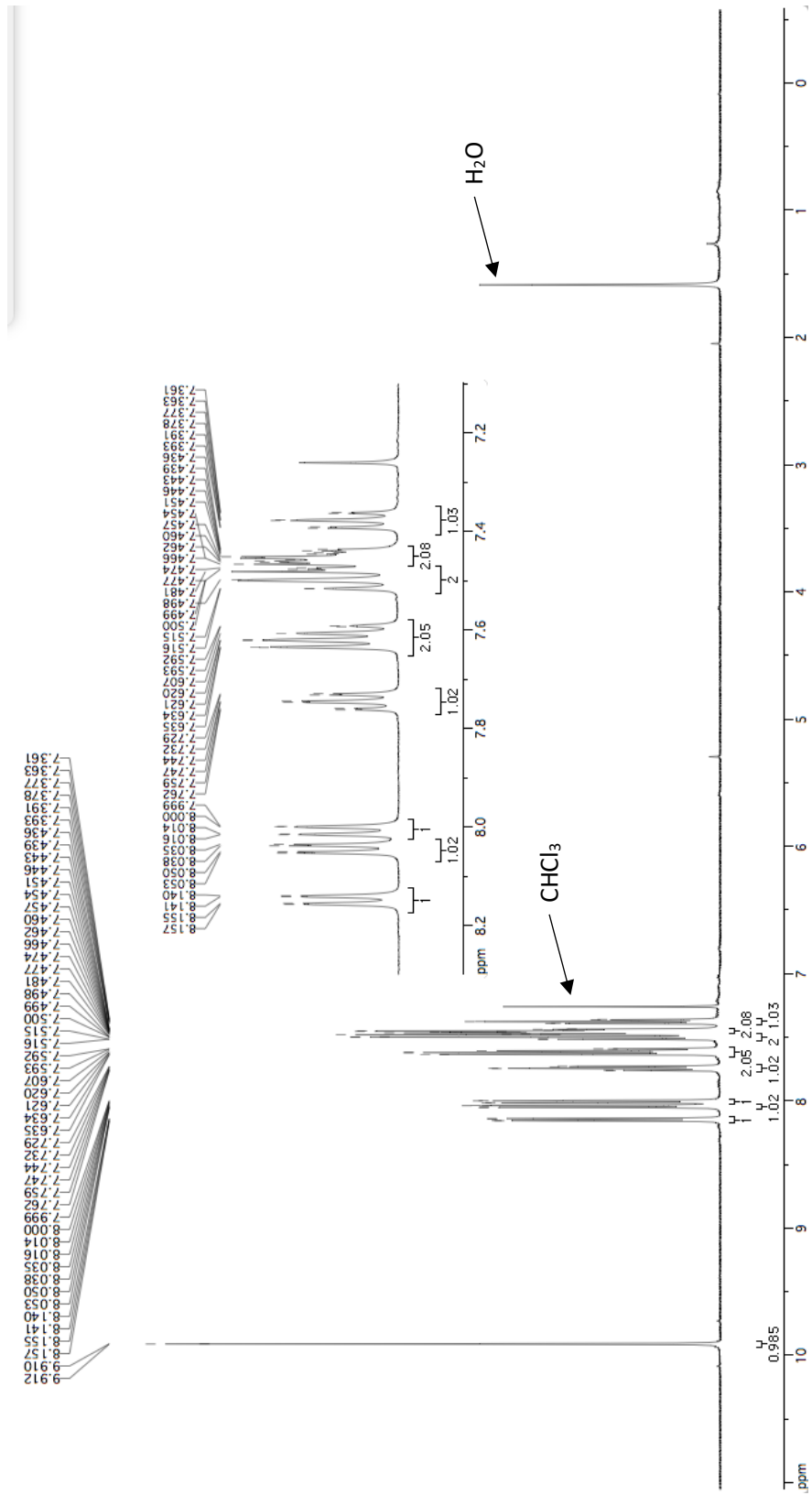


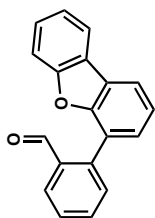
3.92 (¹H NMR, 500 MHz, CDCl₃, 25 °C)



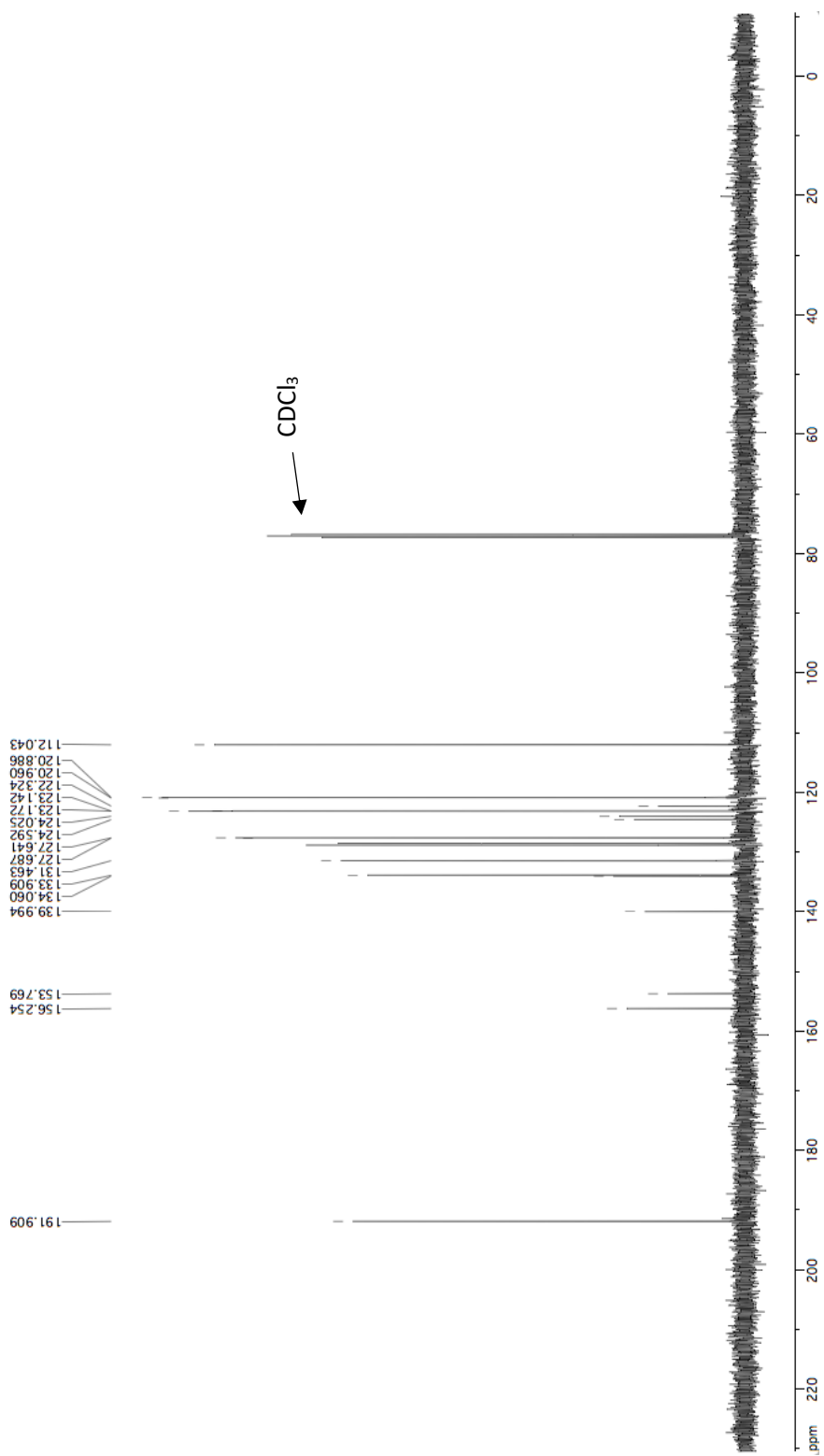


3.94 (¹H NMR, 500 MHz, CDCl₃, 25 °C)



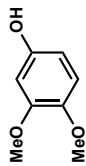


3.94 (¹³C NMR, 126 MHz, CDCl₃, 25 °C)

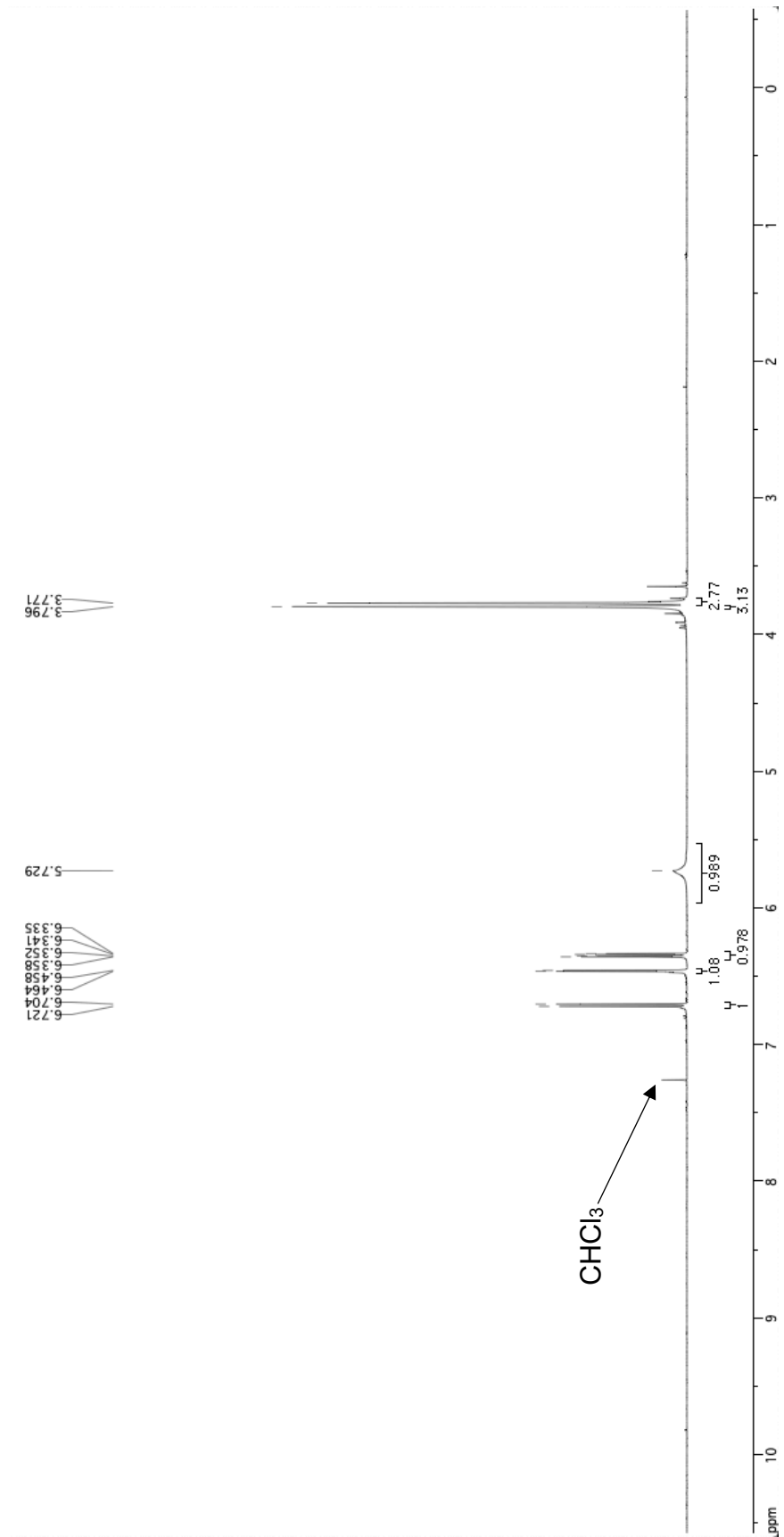


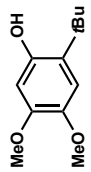
Appendix C: NMR Spectra for Chapter 4

NMR Spectra

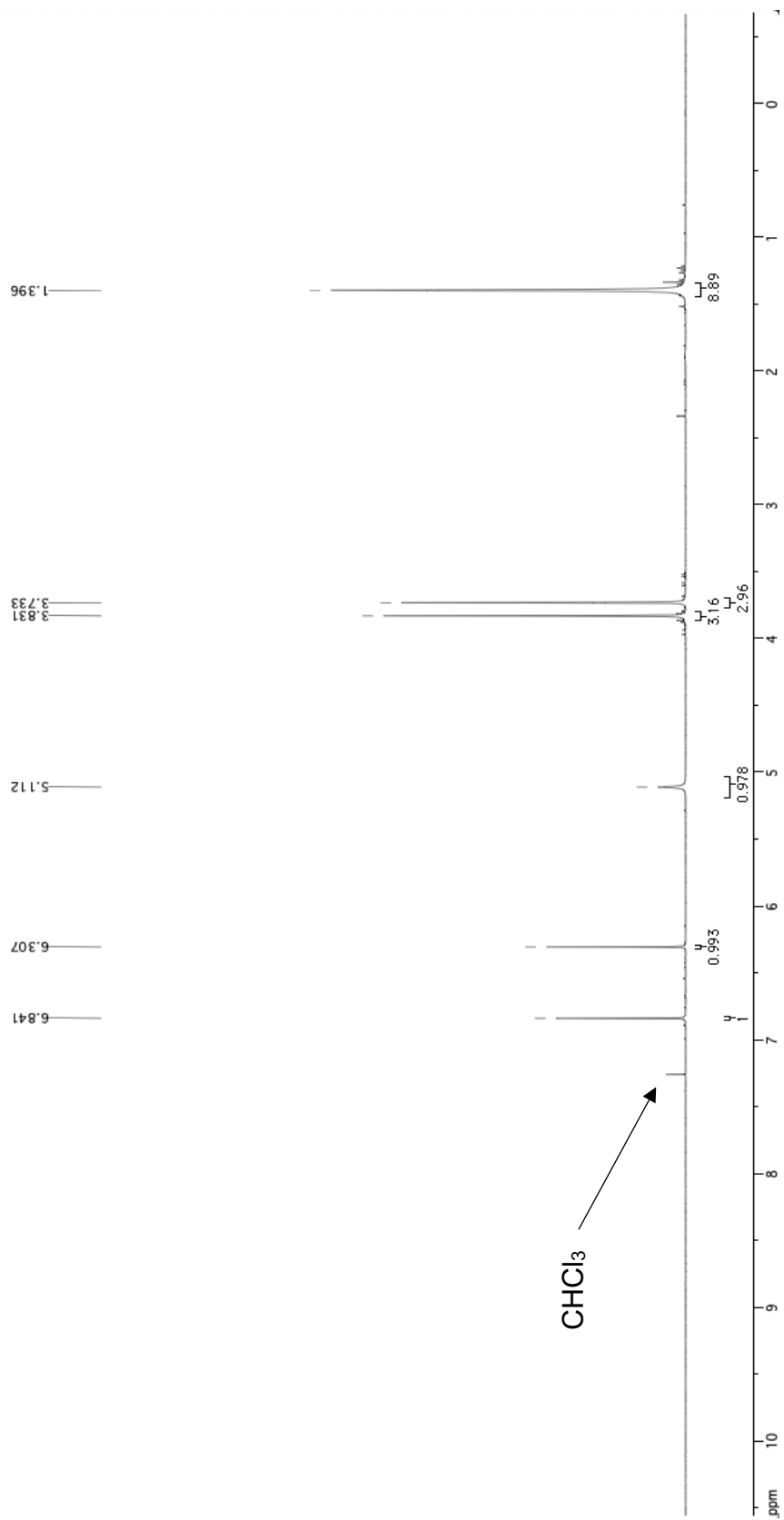


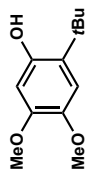
4.96 (¹H NMR, 500 MHz, CDCl₃, 25 °C)



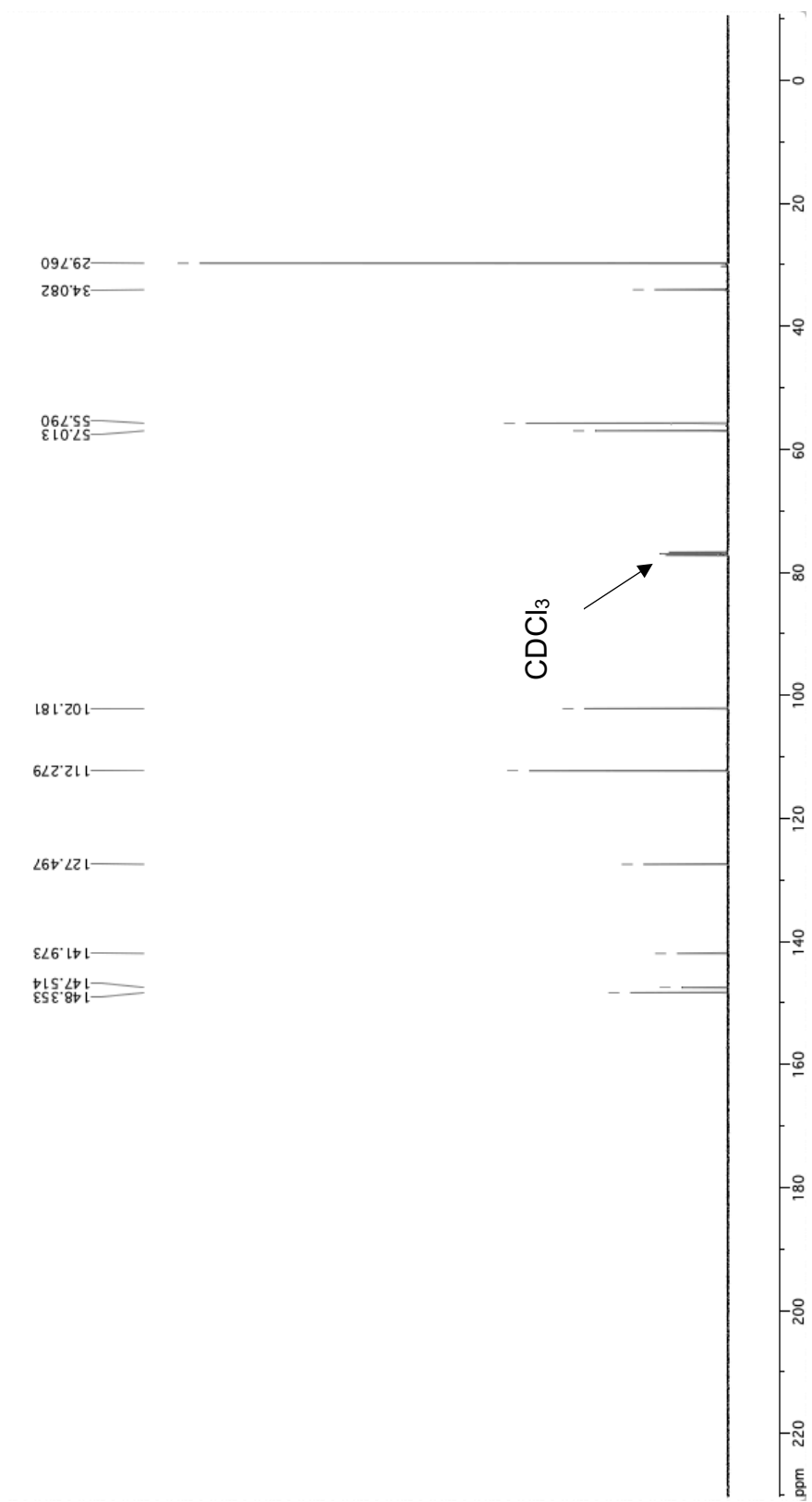


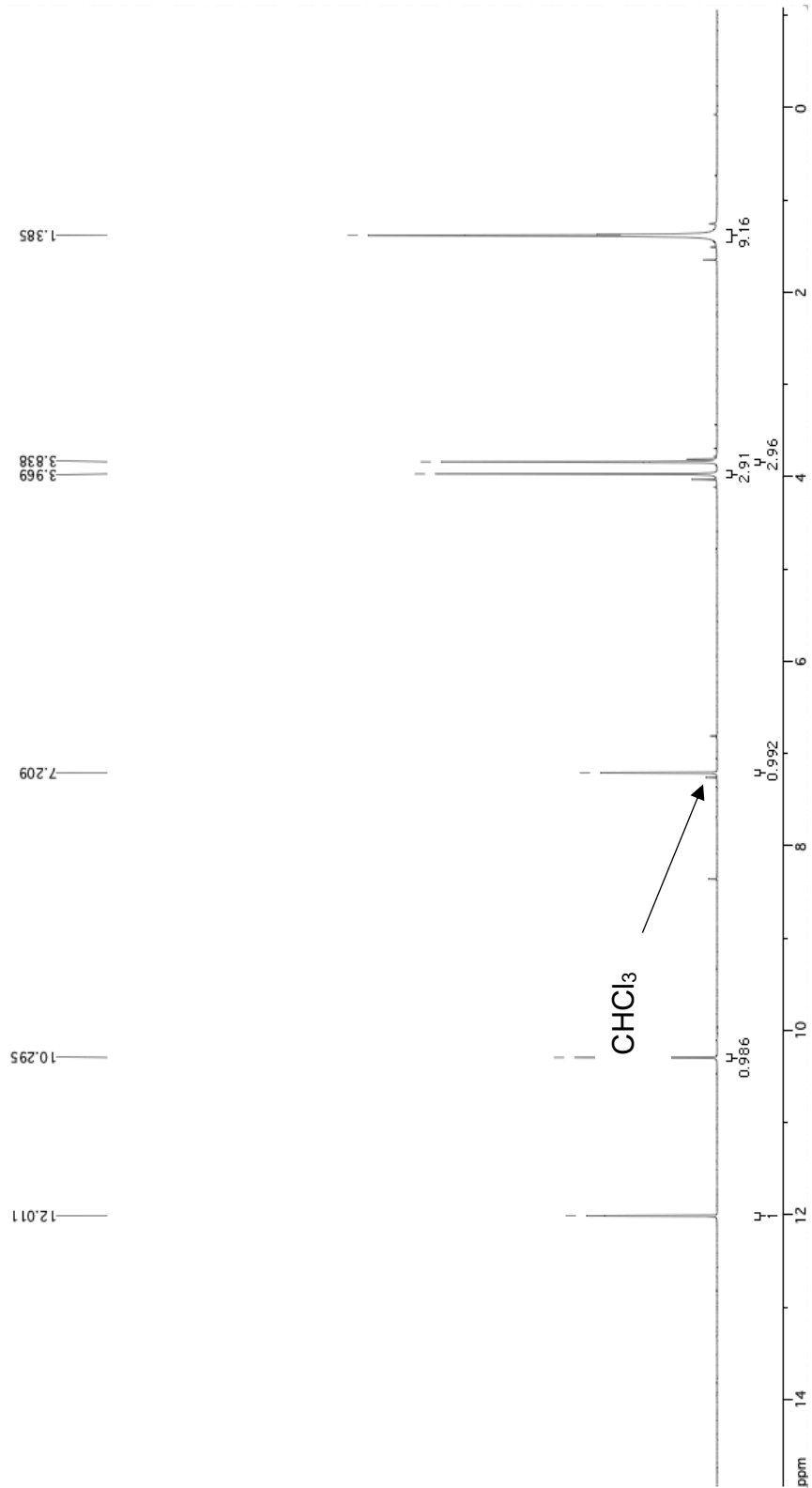
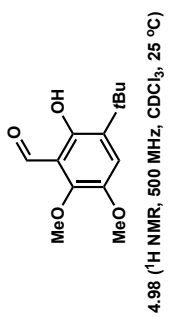
4.97 (¹H NMR, 500 MHz, CDCl₃, 25 °C)

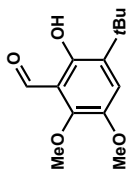




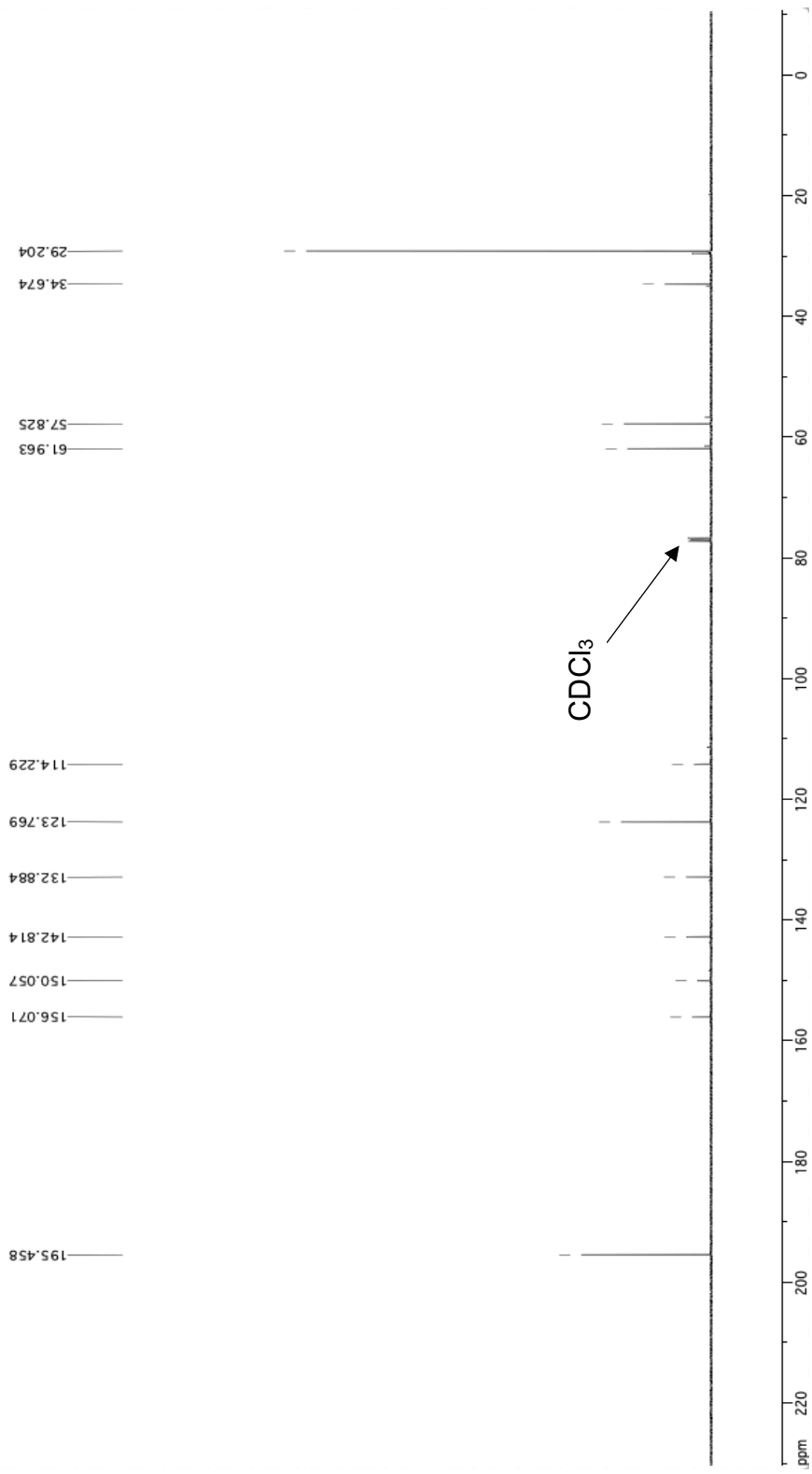
4.97 (¹³C NMR, 126 MHz, CDCl₃, 25 °C)

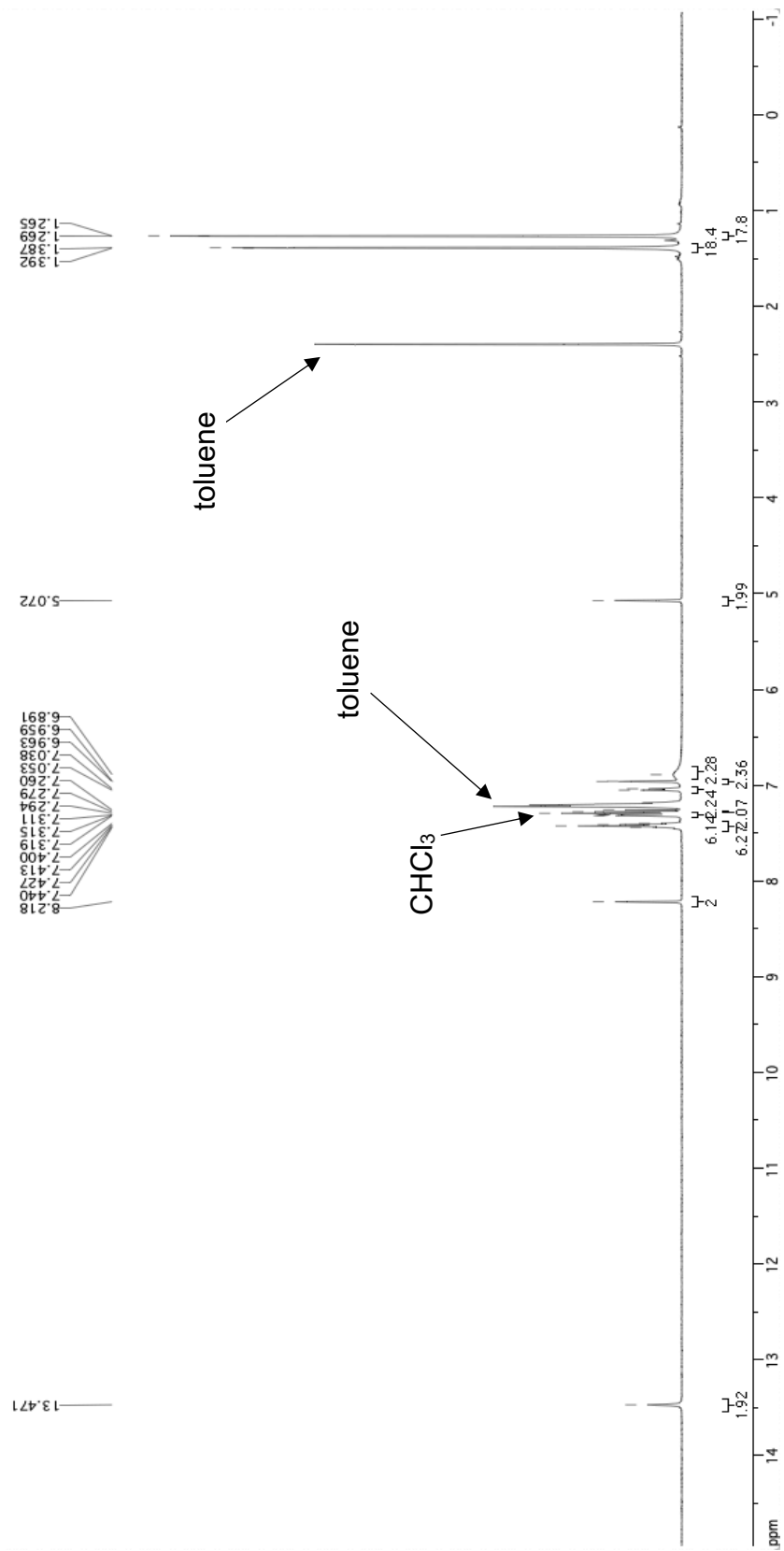
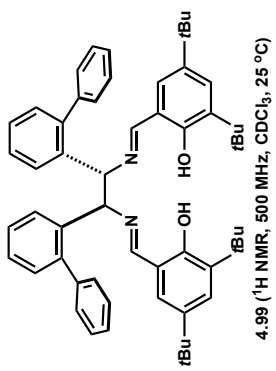


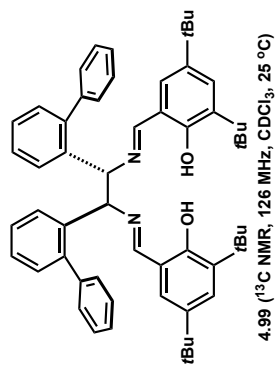




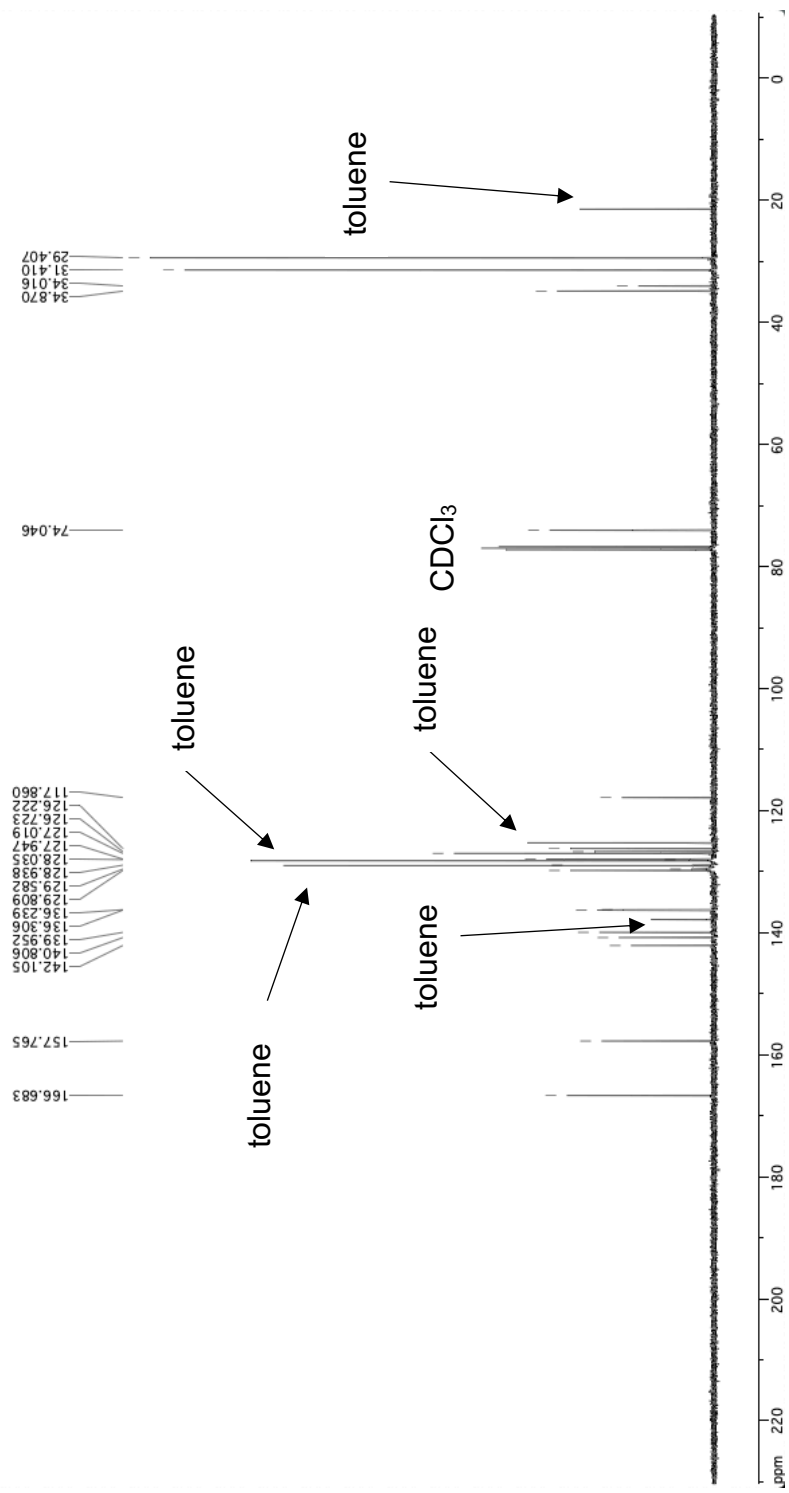
4.98 (¹³C NMR, 126 MHz, CDCl₃, 25 °C)

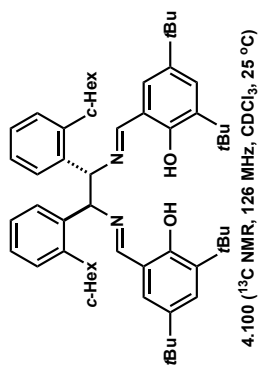






4.99 (¹³C NMR, 126 MHz, CDCl₃, 25 °C)





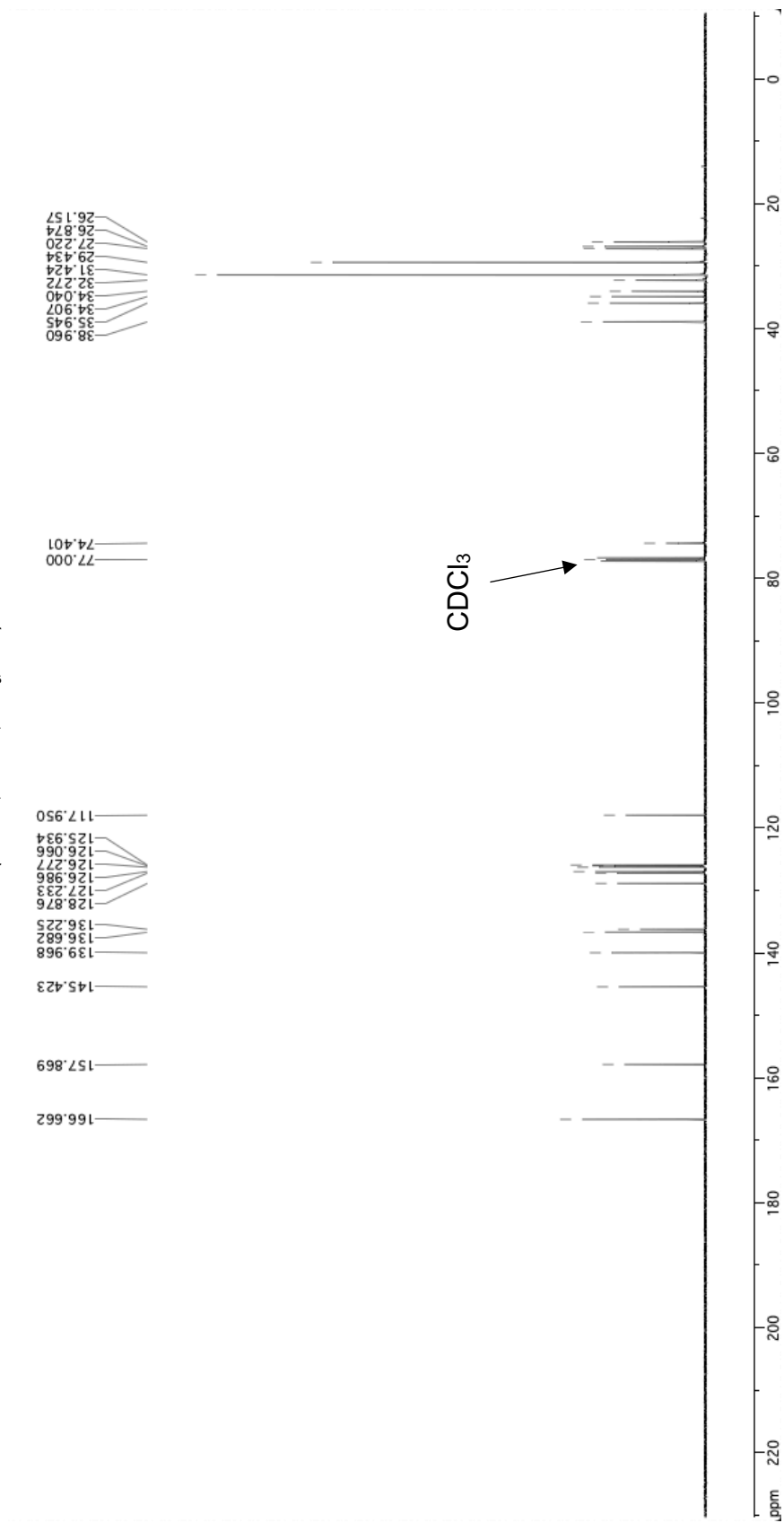
4.100 (¹³C NMR, 126 MHz, CDCl₃, 25 °C)

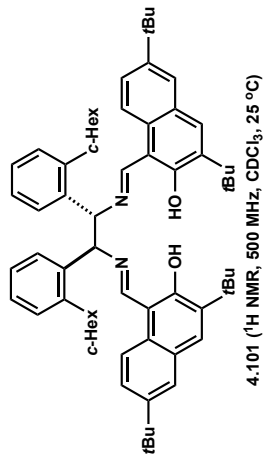
38.960
35.945
34.907
34.040
32.272
31.424
29.434
27.220
26.874
26.157

77.000
74.401

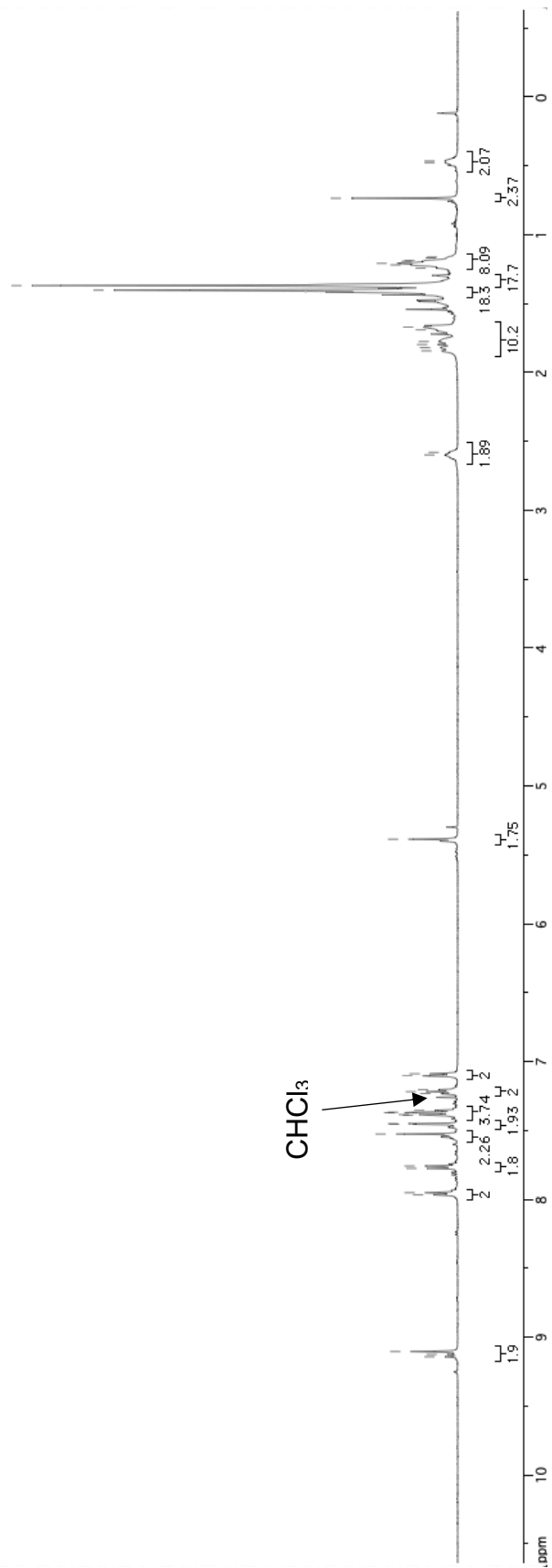
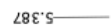
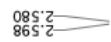
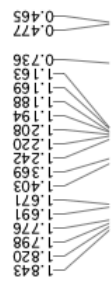
166.662
157.869
145.423
139.968
136.682
136.225
128.876
127.233
126.986
126.277
126.066
125.934
117.950

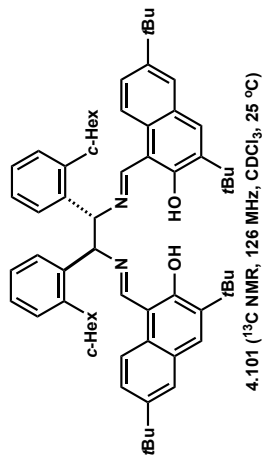
CDCl₃



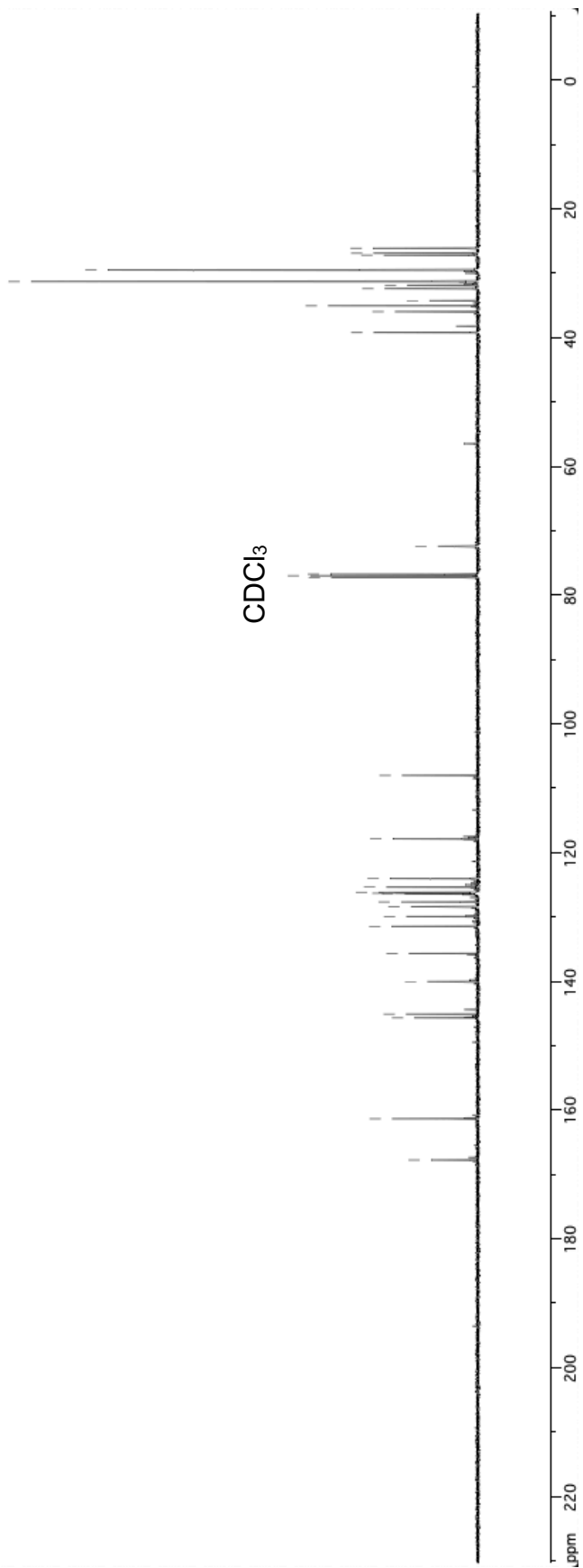


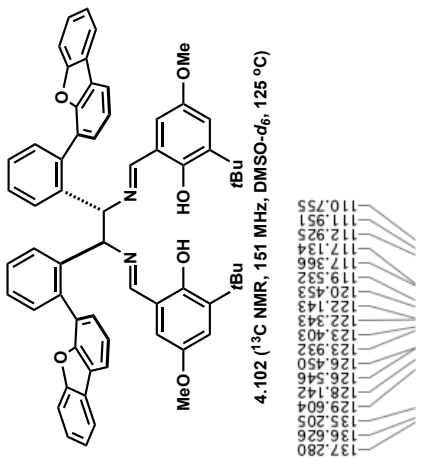
4.101 (¹H NMR, 500 MHz, CDCl₃, 25 °C)



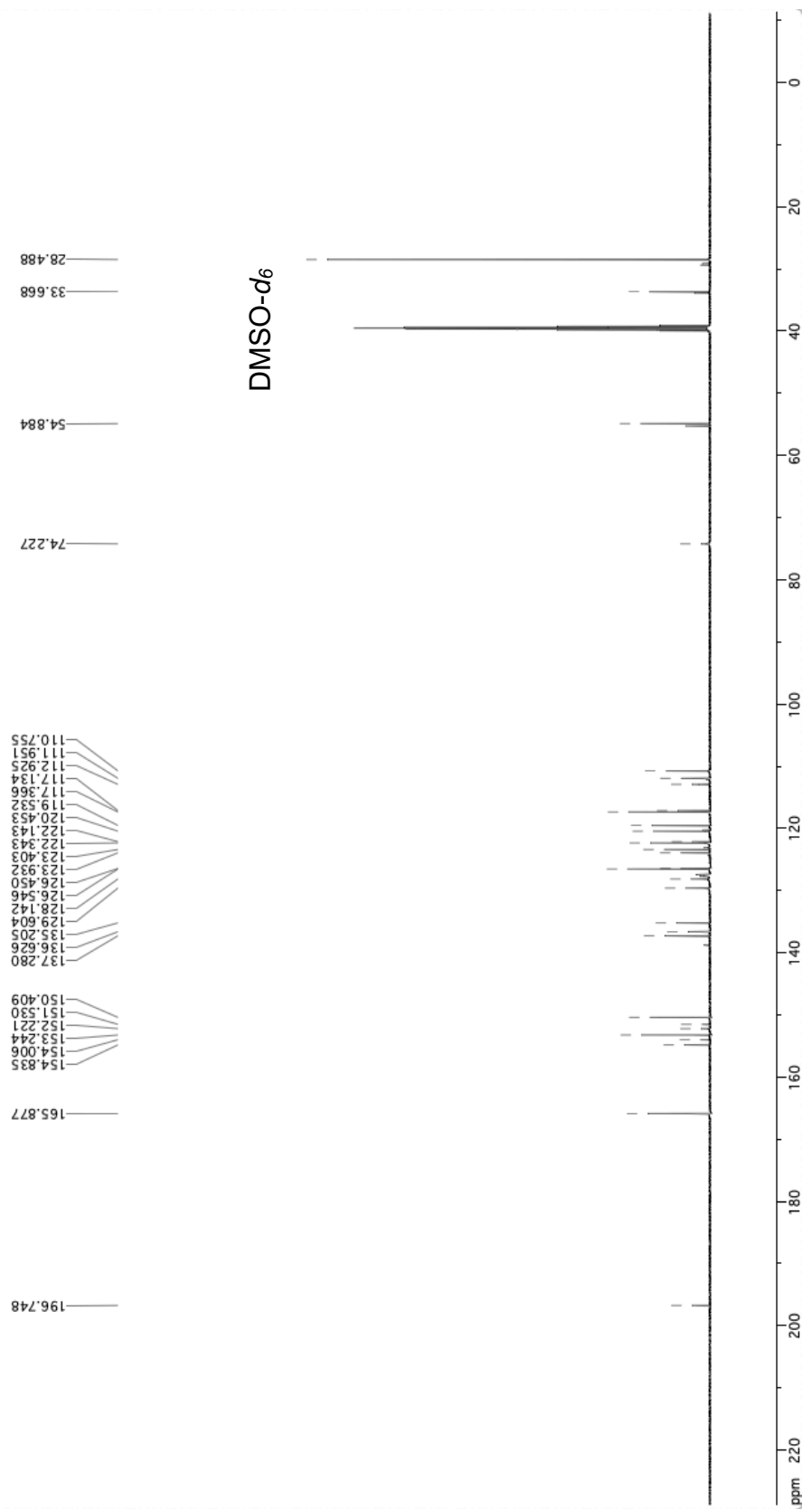


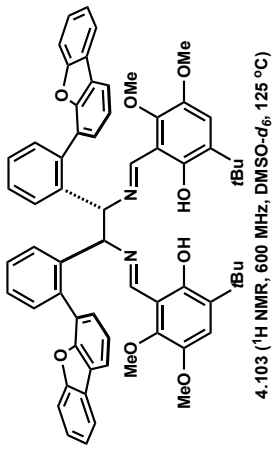
4.101 (¹³C NMR, 126 MHz, CDCl₃, 25 °C)



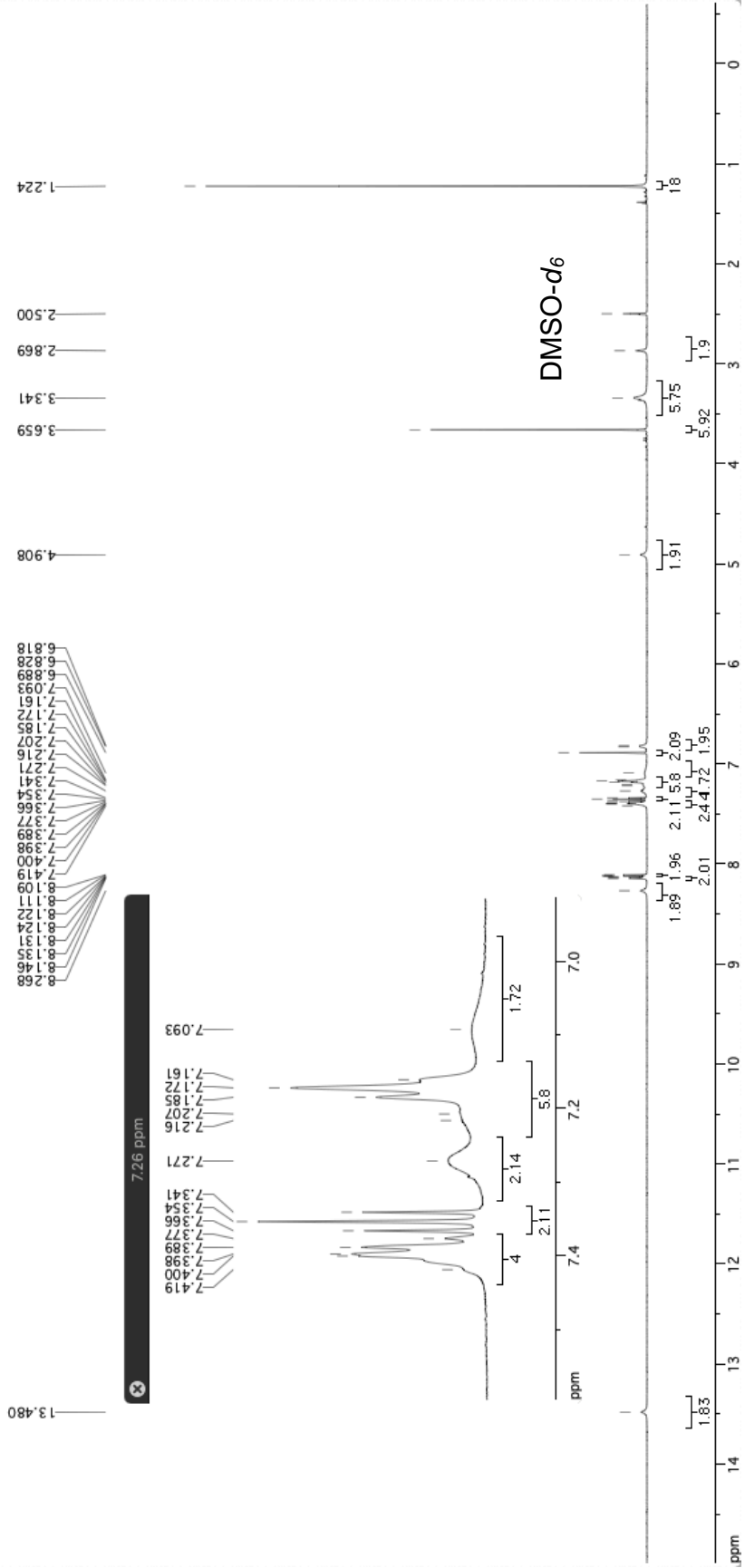


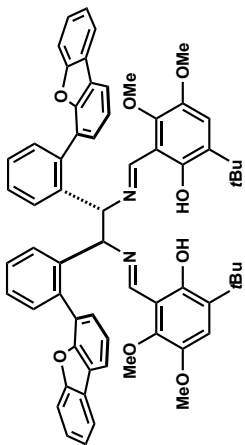
4.102 (¹³C NMR, 151 MHz, DMSO-d₆, 125 °C)



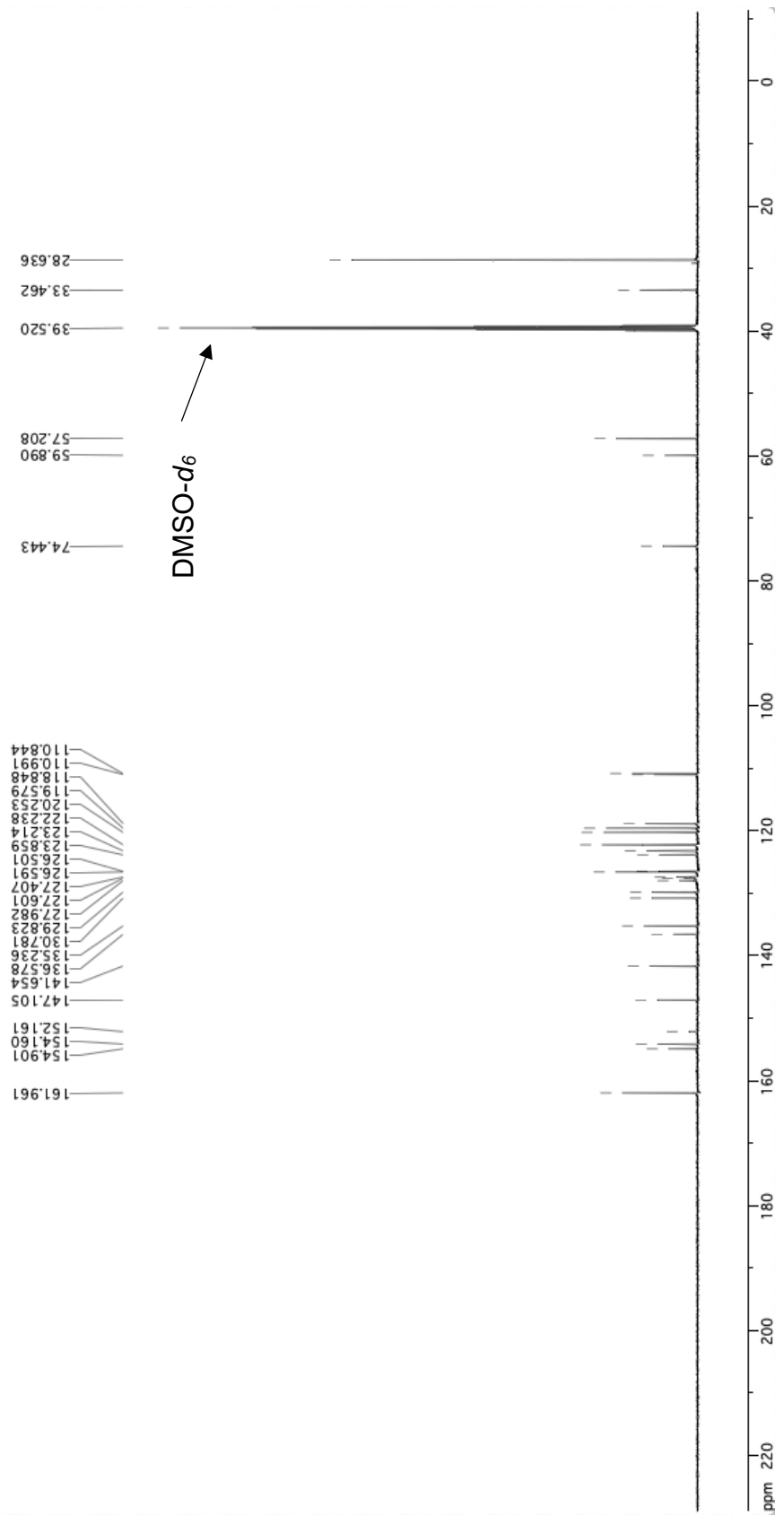


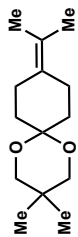
4.103 (¹H NMR, 600 MHz, DMSO-d₆, 125 °C)



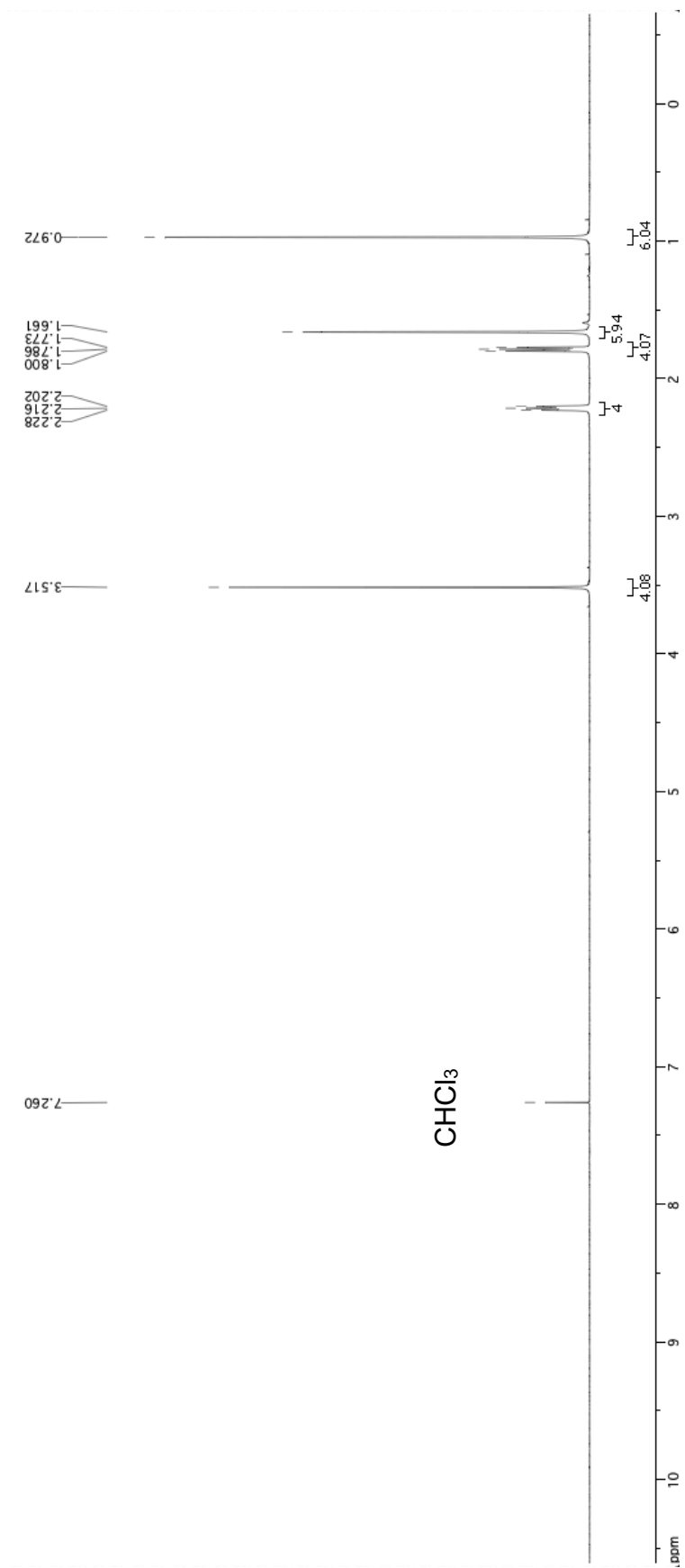


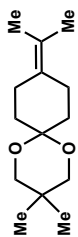
4.103 (¹³C NMR, 151 MHz, DMSO-d₆, 125 °C)



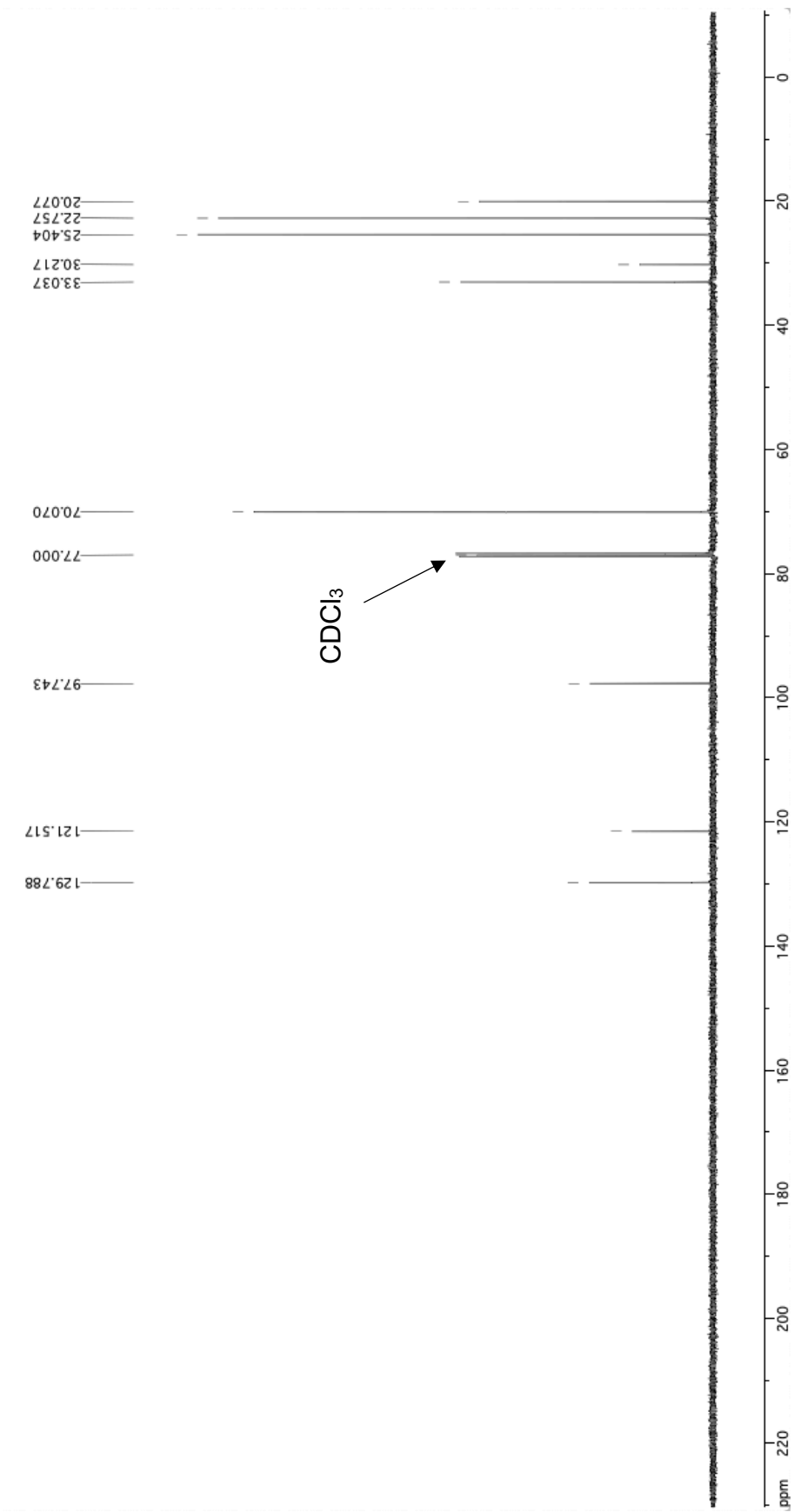


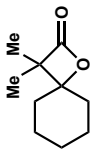
4.41 (¹H NMR, 500 MHz, CDCl₃, 25 °C)



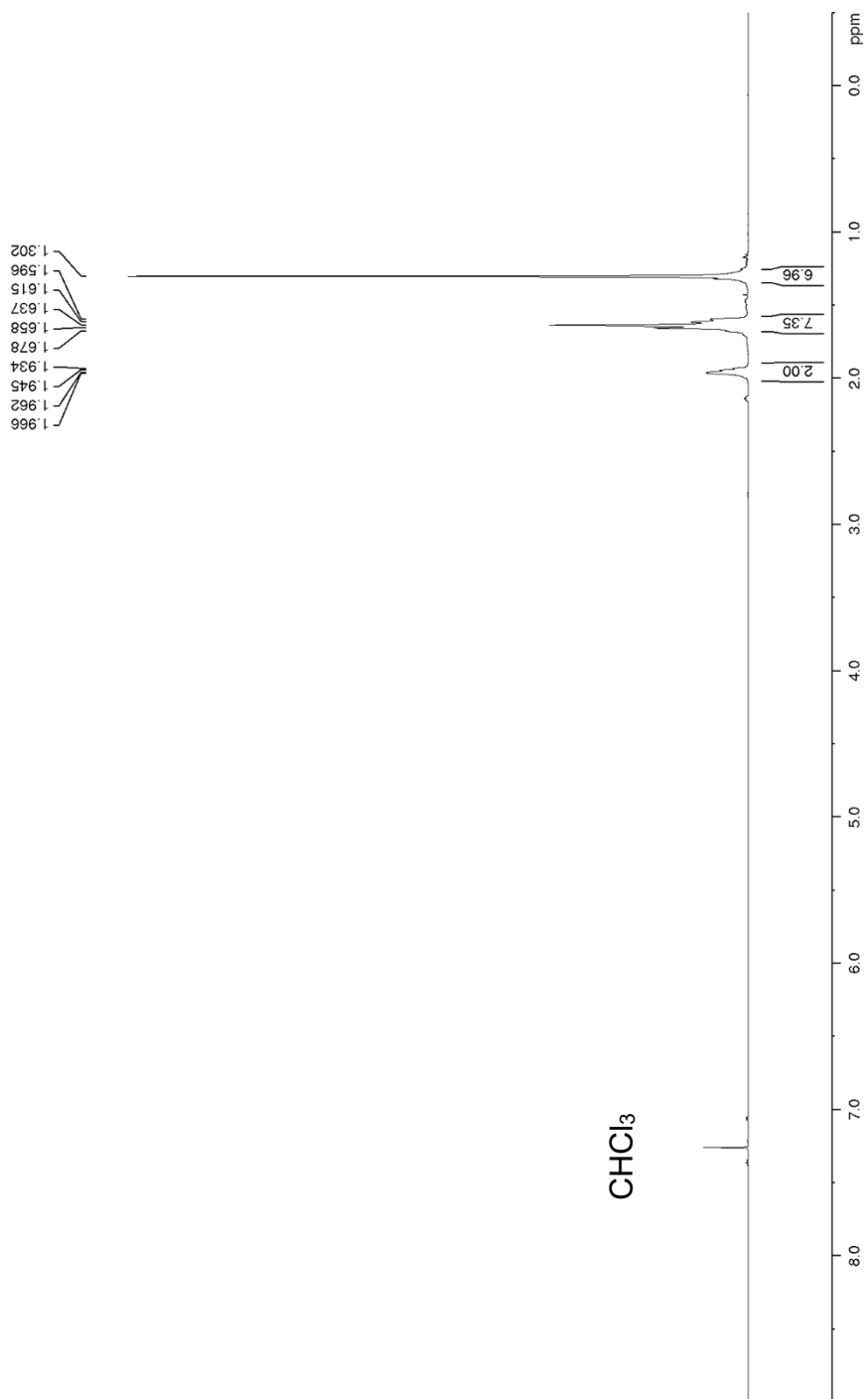


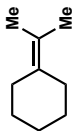
4.41 (¹³C NMR, 126 MHz, CDCl₃, 25 °C)





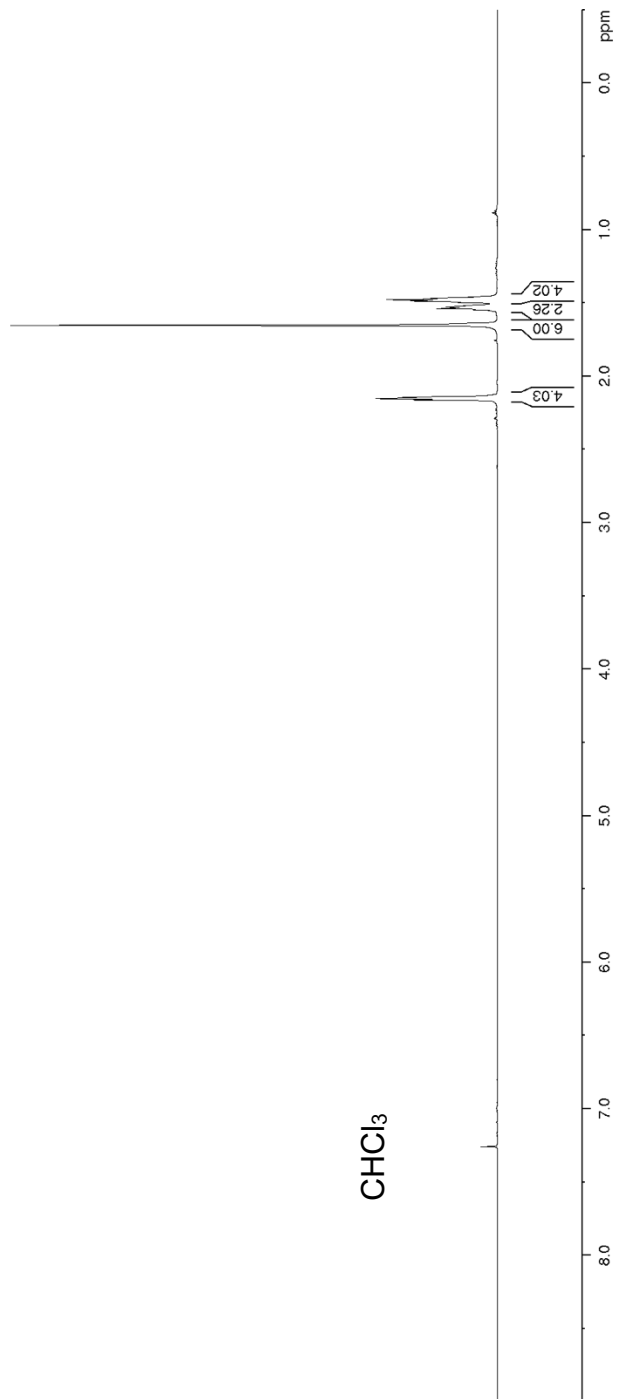
4.104 (¹H NMR, 500 MHz, CDCl₃, 25 °C)

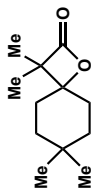




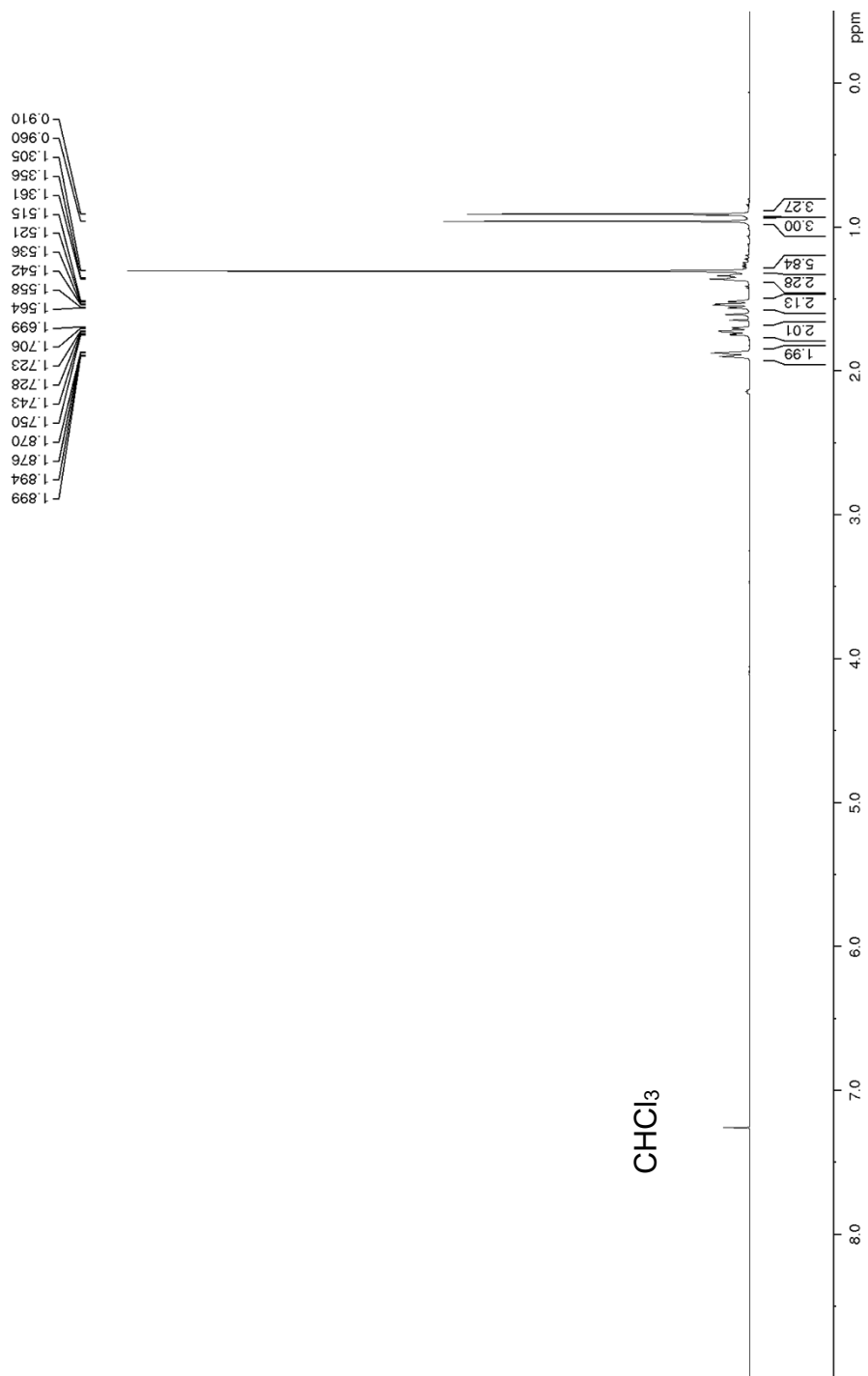
4.105 (¹H NMR, 600 MHz, CDCl₃, 25 °C)

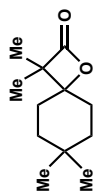
2.160
2.150
2.140
1.655
1.554
1.548
1.541
1.536
1.528
1.523
1.519
1.498
1.489
1.486
1.479
1.469
1.461



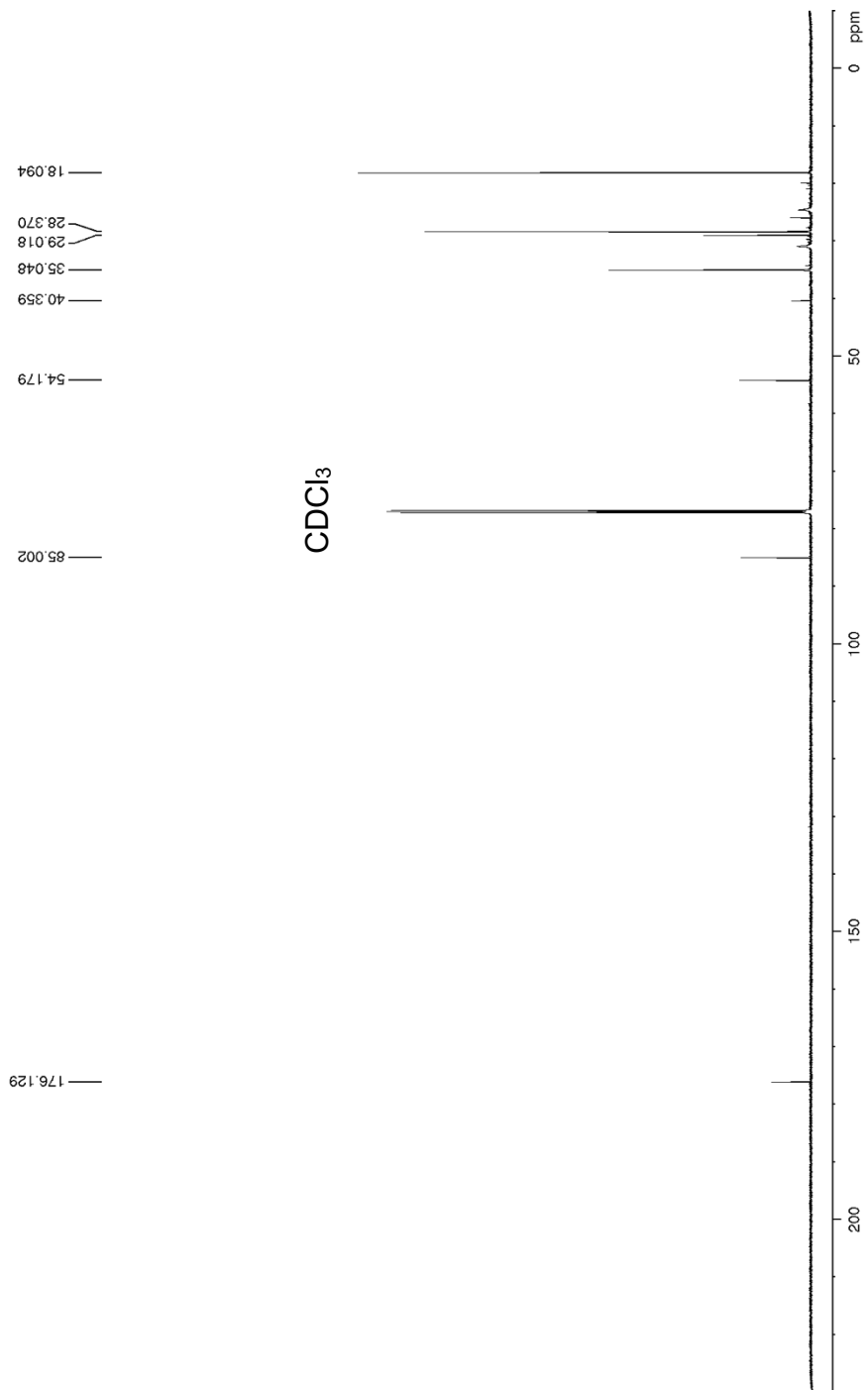


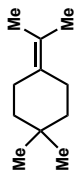
4.106 (¹H NMR, 600 MHz, CDCl₃, 25 °C)



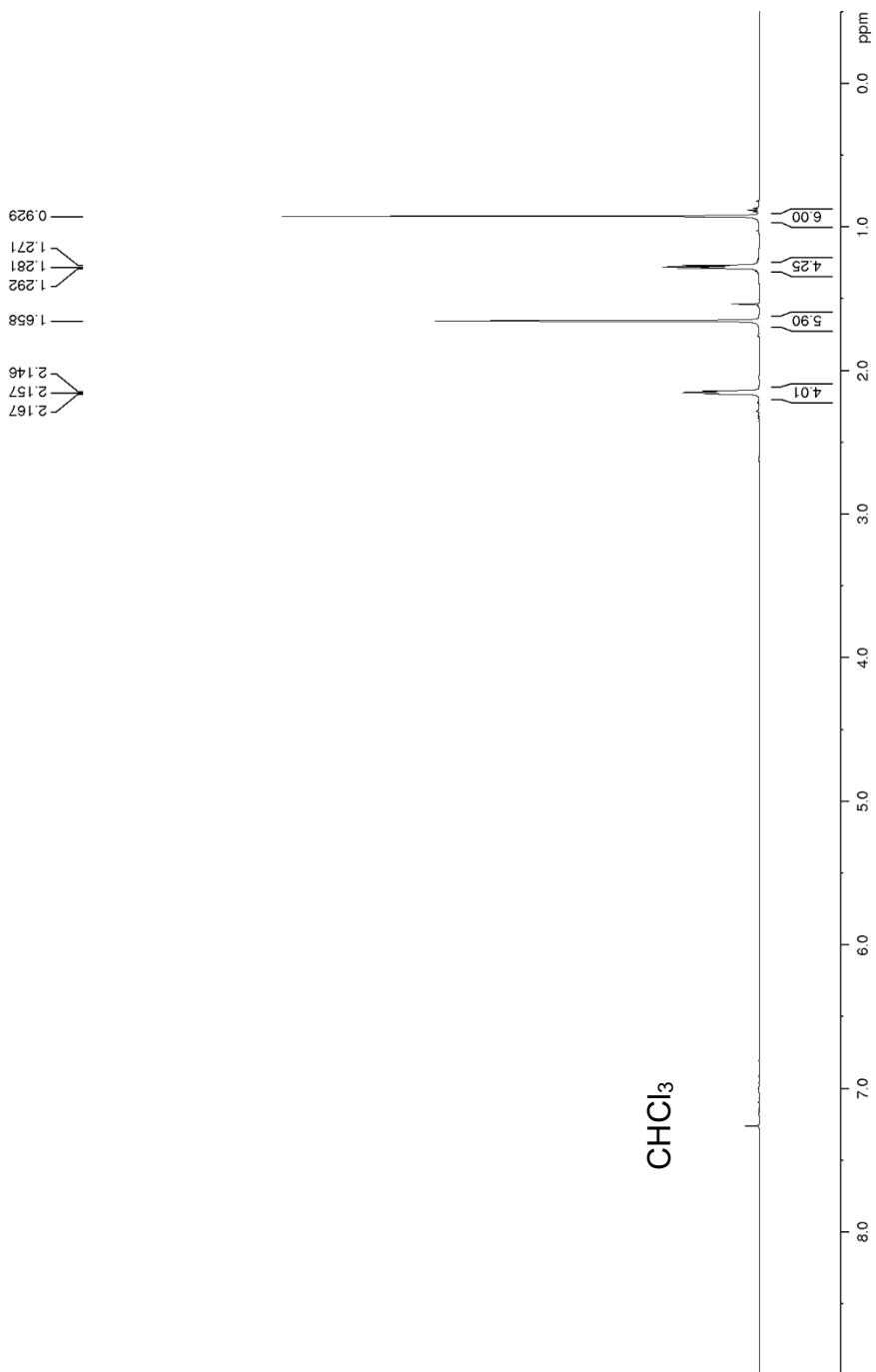


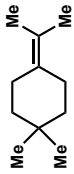
4.106 (^{13}C NMR, 151 MHz, CDCl_3 , 25 °C)



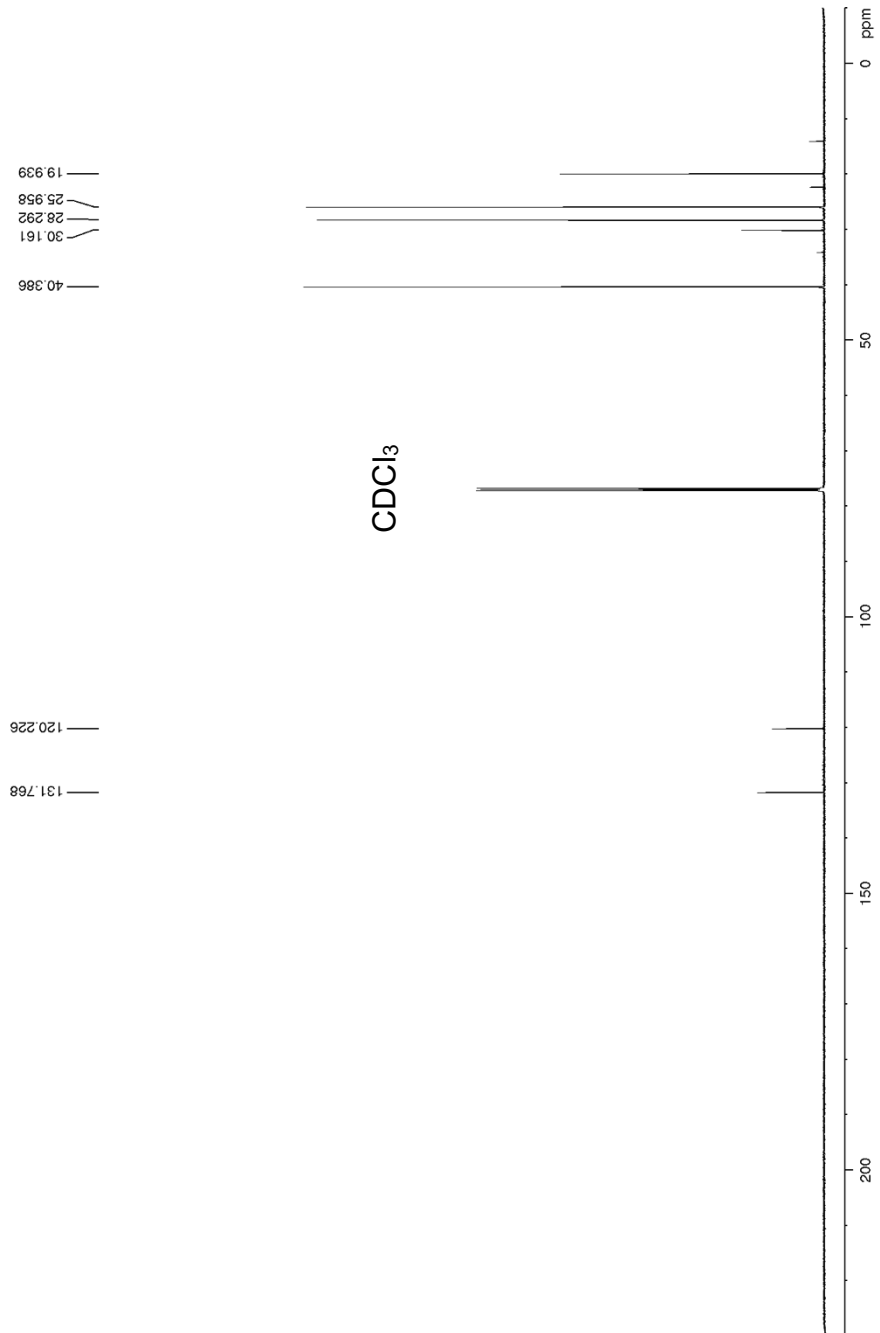


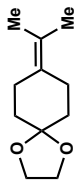
4.107 (¹H NMR, 600 MHz, CDCl₃, 25 °C)



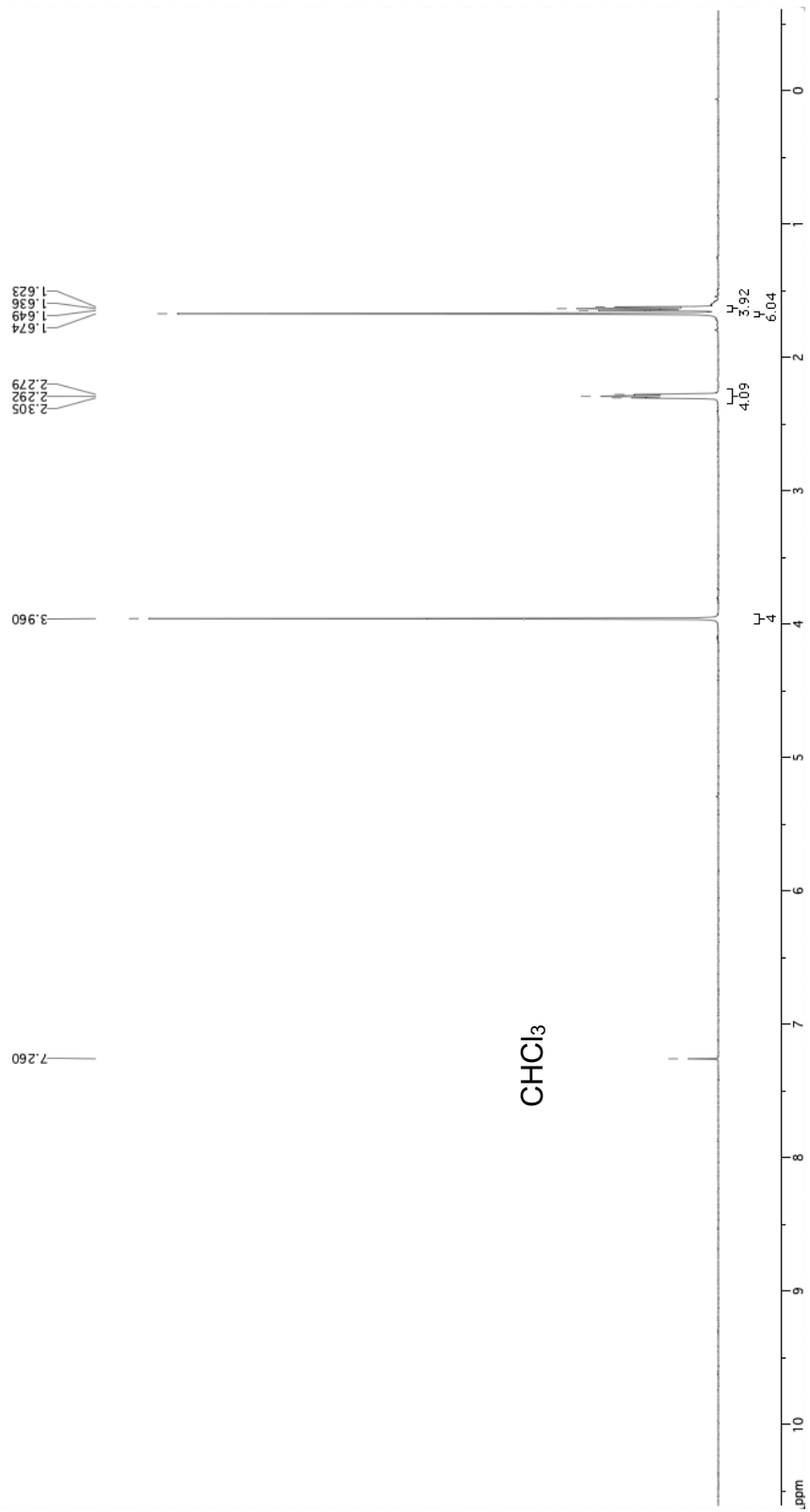


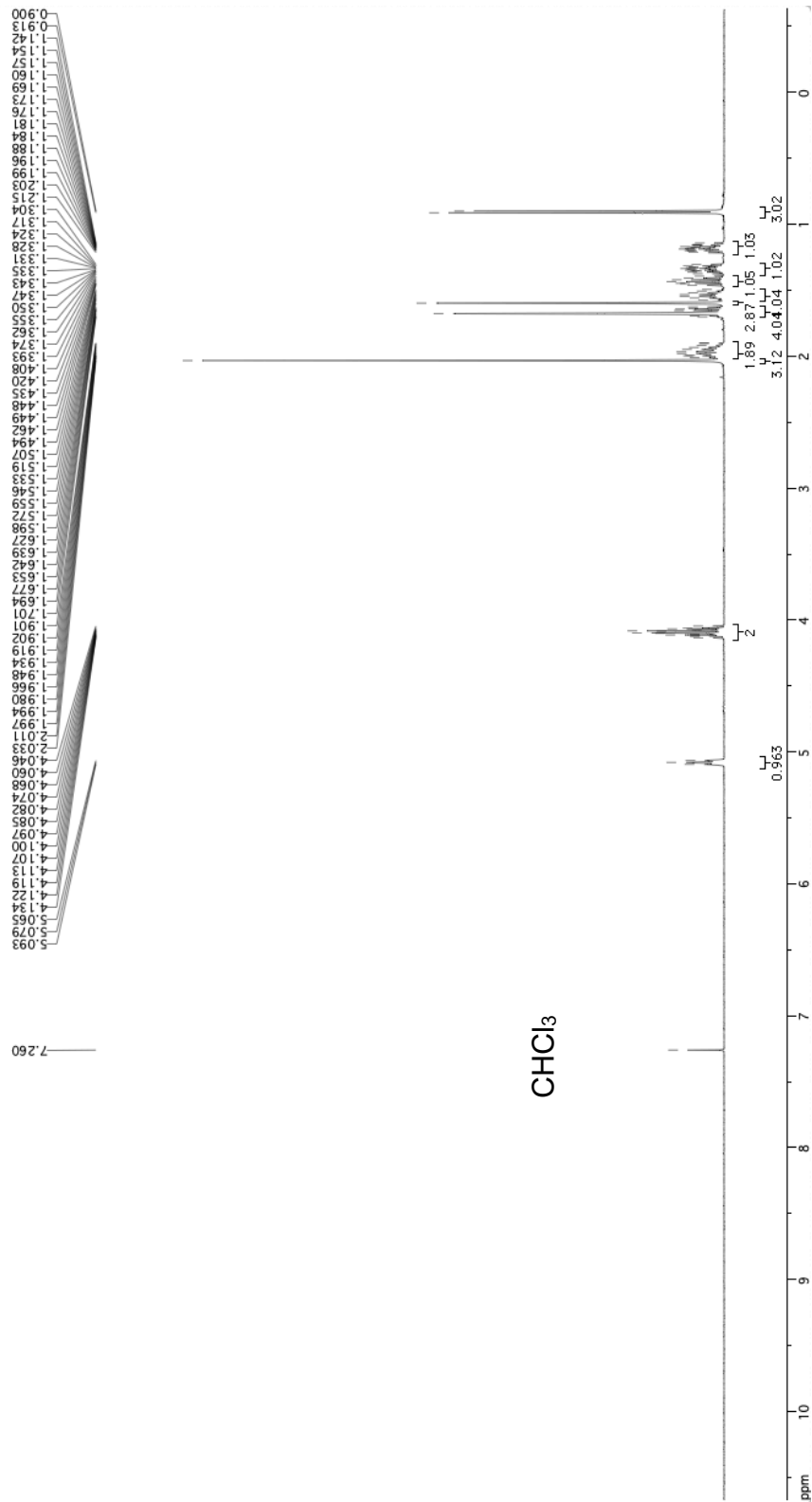
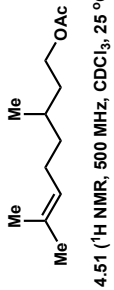
4.107 (¹³C NMR, 151 MHz, CDCl₃, 25 °C)

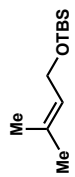




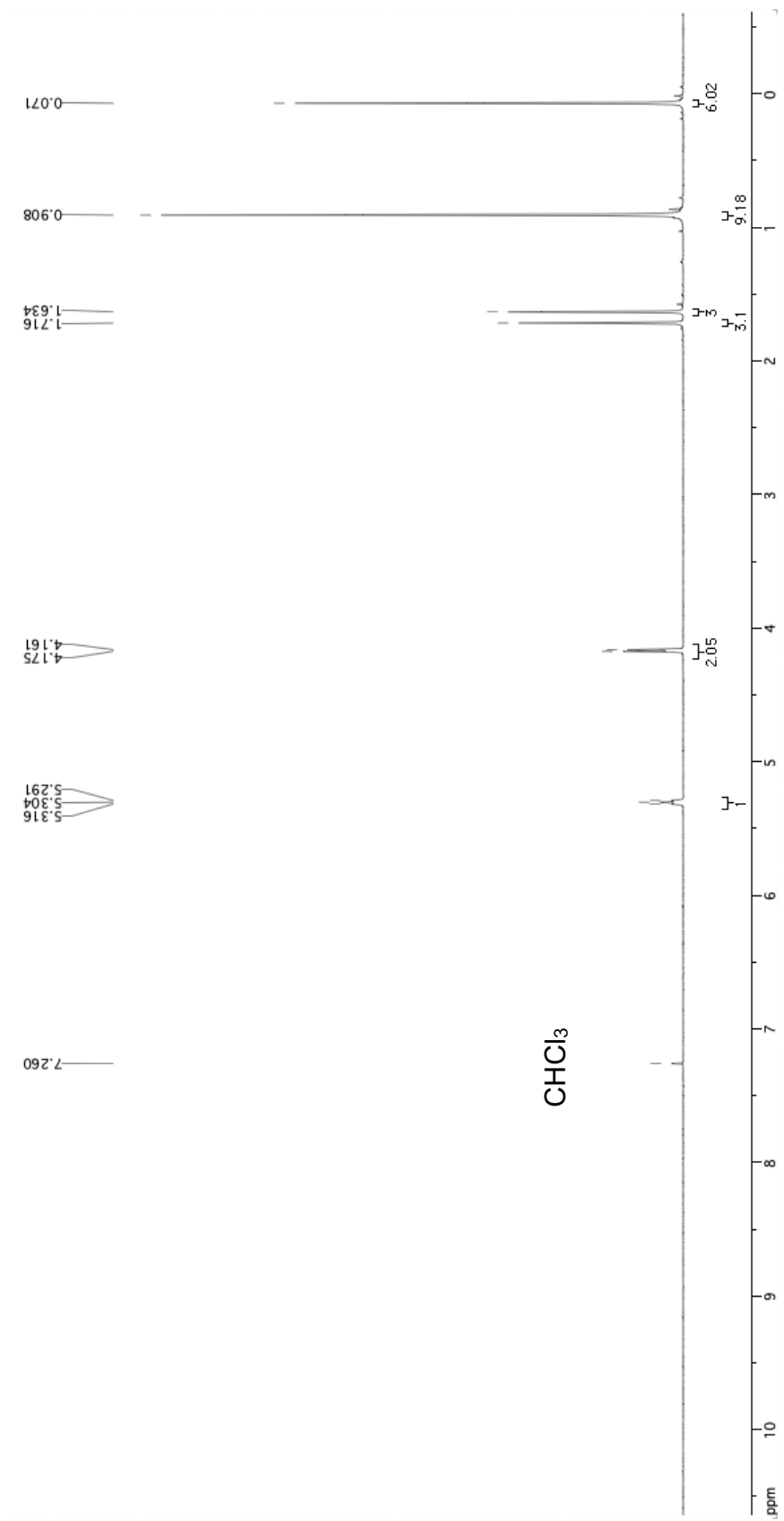
4.108 (¹H NMR, 500 MHz, CDCl₃, 25 °C)

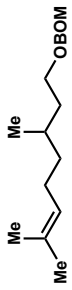




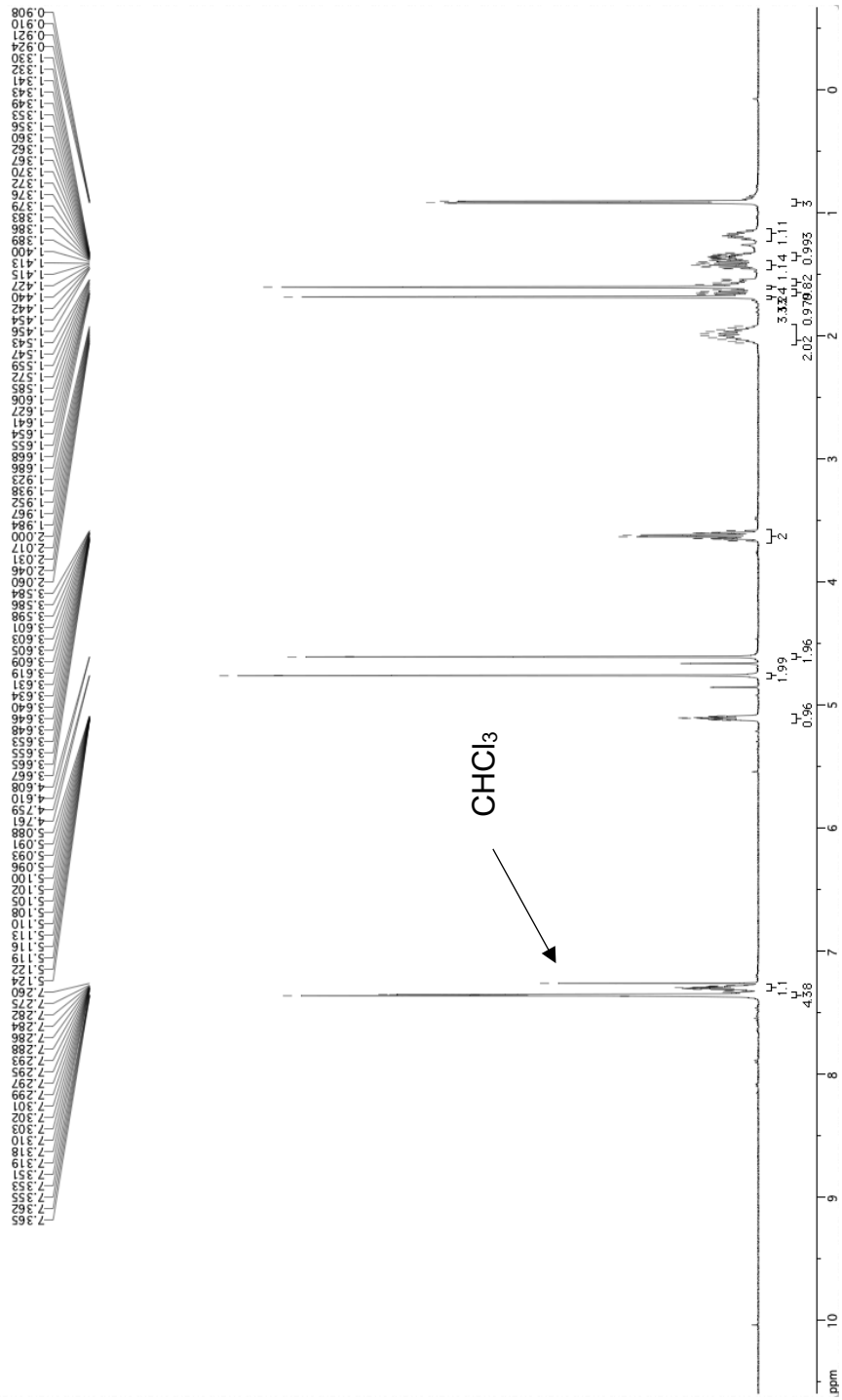


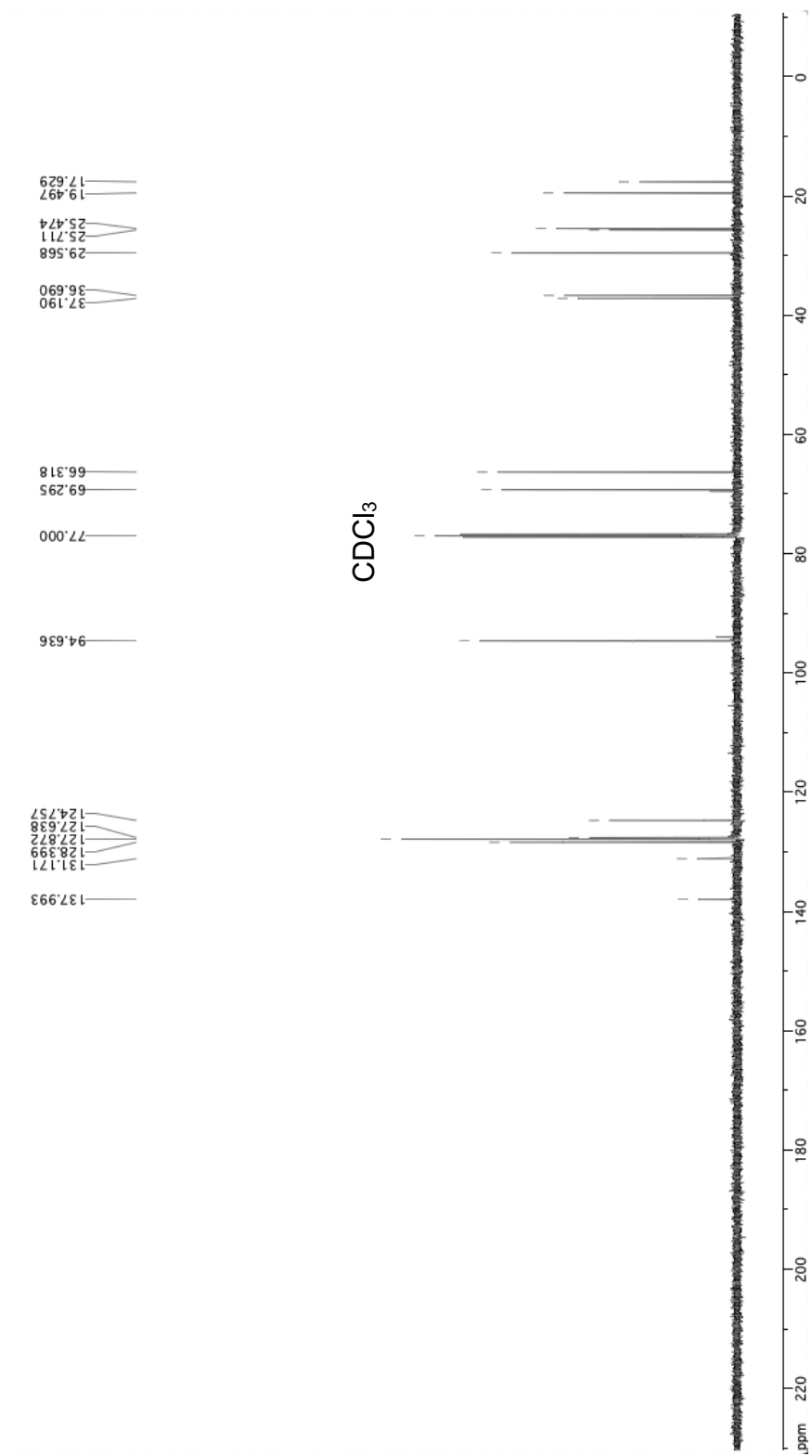
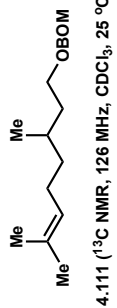
4.109 (¹H NMR, 500 MHz, CDCl₃, 25 °C)

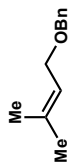




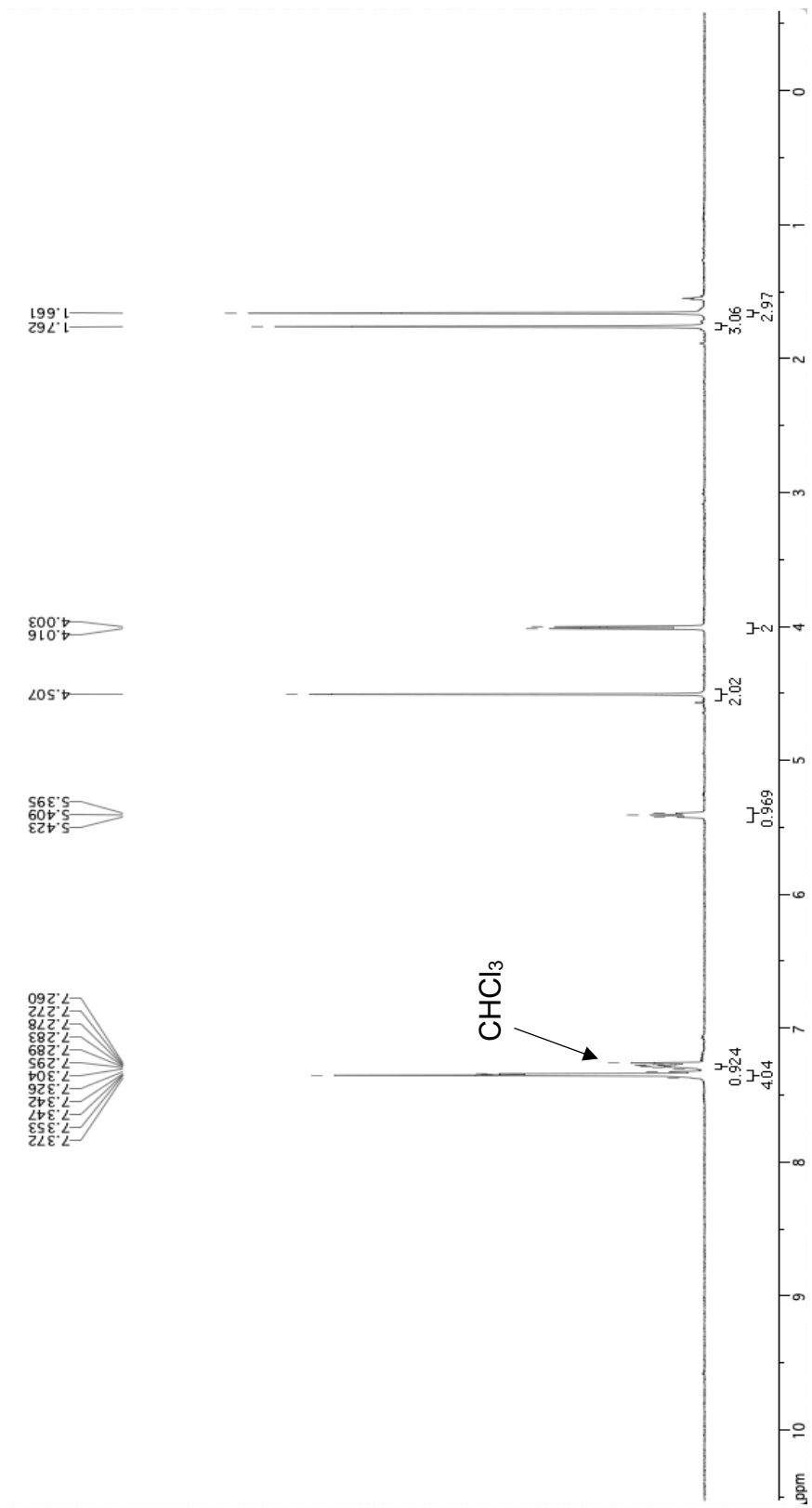
4.111 (¹H NMR, 500 MHz, CDCl₃, 25 °C)

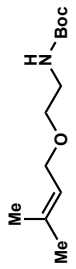




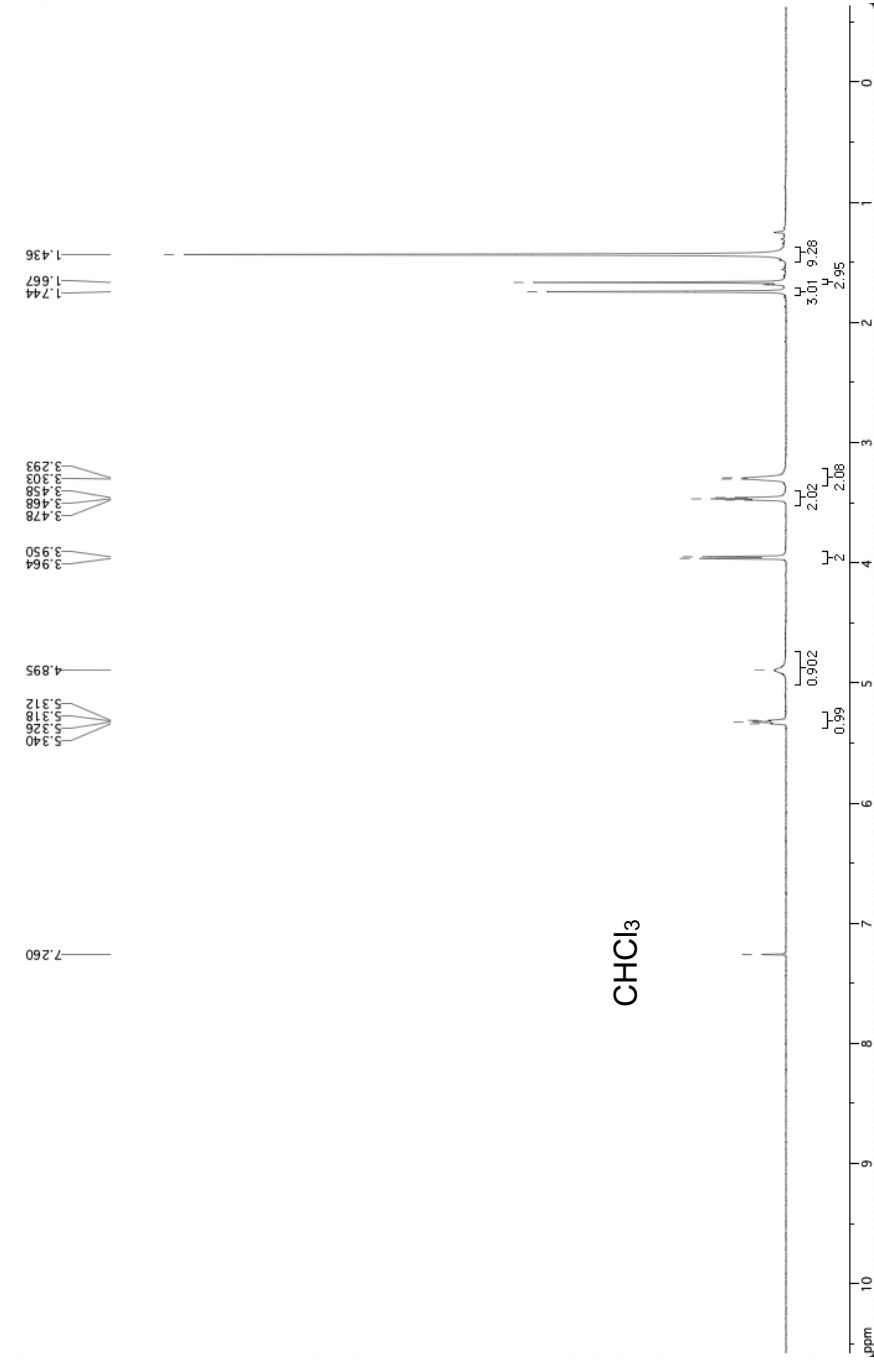


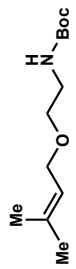
4.112 (¹H NMR, 500 MHz, CDCl₃, 25 °C)



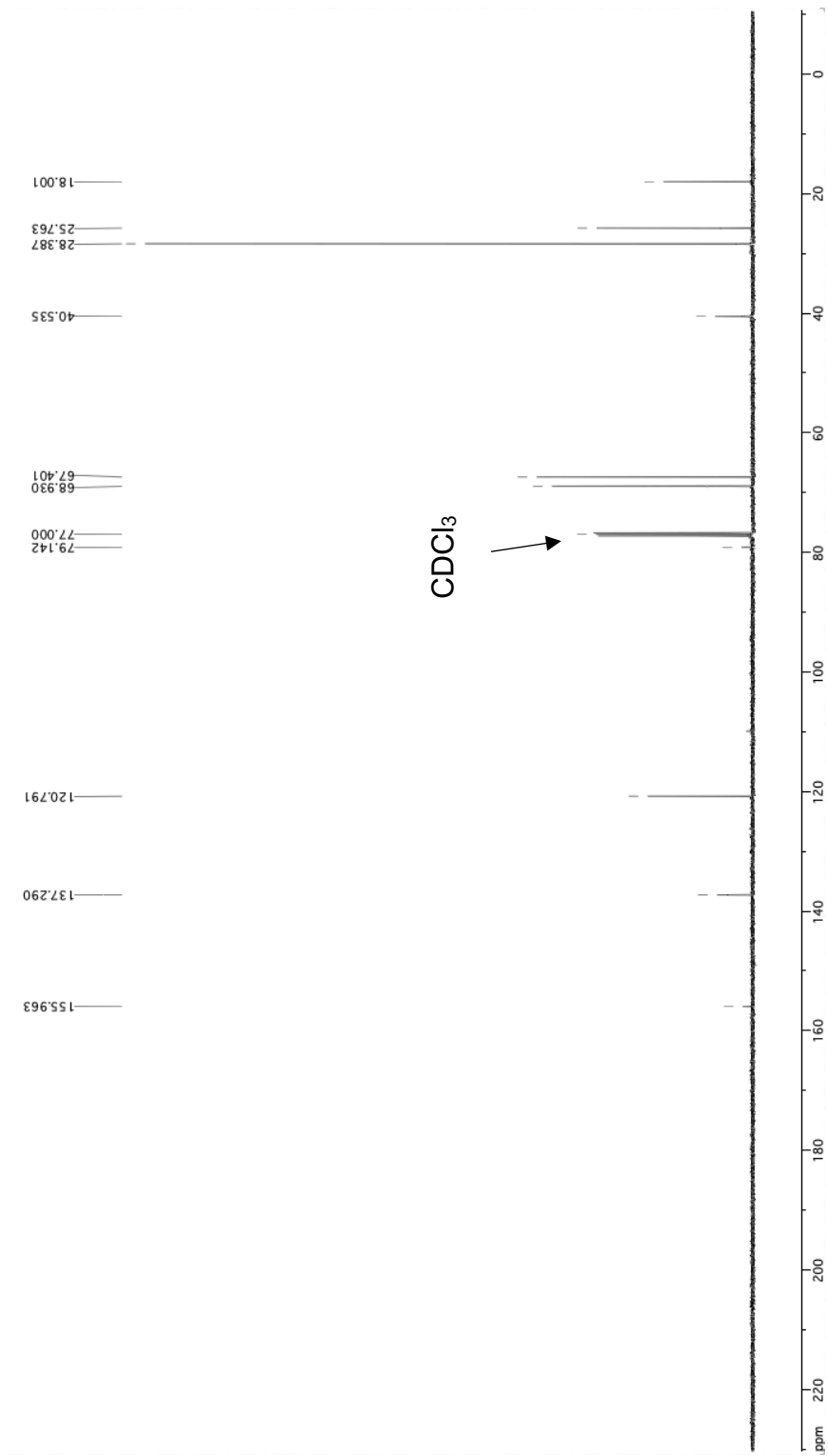


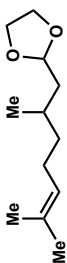
4.113 (¹H NMR, 500 MHz, CDCl₃, 25 °C)



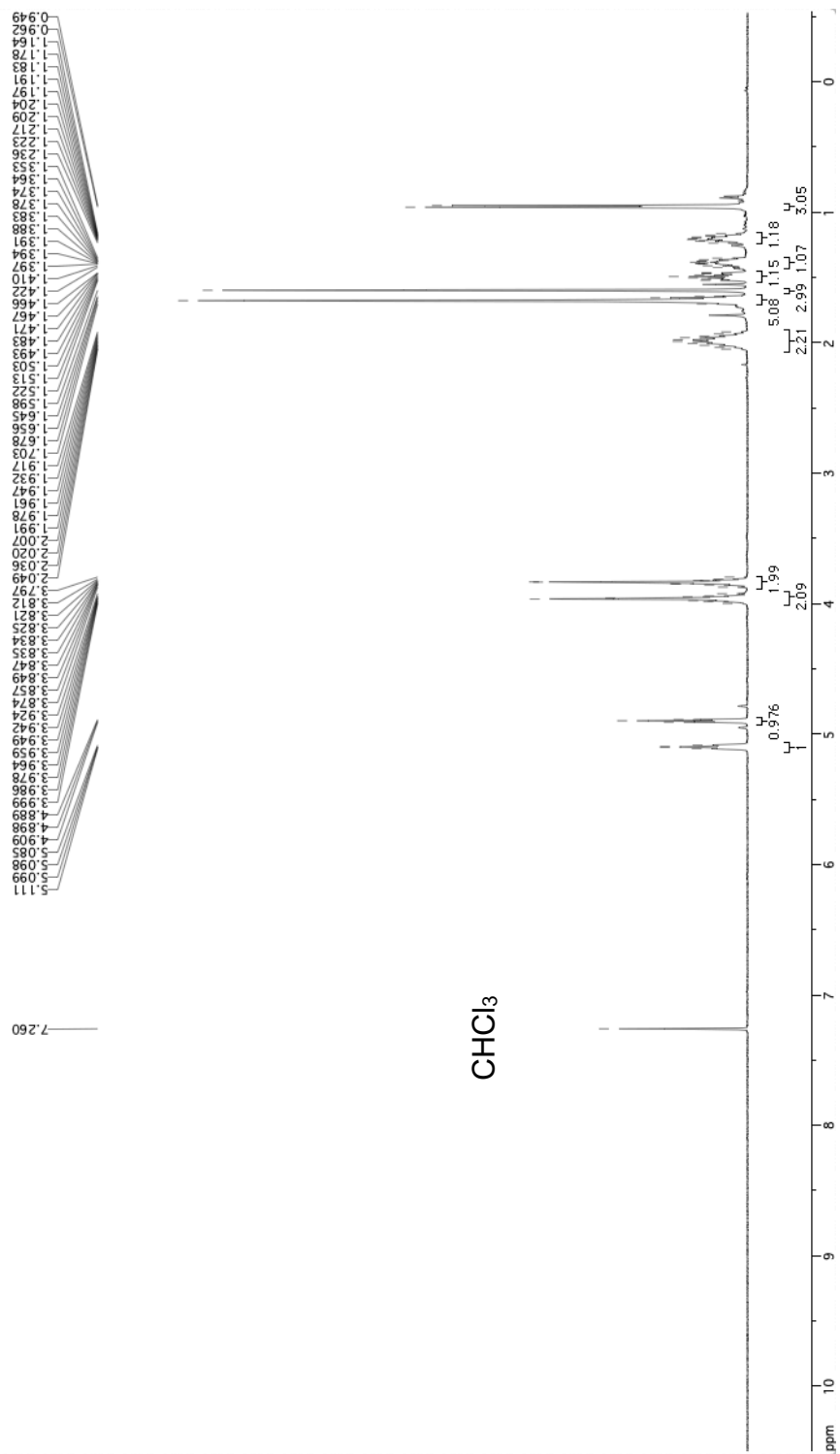


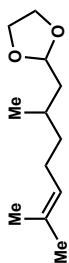
4.113 (¹³C NMR, 126 MHz, CDCl₃, 25 °C)



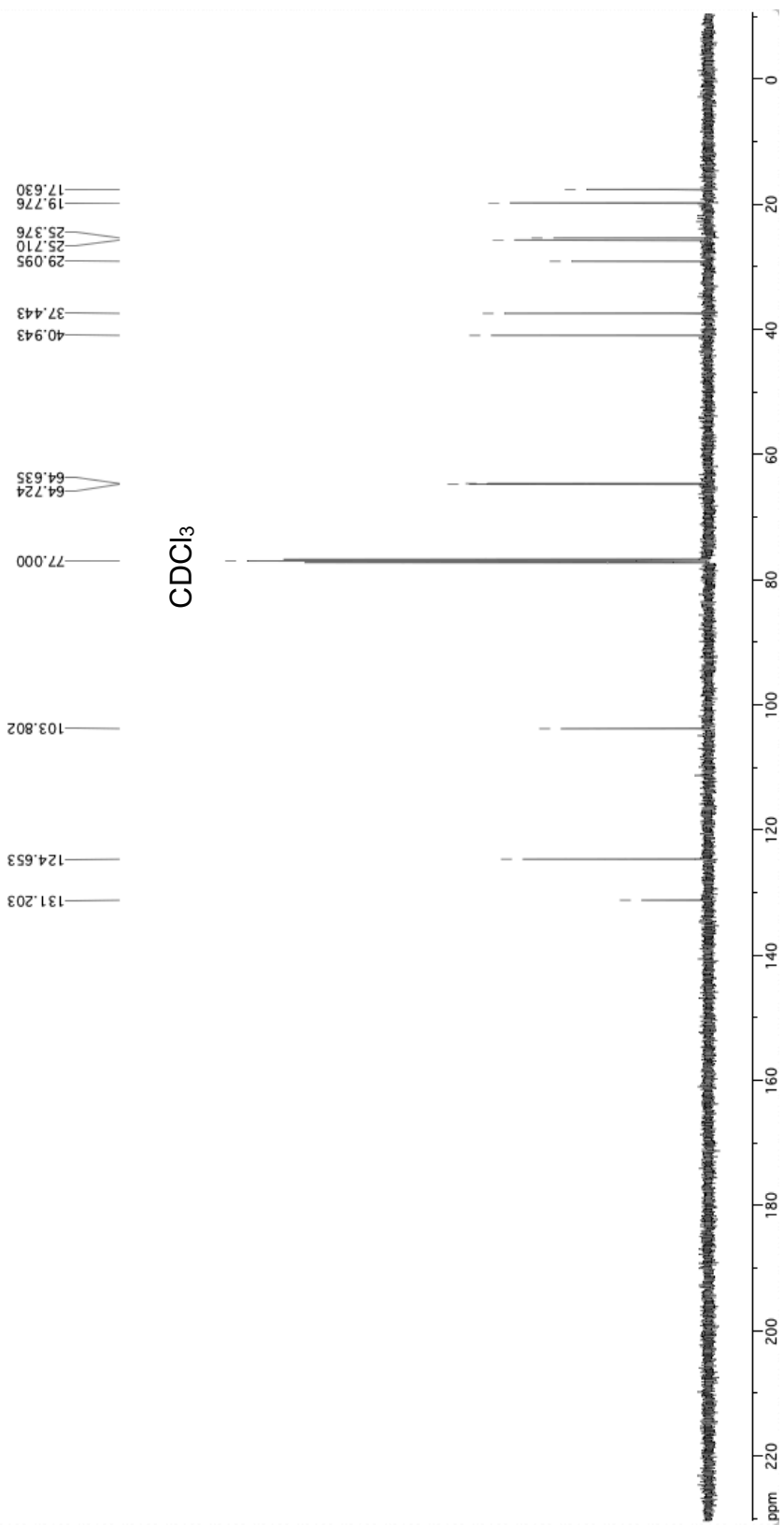


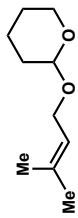
4.114 (¹H NMR, 500 MHz, CDCl₃, 25 °C)



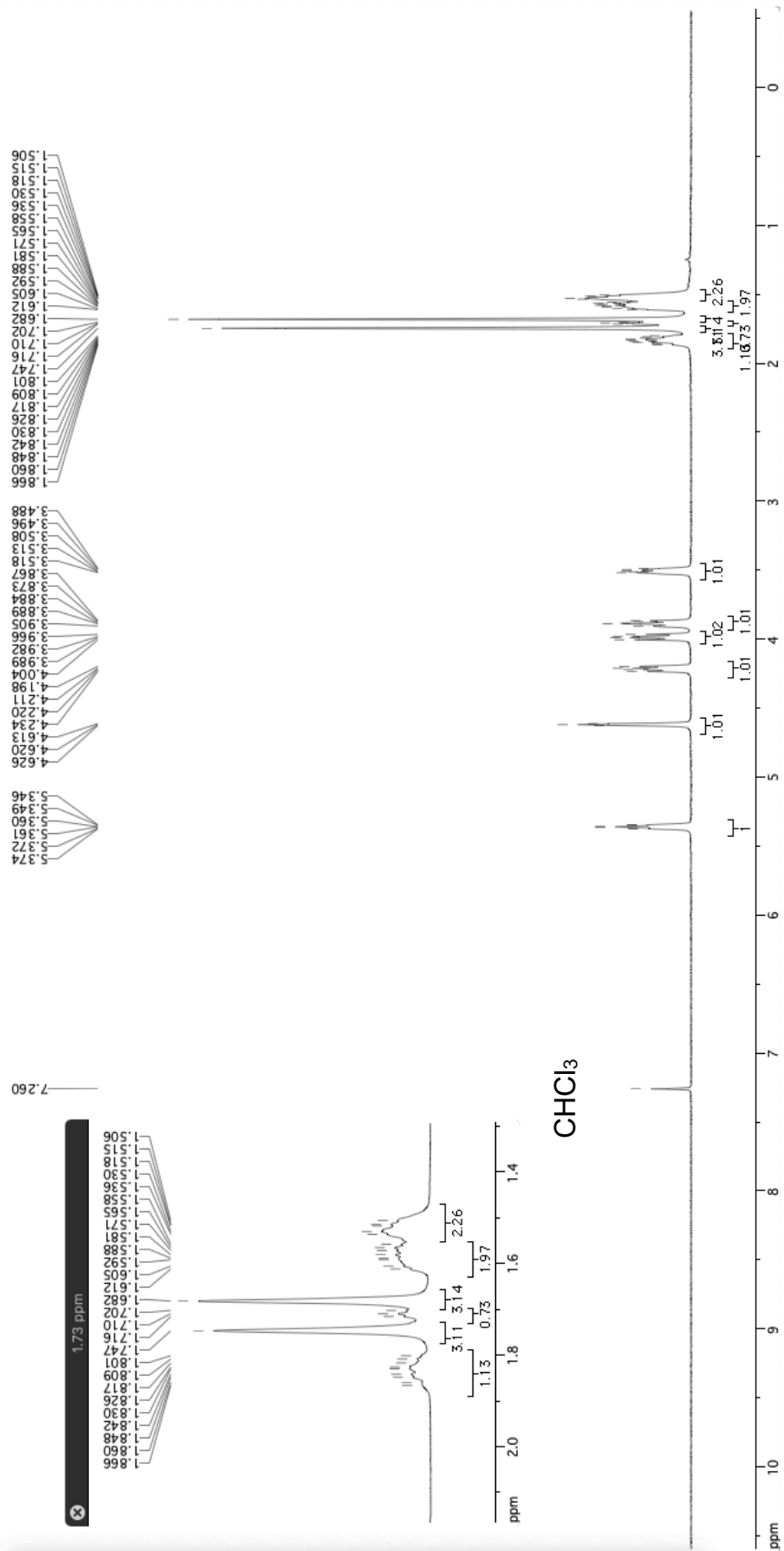


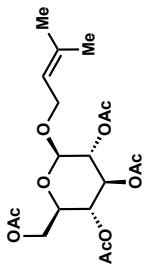
4.114 (¹³C NMR, 126 MHz, CDCl₃, 25 °C)



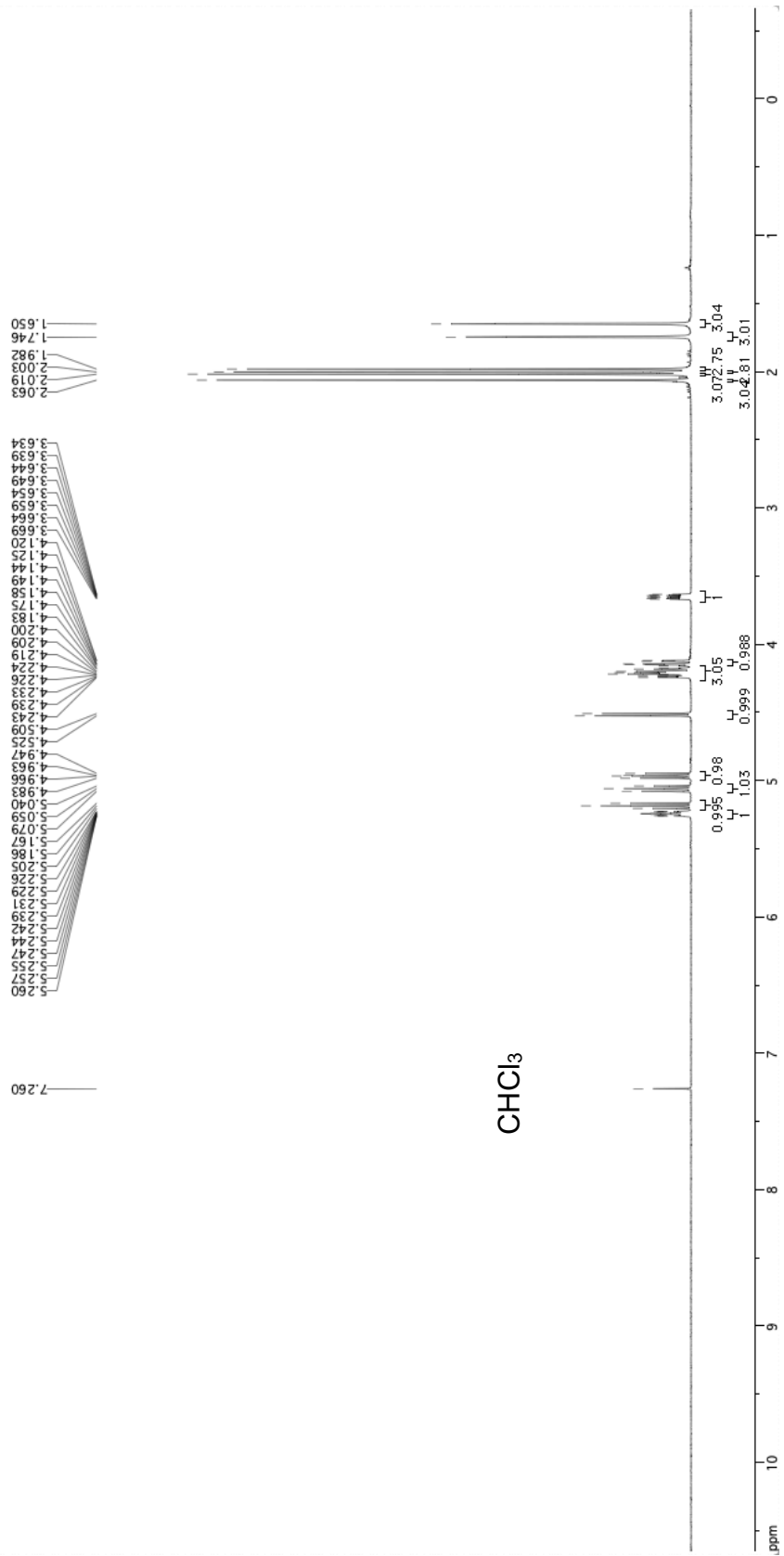


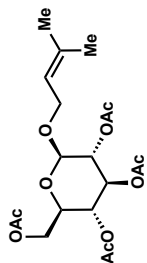
4.115 (¹H NMR, 500 MHz, CDCl₃, 25 °C)



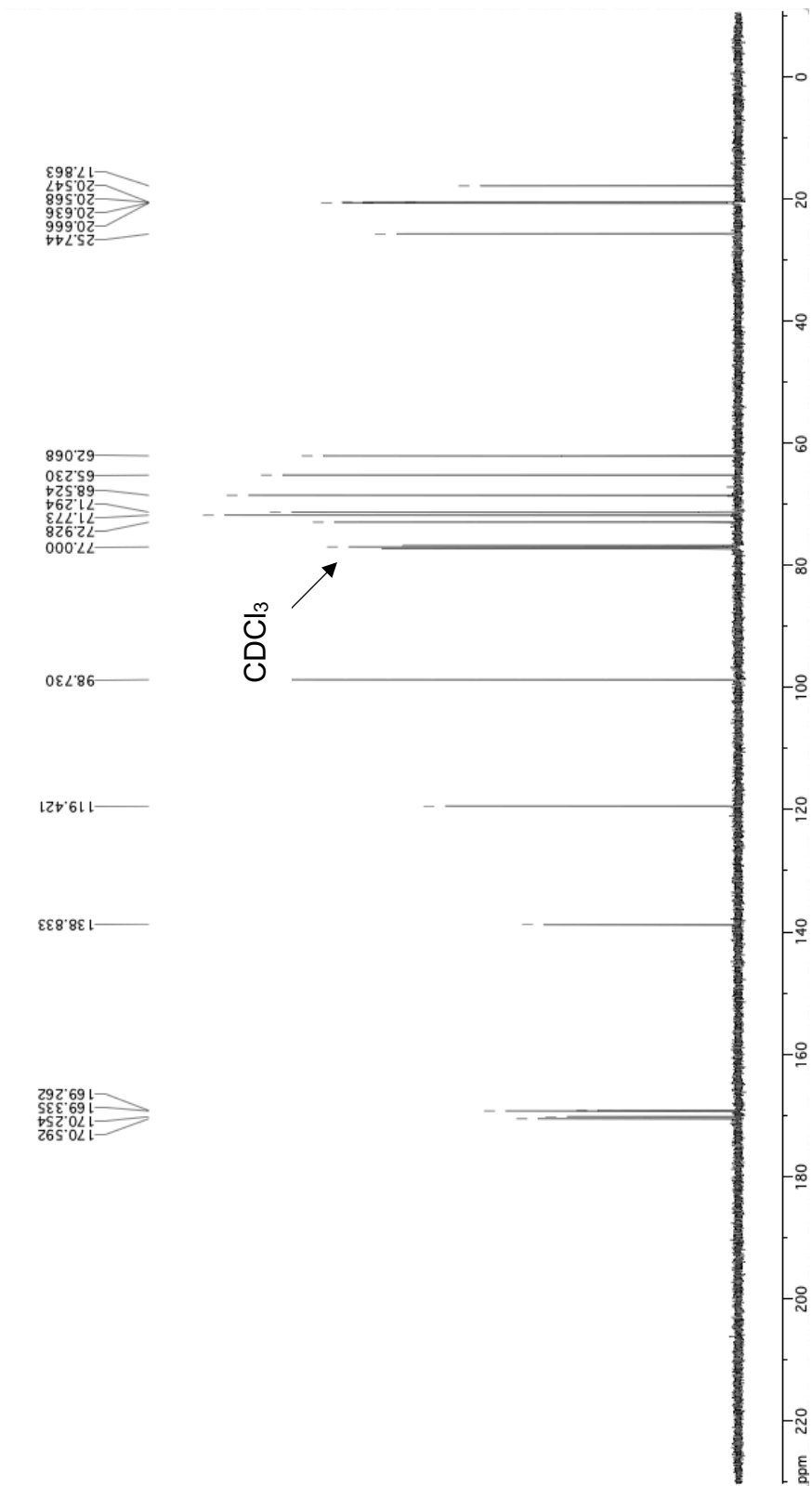


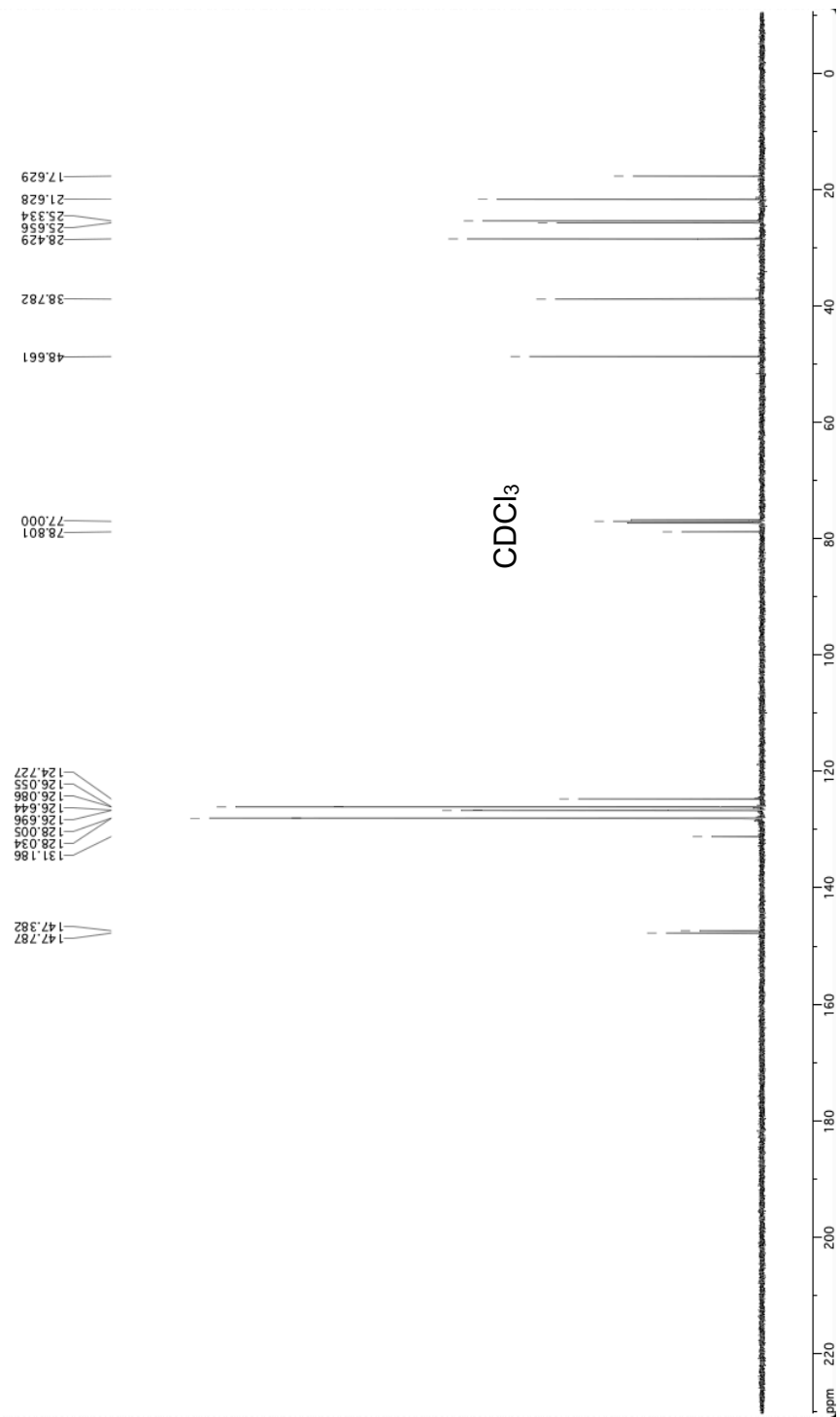
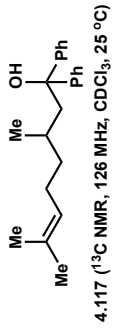
4.116 (¹H NMR, 500 MHz, CDCl₃, 25 °C)

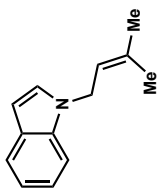




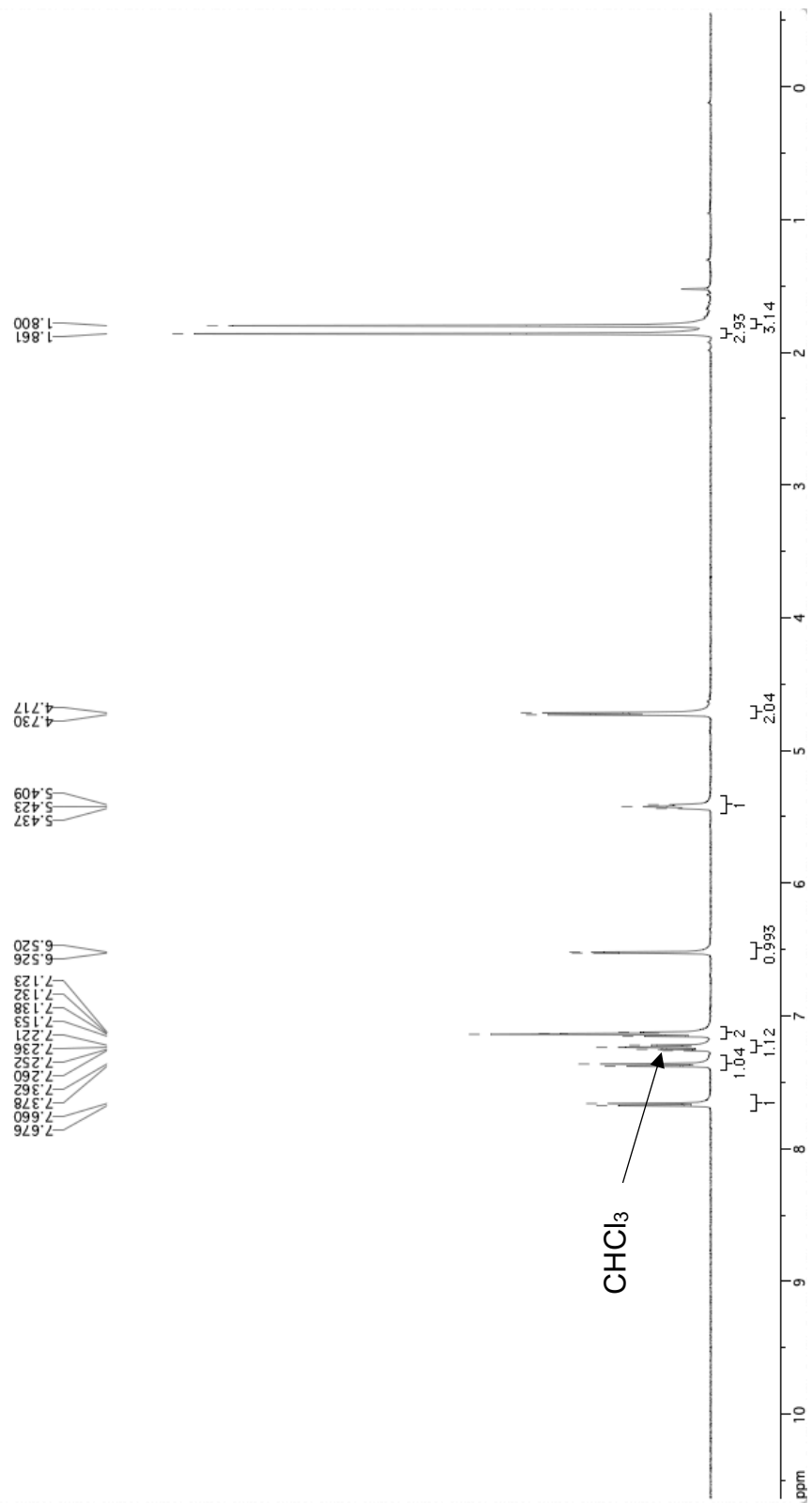
4.116 (^{13}C NMR, 126 MHz, CDCl_3 , 25 $^\circ\text{C}$)

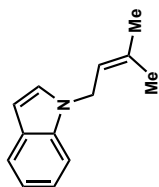




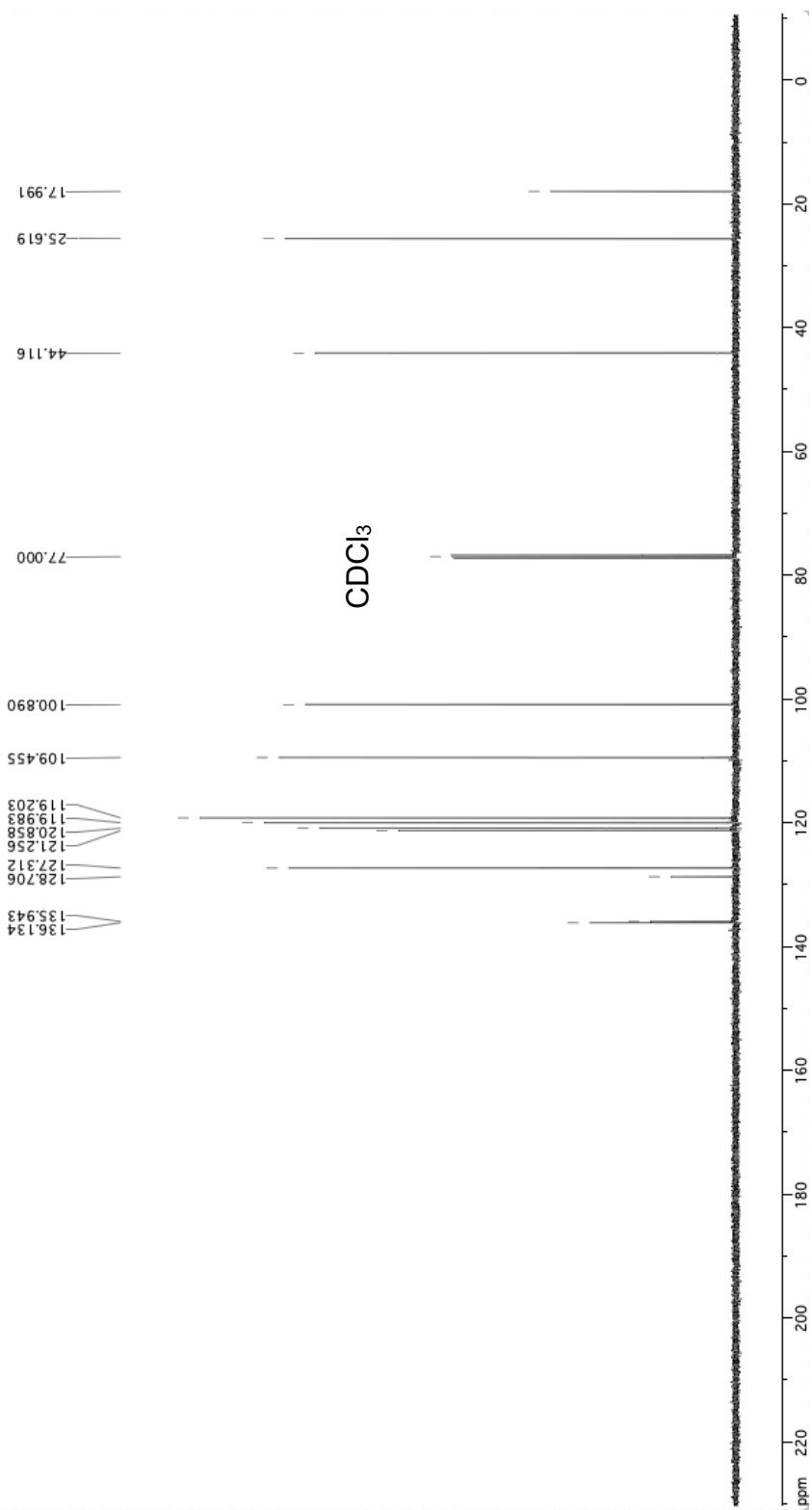


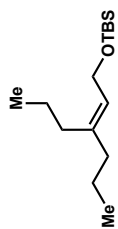
4.119 (¹H NMR, 500 MHz, CDCl₃, 25 °C)



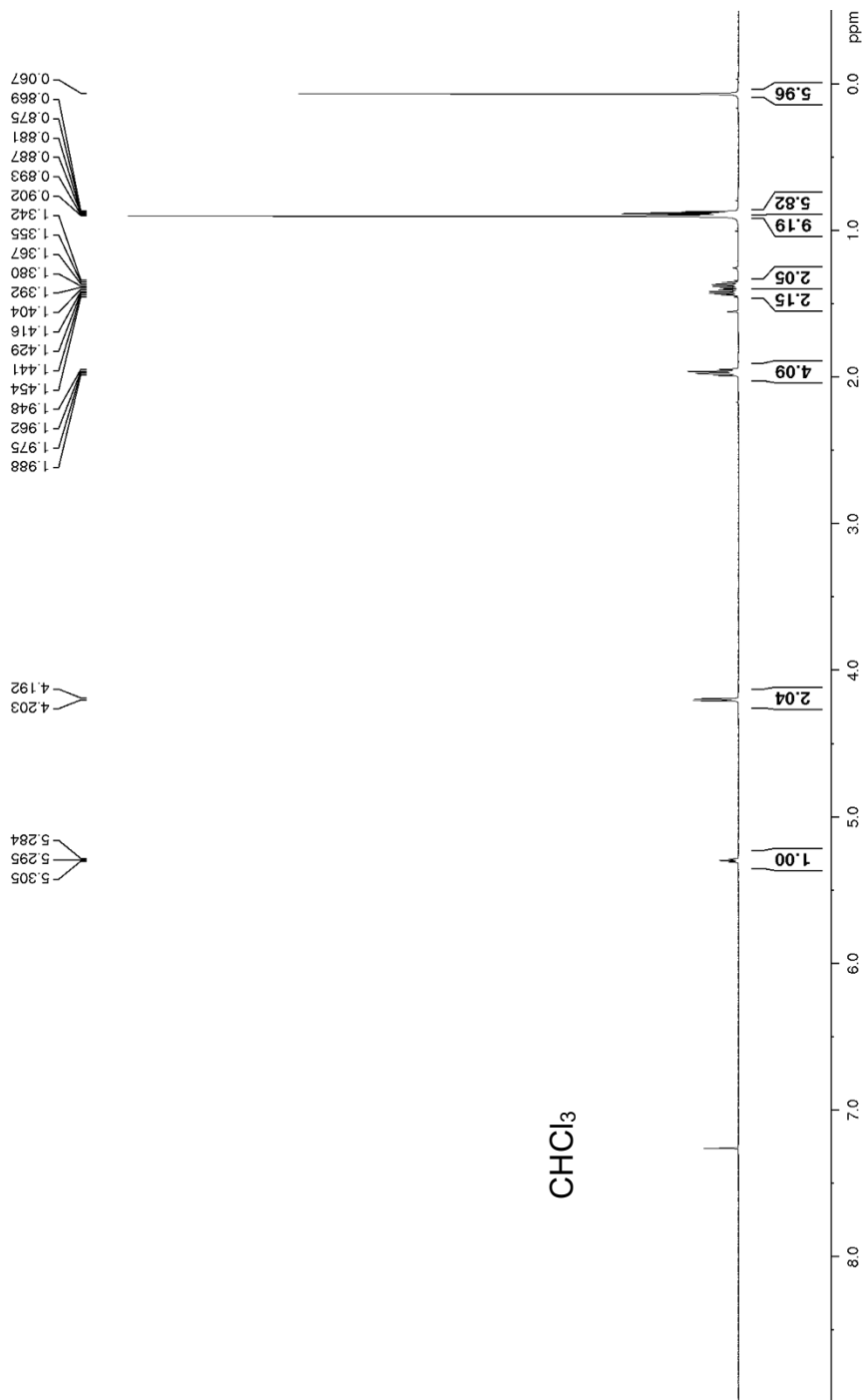


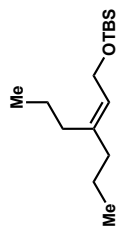
4.119 (¹³C NMR, 126 MHz, CDCl₃, 25 °C)



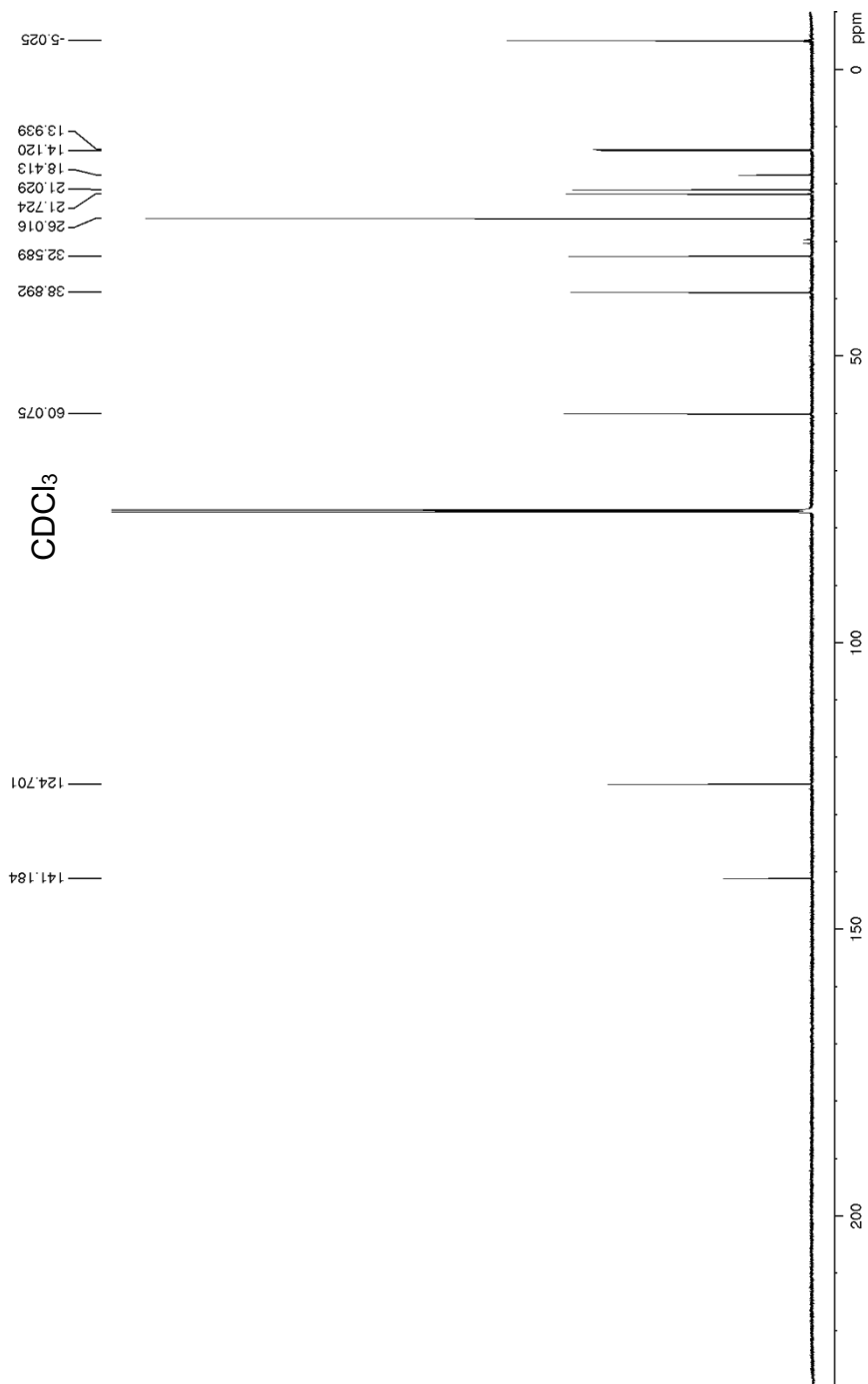


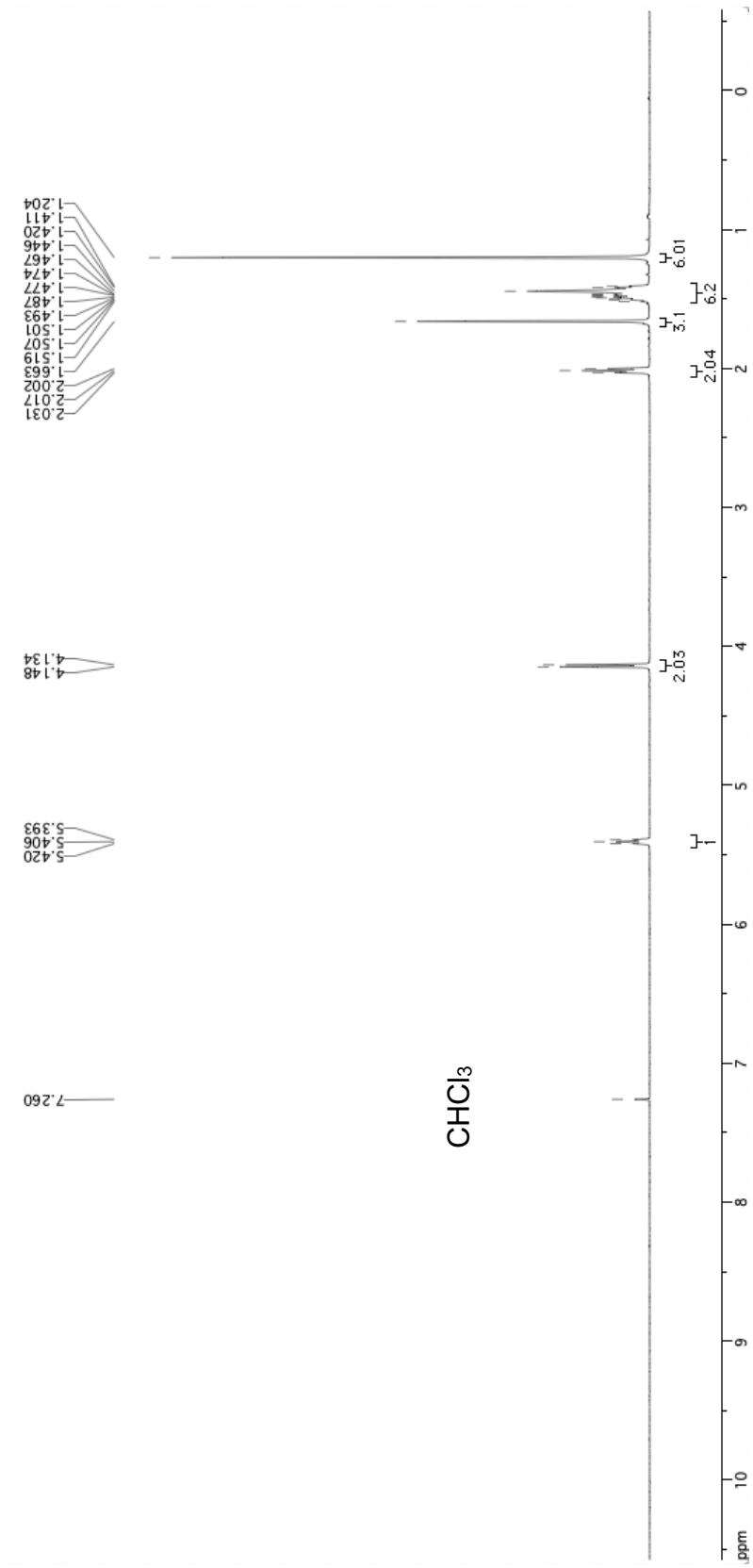
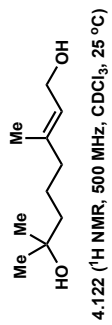
4.121 (¹H NMR, 600 MHz, CDCl₃, 25 °C)

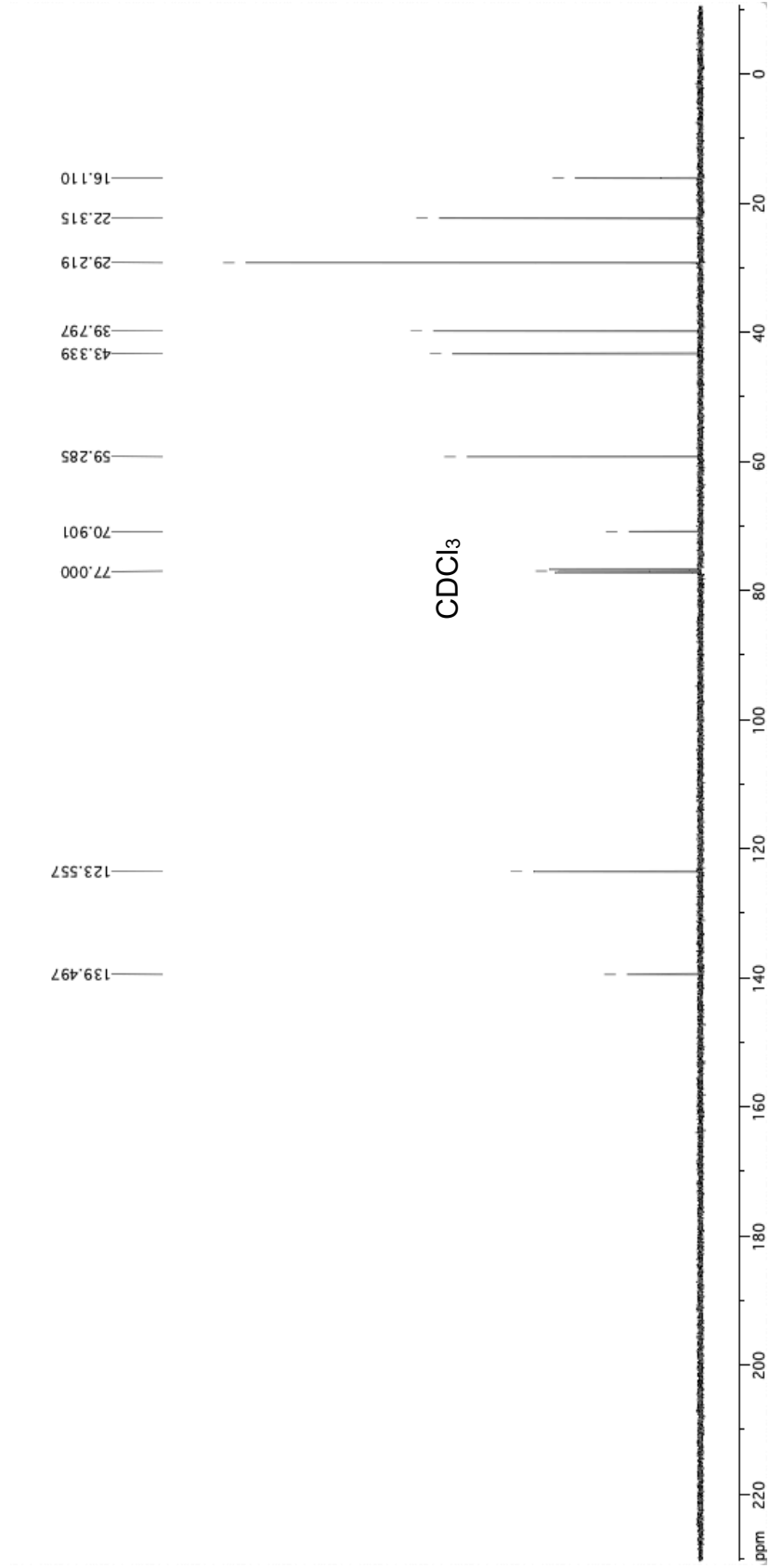
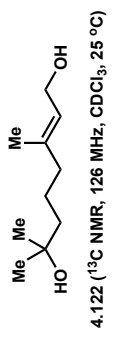


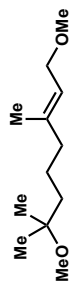


4.121 (¹³C NMR, 151 MHz, CDCl₃, 25 °C)

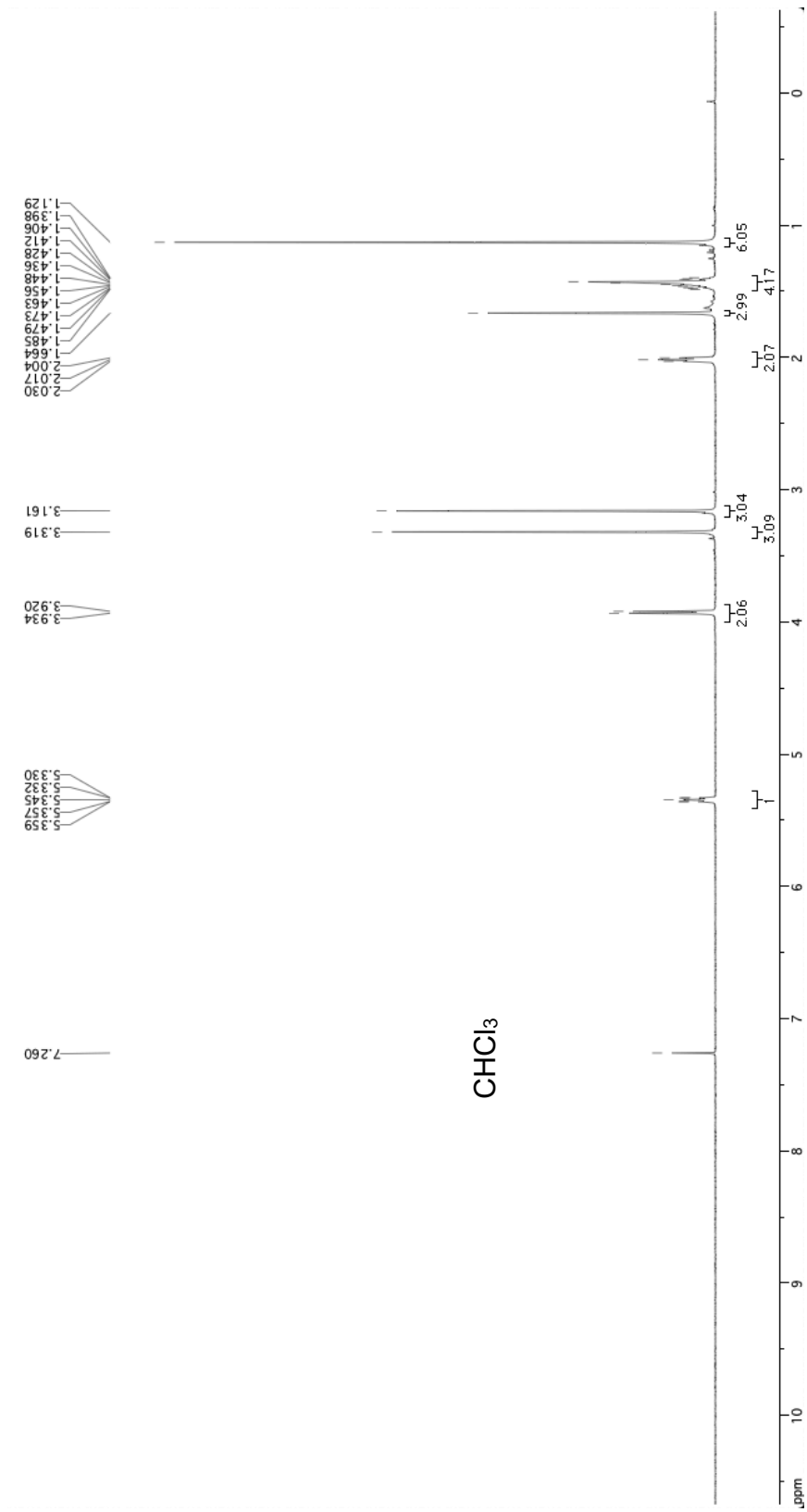


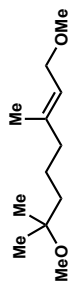




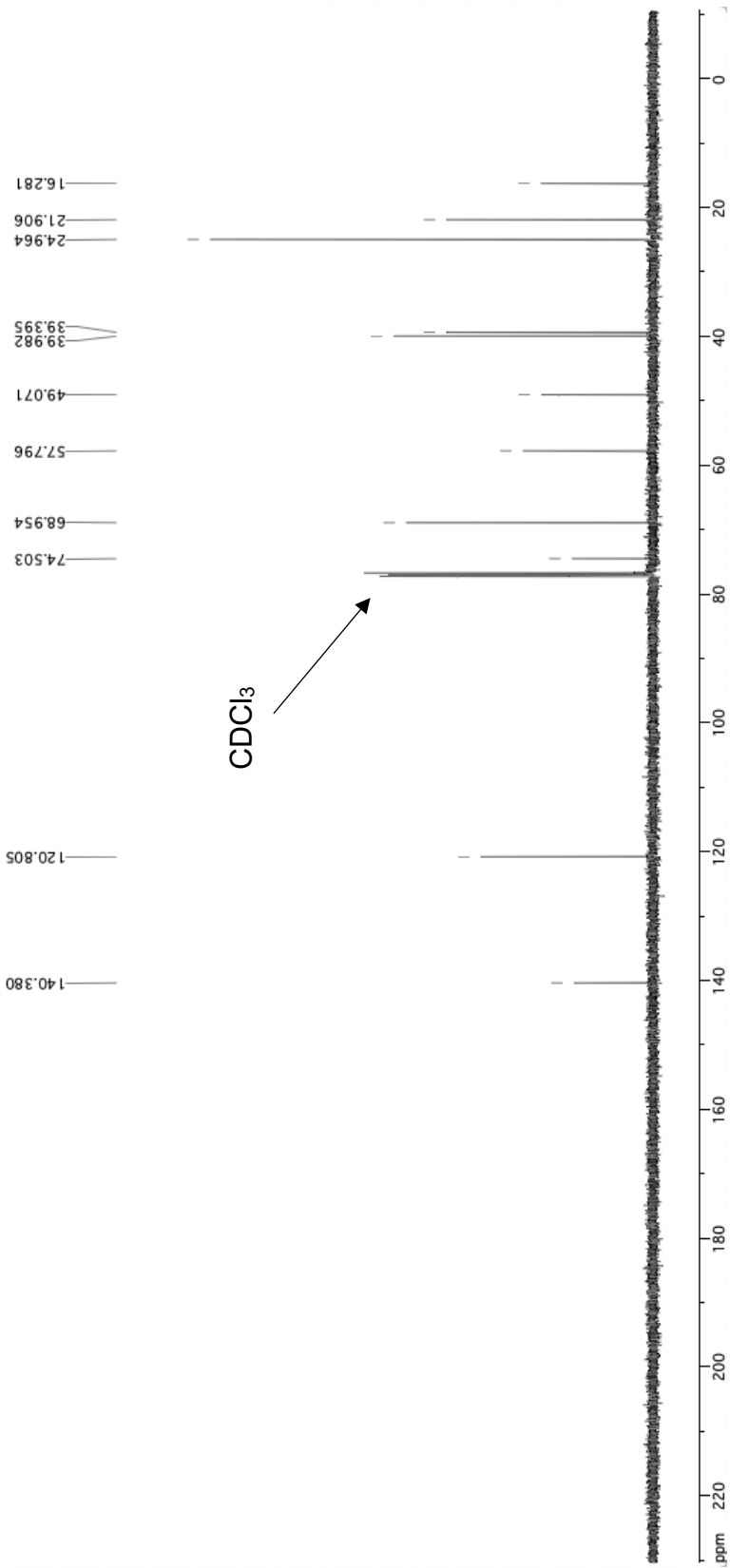


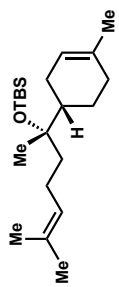
4.123 (¹H NMR, 500 MHz, CDCl₃, 25 °C)



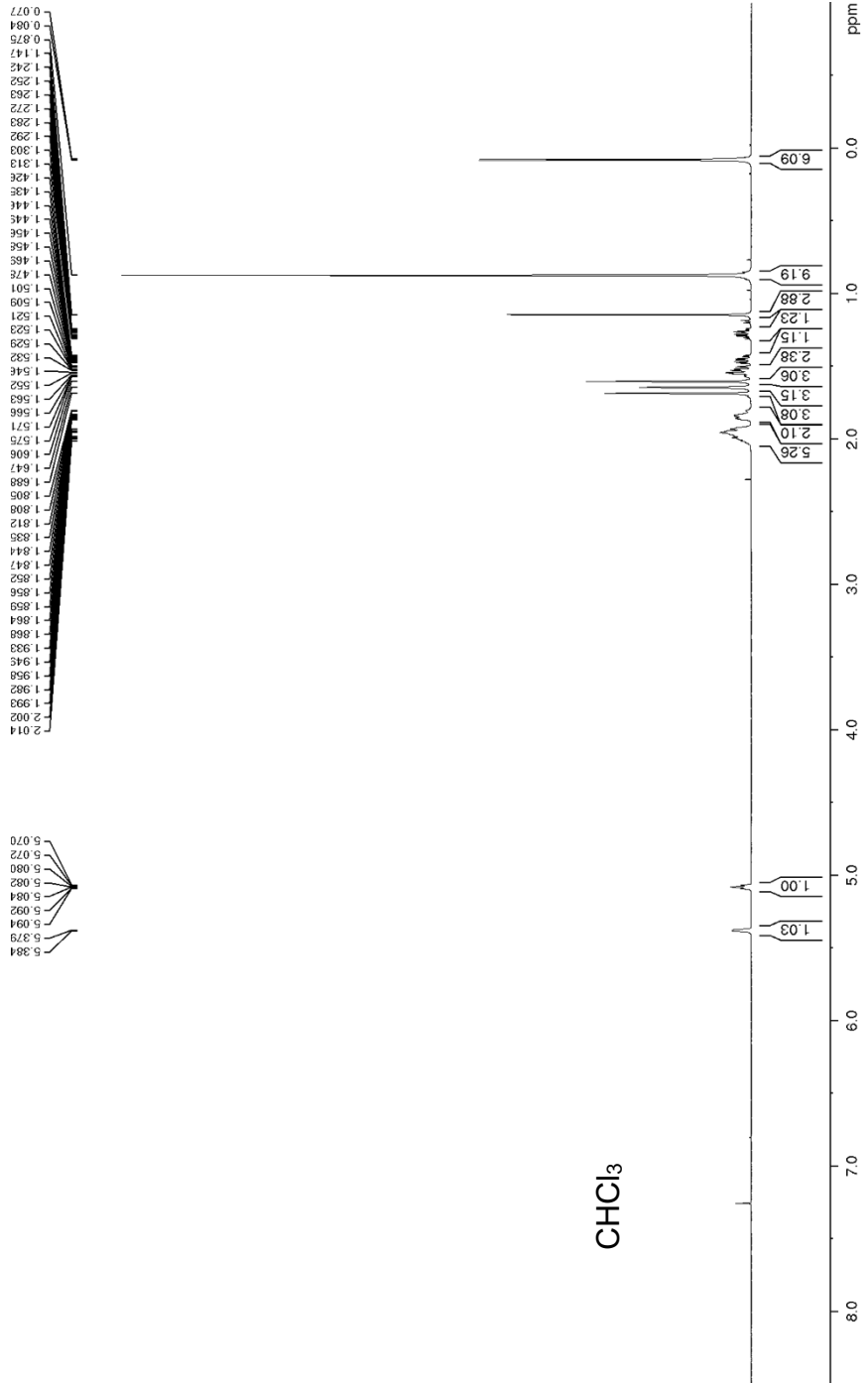


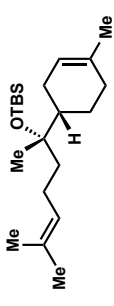
4.123 (¹³C NMR, 126 MHz, CDCl₃, 25 °C)



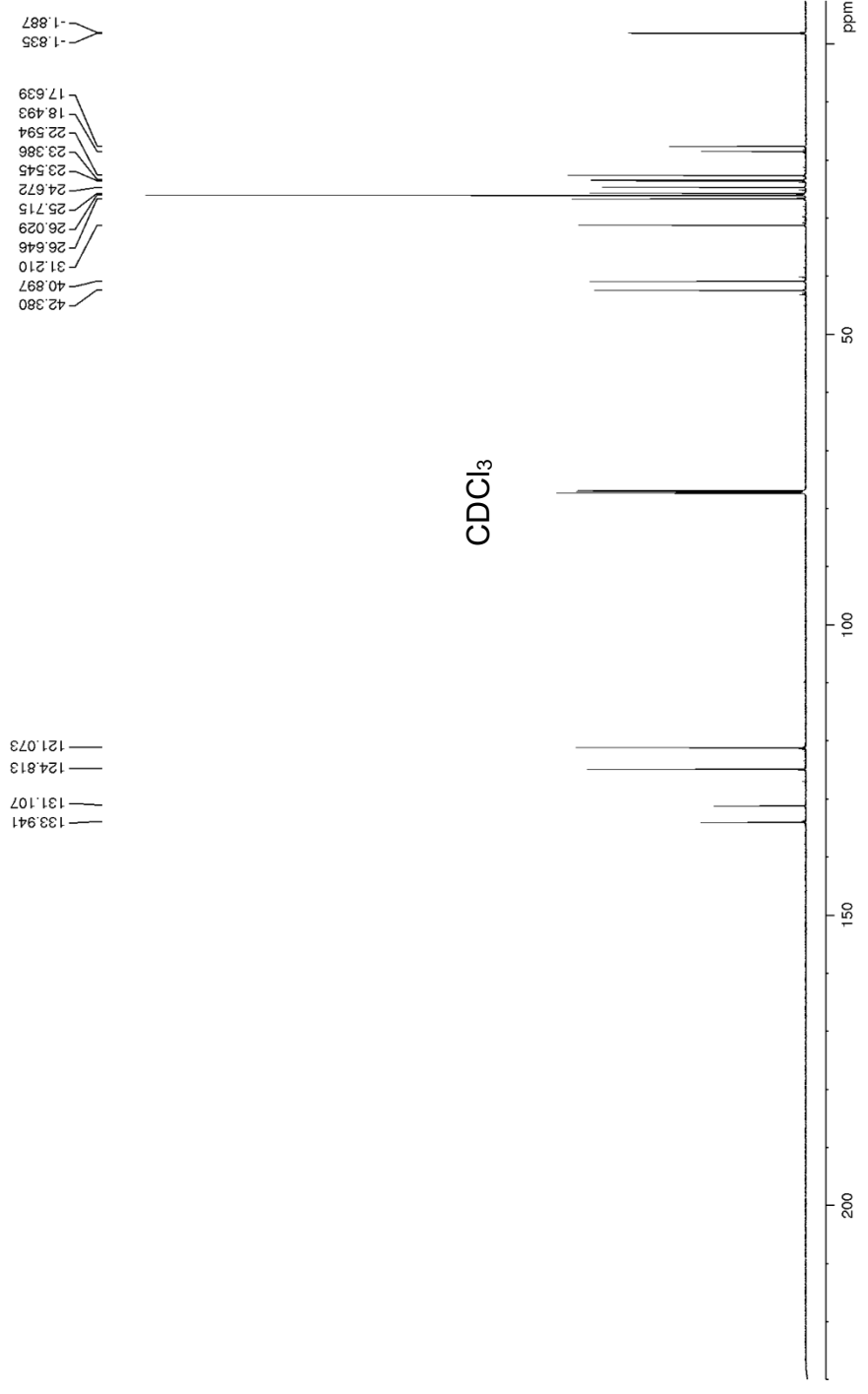


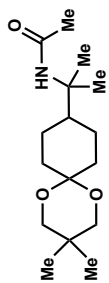
4.124 (¹H NMR, 600 MHz, CDCl₃, 25 °C)



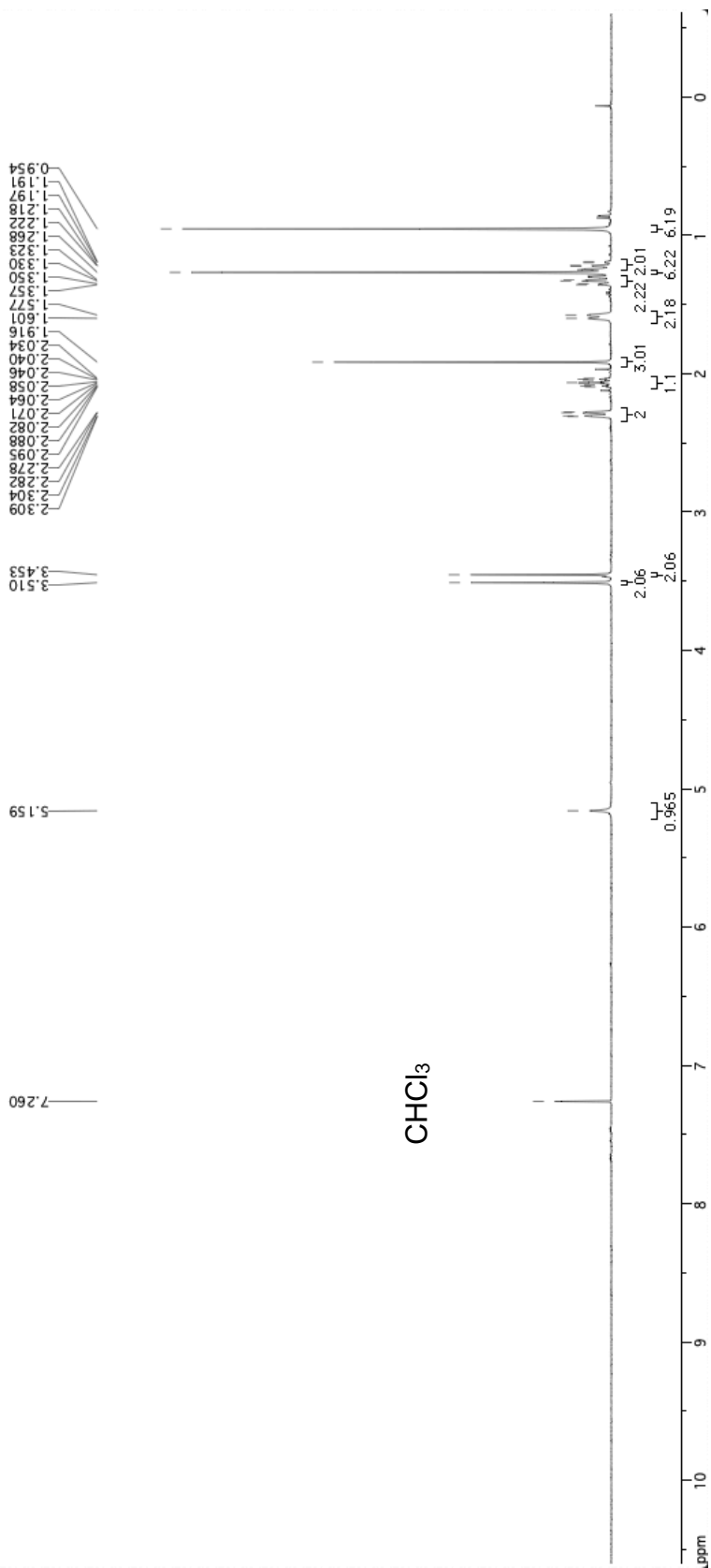


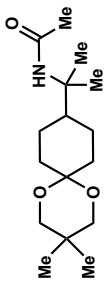
4.124 (¹³C NMR, 151 MHz, CDCl₃, 25 °C)



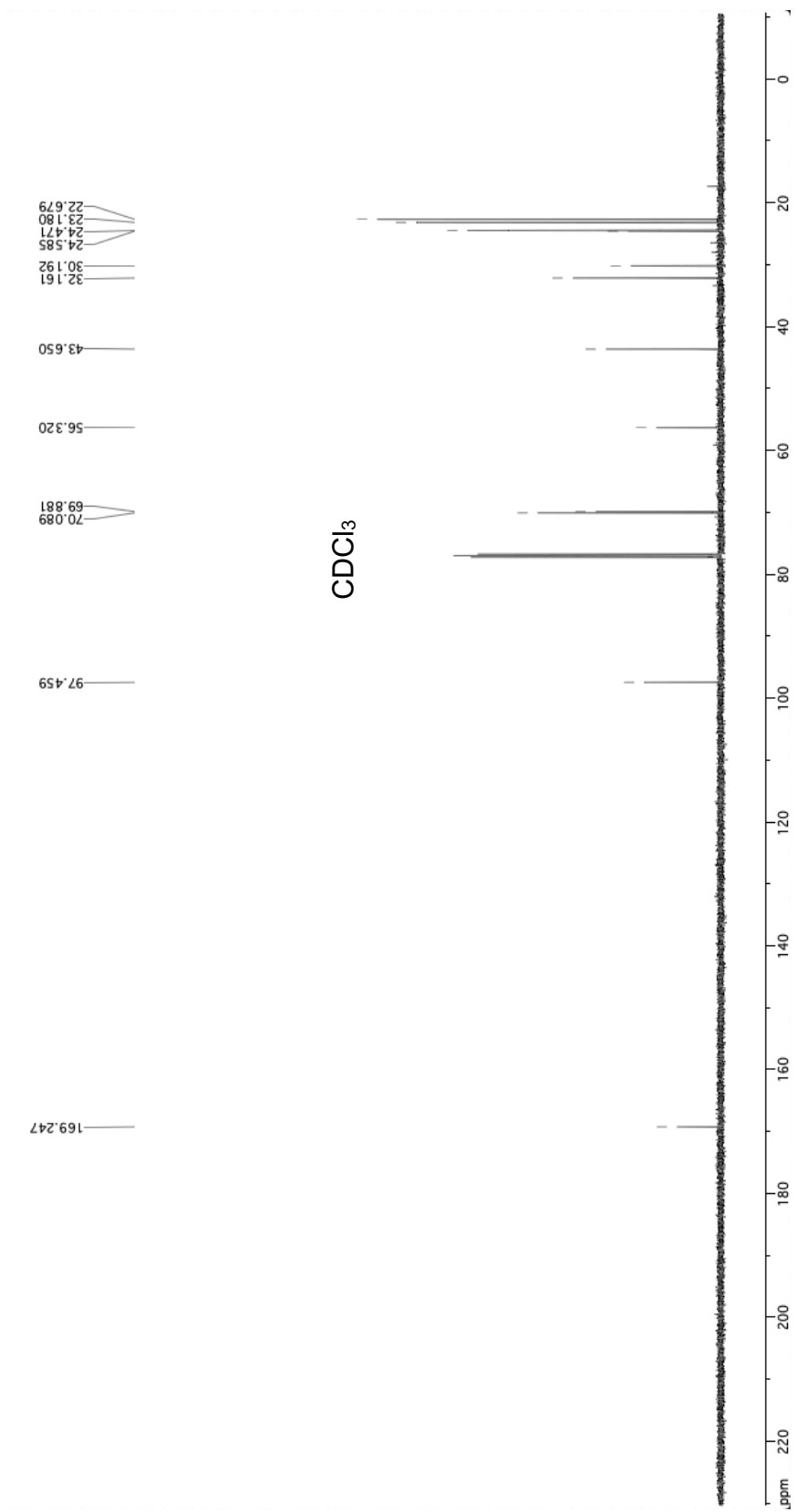


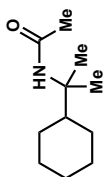
4.42 (¹H NMR, 500 MHz, CDCl₃, 25 °C)



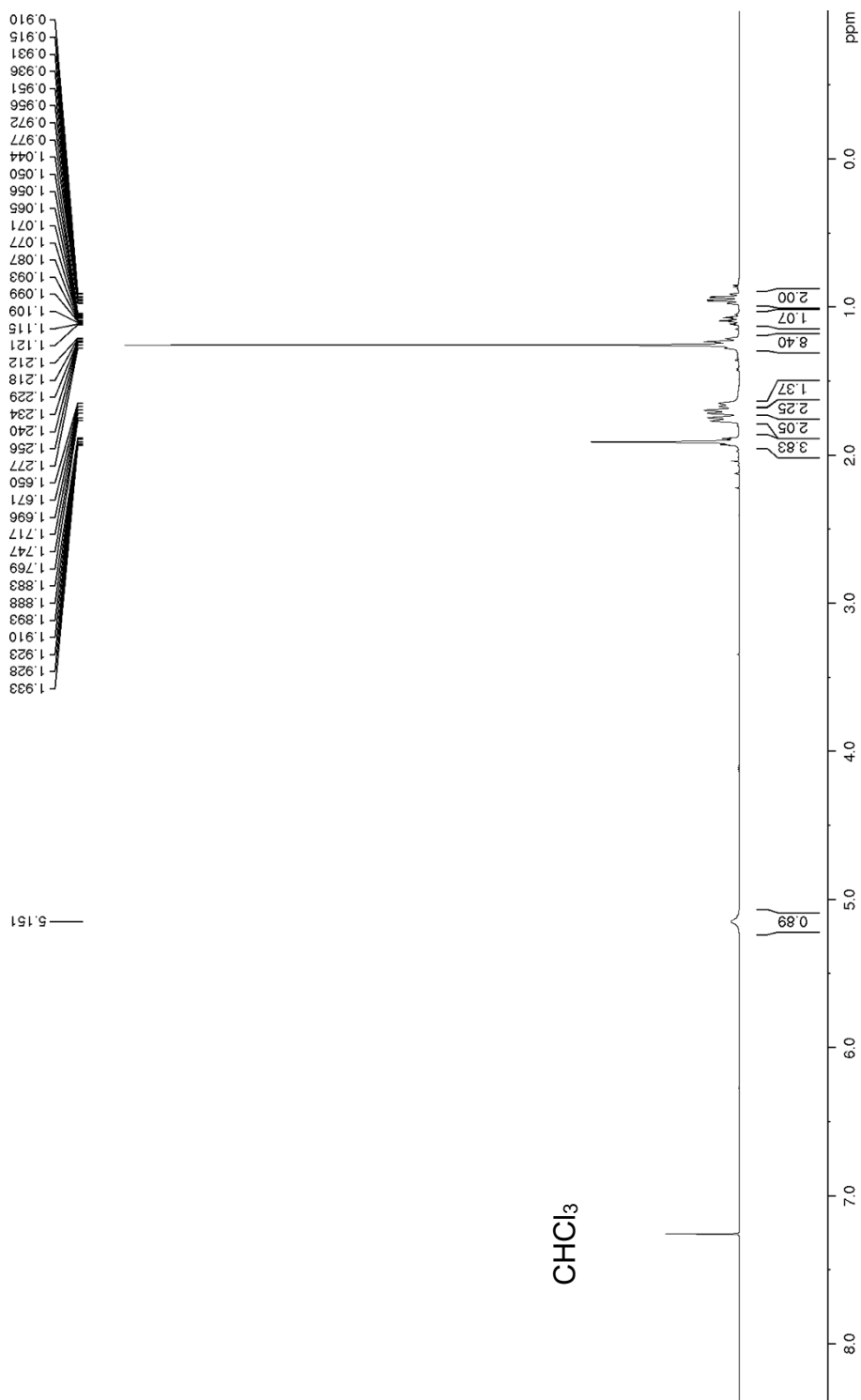


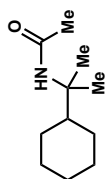
4.42 (¹³C NMR, 126 MHz, CDCl₃, 25 °C)



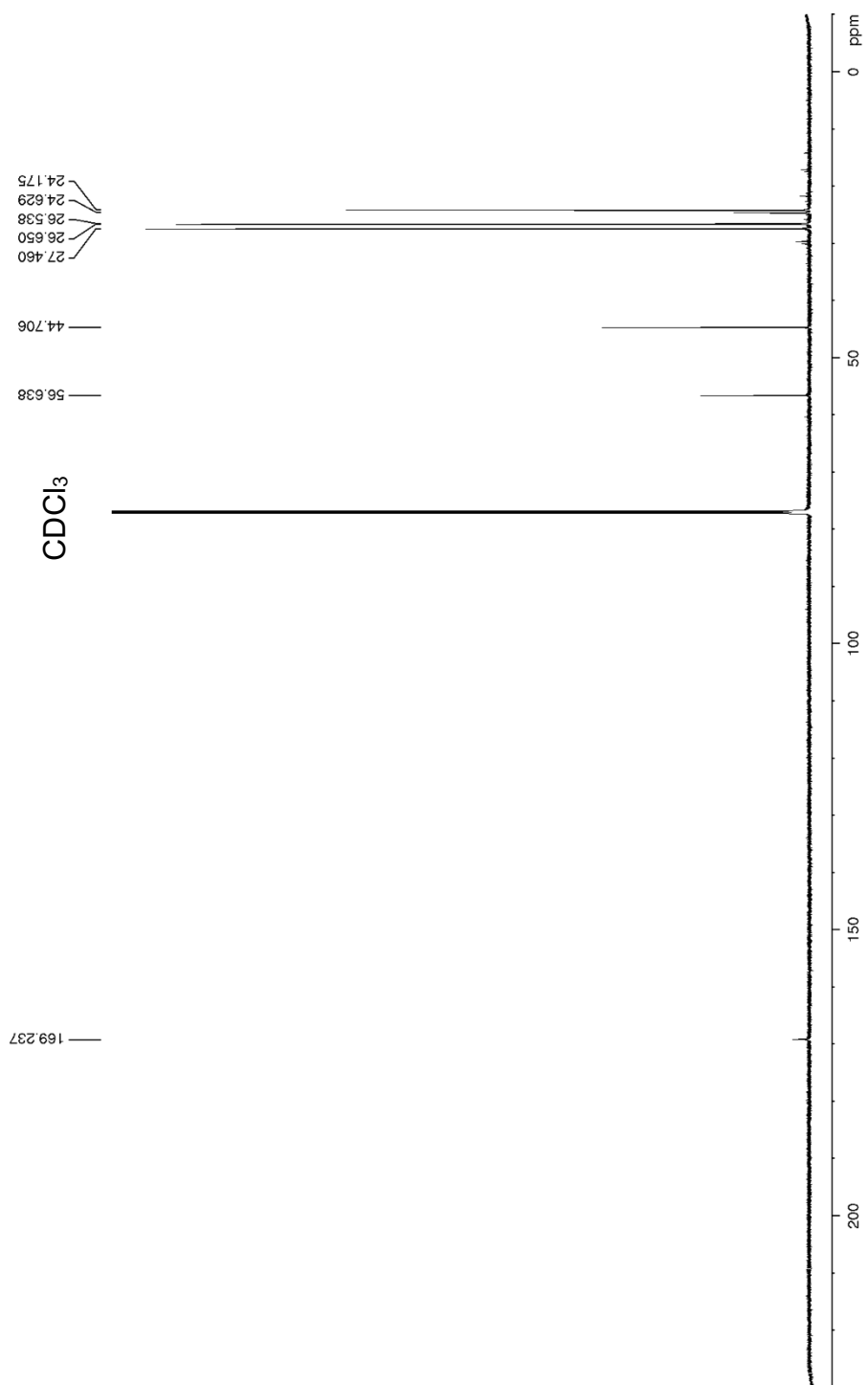


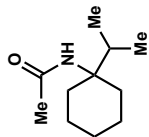
4.56 (¹H NMR, 600 MHz, CDCl₃, 25°C)



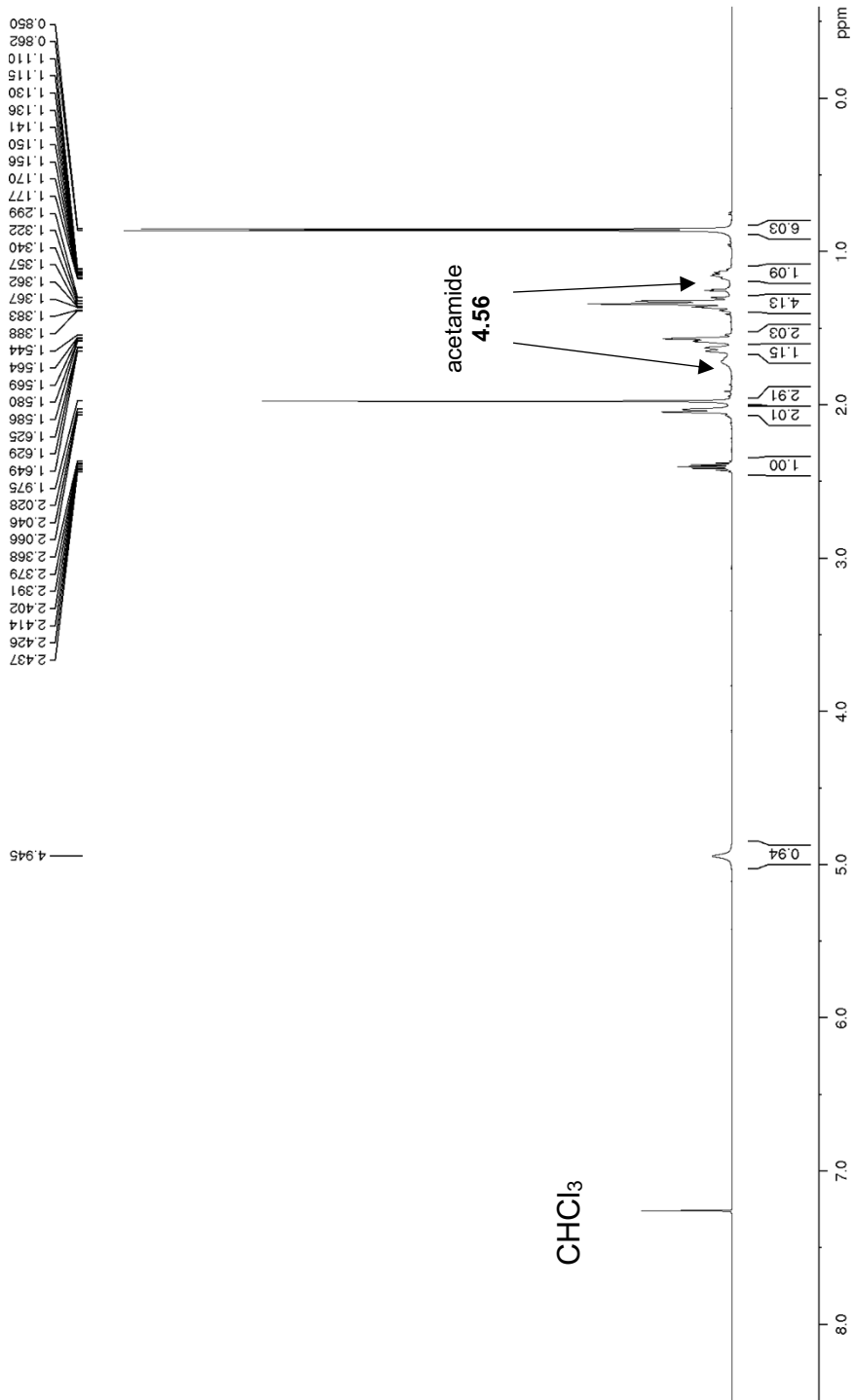


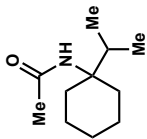
4.56 (¹³C NMR, 151 MHz, CDCl₃, 25°C)



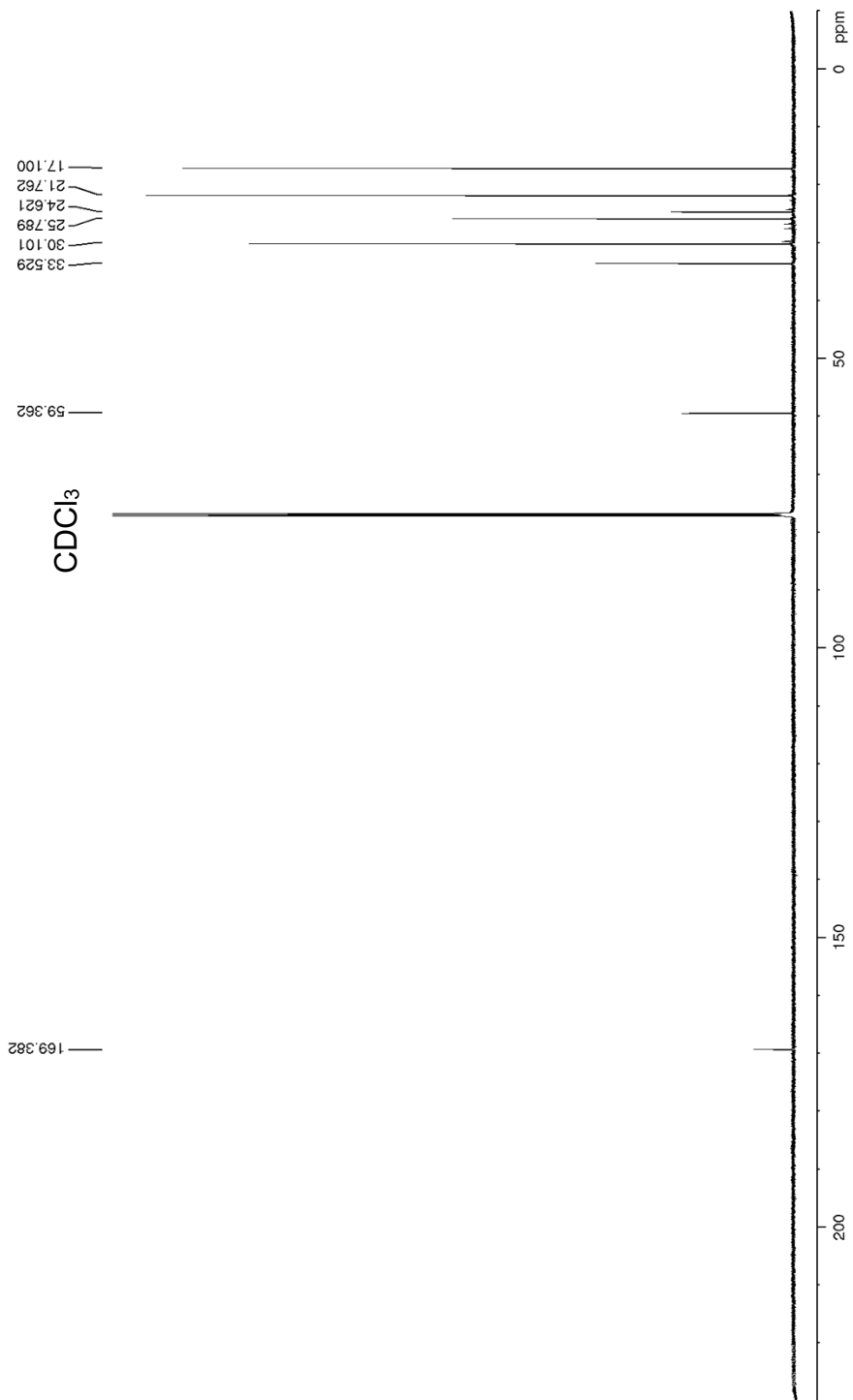


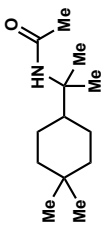
4.56' (¹H NMR, 600 MHz, CDCl₃, 25°C)



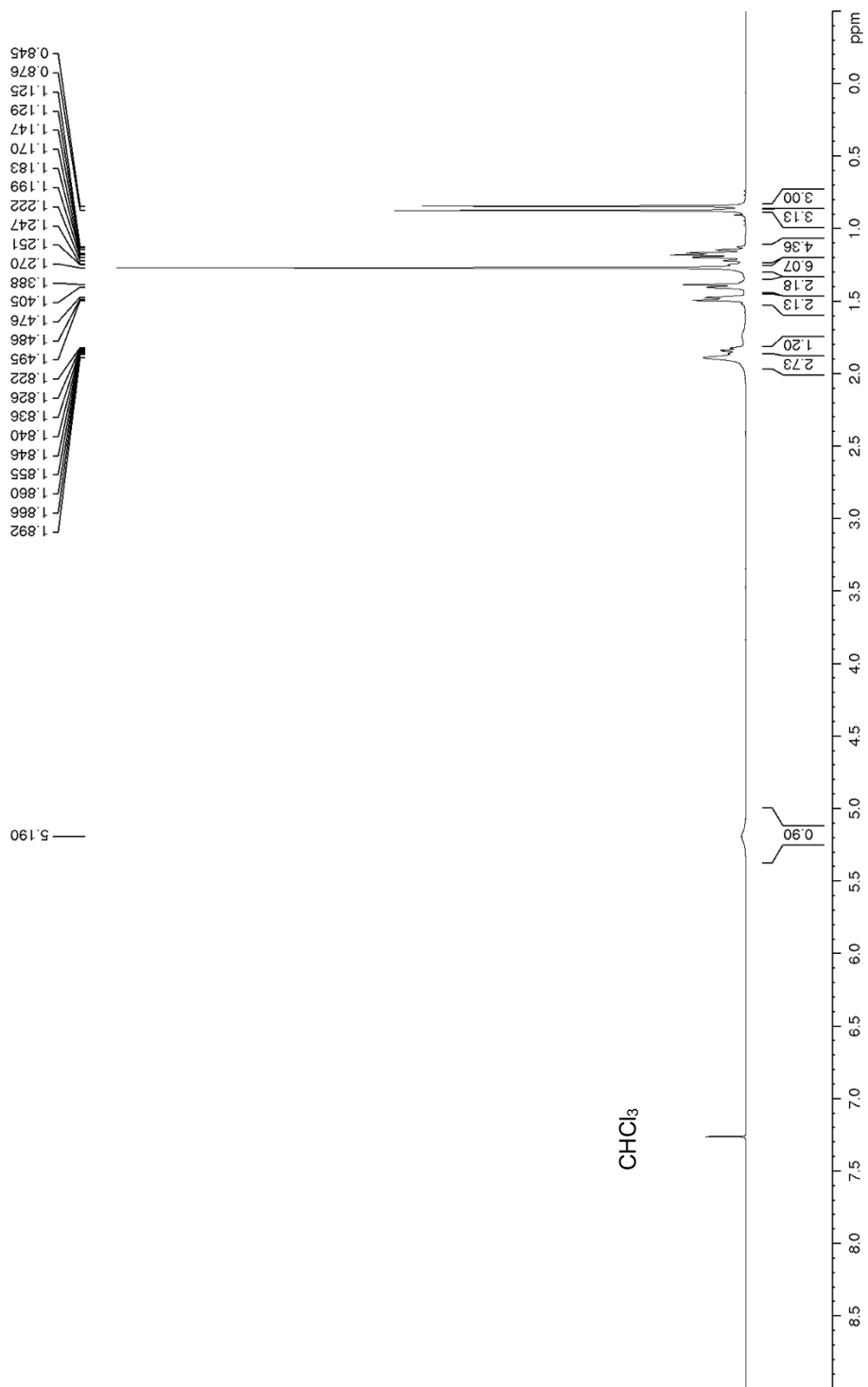


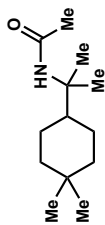
4.56 (¹³C NMR, 151 MHz, CDCl₃, 25°C)



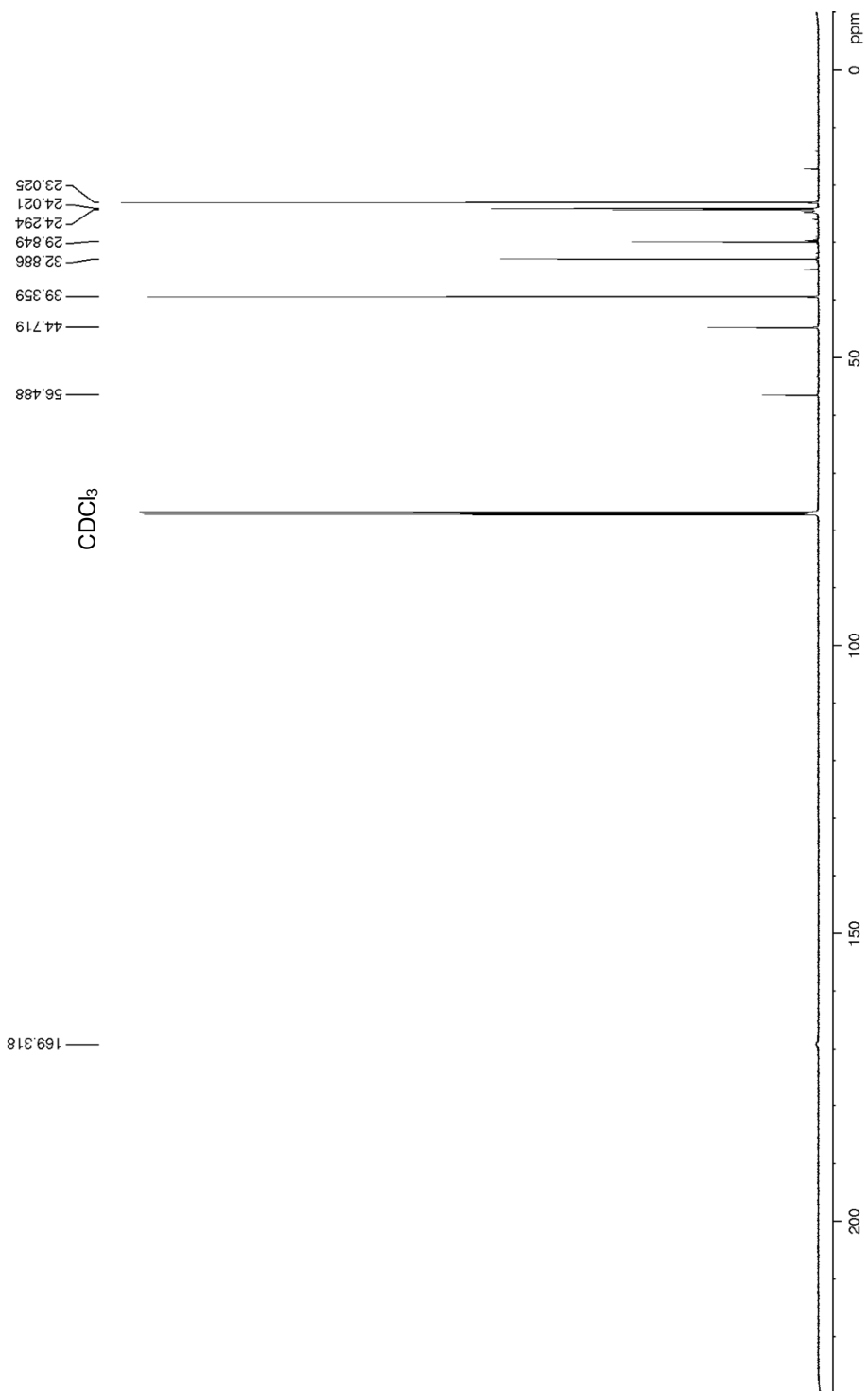


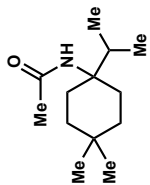
4.57 (¹H NMR, 600 MHz, CDCl₃, 25°C)



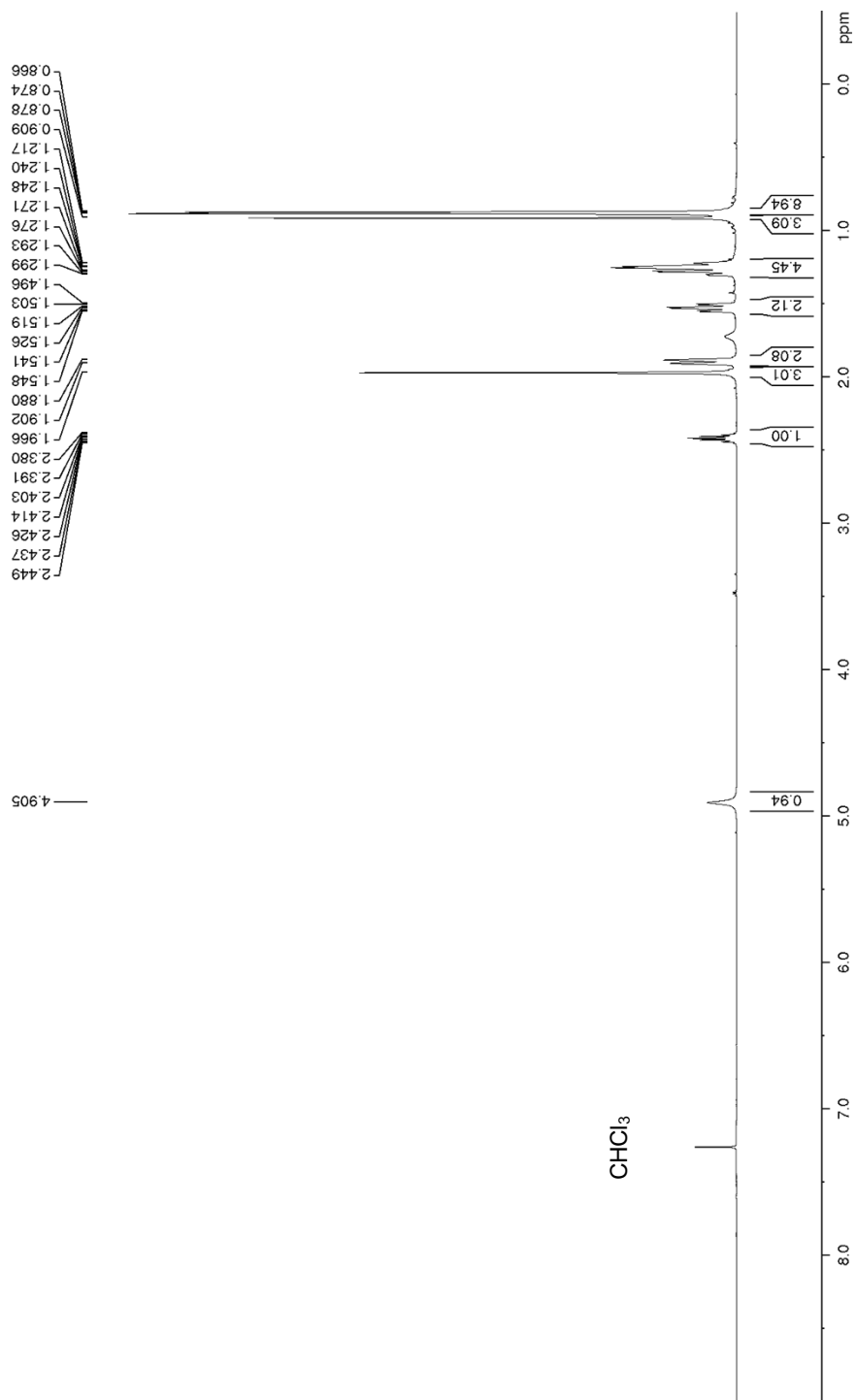


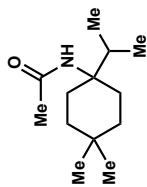
4.57 (¹³C NMR, 151 MHz, CDCl₃, 25°C)



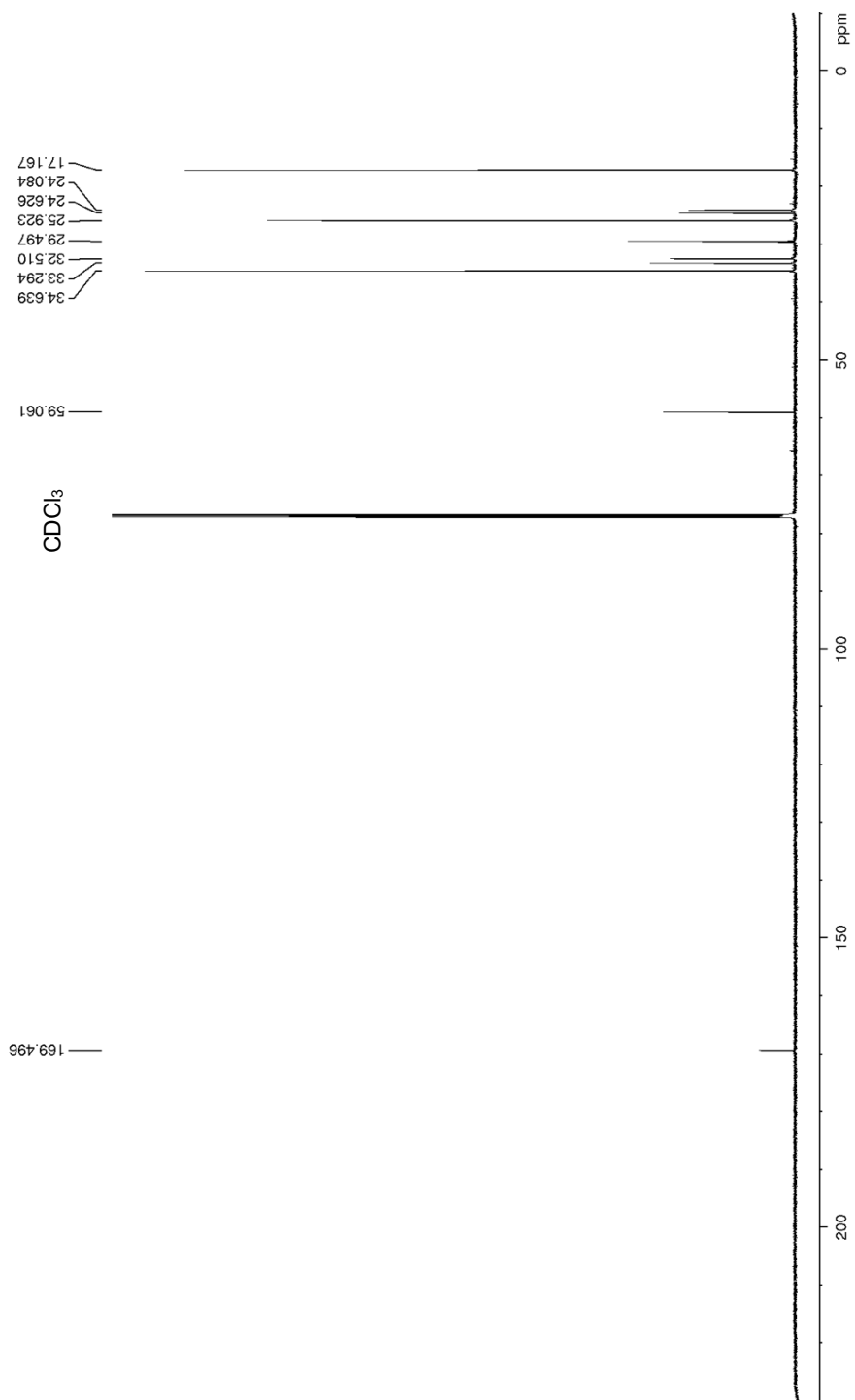


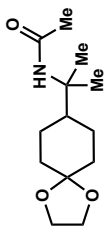
4.57' (¹H NMR, 600 MHz, CDCl₃, 25°C)



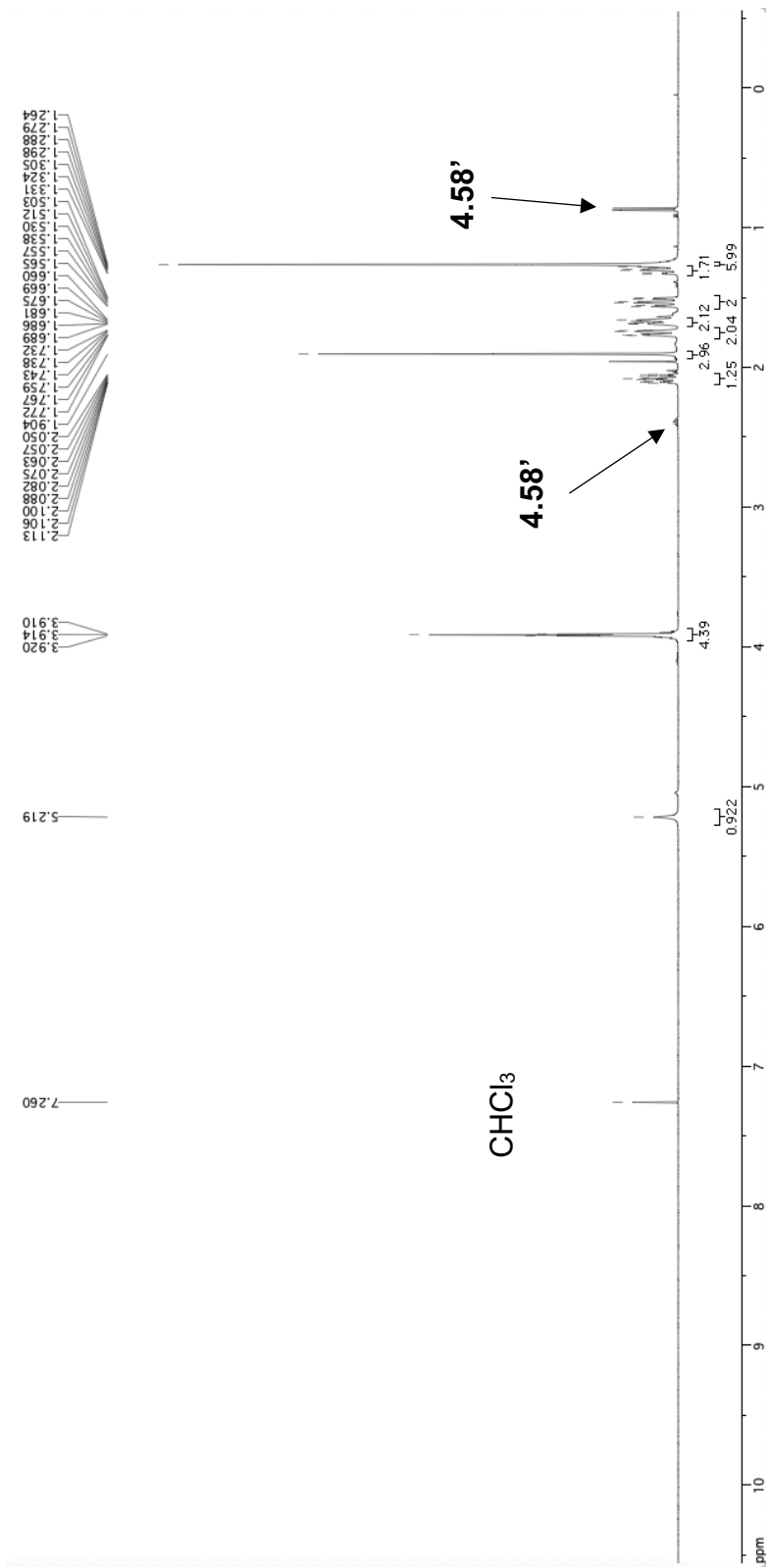


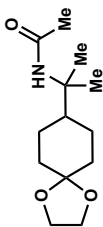
4.57' (¹³C NMR, 151 MHz, CDCl₃, 25°C)



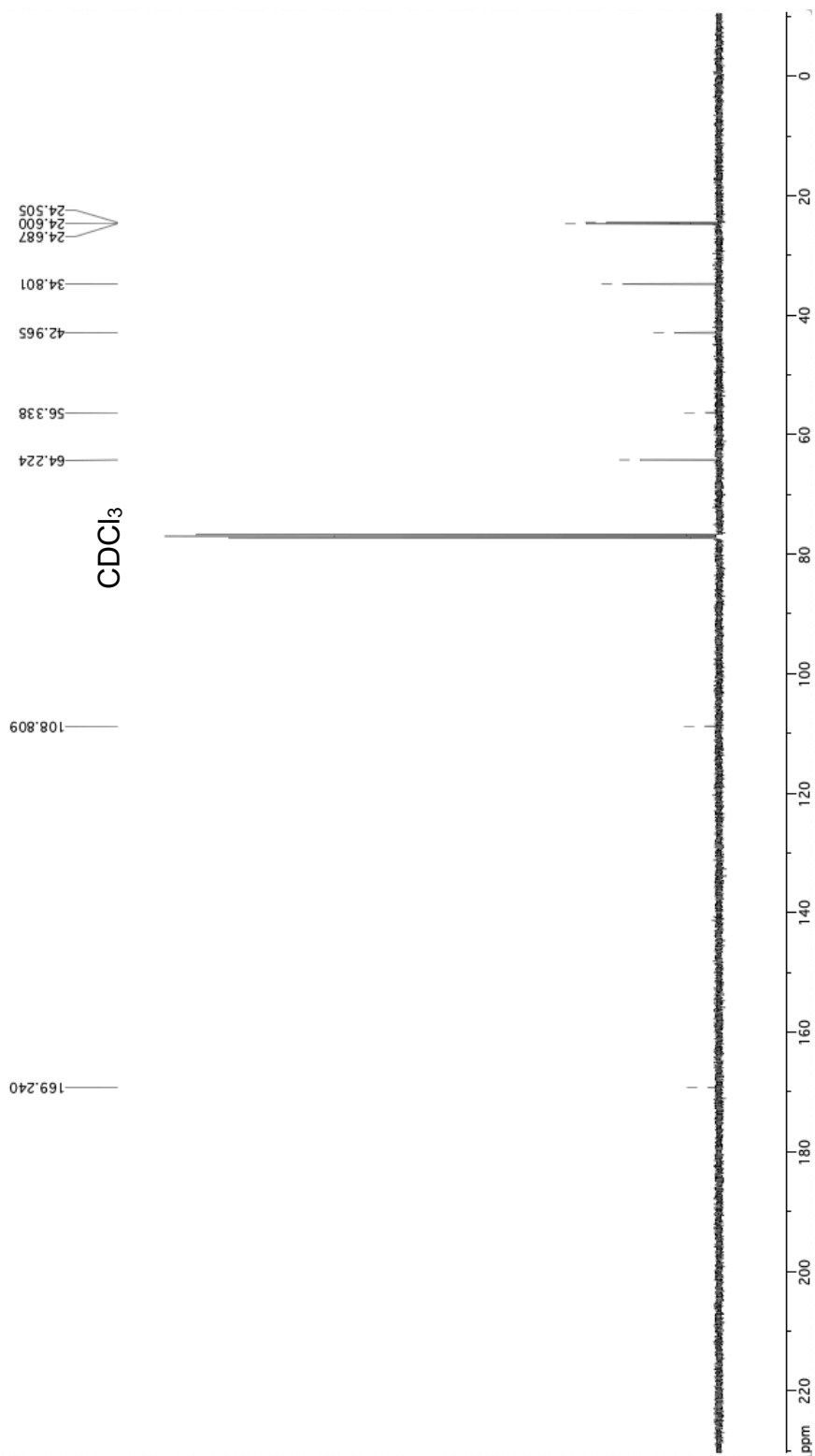


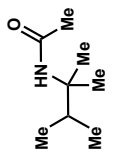
4.58 (¹H NMR, 500 MHz, CDCl₃, 25 °C)



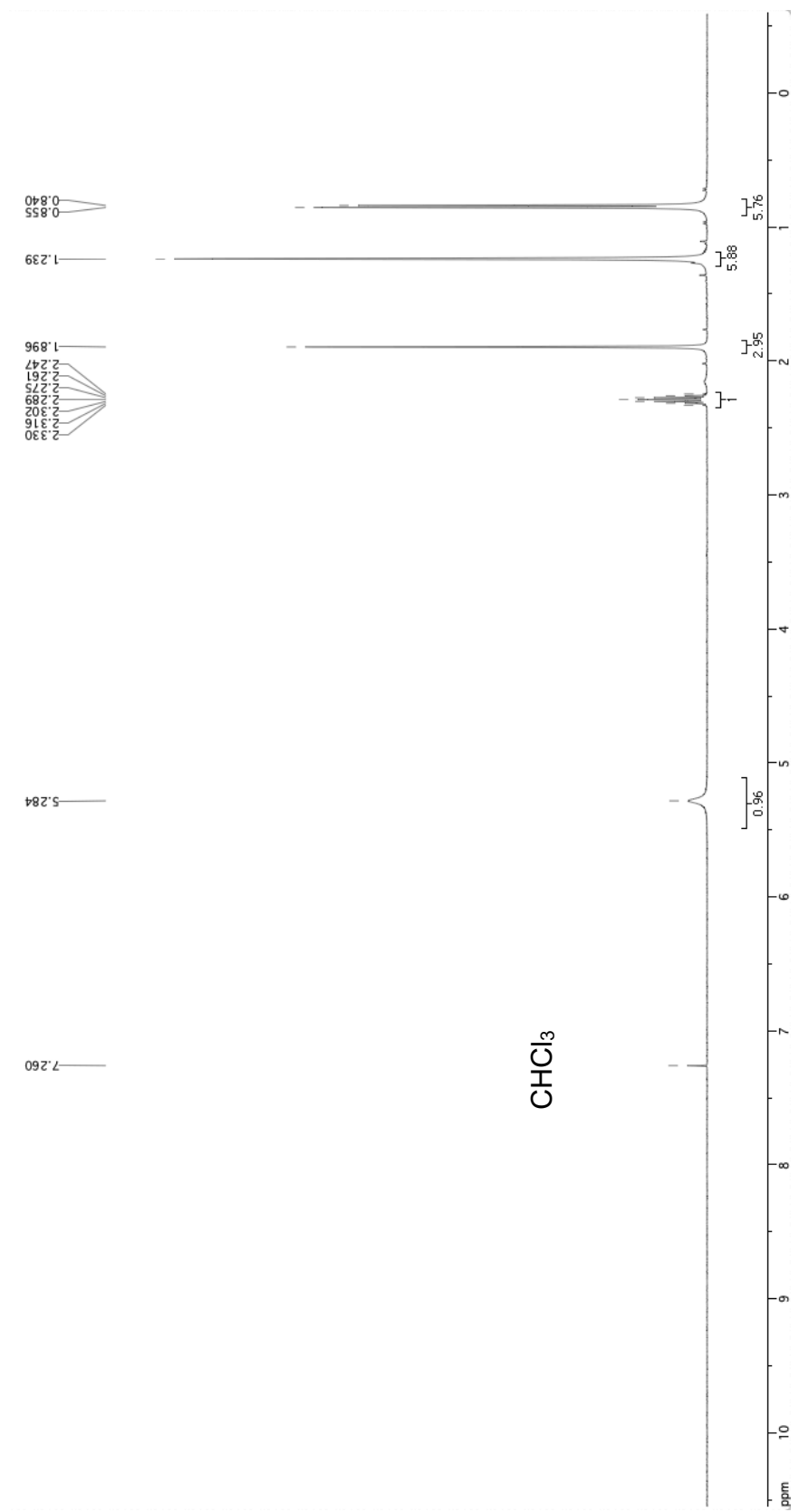


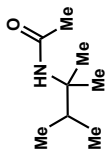
4.58 (¹³C NMR, 126 MHz, CDCl₃, 25 °C)



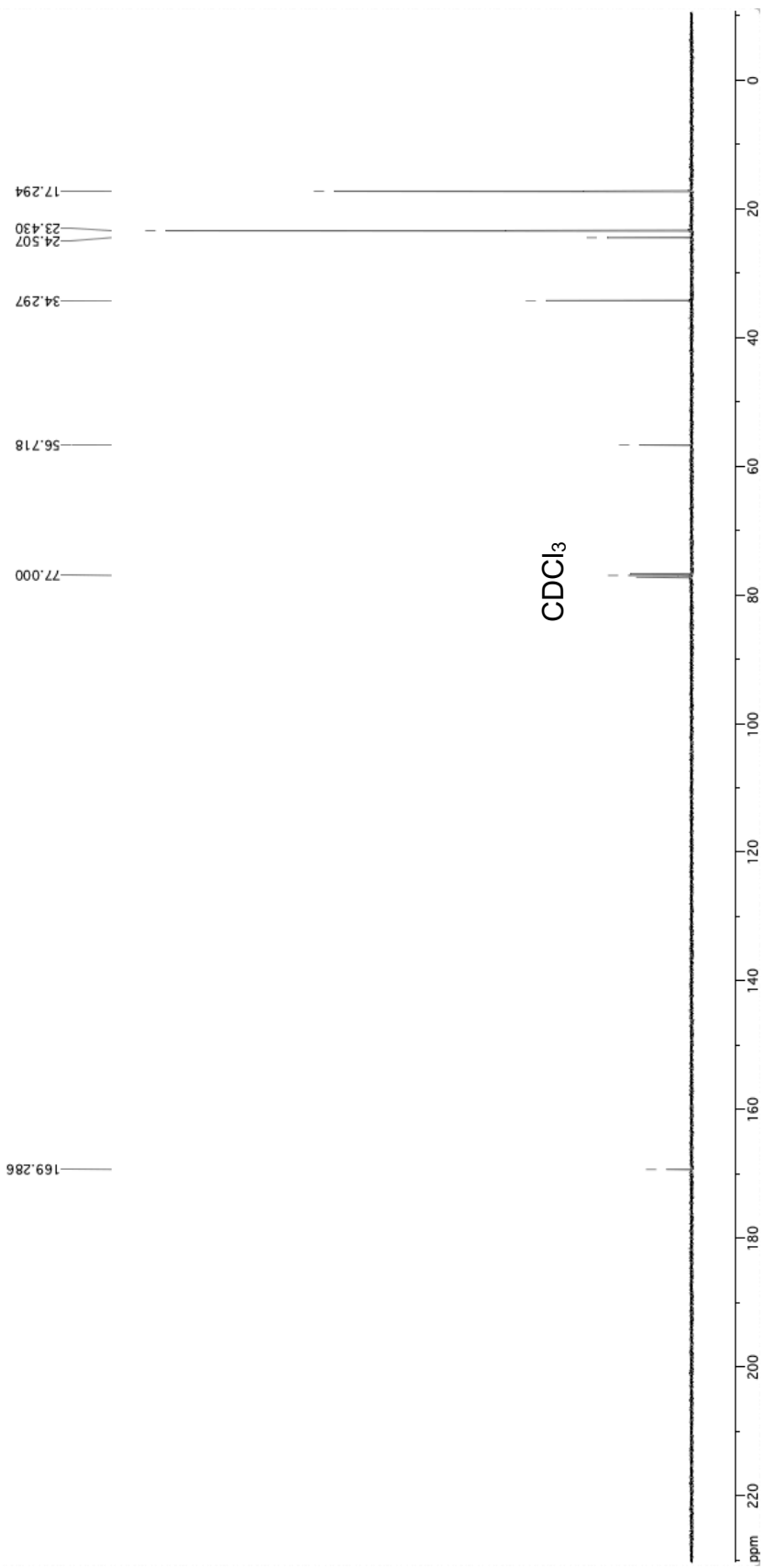


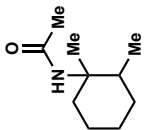
4.59 (¹H NMR, 500 MHz, CDCl₃, 25 °C)



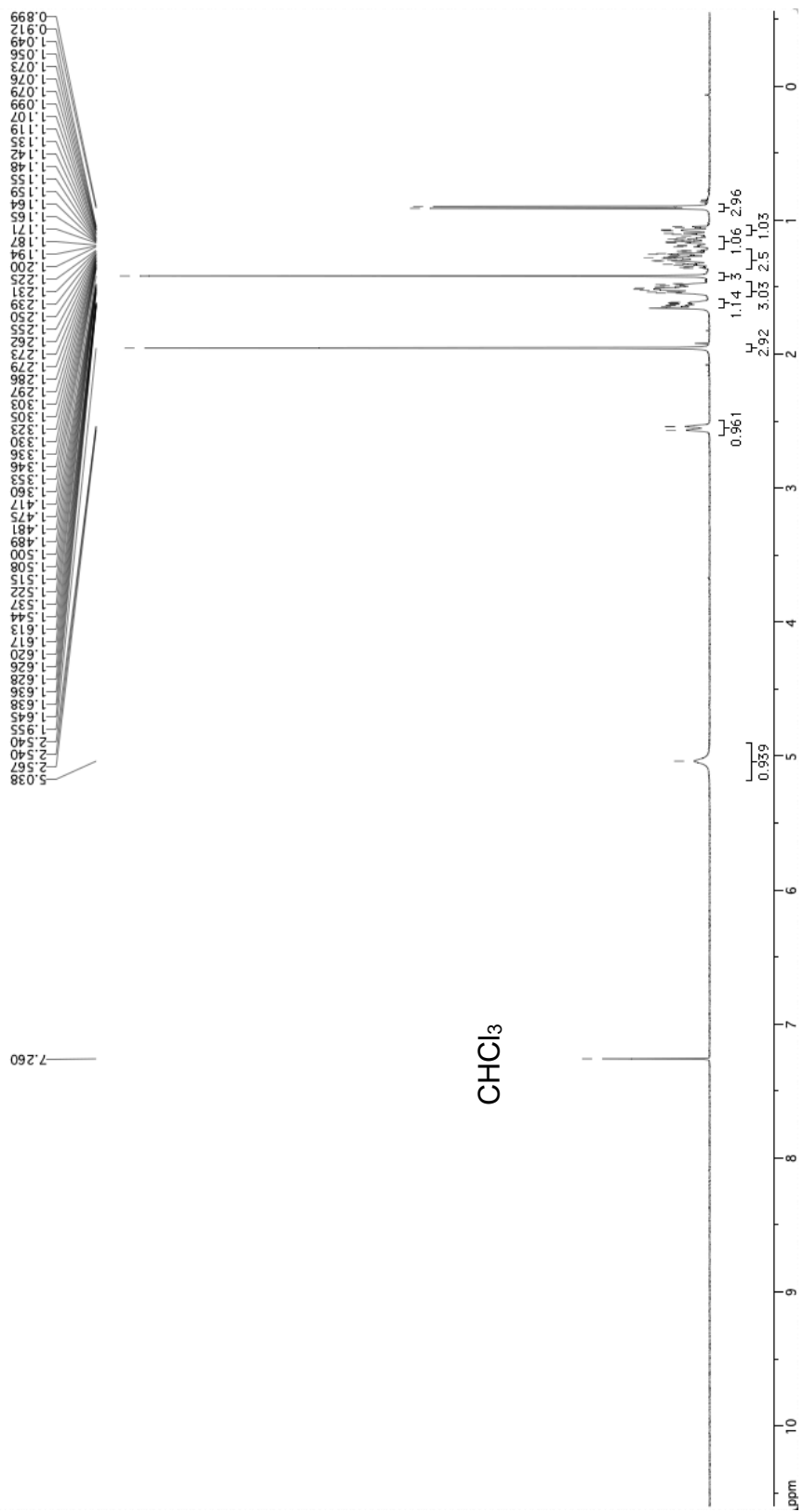


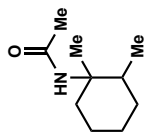
4.59 (¹³C NMR, 126 MHz, CDCl₃, 25 °C)



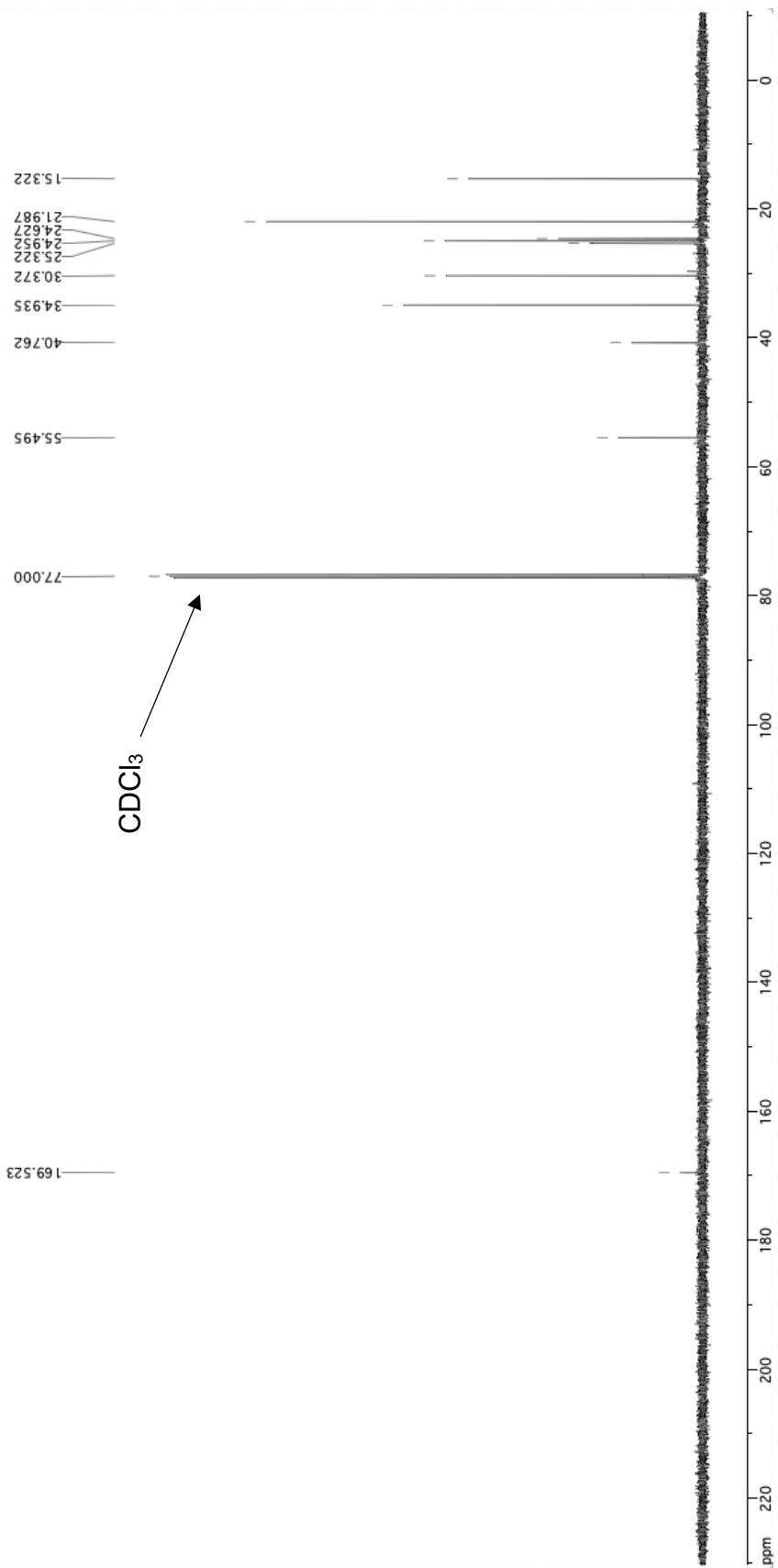


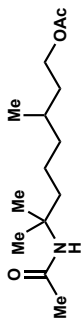
4.60 (¹H NMR, 500 MHz, CDCl₃, 25 °C)



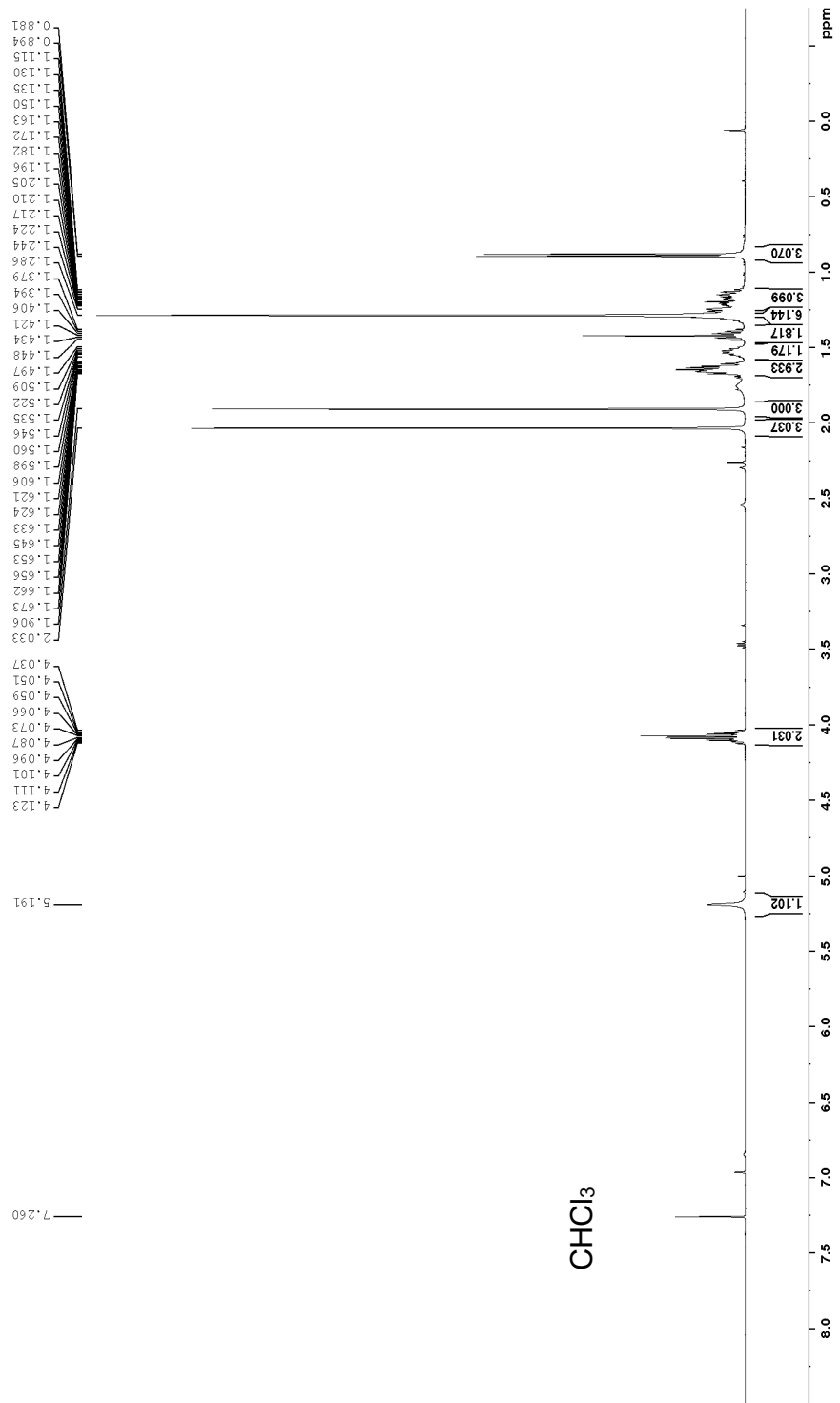


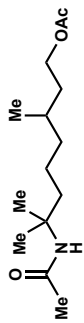
4.60 (¹³C NMR, 126 MHz, CDCl₃, 25 °C)



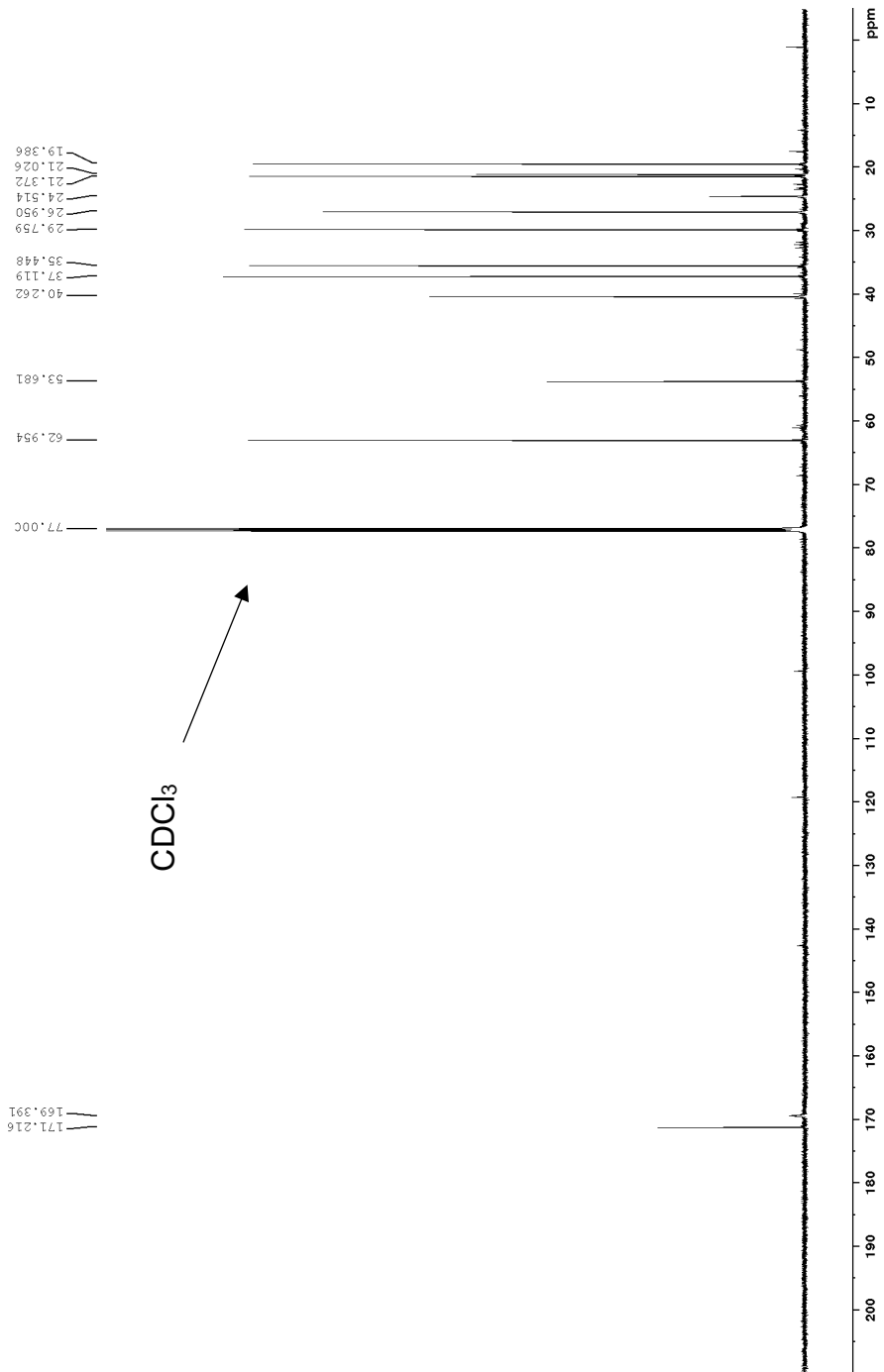


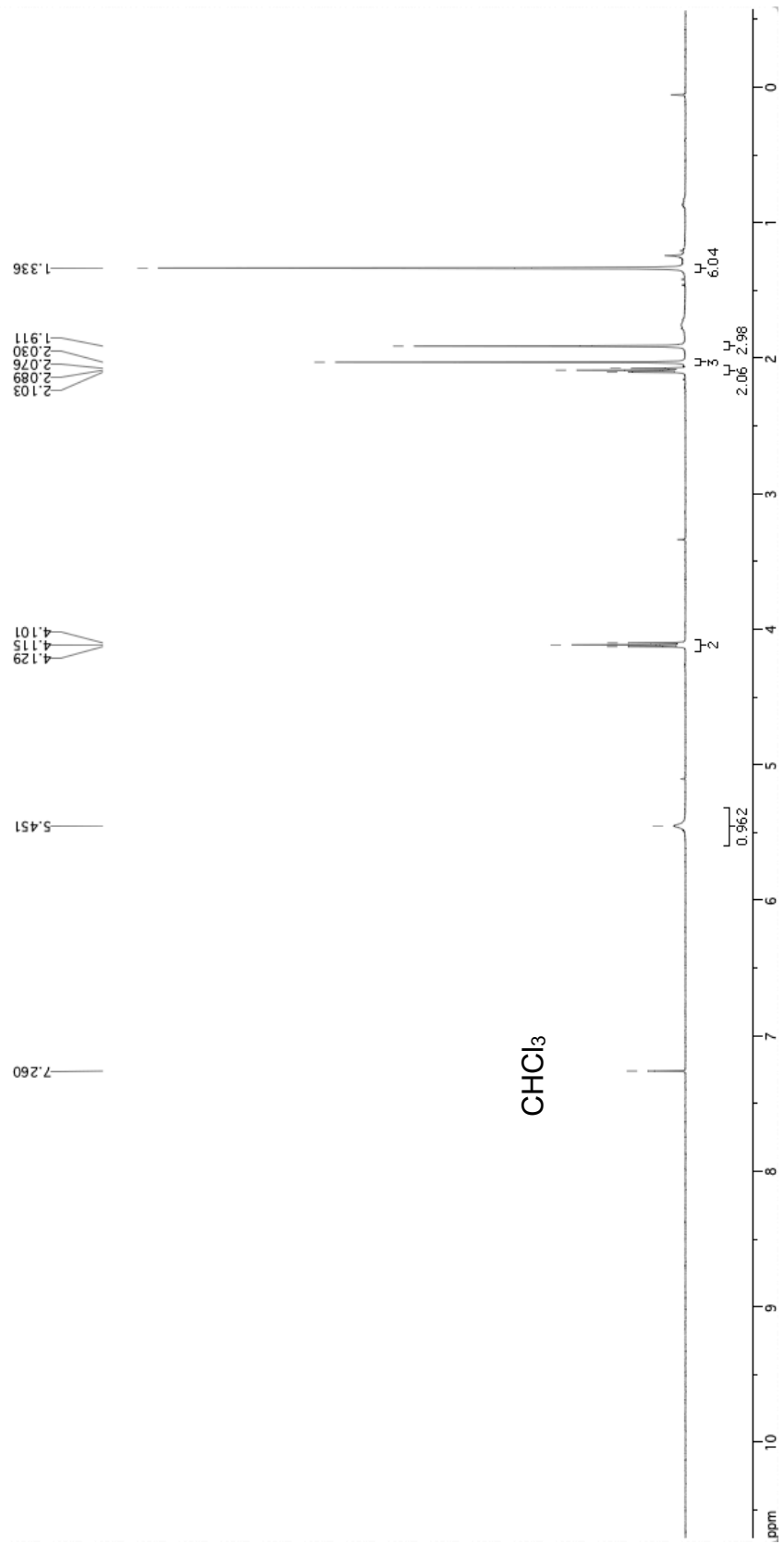
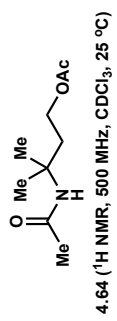
4.52 (1H NMR, 500 MHz, CDCl₃, 25 °C)

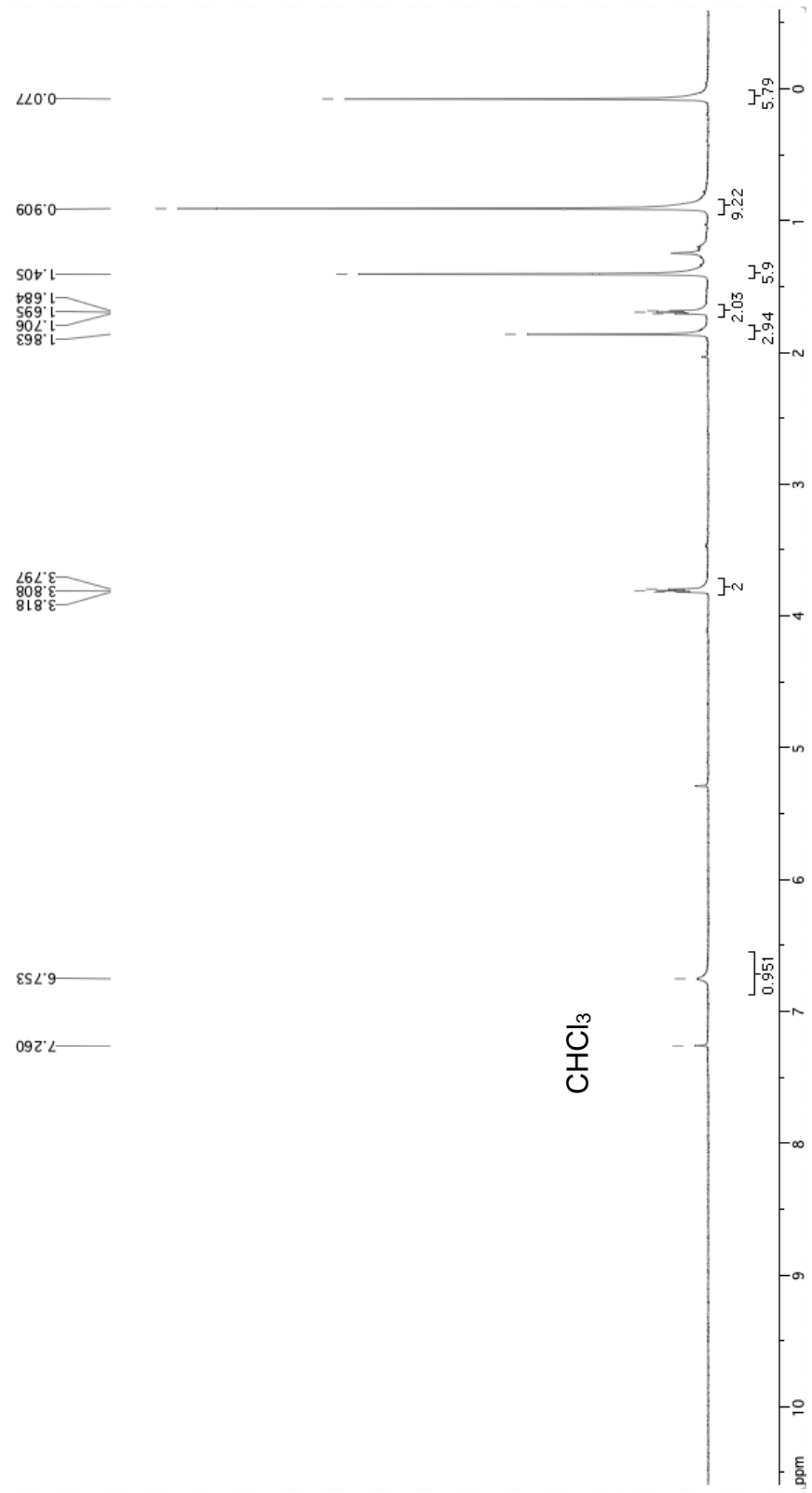
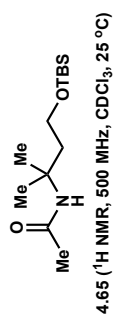


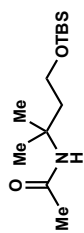


4.52 (¹³C NMR, 126 MHz, CDCl₃, 25 °C)

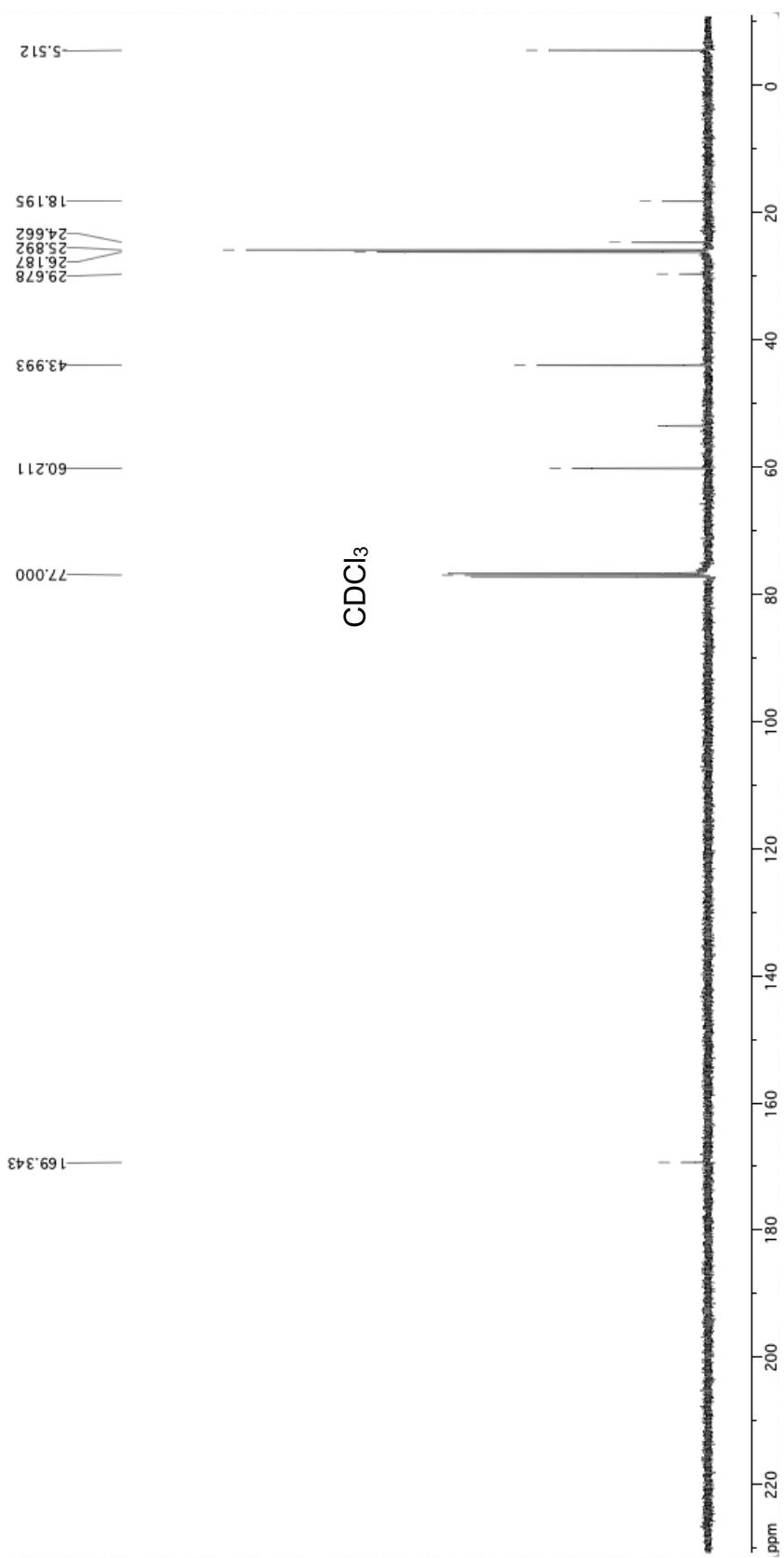


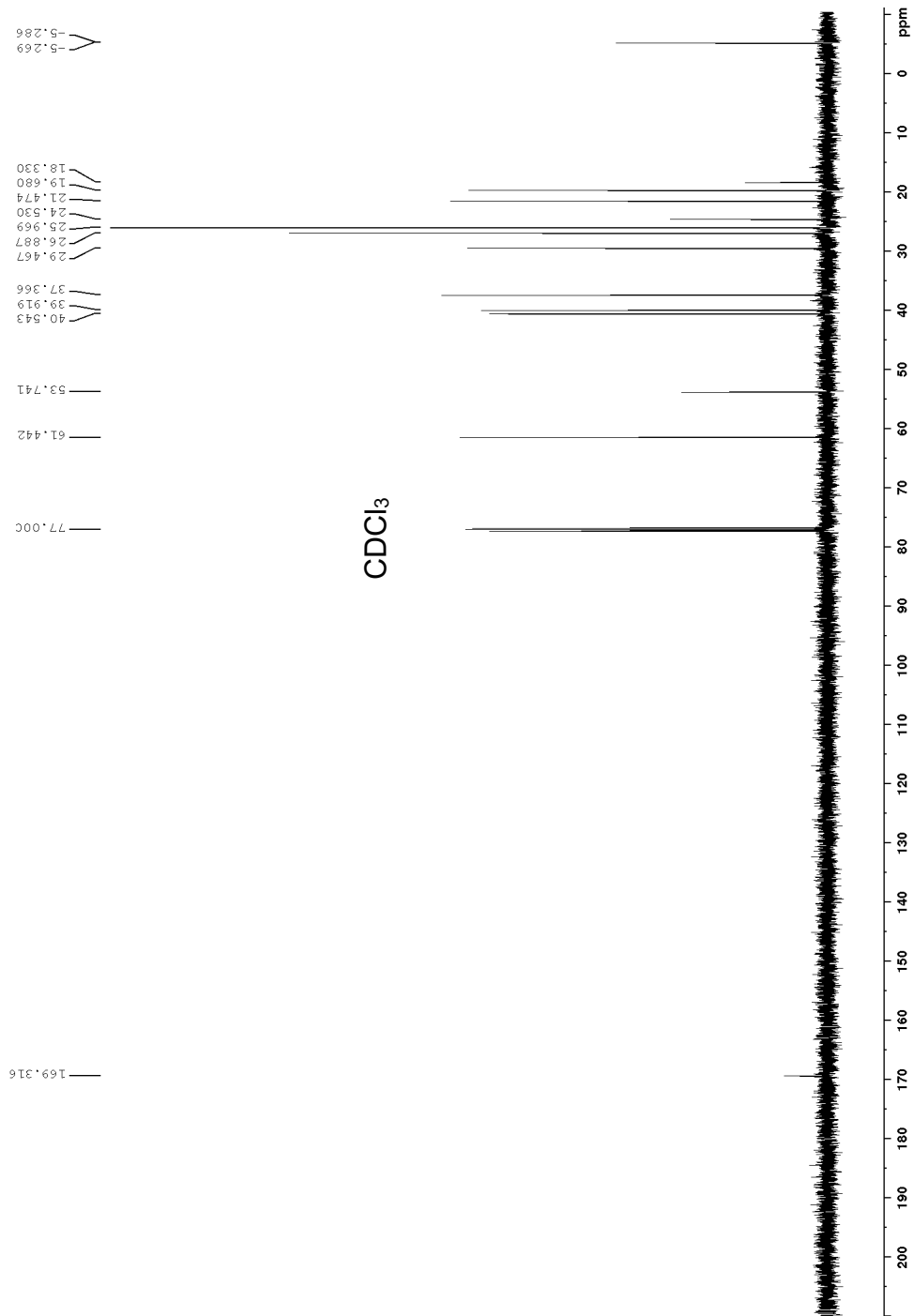
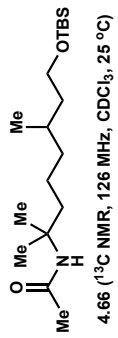


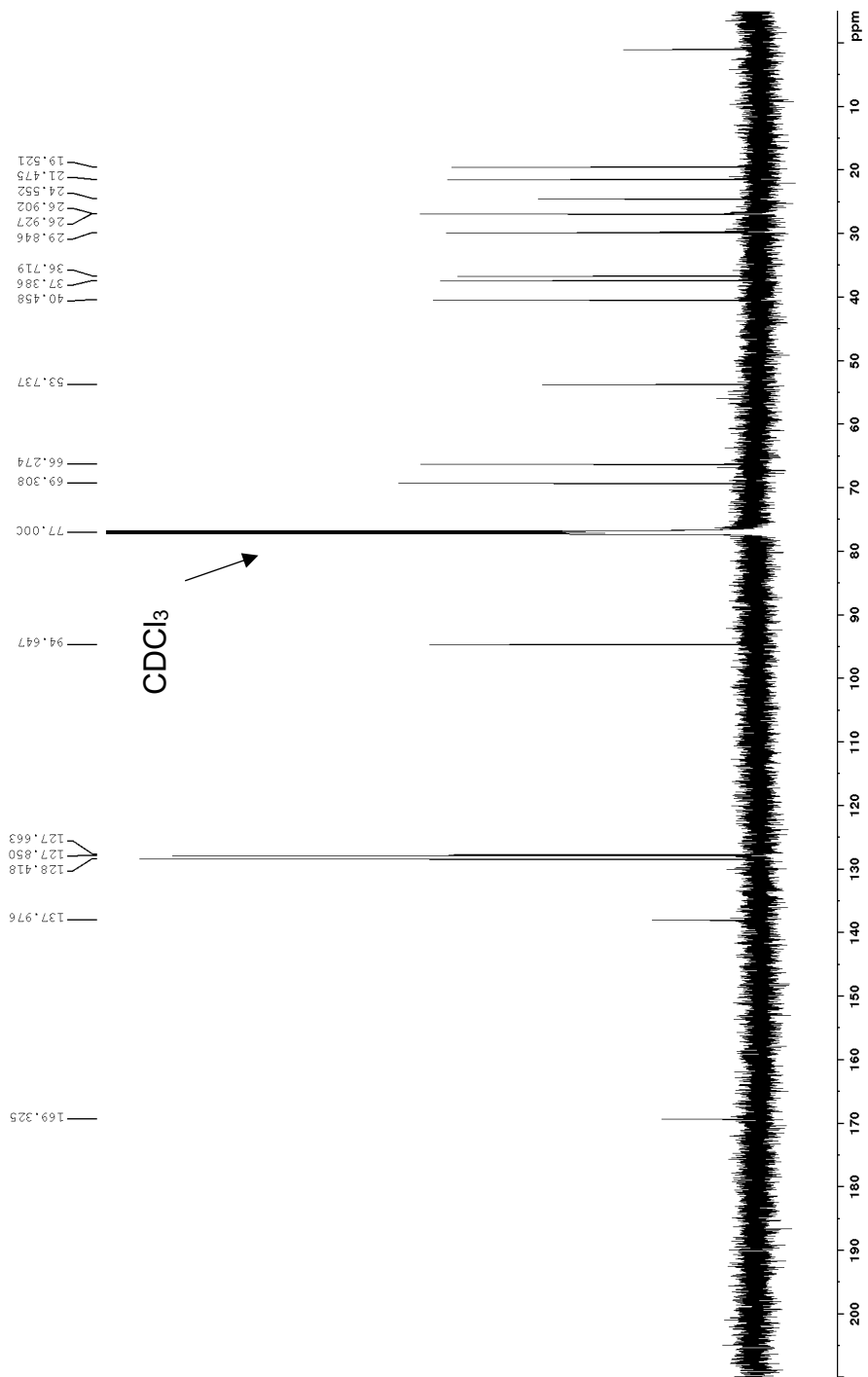
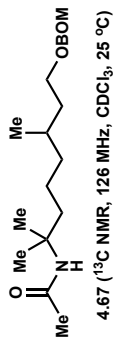


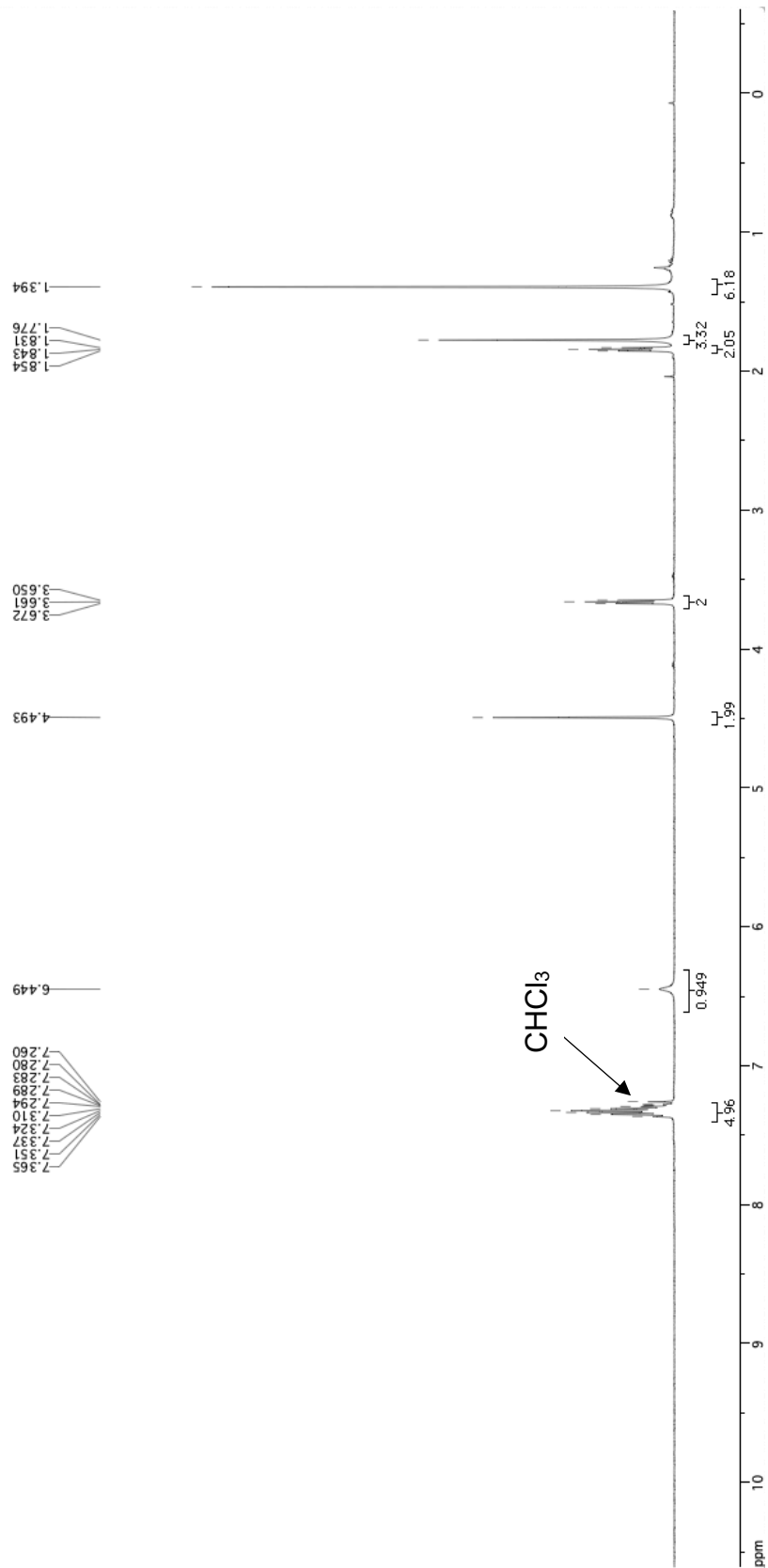
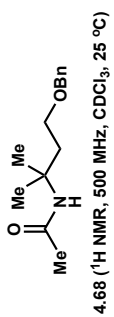


4.65 (¹³C NMR, 126 MHz, CDCl₃, 25 °C)



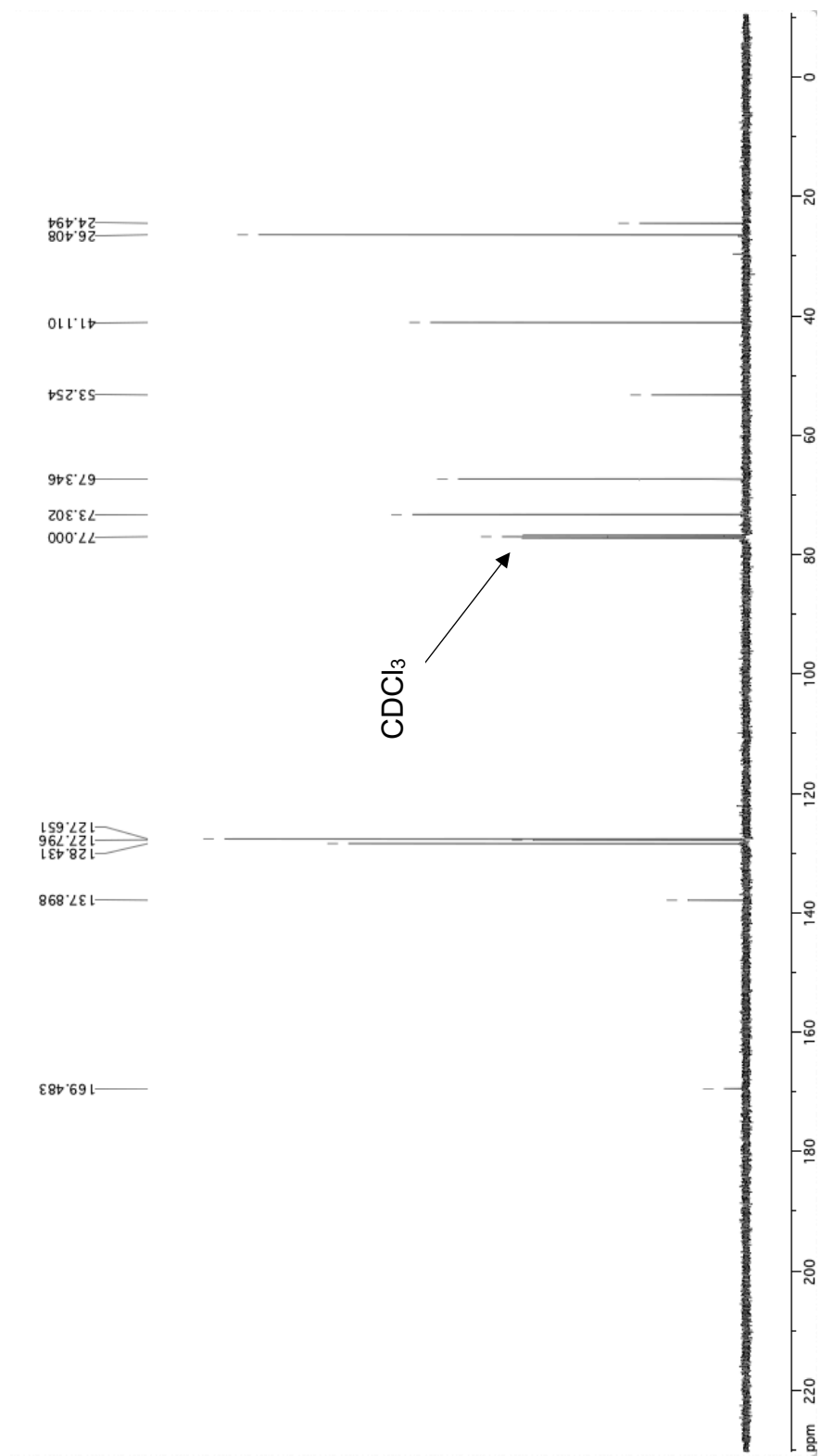


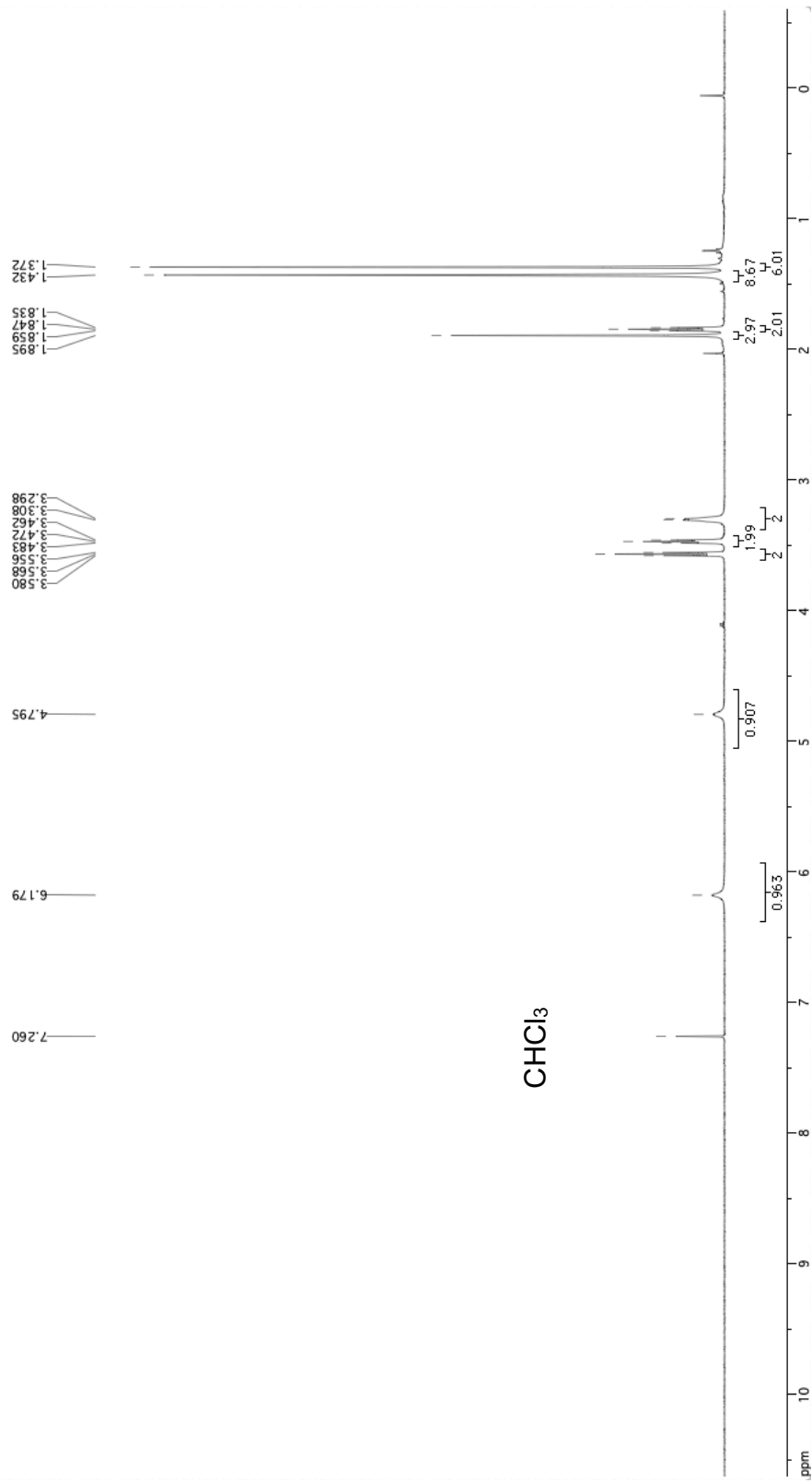
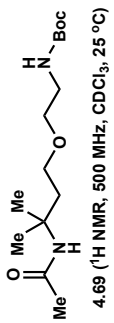


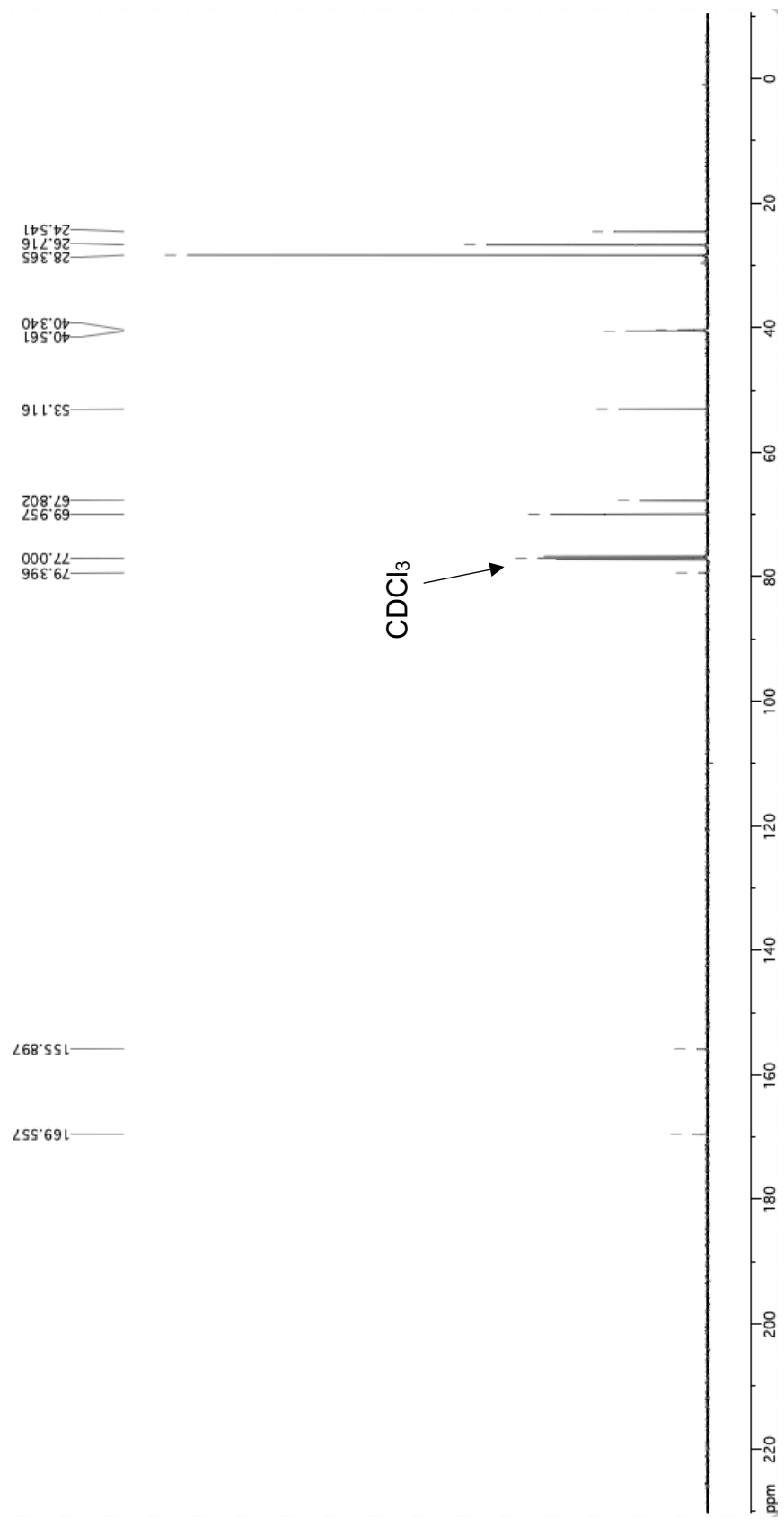
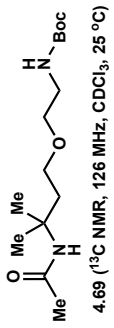


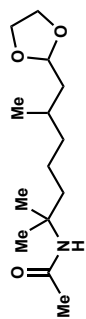


4.68 (¹³C NMR, 126 MHz, CDCl₃, 25 °C)

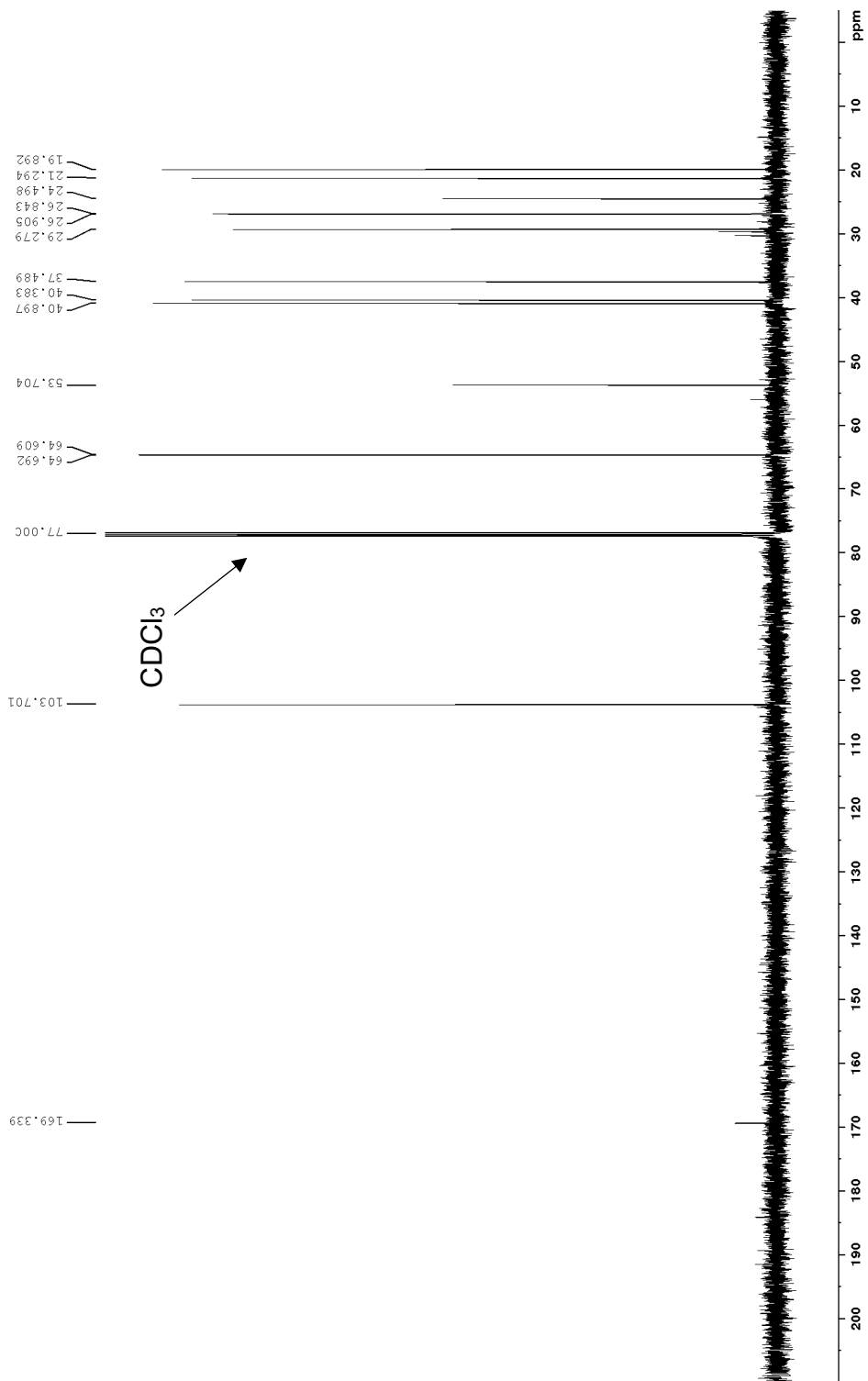


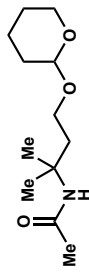




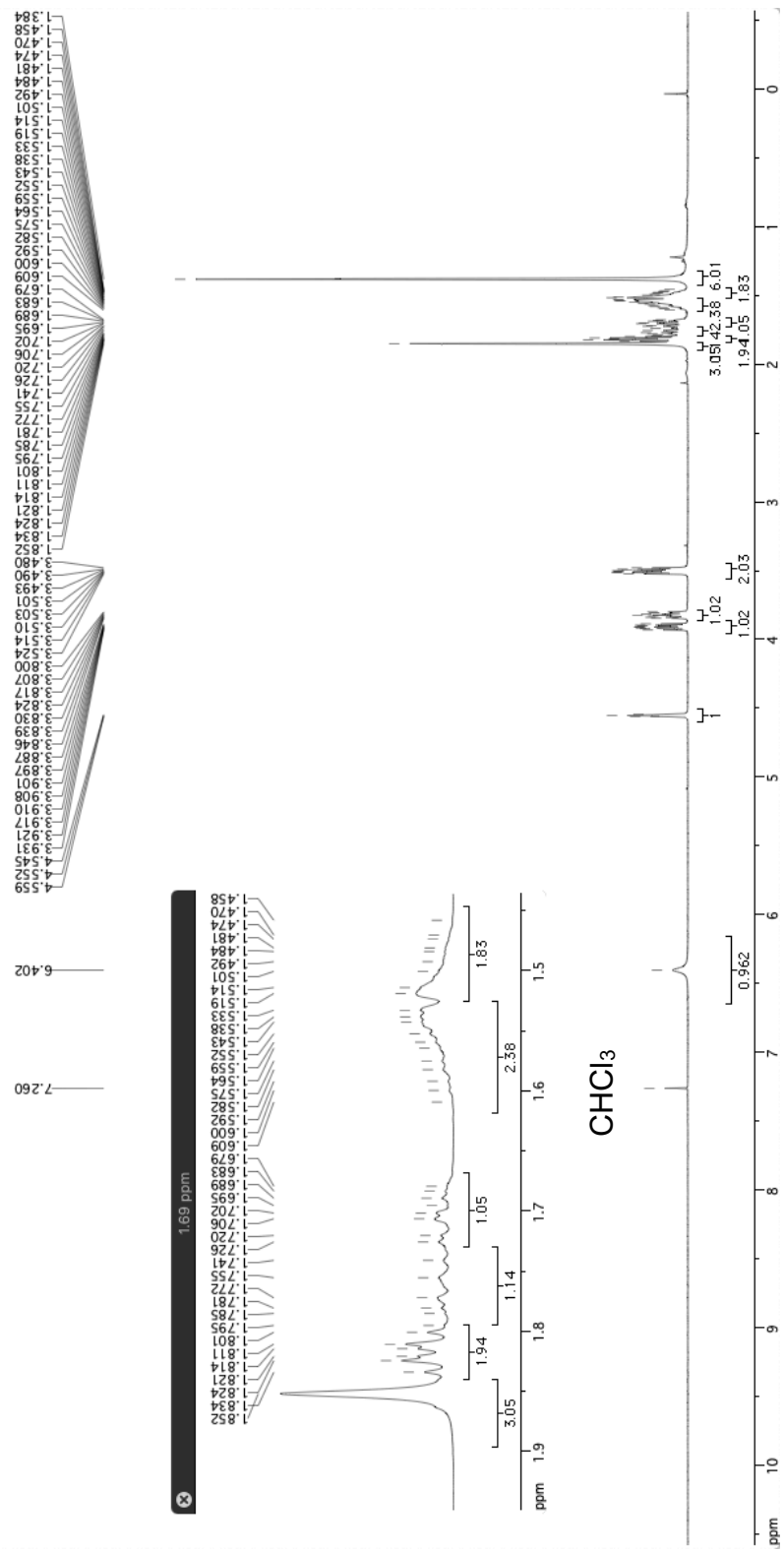


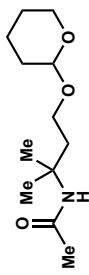
4.70 (¹³C NMR, 126 MHz, CDCl₃, 25 °C)



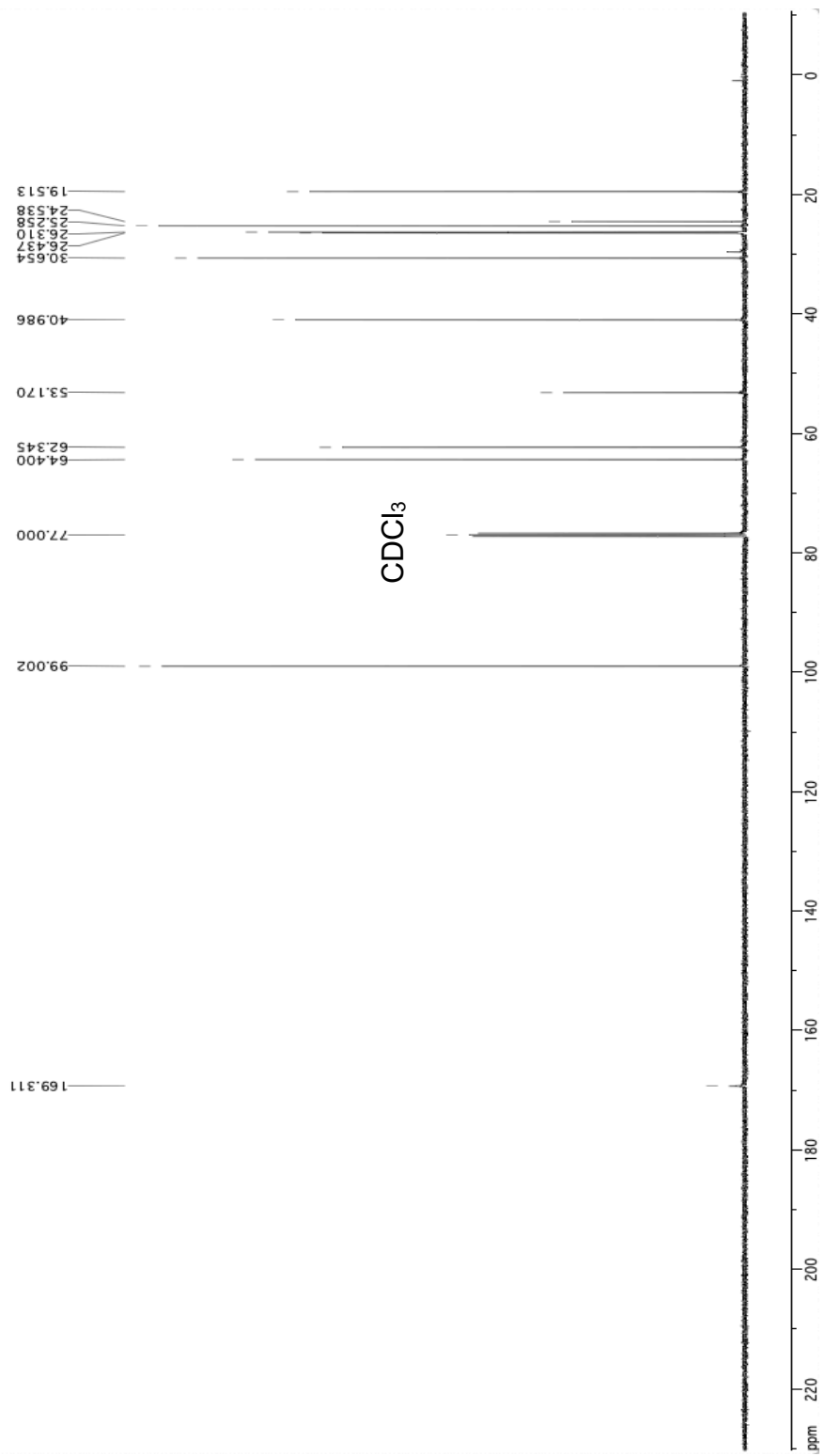


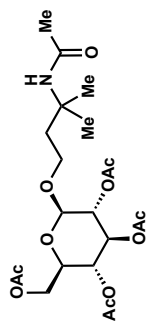
4.71 (1H NMR, 500 MHz, CDCl₃, 25 °C)



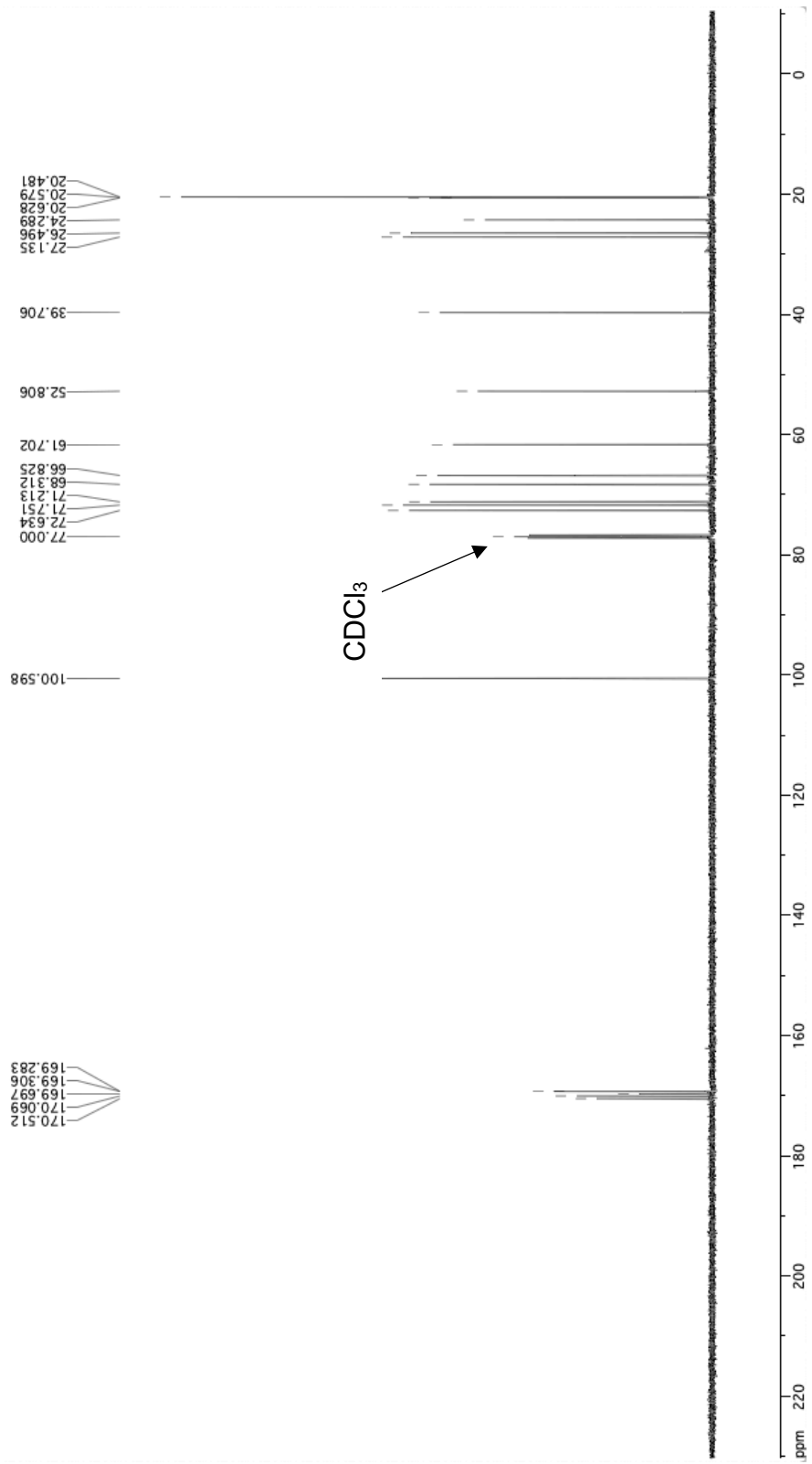


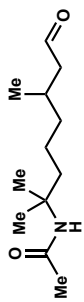
4.71 (¹³C NMR, 126 MHz, CDCl₃, 25 °C)



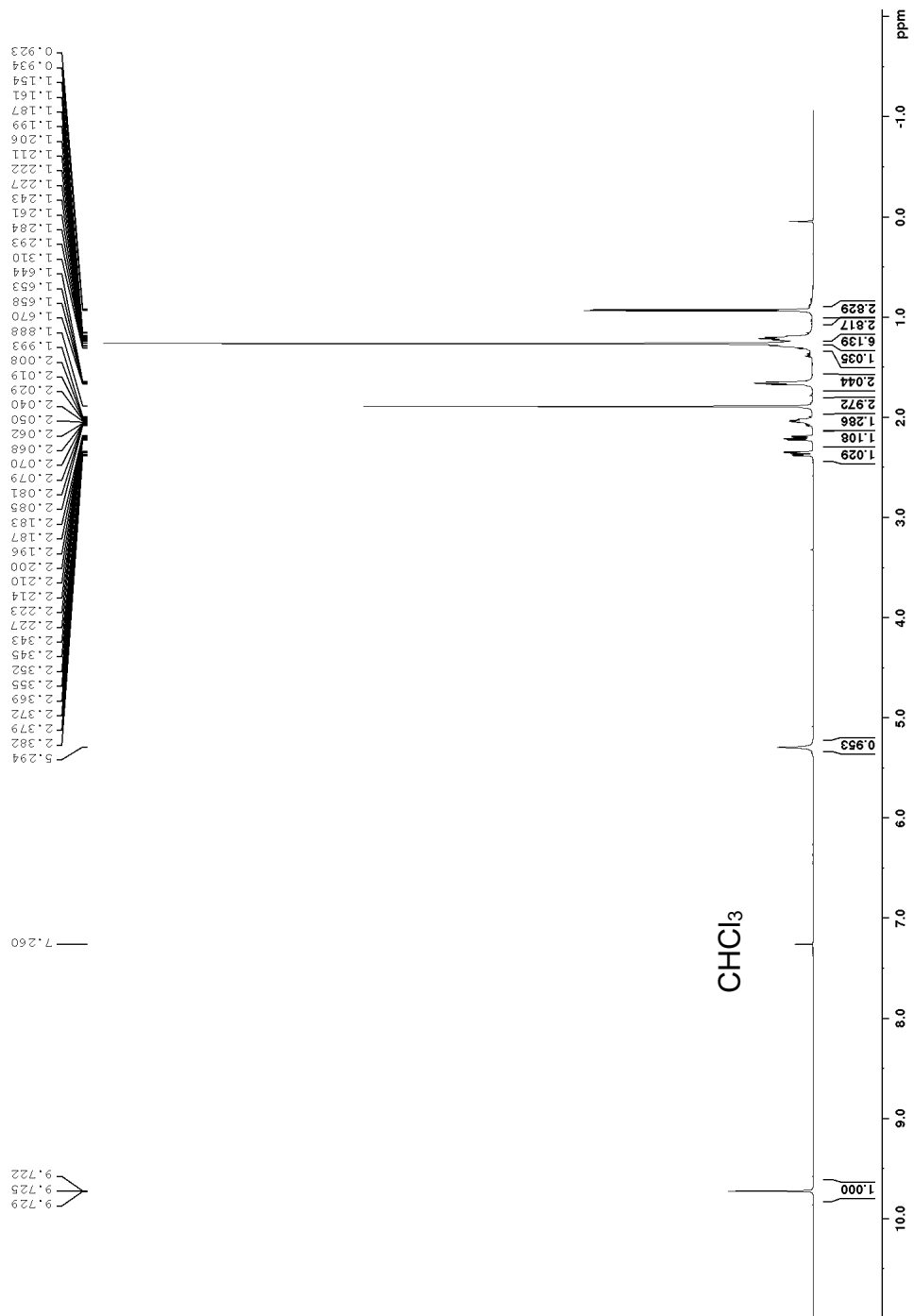


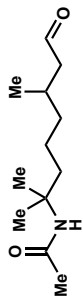
4.72 (^{13}C NMR, 126 MHz, CDCl_3 , 25 °C)



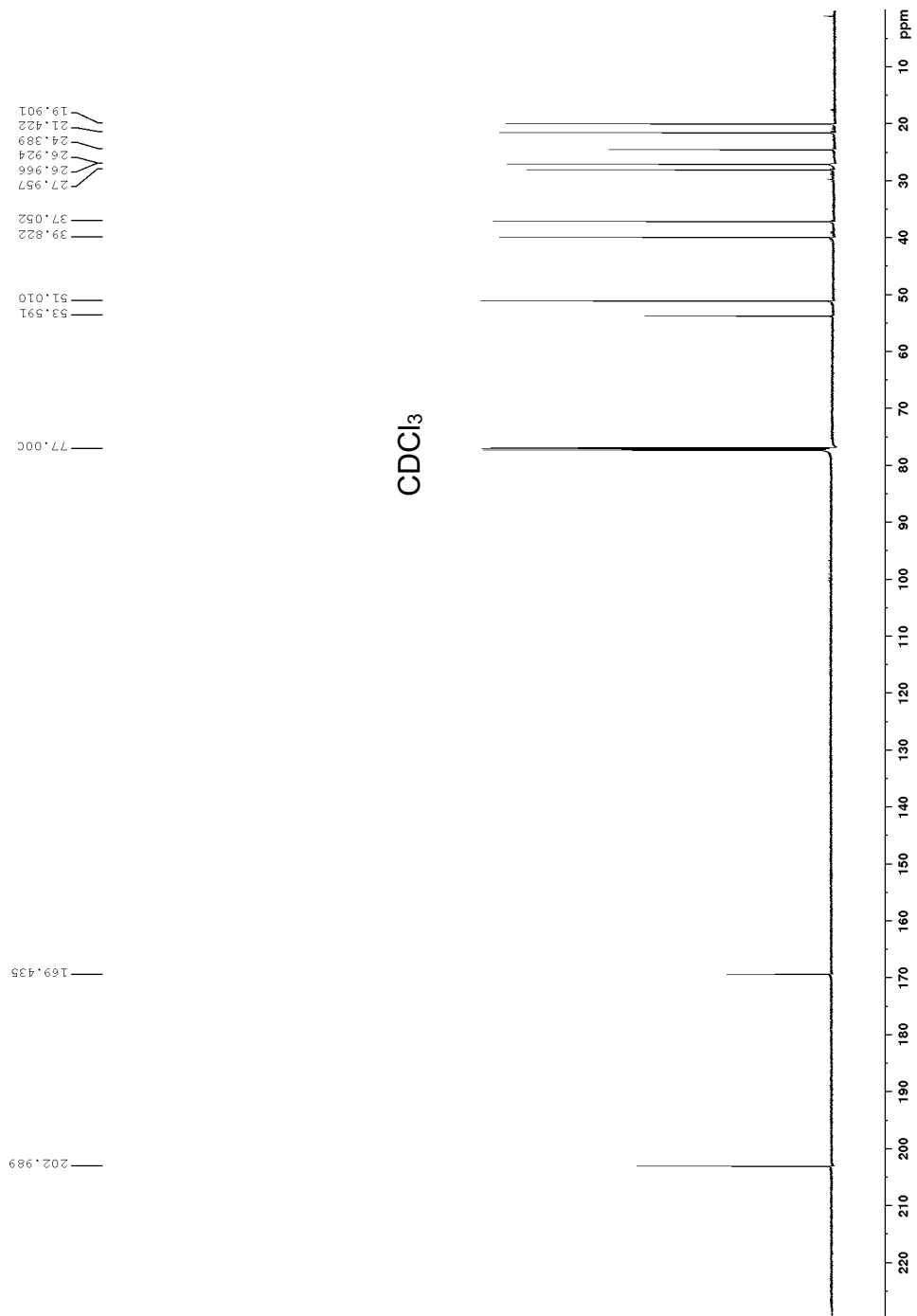


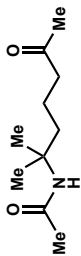
4.76 (¹H NMR, 500 MHz, CDCl₃, 25 °C)



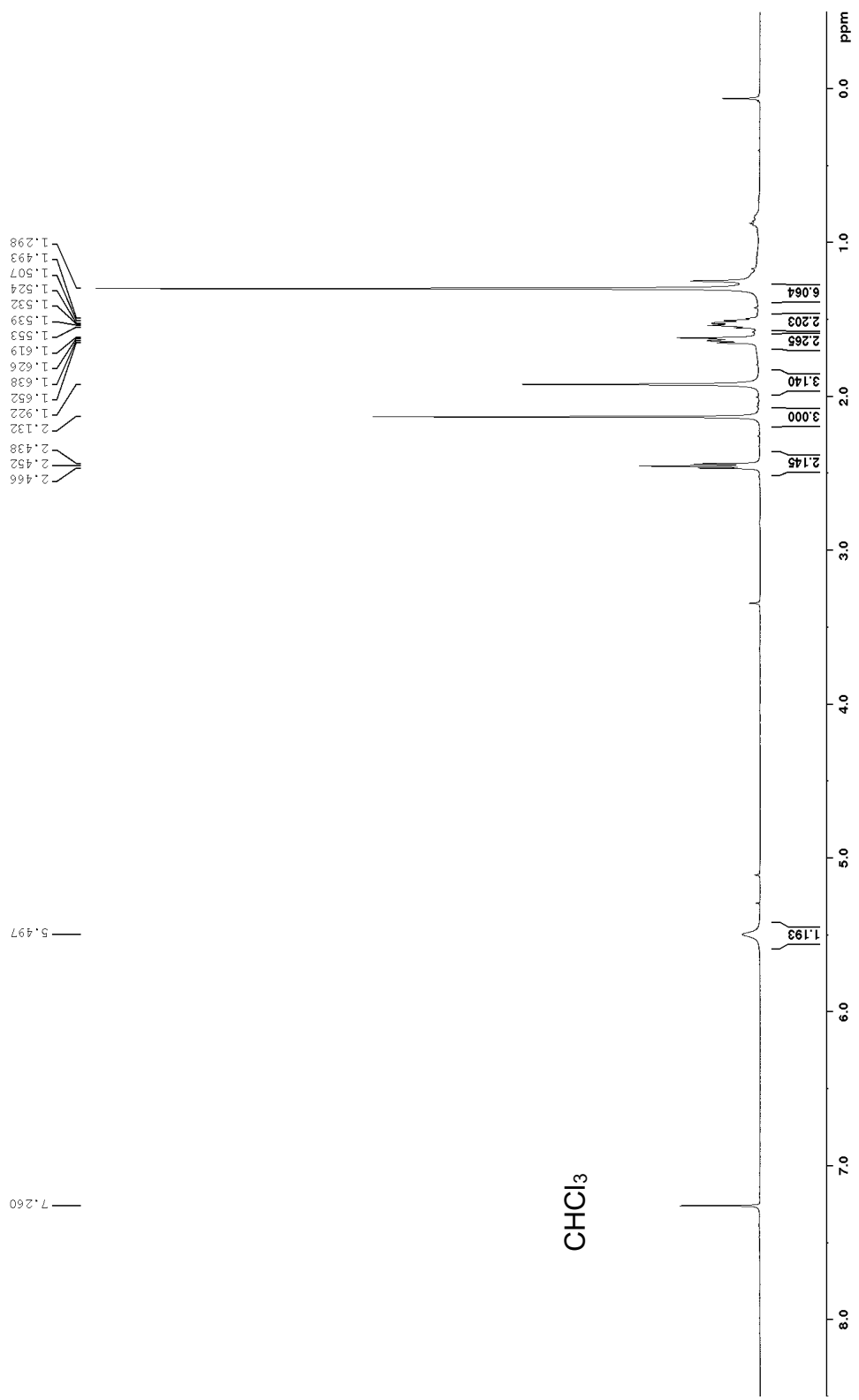


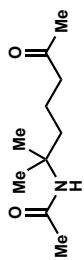
4.76 (¹³C NMR, 126 MHz, CDCl₃, 25 °C)



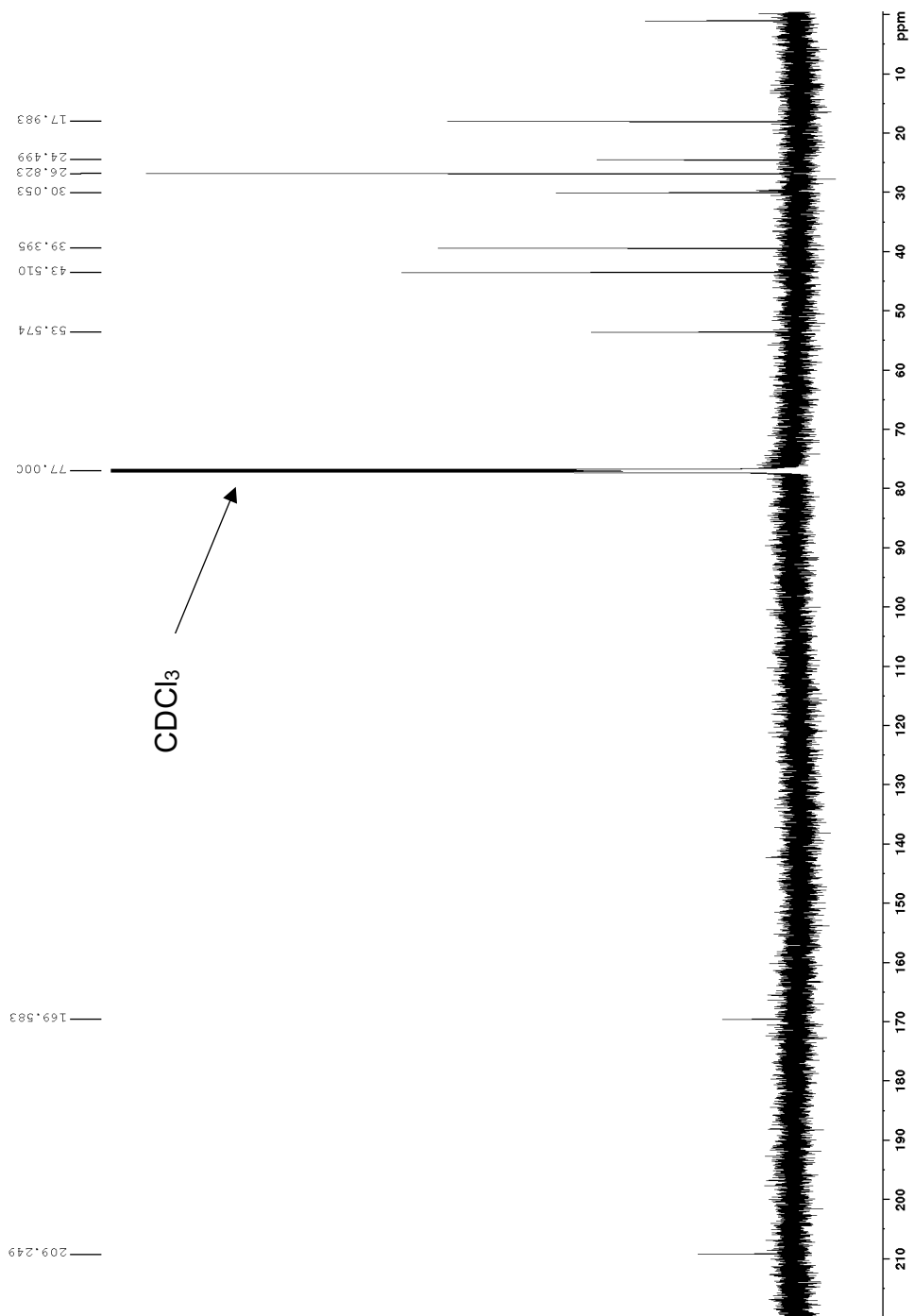


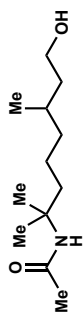
4.77 (1H NMR, 500 MHz, CDCl₃, 25 °C)



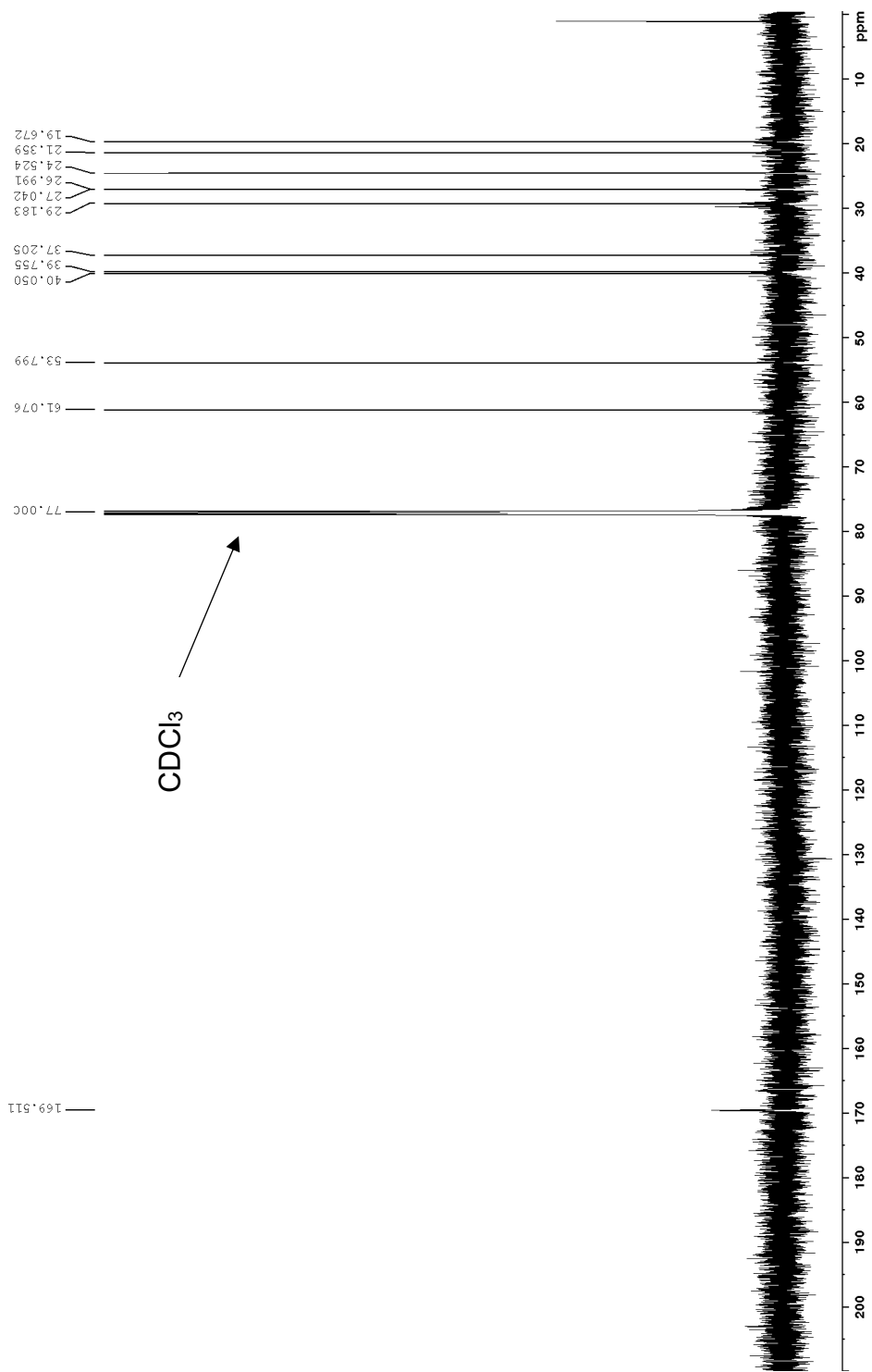


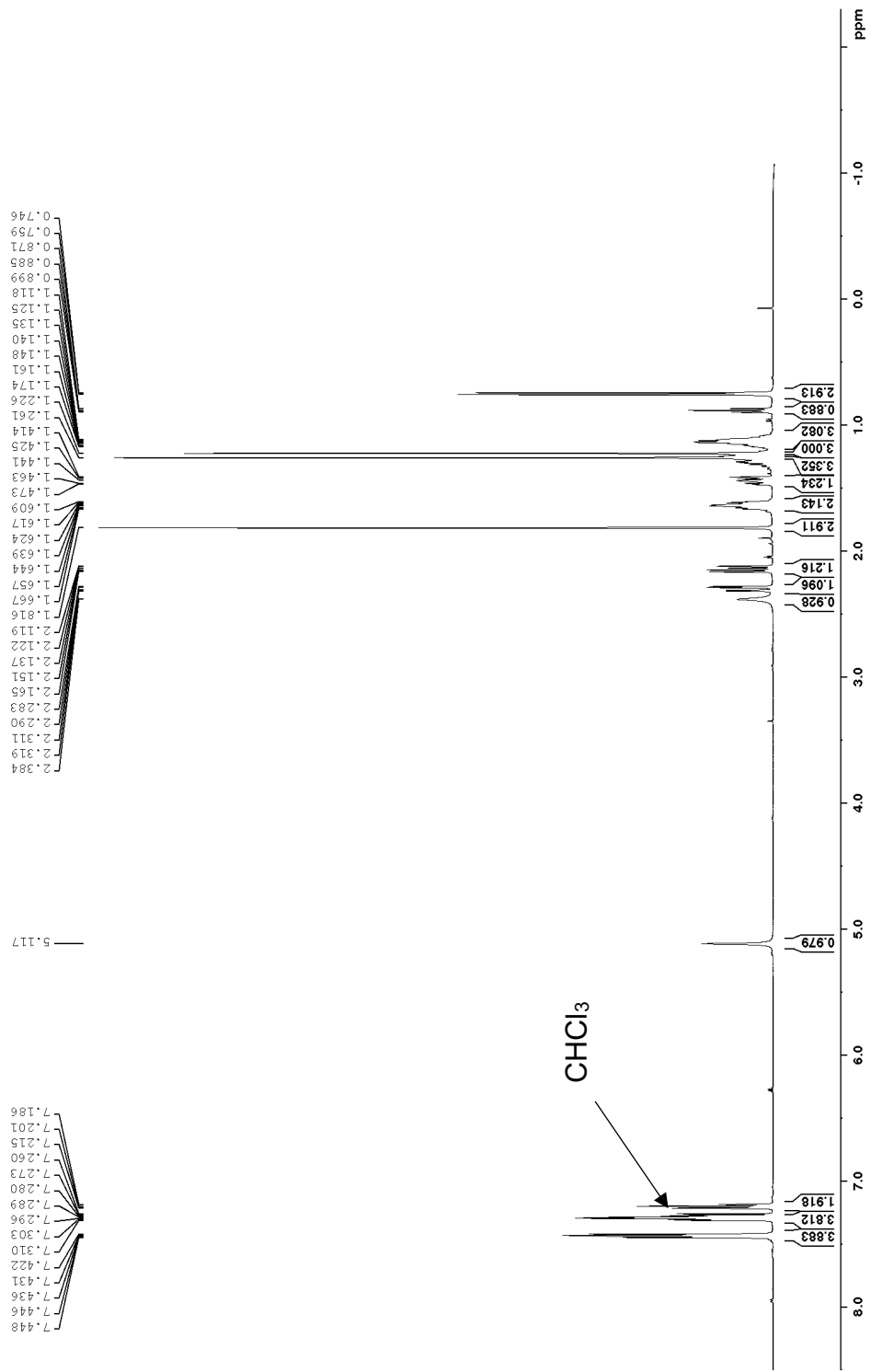
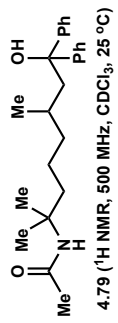
4.77 (¹³C NMR, 126 MHz, CDCl₃, 25 °C)

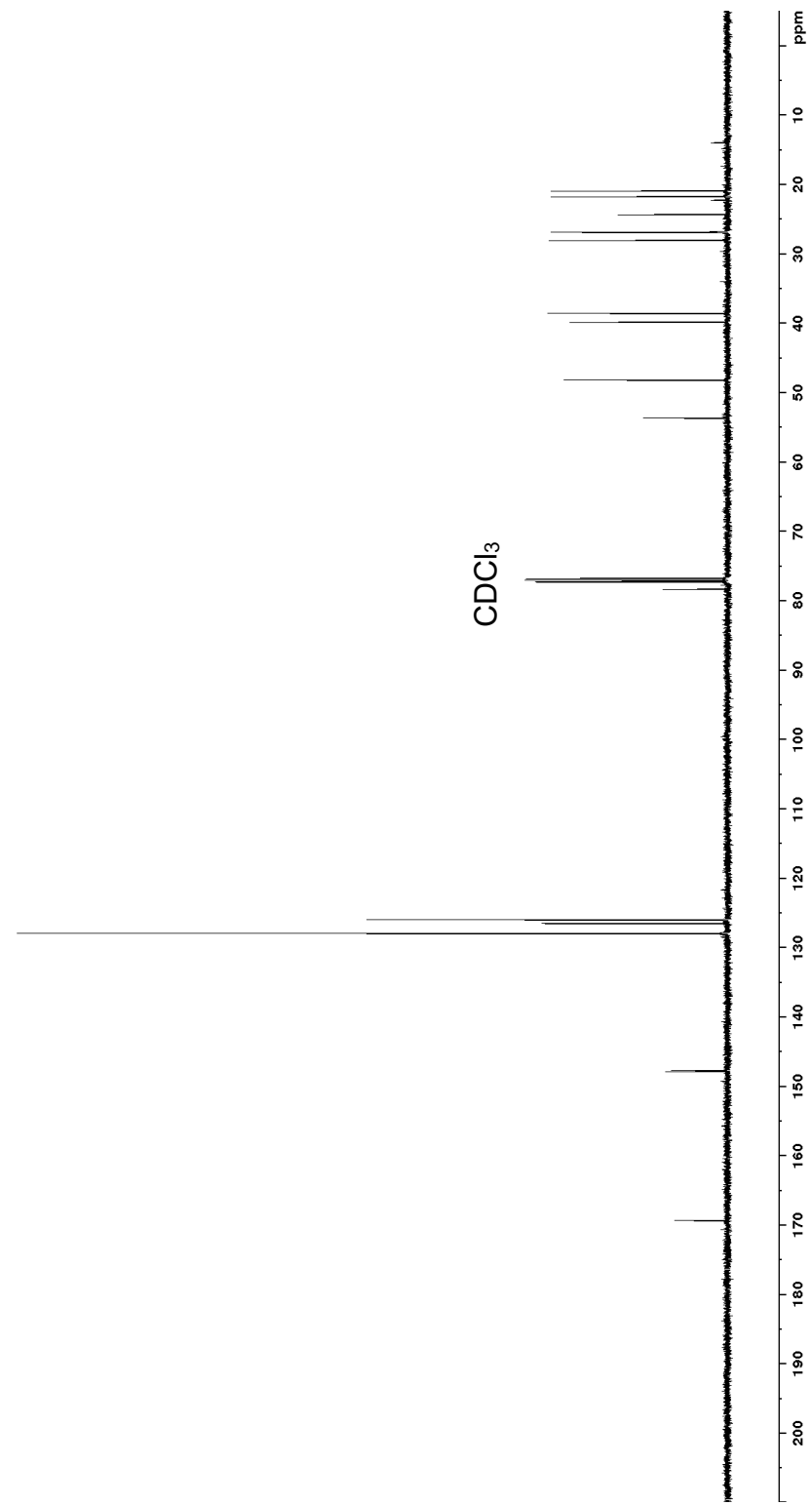
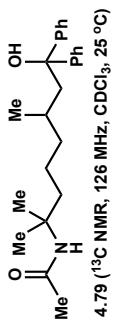


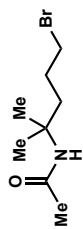


4.78 (¹³C NMR, 126 MHz, CDCl₃, 25 °C)

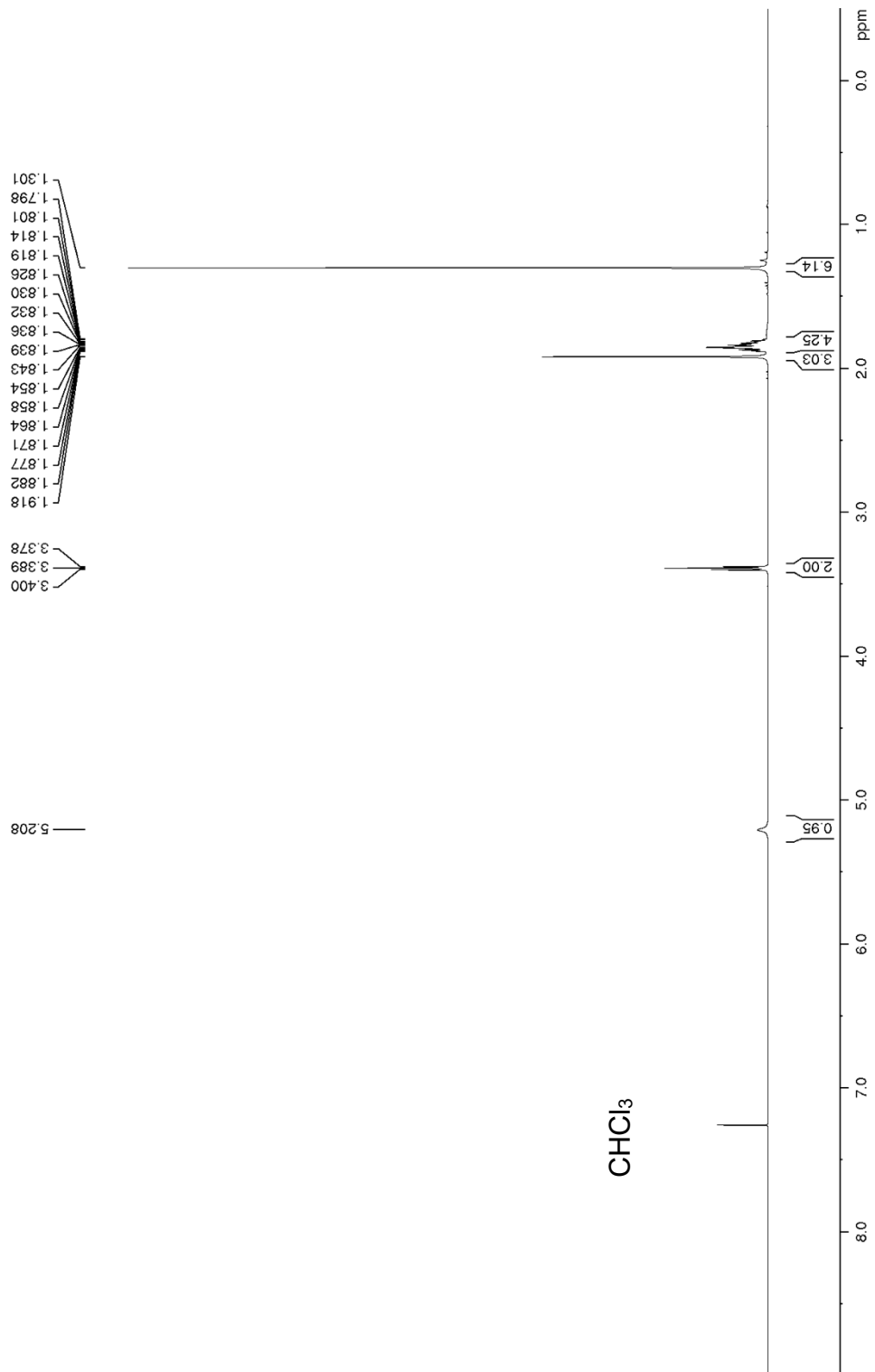


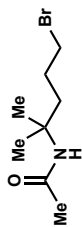




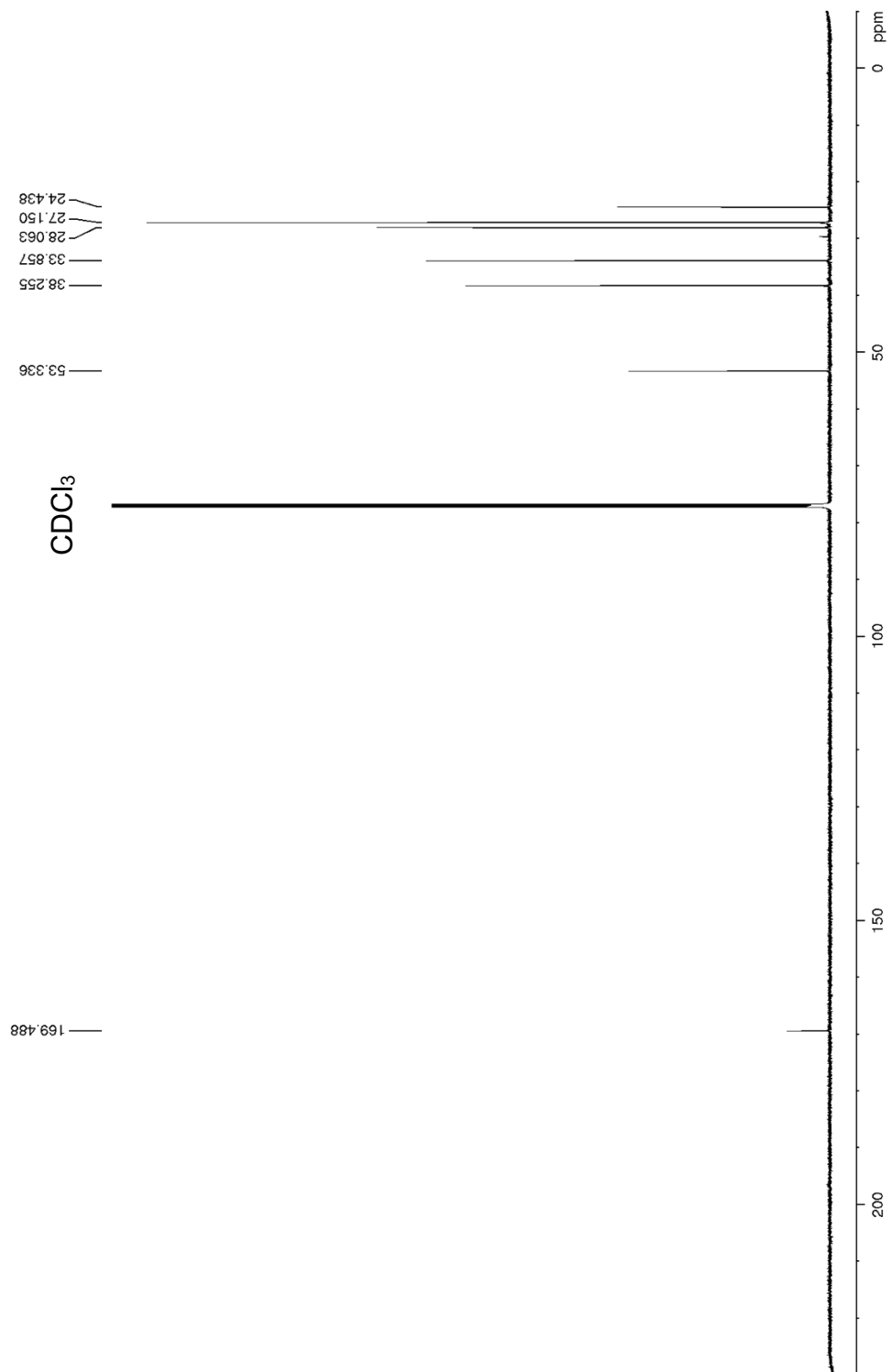


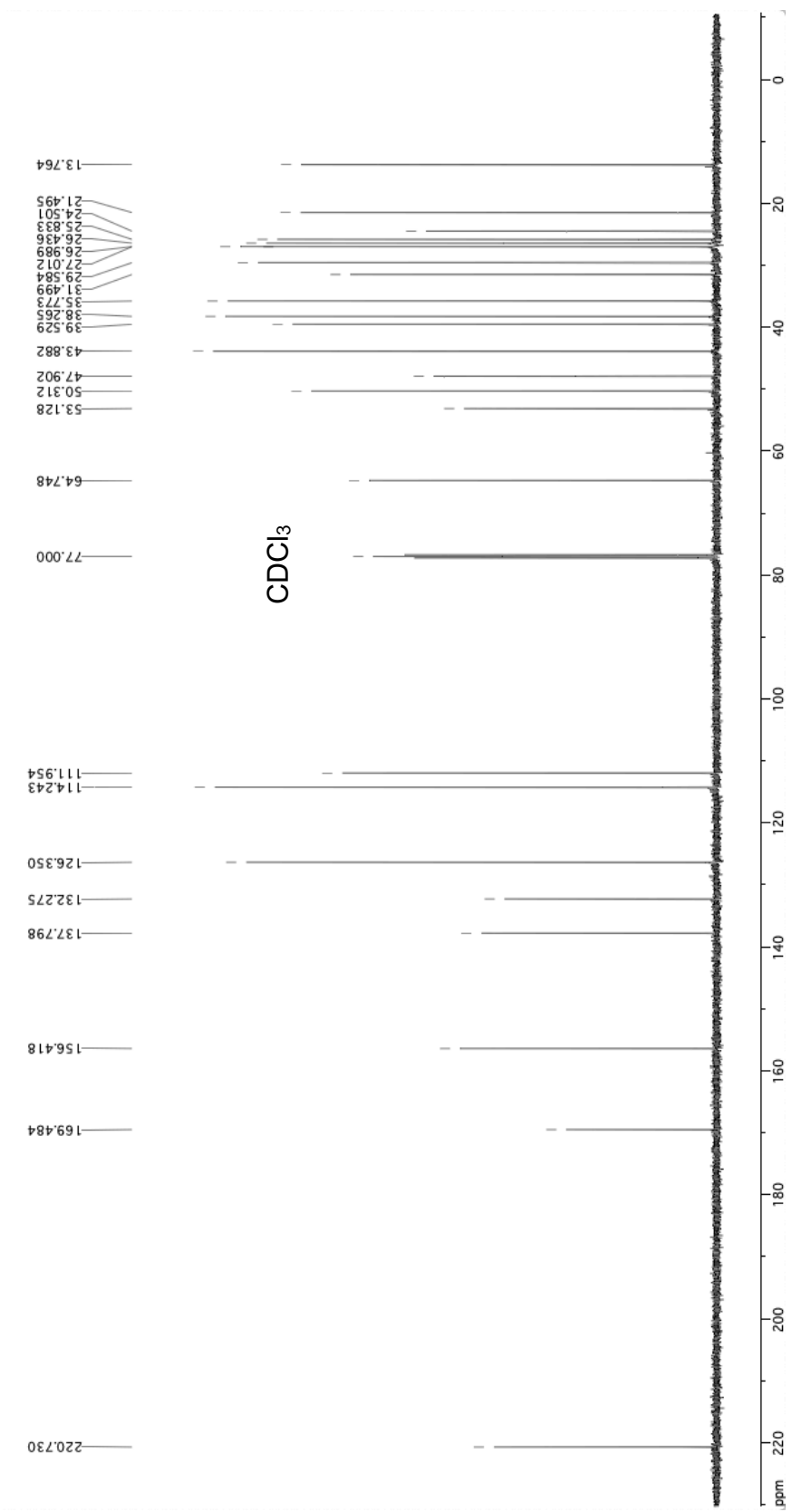
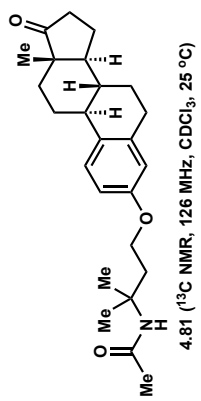
4.80 (¹H NMR, 600 MHz, CDCl₃, 25°C)

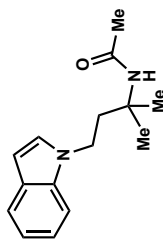




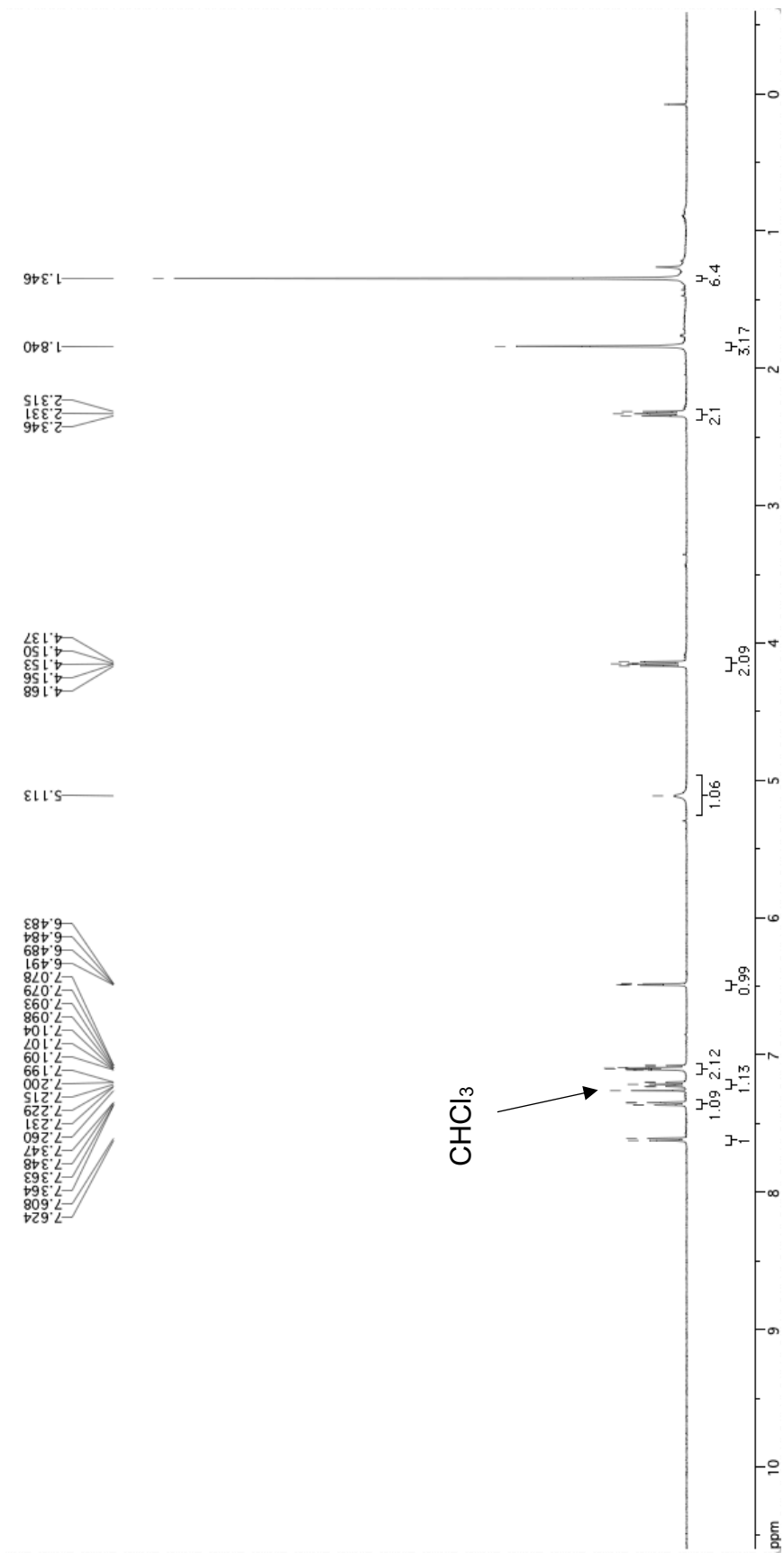
4.80 (¹³C NMR, 151 MHz, CDCl₃, 25°C)

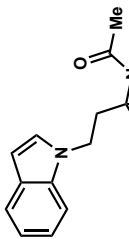




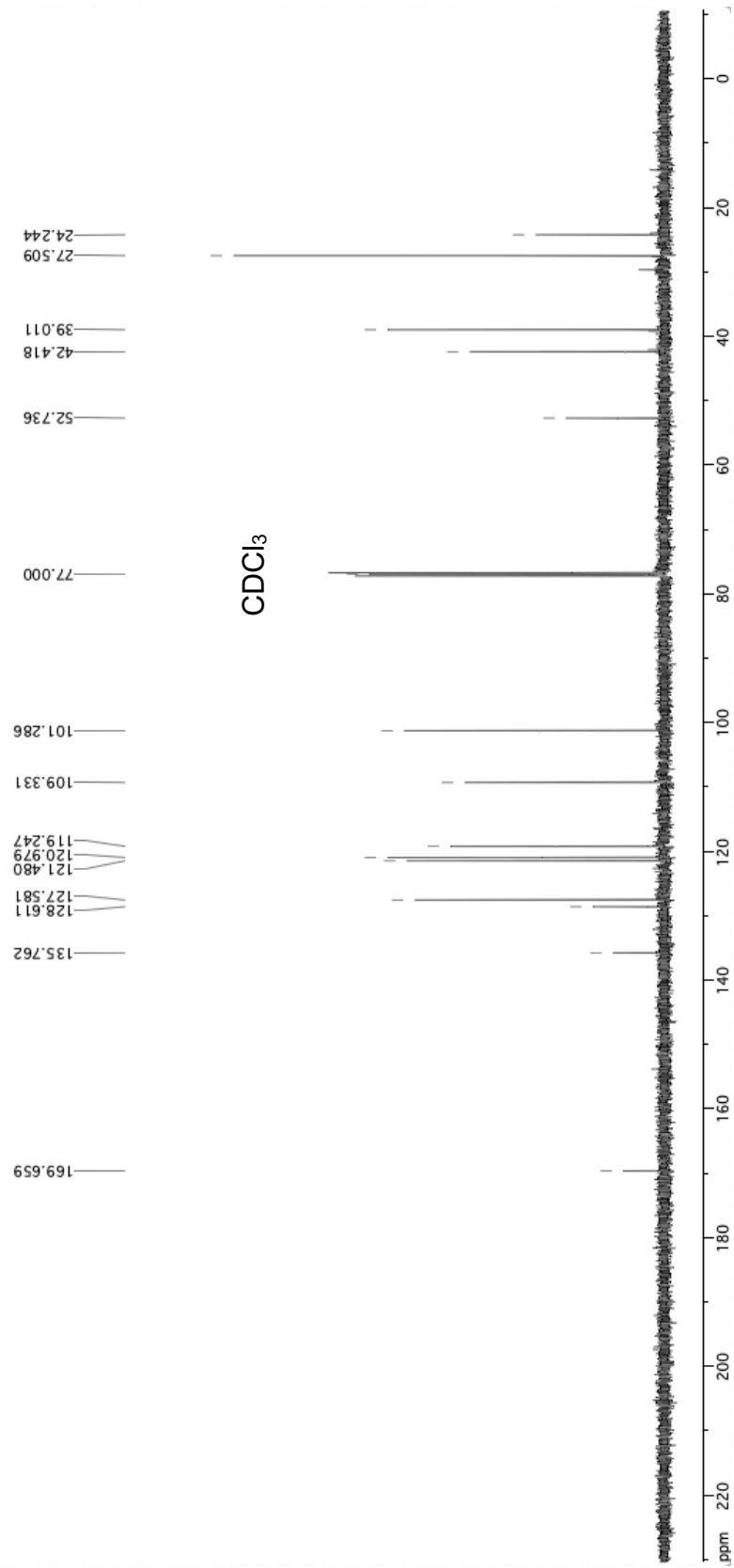


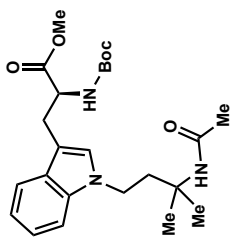
4.82 (¹H NMR, 500 MHz, CDCl₃, 25 °C)



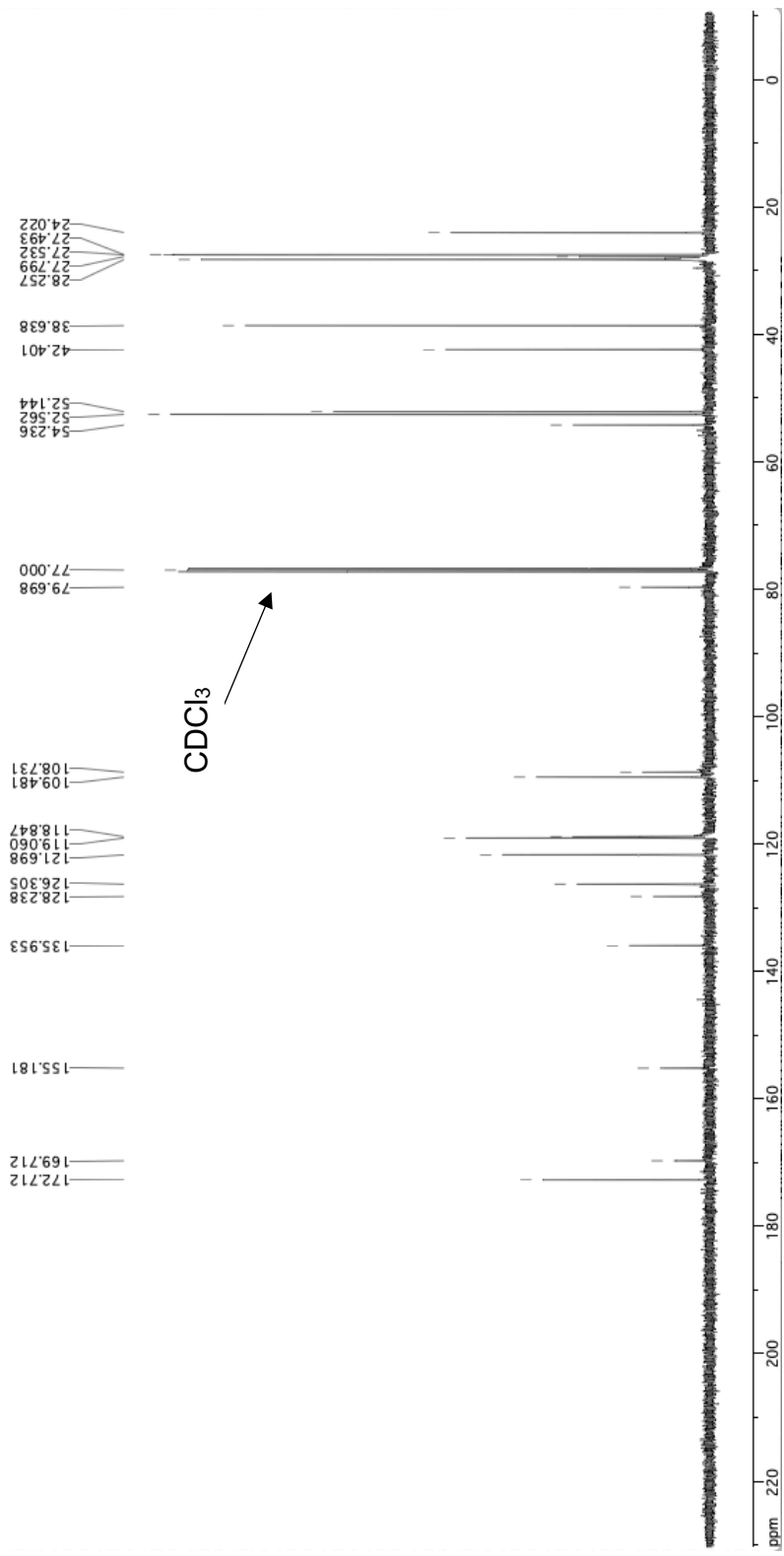


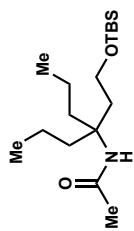
4.82 (¹³C NMR, 126 MHz, CDCl₃, 25 °C)



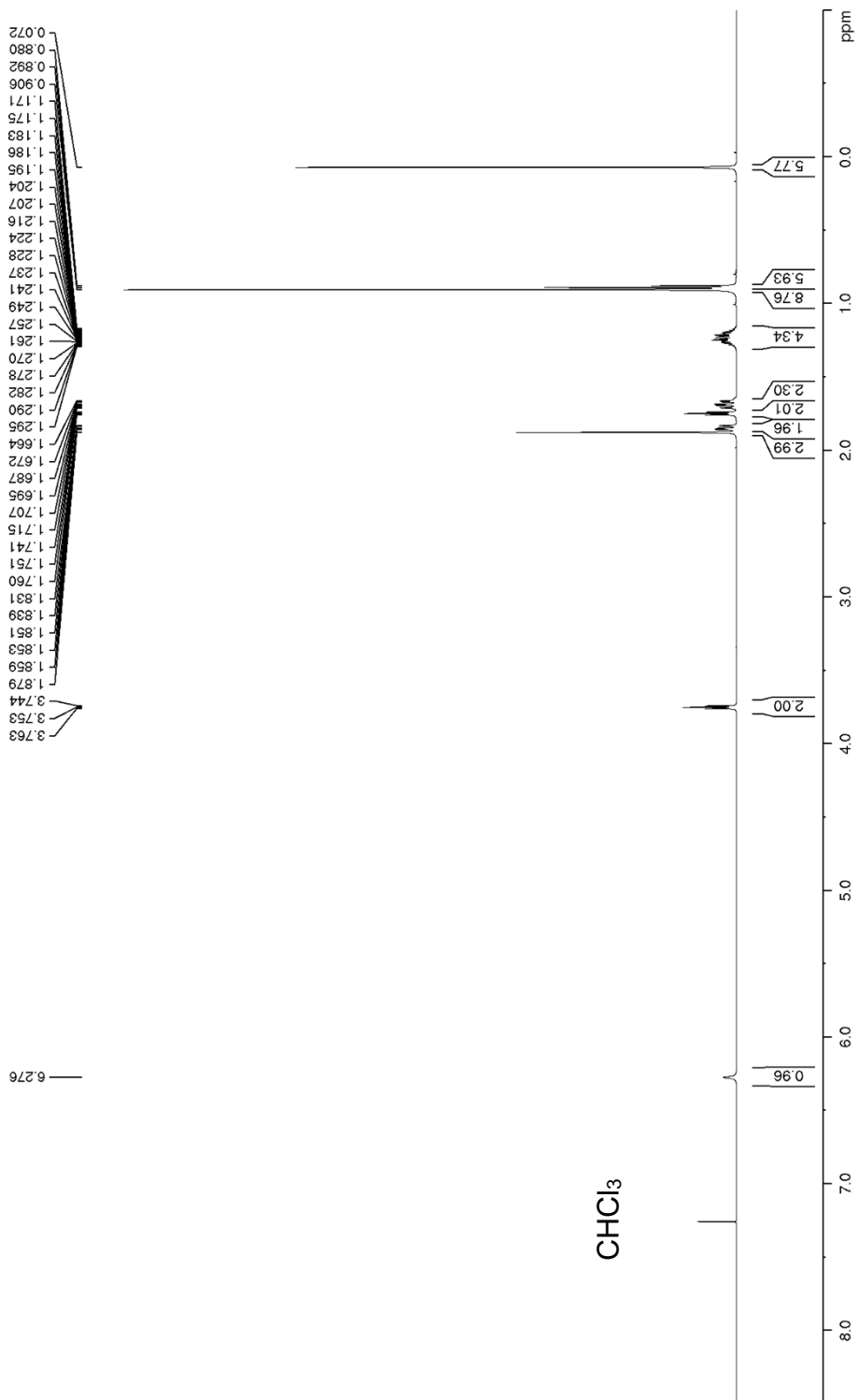


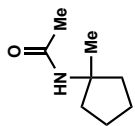
4.83 (^{13}C NMR, 126 MHz, CDCl_3 , 25 $^\circ\text{C}$)



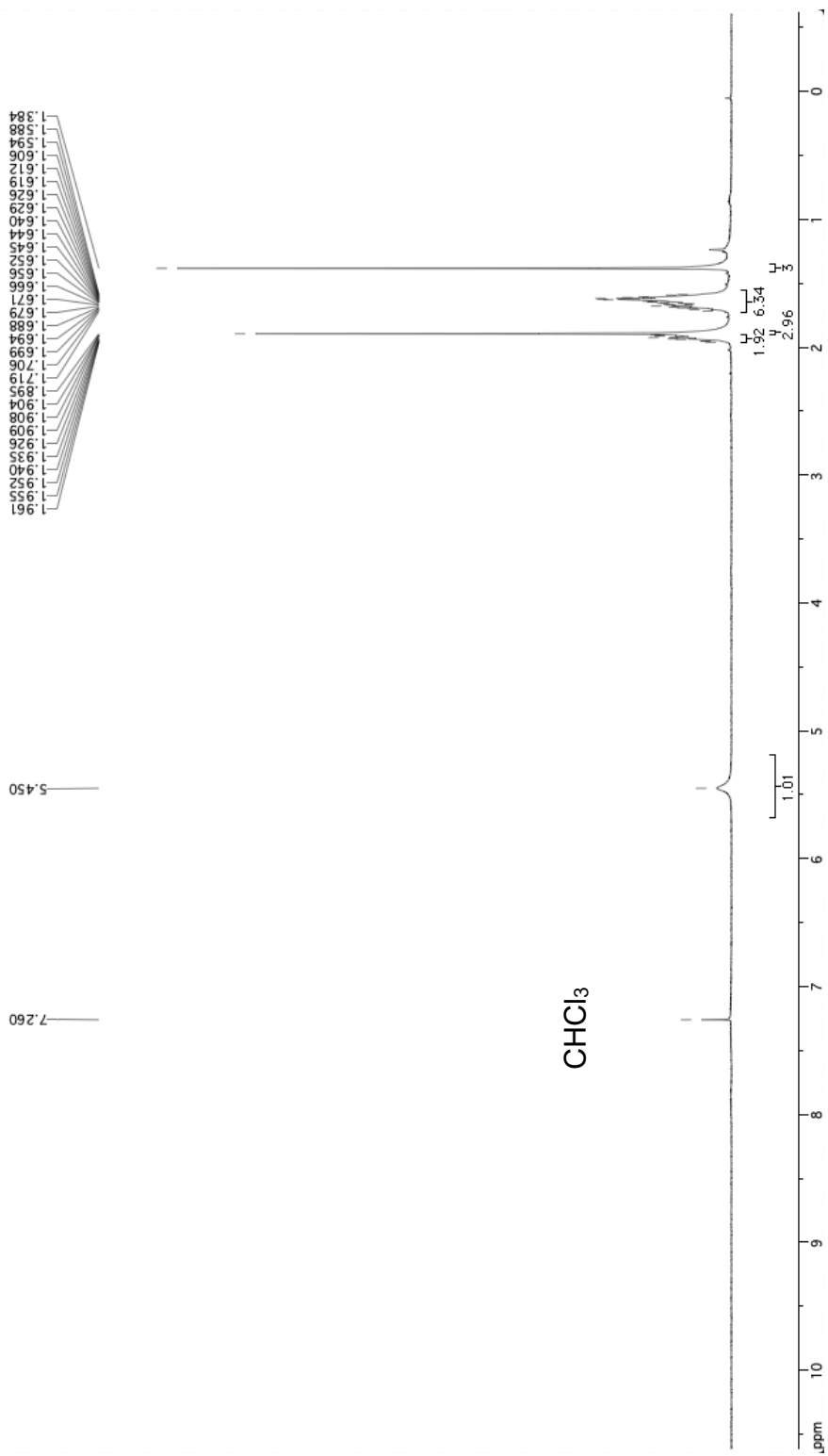


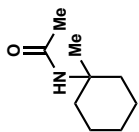
4.85 (¹H NMR, 600 MHz, CDCl₃, 25°C)



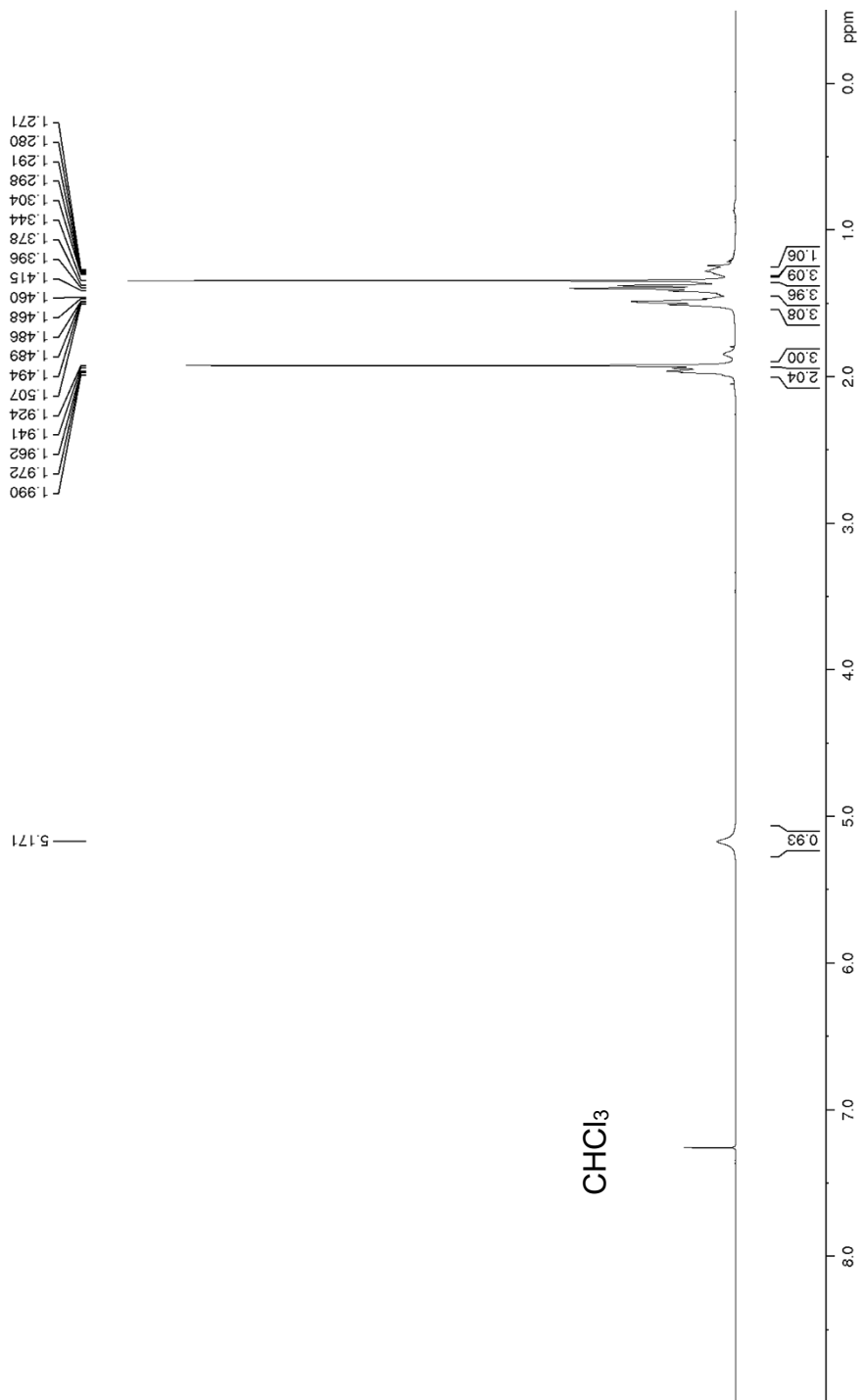


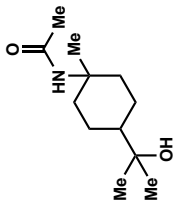
4.86 (¹H NMR, 500 MHz, CDCl₃, 25 °C)





4.87 (¹H NMR, 600 MHz, CDCl₃, 25 °C)





4.88 (¹H NMR, 500 MHz, CDCl₃, 25 °C)

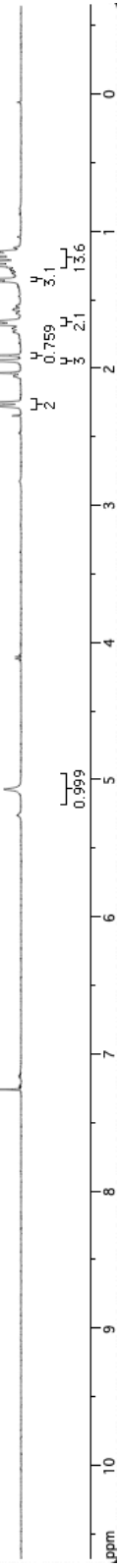
2.274
2.249
1.945
1.682
1.681
1.60
1.659
1.654
1.351
1.263
1.249
1.233
1.26
1.194
1.169
1.147

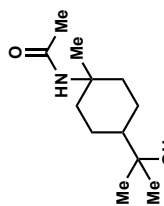
5.070

7.260

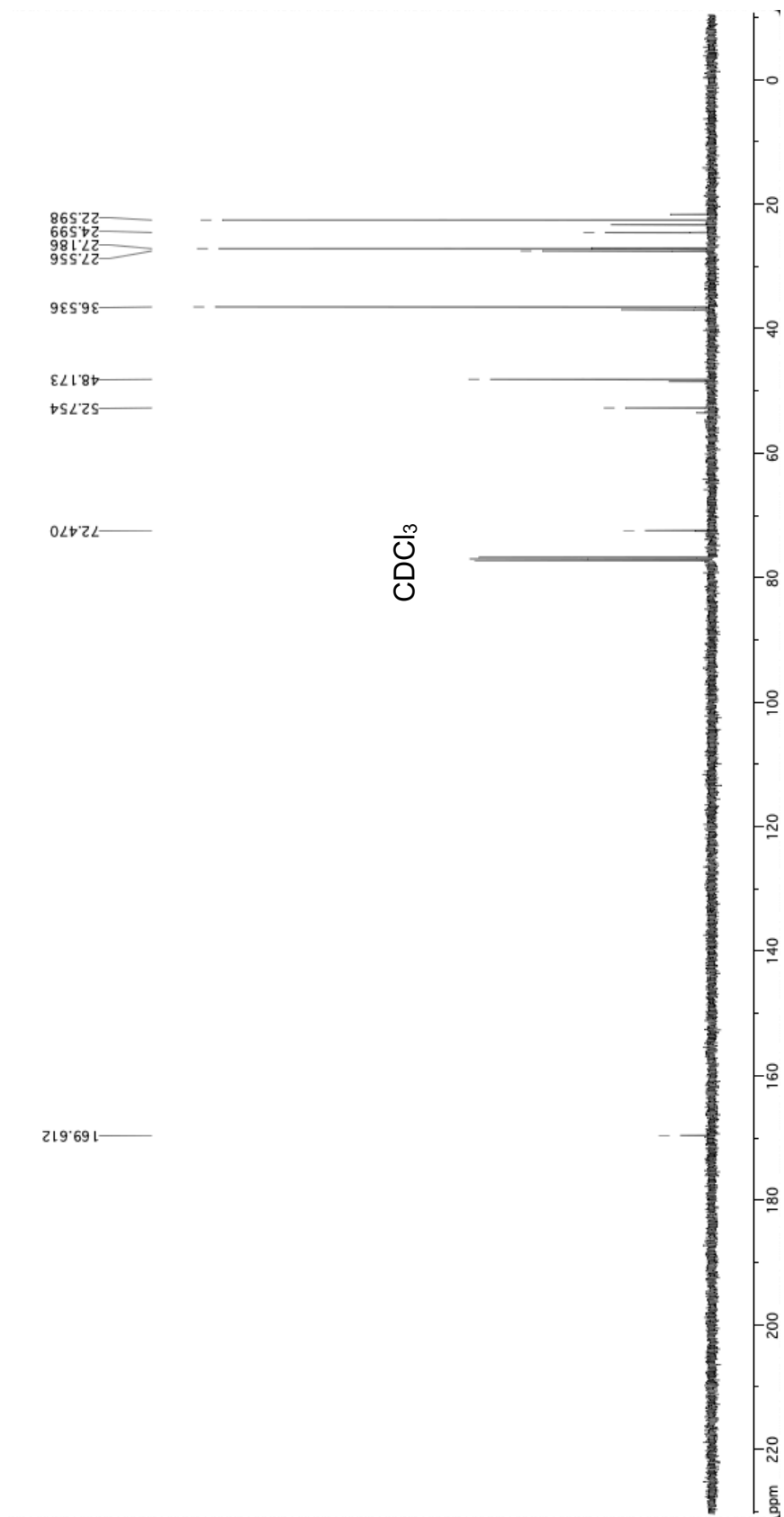
Minor
diastereomer
acetamide methyl

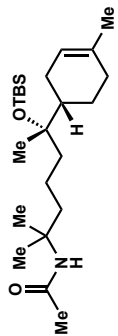
CHCl₃



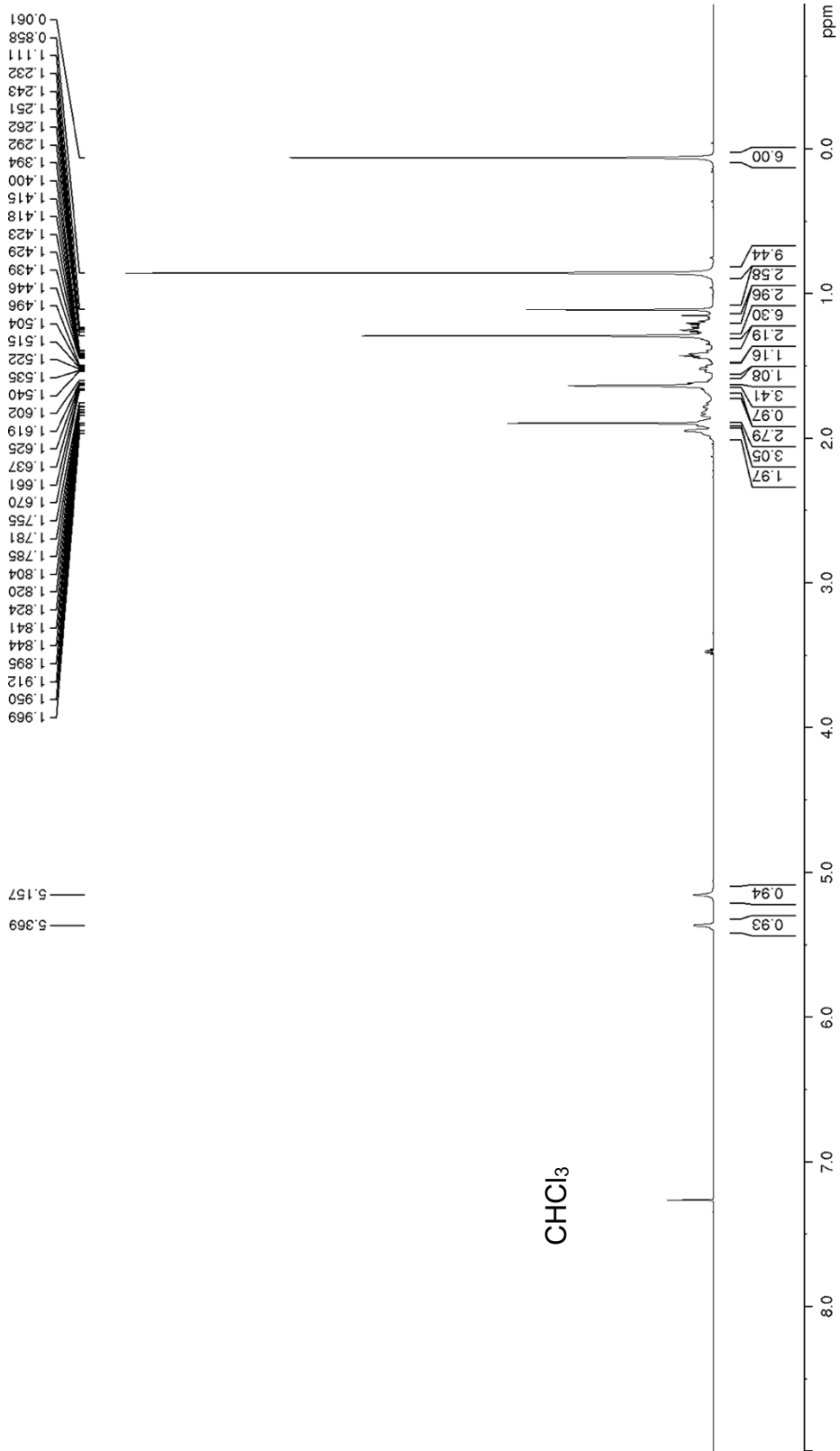


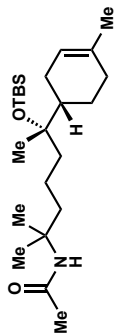
4.88 (¹³C NMR, 126 MHz, CDCl₃, 25 °C)



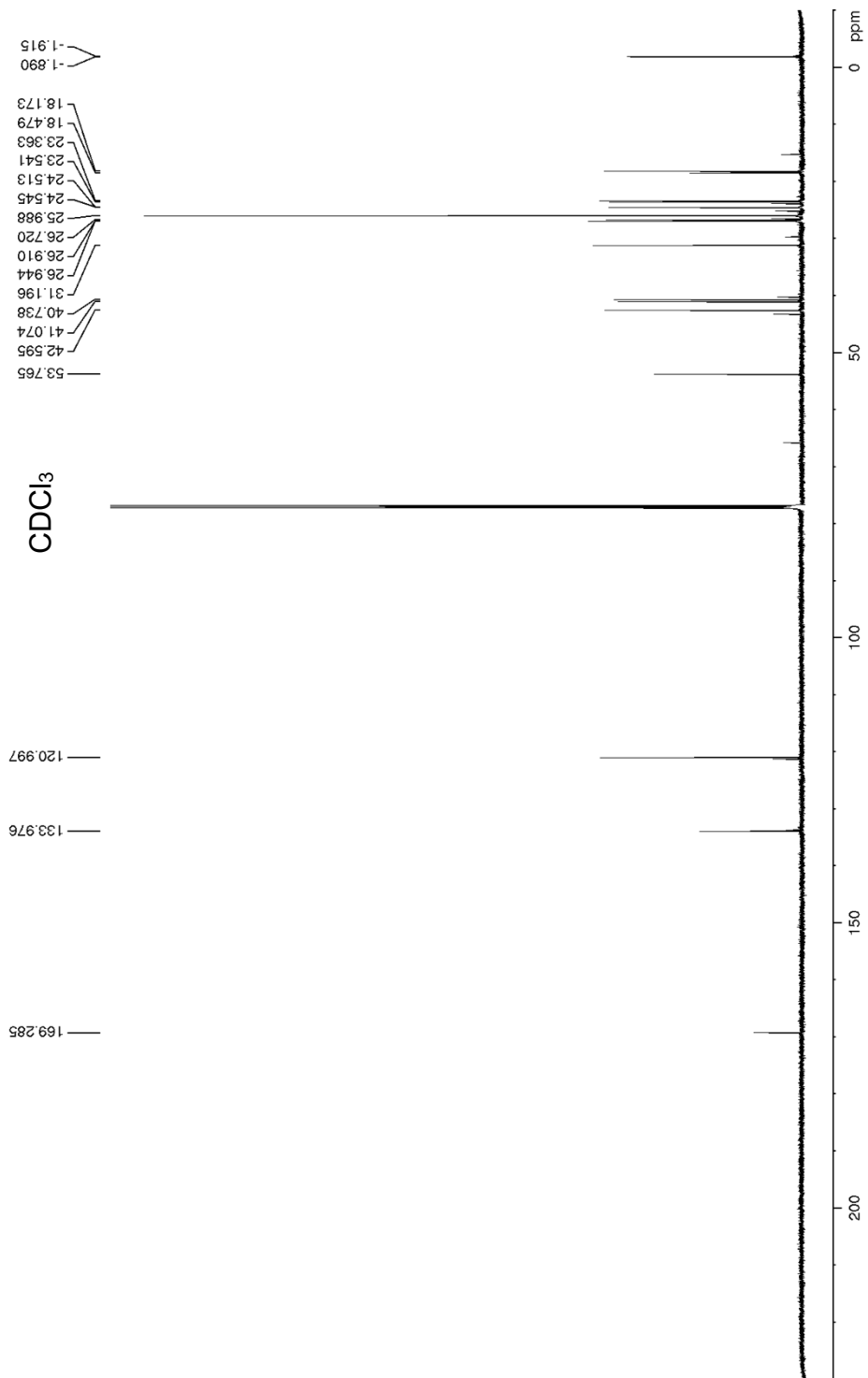


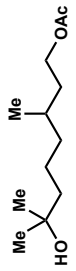
4.89 (¹H NMR, 600 MHz, CDCl₃, 25°C)



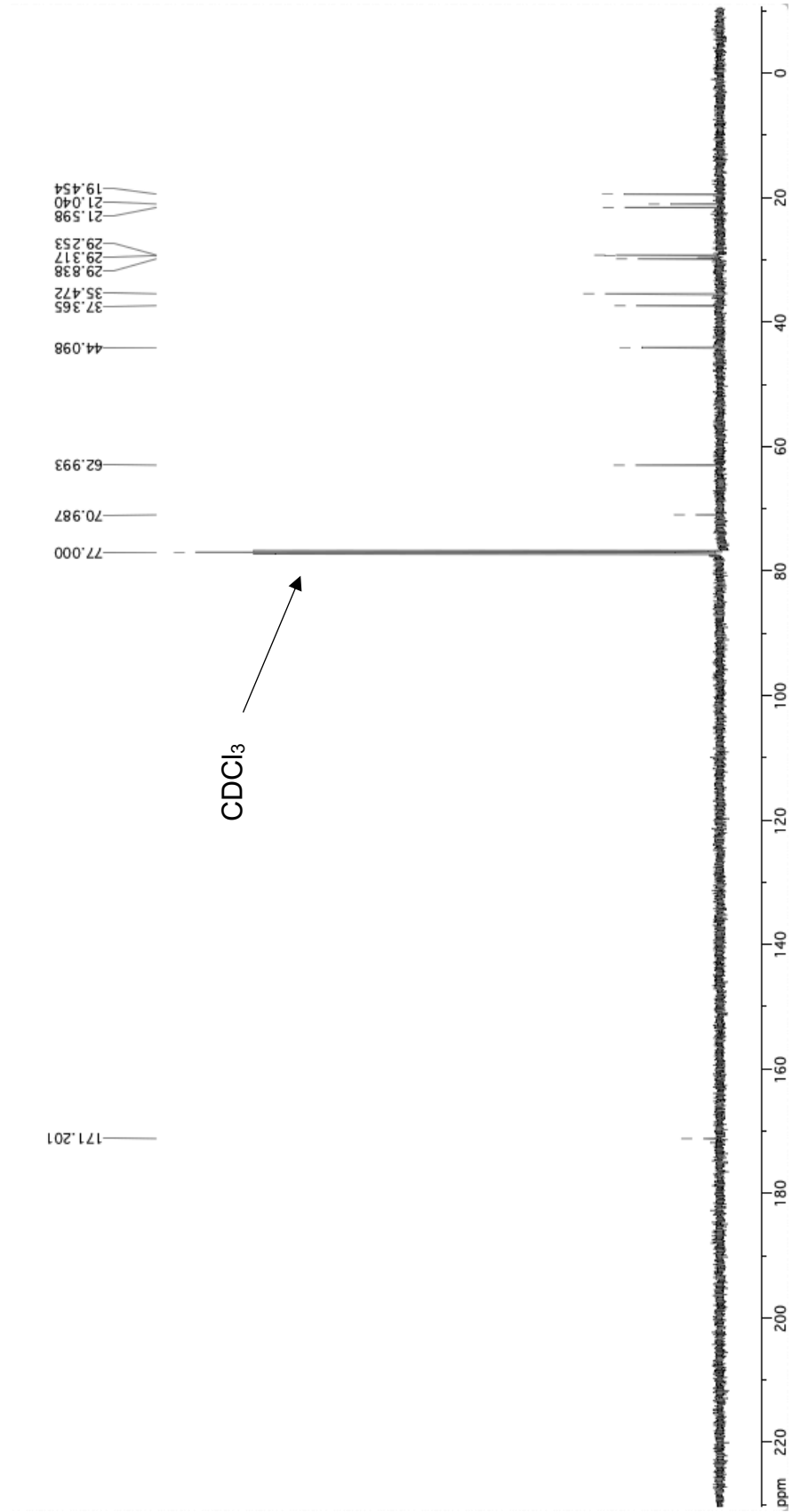


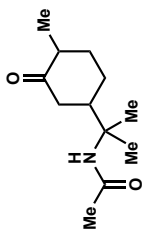
4.89 (^{13}C NMR, 151 MHz, CDCl_3 , 25°C)



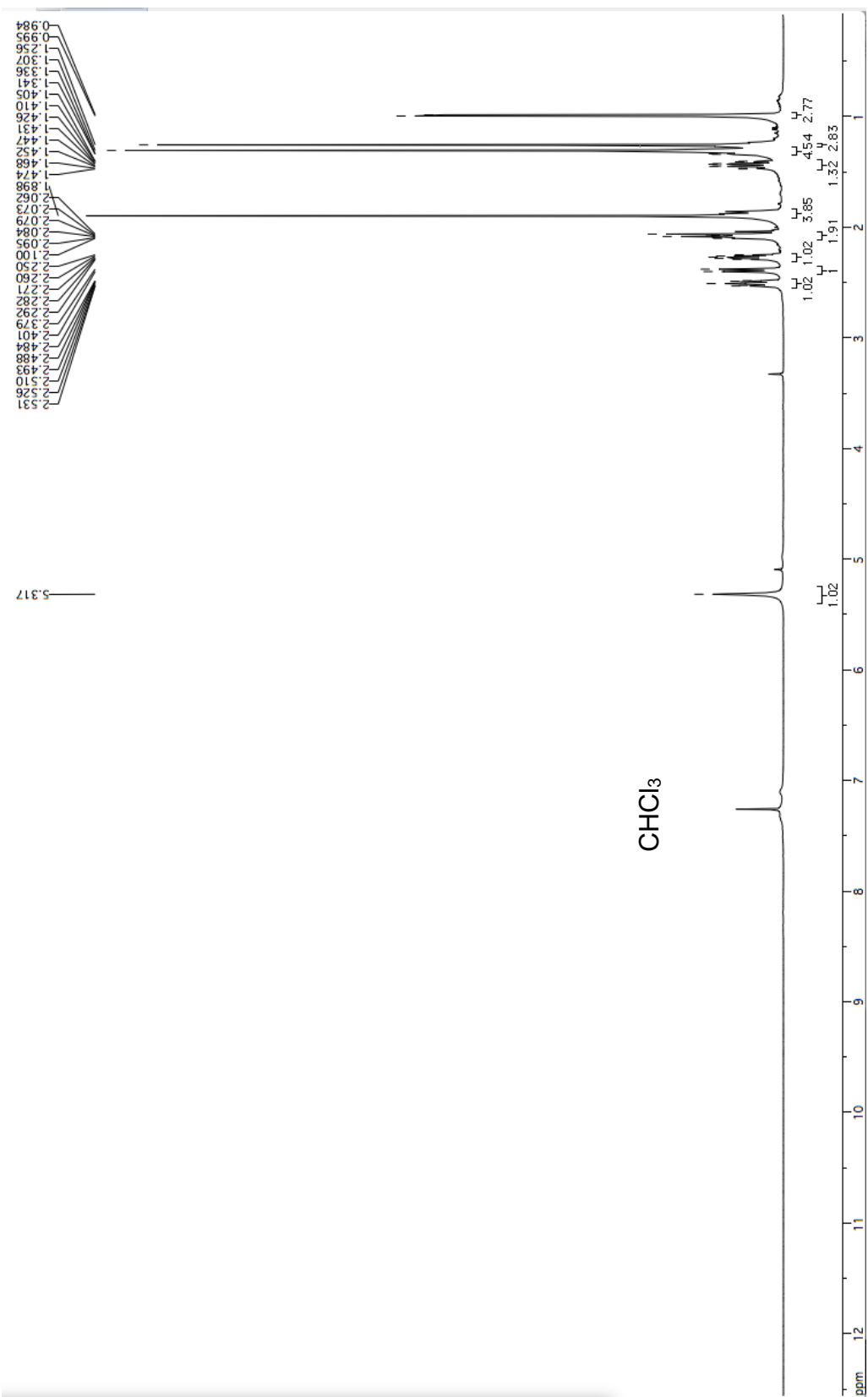


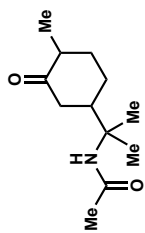
4.90 (¹³C NMR, 126 MHz, CDCl₃, 25 °C)



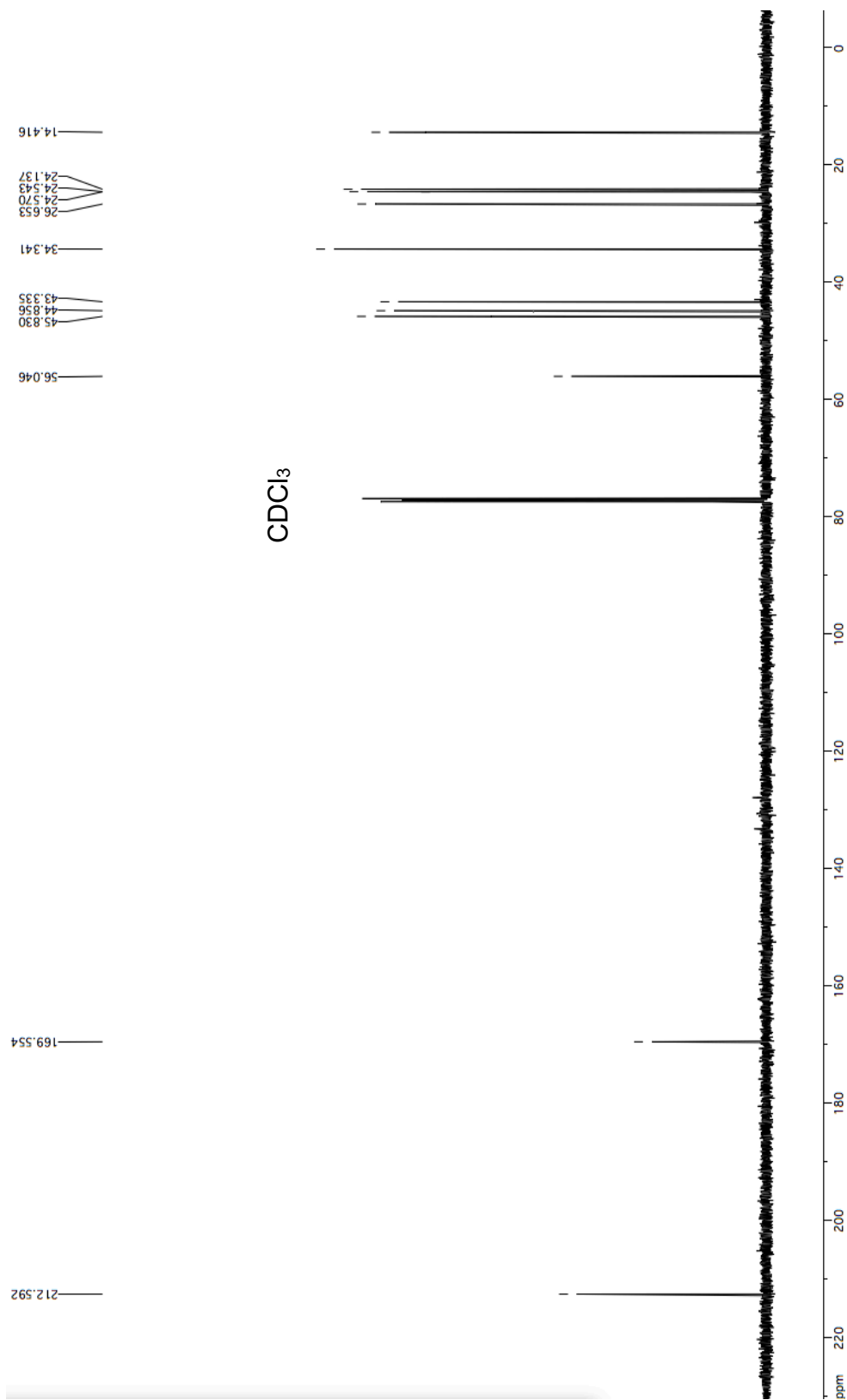


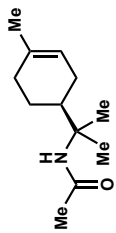
4.18 (¹H NMR, 600 MHz, CDCl₃, 25 °C)



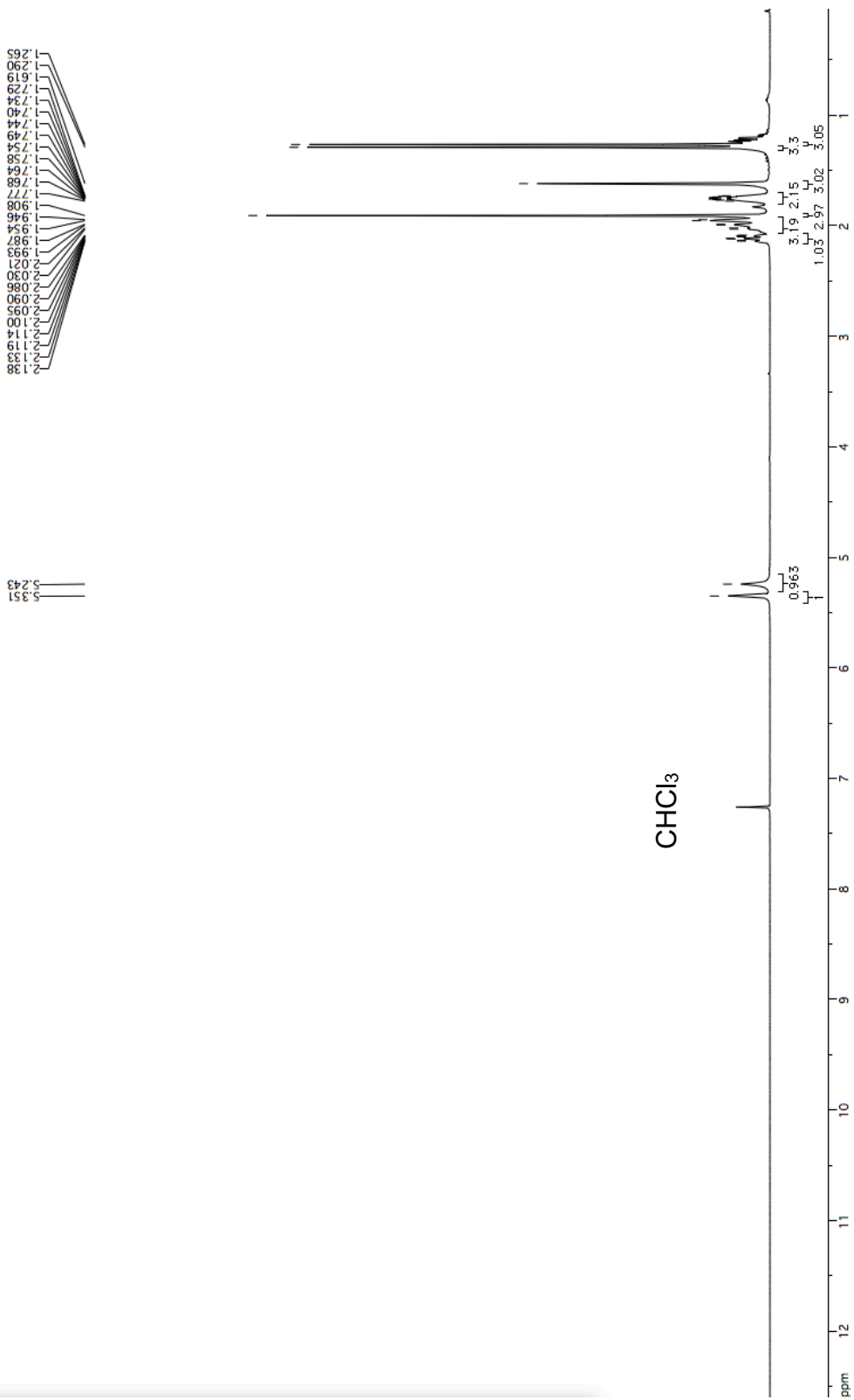


4.18 (^{13}C NMR, 126 MHz, CDCl_3 , 25 $^\circ\text{C}$)



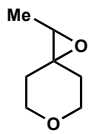


4.19 (¹H NMR, 500 MHz, CDCl₃, 25 °C)

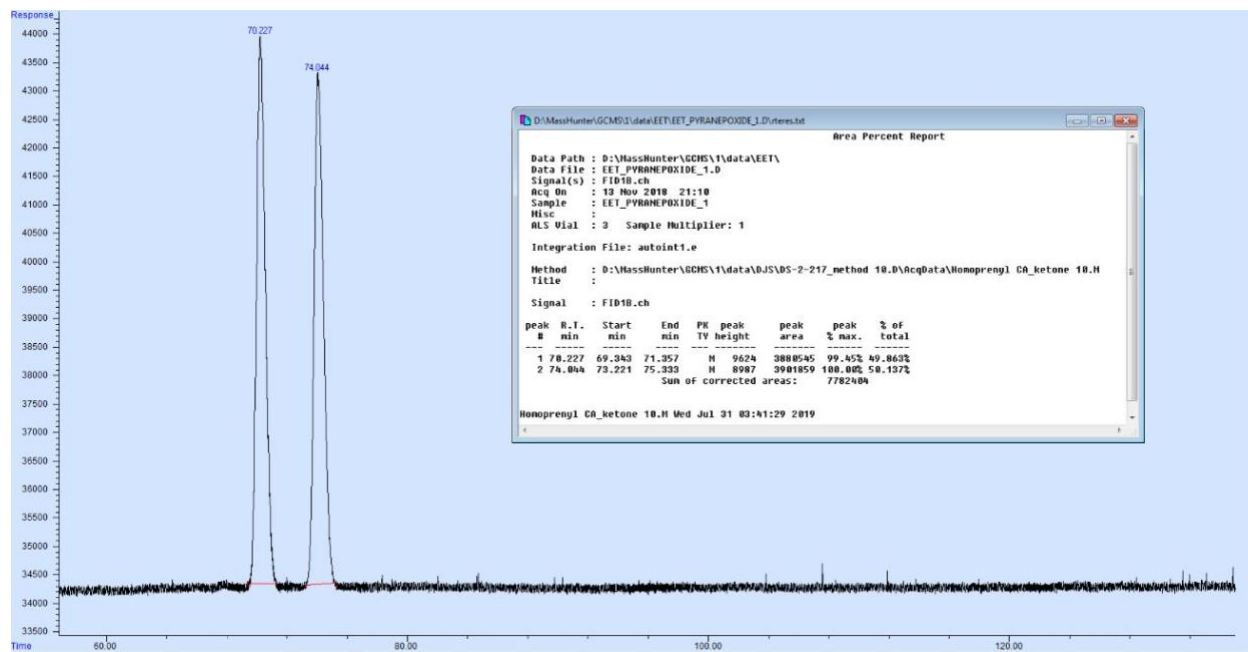


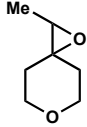
Appendix D: Chiral GC-FID Traces

Chiral GC-FID Traces

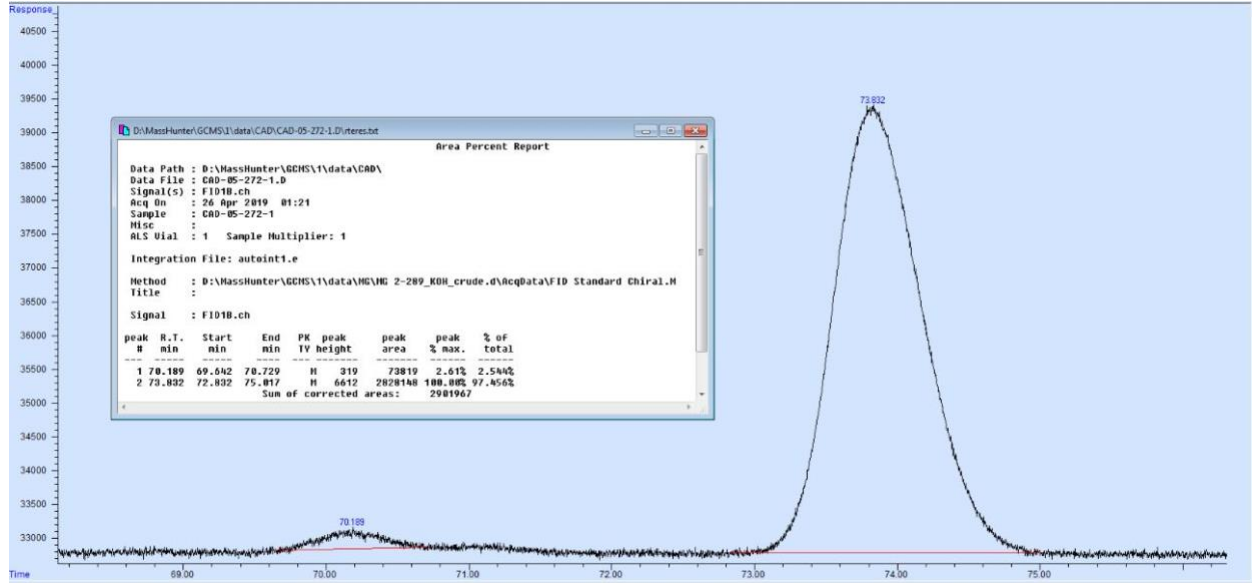


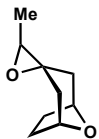
3.52
chiral GC/FID
80 °C, 75 min
racemic



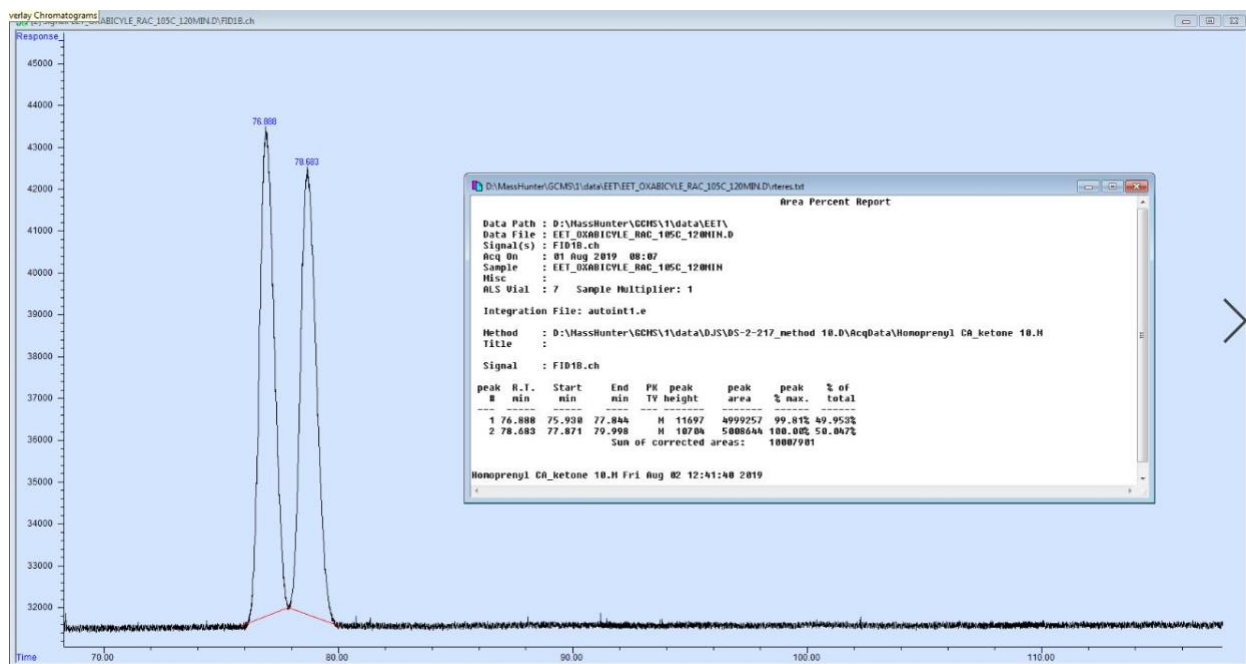


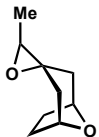
3.52
chiral GC/FID
80 °C, 75 min
enantioenriched
95% ee



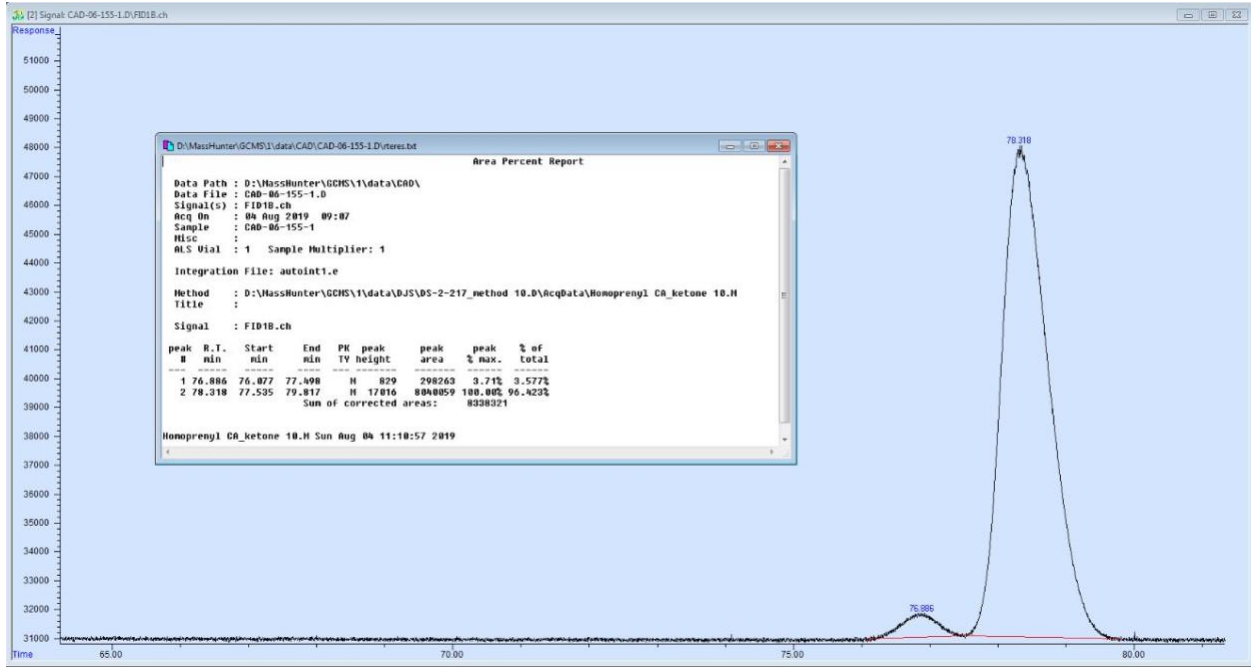


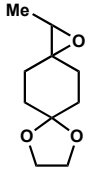
3.63
 chiral GC/FID
 105 °C, 120 min
 racemic



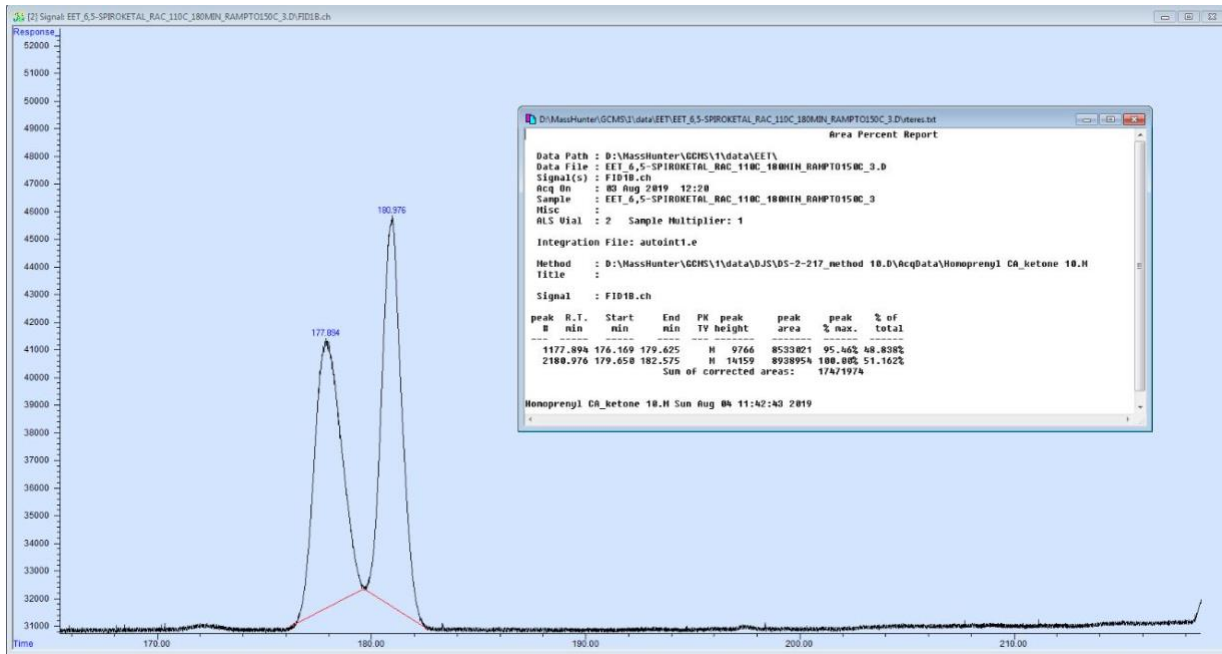


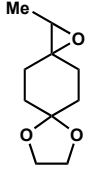
3.63
 chiral GC/FID
 105 °C, 120 min
 enantioenriched
 93% ee



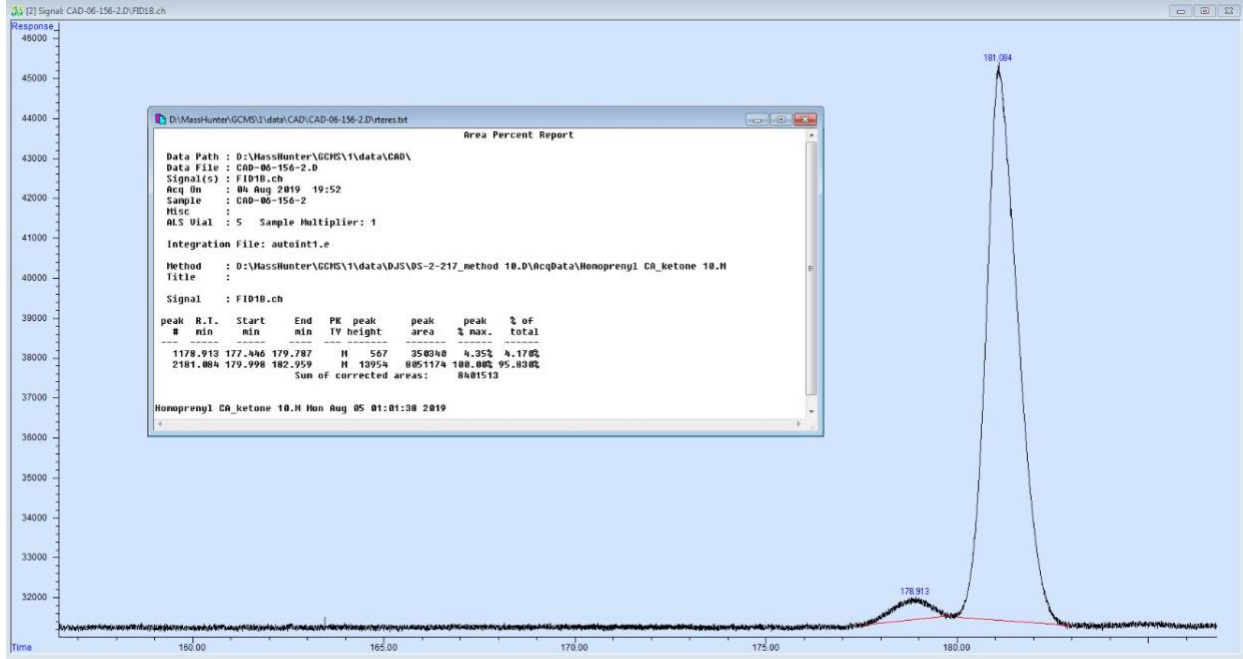


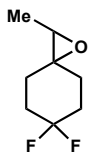
3.66
 chiral GC/FID
 110 °C, 180 min
 ramp to 150 °C, 40 min
 racemic



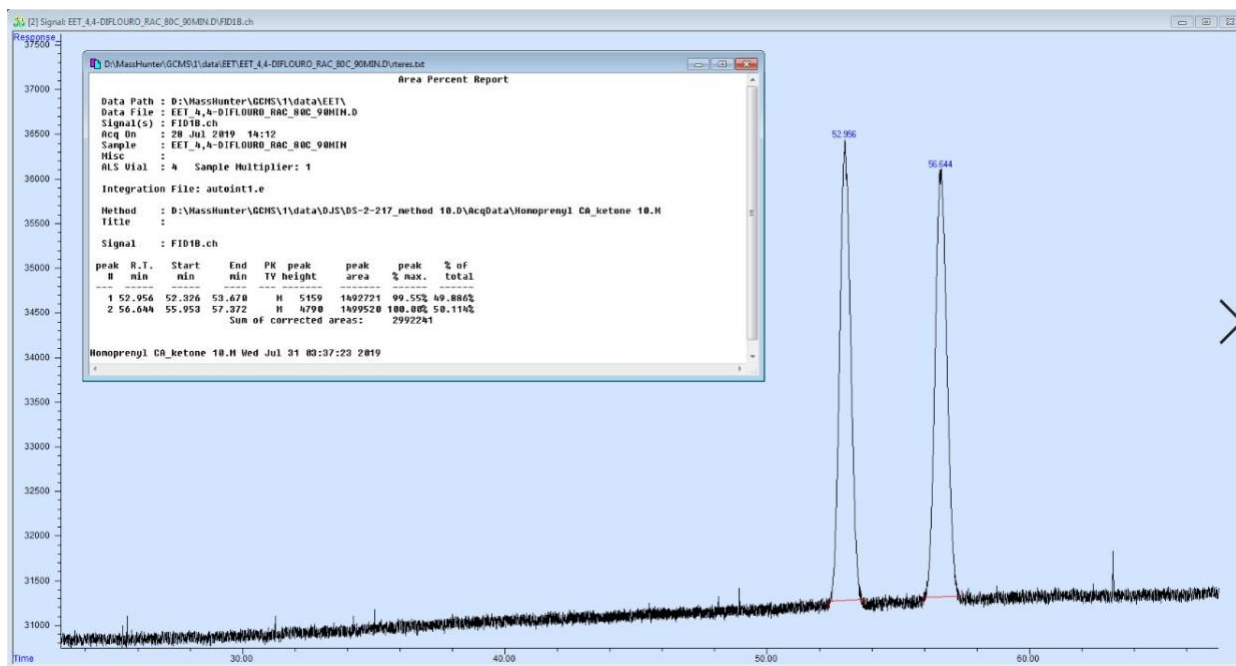


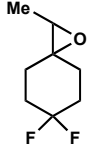
3.66
 chiral GC/FID
 110 °C, 180 min
 ramp to 150 °C, 40 min
 enantioenriched
 92% ee



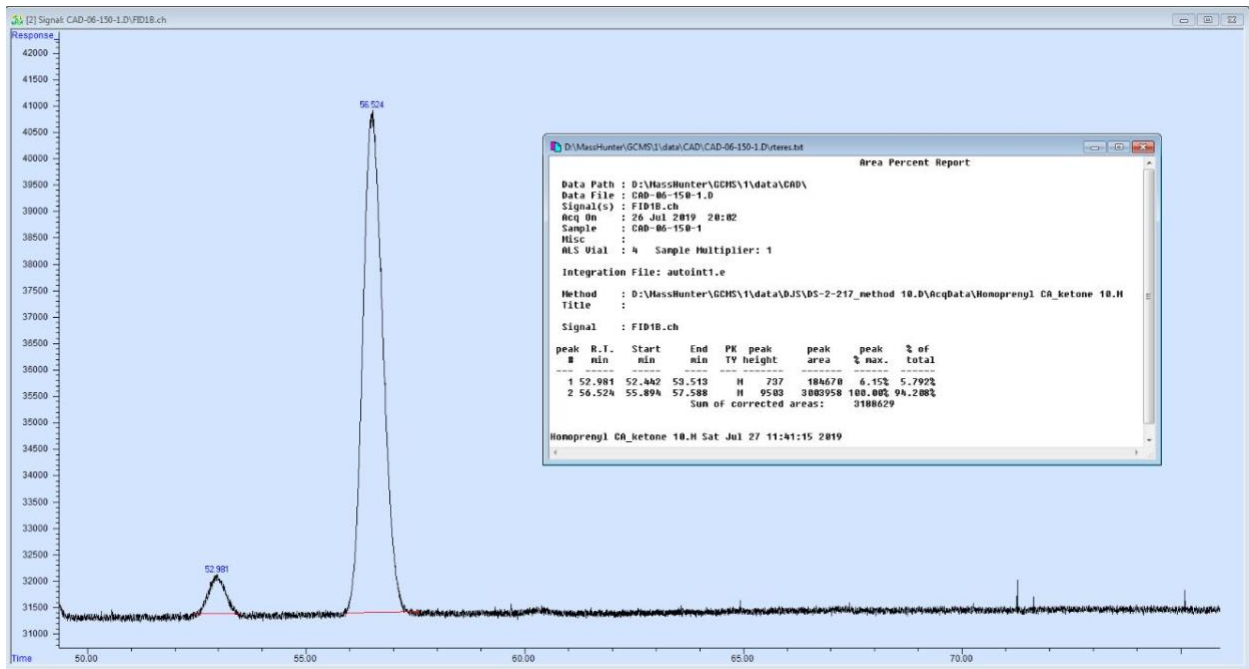


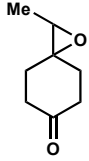
3.65
 chiral GC/FID
 80 °C, 75 min
 racemic



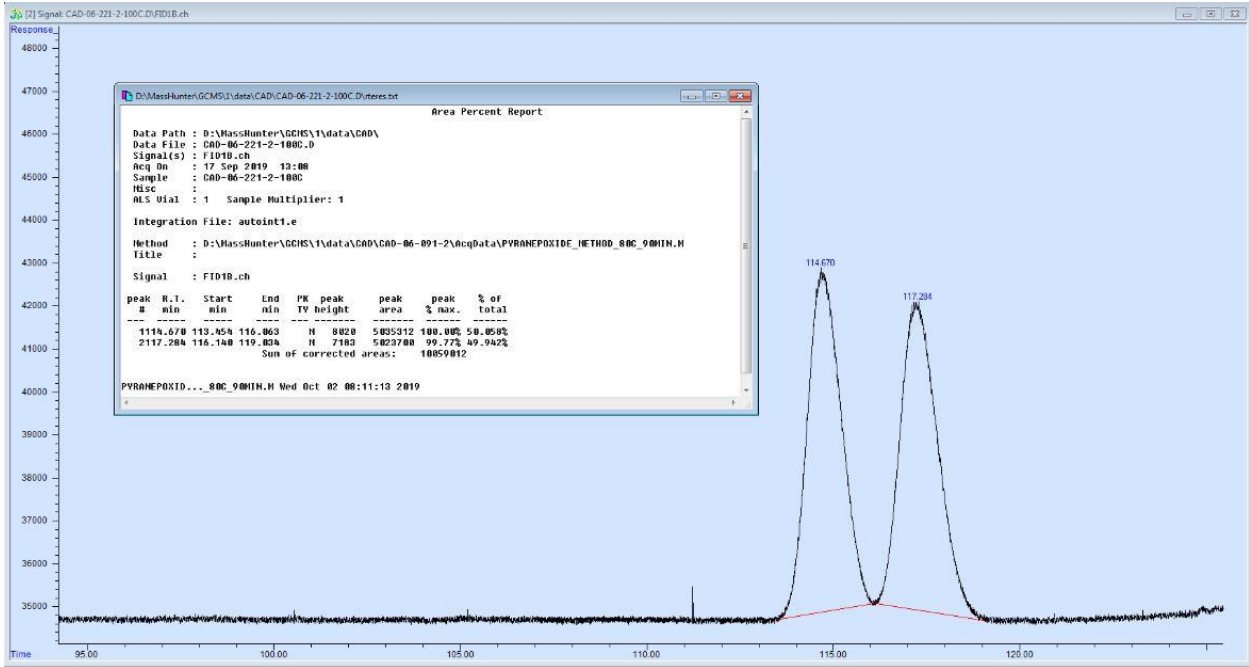


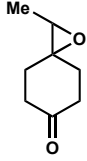
3.65
 chiral GC/FID
 80 °C, 75 min
 enantioenriched
 89% ee



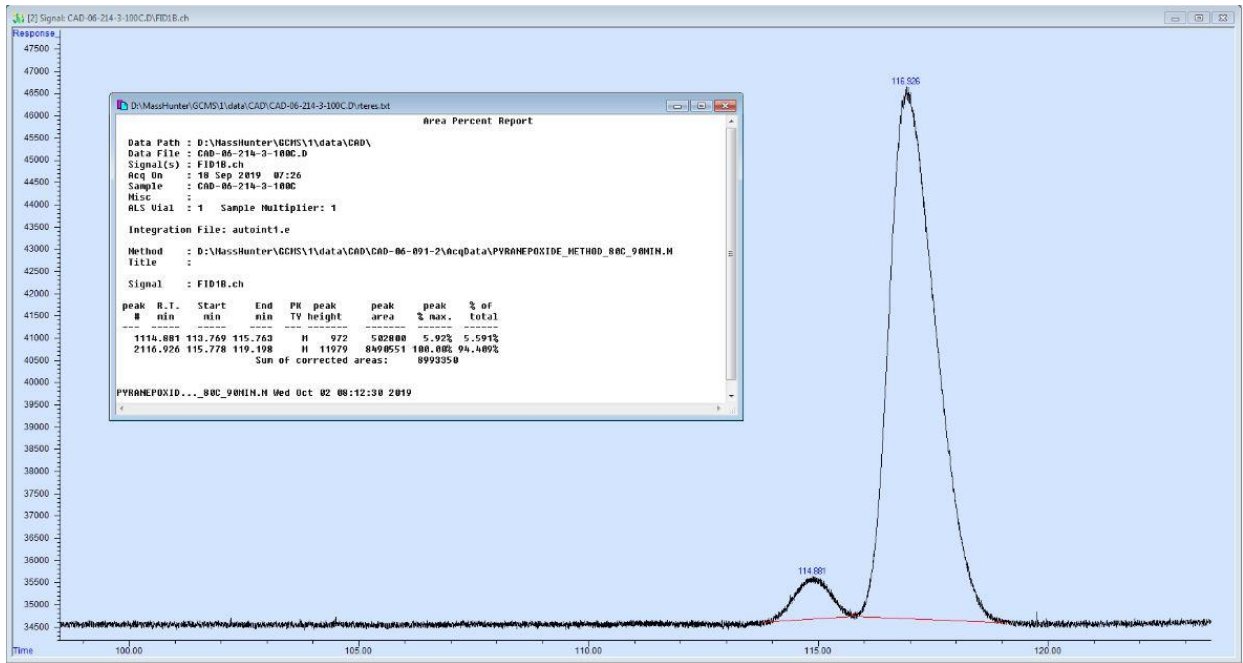


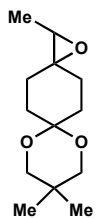
3.68
 chiral GC/FID
 110 °C, 120 min
 racemic



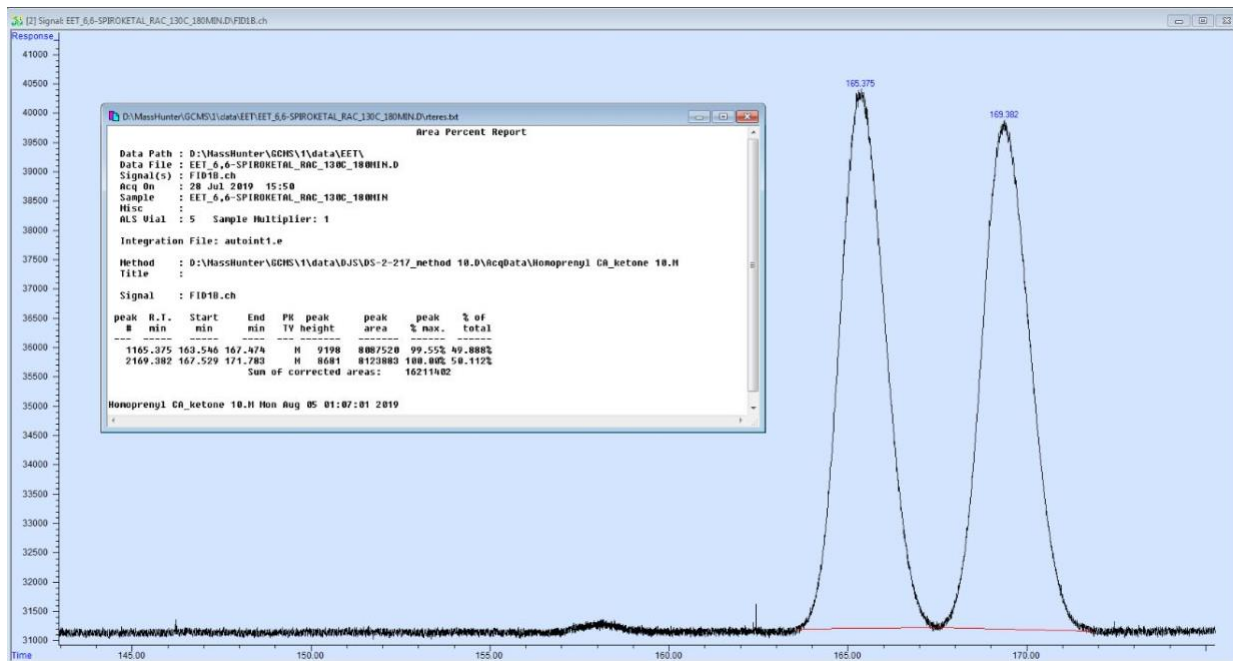


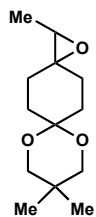
3.68
 chiral GC/FID
 110 °C, 120 min
 enantioenriched
 89% ee



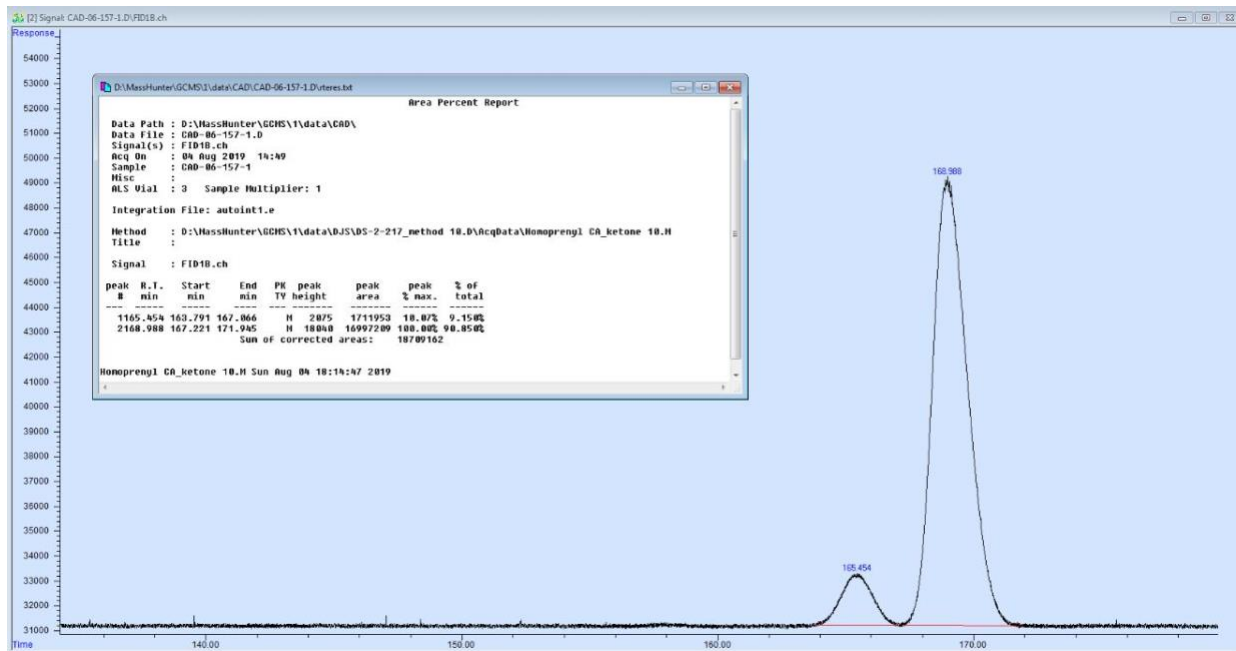


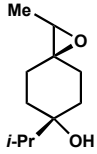
3.67
 chiral GC/FID
 130 °C, 180 min
 racemic



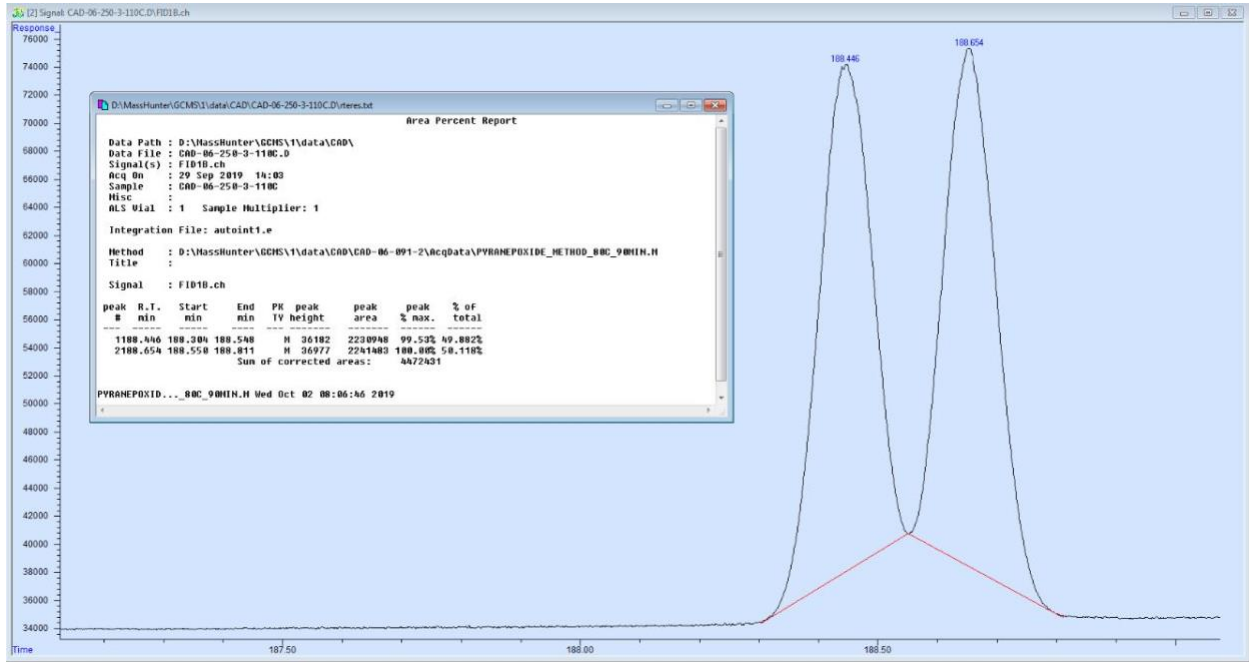


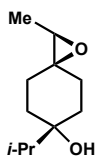
3.67
 chiral GC/FID
 130 °C, 180 min
 enantioenriched
 81% ee



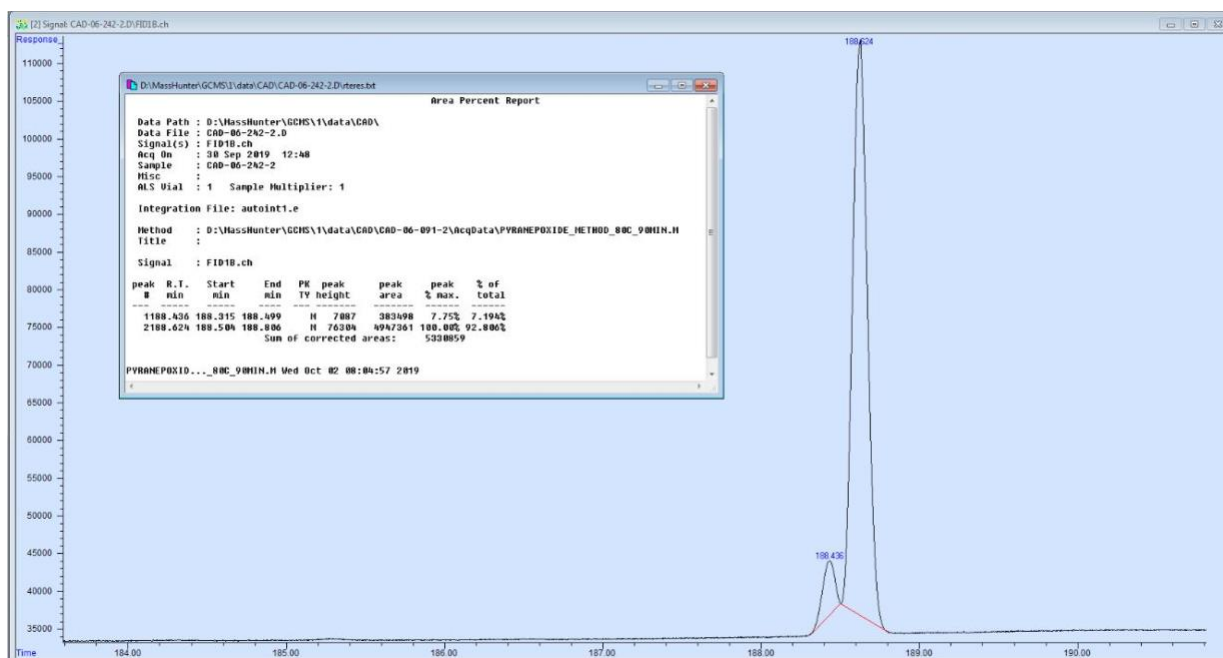


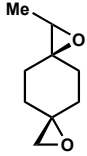
3.69
 chiral GC/FID
 110 °C, 180 min
 then ramp to 200 °C
 at 10 °C per min
 racemic



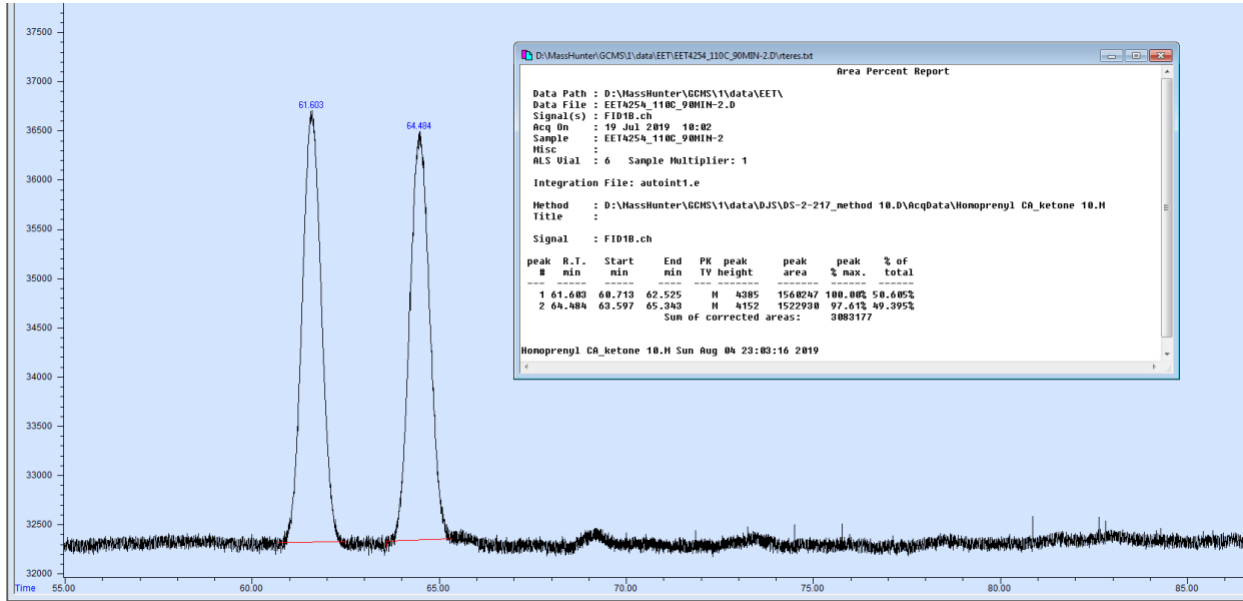


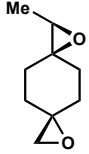
3.69
 chiral GC/FID
 110 °C, 180 min
 then ramp to 200 °C
 at 10 °C per min
 enantioenriched
 86% ee



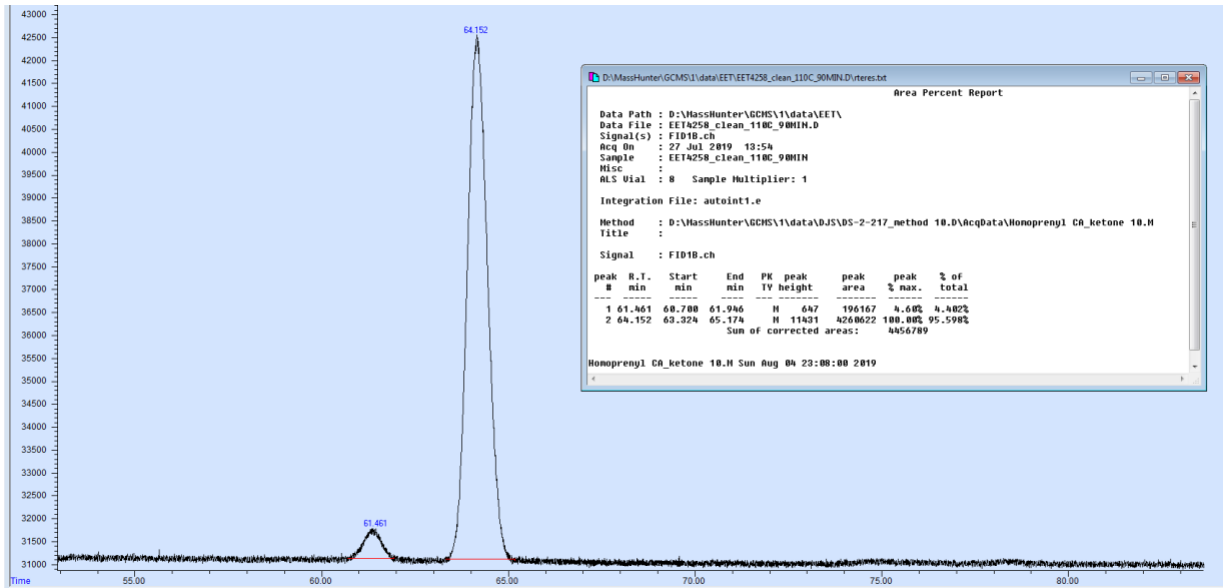


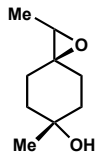
3.71
 chiral GC/FID
 110 °C, 90 min
 racemic



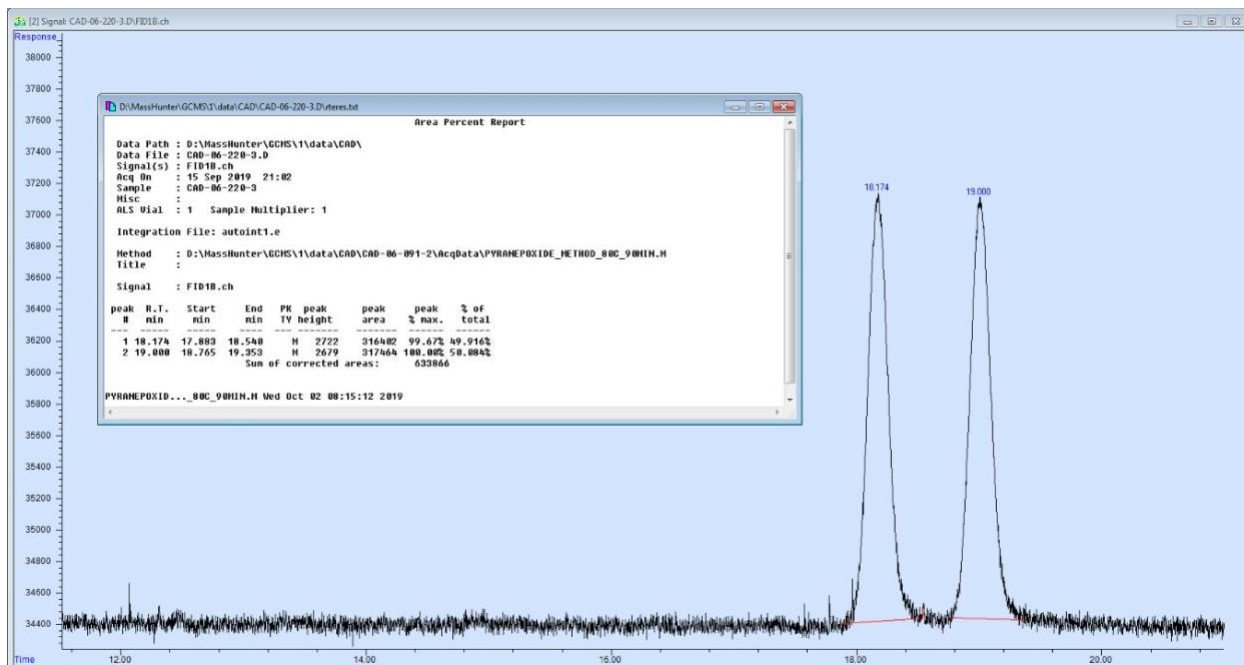


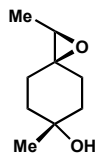
3.71
 chiral GC/FID
 110 °C, 90 min
 enantioenriched
 91% ee



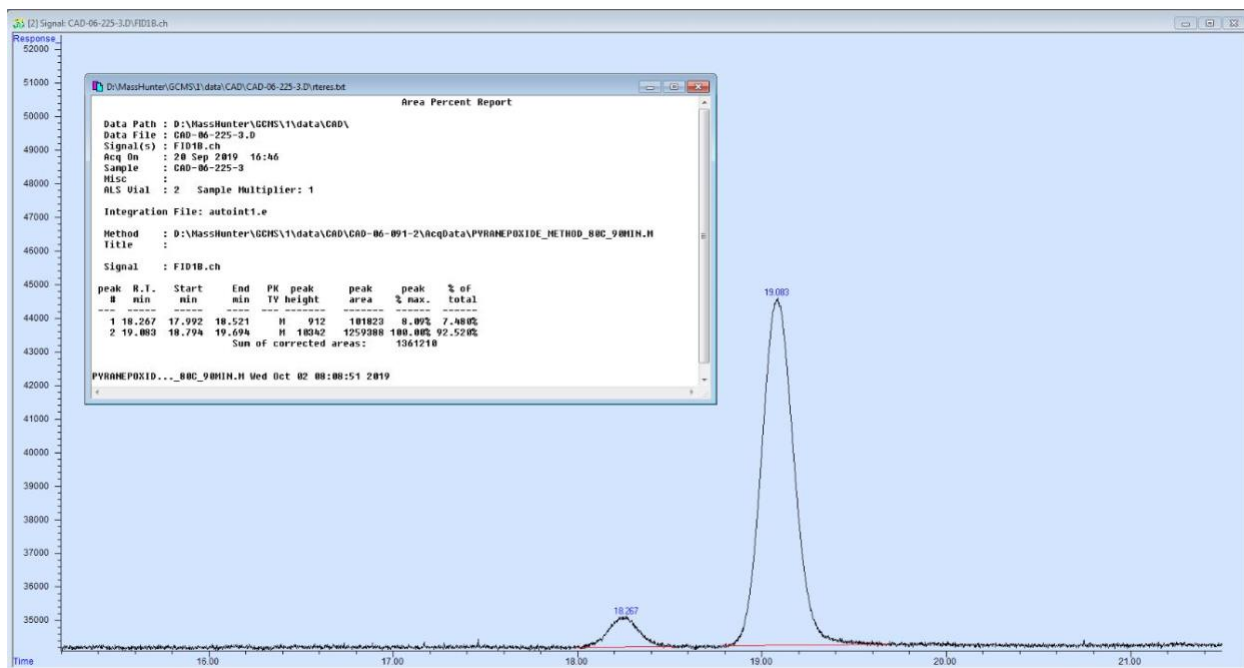


3.70
 chiral GC/FID
 130 °C, 30 min
 racemic



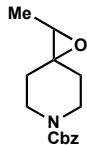


3.70
 chiral GC/FID
 130 °C, 30 min
 enantioenriched
 86% ee

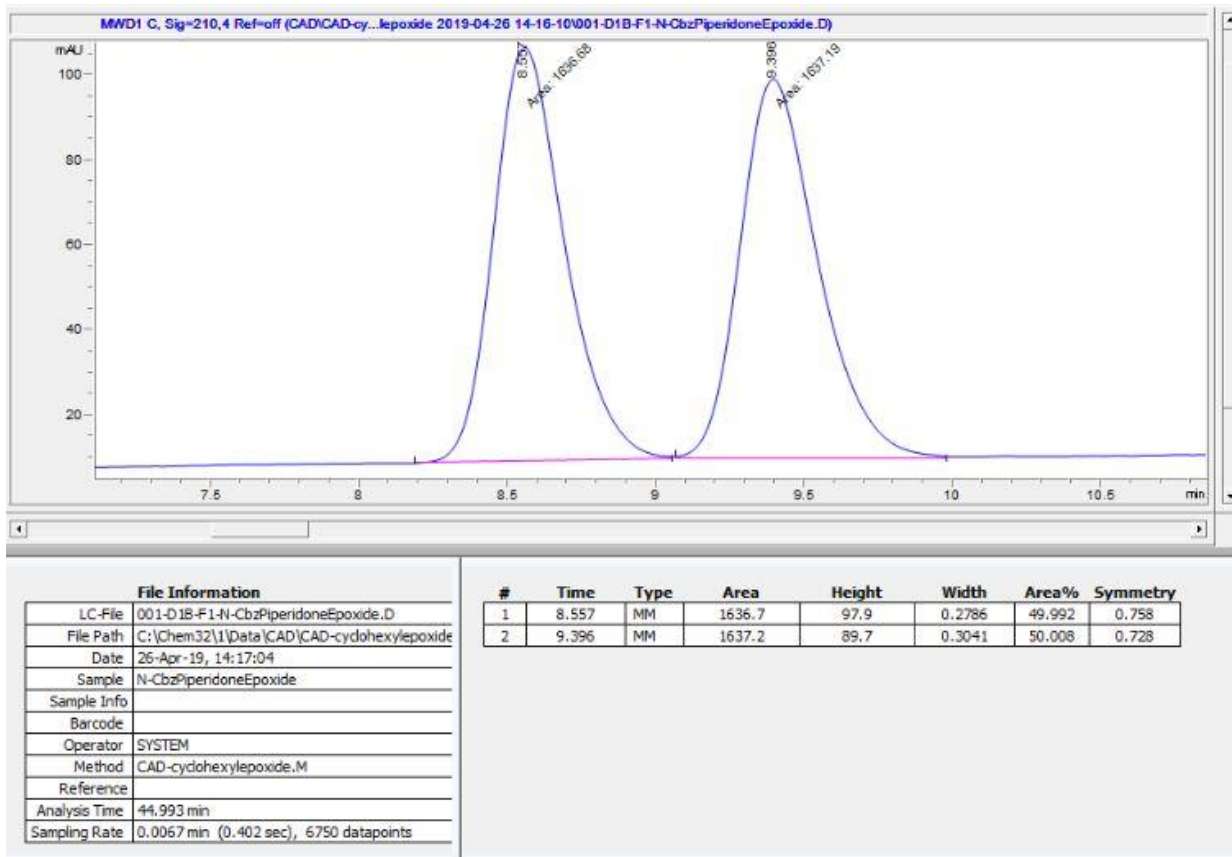


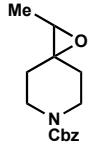
Appendix E: Chiral SFC Traces

Chiral SFC Traces

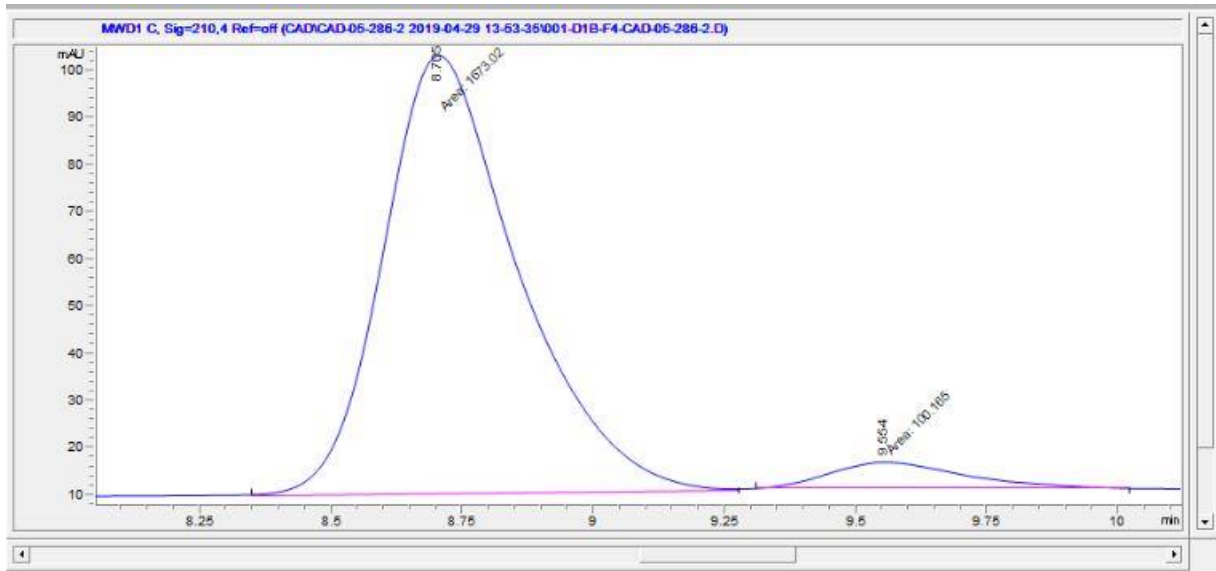


3.60
SFC, OD-H, 5% IPA:CO₂
2 mL/min, 44C, 15 µL
racemic

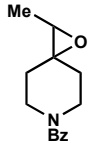




3.60
 SFC, OD-H, 5% IPA:CO₂
 2 mL/min, 44C, 15 µL
 enantioenriched
 89% ee

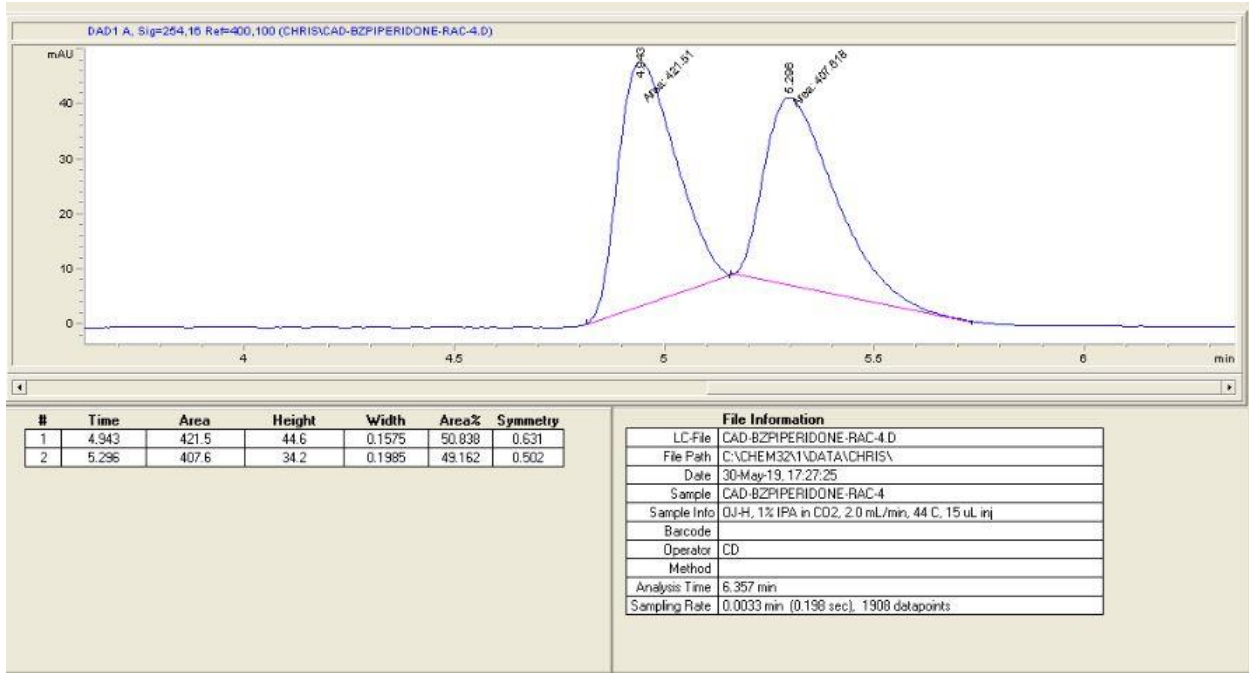


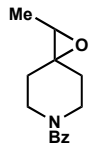
File Information		#	Time	Type	Area	Height	Width	Area%	Symmetry
LC-File	001-D 1B-F4-CAD-05-286-2.D	1	8.705	MM	1673	92.9	0.3	94.351	0.687
File Path	C:\Chem32\1\Data\CAD\CAD-05-286-2 2019-04	2	9.554	MM	100.2	5.6	0.2997	5.649	0.652
Date	29-Apr-19, 13:54:44								
Sample	CAD-05-286-2								
Sample Info									
Barcode									
Operator	SYSTEM								
Method	CAD Ncbz cyclohexyl epoxide.M								
Reference									
Analysis Time	14.993 min								
Sampling Rate	0.0067 min (0.402 sec), 2250 datapoints								



3.62

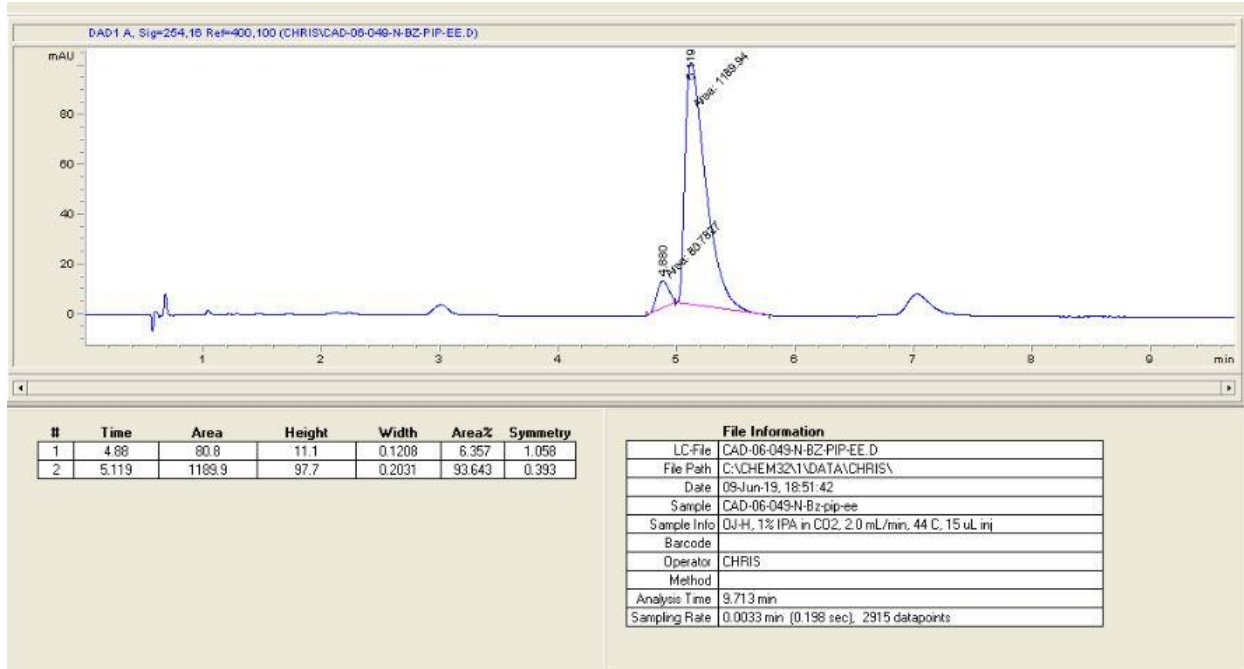
SFC, OJ-H, 1% IPA:CO₂
2 mL/min, 44C, 15 µL
racemic

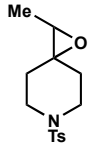




3.62

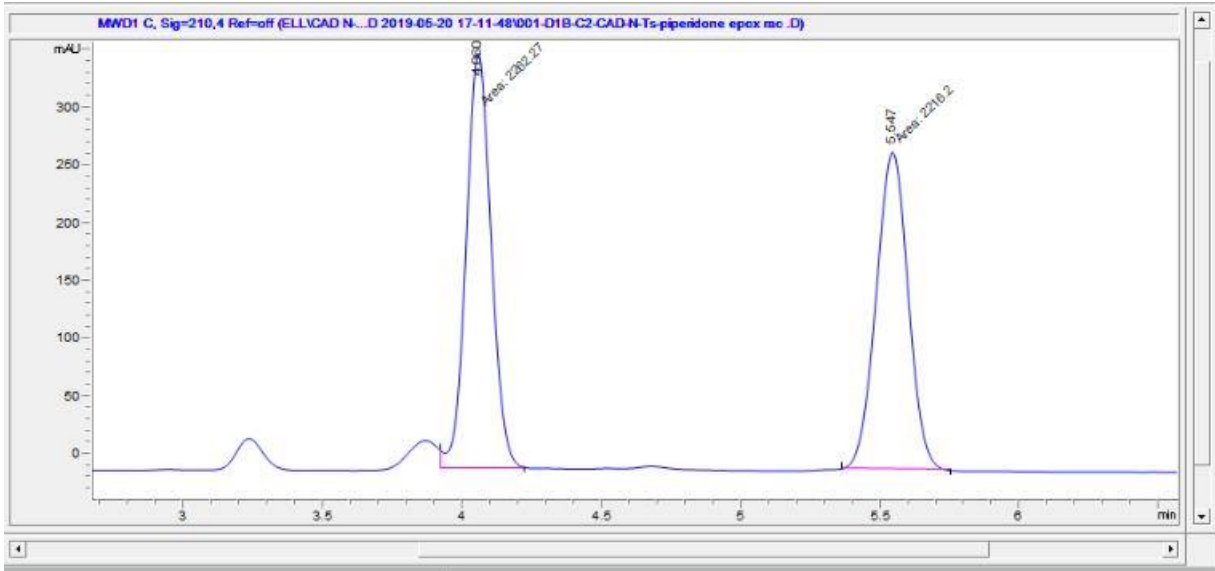
SFC, OJ-H, 1% IPA:CO₂
 2 mL/min, 44C, 15 µL
 enantioenriched
 87% ee



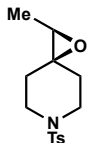


3.61

SFC, AD, 20% IPA:CO₂
2 mL/min, 44C, 15 µL
racemic

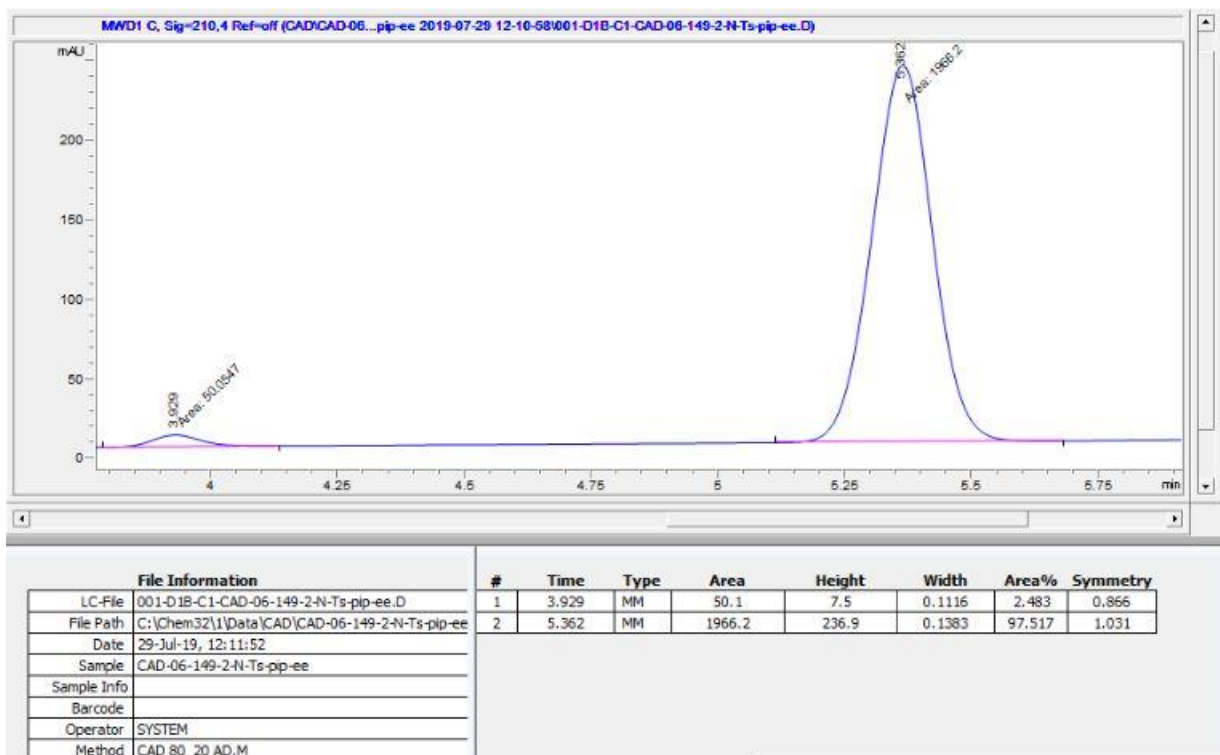


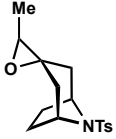
File Information		#	Time	Type	Area	Height	Width	Area%	Symmetry
LC-File	001-D18-C2-CAD-N-Ts-piperidone epox rac .D	1	4.06	MM	2262.3	362.1	0.1041	50.514	0.92
File Path	C:\Chem32\1\Data\ELL\CAD N-Ts piperidone epox	2	5.547	MM	2216.2	276.6	0.1335	49.486	1.028
Date	20-May-19, 17:12:42								
Sample	CAD-N-Ts-piperidone epox rac 80_20 AD-2								
Sample Info									
Barcode									
Operator	SYSTEM								
Method	CAD 80_20 AD.M								
Reference									
Analysis Time	7.74 min								
Sampling Rate	0.0057 min (0.402 sec), 1162 datapoints								



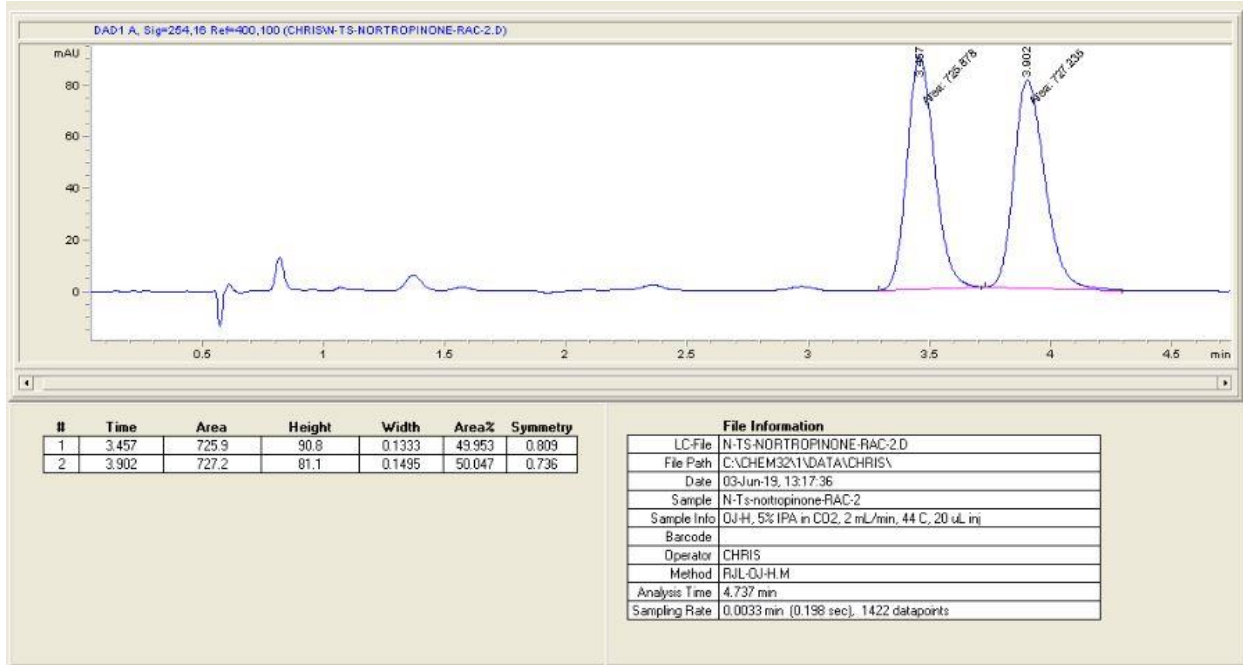
3.61

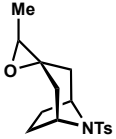
SFC, AD, 20% IPA:CO₂
 2 mL/min, 44C, 15 µL
 enantioenriched
 95% ee



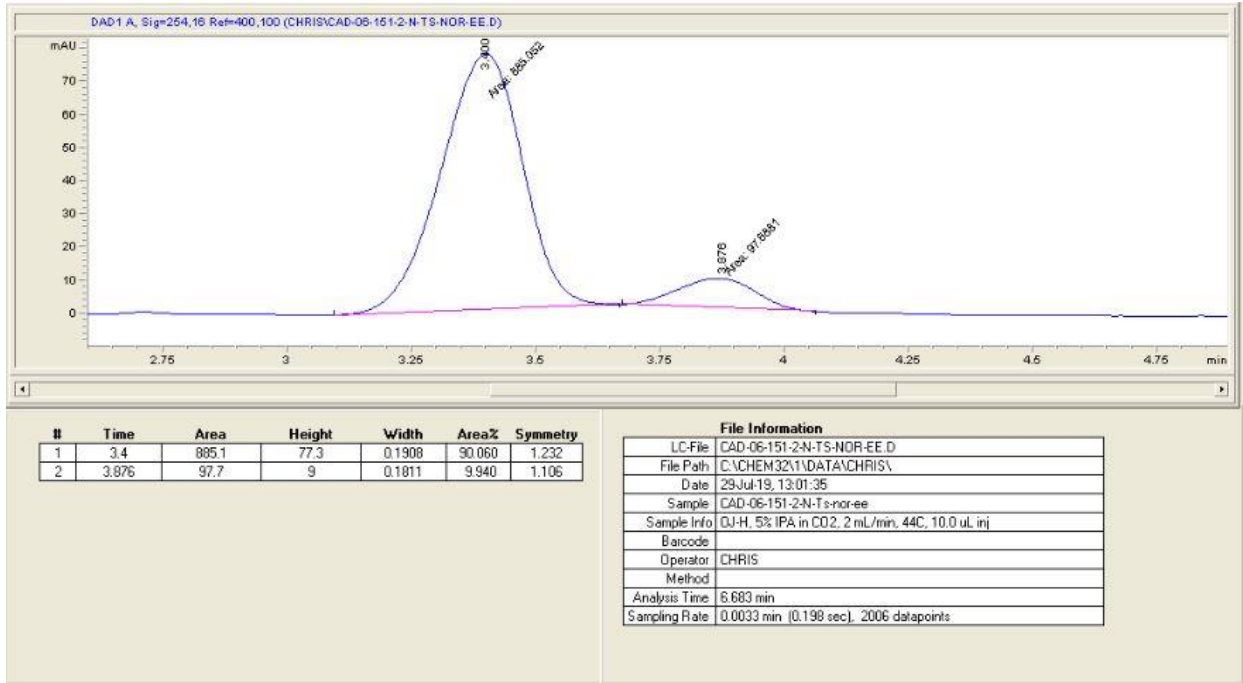


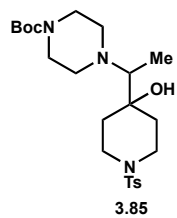
3.64
 SFC, OJ-H, 5% IPA:CO₂
 2 mL/min, 44C, 15 µL
 racemic



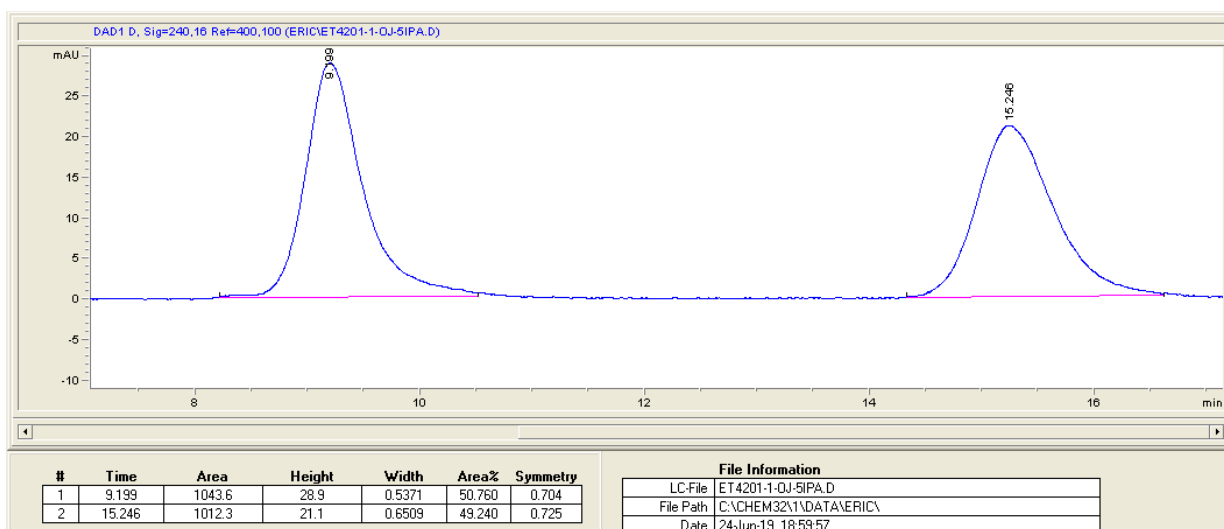


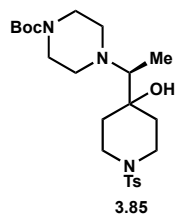
3.64
 SFC, OJ-H, 5% IPA:CO₂
 2 mL/min, 44C, 15 µL
 enantioenriched
 80% ee



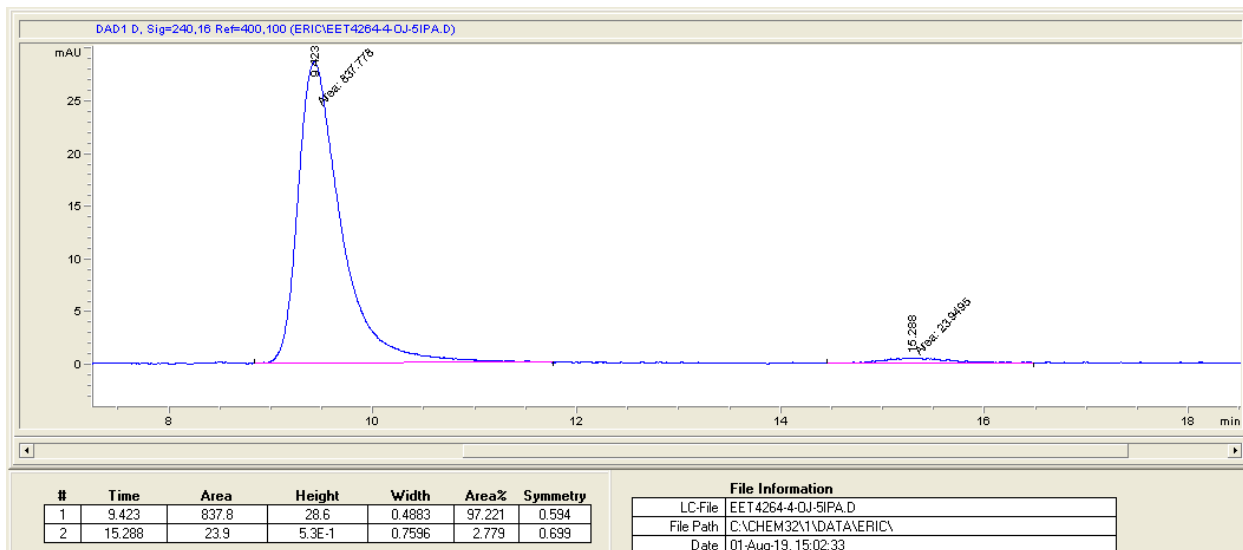


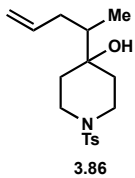
SFC OJ-H, 5% IPA:CO₂
2.0 mL/min
racemic



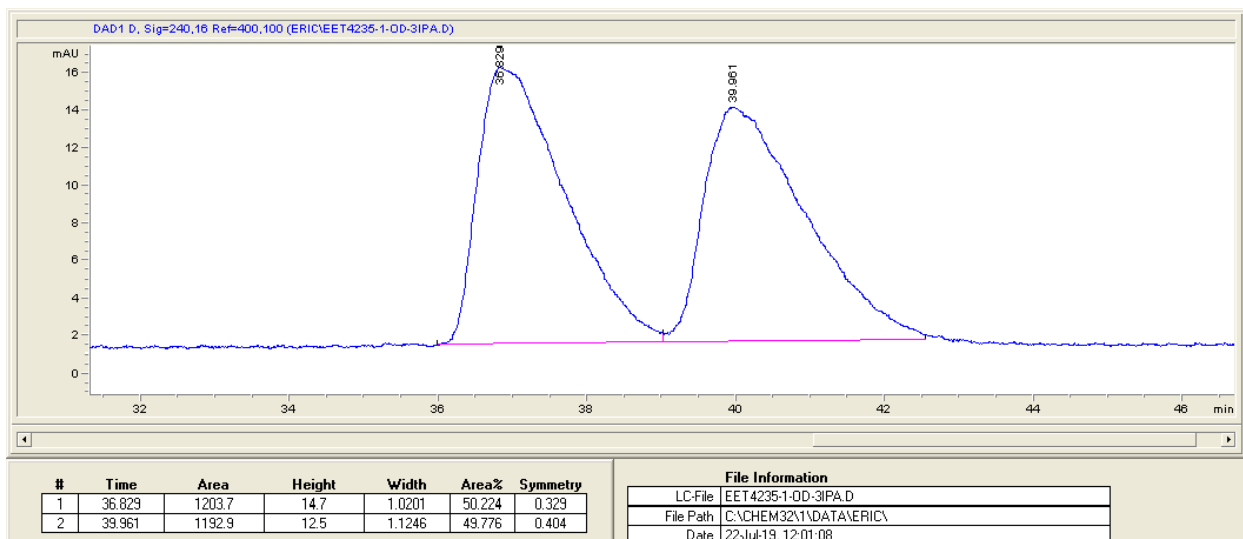


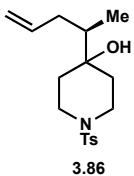
SFC OJ-H, 5% IPA:CO₂
 2.0 mL/min
 enantioenriched
 94% ee



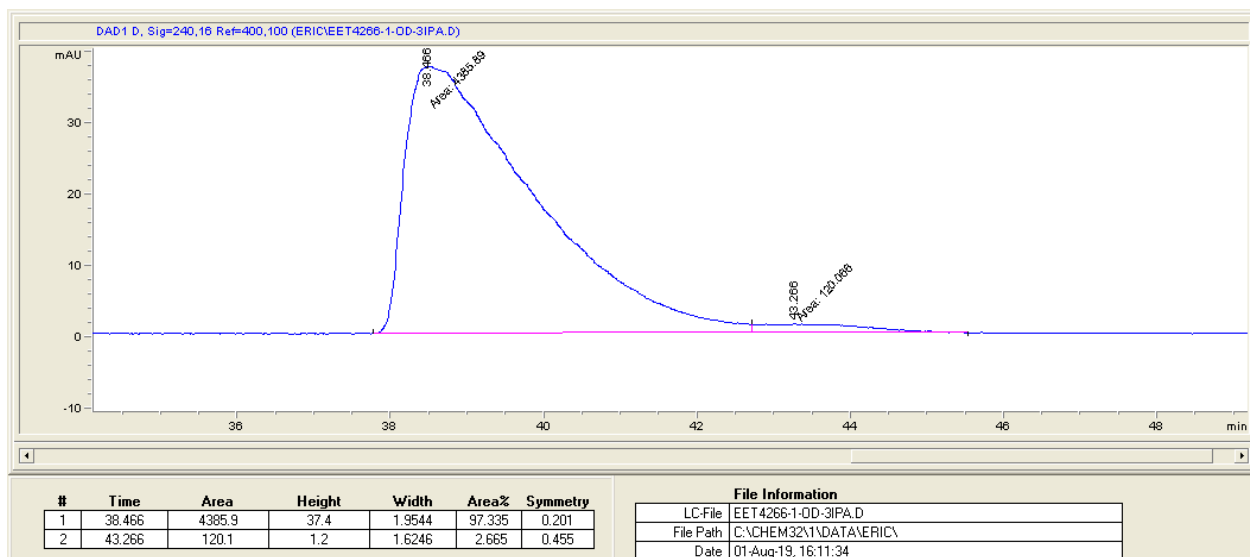


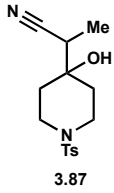
SFC, OD-H, 3% IPA:CO₂
2.0 mL/min
racemic



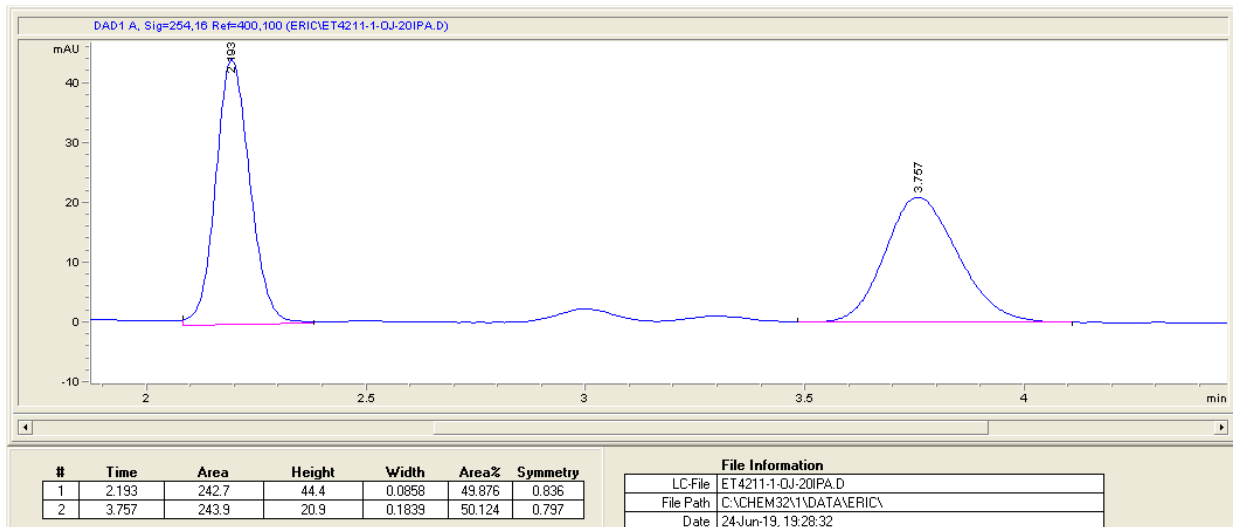


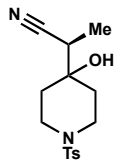
SFC, OD-H, 3% IPA:CO₂
 2.0 mL/min
 enantioenriched
 95% ee





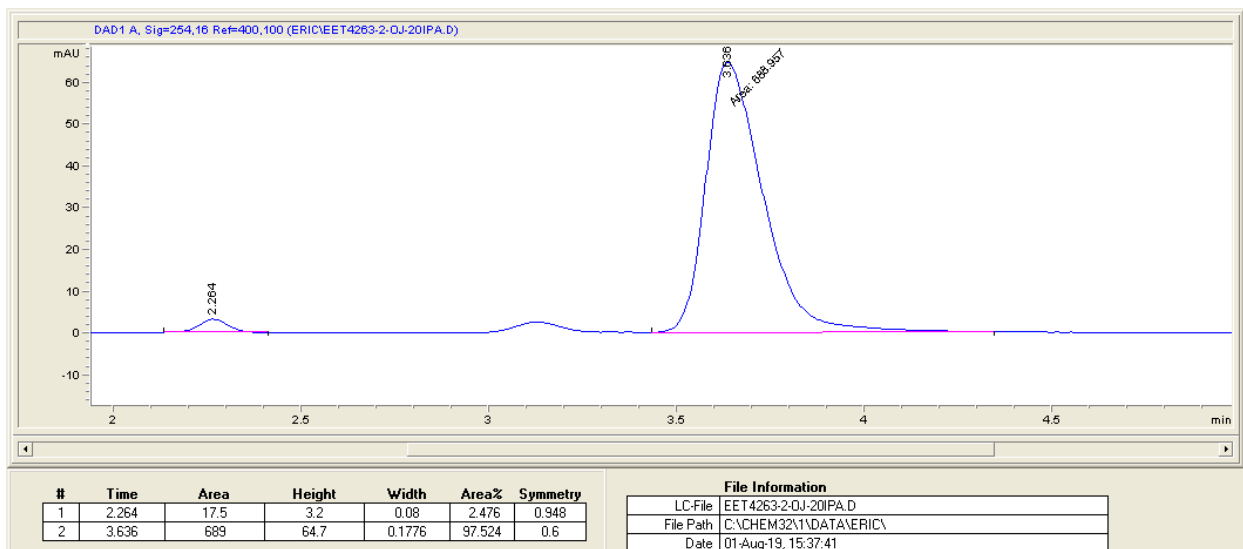
SFC, OJ-H, 20% IPA:CO₂
2.0 mL/min
racemic

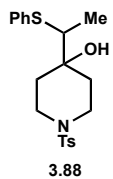




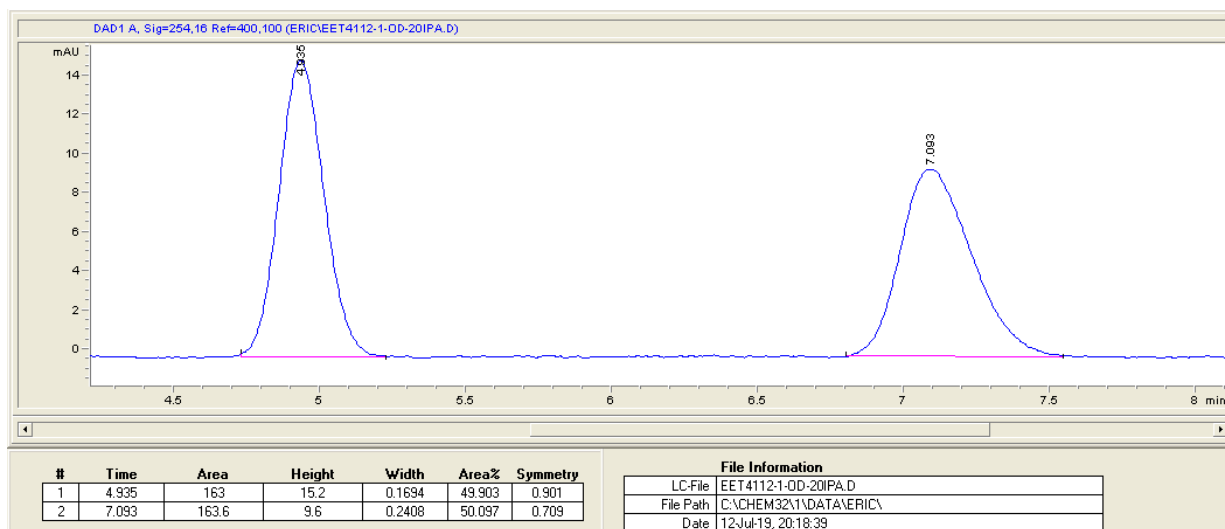
3.87

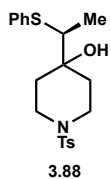
SFC, OJ-H, 20% IPA:CO₂
 2.0 mL/min
 enantioenriched
 95% ee





SFC, OD-H, 20% IPA:CO₂
2.0 mL/min
racemic





SFC, OD-H, 20% IPA:CO₂
 2.0 mL/min
 enantioenriched
 94% ee

